Final report of the
Joint WCRP/SCOR Working Group
on Air-Sea Fluxes
(SCOR Working Group 110)


INTERCOMPARISON AND VALIDATION OF
OCEAN-ATMOSPHERE ENERGY FLUX
FIELDS

by

Members of the WGASF


Edited by P.K.Taylor


Section A – Executive Summary,
and Chapters 1 to 9


June 2000

# TABLE OF CONTENTS

vi.

**PREFACE**

This document is the final report of the Working Group on Air-Sea Fluxes (WGASF) which was jointly sponsored by the World Climate Research Programme (WCRP) and the Scientific Committee on Ocean Research (SCOR). For the WCRP, because the question of surface fluxes is considered central to a number of its scientific projects, the WGASF reported directly to the Joint Scientific Committee. For SCOR, the WGASF was SCOR Working Group 110: "Intercomparison and Validation of Ocean-Atmosphere Energy Flux Fields". This joint sponsorship has impacted the work of the WGASF in a number of ways. On a logistic level, it resulted in more funding being available for meetings than would otherwise have been the case, which was clearly advantageous. However there have been more fundamental effects. In particular, although uniform terms of reference were agreed by WCRP and SCOR, the expectation with regard to the Working Group outcome was somewhat different. Typically a SCOR working group consists of experts in a particular field, chosen to reasonably represent the international membership of SCOR. They are tasked with reviewing a subject in some depth and producing a monograph which may be formally published in book form; often this may take several years. The requirements of the WCRP were somewhat different since the results of the WGASF were expected to have a direct impact on future WCRP projects. Thus the WCRP requirement was for an expert group capable of rapidly concluding its deliberations and of producing one or more reports within a restricted time scale. Fulfilling this last requirement was particularly difficult since the inception of the WGASF coincided with the first dissemination of the results from the "reanalysis" projects at the European Centre for Medium Range Weather Forecasting (ECMWF) and the US National Centers for Environmental Prediction (NCEP); projects which were clearly of major importance with regard to the estimation of air-sea fluxes but which would take time to evaluate. Indeed a first detailed global intercomparison of the various analyses is presented in this report.

It was clear even from the first meeting of the WGASF that, both to justify any evaluation of flux products and also to provide a suitable review for SCOR, it would be necessary first to summarise the requirements for surface fluxes, the state of the art with regard to surface flux estimation, and the methods available for flux validation. The first half of the report deals with these issues. Two later chapters deal with the evaluation of the basic meteorological variables (temperature, wind etc.) and of a number of available flux products. All the chapters have been assembled from many separate sections written by different Working Group members. Inevitably the degree of detail varies considerably; in some cases a comprehensive review has been undertaken, in other cases a point has been made by quoting typical examples. Often Working Group members have relied heavily on their own work - justifiable because it was directly relevant, but also very necessary because there was not the time or resources for a more comprehensive review. Thus this report should not be considered an exhaustive review on air-sea flux research. However the WGASF does believe that the report represents a reasonably balanced assessment of the present state of air sea flux determination.

The conclusions with regard to the relative merits of different flux products are less precise than might have been hoped or originally anticipated. However it must be emphasised that this uncertainty does not stem from a lack of evaluation effort (although more work would clearly be desirable). The detailed discussions presented in the earlier chapters of the report emphasise that there are a number of issues where our knowledge remains inadequate. These include, for example, the question of the correct transfer coefficients for the turbulent fluxes, and the reconciliation of measurements and radiative transfer modelling for the radiation balance. Many of these issues have been the subject of research for many years; however there has recently been significant progress both in measurement techniques and in our understanding. It is likely that, within a few more years, the absolute values of the surface fluxes over the earth's oceans will be much better known. It is hoped that this report represents a positive step toward that aim.

## EXECUTIVE SUMMARY

### The Working Group

The main aims of  the Joint JSC/SCOR Working Group on Air Sea Fluxes[1] were to review the requirements of different scientific disciplines for surface flux data sets,  to catalogue available surface flux data and flux-related data sets,  and to review the strengths and weaknesses of each.   The three meetings of the Working Group were (1)  NOAA Headquarters (Silver Spring,  Maryland,  USA),  22nd to 25th October 1997;   (2) KNMI (De Bilt, The Netherlands) 14th to 17th April 1999;  (3) SOC (Southampton, UK) 6th to 10th December, 1999.   The Working Group's findings are contained in this report, which has been prepared on an accelerated schedule at the request of the JSC.

### The Fluxes Considered

The Fluxes considered by the working group were the transfers of heat, water and momentum between the sea and the air.  The flux products considered were those which: were readily available to all scientists;  were a gridded, derived surface flux or flux related field; covered major ocean basin scales and upwards;  and, were adequately documented.  The Working Group has assembled a catalogue of flux products which meet these criteria.  It will be available on the Internet[2] and described in an appendix to this report.  Given the limited time and resources,  it only proved practicable to evaluate a subset of the more recently available flux products.  The Working Group also summarised the State-of-the-Art with regard to the basic meteorological variables (used in flux calculation),  and other important components of the climate system such as Waves and Sea Ice.

### Requirements and data sources

The Working Group has reviewed the requirements for flux fields and the characteristics of the various data sources available for flux estimation.  The latter include *in situ* data from ships, buoys, rigs, etc.; instruments on satellites either in polar (or other precessing) orbits or geostationary;  and models, run either in operational Numerical Weather Prediction (NWP) or reanalysis modes.   The requirements for surface flux fields are many and diverse.  However the Working Groups review suggests that there are four main types of requirement.

One class of requirement is the need for surface flux fields on high time and space resolution;  typically 3 hours and 50 km.   Such data are needed, for example,  for forcing ocean general circulation models,  for wave modelling and forecasting, and for regional weather nowcasting and prediction.  Such high space/time resolution is only possible at present using models,  however in future,  high resolution satellite products will become available.  The quality of the wind fields is particularly important for these applications and operational satellite-borne scatterometers are expected to make an important contribution.

A second class of requirement is for flux fields on longer space and time scales but with high absolute accuracy, typically within a few W/m$^2$.  Customers for these data include climate and sea-ice modellers.  At present such needs are difficult to satisfy because of the problems of quantifying systematic errors in the flux data.  Only by comparing flux values obtained using different data sources and estimation methods are these stringent accuracy requirements likely to be obtained.

---

[1]  (SCOR Working Group 110: Intercomparison and Validation of Ocean-Atmosphere Energy Flux Fields)

[2]      available from the WG web site: http://www-pcmdi.llnl.gov/airseawg/  (mirrored at http://www.lmd.jussieu.fr/pcmdi-mirror/airseawg/ and at http://www.bom.gov.au/bmrc/clch/pcmdi-mirror/airseawg/ )

Climate variability studies define a third class of requirement. Again high absolute accuracy is desirable, however consistency and continuity of the data over a suitable time period (and spatial domain) is the vital need. The longest time data set available is from the merchant ship observations (as assembled in the Comprehensive Ocean-Atmosphere Data Set, COADS). However the ship data suffers from poor sampling in many regions and time dependent biases due to changing ship characteristics and observational technique. Comparison with the reanalyses suggests that the COADS data can give useful information on interannual variability of monthly mean fluxes in the mid-latitude North Pacific and North Atlantic, and in parts of the South Atlantic; over much of the tropics and the Southern Hemisphere, north of 40S, the COADS data can only define a long-term monthly mean climatology. However, the reanalyses also suffer from time dependent biases because of the assimilation of data from the evolving observational system. Thus, whether using models or observations, the detection of long-term trends in the surface fluxes is difficult if not impossible. Satellite data has now been available for a significant and lengthening time period. Such data has the potential to provide a consistent time record but only if great care is taken to inter-calibrate sensors on successive satellites.

A final flux requirement is for high quality verification data. For example, NWP models need independent estimates of the basic meteorological variables and the fluxes for verification of the model physics. Such estimates must be associated with a realistic error assessment and specification of the true resolution of the data. Similarly Ocean General Circulation Model development would be aided by air-sea interaction experiments with measurements of the fluxes in both atmosphere and ocean, with ocean mixed layer measurements sufficient to allow budget closure. Such high quality measurements are not easy. The "flux buoy" systems are an example of instrumentation capable of providing verification data for both models and satellite - borne instruments.

## Flux Variability

For many applications it is important that a flux product contains accurate information on the variability of the fluxes. In some ways the determination of flux variability is easier than estimating mean flux values; systematic errors are of less importance, and the main spatial scales of longer term variability tend to be large. Numerical weather models tend to perform better with regard to determining the variability than they do in determining the mean; probably because they are targeted at forecasting the weather - the day to day variations in climate.

However despite these considerations, and the undoubted importance of surface flux variability, the Working Group considered that a detailed assessment of variability in the flux products could not be accomplished at this time. The report contains a brief discussion of flux variability to set the context for the flux field evaluations. It was noted that most previous studies had concentrated on the variability of basic variables, such as sea surface temperature (SST), rather than the fluxes themselves, and that further studies focused on the fluxes were desirable. The Working Group concluded that a thorough assessment of the variability of available flux products must remain an important priority for further studies, perhaps by a future working group.

## Direct Flux measurement

Direct measurements of the air-sea fluxes are too few to contribute directly to the calculation of large scale flux fields. Rather they are important for developing, calibrating, and verifying the parameterisation formula used to estimate the fluxes from the basic variables. Thus the accuracy of the direct flux determinations represents an accuracy limit for the indirect estimates. The methods of direct measurement of the radiative fluxes, turbulent fluxes, and precipitation were reviewed.

Accurate measurement of surface radiative fluxes is not easy, and with regard to the instrumentation needed there are contrasting views. Experts in radiation measurement assert

that only sophisticated instruments and procedures,  as defined by the Baseline Surface Radiation Network standards, will provide adequate accuracy.  However such measurements are difficult to implement at sea and will be restricted to very few sites.  In contrast, scientists involved in air-sea interaction studies believe that,  by avoiding known pitfalls,  consistent results can be obtained from simpler instrumentation.  Much depends on the accuracy and time resolution sought.  The simpler instrumentation should be adequate to highlight the biases in the radiative fluxes in many models (presently a few 10's $Wm^{-2}$ in some regions).

Estimation of the turbulent fluxes using fast response instrumentation mounted on research ships or buoys is becoming more common.  The techniques used in the eddy correlation method and the less direct, but more easily implemented, inertial dissipation method are summarised.  When implemented on a ship both methods are prone to errors but of differing nature.   Thus in future it is desirable that both methods be used to fulfil an important requirement,  the determination of the transfer coefficients for flux parameterisation (see below).

Rainfall, particularly that from tropical convection, is highly sporadic both in time and space.  For most applications area averaged values are required.  These can be obtained by ship or aircraft mounted radars on the local scale,  or from satellites in the longer term and on larger scales.  However the sensors and retrieval algorithms need to be verified by reliable ground-truth measurements.  Accurate measurement of rainfall at sea presents difficulties in two respects; there are measurement (instrumental) problems, and sampling problems.   New rain-gauges have been developed for high wind conditions but air-flow distortion by the ship remains a problem.  Even during intensive measurement campaigns the spatial and temporal sampling may be inadequate.  Results of different satellite algorithm intercomparison projects suggest that presently available *in situ* measurements and radar estimates are not representative enough to serve as a verification data source.

## Parameterisation of the fluxes

### *Radiative fluxes*

The parameterisation formulae for obtaining the net surface shortwave and longwave fluxes from ship observations are relatively crude,  relying on the estimate of cloud amount to characterise the effects of cloud on the fluxes.  Satellite based estimates use measurements of the top-of-the-atmosphere radiation,  and radiative transfer models (RTM's) to estimate the surface value.  For clear-sky conditions,  the surface LW values from a sophisticated RTM with *in situ* radiosonde data can be used to check the calibration of pyrgeometers.  However under cloudy conditions longwave RTM's are limited by the information available on both cloud base height and cloud emissivity.   This limits the reliability of satellite estimates of surface longwave; new techniques are being developed but still need evaluation.   Knowledge of atmospheric scattering is essential for shortwave RTM's under both clear and cloudy conditions. Uncertainty in the diffuse component may cause RTM's to over estimate the surface shortwave compared to measurements, possibly by a few percent.  Despite this, satellite estimates of shortwave radiation are more reliable than for longwave.  Atmospheric models (NWP and reanalyses) use simplified RTM schemes for  computational efficiency.  However at present the limiting factor in most models is the representation of clouds and their radiative effects.  In particular, low level stratiform clouds are often poorly modelled.

### *Turbulent fluxes*

The parameterisations for the turbulent fluxes are based on values of basic meteorological variables such as wind speed, temperatures, and humidity.  Since these "bulk formulae" are used for flux estimation from not only *in situ* data, but also satellites, and most models,  they were reviewed at some length by the Working Group.  Despite years of research there is still uncertainty with regard to the behaviour of the various transfer coefficients, in particular for sensible and latent heat at wind speeds over 10 m/s.  For this reason,  some newer parameterisations use wind stress estimates and surface renewal theory to predict the heat

fluxes. However, the variation of the drag coefficient with sea state remains controversial, particularly in sudden storms, or in light wind, swell dominated conditions. The newer algorithms also incorporate treatments of other physical processes, particularly light wind phenomena such as the diurnal warm surface layer and wind gustiness.

## Error Estimation

An important requirement of flux products, which is rarely satisfied, is the realistic estimate of accuracy. The error estimates should consider as many contributing factors as possible, both random and systematic. Representative error estimates may be difficult to determine. The report reviews some theoretical approaches, gives practical examples of quantifying random, systematic, and sampling errors, and shows that it is possible to estimate the cumulative errors.

Many applications need gridded flux fields that are complete both in space, and over some significant time period. The non-uniform sampling of in-situ and remotely-sensed fluxes necessitates the use of an analysis method to interpolate and, sometimes, extrapolate the data. Such techniques alter the error budgets of the flux fields. For example, depending on the choice of method and averaging period, sampling errors in remotely-sensed data may dominate the systematic biases. The advantages and disadvantages of two examples of mapping techniques were discussed. The successive correction technique is computationally simple and has been widely used. However it creates fields with spatially varying resolution, and spreads information so as to degrade the flux values in well sampled areas. In addition, error estimates are difficult to determine. Objective analysis techniques which take proper consideration of observational and sampling errors, and are capable of producing a posteriori error estimates, should be employed instead of the sucessive correction method. In particular, state-of-the-art variational techniques developed in the context of atmospheric and oceanic data assimilation should be applied to the analysis of surface marine fluxes.

## Evaluation of available products

### Methods of evaluation

The methods of evaluation for the basic variables and the flux fields include comparisons to reference data sets (such as direct flux measurements or those from high-quality sources) and intercomparisons between products. For the fluxes it is also possible to use integral constraints such as the global heat and water balance, oceanic transports, and enclosed basin budgets, as well as comparisons with other indirect flux estimates.

### Basic Meteorological Variables

It is important to know the accuracy of our estimates of the basic meteorological variables. Errors in these variables affect the accuracy of the surface flux values. Using the basic variables to verify model and satellite derived estimates avoids uncertainty due to the use of different flux parameterisation formula. As a rough guide, achieving 10 $Wm^{-2}$ accuracy in a heat flux estimate requires knowledge of wind speed to a few tenths m/s, air and sea temperatures to about 0.2K, humidity to about 0.3 g/kg; these requirements vary regionally being generally more stringent in the tropics.

For most of the basic variables, the Working Group reviewed the accuracy of high quality *in situ* measurements, standard *in situ* measurements, and satellite based estimates. The high quality measurements, as might be obtained from research experiments and "flux buoys" are of value for verification and for parameterisation development. The standard *in situ* data, for example from Voluntary Observing Ships (VOS), represent our only near surface measurement of many quantities for use both in flux estimation and model assimilation schemes. As instrumentation and retrieval algorithms improve, the satellite remote sensed data are increasingly being used to define the spatial and temporal variations of a given variable while the *in situ* data are used for verifying the retrievals.

The ocean affects the surface fluxes through the sea surface temperature (SST).  *In situ* observations of "SST" are often made at a few metres depth;  the SST difference due to the cool ocean surface skin can be allowed for,  but significant errors may occur if a near surface diurnal thermocline is present.   Satellite estimates are limited by the effects of cloud and biases due to cloud contamination (particularly at night) and the effects of aerosols.  The better SST analyses use combinations of satellite and *in situ* data. Typical RMS differences between analyses in most regions are a few tenths K,  greater than that in the Southern Ocean, in coastal regions, and in sea ice areas.

Variations of sea surface salinity (SSS) are not significant for air-sea flux calculation (although its mean effect must be allowed for in latent heat flux calculation).   However SSS is important for flux verification and for the freshwater forcing of ocean general circulation models.  *In situ* salinity data remain relatively few but will increase significantly due to projects such as ARGO.   The potential for, and difficulty of,  salinity measurement from space was reviewed.   Useful data may be obtained in regions of large salinity gradients,  however the 0.1 psu accuracy needed by ocean models is unlikely to be achieved by remote sensing in the near future.

Near surface air temperature is not easy to measure accurately in the marine environment.  Biases due to radiative heating of the sensor (or its surroundings), sea spray, etc., are common.   VOS data tends to be biased high, probably by a few tenths K on average, but by several degrees on occasion.  New techniques for estimating air temperature from satellite data have been suggested;  further evaluation is needed.  Fortunately, except in high latitudes,  the sensible heat flux is a minor part of the heat balance.  However air temperature is also needed in all regions for  stability corrections during latent heat flux calculation.

The latent heat flux depends on the humidity of the near surface air.   Humidity measurement on ships is in some ways easier than temperature determination.  However it is likely that VOS data are biased high, particularly where fixed thermometer screens are used.  Methods of determining near surface humidity data from satellites have improved significantly and useful accuracy is obtained in many regions.  However developing an algorithm which performs well both within and outside of tropical regions remains a problem.

There is no accurate absolute standard for near surface wind measurement over the open ocean.  Anemometer-based and visual estimates from ships,  and buoy measurements,  all are subject to systematic and random errors.   "Beaufort scale" values for the visually estimated winds have been calculated which, in the mean,  result in good agreement between visual and anemometer winds.  Importantly, the main reasons for the differences from previous Beaufort Scales are now understood.  Buoy winds may be biased low in high sea state conditions.  Satellite scatterometer winds are considered significantly superior to ship winds but the algorithms were developed using buoy data so biases may still remain.   Passive microwave derived wind speeds are useful for heat flux estimation.  They have the potential to provide good sampling and an increasingly long time series.

Waves are an important climatic variable in their own right and may, to some still uncertain extent,  modulate the surface fluxes.   The amount of wave data from buoys is increasing but the spatial distribution is poor.   Wave data from ship reports is generally considered to be of poor quality;  however it has been used to construct wave climatologies which are still much in use.  One problem is the separate reporting of,  but unclear distinction between, sea and swell.  Satellite altimeters provide verified global estimates of wave height;  algorithms for scatterometer wave estimation are still being developed.  Wave modellers believe that,  given an accurate wind field of high temporal and spatial resolution ( say 3 hours and 50 km), then a good quality wave field can be calculated.

Cloud amount  is used in some radiative flux parameterisations and is also important for the verification of NWP and climate models.  Sources of cloud data reviewed included ship reports and the International Cloud Climatology Project (ISCCP).  Precipitation  also may be estimated from ship weather reports;  however  variable satellite based estimates offer better

future potential. The Global Precipitation Climatology Project (GPCP) and the CPC Merged Analysis of Precipitation (CMAP) have produced precipitation climatologies which merge *in situ* and satellite estimates.

River inflow must not be neglected as a component of the ocean freshwater budget. Data are available through the International Hydrography Program (IHP) which published a Global River Discharge Catalogue, and from the Global Runoff Data Centre (GRDC).

Sea ice is an important climate variable which significantly modifies the surface fluxes and is also a component of the ocean fresh water budget. At present, sea-ice models can reproduce a realistic annual cycle of the global sea-ice cover. Probably this is despite large but opposite errors in the fluxes over sea-ice. Now that multidecadal satellite and submarine records of ice extent and ice thickness are available, the challenge is to understand interannual variability. This will require a higher level of accuracy in estimates of the radiative forcing of the ice surface and data on the interannual variability of snowfall. The errors in reanalysis and satellite-derived surface flux fields must be better characterised and then reduced by more thorough comparisons amongst themselves and with *in situ* observations. Boundary layer formulations need to be examined for their applicability in predominantly stable polar conditions.

*Flux field products*

Newer products based on *in situ* data[3] have benefited from the valuable new data sets constructed by the COADS project. For wind stress the newer climatologies are definitely to be preferred since previous climatologies, such as Hellerman and Rosenstein (1983) or Oberhuber (1988), over estimated the wind stress in most areas. However poor *in situ* sampling in the southern hemisphere, and particularly in the Southern Ocean (where the winds are underestimated in almost all *in situ* climatologies), suggests that the lengthening satellite derived wind data-set is a promising alternative. For the heat fluxes, our inability to balance the long term mean global heat budget together with the uncertainty in the transfer coefficient values, remains a major hindrance to evaluating many of the flux products.

To illustrate the problem: the global heat balance of the SOC climatology was 30Wm[-2]; almost exactly the same as the for the UWM product. This was despite the use of corrections for observation biases in the *in situ* data. In a tuned version of UWM, shortwave radiation was decreased (by about 10%) and latent heat flux increased (by about 14%) resulting in a balanced budget. Previous flux studies have required similar adjustments, often to ensure that the heat transport in the ocean agreed with oceanographic estimates. The satellite estimates of net SW radiation do not support reduction of the shortwave flux (although they in turn may be over-estimated). However by adjusting the other fluxes in various ways a variety of balanced budgets can be produced. As a result, the various estimates span the range of the values from NWP models and reanalyses[4]. The overall conclusion is that for the global balance, and also for zonal averages, the differences between the various flux products are within the uncertainty of the observational estimates (with only one or two outlying exceptions).

Interestingly, almost all adjustments suggest that the latent heat flux must be increased, toward the higher values for latent heat flux predicted by most models. Such an increase would generally worsen the agreement between climatologies (such as UWM or SOC) and the high quality buoy data; however the latter also depend on transfer coefficients to determine the fluxes. Thus while comparisons of fluxes from ship observations and buoys suggest that

---

[3]  Here we will refer to *in situ* climatologies produced at the University of Wisconsin-Milwaukee (UWM), the Southampton Oceanography Centre (SOC) and the Institut f r Meereskunde, Kiel (IfM).

[4]  The reanalyses considered were the ECMWF 15 year reanalysis (ERA15), the NCEP/NCAR reanalyses (NCEP1 and NCEP2) and the Goddard GEOS reanalysis (GEOS1).

NCEP1, NCEP2 and ERA15 evaporation may be too large, we can not be certain. This also reflects the uncertainty in our knowledge of the strength of the hydrological cycle. New satellite based products may help through better estimates of precipitation (although there is a lack of verification data) and global estimates of evaporation. With regard to the latter, the HOAPS climatology[5] suggests that *in situ* climatologies under-estimate evaporation in the Southern Ocean. Further development of these satellite products is needed, for example, the HOAPS latent heat flux is biased low in convective tropical regions.

Other significant differences exist between the different products on a regional level and in some cases the cause can be identified. For example, the reanalyses all appear to have substantial errors in surface radiation fields, reflecting problems both with regard to clouds and clear sky radiation. NCEP1 had errors in the downward shortwave and the albedo which tended to cancel. A major shortcoming for ERA15, GEOS1 and NCEP2 appears to be a lack of low-level stratiform clouds over the eastern subtropical oceans. Satellite Surface Radiation Budget (SRB) short wave radiation appears to have more realistic patterns than the reanalyses, but may have a positive bias. Even the estimates from crude *in situ* parameterisations are in better agreement with SRB than are the models.

*Choice of Product*

Considering the recent, global climatologies based on *in situ* data, UWM and SOC are similar. The SOC climatology gives marginally better agreement with buoy measurements and may be preferred for regional studies. However for a balanced global net heat flux (e.g. for forcing models) then the tuned UWM fluxes must be preferred; these also cover a longer time period. More use should be made of the UWM sensitivity fields for producing new versions of the constrained fluxes. In all cases the sampling density in any particular region must be considered when using these products.

Covering the Atlantic Ocean only, the IFM climatology has used a better mapping technique, has good error estimates, and implies a realistic meridional heat transport. The latter is due to the choice of radiation parameterisations and transfer coefficients which are not generally used for open ocean regions (but are within the bounds of uncertainty). Further verification of this new product is desirable.

The NCEP1, NCEP2 and ERA15 reanalyses appear to have more realistic fluxes than the earlier GEOS1 reanalysis (the GEOS data assimilation system has since been substantially developed). At present the NCEP1 reanalysis covers the longest period and is the most widely distributed and studied. It has the most realistic oceanic low-level stratiform clouds. NCEP2 corrected mistakes in NCEP1 and used improved short wave radiation and boundary layer parameterisations. Its precipitation patterns, downward short wave radiation at the surface, and equatorial wind stress appear superior to NCEP1, but its sensible heat flux over the oceans is lower than all other estimates. ERA15 is the highest resolution reanalysis now available. It appears to produce the most realistic precipitation patterns of the four reanalyses and has more realistic surface downward short wave radiation than NCEP1. Concerning month-to-month variability in surface fluxes, GEOS1 had, in general, the smallest variability, NCEP2 tends to have the largest.

For most of the world ocean, satellite based products are capable of providing much better time and space resolution, and more consistent accuracy, than fluxes based on *in situ* observations. With passing years the restricted time period for which data is available is becoming less of a disadvantage. The surface shortwave flux fields are superior to the model estimates; and presumably also to *in situ* estimates. However on a regional basis the difference between satellite and ship estimates is similar in magnitude to the difference between different satellite fields. The satellite longwave estimates remain less reliable. Satellite scatterometer wind data has significantly less scatter than ship observations. Satellite estimates of the latent

---

[5] Hamburg Ocean Atmosphere Parameters and fluxes from Satellite data.

heat flux have improved substantially but problems still remain in some regions. Satellite precipitation estimates have not been evaluated here other than to review the various comparison projects that have been undertaken by others; lack of verification data is a major problem. For the future, satellite products should exploit combinations of different sensors, preferably flown on a single platform (as for example, the TRMM mission). Combined satellite and *in situ* data products have the potential to provide a data set which is independent from the models.

In summary, all the various flux products that were reviewed in this report have different advantages and disadvantages. However, it is also evident that the various flux products are complementary rather than being in competition, and that the ensemble of air-sea flux estimates that they represent cover the time and space scales that ocean science studies are investigating.

## Specific Recommendations

The main conclusions from the Working Group's endeavours appear throughout the body of the report, are summarised in the final Chapter, and have been described above. At its final meeting, the Working Group also adopted the following specific recommendations:

❍ Reanalyses should be performed every 5-10 years by more than one centre; adequate resources should be provided to the reanalysis efforts to improve their surface fluxes, to carry out and evaluate the reanalyses and to ensure that they are easily available to the entire scientific community. Surface fields should be output every 3 hours .

❍ Evaluation of the surface fields and fluxes from global operational NWP systems will benefit future reanalyses as well as provide critical guidance and product uncertainty estimates to users of these flux products. The WGNE's plans to archive and evaluate the surface fields and fluxes from a number of global NWP systems should therefore be supported.

❍ A network of high quality "flux reference platforms" (combination of long-term moorings and ships) should be established to deliver highly accurate values of stress and all components of the air-sea heat fluxes for, *inter alia*, verification of surface fields and flux estimates from satellites and models, and the long term calibration of satellite sensors.

❍ There is continuing need to compare and assess the quality of fluxes derived from various sources, and to evaluate the parameterisations used. Encouragement should be given to efforts to enhance the reliability of momentum, net heat and freshwater fluxes by combining the best estimates from these various sources.

❍ Support should be provided for the continuing assembly of flux and flux-related data sets (in particular Voluntary Observing Ship-based collections such as COADS and other historical data). Continued efforts are needed to remove non-stationary observational biases in historical data. Basic meteorological variables should be included as well as uncertainties, error estimates and adequate documentation for all flux data sets. A catalogue of flux data sets should be maintained on the Internet.

❍ Research and field experiments are needed to improve boundary layer parameterisations and bulk formulae, especially in regions where our physical understanding is poor. Adequate resources for complete analysis of the resulting data are necessary to realise the full benefits of the field experiments.

# 1  INTRODUCTION

## 1.1  The Surface Flux Field Problem

The extent to which the earth's climate may be changing,  either due to the actions of mankind or natural variability,  is at present a major cause of societal concern.   Numerical models of the earth's climate system are being used to quantify the possible effects of climate change.   A vital test of such models is to verify that the present day climate is correctly simulated.   An important aspect of that simulation is the transfer of energy between the ocean and atmosphere,  the air-sea fluxes of heat, water, and momentum.   These fluxes represent key-processes in the earth's climate system;  they establish links and feedbacks between its main components,  the ocean and the atmosphere.

In recent years there has been significant progress in our knowledge of the surface fluxes.  Air-sea interaction experiments have refined the formulae used for flux calculation,  we have better understanding of the errors in data and the corrections needed,  methods of obtaining fluxes from satellite data have been developed,  and weather forecast models have been used to produce a consistent re-analysis of the past state of the atmosphere.  Unfortunately, despite these advances,  the observational flux data remains limited and various attempts to produce climatologies of the flux fields,  and to describe their climatic variability,  differ in significant aspects.   The major problem is that,  while the magnitude of the flux components is of order a few 100 $W/m^2$,  both the inter-annual variability and the mean heat flux in any region is typically a few 10's $W/m^2$,  and the mean net heat flux must balance to within a only few $W/m^2$.   This places stringent requirements on the accuracy of flux estimates which we are still struggling to meet.   For example Figure 1.1 shows recent estimates of the annual mean distribution of the net heat flux.   Two examples of fluxes calculated from weather forecast models,  which have been used to reanalyse the past weather,  are compared to two climatological estimates based on ship weather observations  ("COADS").   It is obvious that the fluxes calculated from the ship data have more areas where heat is going into the ocean compared to the other estimates.   Since unrealistically large ocean heating would result,   these fluxes cannot be correct and various adjustment schemes have been proposed.   However, where comparisons with high quality buoy data are available,  the ship data often show good agreement - better than that which the models typically achieve.   Thus the bias can not be uniform but must vary both regionally and temporally.   Similarly,  while the heating and cooling calculated by the models is better balanced globally,  in some regions large errors may occur both in the flux components and the net heat flux.

Given this situation,  the main aims of  the Joint WCRP/SCOR Working Group on Air Sea Fluxes  (SCOR Working Group 110: Intercomparison and Validation of Ocean-Atmosphere Energy Flux Fields) are to review the requirements of different scientific disciplines for surface flux data sets,  to catalogue available surface flux data and flux-related data sets,  and to review the strengths and weaknesses of each.   The working group's findings,  contained in this report, will be of particular use for those developing numerical climate models for research and forecasting purposes.

## 1.2  The Joint WCRP/SCOR  Working Group on Air Sea Fluxes

### 1.2.1  Creation of the Working Group

Proposals for co-ordinated activities in the World Climate Research Programme (WCRP) in the area of air-sea fluxes stemmed from the WCRP *Workshop on Air-Sea Flux Fields for Forcing Ocean Models and Validating General Circulation Models* in October 1995 (White, 1996a).   This workshop was a landmark in encouraging interaction and dialogue between the diverse scientific communities involved in producing and using air-sea fluxes; hitherto it had been limited.   Among the principal recommendations from the workshop was the need to continue to foster interdisciplinary consultations in this area,  and to catalogue and

keep under review available surface flux and flux-related data sets.   It was suggested that a limited-life group should be established to carry forward the needed activities.
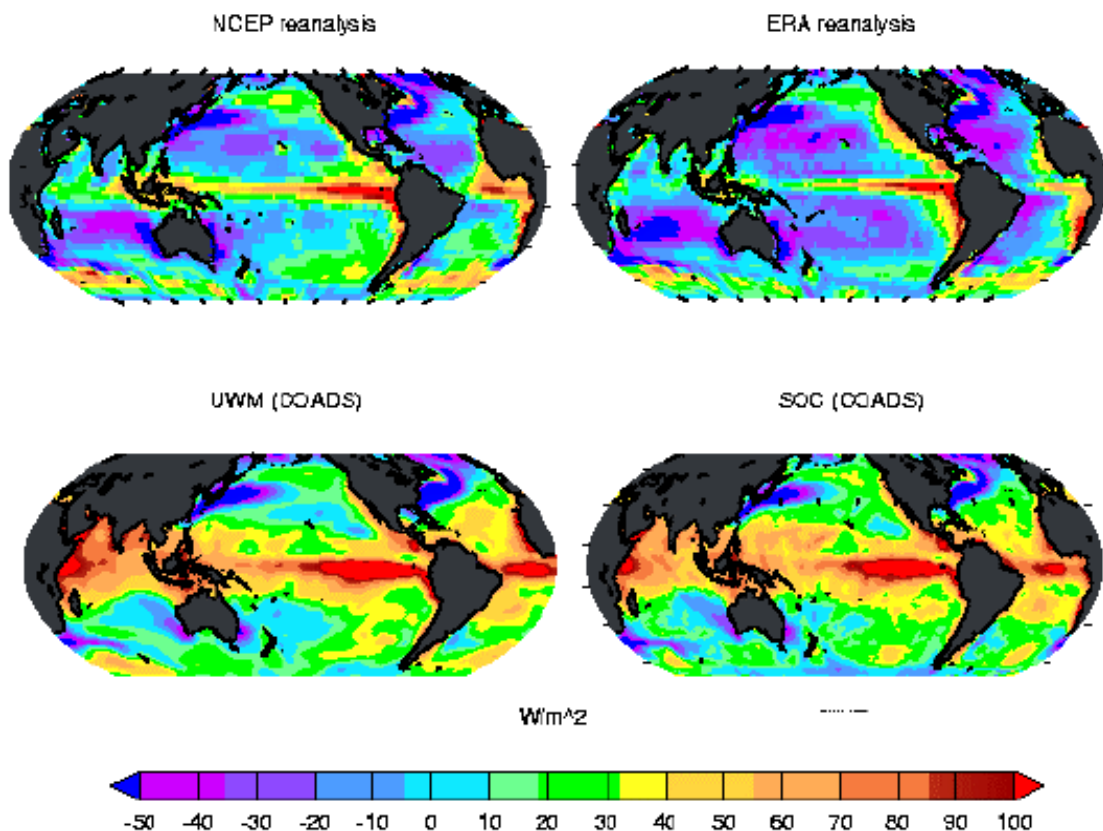


Figure 1.1   The annual mean net surface heat flux from the atmosphere into the ocean (negative implies ocean cooling).  Shown as examples are values from the NCEP/NCAR reanalysis,  the ECMWF reanalysis, and the climatologies based on ship data in the COADS data set as calculated by UWM and SOC (see  Chapter 11 for a detailed discussion)

        The Scientific Committee on Oceanic Research (SCOR) is also very interested in air-sea fluxes,  especially their use in the determination of meridional heat and freshwater transports - basic features of ocean climate.   Therefore a proposal was made to establish a SCOR Working Group on Intercomparison and Validation of Ocean-Atmosphere Flux Fields. Since the roles of the WCRP and SCOR groups overlapped and included several common members,  it was considered reasonable to merge the interests of the WCRP and SCOR in this area and to create a joint **WCRP/SCOR Working Group on Air-Sea Fluxes.**   T h e establishment of the joint group,   its terms of reference and membership were duly endorsed by the Joint Scientific Committee (JSC) for the WCRP at its eighteenth session (Toronto,  March 1997).

*1.2.2  The remit of the Working Group*

The Terms of Reference (TOR) agreed between the JSC and SCOR were:

TOR.1  to review the requirements of different scientific disciplines for surface flux data sets;

TOR.2 to compile a catalogue of available surface flux data and flux-related data sets, including those becoming available from the various reanalysis projects, and to review, in consultation with users and producers, the strengths and weaknesses of these data sets;

TOR.3  to inform the scientific community of the work of the group by the use of the World Wide Web,  by the publication of the final catalogue,  and by convening,  at a suitable time, a scientific workshop;

TOR.4 to keep the JSC and SCOR informed of progress in the area and present recommendations for action as necessary.

*1.2.3  The Working Group's Mode of Working*

The first meeting of the Working Group on Air-Sea Fluxes took place at NOAA Headquarters (Silver Spring, Maryland, USA), during the 22nd to 25th October 1997. The mode of working was agreed and a draft table of contents for the final report was adopted. Over the following 17 months a draft report was assembled from the contributions of working group members. This draft was discussed at the second Working Group meeting held 14th to 17th April 1999, at KNMI (De Bilt, The Netherlands). Although the Working Group had planned to finish its work by summer 2000, in response to a request from the JSC, the schedule was brought forward to produce a completed draft by the end of 1999. Accordingly a third meeting was scheduled to be held at SOC (Southampton, UK) during 6th to 10th December, 1999. At this meeting the report was reviewed and the Working Groups conclusions agreed. The final version of the Working Group report is the result of further editing following that meeting. Because of the shortened time scale it has not proved possible to circulate the report within the air-sea flux community for comment and the final version therefore mainly represents the understanding and beliefs of the Working group members.

## 1.3  The variables to be considered

The basic set of physical fluxes between the atmosphere and ocean are the transfers of shortwave radiation ($Q_{sw}$ - wavelength 0.3 to 3 µm), longwave radiation ($Q_{lw}$ - wavelength 3 to 50 µm), sensible heat ($Q_{sen}$), water vapour ($E$), precipitation ($P$), and momentum ($\tau$ - wind stress). For many purposes the radiative fluxes are characterised by the downwards component of the flux, and the upwards shortwave and longwave fluxes are determined from the surface albedo, A, and the sea surface temperature respectively. Given this basic set of fluxes, other flux variables which couple the atmosphere and ocean can be determined. Thus for the latent heat flux $Q_{lat}$, net heat flux $Q_{net}$, and the freshwater flux, $F_w$, we have:

$$Q_{lat} \propto E \qquad\qquad Q_{net} = Q_{sw} + Q_{lw} + Q_{sen} + Q_{lat} \qquad\qquad F_w = E - P \qquad\qquad (1)$$

The dynamic coupling between atmosphere and ocean depends both on the temporal and spatial variability of the fluxes. Water masses can form at the surface of the ocean in response to the buoyancy flux $F_\rho(Q_{sw}, Q_{lw}, Q_{sen}, E, P)$ and the mixing by the wind, and surface water is also carried into the interior of the ocean by Ekman pumping due to curl $\tau$ and by spatial differences in the ocean's response to the buoyancy forcing. The ocean currents that redistribute heat are driven both at the surface and in the interior by curl $\tau$ and the density gradients that result from the surface buoyancy flux.

The air sea fluxes can be obtained in several ways. The most straightforward, but also most difficult, is the direct measurement of the fluxes. Due to its complexity, direct measurement of fluxes is limited in space and time. However, it provides valuable data for developing formulae to estimate the fluxes and for the validation of fluxes derived from other sources.

Fluxes with a larger coverage of space and time usually come from satellite measurements and/or the application of bulk formulae. Bulk formulae are a parameterisation of fluxes in terms of variables that can be measured more easily, e.g., temperatures. These variables are referred to as *basic variables* in this report (Table 1). Traditionally, they are obtained from ship observations, which have been collected in the COADS data set (Woodruff et al 1993), but nowadays also satellite measurements are used. The same bulk formulae that are applied to measurements are also used in numerical models to calculate fluxes from the basic model variables. Because most of the available flux values are based on parameterisations in terms of the basic variables, large parts of this report are devoted to parameterisation formulae and the measurement of those basic variables.

## 1.4  The flux products assessed

During the first meeting the working group determined that the flux products which would be considered would be those which:

(i)     are readily available to all scientists either routinely or on request;
(ii)    are a gridded, derived surface flux or flux related field;
(iii)   cover major ocean basin scales and upwards;
(iv)    are adequately documented.

The Working Group has assembled a catalogue of flux products which meet these criteria (Appendix C).  However,  given the limited time and resources,  it has only proved practicable to consider a subset of these products.   Nevertheless this subset includes the main recent global flux field products (Table 2).  Other products are included in the Catalogue of Flux products (see Appendix B) but are not considered in the Report,  for example because they are new products that could not be evaluated before the report was finalised (e.g. J-OFURO, Kubota  1999).

Table 1. Summary of the Basic Flux-Related Variables

| | |
|---|---|
| Sea surface temperature (SST) | Waves |
| Sea surface salinity (SSS) | Cloudiness |
| Air temperature | Precipitation |
| Air Humidity (specific humidity, or mixing ratio) | River inflow |
| Wind (speed and direction) | Sea Ice |

Table 2.  Summary of the flux products considered in this report.

| Type | Product | Reference |
|---|---|---|
| *in situ* | UWM (COADS) | da Silva *et al.* (1994) |
| *in situ* | SOC (COADS) | Josey *et al.* (1999) |
| *in situ* | IFM (COADS) | Lindau (2000) |
| model | ECMWF: ERA15 | Gibson *et al.* (1997) |
| model | NCEP/NCAR Re-analysis 1 | Kalnay *et al.* (1996) |
| model | NCEP/NCAR Re-analysis 2 | Kanamitsu *et al.* (2000) |
| model | GEOS1 | Schubert *et al.* (1995) |
| Satellite | HOAPS | Schulz *et al.* (1997) |
| Sat. Rad. | Various US products | |
| Sat. Rad. | New Japanese products | |
| Combined | Residual | Trenberth & Solomon (1994) |

## 1.5  Layout of the report

The different requirements for flux data sets will be summarised in Chapter 2.   In many cases the requirements include knowledge of the variability of the fluxes.  Indeed,  the space-time variability of the fluxes not only defines a set of accuracy requirements,  it also impacts the sampling requirements,  and the accuracy to which the fluxes can be determined.   While

detailed treatment of flux variability was considered beyond the remit of the present working group,  Chapter 3 gives a summary of the state of knowledge of flux variability.  The characteristics of the data sources for either flux values,  or values of flux related variables,  will be considered in Chapter 4.  We will then summarise the state of the art with respect to Direct flux measurement (Chapter 5).  However most flux fields are based on parameterisation formula and these will be considered at some length for the radiative fluxes (Chapter 6) and turbulent fluxes (Chapter 7).  Sources of error in the flux determinations,  such as the sampling density, are considered in Chapter 8.  Chapter 9 discusses methods of evaluating the various available products for fluxes,  and flux related variables.  The state of the art for determining the basic variables will then be reviewed (Chapter 10).  The results of the evaluation of the flux products are given in Chapter 11.  Finally the conclusions (Chapter 12) will include suggestions for future flux related activities.  The working group membership is listed in Appendix A, Appendix B describes the catalogue of flux products , Appendix C lists the acronyms used in the report.

## 2  THE REQUIREMENTS FOR SURFACE FLUX DATA SETS.

### 2.1  Introduction

There are many requirements for surface flux values,  for example,  operational modelling,  nowcasting/forecasting;    climate change studies and diagnostic studies; atmospheric and oceanic synoptic scale case studies;    shelf and coastal seas studies;  oceanic, climate and earth observing systems;  biogenic cycles,  wave forecasting, marine engineering, etc.   To consider the requirements of all of these applications would be a large task and probably not helpful.   However,  the types of surface flux fields considered by the Working Group are large scale,  non-real time,  documented products.   The main requirements for these types of flux fields are those for climate models: atmospheric General Circulation Models (GCM's), oceanic GCM's,  and, for verifying coupled atmosphere ocean GCM's.

This Chapter will discuss the flux requirements for atmospheric and ocean GCM's on a global scale, and also the requirements for some specific applications:  regional applications and studies, wave models,  and sea ice modelling.   The needs of Global Climate Models and Climate Change Studies will also be discussed.  Finally an attempt will be made to summarise all these different requirements for surface flux information.

### 2.2  NWP systems—assimilation and forecasting

#### 2.2.1  Introduction

Atmospheric computer models used in meteorology are based on the laws of physics as expressed in the equations of fluid mechanics (e.g. see Kalnay, 1999).  For both numerical weather prediction (NWP) and climate simulations they are integrated in time from an initial realistic state of the atmosphere obtained through data assimilation.  Climate simulations are integrated long enough (typically months to years) so that the details of the initial conditions are unimportant and are generally run at lower resolution than NWP models.  Climate simulations tend to focus on the atmospheric response to variations in boundary forcing fields; their requirements for air-sea flux fields are discussed elsewhere.

NWP provides the basic guidance for modern weather forecasting on time scales from seconds to years.  Successful forecasting requires both realistic representations of atmospheric processes and accurate initial conditions from data assimilation.  Early NWP models contained very limited or no parameterisation of physical processes; modern NWP models include physical parameterisations that attempt to reproduce all important atmospheric processes, all exchanges of radiation with space and all exchanges of momentum, water and energy with the earth's surface (Pan, 1999).  The increasing sophistication and accuracy of such physical parameterisations has contributed to the tremendous improvement in the skill of weather forecasts over the last 20 years (Kalnay *et al.,* 1998).

Data assimilation creates an initial atmospheric state for NWP (Zupanski and Kalnay, 1999).  It is designed to produce the atmospheric state that will yield the best subsequent forecast.  In operational practice it is used continuously in data assimilation cycles.  In each cycle, usually every 6 hours, a new analysis is produced by a combination of observations and a short-range model forecast from the previous analysis.  The short-range model (first guess) forecast interpolates in space and time between observations and also serves as one of several quality control checks on the observations.  The observations used include:

A. CONVENTIONAL

   1) rawinsondes providing vertical soundings of temperature, moisture and wind.

   2) aircraft observations of wind and temperature at flight level.

   3) surface observations  of pressure, temperature and humidity from land stations, ships and moored drifting buoys.

B. SATELLITE

    1) vertical retrievals of temperature and moisture generated by NOAA/ NESDIS[1] from TOVS vertical sounders on NOAA polar orbiters. Some data assimilation systems, including the NCEP and ECMWF operational systems and the ECMWF ERA reanalysis, now use the radiances observed by TOVS instead of the derived temperature and moisture profiles.

    2) cloud-tracked winds from geostationary weather satellites.

    3) surface winds from scatterometer instruments on polar orbiters.

    4) surface wind speed from SSM/I .

Research is underway on the assimilation of precipitation estimates from satellites and other sources. It is hoped that such assimilation would improve the tropical analysis, particularly the divergence of the wind field. Extensive experimentation with data assimilation systems is now underway investigating the impact of different current and proposed observations on numerical weather prediction. These experiments are designed to guide the design of the future observational system.

The use in data assimilation of a first-guess model forecast acts to make the initial condition of the atmosphere more compatible with the time integration of the model, although two significant errors can develop. One is 'spin-up' during the initial stages of a forecast, reflecting an imbalance between the initial conditions which are influenced by both the forecast model and observations and the atmosphere consistent with the forecast model's physics and dynamics (White and Saha, 1999). This is often manifested as significant changes in the hydrological cycle during the first few hours or days of the forecast. The second error is climate drift, a systematic tendency for atmospheric models to drift away from the actual atmospheric climatology towards their own model climatology (Kalnay, 1999). Several papers document examples of these errors, including Heckley (1985), Arpe and Klinker (1986), Caplan and White (1989), Arpe (1989, 1991) and Klinker and Sardeshmukh (1987).

One problem with NWP data assimilation has been the frequency of changes in the analysis/forecast systems over the years. While the changes have produced greatly improved weather forecasts, they have also caused changes in the analysed fields that can exceed and mask interannual variability. These changes are particularly noticeable in physical fields such as precipitation and air-sea fluxes (Siefridt *et al.*, 1999). To remedy this problem of apparent climate changes due to data assimilation or model changes, several meteorological centres have conducted extensive 'reanalyses' of past atmospheric data using a modern, frozen analysis/forecast system (White and Saha, 1999). The climate change record in the reanalyses can still be contaminated by changes in the observing network over time, such as the introduction of satellite observations in the 1970's (White, 1999).

*2.2.2 The needs of data assimilation systems for flux fields*

Modern data assimilation systems contain atmospheric models that produce flux fields determined by physical parameterisations from surface and near-surface model fields of temperature, moisture and wind. These flux fields are usually generated at each model time-step and accumulated over the length of the first guess forecast or over some other forecast interval. Thus the flux fields from data assimilation are usually from short-term forecasts. These flux fields and flux-related variables need to be carefully verified against independent estimates and observations.

Assimilation systems combine observations with fields from the short-range forecasts and use the short-range forecasts as part of the assessment of the quality of the observations. Data assimilation groups need to know how well their analyses and short-range forecasts agree

---

[1] a comprehensive list of acronyms used in the report can be found in Appendix C.

with the observations and whether their systems draw sufficiently from the information in the observations. Quantitative estimates of the uncertainties in the observations are used in the analysis; better estimates of observation error would be useful. Observations not used in the data assimilation provide an independent check on the analyses. Quantitative estimates of the uncertainties in the independent observations are also useful in order to assess correctly how well the data assimilation fields fit the independent observations.

Independent flux estimates permit a check on the physical parameterisation used in the assimilation system. If the data going into a parameterisation are close to independent estimates, but the fluxes calculated by the parameterisation are not, this could reveal a need to update the parameterisation scheme. Comparison of different flux algorithms could help data assimilation groups improve their parameterisation. Such a comparison of bulk aerodynamic algorithms for computing sea surface fluxes has been carried out by Zeng *et al.* (1998) using TOGA COARE and TAO data. The study led to a change in the thermal roughness length over the ocean in the US National Centers for Environmental Prediction's (NCEP) operational global model.

High quality observations and flux estimates from field experiments such as TOGA COARE can be especially valuable in evaluating the performance of a data assimilation system. Comparisons of the NCEP reanalysis to results from FIFE, a land surface field experiment over the central United States, played an important role in developing a new boundary layer parameterisation that substantially improved the NCEP operational global model (Betts *et al.*, 1996; Hong and Pan, 1996). Comparisons of surface fluxes from the European Centre for Medium-range Weather Forecasts (ECMWF) ERA reanalysis and NCEP reanalysis to surface fluxes from TOGA COARE and other in-situ observational campaigns have also been made (Klinker *et al.*, 1999; Moyer and Weller, 1997; Hendon and Shinoda, 1999). Recent development of single column versions of NWP models makes the comparison of model physics to field experiments easier and more complete. Uncertainty estimates need to be provided. In data assimilation analysis/forecast systems all the physical parameterisations influence each other; adjusting one physical parameterisation to fit one independent estimate or one field experiment too closely may distort other physical fields or the same physical fields in other locations.

The purpose of operational data assimilation at NWP centres is to provide the initial condition that gives the best forecast, not necessarily the initial condition that fits observations most closely nor the initial condition that makes maximum use of all available observations. A few years ago the assimilation of satellite estimates of column-integrated precipitable water was introduced into the NCEP global operational analysis/forecast system. It was subsequently found, however, that the use of this data led to excessive precipitation over the tropical oceans during the first few days of the forecast and, in response, too little precipitation over the tropical continents. The artificial drought over tropical continents amplified with time due to the interaction of precipitation and soil moisture. While there was some evidence of biases in the satellite estimates, the main problem was believed to be incompatibility between the model physics and the satellite estimates of precipitable water. The use of satellite estimates of precipitable water in the NCEP global data assimilation was discontinued. Research on how to use these estimates and how to improve model physics continues at NCEP. This shows how closely coupled data assimilation and model physics are in modern NWP. The assimilation of new data, such as satellite moisture fields or precipitation estimates, may require changes in the physical parameterisations of the model.

Operational NWP serves many users interested in many different phenomena and different forecast lengths. Aviation users of global forecasts are interested in short-range (48 hr or less) forecasts of upper level winds; marine meteorologists are interested in forecasts of weather systems out to 5 days and near-surface winds and resulting ocean waves out to 2 days. Climate Prediction Center meteorologists at NCEP are concerned with forecasts from one week to several seasons in advance. With many different user communities, NWP data assimilation and modelling groups may not focus on air-sea fluxes and may lack expertise in air-sea fluxes,

since personnel resources have not kept pace with increases in the complexity of NWP systems. The focus of the analysis and model developers may be on the effect of changes on the forecast skill of an atmospheric field and on atmospheric fields directly observed, fields whose accuracy they know and have confidence in. The developers may not know what independent estimates of air-sea fluxes are available and how much confidence can be placed in the accuracy of these independent fields. Advice from experts on air-sea fluxes, such as this working group, would be very useful.

Operational NWP groups focus on forecast performance and usually on atmospheric fields. At NCEP a change in the operational analysis/forecast system, while beneficial in many respects, led to too warm low-level temperatures over the summertime Northern Hemisphere continents. After complaints from operational forecasters, the parameterisation of sensible and latent heat was changed and a parameterisation of atmospheric aerosols removed to lower the temperatures; the warm bias was significantly reduced. Operationally, changes in physical parameterisations are often made to improve observable atmospheric fields of importance to weather forecasters; their effect on the surface fluxes is not always as carefully assessed, partly because of a lack of confidence in independent estimates of the surface fluxes.

The complexity of modern NWP analysis/forecast systems makes it difficult to establish with confidence the exact cause of an error. NWP groups often adjust specific parameterisations and measure the success of that adjustment not by whether the parameterised physics is more realistic but by whether specific atmosphere fields (such as precipitation over specific land regions, 500 hPa geopotential height, sea level pressure or winds) are better forecast. This is a reflection not only of the perspective of NWP groups, but of the lack of independent estimates of atmospheric physics whose degree of accuracy is confidently known by NWP groups. The problem with such adjustments is that if the true error is not found a new error may be introduced. The new error may happen to offset an existing error, at least in the test cases. If groups such as this working group can establish what independent estimates of atmospheric physics exist and what their accuracy is, NWP groups could evaluate the effect of changes on the parameterised physics directly as well on the skill of forecasts of specific atmospheric fields.

Data assimilation systems used in operational forecasting are constantly being improved, with substantial changes occurring annually or even more frequently. The effects of these changes on surface fluxes can be considerable. Independent estimates of fluxes could help establish whether these changes have a significant impact and whether they have positive, negative or neutral effects on the accuracy of fluxes. The accuracy of the independent estimates would need to be established so that model developers could have confidence in the independent estimates and in how much uncertainty exists in the independent estimates.

The use of independent estimates of atmospheric physics to assess operational NWP data assimilation is limited by the requirement of timeliness. Many independent estimates of atmospheric physics are based on observations taken one or more years before that have been carefully processed. TOGA COARE atmospheric soundings, for example, have only recently been corrected for moisture biases, more than 6 years after they were taken. NWP systems undergo frequent changes, sometimes to adjust to changes in the observations. The operational data assimilation system may be designed specifically for current observations and not for previous observation systems. A change in satellite data in early 1998, for example, required significant changes in the NCEP operational data assimilation system. A few months later these changes made it extremely difficult to test a higher resolution version of the operational data assimilation/forecast system even on data from 1997. As a result, biases during the Northern Hemisphere summer were not uncovered until after the new system was implemented. At NCEP proposed changes to the operational system are tested for long periods on current observations; a comprehensive archive of output from the tests is available for the last 40 days. To be useful in these tests, independent estimates of atmospheric physics must be available within a month of observation time.

Reanalysis efforts alleviate this problem. By processing several years of past observations with a frozen modern data assimilation system and making the results widely available, reanalysis provides a much larger sample of the results of data assimilation. The results can be compared to a much larger range of independent estimates of atmospheric physics from any time in the last 20 to 50 years by a much larger, more diverse group of scientists. For example, COADS based estimates of air-sea fluxes take considerable time to prepare and are available over many decades; they are more suited for comparison to air-sea fluxes from reanalysis than from operational NWP. The reanalysis effort needs to be periodically repeated. The NCEP/NCAR reanalysis was performed with the operational model introduced in 1995. The NCEP/NCAR operational model has been changed several times since, limiting the applicability of the results of reanalysis to model development. The reanalysis system has been run to test proposed changes to the operational system on past periods. The NCEP/NCAR reanalysis system continues to be run on current data as the Climate Data Assimilation System (CDAS). Comparisons of CDAS to operational analyses and to tests of proposed changes can yield insight into whether known biases in the reanalysis are being reduced or increased.

Global data assimilation systems currently provide air-sea fluxes every six hours, reflecting the length of their assimilation cycle. Users of surface fluxes have requested fields every three hours. Many fields are output from the systems at intervals of 1 hour or less. The current resolution of operational global NWP systems ranges from approximately 40 km (ECMWF) to 210 km (NCEP forecasts beyond day 7). For complete verification and validation, independent air-sea flux fields should have the same spatial and temporal resolution. Independent estimates of air-sea flux fields at lower spatial and temporal resolutions are also very useful, as long as adequate information is given on the true resolution of the data and on any smoothing applied to ensure appropriate comparison.

### 2.2.3 The needs of atmospheric forecast models for flux fields

Since modern data assimilation uses the forecast model as an integral component, most of the needs discussed in the last section also apply here. Short-range forecasts of physical fields can suffer from the effects of 'spin-up'. Independent estimates of physical fields of known accuracy could establish at what forecast lengths the most accurate estimates of physical fields occur and thereby offer insight into the cause of the 'spin-up'. Longer forecasts suffer from systematic model drifts. Independent estimates of physical fields could establish the real error in the forecast physical fields, rather than the departure of the physical fields from their estimated data assimilation values which have errors of their own.

All NWP systems have problems, some common to all or most NWP systems and some unique to the particular system. Diagnosing and remedying these problems has led to major improvements in NWP systems. As an example, problems in the NCEP global model are emphasised here, reflecting the author's experience with the NCEP model. NCEP's operational global forecast model has problems maintaining the correct distribution of tropical precipitation in its forecasts. Tropical precipitation increases during the first 24 hours of model integration, then decreases in the convective maximum in the west equatorial Pacific. The diagnosis of this problem is complicated by the fact that different independent estimates of precipitation, both based on satellite data, give significantly different amounts of precipitation in the western equatorial Pacific (see Sections 10.9.4 and 11.4.14). This makes it difficult to determine at what forecast length the model's precipitation is most correct.

In the NCEP reanalysis, surface winds and stresses in the eastern equatorial Pacific were too weak, even in the analysis phase (White, 1996b). The current NCEP global model has stronger surface stress in the eastern Pacific; however, the equatorial surface stress in the eastern Pacific increases with forecast length. Accurate independent estimates of surface fields and fluxes (such as surface winds from the TOGA TAO buoys) have helped to identify these problems and can help identify which changes to the analysis/forecast system can reduce these problems.

Accurate tropical analyses and forecasts are important not only for tropical forecasts, including hurricanes, but for seasonal forecasts. Seasonal forecasting has received increased emphasis in recent years at NCEP and elsewhere with successful forecasts of dramatic El Nino and La Nina events in the Pacific and their impacts on the United States. Seasonal forecasting often involves the use of an ocean data assimilation and forecast system coupled to the atmospheric model. As a result, at ECMWF, the effects of proposed changes in the operational atmospheric model on air-sea fluxes (and the impact of these changes on the ocean model used in seasonal forecasting) have been carefully examined in pre-implementation testing.

Another problem in the NCEP global model is that the tropical upper tropospheric trough over the Caribbean is weakened significantly in the forecasts. This weakening causes too favourable an environment for hurricanes in the global forecasts, complicating the work of hurricane forecasters. This weakening of the tropical upper tropospheric trough may reflect problems in maintaining the divergent flow in the tropics. Accurate independent estimates of precipitation and surface fluxes could help identify model problems in these fields and lead to improvements in the divergent flow.

Surface fluxes over the Gulf of Mexico and the Gulf Stream play a crucial role in accurate analysis and forecasting of explosive United States east coast cyclogenesis, a major wintertime concern for forecasters. Modern global models often have considerable success in forecasting such events, implying, as do comparisons with COADS-based fluxes (Section 11.4.2 below), that the models' surface fluxes are fairly accurate in these areas. In NCEP's operational meso-scale model, a comparison of air-sea fluxes over the Gulf Stream with COADS-based estimates led to changes in the model's physics.

Some years ago seasonal forecasters at NCEP found large differences in surface radiation between NCEP global model forecasts and independent estimates in the eastern subtropical North Pacific in regions of oceanic low-level stratus clouds. Due to excessive radiative heating rates when cloudiness occurred in thin near-surface layers over land, the NCEP model did not permit low-level clouds anywhere, even when the vertical profiles of humidity and temperature over the subtropical oceans clearly suggested that low-level stratus clouds should be present. Simple changes in the model permitted the occurrence of oceanic stratus clouds and dramatic improvements in the surface radiative budget over the ocean. More recently, the parameterisation of low-level clouds were changed to reduce excessive low-level clouds over the Arabian Sea; this change also affected low-level stratus clouds in the eastern subtropical oceans. Recent tests indicate that low-level stratus clouds can be significantly changed by changes in the vertical and horizontal resolution of the model. Other operational and reanalysis data assimilation systems have problems with stratus clouds (White, 1995; White and da Silva, 1998; section 11.4.7 below).

Comparison of surface net short-wave radiation from the NCEP/NCAR reanalysis to independent estimates by da Silva and White (1996) led to the discovery of an error in the oceanic surface albedo. The error has been corrected in the operational NCEP global model and in the NCEP-2 reanalysis.

### 2.2.4 Regional observing / nowcasting / forecasting systems

Regional operational systems are used for nowcasting and forecasting both the meteorological conditions at the ocean surface and also the dynamics of the upper layer of the ocean. They are characterised by fine spatial and temporal resolution, increasing in the near offshore regions. Thus, for example, the EUROWAVE operational system for diagnosis and forecasting of waves in European coastal areas is running on a 5 km spatial resolution in the off-shore regions and at about 1/4 degree in the open sea. The French operational system for nowcasting of tides and tidal currents in the English channel uses 12 km spatial resolution in operational mode, and twice finer resolution in non-operational mode. Operational models for nowcasting and forecasting of oil spills are running at 0.5 to 2 km resolution in the nearest vicinity to the source and at 5 to 10 km resolution in areas at least 50 km remote from the source. The highest priority parameter required for such systems is wind speed. Since the

majority of operational models have a special focus on coastal regions, the wind fields required have to be provisionally corrected for coastal biases. Further parameters which are very important for these systems are SST and SSS. These are particularly used in oil spill forecasting for describing the interaction between the oil and sea water. Systems running in ice covered areas also require fine resolution sea ice extent data. Many operational forecasting/nowcasting systems use measurements at buoys, these being usually implemented as part of the systems. In this context, a high priority is to provide reasonable estimates of the possible biases between the buoy measurements and the VOS and satellite data assimilated by the models over the larger area. At present, most of systems are focused on the use of downscaled operational analyses from global and regional meteorological centres together with satellite observations. Thus, improvements in accuracy of these two sources of fluxes and flux-related variables, and increased resolution, would contribute considerably to the development of regional operational systems.

### 2.3 Oceanic General Circulation Models (OGCM's)

*2.3.1 Introduction*

The ocean receives energy through the air-sea interface by exchange of momentum, which also represents a source of kinetic energy, and by exchanges of heat and water which locally modify the buoyancy of the fluid and so act as a source of potential energy generating internal pressure forces. Thus ocean models require an accurate representation of the surface flux fields to define their surface boundary conditions. However this alone is not sufficient because of systematic errors in ocean general circulation model (OGCM) solutions which often result in large inconsistencies between the forcing fluxes and the model circulation. For example, mean currents in coarse resolution models are far too broad and slow, and if forced with observed surface heat fluxes they tend to produce unrealistic surface temperatures. Another difficult problem that ocean-atmosphere modellers are confronted with is the interactive nature of air-sea exchanges. Variations in one fluid will force variations in the other, and this raises the question whether it is conceivable to drive one fluid without considering its coupling with the other. Indeed, forcing an ocean model with specified surface fluxes generally produces SST's which are far from the observed sea surface temperature (Rosati and Miyakoda, 1988). Therefore, it is not possible to force an OGCM without some kind of a parameterisation to account for the feedback to the atmosphere.

This feedback issue is not relevant to the wind stress forcing, for which there is not a direct local feedback from the ocean circulation. However, the spatial resolution is of particular importance to the momentum exchange since basin gyres are primarily driven by the wind stress curl, a first order derivative of the wind components. For heat and freshwater, a common OGCM boundary condition is to restore the model surface temperature and salinity to observed climatological values (Cox and Bryan, 1984). The paradox here is that if the model tracer fields agree with observations, there is zero net tracer flux across the air-sea interface. In general, model solutions differ from observations both because they cannot 'keep up' with the changing observations, and because advection introduces a systematic bias (Killworth *et al.*, 2000).

Several parameterisations of the feedback of the ocean to the atmosphere have been developed in the past. It is not the purpose of this report to present an overview of the various way of forcing ocean models. A recent review can be found in Barnier (1998). However, we present here some details of such parameterisations applied to the thermal forcing since they are useful in determining which surface variables are required in the definition of the atmospheric forcing.

*2.3.2  Parameterisation of the thermal feedback*

A.  THERMAL SURFACE BOUNDARY CONDITION.

There are several ways to formulate the forcing of an OGCM based on the primitive equations. A formulation which remains close to the physics of the air-sea interactions is the flux boundary condition. It is assumed that vertical gradient of the ocean temperature at the surface is proportional to the flux across the interface. Thus the advection-diffusion equation for the evolution with time (*t*) of the ocean temperature (*T*) is:

$$\frac{\partial T}{\partial t} = Advection + Diffusion + F_{SOL}(z)$$

(2.1)

which includes a source term, $F_{SOL}(z)$, which represents the depth-dependent heating by the solar heat flux. $F_{SOL}(z)$ is commonly parameterised by an absorption law with depth (*z*) (Paulson and Simpson, 1977). The forcing of the ocean temperature by the non-solar heat flux $Q_{NS}$ (the addition of the net infra-red, latent and sensible heat fluxes) is introduced as a surface (*z=0*) boundary condition:

$$\left( K_v(z) \frac{\partial T}{\partial z} \right)_{z=0} = \frac{Q_{NS}}{\rho_0 C_{pw}}$$

(2.2)

where $K_v$ is a mixing coefficient which depends on the depth *z*. Other parameters are the density ($\rho_0$) and the specific heat ($C_{pw}$) of sea water. This type of formulation is commonly used for mixed-layer models (Gaspar *et al.*, 1990). The parameterisation of the ocean feedback usually occurs through a model dependent definition of the non-solar heat flux $Q_{NS}$.

B.  FEEDBACK PARAMETERIZATION.

There are two methods frequently used to overcome the physical inconsistency due to the lack of air-sea feedbacks in the formulation of the atmospheric forcing of ocean models; a method of flux correction, and a bulk forcing method.

*Flux Correction Method.* This method is based on the pioneer work of Haney (1971) and Han (1984). More recent applications are those of Oberhuber (1988), and Barnier *et al.* (1995). The underlying idea is to express the feedback to the atmosphere as a flux correction which depends upon the model *SST*. Therefore, at a given time step of the model integration, the non solar surface heat flux, $Q_{NS}(t)$, used in boundary condition (2.2) for the temperature is:

$$Q_{NS}(t) = Q_{NS}^{C\lim} + \left( \frac{\partial Q_{NS}}{\partial SST} \right)^{C\lim} \times \left( SST^{C\lim} - SST(t) \right)$$

(2.3)

where:

$Q_{NS}^{C\lim}$ = climatic estimate of the non-solar net heat flux

$SST^{C\lim}$ = climatic estimate of the sea surface temperature used to estimate the air-sea fluxes

$SST(t)$ = instantaneous model sea surface temperature

$\left( \frac{\partial Q_{NS}}{\partial SST} \right)^{C\lim}$ = climatic estimate of the sensitivity of the non-solar heat flux to variations in SST

The second term in the right-hand-side of (2.3) is a feedback term the effect of which is to prevent the model *SST(t)* drifting away from the climatic value used to estimate the forcing fluxes. Thus it is there to drive the model ocean toward a climatic state consistent with the air-sea fluxes. The sensitivity term $\partial Q_{NS}/\partial SST$ can be estimated from atmospheric surface variables using a first order Taylor expansion of the bulk formulas (Barnier *et al.*, 1995). This term calculated from the surface fields provided by the ECMWF re-analysis is shown in Figure 2.1.
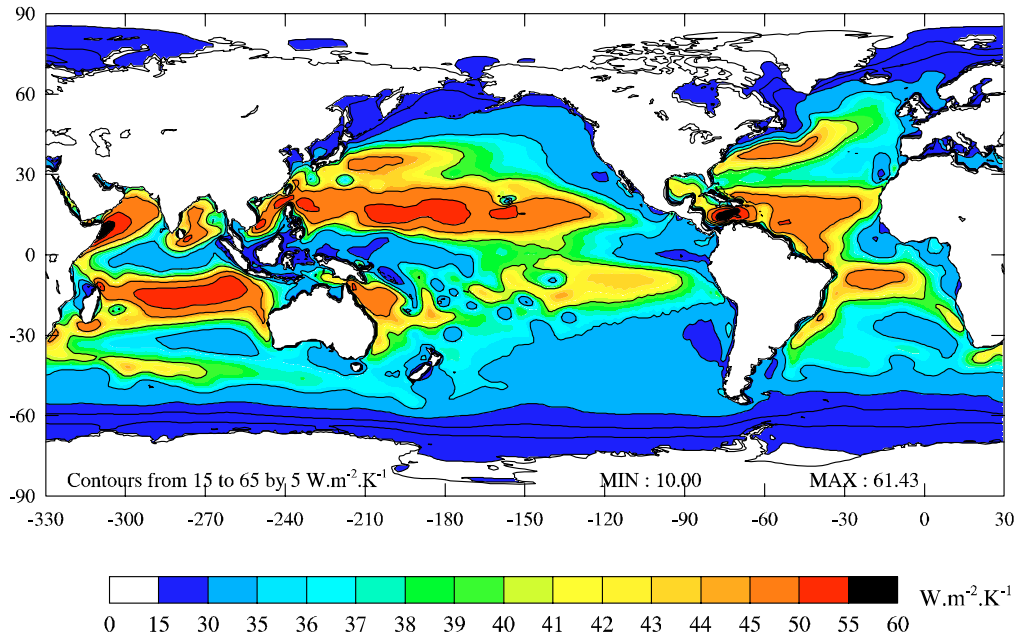
Figure 2.1: Sensitivity term $\partial Q_{NS}/\partial SST$ (Wm$^{-2}$K$^{-1}$) estimated with atmospheric surface variables of the ECMWF re-analysis using the first order Taylor expansion of the bulk formulas proposed by Barnier *et al.* (1995).

To apply this parameterisation of the thermal forcing requires estimates of the various surface heat fluxes and the *SST*. Therefore, this method allows flux estimates to be directly used as components of the forcing; the feedback enters the surface boundary condition through the sensitivity term. This only needs to be estimated once, from a climatology of surface variables.

*Bulk Forcing Method.* In this method, air-sea heat fluxes which enter the flux boundary condition (2.2) are made model dependent by the direct use of the model-computed *SST(t)* in bulk formulations (see Large *et al.*, 1997 for a detailed review of the bulk forcing method). For example, the latent heat loss at a given time $Q_{LAT}(t)$ would be computed by the model according to the bulk formula (with the usual notations)[2]:

$$Q_{LAT}(t) = \rho_a L_E C_E U_{10}\big(q_a - q_s(t)\big)$$
(2.4)

where $q_s(t)$ is the saturated specific humidity estimated with the *SST* predicted by the model at time *t*. All the other variables entering the calculation of (2.4) are obtained from a climatology or from an analysis of surface variables. In addition, the sensible heat flux and longwave radiation are calculated with the model *SST*. The application of this method does not require an estimate of every component of the net heat flux, but rather the knowledge of the net downward radiation (shortwave and longwave), and of surface variables which enter the bulk formulas.

Thus, the requirements for surface variables and air-sea fluxes are different for the Flux Correction compared to the Bulk Forcing methods.

### 2.3.3 Salinity Forcing

The case of salinity forcing is different from that of temperature. The salinity of surface waters vary because the ocean loses or gains water by evaporation, *E*, or precipitation, *P*, river runoff, *R*, and sea-ice production and melt, which causes a variation of the salt concentration in the water. However, the total amount of dissolved salt remains constant. Because OGCM formulation generally assumes a constant volume, the forcing of the salinity equation is

---

[2] see Chapter 7 for a detailed discussion of the bulk formulae.

expressed as a virtual salinity flux which is proportional to the balance *E-P-R* (see Barnier, 1998, for a detailed discussion). The formulation is then similar to the one used for temperature, and a correction term is generally added in the form of a relaxation toward a climatic estimate of the sea surface salinity (*SSS*). However, more OGCM's are now using a free surface formulation, and a more physical formulation of the salinity forcing could be used. This would consider the change in volume implied by the freshwater flux at the surface (Roullet and Madec, 2000). As yet, such a formulation presently is far from being used routinely, and additional restoring to a climatological *SSS* is still included.

### 2.3.4 Geophysical consistency of the ocean forcing function

The section above discussed the two methods most used to overcome the physical inconsistency between the model *SST* and the forcing fluxes which arise from the lack of air-sea feedback in the formulation of the forcing.

However, when applying these methods, it is important to consider the geophysical links that exist between the various components of the atmospheric forcing. This is commonly referred to as the "geophysical consistency" of the model forcing function. Indeed, it is important that the inter-correlation existing between the wind field, the turbulent fluxes, the radiative fluxes, and evaporation and precipitation, are correctly represented. Inconsistencies between the forcing variables may have a dramatic effect on the results of a simulation. This is especially so since the feedback term, which also works to compensate for inaccuracies in the flux estimates, will generally not compensate for such inconsistencies. For example, in the western tropical Pacific the surface salinity of the ocean cannot be correctly calculated if the evaporation (air humidity and wind) and precipitation are not consistent. It is only recently that a bulk forcing which links heat and freshwater forcing through evaporation has been used in a global ocean simulation (Large *et al.*, 1997). Therefore, when using flux estimates from various sources (satellites, NWP analyses, COADS), geophysical correlation between the various components of the forcing should be verified.

The analysis carried out by Garnier *et al.* (1998) on the 15-year flux climatology obtained from the 6-hourly forecast ECMWF re-analysis provides an example of the inconsistencies which may arise. Their global budget calculation indicates that the ocean receives an excess of heat of 8 Wm$^{-2}$, despite a lack of incident short wave radiation in the intertropical zone which is only partly balanced by an excess of incoming short wave radiation at mid-latitudes. In the freshwater budget, evaporation globally dominates precipitation, and the ocean loses, on annual mean, 1.4 Sv (1 Sv $=10^6$ m$^3$s$^{-1}$) of water (runoff estimates being included). For the purpose of forcing an ocean model, corrections to the weak solar radiation reaching the surface in equatorial regions could be sought, but increasing this quantity would increase the global imbalance of heat of 8 Wm$^{-2}$. This could be compensated by an increase in latent heat loss at latitudes where the analysis suggest it could be underestimated, but then the imbalance of the water cycle would be amplified. This contradiction illustrates the difficulty of producing a globally consistent forcing function.

### 2.3.5 Forcing fields

Considering both flux correction and bulk forcing methods, and the fact that geophysical consistency of the forcing variables should be checked, the basic forcing components of a prognostic OGCM include much more than the usual air-sea fluxes. A list of the useful ( if not always necessary) variables to define a forcing function of an OGCM is given below.

### A. FLUXES

The net heat input by solar radiation; the non solar heat flux (the sum of the sensible, latent and infra-red heat fluxes); the components of the wind stress vector; the wind stirring; the evaporation rate; the precipitation rate; the river runoff and sea-ice melt.

B.  OTHER SURFACE VARIABLES

The sea surface temperature; the sea surface salinity; the ocean albedo; the surface wind speed, air temperature and specific humidity at specified height; the mean sea level pressure, the cloud fraction, the sea-ice coverage and growth (or melting) rate.  According to the forcing method which is used, additional parameters, such as exchange coefficients and all variables entering the determination of the stability of the air column may also be necessary.

C.  RESOLUTION ISSUES

The requirements on air-sea flux resolution for modelling the different features of the ocean vary according to the application and the beliefs of the users, from coarse resolution global scale models run over centuries, to eddy resolving models run over a few decades.  For many applications in forthcoming years, monthly means on a one degree grid will be sufficient.  However, the number of applications which have finer requirements is rapidly increasing as ocean model resolution increases with available computer power, and these needs are emphasised here.

Considering time scales, it is now well established that the characteristics of the surface mixed layer are very sensitive to short-term fluctuations of the wind stress which set the amplitude of the vertical shear, and thus determine the intensity of the turbulent vertical mixing.  The inertial frequency needs to be resolved here, and 3 hourly winds are recommended.  Requirements for the heat and freshwater fluxes are not as stringent and six hourly to daily values,  which can presently be achieved by NWP models and geostationery satellites,  are likely to be acceptable.

Considering spatial resolution, again the requirements for the wind are most critical, and a resolution of 50 km, which can already be achieved by scatterometer products,  is a strong requirement to obtain an accurate estimate of the wind stress curl, the primary forcing of ocean gyres. Requirements for the heat and freshwater fluxes could be somewhat looser, but 50 km resolution would allow a better resolution of the gradients across the major ocean currents.

D.  CONSTRAINTS

The various components of the forcing should meet to some degree of accuracy several constraints:
- a global balance constraint
- a global transport constraint
- geophysical consistency

*2.3.6  Discussion*

Having discussed the forcing of ocean models with atmospheric variables, one may briefly comment upon the feedback from ocean observations and ocean general circulation models on the validation of air-sea fluxes.

Ocean hydrographic sections (WOCE) provide estimates of the meridional heat transport across ocean basins (Macdonald and Wunsch, 1996, Ganachaud, 1999), which can be checked against other estimates (derived from satellites, numerical weather prediction centres, or COADS).  However, large uncertainties (in excess of 0.2 PW) are still associated with these transport estimates.

In specific cases (to be carefully controlled), the feedback term can provide valuable information on the consistency of the air-sea flux estimates used to force the model.

Assimilation of ocean surface variables (sea surface height from altimetry and SST) in relation to the heat content of the surface ocean may permit diagnosis of an estimate of the net heat flux at the ocean surface, independent of other estimates.

Coastal oceanography is also concerned with air-sea fluxes.  For such very local applications where the diurnal cycle generally needs to be resolved, air-sea fluxes are of course

important, but the necessary resolution, in particular the high time sampling required for the wind field, are beyond the capabilities of the instrument systems used to observe the global ocean.  Other means could be used, including dedicated instrumentation and atmospheric modelling, since the studied areas are usually limited.

Finally, it is clear that OGCM's will always need to include some parameterisation of the mixed layer.  Validation of mixed layer models requires very accurate estimates of the air-sea fluxes, combined with measurements of the turbulent fluxes and large scale flow in the upper ocean.  Such complete data sets could only be obtained at a few given locations, and would require specific experimental designs.

*2.3.7  Conclusions*

While many applications still call for at least medium spatial (1 degree) and temporal (daily to monthly mean) resolution and global coverage, the demand for high temporal (3 hourly) and fine spatial (50 km) resolution at global scale is rapidly increasing.  Due to the sparseness of observations, these requirements can only be met by numerical or satellite products.  These products, however, have to be carefully checked and validated by comparison with *in situ* measurements.  The specific requirements for development and validation of new parameterisations of mixing in the upper ocean are calling for local but very accurate flux measurements.

## 2.4  Wave Models

Ocean surface waves are generated by the wind blowing over the water.  Wave models thus require the wind vector as input.  Several studies (e.g., Cardone *et al.* 1995, Graber *et al.* 1995, Sterl *et al.* 1998) have shown that the quality of the input wind is crucial for the quality of the modelled wave characteristics.  Empirically it has been found that the significant wave height for fully developed sea is proportional to the square of the wind speed (Sanders 1976, Janssen *et al.* 1984).  Thus, although high waves are rarely fully developed, one may anticipate that errors in the wind speed will be amplified by the wave model.  As very high wind speeds are of limited temporal and spatial extend, a major aspect of "quality" turns out to be the spatial and temporal resolution of the driving wind field.  For example:

Cardone *et al.* (1995) used analysed wind fields from four Numerical Weather Prediction Models and from a kinematic analysis to drive the WAM wave model (Komen *et al.* 1994).  They found that extreme wave heights were only correctly reproduced by the model if the driving wind contained wind-speed peaks of the correct magnitude.

Graber *et al.* (1995) drove the same WAM model by wind fields that were artificially degraded by lowering the spatial and temporal resolution.  They found that in regions of "slowly evolving, nearly linear features" a resolution of 1.5° and 6 hours was satisfactory,  while fronts and rapidly propagating jets required 0.5° and less than 3 hours resolution.

Sterl *et al.* (1998) used the ERA winds to drive a global version of  the WAM model.  They found that with a resolution of 3°,  mean wave heights were severely underestimated, and that,  even at a resolution of 1.5°,  missed peaks in wind speed led to an underestimation of extreme wave heights,  thus corroborating the results of Graber *et al.* (1995).

The conclusion to be drawn from these studies is thus that the resolution of the wind field for wave modelling studies should be of order of half a degree in space and roughly three hours in time.  The spatial extent of the required fields depends,  of course,  on the desired purpose and can vary between regional and global.

Two remarks should be added.

1.    The above estimates have been derived from climatological studies (Sterl *et al.* 1998) or from extratropical storms (Cardone et al 1995, Graber et al 1995).  Due to their much smaller spatial extends, tropical storms (hurricanes) may need even higher resolution. E.g., a resolution of 0.25˚ in space is used in the case study of the WAMDI group (1988).

2.      From the fact that the forcing wind is so important for the quality of wave model results it follows that for *forecasting* wave heights, the quality of the wind forecast is crucial. Improved wind forecasts will automatically lead to improved wave forecasts.

## 2.5  Sea Ice in Ocean Models and Sea-Ice Modelling

Ice-covered and sub-polar oceans play a special role in the global ocean thermohaline circulation - the vertical overturning of the world ocean.  Whereas low-latitude thermohaline processes are controlled both by surface heating and by net evaporation, at polar latitudes these processes are dominated by surface freshwater fluxes, that is, by net precipitation, and to a larger extent by sea ice melting and freezing; sea ice melt water has the same effect on the ocean surface as precipitation.  In the northern hemisphere, large inter-annual variations of the export of ice through the Fram Strait into the GIN (Greenland/Iceland/Norwegian) Seas are modelled (Häkkinen, 1993) and observed (Kwok and Rothrock, 1999).  It is presently hypothesised that abnormally high exports of sea ice in the 60's capped the Labrador Sea with fresh water and limited the production of Labrador Sea Water (Lazier, 1980). This freshening event was called the Great Salinity Anomaly by Dickson *et al.* (1988).  It appears that variations in freshwater input,  both in the form of ice and somewhat less saline upper ocean water from the Arctic Ocean,  influence convective overturning and contribute to interannual variability in the North Atlantic circulation.

In the southern hemisphere, the freezing and melting of sea ice controls the amount and location of deep and bottom water formation in the Weddell Sea and the Ross Sea which are major sources of bottom water of the world ocean.  The appearance and disappearance over long periods of polynyas are thought to force decadal variability in the properties of the flow of Antarctic Bottom Waters into the North Atlantic.  The seasonal melting of sea ice around the Antarctic is responsible for the low salinity of the Antarctic Intermediate Waters, and these water masses are found to intrude far into the North Atlantic with the upper branch of the Atlantic overturning cell.  So, the importance of the freshwater forcing of the global ocean circulation in the form of input of sea ice is quite clear.

We have seen in the previous section that some ocean models use as a surface boundary condition the net surface heating and the net precipitation or ice growth or melt rate.  Others treat separately the penetrating component of solar radiation.  In this latter case, the model requires the ice concentration in order to compute how much radiation penetrates into the water through open water "leads" (openings within the ice cover).  Still others include a full ice model within the ocean model.  In this case, and for modelling sea ice separately from the ocean to determine growth and melt rates as a function of space and time, the specification of global ocean surface fluxes takes on a different character over ice covered oceans.  One can specify or observe the momentum, radiative and turbulent fluxes at the top surface of the ice cover, but of course then one needs to "solve" an ice model in order to translate these into fluxes to the mixed layer of the ocean.  Wind stress pushes the ice which has its own mass and resistance to deformation, and these conspire to apply a somewhat modified stress to the ocean surface.  The same can be said of radiative fluxes; some of the flux goes directly into the ocean through leads, but most of it goes into the heat balance of the sea ice.  The ice cover represents an isothermal boundary condition on the ocean, and turbulent heat fluxes at the ocean surface (and the underside of the ice) are determined by the mixed layer and the vertical mixing at the base of the mixed layer.  The ice conducts heat away from the mixed layer, and ice melt  (or growth) also absorbs heat from (or deposits heat into) the mixed layer. In order to know these quantities, one needs an ice model.

To force today's sea ice models, with or without an underlying ocean model, the following fields are specified:

❍      wind stress, usually taking a bulk drag coefficient as constant;

❍      downwelling solar radiation (the surface albedo and reflected radiation being determined within the ice model);

❍    downwelling longwave radiation (the outgoing being determined within the model by surface temperature);

❍    surface temperature being internal to the model;

❍    the evaporation and latent heat flux, specified as a function of near-surface wind and humidity (determined by the air temperature);

❍    precipitation.

These fields at the sea-ice surface, then, are the proper subject of this working group.

To date, the practice has been to specify fluxes parametrically: downwelling solar radiation in terms of solar geometry and cloud fraction, downwelling longwave in terms of surface air temperature, cloud fraction, and all turbulent fluxes in terms of surface wind and air temperature. It is fair to say that the subject of surface fluxes over sea ice has been taken pretty much for granted by modellers, who have found that the mean annual cycle of sea ice can be modelled satisfactorily with the fluxes specified parametrically years ago by Parkinson and Washington [1979] and have not had cause to examine these inputs much until recently. Now the focus of research is shifting more to interannual variability and climate change, and this has sparked recent interest in data on long-term variability of polar surface fluxes.

A study of the sensitivity of an Arctic sea-ice model (Rothrock and Zhang, 1997) to errors in radiative forcing has shown that an error of +10 $Wm^{-2}$ in the downwelling shortwave produced an error of -20 cm in mean ice thickness in a full thermodynamic-dynamic model (and -60 cm in a radiative model with no ice dynamics). The same error in downwelling longwave radiation produced an error of -50 cm in the full ice model (and -110 cm in the radiative model). The lesser sensitivity to shortwave was due to the high albedo that caused most of the downwelling solar radiation to be reflected. The mean Arctic ice thickness is about 2 m presently, so flux errors of only 10 $Wm^{-2}$ cause a very significant error in modelling the sea ice cover.

## 2.6  Air-Sea Flux Fields and Ocean Data Assimilation

### 2.6.1  Introduction

Data assimilation (sometimes known as "ocean state estimation") is a very powerful tool which is now becoming the tool of choice for all operational centres as well as ongoing (e.g., WOCE AIMS) and future research programs (e.g., GODAE). As is the case for forward ocean models, ocean data assimilation (ODA) is dependent on accurate air-sea fluxes for forcing. However, unlike forward modelling, ODA requires fairly comprehensive error estimates so data-model misfit feedback can be properly partitioned.

### 2.6.2  Ocean Data Assimilation

In general terms, data assimilation techniques are employed to bring, in an extremely efficient way, a model into consistency with the observations, which the forward model by itself predicts. From the resulting misfit between the model and the observations one can determine which uncertain model parameter must be adjusted, and by how much, so as to bring the forward computation into accord with the data. Changes in those fields - often referred to as "control" terms - are determined as a best-fit in a least-squares sense over the full data period. Control terms are usually the model initial conditions, but can likewise include internal model parameters such as friction coefficients and eddy tracer transfers. It is essential to realise that all adjustments of control parameters are enforced to stay in a dynamically acceptable range and that the model equations are otherwise preserved.

Since the observation-model misfits determine the control terms (in a statistical sense), it is critical to have error estimates of the observations in order to correctly partition the misfit

information into each of the control terms.  Additionally, estimates of the ocean circulation depend critically on the quality of the meteorological (forcing) fields.  But error estimates for surface fluxes of momentum, heat and freshwater provided by NWP centres are generally not available.  One way to deal with this situation is to incorporate flux error terms as control parameters into the estimation process.  Nevertheless, prior information about error structures is needed to obtain a statistically consistent solution.

Ocean observing systems are being rapidly developed for the purpose of monitoring the ocean and to allow ocean prediction at global scale.  These are the major objectives of important international programmes such as the Global Ocean Observing System (GOOS) and the Global Ocean Data Assimilation Experiment (GODAE).  For these purposes, an ambitious ocean float program is being implemented (ARGO).  This plans to release more than 3000 profiling lagrangian floats (of P-ALACE and PROVOR types) which will sample the temperature and salinity of the upper ocean with a space-time coverage never attained before.  Assimilation of these data (with additional XBT, SST, and sea surface height observations) into a global model should permit estimation of the net heat flux into the ocean and its variation.  The question remains whether the accuracy of such estimates will approach the few $Wm^{-2}$ required for climate studies.

Information about amplitudes, and spatial and temporal error covariances in momentum, heat and freshwater flux fields, including those from operational centres such as NCEP and ECMWF are necessary.  A concise review is needed of what the atmospheric scientists believe the error in meteorological centre analyses are.  A summary of formal comparisons among different centre estimates would also be valuable if error estimates cannot be given.

### 2.6.3  Example of Ocean Assimilation requirements - GODAE

The requirements which have been stated for  GODAE are as follows.  For SST, GODAE has a requirement for high-resolution global real-time products.  A representative spatial resolution would be 5 to 10 km, and ideally the diurnal cycle should be resolved (implying 6 hour or better time resolution).  The desired accuracy would be 0.1 to 0.2°C.  If sea surface temperature is used as a strong constraint on the ocean models (that is a very small error value is associated with it), then knowledge of the net downward shortwave radiation would complete the determination of the thermal boundary conditions.  The latter is treated as an internal heating source within the model.   Such a product will require careful direct measurements for validation;  for delayed-mode products GODAE would be seeking an accuracy of around 10-15 $Wm^{-2}$.

The availability of suitable surface wind stress products continues to be a major issue for oceanography.   Apart from the need for improved accuracy,  modern ocean data assimilation systems are now demanding estimates of the error in this fields;  without them, the ingested wind data cannot be balanced against other ingested data.   Given the GODAE, emphasis on global, high-resolution, real-time products,  the matter of how to define and obtain a suitable wind field is a matter for urgent debate.

## 2.7  Evaluation of Climate Models

When an Atmospheric General Circulation Model (AGCM) is constrained with prescribed SST's and sea-ice, there is no feedback from the ocean on the simulated atmosphere. If the AGCM is coupled to an Ocean General Circulation Model (OCGM) and a sea-ice model, air-sea feedbacks are present in the resulting (AOGCM) simulations. For this reason,  coupled models are more suitable than AGCM's for studies involving long term variability and offer the most plausible means of predicting anthropogenic climate change. Realistic coupled model simulations depend critically on interactions between the atmosphere, ocean and sea-ice, via the air-sea fluxes of heat, momentum and moisture.  An important motivation for a better understanding of air-sea fluxes (and hence the effort of this Working Group) is the need for an improved means of evaluating air-sea fluxes simulated by coupled models.

       Despite the lack of air-sea feedbacks, studying surface fluxes in AGCM's is often instructive because many deficiencies are so serious that they can be readily identified even with the use of prescribed SST's and sea-ice. Moreover, if the SST simulated by a coupled model is not close to a realistic state, it is difficult to determine if deficient surface fluxes are a direct result of problems in the way fluxes are parameterised, or simply because the basic state of the simulated climate is different from that observed. Detecting problems in coupled model surface fluxes is thus perhaps best done early on in the simulation (before there is much drift in the SST's). However this is complicated by adjustments resulting from incompatibilities in the initial states of the simulated atmosphere and ocean, even when they have been independently 'spun up.' In short, it is useful to evaluate surface fluxes in both coupled and uncoupled climate models, even if the ultimate motivation is improved coupled models. Accurate observationally-based estimates of surface fluxes are fundamental in either case.

       To put the state of affairs in perspective, we take a first cursory look at AGCM simulations recently made (1998-1999) as part of the on-going Atmospheric Model Intercomparison Project (AMIP). Figure 2.1 shows the zonally averaged global ocean net shortwave radiation annual mean climatology of ten models. Also shown are seven observationally based estimates that are described and evaluated in this report. We see that where the fluxes are largest (in low latitudes for the annual mean), there are discrepancies among models on the order of 50 $Wm^{-2}$, and nearly as much among the different observationally based products. The situation for the latent heat flux is perhaps even more troubling, as shown in Figure 2.2, although in this case there seems to be separation between the models and observational products. Gleckler *et al.* (1994) demonstrated how common
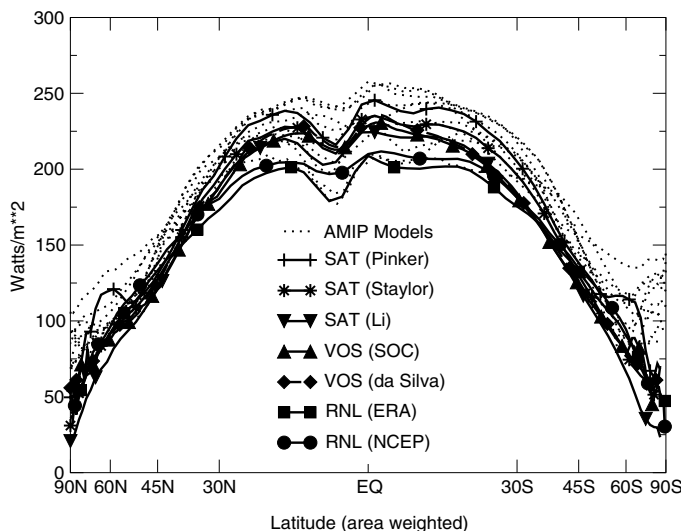


Figure 2.1 Zonal averages of the Global Ocean net SW flux from reanalyses, observations (COADS and satellites) and AMIP2 (1998-99)
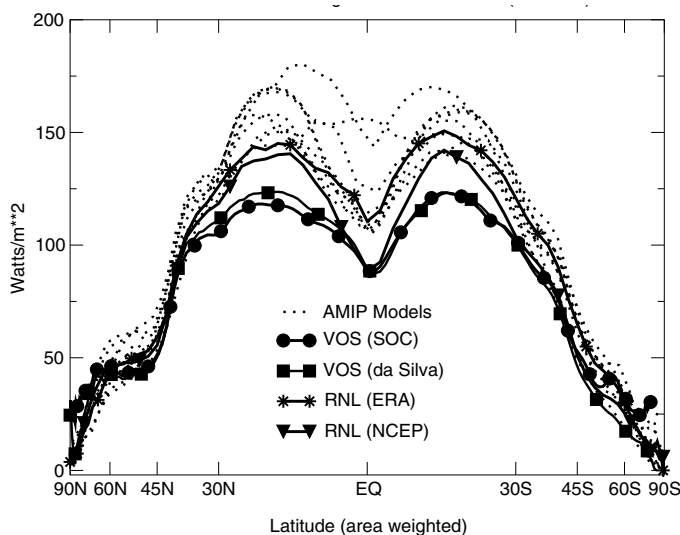


Figure 2.2 Zonal averages of the Global Ocean latent heat flux from reanalyses, observations (COADS) and AMIP2 (1998-99)

deficiencies in modelling the cloud-radiative effects radically altered the implied oceanic heat transport (a common measure of evaluating an AGCM's suitability for coupling). While this was believed for some years to be the primary culprit for coupled model deficiencies, more recently the implied ocean heat transport of the NCAR CCM3 has been shown to be equally as sensitive to the parameterisation of deep convection (Hack, 1998), which principally altered the latent heating. Clearly, the suitability of an AGCM for coupling is critically sensitive to all forms of surface heating, but especially to its surface net shortwave and latent heat flux.

The need for "flux correction" has declined in the last several years (Covey *et al.* 1999) as many teams are having increasing success in reducing climate drift in their coupled models. Encouraging integrations of more than a hundred years with minimal drift have been made by the Hadley Centre (Gordon *et al.* 2000) and NCAR (Boville and Gent, 1998). However a stable simulation with a reasonable SST distribution does not guarantee that surface fluxes are properly simulated. This can only be verified with suitable observations. In Figure 2.3, the 20 year mean (years 60 to 80 of each simulation) net surface heat flux of four simulations taken from the Coupled Model Intercomparison Project are compared with four of the observational products to be evaluated in this report. While there are encouraging similarities, once again we see that even qualitatively there are substantial differences among the observations and methods. The general impression is that the coupled models have large regions where there is a relatively small (less than 20 Wm$^{-2}$) heat flux into the ocean. In comparison ERA shows ocean cooling over many of these areas. The coupled models appear similar to the Residual method results. Compared to the COADS based climatologies they fall somewhere between the SOC climatology and the tuned UWM climatology. Of course, if more of the ocean has net heating, to achieve a global heat balance the coupled models must have significantly greater cooling in the regions where the ocean is loosing heat.

Improving our understanding of, and the accuracy of estimates of, the seasonal cycle of surface fluxes is perhaps the most pressing need for the evaluation of climate models. We have just demonstrated how state-of-the-art climate models still have difficulty in simulating many basic features of this most basic climate variability. Examples include excessive shortwave heating in marine stratus cloud regimes which remains a problem in AGCM's (and which is not apparent in the zonal means), and excessive evaporation with respect to climatologies in low latitudes. High quality estimates (i.e. with low and quantified uncertainty) of global ocean seasonal cycle climatologies of heat, momentum and freshwater are all desperately needed to guide further development of climate models.

Estimates of interannual variability in as many areas as possible are also becoming increasingly valuable in the evaluation process as coupled modellers strive to improve simulated variability in phenomenon such as ENSO, PNA and the NAO. In a recent study by Timmermann *et al.* (1999), it was clearly demonstrated that global coupled models that have 'reasonable' climatologies are doing a poor job at capturing ENSO variability. While there are many other measures of variability to evaluate models with, air-sea interactions are the link between the atmosphere and ocean, and thus there will be an increasing need for reliable estimates of flux variability.

Estimates of global ocean air-sea fluxes derived from in-situ observations, satellite measurements, atmospheric analysis, or potentially some combination of each can all be useful in evaluating climate models. However, climate modellers want to know which is the single best (most accurate) observational data set, and we may not be able to answer that question with absolute confidence. While identifying the strengths and weaknesses of these different products is an important objective of this report, complex uncertainties with temporal-spatial variations are inherent in each of the observationally based estimates and these are not well understood. As described in later sections of this report, the problems differ with each class of flux estimates, and thus the 'best' estimate for the climate modeller may be application dependent. Developers of observationally based flux estimates are beginning to take advantage of the few high quality direct measurements available for evaluating their methods. Climate modellers are

likely to consider this strategy less valuable,  as they are more interested in how their simulations are fairing on the whole,  that is they want maps!
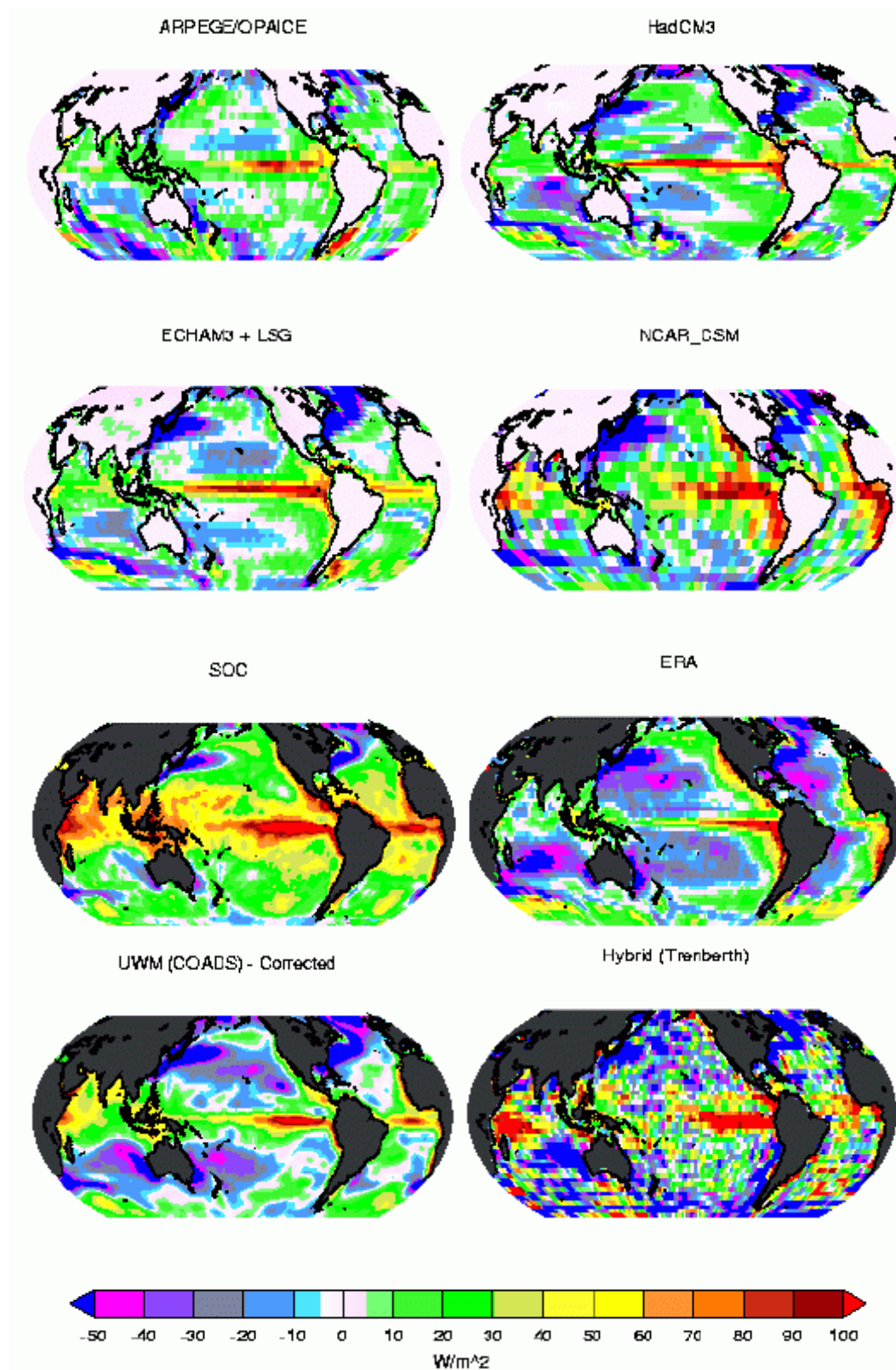


Figure  2.3. The climatological values of the net surface heat flux from four coupled models and four other flux products. Shown are (from top, left) ARPEGE/OPAICE,  HadCM3, ECHAM3 + LSG, NCAR-CSM, the SOC climatology, the ERA15 reanalysis, the tuned UWM/COADS climatology,  and the results from the Residual method (Trenberth and Solomon, 1994)

A better quantitative understanding of our global ocean estimates of heat, momentum and freshwater fluxes is urgently needed for the evaluation of climate models. Accuracy of long-term means and inter-annual variability with medium spatial resolution and global coverage is important. Wind stress, latent and sensible heat, short and long wave radiation, precipitation and evaporation, sea-ice extent and thickness, are all important for long term climate simulations. Despite the difficulties, for the evaluation of coupled models the time is right for a comprehensive examination of state-of-the-art flux products. While it may be years before uncertainties in large scale fluxes can be reduced to a desired level (e.g. <10Wm$^{-2}$ for the net heat flux) it would be of tremendous benefit if a serious attempt is made to identify the strengths and weaknesses of available products, and to the extent possible, quantify their uncertainties (as this Report attempts to do).

## 2.8  Climate change studies

Ocean-atmosphere fluxes establish the link between ocean surface temperature changes and atmospheric circulation variability. On the other hand, they provide the mechanism of by which ocean variability is forced by the atmosphere. Thus accurate knowledge of the flux variability is extremely important for understanding climatological variations in the coupled ocean-atmosphere system. Climate change studies are primarily based on the consideration of gridded flux products with at least monthly temporal resolution. For these products the requirements can be divided into three groups: (1) accuracy requirements; (2) resolution requirements; (3) specific requirements with respect to the reliable description of fluxes in key regions.

With respect to accuracy, the most important requirement of the flux fields is reliable representation of the temporal behaviour of the anomalies of fluxes, rather than closure of the balance either for the globe or for a particular basin. Cayan (1992a-c) and Gulev (1995) stressed that consideration of anomalies avoids a number of errors and uncertainties inherent in consideration of climatological means. On the other hand, variability patterns derived from different data sets are largely influenced by time dependent biases which result from changes in observational techniques and sampling density (for the VOS data) and from the changes in the model configurations and assimilation input (for NWP products).

If we consider interannual and decadal-scale variability, sensible and latent heat are the main contributors to the net flux anomalies in mid- and high latitudes, explaining 70 to 90 % of the magnitude of the net flux anomalies (Cayan 1992a, Gulev 1995, Gulev *et al.* 2000). In the tropics and subtropics, the net flux anomalies are determined by both latent heat and SW radiation. Evaporation minus precipitation anomalies are largely influenced by precipitation in low and high latitudes; in mid latitudes and subtropics, anomalies of evaporation are of similar importance. Rough estimates of the typical magnitudes of the interannual to decadal mid latitudinal winter signals associated with the North-Atlantic Oscillation (NAO) and Pacific-North American Oscillation (PNA) are from 10 to 50 Wm$^{-2}$ (Cayan 1992b,c, Iwasaka and Wallace 1995, Tanimoto *et al.* 1997, Alexander and Scott 1997, Gulev *et al.* 2000). Thus an accuracy of at least 10 to 20 Wm$^{-2}$ is required for mid-latitudinal gridded *anomalies* of fluxes. This estimate does not have a direct link to the accuracy of the mean flux. In the tropics the typical magnitude of the interannual variability, associated with the ENSO signal and the Atlantic subtropical dipole, is somewhat smaller, and we can take 7 to 10 Wm$^{-2}$ as the accuracy requirements for the tropical *anomalies* of latent heat and SW radiation.

For secular changes (with respect to a period of about several decades), the largest observed tendencies vary from 5 to 15 Wm$^{-2}$ per decade for selected locations and from 1 to 5 Wm$^{-2}$ for ocean basins, implying a somewhat higher accuracy for the flux anomaly estimates than is needed for an adequate description of interannual variability. Note however, that all existing estimates of secular climate changes in sea-air fluxes are influenced by the uncertainties inherent in the data used. Thus any given estimates of required accuracy should be considered

as very tentative. This is particularly important with regard to anomalies of wind speed and the wind stress products used to force ocean models. Wind speed based on Voluntary Observing Ship (VOS) observations may be affected by trends which are artificial in nature, resulting from historical changes in observational techniques (such as the relative contribution of Beaufort estimates and anemometer measurements, changing ship size and macrostructure, etc. - Peterson and Hasse, 1987, Cardone *et al.* 1990, Lindau *et al.* 1990, Isemer 1995, Kent and Taylor 1997, Gulev 1999). NWP wind (and stress) products can be also influenced by time-dependent biases due to the impact of VOS and other data on the data assimilation. Changes of wind speed of around 1 $ms^{-1}$ can result, for moderate and strong winds, in an apparent 20 to 25% increase of wind stress, and even larger effects on the mixing parameters (for instance, $u_*^3$) used in ocean modelling. Time dependent biases inherent in the wind fields can strongly affect evaporation estimates, leading to trends in latent heat flux of up to 10 $Wm^{-2}$ per decade or even more. Therefore, accurate evaluation of wind fields free from time dependent biases, would be of great importance for climate research.

The required spatial resolution of the surface flux fields for climate studies is determined by the necessity to resolve the main variability patterns. Although multi-year mean climatologies are available currently at 1° latitude x longitude grid resolution (da Silva *et al.* 1994, Josey *et al.* 1999) the true spatial resolution is worse, typically by a factor of 3 or more (Kent *et al.*, 2000). To require 1° resolution for monthly anomalies would therefore be unreasonable, since it is even more difficult to meet the accuracy requirements for very fine resolution on these time scales. Moreover, taking into account that linear matrix operations, based on SVD and EOF analysis, still constitute the core of most of climate analysis techniques, it is important to avoid continuous gaps in the anomaly fields. On the other hand, the 5° resolution used in the studies of Cayan (1992b,c) and Iwasaka and Wallace (1995) may lead to an inadequate description of a number of key-processes in mid- and high latitudes; in particular those associated with flux variability in the vicinity of SST fronts and sea ice margins. It is probable that the optimal spatial resolution for monthly anomalies of the fluxes is around 2°. That would fit the resolution of the best, present, coupled models but would be hard to achieve from observational data. Furthermore, some key-regions associated with mechanisms which are crucially important for the description of climate variability require finer resolution of the anomalies of the flux fields, and high accuracy. The most remarkable examples are the Labrador Sea and GIN Sea regions which are responsible for deep convection driven primarily by the surface heat and fresh water fluxes. Convection events may occur within quite short periods of around several days, so that both, monthly temporal and 2° spatial resolutions can be too coarse for adequate description of the climatic variability of the sea-air fluxes.

Studies of climate variability in ocean-atmosphere flux fields require accurate description of the sea ice extent. In the presence of ice, the fluxes between the ocean and the atmosphere are changed considerably compared to open water conditions (section 2.5). Moreover, the flux between the ice surface to the air and the flux lost by the ocean are different in the presence of ice, and dependant on the ice thickness. In addition the degree of ice cover strongly affects the ocean-atmosphere fluxes in the vicinity of the ice margins, where the highest local sea-air temperature gradients may be observed. It is known that the ice cover has pronounced decadal scale variability (Hilmer *et al.* 1998). If this is not taken into account (that is if flux producers do not have a time-dependent ice coverage and use a climatological ice mask), large artefacts will affect the computed anomalies of the fluxes.

To summarise, climate studies have some important specific requirements with regard to flux products, relating primarily to the reliability of the anomalies of fluxes. These may not necessarily be properly represented by even the best flux climatologies. In this context, satellite fluxes (when they reach continuity on climatological time scales) will definitely serve as an important data source for reliable anomalies of the fluxes, being expected to have the smallest time-dependent biases.

## 2.9 Conclusions

For NWP models there is clearly a need to continue the observations needed for assimilation into the model. However beyond that, the requirement is for independent estimates of the basic variables and of the fluxes for verification of the model physics. Such estimates must be associated with a realistic error assessment and specification of the true resolution of the data. For regional models the requirement is similar but with increased emphasis on high space/time resolution which at present may only be achieved by using models (although in future high time resolution satellite products may become available).

For OGCM's high resolution forcing fields are needed. For example 3 hourly winds are required to simulate the shear in the mixed layer, and a 50km resolution is sought for the wind stress curl. A useful development for OGCM's would be air-sea interaction experiments where measurements of the fluxes in both atmosphere and ocean are obtained and the ocean mixed layer measurements allow budget closure. Although difficult, such experiments are necessary for parameterisation development.

For wave models, high resolution in space and time is increasingly found to be important, and, for wave forecasting, high quality forecast winds are vital. Time resolution on the order 2 to 4 hours is presently sought and NWP and reanalysis centres are being asked for 3 hourly fields.

For sea ice modelling resolution of the flux fields on synoptic scales is adequate: daily and 50 km resolution. The mean flux values must be known to high accuracy; biases of a few $Wm^{-2}$ can change mean ice thickness substantially. The fraction of open water needs to be known to order 1%.

For climate variability studies the fluxes need to be known to a few $Wm^{-2}$ accuracy but the requirements on spatial resolution can be relaxed; a factor of two coarser than mean climatological fields would generally be adequate. However there are certain vital areas where higher resolution may be required, for example the Labrador Sea. For such areas it is also important to allow for the variability of ice cover; climatological ice masks are not sufficient. For variability studies a long time series of observations is vital. At present such studies are based on the ship data and we must recognise that there are some areas of the ocean, particularly the Southern Ocean, where we really have little idea of what the variability is. Even in better sampled regions such as the Kuroshio there is scope for further studies.

Climate modellers need a reliable data set to compare with - both basic variables and surface fluxes. Climate models tend to be very sensitive to the surface fluxes which are needed to within 10 $Wm^{-2}$. They also need information with regard to sensitivity, for example, how do the fluxes change with changes in the fields of the basic variables?

In summary, for many purposes there is a need for high space time resolution which at present can only be obtained from models (although new satellite products show promise for the future). The models need high quality verification data of known resolution and error characteristics, and also improved representation of the basic physics of air-sea fluxes. Thus it will be argued in this report that the flux products from various sources are complementary rather than being in competition, and that the ensemble of air-sea flux estimates that they represent cover the time and space scales that ocean science studies are investigating.

## 3  SPACE-TIME VARIABILITY OF THE FLUXES

### 3.1  Introduction

The surface air-sea fluxes link oceanic and atmospheric processes, and knowledge of their variability on different space-time scales is crucial for understanding ocean-atmosphere interaction. Accurate quantitative description of the variability of atmosphere-ocean energy exchange is important for process studies and for the development of all types of oceanic and atmospheric models. In addition, accurate knowledge of sea-air flux variability can help to improve the flux fields themselves, since it indicates the accuracy which is required to quantify that variability.

In some respects, determination of the flux variability may be easier than determining the mean flux values; systematic errors are of less importance, and the main spatial scales of longer term variability tend to be large. Similarly, numerical weather models tend to perform better with regard to determining the variability than they do in determining the mean. This is probably because the models are designed to forecast the weather - the day to day variations in climate. However despite these considerations, and the undoubted importance of surface flux variability, the Working Group considered that detailed assessment of the variability of flux products could not be accomplished at this time. Thus, in this chapter, a brief discussion of flux variability will be presented. The aim will be to set the context of the flux field evaluations presented in future chapters rather than to present a complete description of the characteristics of air-sea flux variability. A thorough assessment of the variability characteristics of available flux products must remain an important priority for further studies, perhaps by a future working group.

### 3.2  Synoptic and mesoscale processes

#### 3.2.1  Mid to High latitude variability

A. INTRODUCTION

In the mid and high latitudes, synoptic and mesoscale variability of the sea-air fluxes is primarily determined, on the one hand by the atmospheric synoptic scale transients and their associated high frequency variability, and on the other hand, by mid-latitudinal inhomogeneities of sea surface temperature. Thus SST fronts, together with coastal and marginal ice zones, generate sharp spatial gradients of surface properties which vary little on the time scales of atmospheric synoptic variability. In other words, mid latitudinal synoptic scale ocean-atmosphere energy exchange is characterised by a highly non-stationary atmosphere and a strongly inhomogeneous ocean. The contrast is considerable; atmospheric synoptic variability has spatial scales several times larger than the ocean surface inhomogeneities, and ocean temporal variability on synoptic space scales is several times slower than the atmospheric synoptic time scales.

B. MAGNITUDE OF FLUX VARIABILITY

The typical temporal time scale of mid-latitudinal atmospheric variability is from 1 to 7 days. Atmospheric parameters in different parts of propagating mid-latitudinal cyclones are highly variable. For instance, in winter time, the air temperature in cyclones over the north-west Atlantic and north-west Pacific can vary from 15˚C in the warm sector to strongly negative temperatures behind the cold front. Each winter, the monthly record of wind speed in mid-latitudes shows a range from calm conditions to gale force winds. Thus, mid-latitudinal sensible and latent heat fluxes vary enormously, from heat input into the ocean to very high rates of ocean cooling. As an example, direct measurements during the winter season in the Labrador Sea (The LabSea Group 1998) showed variations of sensible flux between weak ocean warming, of order several tens $Wm^{-2}$, to 600 to 800 $Wm^{-2}$ cooling during a 22 day period.

Extremely high variability of mid-latitudinal fluxes occurs in cold and warm air outbreaks, associated with the propagation of cyclones over SST fronts or ice margin areas. This variability can be further enhanced in rapidly intensifying cyclones ("meteorological bombs" - Rogers and Bosart, 1986), which are characterised by extremely high winds and temperature gradients. Thus, in 12 hours during the development of a rapidly intensifying cyclone in the CASP experiment, Yau and Jean (1989) reported changes of sensible heat flux from -70 $Wm^{-2}$ (ocean warming) to 500 $Wm^{-2}$ (ocean cooling), and changes in the latent heat flux from 30 to 1100 $Wm^{-2}$. Neiman *et al.* (1990) reported about 1000 $Wm^{-2}$ spatial change in the latent flux between the warm and cold sectors of an extra-tropical cyclone propagated along the North American coast. Gulev and Tonkacheev (1996) demonstrated that during a cold air outbreak latent heat fluxes over the Gulf Stream front increased from 20 $Wm^{-2}$ to 500 $Wm^{-2}$ in a distance of 12 km. During the GALE experiment, Bane and Osgood (1989) measured similar spatial gradients of sensible and latent heat fluxes during a cold air outbreak over the Gulf Stream. While the Gulf Stream and Kuroshio are major features, less pronounced frontal zones in the mid-latitudinal and subtropical ocean can be associated with strong local anomalies of surface fluxes (quantified in such experiments as FASINEX and SEMAPHORE). Temperature gradients at the FASINEX front in the subtropics of about 3°C per 20 km were associated with surface latent flux changes from 150 to 300 $Wm^{-2}$ (Friehe *et al.* 1991, Halliwell and Cornillon 1990). Moreover, local anomalies of the turbulent fluxes showed spatial structures with typical horizontal scales of 30 to 60 km.

C.  EFFECTS ON OCEAN AND ATMOSPHERE

The synoptic variability of the fluxes in mid latitudes plays an important role in ocean dynamics and atmospheric synoptic variability. High sensible and latent fluxes from the ocean to the atmosphere, together with strong winds, are responsible for cooling and mixing in the Labrador Sea, Greenland-Iceland-Norway Sea, and in some areas of the Southern Ocean The deep convection events which result are crucially important for the thermohaline circulation of the ocean. These events are associated with flux anomalies on daily to weekly time scales (the LabSea Group 1998), and their description requires accurate knowledge of energy exchange at the ocean surface on those time scales. In the mid-latitudinal open ocean, and in the subtropics, synoptic and meso-scale sea-air flux variability contributes to ventilation and convergence processes in the ocean. These may result in SST and mixed layer temperature changes, and so form long-lived anomalies of upper ocean temperature.

Synoptic variability of mid-latitudinal sea-air fluxes strongly affects the development and propagation of atmospheric synoptic systems, modifying low-level static stability and contributing to local vorticity anomalies. High extremes of the synoptic scale fluxes in mid latitudes can be directly responsible for the intensification and even local generation of marine cyclones. In particular, most rapidly intensifying cyclones with deepening rates more than 1 mb per hour are considered to be directly associated with the highly variable sea-air interaction processes in mid latitudes. Strong spatial gradients of the sea-air fluxes in the vicinity of SST frontal zones can diabatically modify extra-tropical cyclones and thus affect their life cycle (Neiman *et al.* 1990).

D.  MEASURING FLUX VARIABILITY

Accurate quantitative description of synoptic and meso-scale variability of the ocean-atmosphere fluxes cannot be done on the basis of Voluntary Observing Ship (VOS) data, since the sampling is generally insufficient for this task. Ocean weather ship (OWS) data provide a valuable source of information for the analysis of short-period flux variability, if only in a few locations. These data have been analysed in a number of studies (e.g. Josey *et al.* 1995, Gulev 1997a) which quantified synoptic scale variability in the surface fluxes. In this context data from NDBC and JMA buoys located in mid latitudes are also a valuable data source.

It should be noted that, for a number of key synoptic and meso-scale processes such as exchange in the vicinity of sharp SST fronts and ice margin zones, the use of standard bulk

formulae (Chapter 7) may not be valid due to the very strong non-stationarity and intensive local advection effects.   Thus new experiments (like FASINEX, GALE, ERICA, CASP, and LabSea) are very desirable to provide direct measurements of the fluxes in regions of strong gradients of surface temperature and highly variable atmospheric processes.   The high resolution flux fields now available from reanalyses also give an excellent opportunity for global-scale analysis of synoptic variability in the ocean-atmosphere fluxes.   Satellite data also may be used.  For example, Miller and Katsaros (1992) demonstrated the possibility of using SSM/I data for the diagnosis of surface latent heat fluxes in a rapidly deepening marine cyclone in the Atlantic.   Even if the absolute flux values derived from satellites are biased, remotely sensed fluxes may realistically depict the space-time variability on synoptic and mesoscales.

*3.2.2 Variability in the tropics*

        Although synoptic and mesoscale sea-air flux variability in the tropics has smaller magnitude in comparison to mid- and high latitudes, it may play an important role in some key processes in the tropical boundary layer.   Large synoptic variations of tropical evaporation can affect cumulus convection,  contributing to the instability above the 850 mb level.   Note also that in the tropics,  the diurnal cycle in the sea-air fluxes becomes important, especially under calm conditions and considerable insolation (Slingo and Delecluse 1999, Weller and Anderson 1996).   This enhancement of convection,  and the reduction of the magnitude of the diurnal cycle,  is responsible for the transition of tropical convection regimes from primarily continental to marine type.   These effects were studied explicitly in the TOGA-COARE experiment (Slingo and Delecluse 1999).  In general, TOGA-COARE contributed considerably to our knowledge of synoptic and mesoscale sea-air flux variability in the tropics particularly through the extended buoy observational program.   It has been found that tropical synoptic variability can be characterised by 2-3 days dominant time scales.   Weller *et al.* (1999) showed that large variations in sea-air fluxes are associated with a family of convective systems of different origin.   Mesoscale convection can result in 60 and 250 Wm$^{-2}$ peaks in the sensible and latent heat fluxes respectively.   Peaks associated with the sub-mesoscale systems are somewhat smaller, but also pronounced (20 and 150 Wm$^{-2}$).   Esbensen and McPhaden (1996) analysed TAO moorings and IMET buoy data in the TOGA-COARE experiment and found meso-scale variability in the surface heat fluxes, with characteristic ranges of 0-50 Wm$^{-2}$ and 0-300 Wm$^{-2}$ respectively for sensible and latent heat.

**3.3  Climate variability**

*3.3.1 Introduction*

        Climate variability covers time scales from several years to centuries.   Although the number of studies dealing with climate variability in sea-air interaction processes is quite large, these studies are (to date) primarily based on the consideration of anomalies of SST and associated changes in the atmospheric circulation characteristics.  There are very few studies which directly consider the variability of the ocean-atmosphere fluxes.   However, it is through the exchange of heat, moisture and momentum that the atmosphere interacts with the ocean. Thus it is not SST itself, but these energy fluxes to and from the ocean, that actually force the atmospheric circulation and, at the same time, control the ocean temperature.   Reviewing one of the latest results on the mid-latitudinal links between SST and atmospheric circulation (Rodwell *et al.* 1999),  Kushnir (1999) argues that we need *to understand the mechanisms by which the atmosphere 'feels' the SST anomalies*.   Although it is obvious that sea-air fluxes provide more valuable information on these mechanisms in comparison with say, SST, researchers tend to avoid consideration of the climate variability of the fluxes.   This may be explained by the following reasons: (i) flux fields contain more uncertainties and errors (including time dependent biases) than individual variables; (ii) flux fields are characterised by worse sampling in comparison to say SST, and only shorter time series in well sampled ocean basins are available.   Nevertheless, some results for a number of basins have been obtained during the past several years.

*3.3.2  Detection of climate trends*

        The best studied ocean basins are the North Atlantic and the North Pacific,  since these are characterised by better sampling.    Bunker (1982) computed linear trends in the meteorological variables and sea-air fluxes over the Atlantic Ocean from 1948 to 1972 on the basis of the Bunker (1976) data set.    He found significant positive tendencies in winds and evaporation in the tropics and mid latitudes.    However,  in the 1980's and 1990's,  there has been considerable debate on the reliability of wind trends derived from VOS data (Ramage 1987, Peterson and Hasse 1987, Cardone *et al.* 1990, Lindau *et al.* 1990, Ward 1992, Bigg 1993, Isemer 1995, Ward and Hoskins 1996, Gulev 1999).    Changes with time of the fraction of anemometer measurements, growing ship size and other reasons were considered as possible sources of unrealistically high (0.1 to 0.5 ms$^{-1}$ per decade) trends in the wind speed derived from VOS data.    This makes all estimates of secular tendencies in the turbulent fluxes questionable,  since any wind speed bias propagates into the heat flux results through the bulk formulae.    Thus, Wu and Li (1995) found a significant increase in evaporation in a number of the World Ocean basins in the decade of the 1980's,  the same period which showed a sharp increase in wind speed in comparison to earlier decades.    Trends in the sea-air fluxes can also be affected by time-dependent biases in variables other than wind.    For example,  the changing fraction of SST bucket measurements and engine intake readings could result in an artificial SST trend.

        Thus,  at present,  estimation of secular trends in the fluxes is more uncertain compared to other scales of climate variability,  and time dependent biases in the basic meteorological quantities constitute the main contribution to this uncertainty.    Any future efforts in this area should include corrections to the observations (as recommended for example by Kent *et al.*, 1993b; Josey *et al.*, 1999).    However,  such corrections require that additional information be available.    Since that information is not available for every observation,  the sampling errors may be considerably increased,  and this can also affect the estimates of trends.    Now that the reanalyses have become available for periods of several decades,  there is an alternative opportunity to estimate secular changes in the flux fields. However,  although the performance of the models has been kept frozen for the reanalyses,  the assimilation input unavoidably changed with time.    Thus, estimates of secular changes from the reanalyses may also be seriously influenced by the changes in the data assimilation input.    White (1999) reported that the significant increase of satellite data available in the late 1970's could result in artefacts in estimated secular tendencies in SST and precipitation,  especially in the Southern Hemisphere (where the relative role of satellite data in the total amount of observations is very large).    In addition, time dependent biases in the COADS data may propagate into the reanalyses flux products resulting in additional uncertainty of the reanalyses-based trend estimates.    Inspection of linear trends in evaporation and net flux,  derived from the VOS measurements and from NCEP/NCAR reanalysis,  give comparable trend estimates for well sampled areas (e.g., upward tendency of about 15 Wm$^{-2}$ per decade in the North Atlantic mid latitudes and negative trends matching 10 Wm$^{-2}$ per decade in the Gulf Stream area in the subtropics).    However in other areas there are strong disagreements.    In the tropics the VOS fluxes indicate significantly large positive trends,  in disagreement with the NCEP reanalysis fluxes.    In high latitudes (e.g. the Labrador Sea) the NCEP reanalysis fluxes demonstrate strongly positive secular changes which are not supported by estimates based on VOS observations.

        Satellite data sets are already becoming comparable in time span with the reanalyses. In future these will give another alternative data source for estimating secular tendencies, which might reasonably be considered less biased in comparison to VOS and NWP fluxes.    In this sense, satellite data have an advantage because,  even if there are biases in the flux products, these should not be of time-dependent nature and thus should not affect estimates of secular tendencies.    As an example of the application of these data,  White (1999) reported that even for the period from late 1970's to late 1990's (which is considered to have more homogeneous data assimilation input) precipitation trends derived from the NCEP/NCAR reanalysis and satellite data set of Xie and Arkin (1997) have different signs.

*3.3.3 Interannual to decadal scale variability*

A. MID AND HIGH LATITUDES.

We can expect better progress to be achieved when interannual to decadal scale variability is analysed, since the uncertainties present in the mean fields and time dependent biases can be avoided. Cayan (1992a-c) used COADS MSTG products to compute the sea-air flux anomalies for the period 1946-1986 in the North Atlantic and North Pacific and to investigate the links between the flux variability patterns and associated changes in the SST and atmospheric circulation. Iwasaka and Wallace (1995) and later Tanimoto *et al.* (1997) made similar studies of the variability in the ocean-atmosphere fluxes derived from COADS data. All these studies emphasised that the major portion of variance in the surface net fluxes in the North Atlantic and North Pacific is explained by dipole patterns made by subtropical and subpolar centres of action. These patterns mirror corresponding SST patterns on interannual to decadal time scale, and can be linked to the sea level pressure patterns associated with the North Atlantic Oscillation (NAO) in the North Atlantic and with the North Pacific Oscillation and Pacific-North American pattern in the North Pacific. Cayan (1992a) found a typical winter anomaly magnitude of about 30 to 50 $Wm^{-2}$ in the mid-latitudinal North Atlantic and a somewhat smaller anomaly in the North Pacific. Sensible and latent fluxes were primarily responsible for these mid latitudinal anomalies in the net flux.

Although the mid latitudinal variability patterns in the flux fields reported by different authors are quite comparable to each other, careful inspection of the results shows that the spatial features and the flux behaviour in time (usually described in terms of the leading empirical orthogonal functions, EOF's and the corresponding principal components) show differences in different flux products. Whether these observed differences are significant depends on the scientific task considered. For describing the surface flux signal affecting the large scale atmospheric circulation (represented by sea level pressure or 500 mb height patterns), one can be satisfied with similarity of the time series of principal components corresponding to the first EOF, which typically accounts for 20 to 35% of the variance. On the other hand, analysis of relationships between the surface flux variability and behaviour of the mid-latitudinal storm tracks requires consideration of the flux patterns associated with the higher order EOF's. These can reflect differences between products, and may not necessarily be clearly separated one from another because of the errors and uncertainties which again can be different in different data sets. From the view point of forcing the general circulation of the ocean by surface fluxes, even the apparent comparability of the first EOF's in different flux products has to be viewed with caution. For example, for the ocean circulation in the North Atlantic, it is crucially important whether the local flux anomalies in the Labrador Sea, primarily caused by sensible flux, are depicted explicitly. If we consider, for example, the Cayan (1992a) pattern, the Labrador Sea will be characterised by weak anomalies. These are correlated with the anomalies in the centre of the subpolar gyre, which may be partly generated by the spatial interpolation procedures during periods of poor sampling in the Labrador Sea. However, the NCEP/NCAR and ECMWF reanalyses show a pattern characterised by strong anomalies explicitly located over the Labrador Sea and not centred on the subpolar gyre in general (Gulev *et al.* 2000). Exactly this pattern was also found recently by Alexander and Scott (1997) who studied surface flux variability from the atmospheric GCM simulations. The time behaviour of these patterns is highly correlated, however only one of the two products can provide realistic production of Labrador Sea water.

Recently Gulev *et al.* (2000) analysed interannual variability in VOS products derived by using different calculation schemes in comparison to the NWP fluxes taken from the NCEP/NCAR reanalysis. First, the EOF's of the VOS fluxes derived using different parameterisations were computed. They were very comparable to each other. The use of different schemes resulted, as expected, in different magnitudes for the anomalies, but did not affect the estimates of the long-term tendencies and interannual variability. In order to achieve full comparability of the spatial patterns, the anomalies of fluxes derived from different

schemes were projected on the EOF's of a reference product - for example, the Large and Pond (1982) scheme for the turbulent fluxes.   The correlation between the temporal behaviour of the projected fluxes (i.e. the quasi-principal components) and the principal components taken as reference,  showed that different parameterisations did not lead to any qualitative differences in the temporal behaviour of the flux anomalies.   The correlation between different projections was close to one and always over the 0.98 limit.   On the other hand,  the standard deviation of the variability obtained using different parameterisations was quite different,  and the selection of which scheme to apply was important in order to estimate the forcing magnitude (for example for model forcing fields).

This is illustrated in Figure 3.1 (Gulev *et al.* 2000).   Figure 3.1b shows the first EOF's of the net heat flux derived from fluxes computed using individual COADS reports and the observation corrections and parameterisations recommended by Josey *et al.* (1999) - except that for turbulent heat fluxes the Large and Pond (1982) scheme was used instead of Smith (1988). Also shown (Figure 3.1a) are those from the NCEP/NCAR Reanalysis data for the period from 1958 to 1997.   On the first glance, at least in mid latitudes,  the patterns are quite comparable and indicate a north-south dipole made by centres of action in the subpolar gyre and in the Gulf Stream area.   But if we consider the NCEP/NCAR fluxes,  the northern centre of action is centred exactly on the Labrador Sea,  and for the other products we have somewhat more smooth picture with the local maximum located east of Newfoundland.   More comparability is achieved in the southern centre of action.

The observed difference between the VOS and NCEP/NCAR can be influenced by inadequate sampling in the VOS data set, which has a climatological dependence and can affect both long-term trends and interannual variability.   Figure 3.1c shows the first EOF in the modified NCEP/NCAR net flux, which was derived from the original 6-hourly snap-shots by matching them to the dates and hours of the COADS reports used for computing the VOS fluxes. Remarkably enough, this "undersampled" NWP product demonstrates a spatial pattern which is very similar to the original VOS net flux.   In this case,  the importance of good sampling in order to describe variability justifies the use of COADS MSTG products (see also Section 10.12),  at least for investigating climate variations in the flux fields.   Figure 3.1d shows the first EOF in the fluxes derived from the enhanced COADS MSTG, which were taken as trimmed statistics of the basic variables;  the same parameterisations as for the VOS-type of data were applied on a monthly basis.   In comparison to the NCEP fluxes,   the variability over the Labrador Sea is more similar in amplitude when derived from the MSTG rather than from the VOS.   The reason is that the MSTG product is less influenced by undersampling compared to VOS products computed on an individual basis.   This suggests that MSTG can be successfully used for climate studies, especially if some *ad-hoc* corrections are applied to remove,  at least partially,  the time dependent biases inherent in the MSTG.  Figure 3.2 shows the time behaviour of the 1st normalised principal components of different net fluxes in comparison to the NAO index.  The time coefficients for all four products are highly correlated with each other and show quite impressive correlation with the NAO index.

B. TROPICS

The interannual and decadal variability of the fluxes for tropical oceans is significantly influenced by variations in the radiative fluxes in addition to variations of the turbulent fluxes, and this considerably increases the uncertainty of the variability estimates.   Moreover,  the magnitude of flux anomalies in the tropics is smaller in comparison to mid latitudes.   Also, sampling frequency in the tropics is lower than in mid latitudes;  fortunately the smaller synoptic variability in these regions does not require the same sampling as in mid latitudes for adequate description of the anomalies (Weare and Strub 1981).   If we consider the tropical Atlantic Ocean, we can expect that the flux variability should reflect the dominant mode associated with the Atlantic subtropical dipole, characterised by a pronounced decadal cycle in the SST anomalies (Mehta 1998).   In the tropical Pacific the dominant variability is associated with El Niño events.   Although the fluxes are crucially important for understanding the El Niño
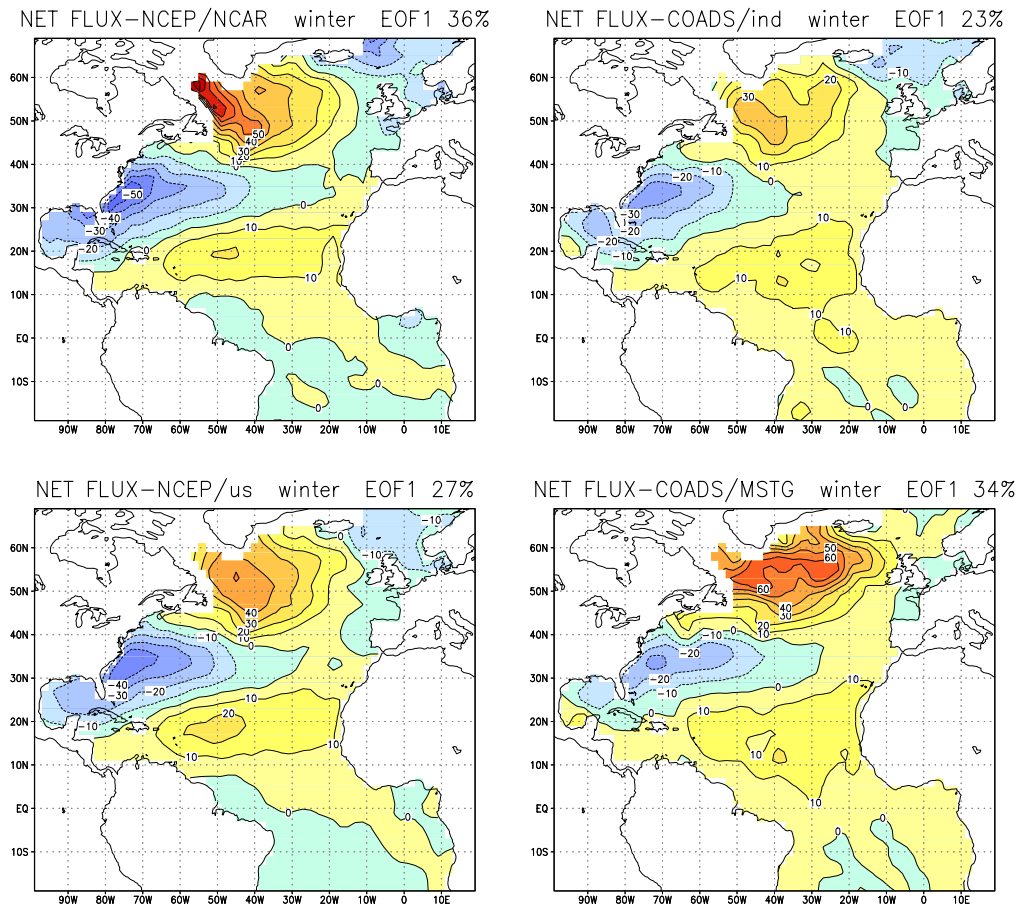
Figure 3.1 First EOF of the net heat flux derived from (a) (top left) NCEP/NCAR reanalysis; (b) (top right) COADS ship reports; (c) (bottom left) the reanalysis sampled at COADS report positions; (d) (bottom right) using COADS MSTG data.
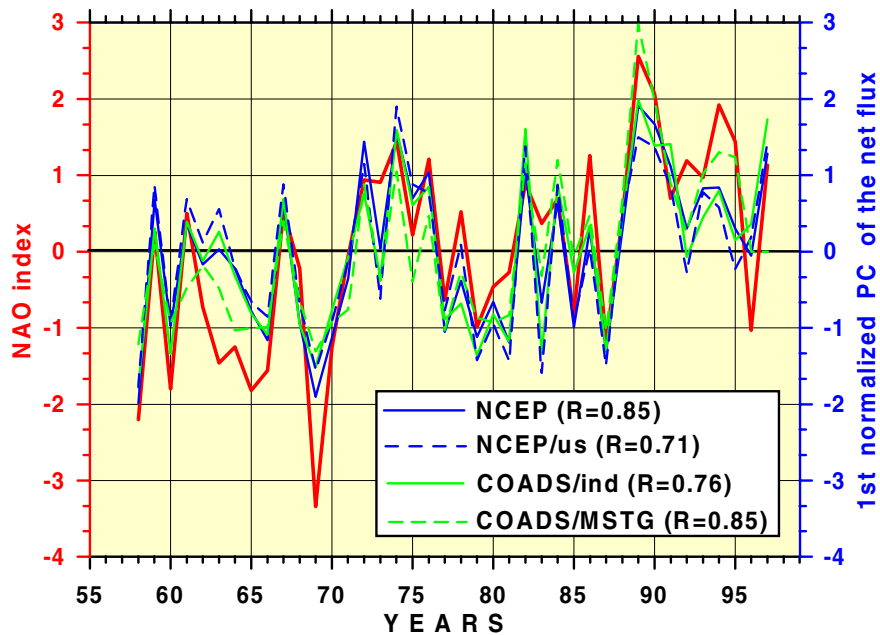


Figure 3.2  Time series of the NAO index (red line) and of the first normalised principal component of the net heat flux from the analyses shown in Figure 3.1. (NCEP/NCAR reanalysis;  NCEP/us is sampled at ship data positions; Individual COADS reports; and COADS MSTG data.)

life cycle on an interseasonal scale,   there is no indication that they can serve better than SST as predictors on longer time scales.   Variability in the Indian Ocean is also poorly quantified. Jones *et al.* (1995) made an EOF analysis of 30-year surface fluxes over the Indian Ocean, using COADS,  and found increasing latent heat flux from the 1960's to 1980's ranging from several Wm$^{-2}$ to several tens of Wm$^{-2}$.

C. SEASONAL VARIABILITY

The interannual variability of flux fields should be considered in the context of seasonal variability since this affects the observed climate changes.   Summer flux anomalies can be primarily driven by net flux components different from those which are crucially important during wintertime.   In particular, radiative fluxes may play a more important role during the warm season.   Tanimoto *et al.* (1997) noted differences in the summer and winter variability patterns in the mid-latitudinal North Pacific.   However, this problem is still has to be fully explored.

## 3.4 Summary

To summarise, our knowledge of the climatic variability of ocean-atmosphere fluxes is still poor.   Results obtained over the last several years have suggested that studies of the variability of the fluxes can potentially tell us much about the surface climate signals on different time scales.   However in practice the signals which have been derived have not proved significantly more valuable for understanding climate variability compared to those obtained by studying the variability of basic variables such as SST.   Nevertheless, development and improvement of different flux products, available from VOS, NWP and satellites,  may improve this situation in the immediate future.

**4  DATA SOURCES FOR FLUXES AND RELATED VARIABLES**

**4.1  Introduction**

        This Chapter will consider the characteristics of the different sources of data for the fluxes and flux related variables.  Each have their advantages and disadvantages.  The main sources of *in situ* data are from ships and buoys.  Merchant ships in the Voluntary Observing Ship programme are the traditional source of flux estimates providing weather observations from which the fluxes can be estimated.   However the sampling is restricted to shipping lanes and many parts of the ocean are rarely observed.  Likewise, intensive field campaigns by research ships (e.g. TOGA-COARE) are too restricted in both sampling time and space, to contribute significantly to the global flux database; however, the resulting high-quality measurements of fluxes and related basic variables are invaluable for verification of systems with broader coverage.  Satellites provide globally distributed data but for a restricted range of variables.  Models can be used to assimilate the various information available, and produce regular gridded fields of flux values. There is continuous effort, using results from the intensive field studies referred to above, to improve the performance of model parameterisations and hence the accuracy of the fluxes. Flux values can also be estimated from what are effectively budget methods, the "residual technique" and assimilation into ocean models. Finally in this Chapter the data sets for determining the fluxes in sea ice regions will be discussed.

**4.2  *in situ* data sources**

*4.2.1  Voluntary Observing Ships*

        Our present understanding of the climate over the global ocean   (e.g. Budyko, 1963; Esbensen and Kushnir, 1981;  Oberhuber, 1988;  da Silva *et al.*, 1994; Josey *et al.* 1999) is based on the meteorological reports from the Voluntary Observing Ships (VOS) of the World Weather Watch.  These merchant ship observations constitute the only quasi-global data set which extends over a number of decades.   In addition,  the range of observations is such that it has been possible to develop parameterisation formulae with which to calculate all the required fluxes.

        A major disadvantage of the ship observations is that adequate coverage is obtained only in areas that are well covered by shipping lanes (Figure 4.1).   For example, in July there are very few observations which enable a latent heat flux estimate to be made south of 40°S. In contrast the North Atlantic and North Pacific are well covered by observations. Inevitably the characteristics of the ship observations (biases,  precision etc.) have changed with time.  There have been, and will continue to be,  changes in instrumentation,  for example,  sea surface temperature buckets (of varying types) are increasingly being replaced by engine room intake readings.  The increasing use of anemometers to  estimate the wind may results in errors due to airflow disturbance and errors in calculating the true wind velocity.  However the major change has been in the size and type of the ships with modern ships typically larger, faster, and travelling on different routes compared to those in past decades.   In recent years our understanding of the resulting biases in these observations has increased significantly (Chapter 10 ) allowing the possibility both of applying correction schemes and implementing improved observational methods.

        Because there are about 7000 VOS,  with ships continually leaving the programme and new ships being recruited,  the instrumentation provided by the Meteorological Agencies has generally been basic and inexpensive.   Kent and Taylor (1991) described  a subset of 46 Voluntary Observing Ships (VOS) operating in the North Atlantic,  and the meteorological instrumentation with which they were equipped.  Typical of this subset would be a container vessel of about 210m length, travelling at about 9 ms$^{-1}$, and loaded with cargo to about 10m to 20m above the main deck.   As an instrument platform, this represents a large object capable of significantly altering the environment to which the meteorological sensors are exposed.   Sea temperatures were measured near the surface using a SST bucket, or,  more likely,  at depths of

3m to 9m using engine intake or hull contact sensors. Air temperature and humidity observations were taken at about 20m to 30m above the sea using a thermometer screen or hand held psychrometer. If carried, the anemometer was mounted at about 30m to 35m above sea level, but, in the North Atlantic, two-thirds of the ships reported visually estimated winds.
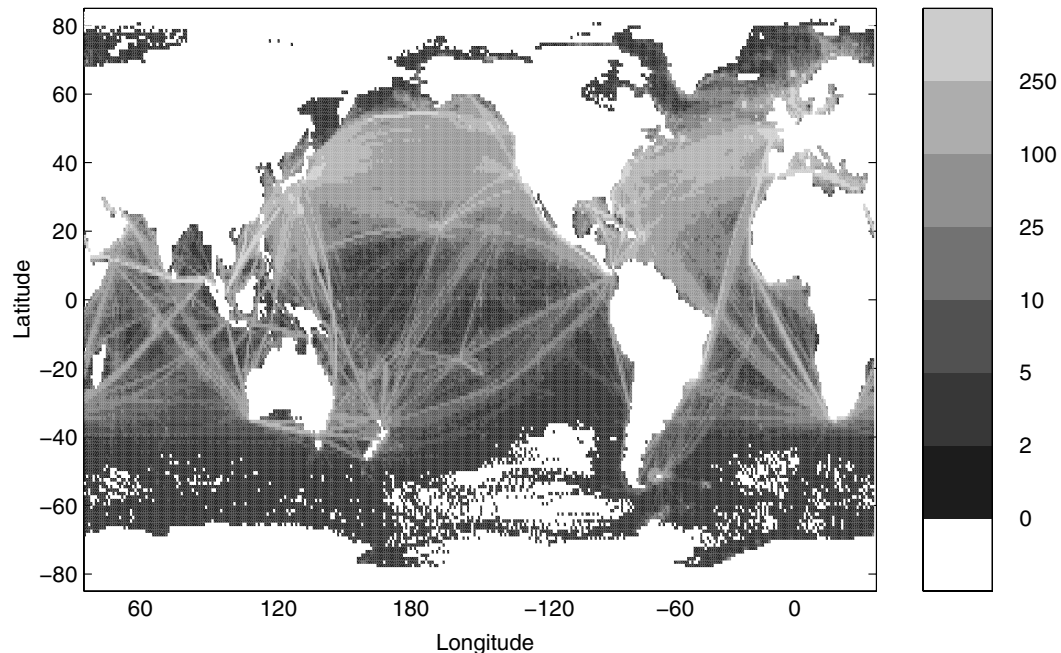


Figure 4.1Global distribution of the number of latent heat flux estimates per 1° x 1° square for the period 1980 - 1993. White indicates that there were no observations over the entire period considered (from Josey *et al.* 1999)

For some time there have been suggestions that improved instrumentation might be placed on a subset of the VOS e.g. (Taylor, 1984). An example is the Improved Meteorological System, IMET (Hosom *et al.*, 1995) developed at Woods Hole Oceanographic Institution (WHOI) which has been installed on a number of the U.S. Research Vessels and is now being placed on U. S. VOS. IMET uses sensors chosen for accuracy, reliability, and their ability to stay in calibration during unattended operation. The present set of IMET modules includes wind speed/direction, air temperature, sea surface temperature, relative humidity, precipitation, incoming shortwave radiation, incoming longwave radiation, and barometric pressure. A data set of automatically recorded meteorological data has been assembled from the research ships operating during the WOCE Hydrographic Programme (1991 - 1998). These ships used IMET or similar systems. Often these ships were away from the main shipping lanes, so these data are potentially of value for flux verification (see Section 9.2.3).

Recently there has been an initiative by the World Weather Watch to establish a VOS Climate Project. The initial aim would be to assemble a set of chosen VOS and to document carefully the instrumentation in use. Data from these ships would undergo detailed analysis in order to estimate any biases on a ship by ship basis. The Working Group considered that such an initiative was to be encouraged since, in time, the resulting data set will form an important asset for verification of both basic variables and flux estimates.

### 4.2.2 Ocean Weather Ships

The array of Ocean Weather Ships was originally subsidised by the commercial aviation sector, and maintained at different sites for varying periods during the years 1945 to 1989 (Table 4.1 and Figure 4.2). Apart from surface and upper air meteorological measurements, the weather ships provided, during various periods, time series of surface radiation budget, surface waves, ocean profiles, and other variables. Valuable climate data were obtained, for example the long time series of data from ocean station Papa. However the

weather ships were implemented for weather forecasting rather than for climate observations and this has implications with regard to the accuracy of the data. Indeed, it should not be considered that the Weather Ship data were immune from systematic errors. For example, Isemer (1994) demonstrates that deriving a long time series of consistent weather ship wind observations is not a trivial task given the many changes in ship type and observing practise. Nevertheless the weather ships form a valuable data resource where a long time series of data is required from specific sites.
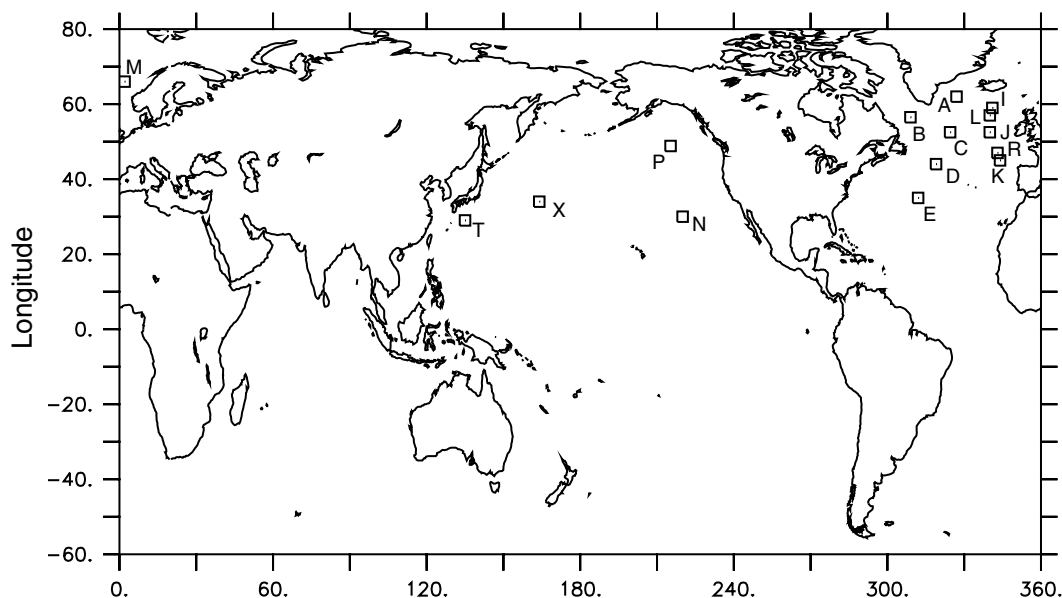


Figure 4.2 Distribution of Weather Ship Stations

Table 4.1 Summary of the Weather ship sites (from Isemer, 1994)

|   | Position | start | end | Country |   | Position | start | end | Country |
|---|----------|-------|-----|---------|---|----------|-------|-----|---------|
| A | 62N 33W | 4/45 | 4/74 | US,F,N, NL,UK | L | 57N 20W | 7/75 | 12/89 | F,NL,UK |
| B | 56.5N 51W | 1/46 | 4/74 | US | M | 66N 2E | 1/49 | 12/89 | F,UK |
| C | 52.5N 35,5W | 11/45 | 12/89 | US, USSR | R | 47N 17W | 7/75 | 12/85 | F |
| D | 44N 41W | 1/46 | 6/73 | US | N | 30N 140W | 6/46 | 4/74 | US |
| E | 35N 48W | 9.49 | 6/73 | US | P | 59N 145W | 10/49 | 6/81 | US,C |
| I | 59N 19W | 9/47 | 6/75 | NL,UK | T | 29N 135E | 9/48 | 10/81 | J |
| J | 52.5N 20W | 8/47 | 6/75 | NL,UK | V | 34N 164E | 3/55 | 1/72 | US |
| K | 45N 16W | 6/49 | 6/75 | F,NL,UK |   |   |   |   |   |

### 4.2.3 Buoys

Buoy data does not allow global estimation of the surface fluxes; however buoys are a good source of verification data for other observing systems. Many countries now operate moored coastal buoy arrays, for example the NDBC (Gilhousen, 1998) and AES (Axys, 1996) buoys off North America, and the ODBS buoys off Japan. Taking as an example the NDBC buoys, these range in type from the very large 12m and 10m discus designs, through the 6m Nomad buoy to the 3m Discus buoy. Over 20 buoy locations have been maintained in both the Atlantic and Pacific with most time series dating from the mid 1970's, or early 1980's, to the

present.   In addition to standard surface meteorological data, spectral wave data and current profiles are available from some locations.   Although primarily established for weather forecasting and now-casting purposes,  these buoys have also proved valuable for the calibration of remotely sensed data from satellites.

Operational buoy arrays have begun to be established away from coasts in the open ocean.   Foremost of these was the TOGA TAO array (McPhaden *et al.*, 1998).   A major responsibility for the western part of the array is now to be assumed by the TRITON programme (Kuroda *et al.*, 1999) and a similar array (PIRATA) is being implemented in the Tropical Atlantic (Servain *et al.*, 1998).   The relatively simple and inexpensive Autonomous Temperature Line Acquisition System (ATLAS) buoys which are used for these arrays measure a basic set of the meteorological variables.   In contrast "Flux buoys" have been developed, principally by a group at WHOI as part of the IMET programme,  to measure all the variables required to estimate the heat, momentum and radiative fluxes.   They have been used in the Subduction experiment in the North Atlantic (Moyer and Weller, 1997),  in the west Pacific during the TOGA COARE experiment (Weller and Anderson, 1996),  in the Arabian Sea (Weller *et al.*, 1998) and elsewhere.   These buoys are a valuable source of data for verifying flux estimates.   Equipped with fast response sensors,  research buoys can also be used to determine the transfer coefficients.
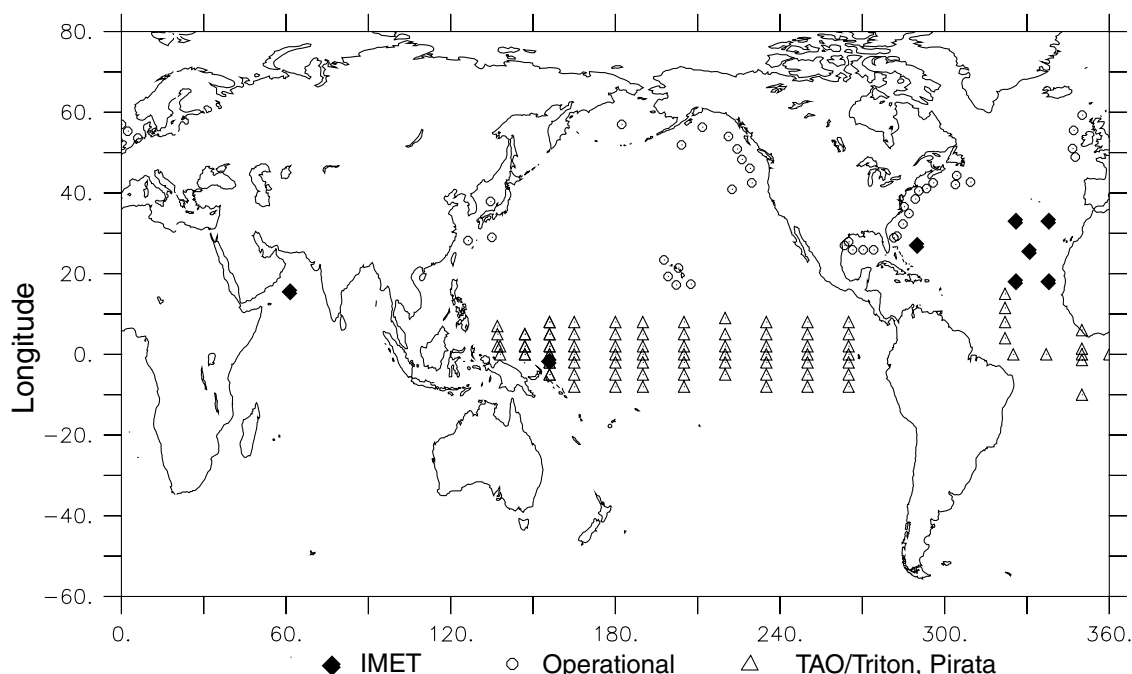


Figure 4.3 Positions of Meteorological buoy arrays (past and present).   (circles: standard meteorological buoys; triangles: TAO/Triton and PIRATA arrays;  black diamonds: Flux buoy sites(IMET) ).  Note that not all of these buoys are still in operation.

Drifting buoys are deployed in significant numbers and are well distributed over the global ocean.   However they measure a too restricted range of variables to allow flux estimation.  Sea temperature is normally measured, air pressure may be measured,  and, on some buoys,  wind speed may also be estimated.

*4.2.4  Platforms, Rigs, etc.*

Fixed platforms, drilling rigs, etc.  generally tend to be poor instrument platforms. Their large size is likely to result in poor instrument exposure.   Instruments,  such as anemometers,  are often mounted several tens of metres above the sea.  If the platform is involved in oil or gas production then there may be strict controls on the type of instrumentation that can be installed and the facilities for access for maintenance.  However,  because some

platforms report meteorological observations on a very frequent basis it may be necessary to ensure that potentially biased observations from a platform do not dominate the climatology of a region. This is also true of coastal observation stations, such as lighthouses, where the data may be significantly influenced by the position of the platform.

An exception to these negative judgements are platforms designed or implemented specifically for meteorological observation, however these are very few in number and confined to coastal regions.

### 4.3 Satellite Data Sources

*4.3.1 Introduction*

Many algorithms have been developed deriving basic state variables like SST, atmospheric surface temperature, wind speed, atmospheric humidity, cloud liquid water, rain rate, longwave and shortwave radiation etc. from satellite data using instruments measuring at different wavelengths. Whereas the radiative fluxes at the surface are derived by measuring radiative fluxes at the top of the atmosphere and using a radiative transfer model (Chapter 6), turbulent fluxes are estimated from the basic state variables using bulk formulae (Chapter 7). Today most of the basic state variables necessary for estimating surface fluxes can be derived from satellite data. These quantities may be directly derived using radar backscatter or from visible, infrared or microwave brightness temperatures. The exception is atmospheric surface air temperature. This variable is important to estimate sensible heat flux, and the transfer coefficients within the bulk formulae, but estimation from satellite data is still troublesome. Previously, some of these retrievals have been used to derive flux climatologies, however mostly they have only been used to derive exemplary fields of the basic state variables over short time periods. However, there has been a remarkable development of new algorithms which is gradually changing the situation.

In this section the major instruments used for flux determination which are presently orbiting are introduced. The orbit and instrument characteristics of the different satellites are identified and discussed. Major demands on the instruments utilised are that they must deliver accurate and relatively stable measurements over a long period. This is only attainable by using on-board calibration, applying algorithms that consider the ageing of the particular radiometer, or by applying ongoing calibration with high quality *in situ* data. A further requirement, for instruments on polar orbiters, is that the swath width must be large enough (over 1000 km) to sample the earth's surface during a couple of days.

*4.3.2 Non geostationary satellites*

The classical instruments that meet the above requirements are the Advanced Very High Resolution Radiometer (AVHRR) and the Special Sensor Microwave/Imager (SSM/I). Measurements of sea surface temperature are best performed in the infrared range where the sea surface has a high emissivity. On the other hand, this high emissivity dominates the signal and prevents the extraction of wind speed or boundary layer water vapour content with high accuracy from infrared measurements. For these parameters the microwave spectral range is much better suited since the ocean surface emissivity is relatively small in the microwave range compared to the infrared. A disadvantage of these considerations was that, before the Tropical Rainfall Measuring Mission (TRMM), it was not possible to obtain energy fluxes from instruments installed on one satellite. Thus, any estimate of a parameterised quantity like latent heat flux will suffer from being derived from estimates of basic variables obtained from different satellites at different times. Fortunately, in general it is expected that this error is relatively small since the sea surface temperature obtained from AVHRR data varies relatively slowly compared to the atmospheric variables obtained from SSM/I measurements. To derive fields of wind speed and rainfall, active instruments like scatterometers and radars may also be used

## A. AVHRR

The AVHRR instrument has been flown on the NOAA satellite series since 1979 and used to construct global fields of sea surface temperature, for example the optimally interpolated SST dataset of Reynolds (Reynolds and Smith, 1994) or the NOAA/NASA Oceans Pathfinder Sea Surface Temperature dataset (Brown *et al.* 1993). Flight periods for the different NOAA satellites are shown in Table 4.2.

The AVHRR instrument measures in five channels, two in the solar spectral range, one in the near infrared, and two located within the infrared atmospheric window. The infrared window channels are best suited for estimates of sea surface temperatures in cloud free cases. Despite the broad swath of approximately 3000 km, a complete coverage of the Earth surface is only achieved within one or two weeks depending on the actual cloud coverage. Some problematic regions, with almost persistent cloud coverage, are the extended stratocumulus fields to the west of Africa, the ITCZ, and Arctic and Antarctic regions during winter. Therefore the quality of an estimation of sea surface temperature is highly dependent on the quality of the implemented aerosol and cloud detection scheme. A description of errors occurring in sea surface temperature, due to the different quality of cloud detection during day and night, can be found in Reynolds (1993). If measurements of sea surface temperature are hampered for weeks by persistent cloudiness (or long periods of darkness as over polar regions) the estimates might become biased due to the more difficult cloud detection in the infrared range. What consequences this has for the combination of AVHRR and SSM/I has not been fully explored.

Table 4.2: Temporal coverage of AVHRR (lighter shading = partial coverage of the year)

| | 78 | 79 | 80 | 81 | 82 | 83 | 84 | 85 | 86 | 87 | 88 | 89 | 90 | 91 | 92 | 93 | 94 | 95 | 96 | 97 | 98 | 99 |
|---|---|---|---|---|---|---|---|---|---|---|---|---|---|---|---|---|---|---|---|---|---|---|
| TIROS-N | | | | | | | | | | | | | | | | | | | | | | |
| NOAA-6 | | | | | | | | | | | | | | | | | | | | | | |
| NOAA-7 | | | | | | | | | | | | | | | | | | | | | | |
| NOAA-8 | | | | | | | | | | | | | | | | | | | | | | |
| NOAA-9 | | | | | | | | | | | | | | | | | | | | | | |
| NOAA-10 | | | | | | | | | | | | | | | | | | | | | | |
| NOAA-11 | | | | | | | | | | | | | | | | | | | | | | |
| NOAA-12 | | | | | | | | | | | | | | | | | | | | | | |
| NOAA-14 | | | | | | | | | | | | | | | | | | | | | | |

## B. ATSR

The Along-Track Scanning Radiometer (ATSR – Zavody *et al.*, 1994) is a visible and infrared radiometer with a built-in calibration system. It provides views of the sea surface at two different incidence angles and hence has the potential to estimate atmospheric transmission effects. In comparison with buoy data, rms scatter better than ±0.25°C has been claimed (see section 10.2.3). However the recent workshop on SST (Arkin, 1999) considered that the ATSR had not yet fully fulfilled its promise for a number of reasons. There had been a failure of one channel on the first instrument (flown on ERS-1) and problems with the cloud clearance algorithm. Because the ATSR was not part of the core payload for the satellites the data were not widely available in operational mode and this had limited their exploitation. A further limitation is that the ATSR has a narrow swath, only 500km, and therefore provides many fewer cloud-clear views of the sea surface compared to AVHRR.

C.  SSM/I

       One of the most advanced sensors for monitoring flux related atmospheric variables and ice cover from space is the SSM/I aboard the satellites of the Defense Meteorological Satellite Program (DMSP). The SSM/I is a passive microwave radiometer measuring emitted radiation from the earth's surface and the atmosphere at four frequencies located at 19.35, 22.235, 37.0, and 85.5 GHz at two polarisations (with the exception of 22 GHz which is only measured at vertical polarisation).  The SSM/I instrument scans conically at a constant earth incidence angle of 53.1° resulting in a swath width of nearly 1400 km,  only half of that of the AVHRR.  However,  cloud coverage is less of a problem within the microwave spectral range, so the determination of flux related variables is only hindered in cases where rain occurs.

       SSM/I data are sampled every 25 km (A-Scan) at the five lower frequencies and every 12.5 km (B-Scan) at 85.5 GHz. Most of the retrieval schemes rely upon the A-scan data and don't consider the effects of different ground resolutions at different frequencies. A more detailed description of the instrument can be found in Hollinger *et al.* (1987).

       SSM/I's have been flown on different DMSP satellites since July 1987 as shown in Table 4.3.   These satellites have different orbits resulting in different local observing times and this can have implications for the construction of a satellite-derived climatology (see section 8.6).   If the data from only one satellite is used (as has been the case to date)  sampling errors can result,  at least in all quantities that have a distinct diurnal cycle, for example,  precipitation.

D.  TRMM

       The Tropical Rainfall Measuring Mission (TRMM) satellite,  dedicated to performing measurements relevant to tropical precipitation and the resulting latent heat release,  was launched in November 1997.   It is a low latitude, precessing satellite carrying five instruments of which three are suitable for the precipitation mission.   These are the TRMM Microwave Imager (TMI), the Visible and Infrared Scanner (VIRS), and the Precipitation Radar (PR).   The TMI is an instrument similar to the SSM/I but with key differences:  an additional channel with vertical and horizontal polarisation at 10.7 GHz,  and a shifted water vapour channel at 21.3 GHz  instead of 22.235 GHz used for the SSM/I which is the centre of the water vapour absorption line).   The latter change should avoid the signal saturation at high atmospheric water vapour contents found within SSM/I measurements.   The VIRS has the same wavelengths and bandwidths as the AVHRR (see above).   The major differences between VIRS and AVHRR are that the VIRS has a post launch calibration unit and a larger instantaneous field of view at nadir of  2.11 km (compared to 1.1 km for the AVHRR).   The PR is an active system working at 13.8 GHz that provides,  for the first time,  information on the vertical distribution of rainfall.   Since the TMI and VIRS are very similar to SSM/I and AVHRR,  in addition to measuring precipitation they may be used to obtain most of flux related atmospheric variables including SST using almost the same algorithms developed for the latter sensors.   A comprehensive description of the different features of all three instruments can be found in Kummerow *et al.* (1998).

Table 4.3: Temporal coverage of SSM/I (lighter shading indicates partial coverage of the year)

| | 87 | 88 | 89 | 90 | 91 | 92 | 93 | 94 | 95 | 96 | 97 | 98 | 99 |
|---|---|---|---|---|---|---|---|---|---|---|---|---|---|
| F-8 | | | | | | | | | | | | | |
| F-10 | | | | | | | | | | | | | |
| F-11 | | | | | | | | | | | | | |
| F-13 | | | | | | | | | | | | | |
| F-14 | | | | | | | | | | | | | |
| F-15 | | | | | | | | | | | | | |

Due to the orbit characteristics, TRMM measurements are only available within ±40° latitude so no global datasets can be derived. In addition, TMI, VIRS, and PR have very different swath widths ranging from 215 km for the PR, 720 km for the VIRS, and 759 km for the TMI, respectively. Thus more time is needed to achieve full coverage compared to the SSM/I and AVHRR. In coming years it is expected that TRMM and SSM/I, together with the new Advanced Scanning Microwave Radiometer (AMSR), will be used to improve and continue satellite-derived products.

E. TOVS

The TIROS Operational Vertical Sounder (TOVS) consists of two components. The High-resolution Infrared Radiation Sounder (HIRS) is the infrared part with 19 channels between 3.7 and 15 μm and a single day-time cloud-detection band in the visible spectral domain. The HIRS is the main vertical sounding component with sixteen temperature and three water vapour channels. Additionally there is the Microwave Sounding Unit (MSU) with for channels arranged between 50.31 and 57.95 GHz. These channels are used for sounding temperature profiles with coarser vertical and horizontal resolution but the ability to obtain data in cloudy cases.

The TOVS package has been flown on the NOAA satellite series, being used to invert temperature and humidity profiles for assimilation into NWP models. Temperature and humidity from the lowest levels of the HIRS derived profiles could be useful for flux calculations but so far have not been used for that purpose. Over ice surface, TOVS data have been used to determine the drag coefients as well as cloud fractions (see Section 10.11.2).

F. Scatterometers (ERS-1,2; NSCAT; QuikScat)

Satellite borne scatterometers have the unique capability of returning estimates of wind speed and direction over the ice-free zones of the global oceans. This is achieved through transmitting microwave signals aimed off-nadir and analyzing backscattered energy from the ocean surface. The magnitude of the backscattered energy indicates wind magnitude while numerous looks at the same ocean surface location provides the wind direction information. The wind direction information is critical for determining ocean-relevant forcings such as wind stress curl. Additionally, wind divergence is an important diagnostic variable indicative of both ocean and atmospheric processes, and can be calculated only with directional information.

Since the first such system was launched aboard SeaSat (1978), there have been significant advances in technology and instrument design to improve the quality of the winds from these instruments. The European spacecraft ERS-1 (replaced by ERS-2) has provided continuous wind measurements over the ocean since 1991. In its scatterometer mode, the ERS platforms provide wind vectors from a single but relatively narrow (500-km) swath with winds provided every 50-km within the swath. Near coastal regions and in ice zones the scatterometer was turned off to facilitate SAR imaging thus limiting wind vector coverage. The NSCAT mission (Oct 96 - June 1997) featured dual swaths of 600-km width each with 25-km grid spacing for the wind retrievals. Continuous scanning over the globe resulted in wind vectors reported over more than 90% of the world's ice-free oceans every two days. A special issue of JGR-Oceans (May 1999 Volume 104, No. C5) contains a number of papers describing the NSCAT mission and scientific results. The next mission, QuikSCAT, was launched in June 1999 and features a radially scanning scatterometer providing a single 1800-km swath of wind vector data covering 90% of the earth's oceans every day.

*4.3.3 Geostationary satellites*

Geostationary satellites like GOES-E, GOES-W, GMS, and METEOSAT typically scan the earth using three bands in the visible, infrared window, and water vapour absorption band at 0.5 – 0.9 μm, 10.5 - 12.5 μm, and 5.7 – 7.1 μm, respectively. These data have been used in combination with data from microwave polar orbiting instruments to enhance the sampling rate - one of the largest error sources for rainfall measurements from space. Since

rainfall estimates from geostationary satellites are inaccurate (because they rely on cloud top temperature) they have been calibrated with the more accurate microwave estimates to develop rainfall products like GPCP or CMAP where the sampling is only improved within the field of view of the geostationary satellites (see Section 10.9).

## 4.4 NWP and Reanalyses

### 4.4.1 Introduction

If one was to design a system to produce the best estimates of air-sea fluxes, the system would use all available observations of the atmosphere and ocean, their exchanges of radiation with space and the exchanges of energy, water and momentum between the atmosphere and the earth's surface.  It would include the effect of data from different observation times and fill in gaps in the data by using the laws of physics as expressed in the equations of fluid mechanics to interpolate in time and space.  The fields actually observed,  and not derived fields,  would be used; thus radiances observed by satellites would be used rather than derived temperature and moisture fields to ensure consistency in physical parameterisation.  This is a data assimilation system.

Such a system would not be identical to a data assimilation system designed for numerical weather prediction, but might well be a modified version of an operational NWP data assimilation system.  As discussed in Section 2.2, data assimilation for NWP is designed to produce the best forecasts, not necessarily the most complete or the most realistic depiction of the atmosphere.  NWP has important timeliness requirements.  Data assimilation for the most realistic estimates of air-sea fluxes could have a longer data cut-off time and in fact might choose to use observations occurring after the analysis time, using a computer model to interpolate both forward and backward in time.  Observations could be used even if their processing took significant time and they had little effect on weather forecasts.  More complete and complex assimilation of satellite measurements could be done than is desirable in operational NWP.  The selection and improvement of parameterisations would be designed to give the more realistic and complete depiction of the atmosphere and its boundary conditions rather than the best forecast.  The system would benefit from a close association with an operational NWP data assimilation effort.

Such a system should not provide the only estimates of air-sea fluxes.  Global estimates of precipitation by Xie and Arkin (1996) (CMAP) include separate estimates of precipitation from each source they use - rain gauges, different satellite methods and data assimilation.   A similar range of estimates for air-sea fluxes could give valuable insight both into the uncertainty of the estimates and also the primary sources of information for the best estimate.

Today,  data assimilation for operational NWP produce complete global analyses of the atmosphere and its interactions with space and with the earth's surface every few hours on a regular grid at fairly high spatial resolution (from 40 to 105 km).  These analyses use large amounts of observations from a wide variety of sources and combine them with highly accurate short-range forecasts.  The analyses are widely distributed a few hours after observation time and are critically scrutinised by many diverse users, including marine forecasters.  Operational data assimilation and NWP modelling groups are made aware every day of the limitations of their analyses and forecasts; they are constantly seeking to improve all aspects of their analyses and forecasts.  Data assimilation systems and NWP models have greatly improved over the last two decades, but the physical parameterisations used are still relatively crude and the physical fields produced by analysis/forecasts systems need to be critically examined to see how close we are to the future system described above.

### 4.4.2 Fluxes from operational data assimilation

A. INTRODUCTION

Physical fields from operational global data assimilation systems, such as surface fluxes of moisture, energy and momentum, are generally accumulated during the short-range six-hour

"first guess" forecast and during longer-range forecasts as well. Meteorological fields such as near-surface winds, temperature and moisture are analysed from a combination of the observations and the first guess forecast and are available at 6 hour intervals as analyses and as 6 hour forecasts. Users of fluxes from data assimilation have requested fields every three hours and global NWP systems may well move to produce analyses every three hours in the near future. Special files for individual points can be prepared in which data is output every hour of the forecast. Model errors can affect the analysed meteorological fields as well as the physical fields through the first guess forecast, especially in data-scarce regions over the oceans. White (1995) compared precipitation and surface fluxes from four operational global NWP analysis/forecast systems: NCEP, ECMWF, the United Kingdom Meteorological Office (UKMO) and the Japanese Meteorological Agency (JMA). Section 11.5 of this report describes a Working Group on Numerical Experimentation (WGNE) proposal to conduct a more extensive comparison of surface fluxes of operational global NWP systems and to establish an ongoing centre for archiving and comparing such fluxes.

There are many operational NWP systems. Pan (1999) describes the parameterisation of subgrid-scale processes in atmospheric models. Phillips (1994) describes the atmospheric models of several centres. This section considers NCEP and ECMWF as examples of operational systems.

B. THE NCEP OPERATIONAL GLOBAL MODEL

**Formulation of the Model:** The home page of the NCEP global modelling branch (http://sgi62.wwb.noaa.gov:8080/research/global2.html) contains information on the formulation and performance of the NCEP operational global analysis/forecast system. A description of the NCEP global analysis/forecast system can be found in Kanamitsu (1989). As an example of an operational global model, the present operational NCEP global model is summarised below (http://sgi62.wwb.noaa.gov:8080/research/mrf.html):

a)  T170 spectral model (equivalent to a horizontal resolution of 75 km).
b)  42 vertical unequally spaced sigma levels. For a surface pressure of 1000 hPa, its lowest level is about 996 hPa.
c)  physics calculated on a Gaussian grid of 512 by 256, approximately 1˚ resolution;
d)  Shortwave radiation is based on work by Chou (1992). Surface solar absorption is determined from the surface albedo. Ocean surface albedo depends on zenith angle.
e)  Longwave radiation follows Fels and Schwarzkopf (1975), Schwarzkopf and Fels (1991). Long-wave emissivity is prescribed to be unity for all surfaces.
f)  Cloud fractions are diagnosed from the relative humidity based on RTNEPH observations.
g)  Over the ocean the Charnock (1955) formula is used to update the momentum roughness from the estimated surface stress. Thermal roughness is based on TOGA COARE observations (Zeng *et al.*, 1998).
h)  The lowest model layer is assumed to be the surface layer (sigma=0.996) and the Monin-Obukhov similarity profile relationship is applied to obtain the surface stress and sensible and latent heat fluxes. The formulation was based on Miyakoda and Sirutis (1996) and has been modified by P. Long in the very stable and very unstable situations. A bulk aerodynamic formula is used to calculate the fluxes once the turbulent exchange coefficients are obtained.
i)  Boundary layer turbulent mixing is a bulk Richardson number based non-local mixing scheme (Troen and Mahrt, 1986; Hong and Pan, 1996). Free atmosphere vertical diffusion uses a local mixing scheme.
j)  Shallow convection by Tiedtke (1983).
k)  Deep convection is a simplified Arakawa-Schubert scheme originally developed by Grell (1993) and modified by Pan and Wu (1995) and Hong and Pan (1996).

l)      Large-scale precipitation is caused by super-saturation removal and by convective adjustment when the sounding is conditionally unstable and supersaturated. Falling rain is evaporated based on Kessler (1969).

**Formulation of the operational analysis:** The analysis seeks to obtain the best fit to the observations and to the six-hour background or first guess forecast (Parrish and Derber, 1992; Derber *et al*., 1991; http://sgi62.wwb.noaa.gov:8080/RTPUB). The analysis is performed as a series of iterative problems in the model's vertical coordinate system and uses the following observations:

a)      rawinsondes and dropwindsondes—winds, temperatures, specific humidity, surface pressure
b)      aircraft reports—winds and temperatures
c)      satellite cloud tracked winds
d)      surface marine observations—winds, temperatures, specific humidity, surface pressure
e)      surface land observations—specific humidity, surface pressure
f)      SSM/I wind speeds over water
g)      Australian sea level pressure bogus
h)      satellite microwave and infrared radiances
i)      hurricane bogus winds
j)      profiler winds
k)      ERS-2 wind speeds and directions over water
l)      SBUV ozone profiles

Observational error statistics vary with each observation type and can vary with location. They contain both instrument error and representativeness error. Background error statistics are used to weight the first guess field and are nearly homogeneous around a latitude band.

C.  THE ECMWF OPERATIONAL SYSTEM

ECMWF currently uses a spectral T319 (about 40 km) model with 60 levels in the vertical. It uses a 4D variational (4DVAR) analysis and processes raw TOVS/ATOVS radiance data. A fully coupled wave model produces surface fluxes dependent on sea state. It currently blacklists ship humidity data; ship wind data makes use of WMO tables for height assignment.

A seasonal forecast system, based on a coupled integration of a T63 and 31 level (as of Oct. 1998) version of the ECMWF atmospheric model and the HOPE ocean model, is run daily. However the model drift tends to be comparable in magnitude to the seasonal anomaly being forecast. Tests of revised physical parameterisations appeared to reduce the drift in SST.

Beljaars (1997) described the parameterisation of atmosphere-ocean exchange in the ECMWF model. Klinker (1997) examined the ECMWF model's surface fluxes. Siefridt *et al.* (1999) examined the effect of parameterisation changes of ECMWF operational fluxes during 1986-95. ECMWF publications can be obtained from the ECMWF Library, also see http://www.ecmwf.int/pressroom/publications.html .

*4.4.3 Fluxes from reanalyses*

A.  INTRODUCTION

In reanalysis a frozen NWP analysis forecast system is used to process data over several years of past data. The advantages of a reanalysis over operational NWP data assimilation is that it offers several years of fields from an unchanging system and that the fields can be more easily obtained. The disadvantage is that by the time the complete reanalysis record is available the system used is lower resolution and uses older, less developed physical parameterisations than the latest operational NWP systems. Several years of results are available from four reanalyses:

a)      ERA15 - ECMWF's reanalysis: 1979-1993.

b)    GEOS1 - Goddard Earth Observing System March :1980-Nov. 1993  (Data Assimilation Office (DAO), Goddard Space Flight Centre (GSFC), National Aeronautics and Space Administration (NASA))

c)    NCEP1 - NCEP/NCAR reanalysis: 1948-present (ongoing as Climate Data Assimilation System (CDAS))

d)    NCEP2 - A rerun of the NCEP/NCAR reanalysis introducing more up-to-date physics and correcting known errors in NCEP-1 (also known as the NCEP/AMIP-II DOE Reanalysis): 1979-Jan. 1996 (as of Nov. 30, 1999). Plans are to continue this up to the present.  Years before 1979 may also be done.

An earlier pilot reanalysis was run by the Centre for Ocean-Land-Atmosphere Studies (COLA). It covered the period April 5, 1982 to Nov. 30, 1983 and is documented at http://grads.iges.org/res/proj5/proj5.html.

The NCEP-1 reanalysis is currently being run on current data as the Climate Data Assimilation System (CDAS).  The Climate Prediction Centre at NCEP is currently considering whether to run NCEP-1 or NCEP-2 or both as the operational CDAS.   ECMWF is preparing to run a new reanalysis (ERA-40) at higher resolution and with improved parameterisation from 1958 to the present.   GEOS has spent several years improving its system from what was used in GEOS-1 and plans to do reanalysis again in the future.

A workshop on the GEOS-1 reanalysis was held in March 1995 (Schubert and Rood, 1995).  The 1st WCRP International Conference on Reanalyses was held in Oct. 1997. Proceedings of the conference are available as WCRP Report 104.  The 2nd International Conference on Reanalyses was held in Aug. 1999 and the proceedings are now available (WCRP, 2000).

B.  NCEP1 SYSTEM FORMULATION

Kalnay *et al*. (1996) and Kistler *et al.* (2000) describe the NCEP1 reanalysis and further information is available from a number of web sites (Table 4.4).

Table 4.4 Web site addresses for the NCEP/NCAR reanalysis

| Contents | URL |
|---|---|
| Official sites for NCEP/NCAR reanalysis | http://wesley.wwb.noaa.gov/reanlysis.html<br>http://www.cdc.noaa.gov/cdc/reanalysis |
| Reanalysis problems | http://wesley.wwb.noaa.gov/reanalysis.html#problem<br>http://www.cdc.noaa.gov/cdc/reanalysis/problems.shtml |
| Reanalysis studies and problem reports by Robert Kistler (technical manager of the NCEP/NCAR reanalysis) | http://lnx21.wwb.noaa.gov/ |
| Examples of the observation and forecast errors used in the reanalysis. | http://lnx21.wwb.noaa.gov/oberr/reanl-obs.html<br>http://lnx21.wwb.noaa.gov/oberr/fcsterr.html |

The NCEP/NCAR reanalysis analysis/forecast system was identical to the NCEP global operational model implemented in Jan. 1995, except that it had a horizontal resolution of T62 (about 210 km).  The vertical resolution was 28 sigma levels, the same as the current operational model.  The physical parameterisations were done on a Gaussian grid of 192 x 94, roughly 2º x 2º latitude.  The radiation grid was a Gaussian grid of 128 x 62.  A time step of 20 minutes was used for computing dynamics and physics, except that the full atmospheric radiation was calculated every 3 hours with corrections at every time step for diurnal variations in short wave fluxes and in surface upward long wave flux.  Mean orographic heights were used.  The radiation used in reanalysis was an older short wave radiation (Lacis and Hansen,

1974) than that used in current operations.  An incorrect, too high,  surface albedo was used over the oceans.  An older boundary layer model,  than that currently used in operations,  was used.  The equation for roughness length for heat in the NCEP bulk flux algorithm used in the reanalysis has been found to be inappropriate under strong wind conditions and to overestimate latent heat flux (Zeng *et al.*, 1998).  It has been changed in the operational model.

The NCEP1 and NCEP2 reanalyses used the following data (Ebisuzaki *et al.*, 1998):

a)    radiosondes, dropsondes, pibals
b)    conventional aircraft winds
c)    ACARS aircraft winds and temperatures
d)    Marine winds, temperature, specific humidity in surface layer
e)    Land surface pressure
f)    Satellite cloud-track winds
g)    NESDIS temperature retrievals
h)    PAOBS
i)    SST and snow-cover analyses

The following data was not used:

a)    precipitation
b)    radar, profilers
c)    SSM/I winds and precipitable water
d)    Land winds, temperature, specific humidity in surface layer
e)    Most cloud information
f)    Radiances from satellite
g)    Satellite humidity estimates
h)    Soil/albedo/snow depth.

The analysis system used was the spectral statistical interpolation (SSI or 3D variational) analysis (Parrish and Derber, 1992; Derber *et al.*, 1991).  Nonlinear normal-mode initialisation was not needed.  Additional details can be found in Kalnay *et al.*, 1996.

Several problems have been found in the reanalysis.  Among them are:

a)    Bogus sea-level pressure observations generated by Australian analysts over the Southern Hemisphere oceans during 1979-92 were misplaced by 180 degrees.  (Reruns of 1979 and Nov.-Dec, 1992 corrected this.)  The problem has little effect north of 40S and little effects on monthly means.  The error is comparable to the difference between ECMWF and NCEP analyses.

b)    The initial attempt to use high-density vertical soundings over the TOGA COARE region from Nov. 92 to Feb. 93 included a failure to convert temperature to virtual temperature and resulted in a cold bias over the TOGA COARE region.  The problem has been corrected, the period rerun, and the archives corrected, but the annual CD-ROM's for 1992 and 1993 include this error for the 4 months.  The effects are limited to the TOGA COARE region and are strongest near the surface.

c)    The snow cover for 1973 was used for 1974-94 as well.

d)    Due to an incorrect parameterisation of the horizontal diffusion of moisture, snow over land tended to fall in valleys.

e)    Discontinuities in radiation fluxes at the International Date Line due to cloud tuning were discovered.

In other instances, portions of observational data sets did not make it into the NCEP1 reanalysis, such as poorly encoded surface observations between 1948 and 1967 and radiosondes in particular regions in particular periods (http://lnx21.wwb.noaa.gov/).  A comparison of ERA and NCEP/NCAR reanalyses for a few months revealed that each contained observations not in the other.  The two sets of observations are being merged.

While the data assimilation system was not changed during the reanalysis (except for some very minor modifications after 1986-89 were processed), the data did change dramatically during the 50 years, as can be seen in Figure 4.4. Satellite temperature soundings became available in significant numbers in 1979, the major change in the data record in the last 50 years, and had a noticeable effect on atmospheric temperatures (Fiorino, 2000). An increase in data in the late 1960's is also evident, as is an increase in the late 1990's due to an increase in satellite winds. In recent years conventional observations have declined, as can be seen in figure 4.5. The number of ship reports increased until the late 1960's and decreased from the late 1980's to 1994. Data from the TAO buoy array in the tropical Pacific in the 1990's is included. White (1999) examined global trends in precipitation and air-sea temperature contrast that could be related to changes in the observational network. It should be noted that the four-dimensional data assimilation systems used in reanalysis can transport information from data rich to data sparse regions; therefore observations can influence regions outside the 2.5° box they were taken in. Ebisuzaki and Kistler (2000) examined the effect of changes in data on reanalysis by comparing fields from NCEP1 and NCEP2 to a rerun of 1998 without PAOBS, aircraft or satellite data.



Figure 4.4. Zonally averaged number of all types of observations available to the NCEP/NCAR reanalysis per 2.5° latitude-longitude box per month from 1946 to 1998. A twelve-month running mean has been applied. Shading indicates more than sixty observations per month.
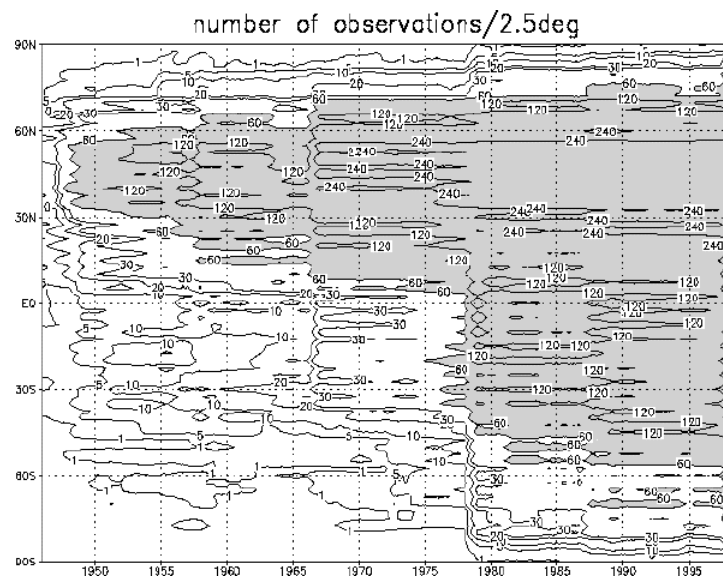


Figure 4.5: Zonally averaged number of ship reports per 2.5° box per month. Oceanic buoys are included.
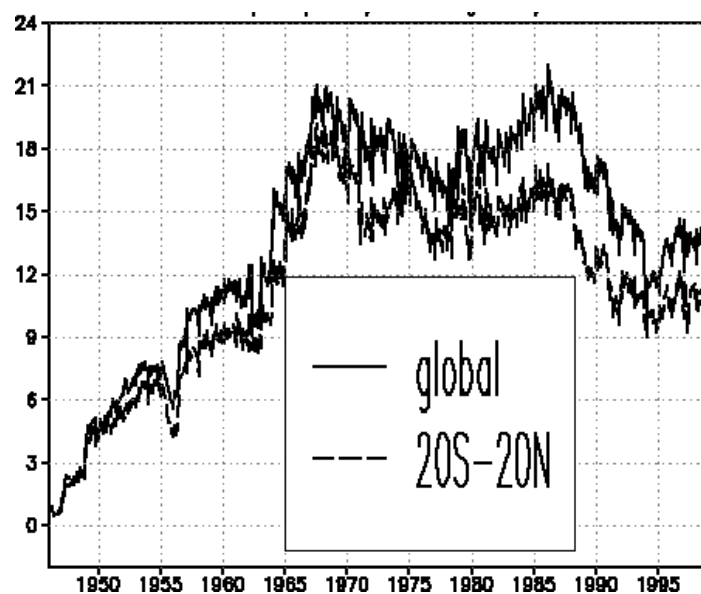
C.  NCEP2 SYSTEM FORMULATION

The NCEP2 reanalysis is documented at http://wesley.wwb.noaa.gov/reanalysis2/index.html.  Papers on the NCEP2 reanalysis were presented at the 2nd International Conference on Reanalyses.  Kanamitsu *et al.* (2000) gave an overview of NCEP2 .  Hnilo *et al.* (2000) compared NCEP1 and NCEP2.  NCEP2 was done with the same data and the same vertical and horizontal resolution as NCEP1.  It corrected the five mistakes listed above as well as the ocean surface albedo.  The following model changes were introduced:

a)  assimilation of five-day mean estimated rainfall from Xie and Arkin to adjust soil moisture
b)  elimination of a nudging of deep layer soil moisture to climatology
c)  a smoother orography than NCEP1
d)  new non-local boundary layer parameterisation of Hong and Pan (1996)
e)  a change to the convective parameterisation
f)  a fix to cloud-top cooling in radiation
g)  updated cloud parameterisation and RH-cloud relationship
h)  radiation code run every hour and on full Gaussian grid
i)  improved desert albedo
j)  improved sea-ice SST fields

NCEP2 did not change the roughness length for heat as suggested by Zeng *et al.* (1998).

D.  ERA15 SYSTEM FORMULATION

An introduction to the ECMWF reanalysis can be found at http://www.ecmwf.int/research/era/index.html.  Reports from the ERA15 reanalysis are available by anonymous ftp at www.ecmwf.int in the /pub/era/era15 directory.  Gibson *et al.* (1997) described the ERA15 reanalysis system, including initial experiments they did.  They tested the effects of a new prognostic cloud parameterisation (Jakob 1994; Teidtke 1993) for one year of data assimilation together with changes in ocean surface albedo and shallow convection.  Compared to an older diagnostic cloud parameterisation similar to the one used in the NCEP reanalyses, the new physics produced quite different surface energy fluxes.  It produced more low clouds over the oceanic storm tracks and near the equator and reduced stratus over the Arctic, all improvements, but decreased low-level stratus over upwelling ocean currents, a disadvantageous impact.  The new scheme increased downward longwave radiation into the ocean by 20-30 Watts/m$^2$ in the latitudes of the storm tracks,  decreased short wave radiation into the ocean at low latitudes,  and decreased evaporation locally by as much as 30 Watts/m$^2$.  The changes,  used in the full reanalysis,  increased energy input into the ocean in the tropics and over the high latitude storm tracks.  These results indicate the sensitivity of reanalyses to changes in the physical parameterisation.

The ERA-15 data assimilation system included:

a)  spectral T106 resolution with 31 vertical hybrid levels (Gaussian grid resolution 1.125° or about 125 km)
b)  Intermittent statistical (optimum interpolation) analysis with 6 hour cycling
c)  One-dimensional variational (1D-Var) physical retrieval of TOVS cloud cleared radiances below 100 hPa.
d)  NESDIS humidity retrieval below 300 hPa over oceans
e)  Diabatic, non-linear normal mode initialisation
f)  3-dimensional semi-Lagrangian advection
g)  Prognostic equations for cloud water and ice content and cloud cover.  Clouds tuned to ISCCP clouds.
h)  ECMWF operational radiation parameterisation with prescribed concentration of aerosols varying geographically (Morcrette, 1991)
i)  ECMWF operational planetary boundary layer parameterisation based on similarity
j)  Mass flux convection scheme by Tiedtke (1989)

k)      Mean orography with a parameterisation of sub-grid scale orography

Kallberg (1997) examined the 15-year mean climate of the reanalysis. He documented the sensitivity of precipitation and surface fluxes to "spin-up" during the first 24 hours of forecasts in the ERA15 reanalysis. He also found evaporation over the ocean to be very sensitive to the observations. Near surface winds observed by ships were generally stronger than either analysed or forecast winds; near surface winds reported by isolated island stations, affected by local effects and not representative of the surrounding oceans, were generally weaker than the analysed and forecast winds. These mismatches generated large increases in evaporation during the first 24 hours of forecasting, locally up to 40 Watts/m$^2$ (the NCEP1 Reanalysis also found suspicious features near isolated island stations; experiments did not find a solution to the problem). ECMWF concluded that the fluxes from 12-24 hour forecasts were better than the fluxes from 0-6 hour forecasts and recommended the use of the former.

ERA15 assimilated TOVS cloud-cleared radiances from a long series of NOAA satellites that suffer from the effects of drift and sudden changes in instruments. In spite of extensive monitoring, quality control and bias correction, the use of radiances resulted in sudden jumps in the time series of analysed temperatures and humidities in the lower troposphere, especially in lower latitudes. The worst jump occurred in Nov. 1986 with an unrealistic large-scale warming and moistening of the Inter-Tropical Convergence Zone (Gibson *et al.*, 1997; Fiorino, 2000).

E.   ERA40 SYSTEM FORMULATION

Plans for the next ERA40 reanalysis were discussed by Uppala *et al.* (2000) at the 2$^{nd}$ International Conference on Reanalyses. ERA40 is still under development. Current plans are to process data from mid-1957 to 2001. In addition to the data in ERA15, this reanalysis will include:

a)      conventional ship and upper air data before 1979 from NCAR,
b)      declassified U. S. Navy data;
c)      full VTPR and TOVS 1b data from 1972 on;
d)      SSM/I radiances;
e)      ERS-1 and ERS-2 data;
f)      updated COADS;
g)      new SST data from UKMO and NCEP with compatible sea ice.

The projected production system will use

a)      spectral T 159 resolution with 60 hybrid vertical levels;
b)      3 dimensional variational (3D-VAR) analysis incorporating physical retrieval of satellite radiance data;
c)      coupling with a 1.5˚ wave model to produce ocean surface fluxes. Analysis of ERS wave altimeter data will be included. The fluxes will be sea-state dependent. (Janssen and Viterbo, 1996);
d)      the Integrated Forecast System (IFS) version of the ECMWF forecast model;
e)      varying carbon dioxide and aerosols;
f)      assimilation of ship winds at 25 m rather than 10 m.

Experiments with the proposed system indicate fewer problems with the near-surface winds over the open ocean and islands, a weaker and slower "spin-up" and more rainfall over the northern hemisphere storm tracks.

F.   GEOS1 SYSTEM FORMULATION

Overviews of the NASA/GSFC DAO GEOS1 reanalysis can be found in Schubert *et al.* (1995) and at a number of web sites (Table 4.5)  Higgins *et al.* (1996) compares the NCEP1 and GEOS1 reanalyses for the period 1985-93. Bony *et al.* (1997) compared the two reanalyses over the tropical oceans.

4 - Data Sources                          53                          **4.4 NWP and reanalysis**
                                                                      **4.5 Residual Methods**
                                                                      **4.6 Ocean data assimilation**

The GEOS1 data assimilation system is described in Takacs *et al.* (1994) and Pfaendtner *et al.* (1995). It employed an optimal interpolation (OI) analysis scheme at a horizontal resolution of 2° latitude by 2.5° longitude at 20 sigma levels. It did not include initialisation and used an Incremental Analysis Update (IAU) procedure by which a fraction of the data increment are added each time step during a rerunning of the forecast (Bloom *et al.*, 1996).

The radiation parameterisations follow those of Harshvardhan *et al.* (1987); a relaxed Arakawa-Schubert scheme (Moorthi and Suarez, 1992) is used for deep convection. The planetary boundary layer is explicitly resolved in a 2 to 4 layer region. Wind, temperature and humidity profiles, in an extended surface layer up to 150 m thick, and the turbulent fluxes at the surface are obtained from Monin-Obukhov similarity theory by selecting similarity functions that approach the convective limit for unstable profiles and agree with observations for very stable profiles. Surface roughness lengths are taken as a function of surface stress over water (Schubert *et al.*, 1995).

The SST data set used in GEOS1 used monthly mean blended sea surface temperature analyses of Reynolds (1988) and Reynolds and Marsico (1993); NCEP used the improved weekly global optimum interpolation SST analyses of Reynolds and Smith (1994). The major differences between the SST analyses are in regions of high SST gradients.

Table 4.5 Web site addresses for the NASA/GSFC DAO GEOS1 reanalysis

| Contents | URL |
|---|---|
| Overviews of the GEOS1 reanalysis | http://dao.gsfc.nasa.gov/experiments/assim54A.html <br> http://www.cdc.noaa.gov/cdc/reanalysis |
| Technical reports on the GEOS-1 reanalysis | http://dao.gsfc.nasa.gov/subpages/tech-reports.html |
| Strengths and weaknesses of GEOS1 | http://dao.gsfc.nasa.gov/experiments/assim54A/assim_prod_evalutaion.html *(sic)* |
| Problems | http://dao.gsfc.nasa.gov/experiments/DATA_PROBLEMS.html. |

## 4.5  Residual methods (TOA + model divergences)

In the residual method (Trenberth and Solomon 1994; Keith 1995) the top of the atmosphere radiation budget and the divergence of the atmospheric energy transport from an numerical model is used to infer the net surface heat flux. Used with the atmospheric moisture budget the net freshwater flux can also be obtained (Trenberth and Guillemot 1998), although the accuracy is crucially dependent on the calculated wind and moisture divergence. A major limitation of this method is the lack of estimates of the individual fluxes and the reliance on atmospheric model data, thus restricting use for model verification.

## 4.6  Ocean Data assimilation

Inverse techniques such as ocean data assimilation can also provide estimates of the surface fluxes of heat, momentum, and freshwater. The approach is straightforward. One constrains (in a least-squares sense) an ocean model (admittedly imperfect or is missing physical parameterisations of ocean processes) to observed temperatures, salinity, or other suitable observations (which have their own errors possibly specified in the inverse methodology) using the flux fields as dependent model parameter fields. Such an approach was demonstrated using a relatively simple tropical Pacific ocean model forced by climatological winds and SST (Yu and O'Brien, 1995). The resulting monthly net heat flux fields had features similar to existing in-situ based climatologies outside the equatorial zone

except the magnitude is not as strong. Similarly, for the Atlantic, seasonally varying ocean temperature and salinity data provided necessary information to estimate surface heat and freshwater flux estimates (Yu and Malonotte-Rizzoli, 1998). Estimates of surface fluxes produced by these inverse methods will improve as ocean modelling evolves.

## 4.7 Data Sources for Fluxes and Flux-Related Variables over Sea Ice

Like other uninhabited and barely frequented areas of the globe, the ice-covered oceans present special problems for observing global phenomena and for estimating global fields. The situations in both polar regions have similarities: a few permanent manned or unmanned stations provide sparse, continual data, but large areas are sampled directly only occasionally. Interpolation is asked to provide information that man did not have the resources to observe.

Winds are specified from pressure fields which in the Arctic have had the benefit since 1979 of a network of drifting buoys, but in the Antarctic have only sporadic buoy data. In the Arctic the buoy and station surface pressure data are assimilated into the NCEP and ECMWF reanalysis fields, making them the best gridded pressure fields. In the Antarctic there is no standing network of buoys, and the reanalysis pressure fields are of lower accuracy but still the best available. Similarly, air temperature fields are recently available from buoys in the Arctic (for example the IABP/POLES 2-m air temperature data set (Rigor *et al.* 2000)), and again rely on more sparse data in the Antarctic. The surface air temperature fields in the reanalyses are not based on surface temperature observations, but use only the first level temperatures from radiosondes, and model physics to estimate surface temperature.

In addition to drifting buoys, an important Arctic data set on surface fluxes, cloud amounts, winds, air-surface temperature differences, snow depths, and radiosondes has been provided by decades of Russian "North Pole" manned drifted stations. Data from these stations have been assembled into long-term climatologies of monthly means (the Arctic Global Radiation (AGR-1 and AGR-2) Data Sets. There have been a number of drifting camps (e.g., Arlis, T-3, AIDJEX, CEAREX, LEADEX, and presently SHEBA) and ship expeditions (Polarstern cruises, and the Arctic Cross-Section), all with observations crucial to parameterising and validating large-scale estimates of surface fluxes.

Satellite data sets are just coming into use. Satellites provide indirect observations of surface variables and fluxes, and much effort goes into trying to make good use of these data. New satellite-derived data products promise good accuracy, better spatial resolution and the resolution of interannual variability. These include the Surface Radiation Balance estimates from ERBE and AVHRR, the ISCCP cloud and albedo data and radiative fluxes derived from them, and Polar Pathfinder data sets from AVHRR and from TOVS.

And of course, global numerical weather prediction models provide fields of many desired variables, some of which are of more value than others. Surface wind and flux fields are available from both the NCEP and ECMWF reanalyses.

As for data on the sea ice state, the most comprehensive record is that of gridded sea ice concentration at both poles are available from 1978 to present, from SMMR and SSM/I passive microwave sensors. Substantial records are available from scatterometers (Ezraty and Cavanié, 1999), ERS-1 and -2 (1991 - 1999), NSCAT (9 months) and QuikSCAT (beginning September 1999), but these are not yet presented as data sets of sea ice variables. Synthetic aperture radar has been used to track ice and infer the ice thickness distribution for ice up to 2 m thick and for ridged ice. These data are produced for the Arctic Ocean by the RADARSAT Geophysical Processor System (RGPS) and will eventually span several years from 1996 on.

## 5  DIRECT FLUX OBSERVATIONS - STATE OF THE ART

### 5.1  Introduction

In general, direct measurements of the air-sea fluxes are too few to contribute directly to the calculation of large scale flux fields.   Rather they are used for developing, calibrating, and verifying the parameterisation formula used to estimate the fluxes from the basic variables. The accuracy of the direct flux determinations thus represents a limit for the accuracy of the indirect estimates.   Methods of direct measurement will therefore be reviewed in this Chapter for the radiative fluxes,  turbulent fluxes,  and precipitation.

## 5.2  Radiative fluxes

*5.2.1 Introduction*

The radiant energy flux to and from the ocean surface comprises the solar (or shortwave) component in the wavelength band 0.3 to 3 $\mu$m, and the terrestrial (longwave or infrared) component from 3 to around 50 $\mu$m.  A good illustration of the sources which contribute to each of these wavebands is given in Figure 1 of Katsaros (1990). For direct measurement of the radiative fluxes at sea, the best compromise between the competing needs of accuracy and practicality is provided by instruments which have been in existence for around half a century, with little modification over that time; namely the pyranometer for shortwave radiation and the pyrgeometer for longwave.  The two instruments are similar in form, both measuring the radiation flux through a hemispherical dome of appropriate spectral transmissivity.  Both experience particular problems in use at sea, contamination of the domes by salt, motion of the ship or buoy and, because it is impossible to screen the sensing element, vulnerability to the many sources of electromagnetic interference aboard ships (e.g. Lind and Katsaros, 1986).  Perversely, to avoid shadowing of the instruments they usually have to be located at the highest place on the ship along with the radio antennae.

Only the top of the range instruments from the various manufacturers are potentially capable of providing radiation data to the accuracy required to close an ocean mixed layer budget, or to validate coupled models or remotely sensed products.  Their use and performance will be discussed in this section. However, instruments of lesser quality are available, and often used when cost is a factor.  More accurate devices, such as the broadband Normal Incidendence Pyrheliometer (NIP), are sometimes used as calibration standards for working instruments, but for reasons given below are generally unsuitable for use at sea.

At the same time, the situation is changing rapidly with the introduction of new knowledge and technology, and the urgent needs of climate research.  Post et al. (1998) describe instruments, several at prototype or research stage of development, which were deployed together during a NOAA-sponsored Combined Sensor Program cruise to the central and western Pacific ocean in March-April 1996.  They included sophisticated radiation instruments, such as the Fourier Transform Infrared Instrument (FTIR) and Atmospheric Emitted Radiance Interferometer (AERI), both of which measure infrared spectra at high resolution over a broad spectral range, and a sun-tracking photometer to obtain solar flux at several filtered visible and infrared wavelengths. The technologies developed to date mostly serve to retrieve variables that can be used to compute fluxes with a radiative transfer code, rather than to observe the fluxes themselves. For example, the humidity field from AERI can be used as one of the inputs needed to compute downwelling LW flux, and the aerosol spectral optical depth from a photometer can be used in the computation of the downwelling broadband SW insolation.  Comprehensive suites of sophisticated and well-maintained radiation instruments are already installed operationally in various climatically important parts of the world (e.g. Pacific islands, Alaska), at some of the Atmospheric Radiation Measurement

(ARM) program's Cloud and Radiation Testbed (CART) sites, and it is likely that ruggedised, affordable versions of such sensors will be in fairly routine use within the next decade.

Determination of radiative components in very high latitudes presents particular problems, partly due to the effects of low temperatures on the instruments, but also because of spatial inhomogeneity of the surface. Sea ice, snow and open leads greatly affect radiative exchange through spatial variability of surface albedo and by selectively insulating the cold atmosphere from relatively warmer water below the ice. To further complicate the issue, it is not usually meaningful to discuss the radiation fields in polar regions without simultaneous consideration of clouds and the various cloud-surface feedbacks. A comprehensive overview of cloud and radiation characteristics in the Arctic, together with discussion of the boundary layer features, is given by Curry et al. (1996). In the following two sections, which deal separately with the general features of shortwave and longwave radiation, and in section 6.5 on albedo, we include comment on the specific problems presented by sea ice.

### 5.2.2 Shortwave radiation

Downwelling shortwave (SW) radiation at the surface (referred to as shortwave irradiance) has a component due to the direct solar beam, and a diffuse component scattered from atmospheric constituents and reflected from clouds. Upwelling shortwave radiation comes from reflection at the surface and the re-emergence of radiation backscattered as it is absorbed through the upper ocean (together referred to as exitance). The terms exitance and irradiance imply hemispheric, broadband radiation, and for the shortwave their ratio is the surface albedo, discussed more fully in section 6.5.

Both irradiance and exitance can be measured with the pyranometer, facing either skyward or towards the sea surface. Modern pyranometers are still based on the Moll-Gorczynski design (Moll 1923) in which radiation falls on a blackened horizontal receiving surface bonded to a thermopile and protected by two concentric precision hemispheric glass domes. The most important factors affecting the accuracy of these instruments are; reliability and stability of calibration, dome temperature effects, cosine response and detector temperature stability. Manufacturers claim temperature stability of 1% over the range –20°C to +40°C, and the same figure for cosine response between 0° and 70° solar zenith angle. The reliability of transfer of the World Radiation Reference (WRR) calibration standard to working instruments is estimated to be 1%. Combined, these sources of error give a basic accuracy for the instrument as 2%, the figure usually quoted. However, Bush et al. (2000) have demonstrated that variability in the temperature of the dome used to shield the detector can affect the observation by several $Wm^{-2}$. The most common manifestation of the impact of dome temperature on the pyranometer is the "night offset"; negative values (typically 1-10 $Wm^{-2}$ and variable with time) for the SW insolation at night. In the ARM Enhanced Shortwave Experiment (ARESE) a first order correction for the dome effect was made by adjusting the diffuse component of the daytime insolation by approximately 5 $Wm^{-2}$ , being largest in clear skies (Alberta and Charlock 1999).

Another source of error, particular to pyranometers used at sea, is caused by the platform motion. For correct measurement the receiving surface must be horizontal, but both ships and buoys can roll through several degrees, or take on a systematic lean caused by wind force or poor trim. For given platform angle the severity of the error depends on several factors; cloudiness, latitude, season and time of day. Katsaros and DeVault (1986) calculate that it can be as large as 10-20% in the daily average for clear skies poleward of 45° in winter if the instrument has a 10° tilt. This is an extreme example, and they point out that the error is considerably less at lower latitudes and that there can be compensating errors, which they have not accounted for, when averages are taken over a whole day. MacWhorter and Weller (1991) also consider the problem. Their experiments simulating symmetrical *rocking* of the platform, without any mean tilt, show that for 10° amplitude the largest error was 2.1% (and for 20°, 5.1%; 30°, 7.8%; 40°, 12%). These figures were for zenith angle of 51° and suggest that for low latitudes and modest seas the effect of platform roll may not be too serious. Even at mid-

latitudes, more severe seas causing greater roll tend to be associated with bad weather and cloudiness, reducing the absolute irradiance (which is also mostly diffuse and therefore less susceptible to tilt error). However, as MacWhorter and Weller (1991) show, a persistent tilt even of only 5° will produce errors between 5% and 16%. Even if the record of ship or buoy motion and all other factors were available, it would be a daunting task to correct the radiation measurement *a postieri.* Both Katsaros and DeVault (1986) and MacWhorter and Weller (1991) recommend that pyranometers be set in gimbals.

During TOGA-COARE a field comparison between several pyranometers on ships, aircraft and a mooring on a clear day, revealed systematic differences up to 3% for the first-class instruments and 8% for one of lower quality, well outside manufacturer's specification. The cause was assumed to be calibration error, subsequently confirmed by laboratory intercalibrations. The instrument's calibration can change through deterioration of the receptor surface (flaking of the paint for example) or of the glass dome (scratching), or some electrical fault within the thermopile system. Manufacturers recommend re-calibration once a year against a WRR standard but hitherto this seems to have been seldom observed. Given the COARE experience, it seems prudent to calibrate before and after each field deployment, and if possible to intercompare instruments in the field.

The issues described above highlight the extreme difficulties of making accurate shortwave measurements at sea, compared with over land. The WCRP has established stringent procedures to apply at each continuous observing site to comply with the Baseline Surface Radiation Network (BSRN) standards for climate monitoring (Gilgen et al., 1995). For measurement of the direct beam these call for the deployment of an NIP, which requires a sun tracking system; rigorous calibration procedures are employed for measurement of the direct beam at stations meeting BSRN protocol. The diffuse component is obtained with a shaded pyranometer; however, there are at present virtually no routine measurements of the diffuse component of downwelling SW insolation whose calibration protocols are sufficiently rigorous for clear sky conditions.

Hence, the only measurement system with the prospect of meeting WCRP observing standards for long-term monitoring of SW insolation at sea would be one deployed on a rigid platform. Neither the NIP sun tracker nor the diffuse system are compatible with unsteady platforms such as ships and moorings. Over land, or on a fixed platform at sea, the diffuse component of short-wave radiation is measured by fitting the pyranometer with a "shadow-band", set to shield the sensing element from the direct solar beam as it tracks across the sky. The position of the band is changed manually to accommodate the variation of solar elevation through the annual cycle. Floating platforms obviously preclude the use of a fixed shadow-band.

Nevertheless, the needs of the modelling community to distinguish between the direct and diffuse components, and to parameterise appropriately, has stimulated efforts to improve the situation. Recently, measurements of the diffuse component have been made from shipboard using a rotating shadow-band which, whatever the relative position of the sun, casts a shadow on the radiation sensor once per revolution. A fast response sensing element, such as a photocell, is required and the diffuse signal determined from the time series and approximate timing. The signal produced by the shadow-band is unambiguous under clear skies, but in conditions of broken cloud can be difficult to recognise. Measurement accuracy is compromised by the poorer quality sensor, although a reference measurement of the direct component is usually provided by a high-quality pyranometer alongside. Descriptions of such instruments are given by Reynolds (1998) and on the ARM web site[1]..

The effect of the above sources of error in terms of absolute energy exchange depends on the latitude and season. Table 5.1 shows the daily averages of downwelling irradiance

---

[1] :http://www.arm.gov/docs/instruments/static/mfrsr.html (mfrsr refers to multi-filter rotating shadow-band radiometer).

observed during field experiments at various latitudes. In terms of the basic 2% accuracy of the pyranometer, instrumental error is seen to be less than 7 $Wm^{-2}$ on daily average, even in the tropics where shortwave irradiance is a dominant component of air-sea energy transfer. However, the dome effect, tilt error and poor calibration can seriously degrade this. Furthermore, at noon on a clear day irradiance in the tropics often reaches 1000 $Wm^{-2}$, and instrumental uncertainty alone increases to 20 $Wm^{-2}$. Such an uncertainty could be unacceptable when trying to model processes in the oceanic and atmospheric mixed layers on the diurnal timescale. Two initiatives by the NASA-Langley group will improve the accuracy of measurement of the marine SW radiation field; Haeffelin et al. (2000) have begun a program to study the physics of the pyranometer; a BSRN-quality measurement site has been established at Chesapeake Lighthouse (36.9N, 75.71W).

Table 5.1 values for the daily average downwelling shortwave irradiance observed during four field experiments.

| Experiment | Dates | Lat. | SW ($Wm^{-2}$) | Reference |
|---|---|---|---|---|
| JASIN | July-Sept. 1978, | 60ºN; | 40 to 270 | (Lind et al., 1984); |
| STREX | November 1980, | 50ºN; | 10 to 60 | (Lind and Katsaros, 1986); |
| FLIP | February 1974, | 35ºN; | 65 to 169 | (Simpson and Paulson, 1979); |
| COARE | Nov.1992-Feb.'93, | 2ºS; | 63 to 330 | (Fairall et al., 1996a). |

While the role of air-sea transfer in forcing global climate has long been recognised in tropical regions, the importance and vulnerability of polar regions has been acknowledged only relatively recently. This has led to increased effort to measure fluxes *in situ* in support of sea-ice modelling and the validation of remotely sensed products. Some intensive measurement expeditions to the arctic, and pointers to data sets are given in section 4.7. The recent Surface Heat Budget of the Arctic Ocean (SHEBA) field experiment[2] involved a year-long deployment, from October 1997, of a comprehensively instrumented ice camp within the perennial Arctic Ocean ice pack. Radiation instruments were included, to augment those on the nearby ARM CART site[3].

Simplicity and availability result in the pyranometer being used as the front-line instrument for measurement of shortwave irradiance in most ocean environments, including the ice-prone waters of the Arctic and Antarctic. However, these regions present three instrumental uncertainties additional to those listed above; whether the instrument calibration holds in temperatures below those specified by the manufacturer; cosine response degrades for solar zenith angles greater than 70°; and frost formation on the dome. The first two problems do not appear to have received much attention, but the third is alleviated in the most recent deployments by blowing air, sometimes heated, across the dome.

Within the Arctic and Antarctic circles (latitudes > 66.5° N and S) shortwave irradiance is either continuous or completely absent for significant periods of the year. There are areas of very high albedo, but variable in space and time. Shine (1984) shows that ignoring multiple reflections between these high albedo surfaces and clouds can lead to errors in shortwave surface flux of 30% over bare ice and 50% over new snow. Although the solar zenith angle is always large, the magnitude of the surface flux is by no means trivial, the average observed for June being around 300 $Wm^{-2}$. Pinto and Curry (1997) point out that this compares with modelled values ranging from 85 to 185 $Wm^{-2}$, ascribed to over-prediction of cloud. They note

---

[2] http://sheba.apl.washington.edu/about/about.html
[3] http://www.arm.gov/docs/sites/nsa/nsaaao.html

that these models may embody parameterisations for clouds and radiative processes which were developed for regions with quite different climatic conditions from those at the poles. The unique features of the shortwave radiation environment in very high latitudes cause problems of simulation and emphasise the need for high-quality validation datasets.

*5.2.3 Longwave radiation.*

Downwelling longwave radiation (longwave irradiance) originates from the emission by atmospheric gases (mainly water vapour, carbon dioxide and ozone), aerosols and clouds. The major component of longwave exitance is emission from the sea surface which depends on the surface emissivity and the skin temperature, augmented by a small contribution due to reflection of the longwave irradiance. Longwave absorption and emission take place in about the top 0.5 mm of water, depending on wavelength.

The pyrgeometer is of similar construction to the pyranometer, but the single dome is made from silicon or similar material transparent to the longwave band, coated on the inside with an interference filter to block shortwave radiation. The longwave irradiance passing through the dome, which we wish to determine, is only one component of the thermal balance of the thermopile. The remaining components come from various parts of the instrument (e.g. Fairall *et al.* (1998) - Figure 1). To isolate the geophysical component, $Q\downarrow_{lw}$ , the manufacturers provide an equation derived by Albrecht *et al.* (1974):

$$Q\downarrow_{lw} = V/s + \varepsilon_p \sigma T_c^4 + B\sigma(T_c^4 - T_d^4) \qquad (5.1)$$

where V is the thermopile output, s the radiometer sensitivity (the calibration factor displayed on the side of the instrument, usually $\mu V/Wm^{-2}$), $\sigma$ the Stefan-Boltzmann constant, B is the ratio of emissivity to transmissivity of the dome material, and $T_c$ and $T_d$ the respective case and dome temperatures (K). Modern instruments are provided with thermistors in the dome and case to enable equation (5.1) to be calculated. $\varepsilon_p$ is the emissivity of the thermopile surface which is, in fact, included incorrectly in this equation (see below).

For completeness, we note that the most common pyrgeometer in use by geophysicists (the Eppley precision infrared radiometer, or PIR), includes a battery-powered resistance network which generates a voltage in series with the thermopile that is the electrical analogue of the second term in (5.1). Thus, providing the observer is prepared to ignore the third (dome heating) term or estimate it using a scheme such as that of Alados-Arboledas *et al.* (1988), longwave irradiance may be recorded with a single output signal, as from the pyranometer. This procedure obviously trades accuracy for simplicity of operation; this is discussed further below.

The performance of pyrgeometers, and particularly the Eppley PIR, has come under close scrutiny recently. Philipona *et al.* (1995) evaluated the thermal balance of the instrument and developed a more complete version of (5.1), retaining three parameters to be determined empirically. To obtain the highest measurement accuracy, they stressed the need to characterise individual instruments and they describe an apparatus designed to obtain the pyrgeometer calibration factor and their three empirical parameters, one of which is closely equivalent to B in (5.1). They also measured significant temperature gradients over the dome, and suggest that a single dome thermistor is inadequate to specify $T_d$ .

Fairall *et al.* (1998) also re-examined the thermal balance of the pyrgeometer and discovered that the factor $\varepsilon_p$ appears erroneously in (5.1). The reason is that Albrecht *et al.* (1974) make the approximation $\varepsilon_p = 1$ ($\varepsilon_p$ is usually quoted as 0.98), but do so inconsistently. Since the second term of (5.1) is usually dominant, the error can be significant. For the COARE data, where $T_c$ was around 300K, it is easy to see that the correction increases the calculated longwave irradiance by about 9 $Wm^{-2}$. Fairall *et al.* (1998) used a radiative transfer model with atmospheric soundings launched from the ship in clear-sky conditions, to calculate longwave irradiance at the surface; the results agreed with simultaneous pyrgeometer measurements within 2 $Wm^{-2}$ in the mean, supporting their revision of (5.1). Persson *et al.* (1997) calculate the impact on various climatically important parameters, of removing the

erroneous $\varepsilon_p$, for example the disappearance of an apparent diurnal cycle of sensible heat flux transfer coefficient.

Like the thermopile calibration factor, the dome heating correction factor, B, is instrument-specific and must be determined empirically, yet a value is not normally provided by the manufacturer. Values from about 2.5 to 4.5 are in common use, their origin usually obscure. The best published determinations are probably those by Philipona *et al.* (1995), using their new calibration system, who obtain values for different instruments ranging from 3.15 to 4.27. Russell *et al.* (1999b) intercompared five Eppley PIR's during SHEBA and reduced the uncertainty in downwelling longwave by mean-normalising values of *s* and B for each instrument. Their adjusted values for B span a very similar range to those quoted above. The significance of this uncertainty can be tested with a rather severe example from the cruise to the equatorial Indian ocean described by Godfrey *et al.* (1999). Around midday on August 26, 1005 Wm$^{-2}$ of solar radiation fell on the pyrgeometer, and $T_d$ - $T_c$ was 2°C, so adopting a nominal B=3.5, the dome heating term was -46 Wm$^{-2}$ from a total longwave irradiance of 407 Wm$^{-2}$. Using B=3.15 the term becomes -42 Wm$^{-2}$, an uncertainty of 4 Wm$^{-2}$ or 1%.

In practice, scatter in the apparent values of B may be due to shortwave leakage through the dome filter. Dickey *et al.* (1994) added such a term to (5.1):

$$Q\downarrow_{lw} = V/s + \varepsilon_p\sigma T_c^4 + B\sigma(T_c^4 - T_d^4) - \lambda Rs_{down} \qquad (5.2)$$

where $\lambda$ is a shortwave leakage factor and $Rs_{down}$ the downward shortwave radiation. Pascal and Josey (2000) showed that this shortwave leakage effect was significant with $\lambda$ varying from instrument to instrument. There was some indication that instruments with smaller leakage factors had larger values for B and vice versa. They found that the differential heating of the radiometer was primarily caused by the incident shortwave radiation, modified slightly by the cooling effect of airflow over the dome.

Over the SHEBA sea-ice, Russell *et al.* (1999a) report frosting of the domes of pyrgeometers and discovered that an ice coating makes the PIR more sensitive to dome temperature, leading in clear conditions to an overestimate of downwelling longwave flux by up to 50 Wm$^{-2}$. They found that ventilation and 10-25 Watts of heating were needed to keep the domes ice-free. Similar differences between ventilated and non-ventilated pyrgeometers were reported by Guest (1998) working in the Antarctic. Guest (1998) compares his longwave observations with the predictions of several empirical formulae, similar to the work of Key *et al.* (1996) for the Arctic, and draws attention to dissimilarities in the processes of ice formation, longwave radiation and cloud effect in the north and south polar regions. However, both Guest's (1998) observations and the (Arctic) satellite analysis by Curry *et al.* (1996) show that downwelling longwave radiation dominates the surface radiation balance, increasing from around 200 Wm$^{-2}$ in winter to 280 Wm$^{-2}$ in summer. For March and April, Russell *et al.* (1999b) report around 260 Wm$^{-2}$ for cloudy conditions but considerably less (~160 Wm$^{-2}$) under clear skies, very similar to those of Guest (1998 - Figure 4).

Philipona *et al.* (1995) conclude that pyrgeometer accuracy can be ±2 Wm$^{-2}$ with careful calibration and operation. The error analysis by Fairall *et al.* (1998) indicates that the basic precision of the instrument is about 1.5% of the total longwave irradiance or about 5 Wm$^{-2}$. They also find that using the battery-compensation circuit leads to errors of at least 5% or 20 Wm$^{-2}$. This is unacceptable in many applications nowadays, and also unnecessary. Fairall *et al.* (1998) discovered that the limitations of the battery-compensated system are well-known to radiation specialists, but not among ocean and atmospheric scientists who acquire pyrgeometers without appreciating the subtleties of their design, and therefore fail to take full advantage of their capability. To do so, however, entails logging three signals and performing regular calibration checks. For data sets where the separate temperatures have not been logged, Pascal and Josey (2000), suggest that correction is still possible if the factors B and $\lambda$ are known for the specific radiometer and the available data set contains values for the incident solar radiation and wind speed.

Calibrating facilities for infrared instruments are more complicated and therefore less common than those for solar radiation, and require careful technique. Fairall *et al.* (1998) recommend field intercomparisons if several instruments are available (e.g. Russell *et al.* 1999a,b). They also suggest that calculations from a modern radiative transfer model (RTM), using on-site atmospheric soundings in clear-sky conditions, would provide an absolute reference for longwave irradiance within about 2 Wm⁻² ; Miskolczi (1994) comes to a similar conclusion (aspects of RTM's are discussed in Section 6.3). RTM's are not as rigorously validated for cloudy sky conditions, however. The calculation of the downwelling longwave flux under a cloud requires knowledge of both cloud base height and emissivity. Cloud base height may be measured with active systems such as a MicroPulse lidar (Spinhirne, 1993) or a cloud profiling radar, although an infrared radiometer (such as the pyrgeometer) would still be needed to estimate cloud emissivity. The requirement for downward LW under cloudy skies argues for continued deployment of pyrgeometers on research ships.

The pyrgeometer can be faced downward to measure longwave exitance, but for either a ship or buoy would need to be mounted at the end of a fairly long boom to exclude the platform itself from the field of view. There are obviously practical problems to this arrangement, and it is preferable and probably more accurate, to measure sea temperature and use the Stefan-Bolzmann law, remembering to include the small component of longwave reflected from the sea surface. Then:

$$Q\uparrow_{lw} = \varepsilon\sigma T_s^4 + (1-\varepsilon)Q\downarrow_{lw} \qquad (5.3)$$

where $\varepsilon$ is the emissivity of the sea surface, and $T_s$ the skin temperature of the water, as would be measured by an infrared radiometer. This immediately raises a problem, because accurate IR radiometers are not usually available, and the sea temperature measured at some depth may be considerably different from $T_s$ (see Section 10.2).

## 5.3 Turbulent fluxes

### 5.3.1 The Eddy correlation method

In a turbulent atmosphere, the instantaneous vertical transport of some atmospheric constituent is given by the product of its concentration, $C$, with the vertical wind velocity, $W$. It is customary to write these quantities in terms of their mean values over some convenient period (10 minutes to 1 hour), plus their instantaneous fluctuation from that mean. Thus, $C = \bar{c} + c'$ and $W = \bar{w} + w'$; multiplying and performing the usual Reynolds averaging we have, for the vertical flux of constituent $C$:

$$F_c = \overline{WC} = \overline{w}\,\overline{c} + \overline{w'c'} \qquad (5.4)$$

When the site is horizontally uniform, and atmospheric conditions steady over the averaging period, it is expected that $\bar{w}$ is zero, so that the flux is given by the last term of (5.4). Measurement of the fluctuating quantities $w'$ and $c'$ with fast-response sensors, and calculating the covariance, is therefore a direct way of obtaining the fluxes. The covariance must embrace a frequency range from the turbulence dissipation scale (see below) to a period long enough to include all flux-carrying wavelengths. In practice this entails recording continuous time-series at a resolution of 10-20 Hz. See Friehe *et al.* (1991) for a discussion of this, and some practical aspects of the flux calculation.

Referred to as the eddy-correlation method, rapid advances in the development of sonic anemometers and fast-response temperature and humidity sensors have made measurement of covariance fluxes over land routine for almost two decades. However, measurements at sea are complicated by contamination of the complex sensors by salt and sea spray, by ship motion, and air-flow distortion. Eddy-flux equipment has been operated from bottom mounted towers and research platforms, but necessarily these are shallow water sites. Aboard ship, the need to locate turbulence sensors well clear of obstructions is even more critical than with other

instruments, because distortion to the wind flow and wakes from even small objects upstream can significantly modify the turbulent field. More importantly, pitching and rolling of the ship usually dominates the observed wind signals, and the 3-dimensional motion of the wind sensor relative to the surface must be recorded and subtracted *post-facto* from the recorded wind signals (Edson *et al.* 1998).

Nevertheless, it's value as a direct method of flux determination to validate indirect methods such as the bulk and inertial dissipation (see below), has spurred increased effort to overcome these inherent difficulties. Following the pioneering work of Fujitani (1985), instruments and computational methods have been improved, and several investigators report successful motion-corrected covariance fluxes from ships (Tsukamoto and Ishida 1995; Fairall *et al.* 1996a; Fairall *et al.* 1997; Edson *et al.* 1998). The greatest difficulty arises in the case of momentum flux, or stress $\tau = \overline{\rho u'w'}$ where the spurious horizontal and vertical wind signals in $w'$ and $u'$ are themselves correlated. The sensible and latent heat fluxes,

$H = \rho C_p \overline{w'\theta'}$ and $E = \rho L \overline{w'q'}$ respectively,

are less susceptible to slight errors in the motion correction, because the scalar concentrations are only linked to the movement of the sensor as it pitches through the vertical gradients of temperature and humidity, which are generally small at sensor height.

In the context of a 10 Wm$^{-2}$ heat flux accuracy goal as specified for TOGA COARE, the small correction to the fluxes of water vapour (and other trace gases) described by Webb *et al.* (1980) may be significant. They point out that; "If the heat flux is upwards (positive) then rising parcels of air are on average warmer than descending parcels, so on the assumption of zero mean vertical mass flow of air there must exist a small mean upward velocity component.". In this case the first term on the right hand side of (5.4) may not be negligible. This vertical velocity is given by;

$$\overline{w} = 1.61\overline{w'q'} + (1+1.61q)\overline{w'\theta'}/T \qquad (5.5)$$

and the consequent correction to the latent heat flux is:

$$E_{Webb} = \rho L \overline{w}q \qquad (5.6)$$

Over the COARE 4-month Intensive Observation Period, the "Webb" effect averaged 4 Wm$^{-2}$. During strong wind periods, with large sensible and latent heat fluxes, Webb corrections of order 20 Wm$^{-2}$ were observed.

Although much progress has been made with the measurement of eddy-fluxes from ships in the open ocean, and the effort continues to make such measurements more common (Fairall *et al.* 1997; Edson *et al.* 1998), it is likely that their role will remain as a research or validation tool for some time to come. However, the so-called inertial dissipation technique, which employs essentially the same fast-response wind, temperature and water vapour sensors as the eddy-correlation method, may be more readily developed as an operational facility (Fairall *et al.* 1990, Yelland and Taylor 1996).

### 5.3.2 The inertial dissipation method

A. MOMENTUM FLUX

The inertial dissipation method has been favoured for use on ships for two main reasons. The turbulence measurements required can be made at frequencies (a few Hz) above those affected by the motion of the ship, and the implied short spatial scale of the turbulence reduces the errors due to airflow distortion. However since various assumptions are necessary to determine the fluxes, the inertial dissipation method is less direct than the use of eddy correlation. The underlying theory will be outlined using, as an example, the momentum flux.

Based on the Kolmogorov hypothesis, the power spectral density, $S_{uu}(n)$, of the downstream wind component, $u$, can, in the inertial subrange, be related to the dissipation rate $\varepsilon$ via the wave number, $n$:

$$S_{uu}(n) = K\varepsilon^{2/3}n^{-5/3} \tag{5.7}$$

where $K$ is the one-dimensional Kolmogorov constant. Henjes (1998) has shown that (5.7) is valid for use in the inertial dissipation method provided the spectrum of the turbulence is homogeneous and isotropic for wave numbers in the inertial subrange. Using Taylor's hypothesis, that is assuming "frozen" turbulence, (5.7) becomes:

$$S_{uu}(f) = K\varepsilon^{2/3}f^{-5/3}\left(U_{rel}/2\pi\right)^{2/3} \tag{5.8}$$

where $U_{rel}$ is the wind speed as measured by the anemometer, and $f$ is the measurement frequency. Hence the dissipation rate can be obtained by calculating the mean value of $f^{5/3}S_{uu}(f)$ over an appropriate frequency range.

The wind stress is derived from the dissipation rate using the turbulent kinetic energy budget (see for example (Busch, 1972)) which for steady state, horizontally homogeneous turbulence, can be written as:

$$u_*^2\frac{\partial\langle u'\rangle}{\partial z} + g\frac{\langle w'T_v'\rangle}{T_v} - \frac{\partial}{\partial z}\langle w'e'\rangle + \frac{1}{\rho}\frac{\partial}{\partial z}\langle w'p'\rangle = \varepsilon \tag{5.9}$$

or

$$P \quad + \quad B \quad - \quad D_t \quad + \quad D_p \quad = \quad \varepsilon \tag{5.10}$$

where primes indicate fluctuations and $<>$ indicates mean quantities. In (5.10) $P$ is the mechanical production, $B$ the buoyant production, $D_t$ and $D_p$ are the vertical divergence of the turbulent transport and pressure transport terms, and $\varepsilon$ is the dissipation. Equation (5.9) can be made dimensionless by multiplying by the Monin-Obukhov surface layer scaling parameter $kz/u_*^3$ giving:

$$\phi_m - \frac{z}{L} - \phi_t + \phi_p = \frac{\varepsilon kz}{u_*^3} = \phi_\varepsilon \tag{5.11}$$

where the Obukhov length, $L$, is:

$$L = \frac{-u_*^3 T_v}{\left(gk\langle T_v'w'\rangle_0\right)} \tag{5.12}$$

and each of the dimensionless profiles $\phi_m$, $\phi_t$ and $\phi_p$ are expected to be universal functions of $\zeta$ ( $= z/L$). Equation (5.11) defines the dimensionless dissipation function $\phi_\varepsilon$. If the terms on the left-hand side of (5.11) are known (or equivalently the form of $\phi_\varepsilon(\zeta)$), the friction velocity can be evaluated from an estimate of the dissipation. Thus :

$$u_* = \left[\frac{fS_u(f)}{K}\right]^{1/2}\left[\frac{2\pi}{U_{rel}}\frac{kz}{\left(\phi_m - (z/L) - \phi_D\right)}f\right]^{1/3} \tag{5.13}$$

Unfortunately, the exact forms of $\phi_m(\zeta)$, $\phi_t(\zeta)$ and $\phi_p(\zeta)$ are not well known (Fairall and Larsen, 1986), and previous authors have made various assumptions as to their magnitude for turbulence over the sea. The form of $\phi_m(\zeta)$ will be discussed in Section 7.2; with regard to the vertical divergence terms, Large (1979) argued that the available evidence suggested that

$$\phi_t \approx -\phi_p \tag{5.14}$$

This leads to a balance between dissipation and the sum of mechanical and buoyant production:

$$\phi_\varepsilon = \left( \phi_m - \frac{z}{L} \right) \tag{5.15}$$

However, other authors suggest that there is an imbalance between production and dissipation. Thus:

$$\phi_\varepsilon = \left( \phi_m - \frac{z}{L} - \phi_D \right) \tag{5.16}$$

Deacon (1988) argued that the value of the Kolmogorov constant used in the inertial dissipation method is not the true value, but rather an effective value which corrects for the $\phi_D$ term at neutral stability. Edson *et al.* (1991) and Edson and Fairall (1998) have estimated that this correction might be of order 10 to 20%. By evaluating the friction velocity to wind speed relationship for different stability ranges Yelland & Taylor (1996) and Dupuis *et al.* (1997) evaluated the variation of the apparent imbalance term with $\zeta$. However Taylor and Yelland (2000a) have shown that much of that apparent imbalance was mainly caused by random errors in the data which caused errors in the calculated stability. The implication is that the true magnitude of any imbalance may well be smaller than previously estimated, thus giving more confidence in results from the inertial dissipation method.

As formulated above, the inertial dissipation technique requires assumptions with regard to the values of the von Karman constant, $k$, the Kolmogorov constant $K$, and the form of the dimensionless functions $\phi_m(\zeta)$ and $\phi_\varepsilon(\zeta)$. These constants and functions are not independent and Fairall and Larsen (1986) have suggested a different formalisation of the inertial dissipation method in terms of turbulence structure functions. As implemented by Edson *et al.* (1991), this requires determination of $\phi_m(\zeta)$ and the dimensionless structure function parameter $f_m(\zeta)$ but does not require an explicit Kolmogorov constant value. We have described the above formulation because it follows that of Large (1979) and Large and Pond (1981,1982) which represent the main verification of the inertial dissipation method over the open ocean.

B. SCALAR FLUXES

For other variables the inertial dissipation method consists of determining the spectral level of the fluctuations in the inertial subrange and then solving the budget equation for the variance of that quantity. Thus:

$$\left| \langle w' \gamma' \rangle \right| = \left[ \frac{K}{\beta} \frac{\phi_\varepsilon}{\phi_{N_\gamma}} \frac{f S_\gamma(f)}{f S_u(f)} \right]^{1/2} u_*^2 \tag{4.17}$$

where $\gamma$ signifies any passive scalar and $\phi_{N_\gamma}$, $\beta$ are respectively the dissipation function and Kolmogorov constant pertaining to $\gamma$.

## 5.4 Precipitation Flux

### 5.4.1 Introduction

The determination of precipitation flux over the oceans is a critical requirement for studies of the hydrological cycle, ocean stratification and mixing, and for the development of coupled ocean-atmosphere GCM's. However, accurate measurement of rainfall at sea presents difficulties in two respects; there are measurement (instrumental) problems, and sampling problems. Rainfall, particularly in storms associated with tropical convection, is perhaps the "patchiest" of all meteorological variables. For most applications, over land or sea, single point observations of rainfall are generally less relevant than area-averaged values or spatial characteristics. Whereas over land these quantities may be derived from an appropriately-spaced network of surface raingauges, at sea both spatial and temporal sampling by

conventional means is usually quite inadequate, even during intensive measurement campaigns (see Section 10.9.1). Remote sensing can provide areal coverage, by ship or aircraft mounted radars on the local scale, or from satellites in the longer term and globally. The sensors and recovery algorithms should, however, be verified by reliable ground-truth measurements. Results of different algorithm intercomparison projects (see Section 10.9.4) have shown that this is rather difficult because the *in situ* and radar measurements are generally not representative enough to serve as a verification data source.

For the TRMM satellite (see Section 4.3.2) an intensive validation experiment (KWAJEX) was conducted around the island of Kwajalein (Marshall Islands) from July to September 1999[4]. Ground-truth instruments were deployed on the island, on aircraft and ship-borne. When available, the results of this experiment will add to our knowledge of the performance of various instruments in common use to determine precipitation at sea. Development in this area has been much needed, because, as will be discussed next, there are significant problems with using conventional funnel rain-gauges on ships.

*5.4.2  in situ rainfall using Funnel raingauges.*

A.  INTRODUCTION

The use of conventional rain-collecting instruments, designed for land use, results in uncertainties which are of the same order of magnitude as the mean precipitation estimates. Hasse *et al.* (1998) stressed two main sources of the uncertainties of precipitation measurements using traditional land rain gauges at ships and buoys: (i) the effect of the flow around the ship's overall structure which can lead to undercatch or overcatch depending on the location of gauge; (ii) the effect of the flow in the close vicinity of the rain-gauge, which tends to carry the rain above the orifice of the gauge and leads to a wind speed dependent undercatch. Corrections of measurements for the wind speed, and proper installation of rain gauges, can slightly improve the accuracy, but do not resolve the problem in general (Olbrueck 1979, Ruprecht 1993, Hasse *et al.* 1998). There is also the problem that conventional tipping bucket raingauges do not work on board ships or moorings because of the platform motion.

B.  FUNNEL DESIGN

A serious source of error is loss of catch due to the deflection of raindrops away from the opening of funnel-type gauges during strong winds. This phenomenon is well-known in funnel gauges used over land. It was first documented by Heberden (1769) who observed the difference between rainfall measured in the garden of Westminster Abbey, and that measured on the roof. Jevons (1861) explained the problem analytically and Koschmeider (1934) devised a simple empirical wind-speed dependent correction. In about 1980 the WMO Commission for Instruments and Methods of Observation (CIMO) initiated a series of workshops and a monitoring program designed to standardise international practice in the form and exposure of operational gauges (WMO 1985, 1989). A recent contribution to this effort is described by Yang *et al.* (1998). Folland (1988) developed a theory for loss of catch based on the pattern of fluid flow past cylindrical obstacles, and involving droplet size and rainrate. The lighter the rainfall and the smaller the drop, the more likely will it be swept past the funnel instead of dropping in. Folland adopted the drop size distribution (DSD) of Best (1950) rather than the better-known DSD of Marshall and Palmer (1948) on the grounds that the latter overestimated the number of small drops. Folland's model agrees fairly well with field observations, but covers rainrates from 0.1 to only 10 mm hr$^{-1}$ which may be adequate for most rainfall over land in Europe, but is at the low end of rainfall at sea and far short of tropical storms. With a 10 ms$^{-1}$ wind and 10 mm hr$^{-1}$ rainrate, the model predicts about 10% loss. But other empirical studies hint at the possibility of much larger effects; 5-80% loss (Kurtyka, 1953), 50% loss for 1-2mm drops at 12 ms$^{-1}$ in a wind tunnel (Mueller and Kidder, 1972), annual loss 20% and "considerably greater" with taller gauges (Rodda and Smith, 1986).

According to Folland's (1988) model, for the large drop sizes and high rainrates of a tropical storm loss of catch would be negligible. However, the problem is much more severe on

ships because, to avoid obstructions, raingauges are usually mounted aloft where winds can be augmented by the ship's speed.  Further, the wind flow distortion is over the entire vessel, not just the gauge itself.   The problem has been investigated in respect of the COARE rainfall data, and extended to studies of measurement variability at various locations on the ship during subsequent cruises.  This will be discussed in more detail below, but here we simply observe that even in heavy rainstorms,  raindrops were seen to be deflected upward away from the funnel in some locations.   For funnel gauges mounted in more favourable positions, Koschmeider's (1934) empirical wind-speed dependent correction, brought the siphon rainfall values close to the corrected optical raingauge values in the COARE, MCTEX and Indian ocean cruises (Bradley, *pers. comm.*; Godfrey *et al.* 1999).

Hasse *et al.* (1998) have designed a rain gauge for use on ships specifically to overcome the wind loss problem, using a "dual collector" arrangement.  The top funnel is of similar shape to the "champagne glass" design recommended by Folland (1988), and feeds to a calibrated orifice from which drops are counted.  Rain blown against the side of the instrument is trapped, funnelled down into a separate collector, and its contribution weighted according to wind speed measured by a co-located anemometer.  This instrument has been tested for some years on land against standard gauges, and on ships against an optical disdrometer achieving an accuracy of about 3% for 6-hourly sums. (Grossklaus *et al.* 1998).  Tests continue on various ships, including a 2-year operational pilot project on ship lines in the Baltic Sea.   Its performance must be judged eventually against a consensus of experience with other instruments, all of which carry some measure of uncertainty when used at sea.   Taking into account the relatively low cost of the gauge and computer interface for data storage (in operational design mode), its operational use on ships would appear feasible.

C.  MEASUREMENT METHOD

The most common type of funnel gauge used aboard ships and moorings is the siphon gauge.  This has a reservoir which steadily fills with rainfall to its capacity, when it siphons automatically and starts filling again.  Some electronic system (e.g. capacitance) is used to keep track of the level of water in the gauge, and provide an analogue output; a common specification is capacity equivalent to 50 mm rainfall with resolution 0.01 mm.  The siphon system is relatively, but not completely, independent of ship motion.  There is also loss of rainfall registration while the instrument is siphoning; since this point is frequently reached during a period of particularly heavy rainfall, the loss can be significant.

*5.4.3  Other methods of in situ measurement*

A.  OPTICAL RAINGAUGES

The most common optical raingauge (ORG) in use was developed partly to address the problems of measurement in the remote, marine environment.  It has no moving parts, is robust and completely sealed, and provides an analogue output which is a simple function of the rainrate.  These ORG's measure rainrate directly by detecting the intensity of scintillations caused by raindrops passing through a partially coherent beam of infrared radiation.  The instrument, and the theoretical basis of its optical scintillation system are described by Wang *et al.* (1978, 1979) and Crosby (1994).  Some ORG's were provided by the NASA-TRMM office to ships and moorings participating in TOGA-COARE, in support of the TRMM satellite validation program.

At the 1994 Toulouse COARE data workshop (Chinman *et al.* 1995, page 26), disagreement between various rainfall estimates was found to be worse than a factor of two, which led to a comprehensive study of  rainfall measurement. The methods under scrutiny, and their Intensive Observation Phase (IOP) average rainfall estimates were reported at a COARE Flux Group workshop (Bradley and Weller 1995a, page 14).  Leaving aside the broad range of satellite estimates, these results seemed to form two groups; the radars, atmospheric budgets and siphon gauges supporting an IOP-average rainfall of around 5-6 mm day$^{-1}$ with the ORG's indicating about twice that value.  Being a relatively new and untried instrument, the ORG was

suspected of overestimating relative to the more conventional systems. Suggested defects were errors in calibration, sensitivity to ship vibration, and inappropriate response to the intensity and DSD of tropical rainstorms.

All of these possibilities were studied on three of the COARE ORG's, using an artificial rain facility (or rain-tower) in which a uniform distribution of raindrops fell to terminal velocity, and rainrate could be varied over the range 20-200 mm hr$^{-1}$. An ORG was subjected to quite severe vibration in the rain tower, but no spurious signals appeared either with or without rainfall. Neither was any dependence on DSD found, agreeing with the conclusions of Nystuen *et al.* (1996). The calibration slopes of all three ORG's tested agreed with the factory specification and was linear over the entire range of rainrate, but for two of the three there was a constant offset of a few mm hr$^{-1}$. This could lead to large percentage errors at low rain rates.

The only other defect found was an imperfect cosine response, such that the vertical component of rain falling through the ORG beam is overestimated. This can be a significant effect on board ship, where the relative rainfall angles are accentuated by the ship's speed. Given relative wind speed and direction measured on the ship, this can be allowed for; the correction lowers the originally reported COARE ORG rain rates, typically by 15%. ORG rainrates were used to obtain closure of the freshwater budget over the R/V *Wecoma* COARE cruise area by Feng *et al.* (1998) and in the tropical Indian Ocean by Godfrey *et al.* (1999), providing further support for their performance. The test ORG's have been deployed on the ship and a drifting buoy during several cruises of R/V *Franklin*, and recently on R/V *R.H. Brown*.

B. DISDROMETERS

The primary purpose of a disdrometer is the measurement of drop size, and drop size distribution in rainfall. Automated designs may also serve to record rainrate continuously and, by integration, total rainfall. Among some precipitation investigators the disdrometer is regarded as the reference instrument. However Post *et al.* (1998) comment that disdrometers were used during the Combined Sensor Program cruise and appeared to work satisfactorily, but that after the cruise, serious concerns about calibration and linearity raised doubts that any of the rain data could be used quantitatively.

The most usual disdrometer is an acoustic device (effectively a microphone) which converts the sound of impact of raindrops hitting a sensor surface into an electrical signal related to the size of the drop (Joss and Waldvogel, 1967). One commercial instrument has a sensor area of 50 cm$^2$ and sorts the signals into 20 drop size categories covering the range 0.3 to 5.5 mm diameter. Improved calibration boundaries by Sheppard (1990) and Sheppard and Joe (1994) improved its response to rainfall which contained a high proportion of large drops. Not surprisingly, the instrument is sensitive to ambient acoustical noise, including noise from rain hitting nearby surfaces, so special measures have to be taken to isolate the instrument (Nysteun *et al.*,1996). For the TRMM project, improved impact disdrometers are being developed following the design of Roland (1976).

Optical disdrometers, which measure the light extinction by raindrops falling through a sensitive volume, have been described by Bradley and Stow (1974), Illingworth and Stevens (1987) and Grossklaus *et al.* (1998). The latter, designed particularly for use at sea, has a higher 128-bin resolution. The incidence of multiple drops and grazing incidence on the sensitive volume are considered. Rainrates are determined from droplet spectra by assuming terminal velocity according to drop size. The resolution is 0.05 mm diameter.

C. ACOUSTIC METHODS

Another acoustical method of rainfall measurement at sea uses the underwater sound produced by raindrops impacting on the surface. Rainfall produces a unique acoustic signal which may be readily distinguished from other common sound signals (breaking waves, biological sources, etc.), and is typically louder by orders of magnitude than these other sources (Nystuen, 1996). Acoustic signatures have been identified for different raindrop sizes (Medwin

*et al.*, 1992), enabling estimation of  DSD within the rain and hence rainrate.  An "Acoustic Rain Gauge" employing these principles has been described by Nystuen (1999), and deployed on ocean moorings during SCSMEX and on the TOGA-TAO array (Nystuen et al., 2000).

## 6  PARAMETRISATION OF RADIATIVE FLUXES

### 6.1  Introduction

　　　　Shortwave (SW) is considered as radiation whose source is the sun. Longwave (LW) is considered as radiation whose source is the emission of thermal infrared by the atmosphere and surface. SW (LW) is generally below (above) 3 μm in wavelength;  the maximum overlap at the surface is well below 10 Wm$^{-2}$. LW forcing to the climate system by concentrations of trace gases can be computed more confidently than it can be directly measured;  the trace gases can be measured accurately and their spectroscopic characteristics are fairly well known. Unfortunately the exception is water vapour – which is the most important radiatively.  SW forcing to the climate system by aerosols (direct scattering, absorption, and some thermal emission; indirect through clouds) and changes in land use (surface albedo) is uncertain and cannot be measured in a straightforward manner; theoretical calculations of SW forcing could be validated by comparing a time history of computed and measured fluxes (provided that the measurements are sufficiently stable).  Because  at present the computed and measured SW fluxes do not match, the uncertainty in SW forcing is a significant problem for IPCC assessments of anthropogenic impacts on climate.

### 6.2  Radiative fluxes from ship data

#### 6.2.1  Parameterisation of SW flux

　　　　Because the radiation community has generally considered that acceptable accuracy would not be obtained,  merchant ships are not equipped to measure the incoming shortwave radiation. Instead the insolation must be estimated from information on the ship's position and the cloud information visually estimated by the ship's officer.  Such an estimate has to be considered relatively crude and it might be argued that the deployment of pyranometers (and pyrgeometers) on at least a subset of the VOS would be advantageous.

　　　　In general, the short-wave radiation flux on the sea surface may be parameterised as:

$$Q\downarrow_{sw} = Q_t T_F \tag{6.1}$$

where $Q_t$ is the SW radiation at the top of the atmosphere, equal to $Q_t = S_0 \cos h$, where $S_0$ is the solar constant, and $h$ is solar altitude. $T_F$ represents the transmission factor of the atmosphere and has to be parameterised in terms of the cloud cover and thermodynamic parameters of the atmosphere.  There are few parameterisations which use this very general approach (see for example the reviews of Lind *et al.*, 1984; Dobson and Smith 1988).  However, the accuracy of this approach is not very high because it requires consideration of the radiation transfer in the whole atmospheric column. Parameterisations based on ship data are usually poorly determined because of the very complicated and uncertain dependency of the transmission factor on the surface parameters available from marine data. To avoid this very large uncertainty, it is more helpful to parse the transmission factor into two terms.  One represents the modification of short-wave radiation under clear sky conditions (astronomy, temperature, humidity, and aerosols are the main agents of these modification). The other is the cloud modification of the clear sky radiation.  In this case,  the general formula for the short-wave radiation becomes:

$$Q\downarrow_{sw} = Q_0 F(n, T, h) \tag{6.2}$$

where $Q_0$ is clear sky solar radiation at sea surface, $F(n, T, h)$ is the empirical function of the fractional cloud cover $n$, air temperature $T$, and solar altitude $h$ (in general case). Clear sky solar radiation is assumed to be a function of the astronomy and of the transmission for the clear sky atmosphere.  In most schemes,  these two factors are parameterised through the purely astronomical characteristics (latitude and solar altitude) and empirical coefficients which account for the atmospheric air transparency under clear skies (Seckel and Beaudry 1973; Lumb 1964; and others).  There are only a few parameterisations which directly include surface atmospheric parameters into the clear sky radiation formula. Thus, Malevskii *et al.* (1992) suggested to use for $Q_0$ the parameterisation:

$$Q_0 = c(\sinh)^d \tag{6.3}$$

where $c$ and $d$ are empirical coefficients, which depend on the atmospheric transmission for the optical mass number $2P_2$. $P_2$ itself is a function of atmospheric surface humidity, although Malevskii *et al.* (1992) also gives formulae using air temperature, when humidity measurements are not available.

Quantitative estimation of the cloud reduction factor $F$ is given in many works, reviewed by for instance Dobson and Smith (1988). The most frequently used parameterisations are the result of a compromise between the complexity of the radiation transfer in the cloudy atmosphere and the availability of data to describe this complexity. Thus it is obvious that a universal parameterisation of the cloud modification of radiation should be based on the consideration of cloud types and heights. Against that it is often considered that the only reliable parameter in the VOS data is the amount of cloud cover. Attempting to fit the limited data set of direct measurements using this parameter obviously leads to a dependency of the fits on the region and time of the year, and results in the different parameterisations suggested by different authors. As a good example, Dobson and Smith (1988) found pronounced differences fitting their formulae using the data from OWS Papa and Sable Island.

However for this flux there is a further potential problem; most ship's report at most 4 times per day and the most reports occur at the standard reporting hour closest to local noon. To avoid introducing bias, the Reed (1977) formulae for the daily mean net shortwave flux $Q_{SW}$ uses the calculated monthly mean values for the fractional cloud cover $n$, and the noon solar elevation in degrees, $\phi$. Hence:

$$Q_{sw} = Q_{sw_0}\left(1 - c_n n + 0.0019\phi\right)(1 - \alpha) \tag{6.4}$$

where $c_n = 0.62$ the cloud attenuation factor, and $\alpha$ the albedo (Payne 1972). $Q_{sw_0}$ is the shortwave insolation at the surface under clear skies (Seckel and Beaudry 1973). The Reed formula (6.4) should only be used for $0.3 \leq n \leq 1$, and $Q_{sw} = Q_{sw_0}$ should be used for $n < 0.3$ (Gilman and Garrett, 1994).

Being based only on the mean monthly estimated cloud amount, (6.4) is a crude method of estimation. However it was recommended by the comparative studies of Frouin *et al.* (1988) and Dobson and Smith (1988) who found a site dependant long term bias of -1 to +12 Wm$^{-2}$ and a monthly mean rms error of about 8 Wm$^{-2}$. In contrast, using comparisons with data from several air-sea interaction experiments, Katsaros (1990) and Godfrey *et al.* (1991) found the Reed formula to be biased high by about 20Wm$^{-2}$.

Malevskii *et al.* (1992) suggested formulae for the use of the low and total cloud cover as available from the VOS reports (although the quality of the low cloud cover estimates can be questioned). Their two level scheme uses the low cloud amount and total cloud amount, while their one level scheme just uses the total cloud amount. Intercomparison of these parameterisations with Reed (1977) and Dobson and Smith (1988) as well as with instrumental measurements shows that the two-level Malevskii *et al.* (1992) scheme gives the least biases at least in the mid latitudes (Niekamp 1992).

An important problem of the validation of the SW schemes is that the most of continuous instrumental measurements were undertaken in mid latitudes. However the tropical cloudiness is characterised by very different transmission characteristics. An effect in high latitudes, still poorly understood, is the secondary reflection of radiation from the cloud margins under low declinations and small cloud cover. Note here, that the Dobson and Smith (1988) and Malevskii *et al.* (1992) schemes assume the possibility for the cloud "reduction" coefficients to be greater than 1, partially accounting for this effect.

We should note that the atmospheric radiation community generally avoids the use of expressions such as (6.4). This is because the optical depth (optical thickness) in (6.4) is implicitly constant. In a formal radiative transfer model (RTM - Section 6.3) the perturbation to TOA albedo and surface insolation induced by overcast cloud ($n = 1$ in 6.4) over a dark ocean

can vary widely, depending primarily on the optical depth of the cloud. Thus, a thin veil of cirrus may increase the albedo by 0.10, while thick altostratus may increase the albedo by 0.60. For similar reasons, remote sensing of cloud cover $n$ and cloud optical depth with satellite data are equally challenging problems. Nevertheless, expressions such as (6.4) will continue to be useful for some applications, since they allow changes in the surface insolation and TOA albedo to be simply estimated from changes in cloud cover $n$ noted by routine visual observation.

One of the more difficult issues faced by the RTM community is indirect aerosol forcing: the changes to cloud optical depth and reflectivity that are caused by increases in the concentration of cloud condensation nuclei (CCN). A group of radiation experts (Hanen *et al.*, 1998) has used historical records of cloud cover $n$ over the US in this century to estimate the change in radiative forcing (i.e., the output of an RTM using optical depth as input) due to increases in CCN.

### 6.2.2 Parameterisation of LW flux

As for short wave radiation, the incoming longwave radiation is not measured but must be estimated from the visually estimated cloud amount. Other parameters are the air temperature and humidity and, for determining the net longwave flux, the sea temperature. For example (Clark *et al.*, 1974):

$$Q_{LW} = \varepsilon\sigma\, T_S^4 (0.39 - 0.05 e^{0.5})(1 - \lambda n^2) + 4\varepsilon\sigma\, T_S^3 (T_s - T_a) \qquad (6.5)$$

where $\varepsilon$ (= 0.98) is the spectrally integrated emittance, $\sigma$ (= 5.67 x 10$^{-8}$ Wm$^{-2}$K$^{-4}$) the Stefan-Boltzmann constant, $e$ the water vapour pressure, $n$ the fractional cloud cover, and $T_a$ and $T_s$ are the air and sea temperatures in K. The cloud cover coefficient $\lambda$ varies with latitude. Equation (6.5) is essentially a simple parameterisation of the RTM's for clear sky conditions (Section 6.3).

The latitude-based adjustment $\lambda$ accounts for the variation of cloud based height and emissivity, both of which may vary enormously within a latitude zone. Thus it is perhaps not surprising that the global validity of (6.5) and similar formulae has recently been questioned. For the Mediterranean, Gilman and Garrett (1994) found that this class of formulae underestimated $Q_{lw}$ by about 17 Wm$^{-2}$ and, based on Mediterranean data, Bignami *et al.* (1995) proposed a new formulae which, for mid-latitude regions, gives $Q_{lw}$ values some 25 Wm$^{-2}$ greater than (6.5) (see Section 9.4.3B). In contrast the review of Katsaros (1990) found that (6.5) underestimated the mean by only 5.5 Wm$^{-2}$ and comparisons with ship measurements from the Atlantic and Southern Ocean (Josey *et al.* 1997) have shown agreement typically to within 5 Wm$^{-2}$ on timescales of order one month. In the tropical western Pacific, Godfrey et al. (1991) found (6.5) to be the best of four such formulae, showing no systematic bias compared with pyrgeometer measurements.

## 6.3 Radiative Transfer Models - RTM's

### 6.3.1 Longwave radiative flux (LW)

In a cloud-free atmosphere, the net longwave flux density at any height may be calculated from an atmospheric temperature profile, with knowledge of the thermal absorption and emission characteristics of the atmospheric gaseous constituents, via an appropriate radiative transfer model, RTM (see e.g. Paltridge and Platt 1976, chapter 7). RTM's require as input the vertical concentration profiles of the atmospheric gases, the most important for infrared transfer being water vapour, carbon dioxide and ozone. Most exact are the Line-By-Line Radiative Transfer Models (LBLRTM) which, as their name implies, compute transfer of each constituent for each emission and absorption spectral line at many levels throughout the profile. Their computational burden is therefore large, which makes them unsuitable for routine use in numerical models Over the years therefore, many broadband RTM's have been developed, increasing in accuracy and efficiency with improved parameterisations and increased computer power. Such models are widely applied in climate modelling, and in flux retrieval from direct and remotely sensed atmospheric variables.

Longwave irradiance at the surface may thus be obtained by integrating the calculations from an RTM through the atmosphere. Dutton (1993) used LOWTRAN7 (Kneizys *et al.* 1988) to determine longwave irradiance from two radiosonde launches per day at each of four sites spread from the South Pole to the tropics, over the course of a year, selecting the clear-sky occasions. His purpose was comparison with simultaneous pyrgeometer readings, and they agreed overall within 5 $Wm^{-2}$. Dutton (1993) was careful to stress that the result demonstrated internal consistency of the two methods, and claimed absolute accuracy for neither, but his work illustrated convincingly the potential value of RTM's for obtaining accurate global flux fields from routine meteorological observations.

Miskolczi (1994) also used an RTM to compare with pyrgeometer measurements and, as noted in Section 5.2.3, Fairall *et al.* (1998) used the Rapid Radiative Transfer Model (RRTM) developed for the Atmospheric Radiation Measurement Program (ARM) science team by Mlawer *et al.* (1997) for comparison with the Moana Wave pyrgeometer measurements. This particular model allows for the use of up to 35 molecular species, defaulting to the seven most important, $H_2O$, $CO_2$, $O_3$, $N_2O$, CO, $CH_4$ and NO. Mlawer *et al.* (1997) verified RRTM against a LBLRTM (Clough *et al.* 1992), and relied on LBLRTM verifications against measurement. They claim that RRTM and LBLRTM longwave calculations differ by less than 1.0 $Wm^{-2}$ at any altitude and, based on a large number of validations with well specified water vapour profiles (the SPECTRE data), that LBLRTM has an accuracy of 2 $Wm^{-2}$.

The parameterisations used in RTM's steadily improve as new observational technology provides better validation data. For example, in collaboration with COARE, the ARM program operated the Pilot Radiation Observation Experiment (PROBE) which was equipped with a Fourier Transform Infrared Radiometer (FTIR, Shaw *et al.* 1991) (see section 5.2.1). One of the primary goals of PROBE was to compare radiance spectra measured with the FTIR with the predictions of a LBLRTM based on radiosonde observations of temperature, water vapour and pressure. In the water vapour window region (830 to 1250 $cm^{-1}$), the calculations were lower than measurements by about 5%, which enabled revision of the water vapour continuum formulation used in the model (Clough 1995). Post *et al.* (1998, their Figure 10) illustrate the effect of this improvement. Tobin (1999) notes that recent refinements to the parameterisation of the water vapour continuum (Clough *et al.*, 1992) improve accuracy by 1-2 $Wm^{-2}$. However, the continuum itself is not rigorously understood in terms of basic physics.

The computation of LW flux with the best high spectral resolution codes under clear conditions is at an advanced state. Further advances will depend upon developments in sensor technology in the far infrared (wavelengths exceeding ~ 20μm). Accurate computation of LW under clear skies requires a treatment of surface emissivity, to account for scattering as well as absorption and emission. Some rapid codes (e.g., Fu and Liou, 1993) include this. For cloudy sky conditions, however, RTM's are not well validated. The calculation of the downwelling longwave flux under a cloud requires knowledge of both cloud base height and emissivity. Cloud base height may be measured with active systems such as a MicroPulse lidar (Spinhirne, 1993) or a cloud profiling radar, although an infrared radiometer (such as the pyrgeometer) would still be needed to estimate cloud emissivity. RTM's designed for GCM calculations (e.g., Morcrette, 1991; Chou et al., 1995a; Fu and Liou, 1993) are compared with higher spectral resolution codes in the Intercomparison of Radiation Codes in Climate Models (ICRCCM, Ellingson *et al.*, 1991; Ellingson and Fouquart, 1991).

### 6.3.2 Shortwave radiative flux (SW)

Knowledge of atmospheric scattering is essential for shortwave RTM's under both clear and cloudy conditions. Recent studies with SW RTM's under clear skies have indicated significant discrepancies when compared with measurements (e.g., Wild *et al.* 1995; Charlock and Alberta, 1996); computed insolation values are too high, suggesting that the real atmosphere absorbs more than is predicted by theory. A thorough study by ARM (Kato *et al.*, 1997) has demonstrated that under clear skies, the discrepancy is in the diffuse component. Zender *et al.* (1997) used alternate radiometers (Valero *et al.*, 1982) and do not regard their excess in

computed versus observed flux as "significant", although their discrepancies are of order 10 $Wm^{-2}$. One recent study (Wild, 1999) found no discrepancy for clear skies at Payerne; but personal communication with one of the authors revealed that a "model" aerosol profile was employed. The aforementioned ARM studies used measured spectral optical depth. Some ocean studies (Chou and Zhao, 1997; Waliser *et al.*, 1996) have also reported no discrepancies for clear skies, but their measurements were made with unshaded pyranometers. Similarly, many measurements of surface shortwave irradiance (i.e., most of those in the Global Energy Balance Archive (GEBA), have been made with pyranometers only. Under clear skies, the errors with a pyranometer can be quite large (DeLuisi *et al.*, 1991); for the most accurate results, the correct procedure is measurement of the direct beam with a normal incidence pyrheliometer (NIP) and the diffuse component with a shaded pyranometer (see Section 5.2.2). A strict measurement and calibration protocol has been developed under WCRP to guide the Baseline Surface Radiation Network (BSRN, Gilgen *et al.*, 1995). At present, no ship-borne system subscribes to the BSRN protocol.

The importance of such a protocol is illustrated with the following results from the comprehensive ARM Program (Stokes and Schwartz, 1994) in Oklahoma under clear skies in October, 1995. ARM measurements for aerosols, cloud screening, soundings, and other parameters were thorough.

Table 6.1. Results from the Atmospheric Radiation Measurement (ARM) Program

| *Mean incoming at TOA for SW* | *794 $Wm^{-2}$* |
|---|---|
| Surface SW Insolation: | |
| Pyranometer only | 549 $Wm^{-2}$ |
| NIP + shaded pyranometer | 571 $Wm^{-2}$ |
| RAMS (Valero radiometer) | 585 $Wm^{-2}$ |
| Theory (Fu-Liou code) | 617 $Wm^{-2}$ |

The theoretical calculation with the Fu-Liou code is 32 $Wm^{-2}$ larger than the measurement with the sophisticated RAMS radiometer (Pilewskie and Valero, 1995). A similar bias has been found by many teams in ARM, with most of the discrepancy in the diffuse component. The NIP + shaded pyranometer set-up approximates BSRN protocol; the NIP has already been corrected by over 2% following special cavity radiometer measurements (Michalsky *et al.*, 1997). The measurement with the pyranometer only (which would be typical for an ocean measurement but without the additional errors listed in Section 5.2.2) is the outlier; the bias depends upon the angular distribution of the radiation and is not constant. There are several possible reasons for this. Taking the NIP + diffuse measurement as a calibration reference, it may be that the particular pyranometer here was poorly calibrated by the manufacturer, or had changed subsequently. In Section 5.2.2 we discuss this question and note that systematic differences of 3% were found among first-class pyranometers used in COARE.

GCM's use fast RTM's to compute SW under clear and cloudy skies. Well regarded GCM-type codes include Morcrette (1991), Chou et al. (1995a), and Fu and Liou (1993). It is well known that faster codes, which employ techniques such as 2-stream, delta-Eddington, and 4-stream, are not as accurate as the higher order plane parallel codes such as discrete ordinate (Stamnes et al. 1988) and adding-doubling; errors of several per cent can be expected (Liou, 1992). But few clouds are plane parallel. With finite geometry, more computationally intensive routines like Monte Carlo and the ingenious spherical harmonics discrete ordinate (Evans, 1998) are more appropriate for estimating an instantaneous flux. Finite geometry is appropriate for some LW applications, too (e.g. Takara and Ellingson, 2000). Finite cloud geometry often has a dramatic effect on the albedo at the top of the atmosphere (TOA) and the transmission to the surface; Stephens and Greenwald, (1991) have pointed out that cloud macrostructure (i.e. finite geometry) can be more important than cloud microphysics. But the

surprising general result is that when the TOA albedos of plane parallel and finite cloud RTM's agree, the surface insolation in the RTM's often differs by only a few Wm$^{-2}$. While finite cloud (2-D or 3-D) geometry can either increase or decrease the atmospheric absorption relative to plane parallel for particular cases, ensemble means generally show a small effect - at least in RTM's. Cloud finite geometry appears to be much more critical for the retrieval of the physical and optical properties of clouds than for the computation of time-mean radiative flux.

But if theoretical 3-D and 1-D clouds with the same albedos also have approximately the same atmospheric absorption, do 3-D effects account for the strong "anomalous SW absorption by clouds" which has been reported? The existence of such absorption is a matter of debate. For example, Cess *et al.* (1995), Ramanathan *et al.* (1995), and Pilewskie and Valero (1995) have found significant discrepancies between computed and measured SW radiation for cloudy skies, as was noted earlier by Stephens and Tsay (1990). From Cess *et al.* (1995), we would infer that if a plane-parallel (GCM) code produced an albedo at the TOA that matched observations, it should have a global mean error of approximately 25 Wm$^{-2}$ for the atmosphere (and hence also for the surface). Over Oklahoma, matched aircraft observations by Valero *et al.* (1997; 2000) found a strongly absorbing cloud, corroborating the finding of Pilewskie and Valero (1995) in the Pacific Ocean; both studies used the broadband RAMS instrument, rather than Eppley or Kipp and Zonen radiometers, and were based on a few hours of measurement. The brief aircraft-based results of Valero *et al.* (1992) have been seconded (Charlock *et al.*, 1998) with narrow band (GOES-8) satellite data (Minnis *et al.*, 1995) but only for short periods; when the domain is extended to several weeks, observed absorption by the clear and cloudy atmospheres both exceed theoretical values by approximately the same amount (i.e. there is a little anomalous absorption – but in both clear and cloudy skies). Cess *et al.* (1995) and Ramanathan *et al.* (1995) used longer records of broadband Earth Radiation Budget Experiment, ERBE, data (which is more reliable than GOES) at the TOA and broadband radiometers at the surface to infer anomalous SW absorption by clouds; most of their surface observations, however, were not based on separate measurements of the direct (NIP) and diffuse (shaded pyranometer) components, as recommended by BSRN. An intensive study (Charlock *et al.*, 1999) with the newly released broadband CERES data and separate direct and diffuse surface measurements at a score of ARM Southern Great Plains (SGP) sites for January-August 1998 found no support for the level of cloud forcing to atmospheric absorption reported by Cess *et al.* (1995) and Ramanathan *et al.* (1995). A similar study by Trischencko *et al.* (1999) also found no support for anomalous absorption by clouds over long time periods in either ERBE, CERES, or ScaRaB (Scanner for Radiation Budget) data that was matched with surface data.

*6.3.3 COARE atmospheric soundings*

Clearly, however good its internal physics and parameterisations, the accuracy with which an RTM can deliver radiative fluxes depends directly on the reliability of the atmospheric soundings used as input. Following COARE, several research groups, came to suspect that the majority of COARE soundings were in error, in particular that the humidities seemed about 1 g kg$^{-1}$ too low (Bradley and Weller 1997; Zipser and Johnson 1998). This was initially based on anomalous north-south gradients of humidity and Convective Available Potential Energy (CAPE), which did not correspond with any observed surface meteorology or SST gradient. Other signals appeared to reinforce this view; a step-function was evident in humidity time-series when the brand of radiosonde was changed; budget calculations based on the soundings predicted that some visibly rainy regions ought to have been cloud-free; during the pyrgeometer/RRTM comparisons described in Section 5.2.3, only two sets of independent soundings known to be reliable could be used, while the others clearly underestimated the longwave irradiance. Working with the radiosonde manufacturers, NCAR-ATD have found the source of the problem: calibration drift due to contamination of the radiosonde by its packaging material. A time-dependent correction algorithm has been developed (Cole and Miller 1999), and a schedule has been worked out for recalculation of the entire COARE soundings dataset. Guichard *et al.* (2000) confirm that the impact of this bias on the calculation of convective available potential energy (CAPE) in the tropics can be quite large. Meanwhile, ECMWF and

NCEP have postponed their planned high-resolution reanalysis of the COARE period pending this process. The consequences may well reach beyond COARE into other areas of climate research, reanalysis and data assimilation, which make use of historical atmospheric soundings.

The impacts of these humidity biases are likely to be enormous for numerical weather prediction models, which attempt to predict wind fields modulated by convection, responding to the observed thermodynamic profile. The observed errors would seriously distort the convection field in space and time, and produce unrealistic ocean-atmosphere coupling. An incorrect moisture field would certainly affect the dynamics of cloud-resolving models. The impact would also be of first order for the calculation of moisture budgets, particularly during light rainfall periods. However, the effect on longwave irradiance computed from RRTM using the COARE data (see Section 5.2.3) was not large; with humidity in the lowest 300m of the profile increased by the full 1g kg$^{-1}$, downwelling longwave was increased by only 1.5 Wm$^{-2}$. This calculation was for a tropical atmosphere, of course; in a drier atmosphere, the same increase of specific humidity would have a larger effect on the flux.

A similar problem has also recently been identified by ARM scientists with their CLASS radiosondes. They find that the new generation of high technology sensors, such as the microwave radiometer, can be used to detect radiosonde problems. At the ARM Southern Great Plains Central Facility, data from a Microwave Water Substance Radiometer (MWSR) is now used to scale radiosonde moisture profiles.

## 6.4 Radiative Fluxes by Remote Sensing

### 6.4.1 SW and LW fluxes from TOA radiances

The determination of the surface radiation budget (SRB) from satellite data involves measuring the radiative fluxes at the top of the atmosphere (TOA) and accounting for the effects of the atmosphere using a radiative transfer model (RTM). An obvious problem is allowing for the effects of clouds. It has proved easier to model the scattering and absorption of SW radiation than to model the effects of clouds on the LW radiation. The problem for LW is that the surface budget is dependent on the height of the lowest cloud, a quantity not easily determined by satellite. As a result there are significantly more products for surface SW than there are for LW.

The different algorithms differ in the cloud information used and the sophistication of the RTM. While various methods have been proposed that use the narrow band (visible) satellite radiances directly together with an RTM (e.g., Tarpley, 1979; Gautier *et al.*, 1980; Dedieu *et al.*, 1987; Stuhlmann *et al.*, 1990; Pinker and Laszlo, 1992) no extensive datasets have been produced. Most data sets are based on algorithms which have used cloud information from ISCCP. These cloud data have been retrieved from the narrow band satellite radiances using a method based on a radiative transfer model. Examples are the SW products from GEWEX SRB-1 (Whitlock *et al.*, 1995), and Bishop *et al.* (1997), and the SW and LW products of Rossow and Zhang (1995), Gupta *et al.*, (1999). While each of these products has used the ISCCP C1 data (280 by 280 km equivalent area grid boxes; 2.5 by 2.5 degree at the equator; number of grid boxes changing with latitude), the GEWEX SRB Version 2 will be based on ISCCP DX (pixel scale) data with correspondingly high resolution.

The goal of the CERES SRB is to reduce the error in the GEWEX SRB by a factor of two. In addition to the CERES broadband scanning instruments, the CERES data will be processed with simultaneous cloud imager data (VIRS on TRMM and MODIS on EOS-AM1); 3-hourly GEOS 2-3 meteorology (Schubert *et al.*, 1995); and 3-hourly operational geostationary satellite data. SRB retrievals will be validated and released 2-3 years after launch. Gridded products (1x1 degree) will eventually be available 3-hourly, daily, and monthly. Instantaneous SRB at the individual "footprints" of the broadband CERES scanner will typically have diameters of 10-50 km. One set of CERES retrievals of the SRB will be based on fast "surface-only" algorithms for SW (Li and Leighton, 1993) and LW (Inamdar and Ramanathan,

1997; Gupta *et al.* 1992); a second set will be based on "full-physics" radiative transfer (Fu and Liou, 1993), balancing CERES broadband TOA measurements (Charlock *et al.*, 1997).

More details of each of these various satellite based radiation products will be given in Section 11.3.3 where the products are evaluated.

*6.4.2 Longwave Net Flux from a combination of AVHRR and SSM/I*

This section describes a method to compute the longwave net flux, $R_L$, at the sea surface from a combination of AVHRR-derived sea surface temperature and SSM/I-derived atmospheric back radiation. For sea surface temperature $T_S$:

$$R_L = \bar{\varepsilon} R_L^{\downarrow} - \bar{\varepsilon} \sigma T_S^4 \qquad (6.6)$$

where $\bar{\varepsilon}$ is the spectrally integrated surface emissivity (which is close to 0.98, Gardashov *et al.*, 1988) and $\sigma$ is the Stefan-Boltzmann constant (see also equation 5.3).

Schlüssel *et al.* (1995) described a retrieval scheme of the atmospheric back radiation under clear and cloudy conditions from SSM/I measurements using three channels at 22, 37, and 85 GHz. This retrieval is based on the following consideration: about 80 % of the downwelling irradiance is emitted from the lower 500 m of the atmosphere (Schmetz, 1989) and is mostly emitted in the water vapour bands near 6.3 μm and above 20 μm, and to a lesser extent in the $CO_2$ band at 15 μm. As shown by Schulz *et al.* (1993) the SSM/I measurements contain information on the boundary layer water vapour content. Schlüssel *et al.* (1995) conclude that the irradiance emerging from the lower 500 m should be proportional to the product of the mean layer temperature and the absorption by the columnar water-vapour content of this layer, since the emitted flux density is proportional to the fourth power of the temperature according to the Stefan-Boltzmann law. Radiative transport calculations then showed that functions $f_1$ and $f_2$ are in fact closely correlated:

$$f(T_{22v}, T_{37h}) = \sigma(T_{22v}^4 - T_{37h}^4) \propto f_2(T_S, w_l) = \sigma T_S^4 (1 - e^{-w_l}) \qquad (6.7)$$

where $T_{22v}$ and $T_{37h}$ are the brightness temperatures for the 22Ghz vertically polarised and 37 GHz horizontally polarised channels respectively.

The RMS error for the retrieval scheme has been theoretically estimated to be 30 Wm$^{-2}$. It has been partly verified using simultaneously obtained pyrgeometer measurements, radiosonde data, and cloud observations from the TOGA-COARE and CEPEX experiments. The radiosonde data and the cloud observations have been used within radiative transfer simulations as another means for comparison. Considering hourly means, Schanz and Schlüssel (1997) stated a bias of -3 Wm$^{-2}$ and a standard deviation of 14 Wm$^{-2}$ for the comparison of pyrgeometer measurements and satellite retrieval and a bias of +3 Wm$^{-2}$ and the same standard deviation for the comparison of radiative transfer simulations with satellite retrieval. For monthly averages a RMS error of around 10 Wm$^{-2}$ is expected.

Combining the back-radiation retrieval with AVHRR derived sea surface temperature using equation (6.6) gives the net flux at the sea surface. This scheme has been used within HOAPS (Hamburg Ocean Atmosphere Parameters and Fluxes from Satellite Data) to retrieve longwave net fluxes with the same sampling as evaporation and precipitation.

An alternative method estimating net longwave fluxes $R_L$ directly from SSM/I measurements using neural networks has been published by Liu *et al.* (1997). The neural network technique has been used to better account for the non linearity between $R_L$ and the measured brightness temperatures. Validation attempts were restricted to 5 clear sky and 14 cloudy cases during the International Cirrus Experiment (ICE) in October 1989 over the North Sea. The comparison of the technique with pyrgeometer measurements revealed small errors for the clear sky cases but a large standard error (24 Wm$^{-2}$) for the cloudy cases. Liu *et al.* (1997) claimed that this error is probably caused by the spatial inhomogeneity of clouds in the field of view of the SSM/I. However a likely further source of error was the use by Liu *et al.* (1997) of an algorithm which excluded the 85 GHz channels (due to the malfunctioning of these

channels during 1989). However those channels are the most sensitive SSM/I channels to cloud particles and act as main predictors for the cloud signal in the Schlüssel *et al.* (1995) algorithm.

A comparison of the monthly mean of $R_L$ over the Atlantic for October 1989 reveals the best agreement with climatological values from Lindau (2000), but large discrepancies with the Isemer and Hasse (1985) climatology, and also with an ISCCP derived dataset (Darnell *et al.*, 1992), especially in regions with quasi-persistent maritime stratocumulus over the Atlantic west of the African coast. It can be argued that factors such as the solar breakup of stratocumulus during the day, which is not considered in ISCCP, account for a certain amount of this difference.

## 6.5  Surface Albedo

### 6.5.1  Ocean Surface Albedo

As mentioned in Section 5.2.2, sea surface albedo is the ratio of shortwave exitance to irradiance. The *broadband* albedo can be measured with a pair of pyranometers, one facing upward and the other downward, but as with upwelling longwave the latter must be mounted on a boom so that it does not "see" the platform. This presents obvious difficulties for ships on the open ocean. The seminal study of sea surface albedo is that of Payne (1972), who made comprehensive measurements from a platform in Buzzards Bay, MA (41°N), expressing the results in terms of only two parameters, solar altitude and atmospheric transmittance. The latter is the ratio of solar irradiance actually measured at the surface to that incident at the TOA, which can be simply calculated from knowledge of the solar constant, date, time and location (Paltridge and Platt 1976). Solar transmittance is affected by absorption or scattering from atmospheric constituents, mainly water vapour, ozone, aerosols and clouds. Thus, Payne's (1972) parameterisation actually relates to the varying ratio of diffuse to direct shortwave radiation. The Fresnel laws predict (and common observation confirms) that reflectivity at a water surface increases toward glancing angles of incidence. Generally speaking then, for high solar altitude and clear skies the albedo is small, but any increase in the diffuse component due to cloudiness will reduce the average angle of incidence and increase the albedo. For low solar altitude, the addition of cloudiness has the opposite effect.

Katsaros *et al.* (1985) confirmed Payne's albedo results during GATE at 7°N and JASIN at 60°N (both during summer), and their Figure 1 provides an excellent illustration of the effects of diffuse radiation, solar altitude and surface roughness on surface albedo. Albedo is expected to depend on wind speed through changing sea roughness, but Payne (1972) showed theoretically that the effect is small excepting for solar altitudes less than 30° with a clear sky. Within this restricted regime, Katsaros *et al.* (1985) combined Payne's observations with their own, and those of Simpson and Paulson (1979), to estimate that albedo decreased by 3.6% per ms$^{-1}$ for winds less than 12 ms$^{-1}$. At wind speeds above about 15 ms$^{-1}$, albedo increases due to the presence of whitecaps (Monahan and O'Muircheartaigh 1987).

Payne's (1972) empirical relationships are widely used in ocean-atmosphere studies, and to parameterise broadband albedo in numerical models. They were confirmed over the deep ocean with direct albedo measurements from a boom mounted forward of the bow of R/V Franklin over 20 days during COARE in the vicinity of 2°S. To avoid undue bias from the very large albedos at low sun elevations, daily average values were calculated as the ratio of total upwelling to downwelling radiant energy. For the typical conditions of predominantly light winds and relatively smooth seas, a constant albedo of 0.058 was found to apply to daily averaged air-sea heat flux with negligible error over using the diurnally variable values. This is the value incorporated into the COARE bulk flux algorithm (Section 7.4.1).

As the broadband albedo of the sea is a ratio of upwelling to downwelling flux, it is not an appropriate input for the spectrally resolved theoretical radiative transfer calculations made in GCM's or satellite-based retrieval algorithms. Rather, a radiative transfer model uses a spectral reflectance as an input, and the broadband albedo is determined from the ratio of its output fluxes. For example, the CERES retrievals of surface fluxes use the Fu and Liou (1993)

code and assume, following Bowker *et al.* (1985) and Payne (1972), spectral reflectances for diffuse SW:  0.0878 (0.2 to 0.7 μm), 0.0505 (0.7 to 1.3 μm), and 0.0163 (above 1.3 μm). Under clear conditions, these are adjusted with solar zenith angle.   A more rigorous treatment of the spectral bi-directional reflectance function (BRDF) of the sea has been developed by Hu (2000, *pers comm.*) using the Cox-Munk wind-speed wave distribution and a modified discrete ordinates scheme with 100 streams;  this is to be validated at the Chesapeake Lighthouse with measurements of upwelling spectral radiance.

Using data from aircraft-mounted instruments during the JASIN experiment (flight level 50m and solar altitude about 50°),  Katsaros *et al.* (1985) determined the sea surface albedo in three spectral bands.    In the shortest waveband (0.28 to 0.53 μm) albedo was almost independent of cloudiness at around 0.07,  whereas in the remaining visible (0.53 to 0.70 μm) and near-infrared (0.70 to 2.8 μm) bands albedo increased with cloudiness.   Observations that the broadband surface albedo under clouds exceeds the clear-sky value are widely reported. There are two main reasons; the change to the diffuse component referred to above, and the selective absorption of solar radiation by clouds at wavelengths greater than about 0.7 μm (Lindsay and Rothrock, 1994; Curry *et al.*, 1996).

*6.5.2  Albedo over sea ice*

The variability of albedo,  including its spectral dependence,  take on particular significance at high latitudes.   Lindsay and Rothrock (1994) tabulate values of albedo within pack ice ranging from 0.06 for smooth water, through 0.32 – 0.68 for various forms of melting ice, to 0.87 for fresh snow.   The effective albedo over a given region will depend on the relative areas of each type of surface present.    At these predominantly large solar zenith angles the proportion of ice to water is particularly critical.    It creates obvious problems for both representative measurement and modelling, leading Lindsay and Rothrock (1994) to devise an equivalent "potential open water fraction" based on surface temperature and albedo.   Drawing on a large number of previous studies, Ebert and Curry (1993) developed a surface albedo parameterisation which considers both spectral variation and solar zenith angle dependence. They find that the annual cycle of Arctic ocean broadband surface albedo ranges from about 0.48 during summer to 0.83 in winter.

Several authors (e.g. Shine, 1984; Lindsay and Rothrock,1994: Curry et al, 1996) emphasise the particular importance over high albedo surfaces of multiple reflections between the surface and cloud base,  which contribute substantially to the downward flux.   Shine (1984) presents a calculation method which takes account of this and finds that,  for reasonable cloud thickness, neglecting multiple reflections can incur errors in the surface net flux of 30% over bare ice and 50% over new snow.   On the other hand,  neglecting spectral variability of albedo seems to generate errors no greater than 1.5% in surface flux.   Pinto and Curry (1997) note that multiply reflected shortwave radiation from the high albedo surface will change the heating rate within the cloud layer, as well as modifying the flux at the surface itself.

**6.6  Summary - Parameterisation of Radiative fluxes**

In summary, parameterisations of both SW and LW radiation result in wide range of estimates of radiative fluxes.   More in-situ observations of radiative fluxes are needed in different regions, especially in the tropics to verify the parameterisations.   Although cloud correction is the most uncertain point of SW parameterisations developed for use with VOS data,  large uncertainties also result from the formulation of clear sky radiation. Use of two-level cloud cover can improve parameterisations of SW radiation, but there are still relatively few VOS reports which provide both total and low level cloud cover information. LW radiation estimates computed with different parameterisations largely depend on the data used to produce particular formula. These data are affected by regional variations in cloud conditions.

# 7  PARAMETERISATION OF TURBULENT FLUXES

## 7.1  Introduction

The parameterisation formulae are used for determining the turbulent fluxes from the basic variables such as wind speed, air temperature, etc.  The same "bulk formulae" are applicable whether the basic variables have been obtained by *in situ* measurement or by remote sensing,  or have been calculated by a numerical atmospheric model.   Thus these formulae are fundamental to flux estimation and therefore they will be discussed in some detail in this Chapter.

Until recently there was general agreement as to the form of the bulk formulae which, at the simplest,   could be written: $F \propto u_z \, C_z \, (\Delta s_z)$ where $F$ is the flux, $u_z$ is the wind speed measured at height $z$, and $\Delta s_z$ is the difference in value of the appropriate basic variable between height $z$ and the sea surface.   Written in this form,  most of the physical processes have been parameterised by the transfer coefficient $C_z$ which will vary with height, and stability (and possibly wind speed and other factors).   Since the form of the stability correction is thought to be reasonably well known, $C_z$ is normally represented by $C_{10n}$, the 10m neutral value (defined as that which would give the same flux given measurements at 10m height obtained under neutral atmospheric stability).   Depending on which flux is to be calculated (and the state of our knowledge),  $C_{10n}$ may be taken to be a constant value,  to have a simple wind speed dependence, or to have a more complicated variation with sea state and other factors.

While the standard bulk formula is designed to model turbulent transfers near a rough surface, in recent years experiments such as TOGA COARE have resulted in formulae which attempt to also take into account other physical processes. Now many versions of the formulae exist and new formulae are constantly being developed. At the same time,  many models have for many years used the older versions of the formulae, partly because "that is what they have always used" and there is the possibility that other processes in the model may have become tuned to the resulting flux values.

To try to bring some order to the present situation,  in this Chapter we will first describe the derivation of a "traditional" bulk formula for the surface fluxes. We will then summarise the present state of knowledge with regard to the roughness lengths (which determine the transfer coefficients).  Recent algorithms for the bulk formula will then be described.  Although many of the modifications have attempted to deal with low wind phenomena, these new formulae are being applied more generally.  Finally we will consider transfers in strong wind conditions.

## 7.2  Example of traditional "Bulk Aerodynamic" formulae

The aim of the stability dependent bulk formulae is to calculate the air-sea flux of momentum, sensible, or latent heat from mean values of the meteorological variables (wind speed $u$, air temperature $t$,  and humidity $q$) measured at some height $z$ above the surface, together with values of the sea surface temperature, $t_s$.  Although often considered to be purely empirical,  the formulae used can be derived from the dimensionless profile equations (which can themselves be derived using dimensional considerations and "similarity theory",  see for example Geernaert (1990) for a more detailed treatment):

$$\frac{kz}{u_*} \frac{\partial <u>}{\partial z} = \phi_m$$

(7.1a)

$$\frac{kz}{t_*} \frac{\partial <t>}{\partial z} = \phi_t$$

(7.1b)

$$\frac{kz}{q_*} \frac{\partial <q>}{\partial z} = \phi_q$$

(7.1c)

where $k$ is the von Karman constant, and the dimensionless profiles $\phi_x$ are each functions of the stability parameter $\zeta$ ($= z/L$ ). Here $L$ is the Monin-Obukhov length, defined by (e.g. Stull, 1988 p.180):

$$ L = \frac{T_v u_*^3}{g k \langle w' T_v' \rangle} $$

(7.2)

where $T_v$ is the virtual temperature of the air. The dimensionless profile functions have been determined experimentally. The correct form is critically dependent on the assumed value for k (Frenzen and Vogel, 1994). Edson *et al.* (1991) review several formulations for $\phi_m(z/L)$, modified where necessary on the assumption $k = 0.4$. The best performing formulae could be summarised by:

$$ \phi_m = \left(1 - \alpha(z/L)\right)^{-\beta} \qquad\qquad \zeta < 0 \qquad (7.3a) $$

$$ \phi_m = 1 + \gamma(z/L) \qquad\qquad \zeta > 0 \qquad (7.3b) $$

where values of $\alpha$ ranging from 16 to 28 all fitted the data to a similar degree and a value $\alpha = 20$ was chosen because it gave the best overall fit with $\gamma = 8$. In most formulations $\beta$ is 1/4 but some authors have suggested $\beta = 1/3$ as theoretically more consistent. For temperature and humidity (referred to by many authors as the scalar variables), it will be assumed that:

$$ \phi_t = \phi_q = \phi_m^2 \qquad\qquad \zeta < 0 \qquad (7.4a) $$

$$ \phi_t = \phi_q = \phi_m \qquad\qquad \zeta > 0 \qquad (7.4b) $$

where the $\phi_t$ relationship follows Paulson (1970). The assumption that $\phi_q = \phi_t$ seems reasonable but is based on very little evidence. In (7.1) the scale variables $u_*$, $t_*$ and $q_*$ are defined, using dimensional reasoning, by reference to the surface fluxes:

$$ u_*^2 = \langle u' w' \rangle = \frac{\tau}{\rho} $$

(7.5a)

$$ u_* t_* = \langle t' w' \rangle = \frac{H}{\rho c_p} $$

(7.5b)

$$ u_* q_* = \langle q' w' \rangle = \frac{E}{\rho L_v} $$

(7.5c)

Remembering that we need the formulae to allow the fluxes to be determined from measurements at some height $z$, (7.1) is integrated between the surface and the measurement height to give:

$$ u_z = u_0 + \frac{u_*}{k}\left( \ln\left(\frac{z_u}{z_0}\right) - \Psi_m \right) $$

(7.6a)

$$ t_z = t_0 + \frac{t_*}{k}\left( \ln\left(\frac{z_t}{z_{ot}}\right) - \Psi_t \right) $$

(7.6b)

$$ q_z = q_0 + \frac{q_*}{k}\left( \ln\left(\frac{z_q}{z_{oq}}\right) - \Psi_q \right) $$

(7.6c)

where $u_o$, $t_o$, and $q_o$ are the surface values and the stratification functions $\Psi_i$ represent the stability corrections to the profiles and are the integrals of the dimensionless profiles $\phi_i$ (Paulson, 1970):

$$\Psi_m = 2\ln\left(\frac{1+\phi_m^{-1}}{2}\right) + \ln\left(\frac{1+\phi_m^{-2}}{2}\right) - 2\tan^{-1}\phi_m^{-1} + \frac{\pi}{2}$$

$$\zeta < 0 \qquad (7.7a)$$

$$\Psi_m = 1 - \phi_m \qquad\qquad\qquad\qquad\qquad \zeta > 0 \qquad (7.7b)$$

$$\Psi_t = \Psi_q = 2\ln\left(\frac{1+\phi_t^{-1}}{2}\right)$$

$$\zeta < 0 \qquad (7.7c)$$

$$\Psi_t = \Psi_q = 1 - \phi_t \qquad\qquad\qquad\qquad \zeta > 0 \qquad (7.7d)$$

Note that in neutral stability $\phi_i = 1$ and $\Psi_i = 0$  Using Equation 7.6(a-c) to substitute for $u_*$, $t_*$ and $q_*$ in 7.5 (a-c) we can derive the bulk formulae:

$$u_*^2 = C_D\left(u_z - u_0\right)^2 \qquad\qquad\qquad (7.8a)$$

$$u_* t_* = C_H\left(u_z - u_0\right)\left(t_z - t_0\right) \qquad\qquad (7.8b)$$

$$u_* q_* = C_E\left(u_z - u_0\right)\left(q_z - q_0\right) \qquad\qquad (7.8c)$$

which define the transfer coefficients as the expressions:

$$C_D = k^2\left(\ln\left(\frac{z_u}{z_0}\right) - \Psi_m\right)^{-2}$$

$$(7.9a)$$

$$C_H = k^2\left(\ln\left(\frac{z_t}{z_{0t}}\right) - \Psi_t\right)^{-1}\left(\ln\left(\frac{z_u}{z_0}\right) - \Psi_m\right)^{-1}$$

$$(7.9b)$$

$$C_E = k^2\left(\ln\left(\frac{z_q}{z_{0q}}\right) - \Psi_q\right)^{-1}\left(\ln\left(\frac{z_u}{z_0}\right) - \Psi_m\right)^{-1} \qquad (7.9c)$$

From (7.9) it can be seen that the 10m neutral drag coefficient is:

$$C_{D10n} = k^2\left(\ln\left(\frac{10}{z_0}\right)\right)^{-2}$$

$$(7.10a)$$

which emphasises that the drag coefficient is directly related to the roughness length;  the two are interchangeable.  The transfer coefficients for heat and water vapour (the Stanton and Dalton numbers, respectively) depend on both the momentum roughness length and the heat and moisture roughness lengths:

$$C_{H10n} = k^2\left(\ln\left(\frac{10}{z_{0t}}\right)\right)^{-1}\left(\ln\left(\frac{10}{z_0}\right)\right)^{-1}$$

$$(7.10b)$$

$$C_{E10n} = k^2\left(\ln\left(\frac{10}{z_{0q}}\right)\right)^{-1}\left(\ln\left(\frac{10}{z_0}\right)\right)^{-1}$$

$$(7.10c)$$

## 7.3  Determining the Transfer Coefficients

### 7.3.1  Traditional bulk formulae

A. INTRODUCTION

The above discussion suggests that the transfer coefficients could be determined by obtaining, in some way, the various roughness lengths (7.10).   However in the traditional approach the transfer coefficients have been obtained by measuring the surface fluxes, using one of several techniques, together with measurement of the mean physical variables required (7.8).

Early work on air-sea exchange tended to focus on the momentum transfer between atmosphere and ocean. Synoptic methods, such as the slope of the surface or the geostrophic departure of the wind field, were used to estimate the wind stress on the ocean and obtain a drag coefficient. Later, application of classical boundary-layer laws relating the momentum flux (or stress) to the vertical wind gradient (e.g. (7.6a)), allowed a drag coefficient to be generated entirely from measurements of the vertical wind profile. Semi-empirical expressions for the diabatic flux-profile relationships established over land sites (e.g. Businger *et al.* 1971) enabled correction of the measured drag coefficient to its equivalent neutral value, and also to a standard reference height of 10m above the water surface, as set out in the previous section. Experimental studies on wind/wave interaction and the ocean drag coefficient proliferated, so that by the time Garratt (1977) published his comprehensive review of the subject, he was able to quote five previous reviews between 1951 and 1969 (his Table 1). Garratt (1977) goes on to list seventeen determinations of $C_{D10n}$ between 1967 and 1975, most of which obtained the stress by the direct method, covariance (see Section 5.3.1).

For the scalar (sensible and latent heat) fluxes, Pond et al (1974) examined results for $C_{H10n}$ and $C_{E10n}$ determined from profile measurements, while Friehe and Schmitt (1976) compiled data from nine experiments all using covariance fluxes. However, it was the much-quoted comparison of ten common bulk transfer coefficient schemes by Blanc (1985) which drew attention to the substantial differences between these schemes, and quantified the consequent uncertainty in flux estimates. This review also highlighted the limited wind speed range over which many of the schemes had been verified. There were virtually no determinations above 14 ms$^{-1}$, where exchange of heat and moisture begin to be complicated by spray droplets, or below 4 ms$^{-1}$, a common situation in the climatically important region of the tropical oceans. Improved parameterisation of the fluxes in both of these regimes was badly needed for numerical climate models.

Some of the more frequently used results from recent traditional determinations of the exchange coefficients are discussed briefly below. It is common practice to plot the neutral exchange coefficients against the 10m wind, as Blanc (1985) does, although the possibly of dependence on other factors should be borne in mind.

B. WIND STRESS

For wind stress, the drag coefficient values used in many past studies were those obtained by Large and Pond (1981, 1982) or Smith (1980, 1988). Although these studies used both eddy correlation and inertial dissipation stress data, the bulk of the Large and Pond results were obtained with the latter technique (see Section 5.3.2). For 10m wind speeds $u_{10}$ between 3 and 10 ms$^{-1}$ they found a constant value ($10^3 C_{D10n} = 1.12 \pm 0.2$), and for $u_{10}$ between 10 and 25 ms$^{-1}$ suggest a linear increase given by ($10^3 C_{D10n} = 0.49 + 0.065 u_{10}$). Other schemes suggest a linear relation over the entire range of validity; Garratt (1977) gives ($10^3 C_{D10n} = 0.75 + 0.067 u_{10}$) valid from 4-21 ms$^{-1}$ and Smith (1980) gives ($10^3 C_{D10n} = 0.61 + 0.063 u_{10}$) from 6-22 ms$^{-1}$ (Figure 7.1).

These upper wind speed limits are supported by very few observations, and are best regarded as extrapolations from the lower wind regime where data is more plentiful and more reliable. However Yelland *et al.* (1998) used a large data set from the Southern Ocean, obtained using the inertial dissipation technique, to effectively confirm the Smith (1980) eddy correlation derived formula for open ocean wind stress for wind speeds between about 6 and 20 ms$^{-1}$. Above 20 ms$^{-1}$ the Smith (1980) formula possibly underestimates the wind stress, the Smith (1988) formulation (a reinterpretation of the 1980 results based on the Charnock formula, and presented in tabular form) under-estimates significantly at higher wind speeds.

As the wind decreases below about 2 ms$^{-1}$, Smith (1988) suggested that $C_{D10n}$ would increase due to viscous effects. However, the significantly greater $C_{D10n}$ values for winds below about 5 ms$^{-1}$ predicted by Wu (1994) appear to be a better fit to the data of Bradley *et al.* (1991) and Yelland and Taylor (1996) (however see discussion in section 7.4.2B).

Figure 7.1 Examples for the Drag Coefficient, $C_{D10n}$ ,plotted as a function of wind speed, $U_{10n}$
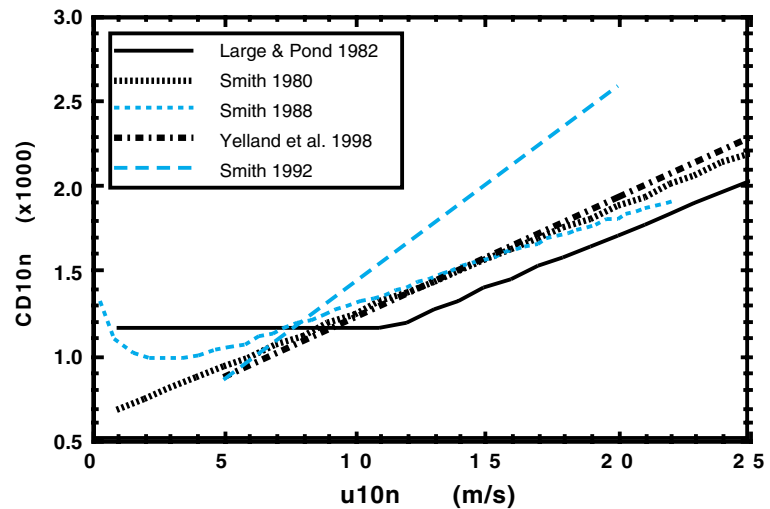
## C. SENSIBLE AND LATENT HEAT

Unlike the drag coefficient, traditional estimates of $C_{E10n}$ and $C_{H10n}$ over the ocean tend to support a fairly constant value over a wide range of wind speed.  Instrumentation problems, partly caused by exposure to the salt environment, have limited the number of reliable determinations and there is still at least 10% uncertainty in their values and hence in the derived fluxes.  Friehe and Schmitt (1976) recommend a constant Dalton number ($10^3 \ C_{E10n}$ =1.32 $\pm$ 0.07) on the basis of several turbulence-based datasets where the highest wind speed was 4 ms$^{-1}$.  After a critical assessment of previous studies, Smith (1989) also suggested a constant "consensus" value ($10^3 \ C_{E10n}$ =1.2 $\pm$ 0.1) for winds between 4 and 14 ms$^{-1}$.   The Humidity EXchange Over the Sea (HEXOS) experiment results (DeCosmo *et al.*, 1996)  also suggest a near constant value (any increase being less than 15 to 20%)  with ($10^3 C_{E10n}$ , = 1.12 $\pm$ 0.24 ) for winds up to 18 ms$^{-1}$.

For the Stanton number, Friehe and Schmitt (1976) obtained slightly different values for unstable and stable conditions ($10^3 \ C_{H10n}$  =  0.97 and 0.86 respectively), and proposed that the dissimilarity with their Dalton number was partially an effect of the classical ratio of the thermal to species diffusivities (Prandtl/Schmidt numbers),  $C_E/C_H$ = 1.16.   Smith (1988) suggested $10^3 \ C_{H10n}$ = 1.0 which is consistent with this ratio and his value of  $C_{E10n}$ .  In contrast DeCosmo *et al.* (1995) suggest that ( $C_{E10n} \approx C_{H10n}$) for the high wind HEXOS results, to the accuracy of their determination.

Given that the drag coefficient, and hence the roughness length, increases with wind speed, a constant value for the Dalton number,  implies that the humidity roughness length decreases with increasing wind speed (see (7.10b,c)).   In explanation,  Liu *et al.* (1979) suggested that, whereas momentum is transferred by pressure differences as well as by molecular forces, heat and moisture are transferred only by molecular diffusion which becomes less efficient as the roughness increases and sheltering occurs between the wave troughs.

For the low wind speed regime, the transfer coefficients,   $C_{E10n}$ and $C_{H10n}$, have been found to increase as the wind decreases below about 2 ms$^{-1}$ (Bradley  *et al.*, 1991) as predicted by Liu *et al.* (1979) (see section  7.3.2C).

### 7.3.2 *New bulk formulae*

## A INTRODUCTION

The remaining uncertainty in the specification of transfer coefficients, and the consequent limited accuracy with which fluxes could be calculated from bulk formulae, became unacceptable in the context of climate models and particularly in attempts to couple ocean and

atmospheric models. Along with improved instruments and further experimental studies, new bulk formulae have been developed aimed at incorporating better physical descriptions of the transfer process. These newer bulk formulae differ from the traditional approach with regard to the transfer coefficients in several ways. Typically, the momentum roughness length, $z_o$ , is obtained from a formula which takes sea state into account, and the roughness lengths for temperature and humidity are calculated from $z_o$ by considering the transfer of heat through the interfacial boundary layers, so-called "surface renewal theory" (Liu and Businger 1975; Brutsaert 1975). They also seek to extend the wind speed range over which the algorithm is applicable, particularly into the climatically important low-wind, convective regime. In this respect, improved convective flux/gradient relationships have been incorporated, and steps taken to overcome the fundamental singularity in the bulk formula as the wind speed approaches zero.

### B MOMENTUM ROUGHNESS LENGTH, $Z_0$

The aerodynamic roughness length, $z_o$ , appears as the integration constant in (7.6a); it is the height at which the wind velocity extrapolates to zero on the logarithmic wind profile under neutral conditions. Considerable efforts have been made in the disciplines of fluid mechanics, engineering and micrometeorology to relate $z_o$ to the geometrical properties of various natural and fabricated surfaces and some empirical generalities have emerged (e.g. Figure 4.1 of Garratt 1992). Over most rigid land surfaces $z_o$ may be obtained from the neutral wind profile (and its value is nowadays cross-checked by measuring all the other quantities in (7.6a)). Panofsky and Dutton (1984) give values of $z_o$ for various surfaces, from which we note that the sea is very "smooth". The associated small velocity gradient make both $z_o$ and $u_*$ extremely difficult to measure accurately using the profile method, especially from shipboard. Furthermore, the sea surface geometry and roughness alter continuously with varying windspeed. It has therefore become common practice to specify the roughness length independently, drawing on the methods of classical fluid dynamics (Schlichting, 1968, Chapter XX).

Kraus and Businger (1994, Chapter 5) describe in detail the application of this work to the air-sea interface, so we discuss only the basic issues here as they relate to current flux algorithms. It is common to characterise the surface and the wind flow regime in terms of the roughness Reynolds number:

$$R_r = u_* z_0 / v \qquad (7.11)$$

where $v$ is the kinematic viscosity of air. When $R_r < 0.13$, aerodynamically "smooth" flow exists when the roughness elements lie entirely within the viscous sublayer at the surface. The concept of a viscosity dependent transfer regime is important in the context of surface renewal discussed below. In smooth flow, classical experiments show that:

$$z_0 = 0.11 v / u_* \qquad (7.12)$$

With increasing windspeed the flow becomes aerodynamically "rough" when $R_r > 2.5$, as the stress is dominated by pressure and viscous forces around the surface roughness elements. In this regime over a rigid surface, $z_o$ (and $C_{Dz}$) is independent of windspeed, but a water surface responds to the varying wind stress continuously by changing its roughness. Charnock (1955) argued for proportionality of the two quantities, and on dimensional grounds proposed a relation for rough flow over the sea:

$$z_0 = \alpha_c u_*^2 / g \qquad (7.13)$$

where $\alpha_c$ is referred to as Charnock's constant, for which values between 0.010 and 0.035 can typically be found in the literature (Garratt 1992, Table 4.1). Fairall et al. (1996a) present values of $\alpha_c$ as a function of $R_r$ and conclude that the "best" value to use in the COARE bulk flux algorithm (see below) was 0.011. However in the open ocean, the near linear increase of $C_{D10n}$ with wind speed (Yelland et al. 1998) implies that $\alpha_c$ increases to around 0.018 at about 20 ms$^{-1}$ (Hare et al. 1999).

Roughly speaking, flow over the ocean is smooth below a 10 m windspeed of about 2 ms$^{-1}$ and fully rough above 8 ms$^{-1}$; between these limits there is a transition regime. Smith (1988) therefore proposed:

$$z_0 = \alpha_c \frac{u_*^2}{g} + 0.11 \frac{v}{u_*}$$

(7.14)

valid for the entire smooth to rough flow regime, a scheme which is being increasingly adopted in bulk flux algorithms (Fairall *et al.* 1996a; Zeng *et al.* 1998). Kraus and Businger (1994, figure 5.3) illustrate the form of this relationship.

The wide range of empirical values found for $\alpha_c$ have led to suggestions that it is not a constant, but dependent on what may loosely be called "sea state". The complicated topography of the ocean surface depends strongly on the interaction between wind and waves, which has been an active field of study and controversy for the past half-century. Claims have been made for relationships between the drag coefficient (or equivalently $z_0$) and various wave characteristics and influences. For example, several sets of observations over shallow water sites appear to give higher drag coefficient values than those over the open ocean (Geernaert 1990, Figure 8). This has prompted modification of Charnock's relationship to make $\alpha_c$ dependent on wave parameters, particularly the wave age:

$$w_a = c_p / u_*$$

(7.15)

where $c_p$ is the phase speed of the dominant waves at the peak of the locally wind-driven wave spectrum (Melville 1977, Nordeng 1991, Donelan *et al.* 1993). The notion is that younger waves, developing as a result of limited coastal fetch, limited duration, or steepening due to shallowing depth, travel slower than the wind and absorb more momentum, therefore appearing to be rougher.

Wu (1968) rationalised Charnock's expression as an "equation of state characterising equilibrium interaction between the wind and waves with gravity waves as the roughness elements", and suggested that capillary waves contribute significantly to the stress at intermediate wind speeds, implying a dependence on surface tension and viscosity of the water. On this basis Wu (1968) proposed an expression for $z_0$ due to capillary waves, and subsequently (Wu 1980) a further refinement to the Charnock relationship for separating flow behind "short waves superimposed on the dominant waves in the ocean".

During the HEXOS experiment near the coast of Holland, Smith *et al.* (1992) found the relationship:

$$z_0 = \frac{0.48}{w_a} \frac{u_*^2}{g}$$

(7.16)

effectively modifying the Charnock "constant" to accommodate the range from very young waves ($w_a \approx 5$ ; $\alpha_c = 0.096$) to mature waves ($w_a \approx 30$ ; $\alpha_c = 0.016$). Komen *et al.* (1998) reviewed various formulations for the Charnock parameter and concluded that, of those available the HEXOS relationship (7.16) had the advantage of fitting data sets ranging from the open ocean to the short fetch Lake Ontario data of Donelan (1982). However reanalyses of the HEXOS data by Janssen (1997) and Oost (1998) questioned the validity of (7.16). For example, Oost (1998) suggested that at least some of the enhanced stress values were caused by shoaling waves. When those data were excluded, Equation (7.16) was valid only for the youngest waves ($w_a < 13$). Similarly, Yelland (2000) found little difference in stress values for the open North Atlantic and the region of the HEXOS experiment. However data collected from the shallower North Sea regions did show higher stress values.

Bourassa *et al.*(1999) proposed an air-sea interaction model which, for $z_o$, used the root-sum-of-squares of Wu's (1968) capillary wave parameterisation and the wave-age modified Charnock expression of Smith *et al.* (1992):

$$z_0 = \left[ (\beta_c \frac{b\sigma}{u_*^2 \rho_w})^2 + (\beta_g \frac{0.48}{w_a} \frac{u_*^2}{g})^2 \right]^{1/2}$$

(7.17)

Here $\sigma$ is surface tension, $\rho_w$ the water density, $b$ is Wu's parameter (modified by Bourassa *et al.*), and $\beta_c$, $\beta_g$ are weights for capillary and gravity waves respectively, based on physical factors. Capillary waves are the dominant roughness for windspeed < 7 ms^{-1} and short gravity waves for wind > 7 ms^{-1}. Other aspects of the bulk flux model of Bourassa *et al.* (1999) will be discussed below (section 7.4.2B).

Wave age is not necessarily a function of fetch alone; in the open ocean a sudden change in windspeed due to passage of a frontal system, for example, can produce a non-equilibrium wave/stress situation. Indeed, the effects of wave age as predicted by (7.16) can be significant. For example Gulev and Hasse (1998) estimated sea state dependent wind stress, by computing wave age from the wave periods reported by Voluntary Observing Ships. They used the sea period, arguing that, by definition, swell is not related to the local wind, and that it is the interaction of the local wind with wind sea that determines the part of the wind stress caused by waves. Computing the drag coefficient from (7.16) they found differences between wave-age-based and traditional estimates to be quite pronounced in the mid latitudes and tropics, with wave induced stress contributing up to 20 % of the total stress estimate in wintertime.

The occasionally large $C_{D10n}$ values predicted by wave age based formulae have led Yelland *et al.* (1998) to question whether the roughness depends on wave age. Their large dataset obtained during three cruises to the Southern Ocean showed no evidence for wave-age dependence of the wind stress nor of the high values predicted for storms. Furthermore, using a buoy mounted sonic anemometer system, Taylor *et al.* (1999b) found no variation of roughness for wave ages from 10 to over 30. Janssen (1999) suggested that this was because the data were obtained using the inertial dissipation method, but this was disputed by Taylor and Yelland (2000b) who emphasised that Janssen's arguments, if true, would have led to an enhanced wave age dependence in their data set. Examining the published data from a number of field experiments, Taylor and Yelland (2000c) proposed a different roughness length formulation:

$$\frac{z_o}{H_S} = A \left( \frac{H_S}{L_p} \right)^B$$

(7.18)

where $H_s$ and $L_p$ were defined as the significant wave height and peak wavelength for the combined sea and swell spectrum. The suggested values for the coefficients were $A$ = 1200, $B$ = 4.5. The character of the $C_{D10n}$ values derived from (7.18) are significantly different from those predicted by wave age based formulae. Short duration or fetch do not result in enhancement of the roughness. Thus the $C_{D10n}$ values predicted for a pure wind sea always have a similar relationship to the wind speed. At most wind speeds these pure wind sea values were higher than is observed in the open ocean. However the typical mean open ocean values were predicted when (7.18) was applied to wave measurements which were dominated by mixed wind sea and swell. Thus Taylor and Yelland (2000c) claimed that (7.18) successfully predicted the observed values of $C_{D10n}$ for the open ocean, coastal seas, lakes, and even wind-wave flumes. This is a wider range of conditions than those for which wave age based formulae have been found to hold. However they were unable to predict the large $C_{D10n}$ values observed by Donelan (1982) at very short fetch on Lake Ontario and questioned whether the upwind roughness over land had affected these data.

In summary the present position is that, despite decades of work on wind-wave interactions, the parameterisation of $z_0$ in terms of sea state is still a matter of considerable controversy. A problem is that, for the wave age based formulae to be valid, there must be a wave age dependence of the short waves (wavelength $\approx$ 10cm). However, at present, there is no direct proof for or against this (Komen *et al.* 1998). This uncertainty in $z_0$ also affects our knowledge of $C_E$ and $C_H$.

C  SURFACE RENEWAL THEORY

Analogous to the momentum roughness length, surface length scales for the scalar quantities appear in the equations involving temperature and humidity (Section 7.2). The model of Liu *et al.* (1979) was one of the first to deal with air-sea transfer in the low wind-speed regime, and to derive the scalar roughness lengths from the principles of "surface renewal theory". This theory was introduced many years ago in chemical engineering applications, and applied to the air-sea interface by Liu and Businger (1975) and independently by Brutsaert (1975). Here we will briefly outline the development leading to the Liu *et al.* (1979) bulk algorithm (hereafter LKB).

Whereas the atmospheric (and oceanic) surface boundary layer transports heat, mass and momentum to the interface by turbulent motions, at the surface itself there exists an interfacial layer of order 1 mm thick, in which molecular diffusion plays a significant role in the transport. The idea behind surface renewal theory is that, across this interfacial layer, small eddies of air transfer heat randomly and intermittently between the "bulk" turbulent fluid, of temperature $T_b$, and the surface itself which therefore warms or cools by conduction from the eddies. The temperature gradient and the surface heat flux are determined by the heat conduction equation:

$$\frac{\partial T}{\partial t} = \kappa \frac{\partial^2 T}{\partial z^2}$$

(7.19)

where $\kappa$ is the thermal diffusivity. The solution for initial condition $T(t=0) = T_b$ = constant, and surface temperature $T(z=0) = T_s$ = constant (Carslaw and Jaeger, 1959) gives the surface heat flux :

$$H(0,t) = -\kappa \rho C_p (\frac{\partial T}{\partial z})_{z=0} = \frac{\kappa \rho C_p (T_s - T_b)}{(\pi \kappa t)^{1/2}}$$

(7.20)

Liu and Businger (1975) define a distribution function to describe the areal fraction of eddies which have been in contact with the surface for time $t$, and assume a characteristic time, $t_c$, for which an eddy remains in contact with the surface before breaking away. For constant $T_s$ and a random distribution of contact duration they determine the time-averaged temperature profile in the interfacial layer as:

$$\frac{(T - T_s)}{(T_b - T_s)} = 1 - \exp\left(\frac{z}{(\kappa t_c)^{1/2}}\right)$$

(7.21)

and average heat flux:

$$H = \frac{\kappa \rho C_p (T_s - T_b)}{(\kappa t_c)^{1/2}}$$

(7.22)

For the scaling length $(\kappa t_c)^{1/2}$ , LKB substitute $\delta T$, the thickness of a layer in which the same heat flux and temperature difference would be maintained solely by molecular diffusion.

Similar relations to (7.21) and (7.22) can be derived for moisture and momentum transport:

$$\frac{Q - Q_s}{Q_b - Q_s} = 1 - \exp(-\frac{z}{\delta_Q}); \quad \delta_Q = \varepsilon \rho (Q_s - Q_b) / E = (\varepsilon t_c)^{1/2} \qquad (7.23a)$$

$$\frac{U - U_s}{U_b - U_s} = 1 - \exp(-\frac{z}{\delta_U}); \quad \delta_U = \nu \rho (U_s - U_b) / \tau = (\nu t_c)^{1/2} \qquad (7.23b)$$

where $\varepsilon$ is the molecular diffusivity of water vapour and $\nu$ the kinematic viscosity. With the scale variables, $u_*$ , $t_*$ , $q_*$ as defined in (7.5), the above relations can be written:

$$(T - T_s) / t_* = S[1 - \exp(-zu_* / S\kappa)]$$

(7.24a)

$$(Q - Q_s) / q_* = D[1 - \exp(-zu_* / D\varepsilon)] \qquad (7.24b)$$

$$(U - U_s) / u_* = C[1 - \exp(-zu_* / Cv)] \qquad (7.24c)$$

where "sublayer parameters", sometimes referred to as inverse interfacial Stanton and Dalton numbers (Brutsaert 1982) are given by:

$$S = (T_b - T_s) / t_* = \delta_T u_* / \kappa \qquad (7.25a)$$

$$D = (Q_b - Q_s) / q_* = \delta_Q u_* / \varepsilon \qquad (7.25b)$$

and the inverse interfacial drag coefficient:

$$C = (U_b - U_s) / u_* = \delta_U u_* / v \qquad (7.25c)$$

Brutsaert (1975) suggested that the renewal time scale $t_c$ be proportional to the time scale of Kolmogorov eddies:

$$t_c = (v z_o / u_*^3)^{1/2} \qquad (7.26)$$

which, combined with the relations for sublayer thickness (7.21) indicates that the sublayer parameters can be expressed in terms of the roughness Reynolds number (7.11)), the Prandtl number, $Pr$ (= $v/\kappa$) and the Schmidt number, $Sc$ (= $v/\varepsilon$).

$$S = GRr^{1/4} Pr^{1/2}$$

$$D = GRr^{1/4} Sc^{1/2}$$

$$C = GRr^{1/4} \qquad (7.27)$$

where $G$ is a proportionality constant determined empirically by LKB as 9.3.

LKB match the exponential sublayer profiles (7.24) smoothly with the slope of the outer turbulent logarithmic profiles (7.6) via a transition layer. This leads to a relationship between the scalar roughness lengths ($z_{0T}$, $z_{0Q}$) and the momentum roughness length via the roughness Reynolds number. As they show, the resulting continuous temperature and velocity profiles agree well with laboratory and field experiments; the profile for moisture (and other scalar quantities) is assumed similar to temperature. LKB (their Figs. 6 and 7) illustrate their model for the roughness scalar lengths compared with a small number of field measurements, and parameterise the relationship in the form:

$$R_t = \frac{z_{ot} u_*}{v} = a R_r^{b} \qquad (7.28a)$$

$$R_q = \frac{z_{oq} u_*}{v} = c R_r^{d} \qquad (7.28b)$$

where the values $a$, $b$, $c$ and $d$ were determined from field experiments by LKB and given in tabular form.

Brutsaert (1982) also matched the sublayer and logarithmic profiles, but assumed different sublayer constants and velocity behaviour. This leads to significant differences between his model and that of LKB, as illustrated by Fairall *et al.* (1996a) for the neutral moisture exchange coefficients and for the functional dependence of $R_q$ and $R_r$. Other variations on the application of surface renewal theory will be discussed below in the context of recent bulk flux models.

The physics and thermodynamics of the interfacial sublayers applies at both sides of the interface. Soloviev and Schlüssel (1994, 1996) have developed models of ocean-atmosphere gas transfer, applying surface renewal theory to the sublayer on the ocean side of the interface, otherwise referred to as the cool skin. They explore the sources of convective instability which control the sweeping and breaking away of the turbulent eddies. In this case, both heat and salinity fluxes play a role; Soloviev and Schlüssel (1996) point out that under low wind speed conditions, solar heating can damp the convective instability, increasing the renewal time and reducing gas transfer across the sublayer.

## 7.4 Bulk formulae for light to moderate wind conditions

### 7.4.1 *The TOGA COARE algorithm*

A. BACKGROUND

Process studies such as GATE, COARE, ASTEX, HEXOS etc. are closely focussed experiments designed to describe, improve our knowledge of, and to quantify certain aspects of the ocean-atmosphere climate system. While they may be limited in extent and scope in global terms, they nevertheless provide the basic relationships and parameterisations of physical processes needed within the broader framework of global atmospheric and oceanic studies, and of climate models. Thus, within the overall aims of TOGA, TOGA-COARE was designed to answer specific questions about energy exchange, convective processes and scale interactions in the west Pacific warm pool (Webster and Lukas 1992). Various considerations led to the requirement that the net air-sea energy exchange be specified to an accuracy of about 10 $Wm^{-2}$ of which the allowable uncertainty in the turbulent flux components would be 6-7 $Wm^{-2}$ . This leads to limits on permitted errors in the mean variables used to calculate bulk fluxes, wind speed = 0.2 $ms^{-1}$, sea and air temperatures $T_s$ , $T_a$ = 0.2 K, specific humidity $q$ = 0.2 g $kg^{-1}$, assuming that they are independent.

It is likely that the COARE surface observations have experienced closer scrutiny and more rigorous quality control than any previous similar data set. Details are given in the various Flux Group workshop reports (Bradley and Weller 1995a, b; 1997; Bradley *et al.* 1997) (also on the COARE Data Users web site: http://www.ncdc.noaa.gov/coare/ ). These observations have been used as a benchmark to develop and validate various models of the tropical ocean-atmosphere climate system, including remote sensing and surface flux bulk algorithms. The TOGA-COARE algorithm was developed early in the post-experiment analysis, by Fairall *et al.* (1996a), to provide common code for use by the COARE research community

B. ALGORITHM HISTORY

The algorithm was based on the model of Liu *et al.* (1979, LKB), to take account of the light wind, strongly convective conditions commonly found over tropical oceans. Some additional physics has been incorporated and, on the basis of data from COARE and other recent field programmes, some empirical constants have been adjusted. Version 1.0 was released in November 1993, and included various modifications to the basic LKB code. Following Smith (1988) the momentum roughness length (and hence $C_{d10n}$) was specified as the sum of the Charnock formula and a smooth flow limit; i.e. (7.14), with the value $\alpha_c$ = 0.011 evaluated from the Moana Wave direct flux measurements. The interfacial specific humidity was calculated from the saturated vapour pressure at sea surface temperature, appropriate to a salinity of 34 psu; i.e. reduced by 2% relative to the saturated vapour pressure over fresh water at the same temperature (Kraus and Businger 1994).

Like LKB the Monin-Obukhov stability length, $L$ (7.2), was calculated using virtual potential temperature, defined in full here to emphasise the point that the contribution of moisture to buoyancy is usually of first order over tropical oceans:

$$L = \frac{T(1+0.61q)u_*^2}{gk\left[t_*(1+0.61q)+0.61Tq_*\right]} \qquad (7.29)$$

where the scaling parameters, $u_*$ , $t_*$ , $q_*$ , were defined in. (7.5). However, the dimensionless profile functions were given a form that asymptotically approached the proper convective limit as wind speed goes to zero (Garratt 1992). In this "free convection" regime, the dimensionless scalar profile functions are expected to follow a $(z/L)^{-1/3}$ dependence. The form:

$$y = \left[1 - \gamma(z/L)\right]^{-1/3} \qquad (7.30)$$

was adopted for both velocity and scalar dimensionless profiles, with the empirical constant $\gamma$ = 12.87, which leads to stratification functions of the form,

$$\psi_c = 1.5 \ln\left[\frac{y^2 + y + 1}{3}\right] - \sqrt{3} \arctan\left[\frac{2y + 1}{\sqrt{3}}\right] + \frac{\pi}{\sqrt{3}} \qquad (7.31)$$

As stability approaches neutral conditions, the function was blended to a standard Kansas type (7.7) (Businger *et al.* 1971). For stable conditions, the Kansas form $\psi = -4.7(z/L)$, which follows from (7.3b) with $\gamma = 4.7$, is used for both momentum and scalar profiles.

Following Godfrey and Beljaars (1991), the wind speed in the bulk expression was augmented by a gustiness velocity, $W_g$, such that the wind speed, $S_U$, becomes:

$$S_U = u_x^2 + u_y^2 + W_g^2 = U^2 + W_g^2 \qquad (7.32)$$

where $u_x$ and $u_y$ are the mean wind components (i.e., magnitude of the mean wind vector) and $W_g$ is proportional to the convective scaling velocity, $W_*$ (Deardorff 1970):

$$W_*^3 = \frac{g}{T}\left[\frac{H}{\rho C_p} + 0.61T\frac{E}{\rho L_V}\right]z_i . \qquad (7.33)$$

where $z_i$ is the depth of the convective boundary layer. Thus $W_g = \beta W_*$, and a value $\beta = 1.2$ was adopted on the basis of the Moana Wave direct flux measurements in COARE. A reasonable default value for the depth of the marine boundary layer in the tropics is $z_i = 600$m.

The major modification for Version 2.0 (August 1994) was the inclusion of optional models for the cool skin temperature effect and the diurnal thermocline to correct bulk water temperatures to true SST. The cool skin model was based on Saunders (1967) with a modification to include the effects of buoyancy flux. This indicates a cool skin of about 0.3°K during the night. During the day the cool skin may be reduced or apparently eliminated entirely by solar heating in the upper layer of the ocean (Soloviev and Schlüssel 1994). A warm layer model was added to correct bulk water temperature measurements made at some depth, $z_b$. The idea is that ship intake and buoy temperature sensors at a metre or so depth are unable to resolve the diurnal warm layer which commonly forms in the upper tropical oceans under light wind conditions. This model was based on a simplified scaling version of the Price, Weller and Pinkel (1986) mixing model. If daytime solar heating is sufficient, a stable near-surface layer is formed causing the surface temperature to increase. Linear profiles of temperature and current are assumed. The depth is determined by a critical Richardson number and the profile of absorption of solar energy in the water (Paulson and Simpson 1981). The physics of both the cool skin and warm layer models are described in Fairall *et al.* (1996b)

Under very light wind conditions, peak solar warming as great as 4°K is produced with a warm layer depth of about 0.25 m. Once the warm layer forms, its depth and intensity are determined by integrating the accumulated momentum and heat input in the layer. Thus, this model requires a complete time series of data throughout the diurnal cycle; appropriate time resolution is from ten minutes to one hour. Both the cool skin and warm layer models can be disabled if true skin surface temperature is available (e.g. from aircraft or satellites with IR radiometers).

Calculation of fluxes of momentum (Caldwell and Elliott, 1971) and sensible heat due to rainfall were included, with raindrops assumed to be 0.2°K cooler than the surface wet-bulb temperature (Gosnell, Fairall and Webster, 1995). The so-called Webb correction to latent heat flux, which arises from the requirement that the net dry mass flux be zero (Webb *et al.*, 1980), is also calculated in the algorithm.

The last major modifications to the algorithm were made at the COARE Air-Sea Interaction (Flux) Group Workshop in Honolulu, 2-4 August 1995 (Bradley and Weller, 1995b). Transfer coefficients were adjusted by six percent to give better average agreement with covariance latent heat fluxes from several COARE ships. At the Woods Hole workshop, 9-11 October 1996 (Bradley and Weller, 1997) it was agreed that no further development would be attempted to the community version of the COARE Bulk Flux Algorithm, and that a version

2.5b bulk algorithm "package" would be made available, consisting of the Fortran source code and a test data set. This was released at a meeting of the Flux Group at NCAR, 14-16 May 1997 (Bradley *et al*., 1997)[1].

The formalism of the COARE algorithm is fully described in Fairall *et al*. (1996a). It has been used with success in subsequent field observations from ships and aircraft, both in equatorial and mid-latitude regions; a sample list of publications in which the COARE algorithm has been used appears in Bradley *et al*. (1997). During an ocean mixed layer heat budget experiment by R/V Franklin in the Indian ocean in 1996, using the COARE algorithm for the sensible and latent heat fluxes, closure was obtained to within the equivalent of about 3 $Wm^{-2}$ over a 7-day period (Godfrey *et al*. 1999).

The major limitation of the COARE algorithm is that it has not been verified above about 12 $ms^{-1}$ windspeed. In it's published form there are two factors which could impede its use in numerical models. Although the iteration around exchange coefficients, stability and fluxes normally converges within 5 iterations, except for very stable conditions, the code still retains the original 20 loops. Also, the use of complete functional forms for parameters such as $g$, $L_v$ and $v$, and the inclusion of all minor flux corrections in pursuit of the COARE 10 $Wm^{-2}$ accuracy goal, may be regarded as superfluous at this stage.

The authors have released[2] for trial a new version 2.6 (Bradley *et al*. 2000) which addresses these limitations and introduces other recent analytical developments, as follows:

1.     The empirical constants in the convective portion of the profile functions have been changed for improved matching to direct profile observations (Grachev *et al*., 2000)

2.     The Kansas stable profile functions have been replaced by those from Beljaars and Holtslag (1991) based on new profile data taken over the Arctic ice cap.

3.     A fixed value of the Charnock parameter ($\alpha_c$= 0.011) has been replaced by a formulation with a simple wind-speed dependence above 10 $ms^{-1}$ based on data from Yelland and Taylor (1996) and Hare *et al*. (1999).

4.     The Liu *et al*. (1979) scalar roughness relationship [$f_x(R_r)$] has been replaced with a simple analytic form which fits both the COARE and HEXMAX data bases.

5.     The stability iteration loop has been reduced from 20 to 3 using bulk Richardson number parameterisation for an improved first guess (Grachev and Fairall, 1997).

6.     The latent heat flux has been reformulated in terms of mixing ratio instead of water vapour density to eliminate the need for a Webb *et al*. (1980) correction.

7.     Gustiness velocity has been expanded to include the effects of mesoscale variability associated with convective precipitation using the approach of Jabouille *et al*. (1995) or Redelsperger *et al*. (2000).

For a later release, two options are being considered to make the COARE algorithm more useful for applications to more limited data sets and for implementation in numerical models. The first is the addition of simple parameterisations to furnish downward IR and/or solar radiative fluxes when they are not available by direct measurement (e.g., COADS data). These would be standard parameterisations available in the literature (see Josey *et al*. 1999 for examples or refer to Section 6.2). The second is the addition of a parameterised form of the warm layer effect, probably based on Webster *et al*. (1996). This has the great advantage that

---

[1] Available at: http://www.ncdc.noaa.gov/coare/catalog/data/atmosphere_large_scale/bulk.html or by ftp from the NCAR site:ftp://ncardata.ucar.edu/datasets/ds606.1/flux_algorithm/

[2] The new algorithm is available at ftp://ftp.etl.noaa.gov/pub/et7/users/cwf/bulkalg/

the fluxes would be a pure function of a single record of data, rather than an integral of the previous time series. A major addition is being considered to account for the effects of waves on the fluxes. This would allow the algorithm to be applied in coastal/shallow water areas such as much of the Gulf of Mexico. The new model from Taylor and Yelland (2000c) is a primary candidate with the surface roughness parameterised in terms of the significant wave height and the peak wavelength (or, equivalently the wave period) both of which are observable from satellites.

*7.4.2 Other Algorithms*

A.  ZENG, ZHAO AND DICKINSON (1998)

The algorithm described by Zeng *et al.* (1998, ZZD) takes essentially the same path as the COARE algorithm, but uses different stability functions for the velocity and scalar profiles, and a different form for the scalar roughness lengths. The various empirical constants are given values which ensure reasonable agreement with observation over the wind speed range 0 -18 ms$^{-1}$. The observations used are the COARE Moana Wave dataset for low to moderate wind speeds (0-12 ms$^{-1}$) and the HEXOS data up to 18 ms$^{-1}$.

Like Fairall *et al.* (1996a), ZZD use the Kansas expressions for near-neutral atmospheric stability and the stable case (with $\gamma = 5$ in (7.3b)) but, as stability increases beyond $z/L = 1$, the expression of Holtslag *et al.* (1990) is adopted :

$$\phi_m = \phi_t = \phi_q = 5 + z/L \qquad (7.34)$$

which prevents $\phi$ from becoming too large in very stable conditions. For convective conditions ZZD use the expressions of Kader and Yaglom (1990, see their Figure 1):

$$\phi_m = 0.7k^{2/3}\left(-\frac{z}{L}\right)^{1/3} and \quad \phi_t = \phi_q = 0.9k^{4/3}\left(-\frac{z}{L}\right)^{-1/3} \qquad (7.35)$$

which lead to simpler integrals than those given in (7.30) and which are therefore more suitable for incorporation into numerical models. ZZD match the near-neutral to convective forms at $z/L = -1.574$ for momentum and $z/L = -0.465$ for the scalars.

They also use the functional form of Smith (1988) for the momentum roughness length, but their analysis of the Moana Wave COARE data suggests a value for the Charnock constant $\alpha_c = 0.013$. For the scalar roughness lengths they use the expression given by Brutsaert (1982):

$$\ln\left(\frac{z_0}{z_{0T}}\right) = \ln\left(\frac{z_0}{z_{0Q}}\right) = b_1 Rr^{1/4} + b_2 \qquad (7.36)$$

where the constants determined empirically by ZZD ($b_1 = -2.57$ and $b_2 = 2.67$) differ slightly from those given by Brutsaert (1982). This is partly because they are optimised to provide a continuous fit to both the COARE and HEXOS datasets.

Other similarities with the COARE algorithm include allowance for the 2% reduction in saturated specific humidity over sea water, which ZZD find decreases latent heat flux by 20% at 14 ms$^{-1}$, and the "gustiness" correction at low wind speeds. However, they adopt a value $\beta = 1.0$, rather than the value 1.2 which Fairall *et al.* (1996a) prefer. ZZD does not include the contributions to sensible heat and momentum due to rainfall, nor models for the cool skin and diurnal thermocline, so input data for the algorithm must be either measured or derived skin surface temperature. Zeng *et al.* (1999) have developed an hourly dataset from the Pacific ocean TOGA-TAO mooring array for use with their algorithm, which includes such a derived surface skin temperature field.

ZZD compare their algorithm with COARE 2.5b, and with those embodied in several research and operational numerical climate models, NCAR's CCM3, the ECMWF forecast model, the NCEP medium range forecast model and the GEOS DAS model.

B.  BOURASSA-VINCENT-WOOD (1999) FLUX AND SEA STATE MODEL

The main innovation of the Bourassa *et al.* (1999, BVW) model is a scheme to relate roughness lengths ($z_0$, and by implication the neutral exchange coefficients) to the various constituents of "sea state", particularly drawing the distinction between the effects of capillary waves and gravity waves.  BVW also note that, particularly under low to moderate wind conditions with swell, the wind, stress and current directions are not necessarily parallel, and their algorithm allows the cross-wind component of stress to be calculated.  BWV contend that with the co-existence of these different wave types, and interactions between them, it is unclear what the proper coordinate frame of reference should be for the wind and water velocities, and for $z_0$, and question whether the surface current is the appropriate reference velocity (see Section 10.6.2).  They argue that wind parallel to the crests of swell will not "feel" the swell as roughness, citing the observations of Donelan *et al.* (1997), who measured much larger drag coefficients in the presence of counter and cross-swells, than would be expected over a pure wind sea.

BVW distinguish between aerodynamically smooth and rough regimes with a Smith (1988) type roughness length expression (c.f. 7.14) :

$$z_0 = s_v \frac{0.11\nu}{u_*} + \left[ (s_c \beta_c \frac{b\sigma}{u_*^2 \rho_w})^2 + (s_g \beta_g \frac{u_*^2}{g})^2 \right]^{1/2} \qquad (7.37).$$

Each term includes a binary switch, $s_x$, to exclude any surface type which is not contributing to the roughness at that time.   Thus for smooth flow $s_v = 1$ and $s_c = s_g = 0$, the criterion for which is that the calculated phase speed, $c_p$, for the dominant wave be less than the minimum phase speed for surface waves:

$$c_{p\min} = (4g\sigma / \rho_w)^{1/4} \qquad (7.38)$$

which is approximately 0.23 ms$^{-1}$.  Above this windspeed surface waves are assumed to exist, and $s_v$ becomes zero.   This is the basis for the BVW claim to distinguish between aerodynamically smooth and rough flow.  Capillary waves appear above a windspeed $U_{10} \approx 1.8$ ms$^{-1}$, referred to as the "capillary cutoff".  BVW re-evaluate Wu's (1968) parameter, $b$, on the premise that Wu failed to take account of a zero-displacement correction when using the profile method for $z_0$ and $u_*$, and Wu (1994) failed to correct for the increase in drag coefficient for the low wind, strongly unstable regime of the Bradley *et al.* (1991) observations which he used to verify his value of $b$ for field conditions.  Their re-evaluation reduces $b$ from Wu's 0.18 to 0.06, which agrees with their mean value of 0.05 using the wave age and phase speed data from NOAA's San Clemente Ocean Probing Experiment (SCOPE) on R/P FLIP (Kropfli and Clifford, 1994).

The weighting parameters, $\beta_c$ and $\beta_g$, account for the two effects referred to above, namely the correct frame of reference for velocities and $z_0$ and the non-parallel wind and stress vectors.  Not much detail of the structure of these weights is provided, although two examples are given; the correction to $u_0$ (7.8a) for the velocity of capillary waves superimposed on a gravity wave field, and for gravity waves propagating in different directions relative to the wind.  Then :

$$\beta_c = \exp(-\kappa U_c c_p / u_*) \qquad (7.39)$$

for simplicity not written here in the vector form used by BVW.  The shift in velocity, $U_c$, is an empirically determined fraction of the orbital speed ($U_{orb} = \pi H_s/T_p$), where the significant wave height, $H_s$, and the wave period, $T_p$, are estimated from the "3/2"relationship of Toba *et al.* (1990) :

$$\left( H_s = B(gu_*)^{1/2} T_p^{3/2} \right) \qquad (7.40)$$

with $B$ = 0.62.   For the gravity wave roughness length $z_{og}$, BVW use the weighting $\beta_g$ =0.48/$(c_p/u_*)$ (the HEXOS result, see equation 7.16) rather than the form which may be a better physical representation :

$$\beta_g = \exp(-\kappa \Psi c_P / u_*) \tag{7.41}$$

because of the lack of data to determine the scaling parameter $\Psi$. This shortcoming in the gravity wave parameterisation leads to an overestimation of stresses for rising seas, and a very small underestimation of fluxes for falling seas (e.g. those examined by Fairall *et al.* (1996c)). However data from a directional Waverider and a buoy mounted anemometer (Dobson *et al.* 1999; Taylor *et al.*, 1999b) showed that the BVW model significantly overestimated stress for conditions of growing seas, with the larger errors occurring for $U_{10} > 12$ ms$^{-1}$ (which presumably corresponds to larger departures from local equilibrium).

BVW go on to express the wind profile, roughness length components, and wave age in vector form, so that their working form of (7.37) is written in terms of parallel and crosswind components of stress. For aerodynamically smooth or rough flow, the BVW scalar roughness lengths are adopted from the forms of Brutsaert (1982, Section 7.3.2C) :

$$z_{0T} = \frac{0.40\nu}{u_*} \quad ; \quad z_{0Q} = \frac{0.62\nu}{u_*} \tag{7.42}$$

and, citing Smith (1988, 1989) apply them to both smooth and rough flow conditions.

For the profile stability functions, BVW depart from tradition in respect of both stable and unstable forms. We detail these here because Clayson *et al.* (1996), whose algorithm is described in the next section, use the same functions. Beljaars and Holtslag (1991) point out that the Webb (1970) stable relation ($\Psi_m = \Psi_t = \Psi_q = -5z/L$ see (7.3b, 7.4b)) is fairly consistent with most data for $0 < z/L < 0.5$, but produced unrealistic results when used in a weather forecast model (Louis 1979). On the basis of several sets of very stable data they propose the following :

$$-\psi_m = a\frac{z}{L} + b\left(\frac{z}{L} - \frac{c}{d}\right)\exp\left(-d\frac{z}{L}\right) + \frac{bc}{d} \tag{7.43}$$

and

$$-\psi_t = -\psi_q = \left(1 + \frac{2}{3}\frac{az}{L}\right)^{3/2} + b\left(\frac{z}{L} - \frac{c}{d}\right)\exp\left(-d\frac{z}{L}\right) + \frac{bc}{d} - 1 \tag{7.44}$$

valid over the range $0 < z/L < {\sim}10$, with $a = 1$, $b = 0.667$, $c = 5$ and $d = 0.35$ in both expressions.

In place of the standard Kansas expressions for the unstable case, BVW and Clayson et al (1996) adopt the expressions of Benoit (1977) :

$$-\psi_m = \ell n\left[\frac{(\zeta_0^2 + 1)(\zeta_0 + 1)^2}{(\zeta^2 + 1)(\zeta + 1)^2}\right] + 2\left[\tan^{-1}(\zeta) - \tan^{-1}(\zeta_0)\right] \tag{7.45a}$$

$$-\psi_t = -\psi_q = 2\ell n\left[\frac{\lambda_0 + 1}{\lambda + 1}\right] \tag{7.45b}$$

where

$$\zeta = (1 - 16z/L)^{1/4} \quad ; \quad \zeta_0 = (1 - 16z_0/L)^{1/4} \tag{7.46}$$

and

$$\lambda = (1 - 16z/L)^{1/2} \quad ; \quad \lambda_0 = (1 - 16z/L)^{1/2} \tag{7.47}$$

which have the correct analytical limit as $z/L$ tends to zero and are stable numerically. BVW adopt the "gustiness" correction for low wind speeds, using the same value of $\beta = 1.25$ as in the COARE algorithm.

There are few open ocean data for low to moderate wind speed, including wave measurements, with which the BVW model can be compared. The model results show minima

in the neutral drag coefficient ($C_{DN}$) for windspeed just below the capillary cutoff (~1.8 ms$^{-1}$). For aerodynamically rough surfaces there is a local minimum in $C_{DN}(U_{10})$ for $c_p/u_* = 5$. This is qualitatively in accord with measurements by Bradley *et al.* (1991), Dupuis *et al.* (1997) and a composite result by Large *et al.* (1995). In other words, if capillary waves exist, below 4 ms$^{-1}$ the drag coefficients are much larger than those for an aerodynamically smooth surface. On the other hand, Grachev *et al.* (1998) have suggested that the traditional stability formulae over estimate the drag coefficient at wind speeds below about 2 ms$^{-1}$ and Taylor and Yelland (2000a) suggest that many low wind speed data may be biased high. These studies suggest that the minimum drag coefficient occurs at lower wind speeds, possibly at 3 ms$^{-1}$ as predicted by Smith (1988).

The BVW comparison of modelled stress with the bulk of the COARE observations is not unreasonable, most of the serious disagreements being underestimates on the part of the model. The SCOPE observations are nearly all underestimated. BVW speculate that this is due to lack of wave information to put in the model, and the probability of large angles between the wind direction and that of wave propagation. The model predicts that the stress (and drag coefficient) are least when these directions are parallel, in accord with the findings of Donelan *et al.* (1997).

The BVW model predicts that the influence of capillary waves on surface fluxes is very significant for winds less than 7 ms$^{-1}$ down to the capillary "cutoff" around 2 ms$^{-1}$. On the basis of the Franklin (Bradley et al, 1991) low windspeed observations they calculate that, near the cutoff, capillary waves contribute about 10 Wm$^{-2}$ to the latent heat flux compared with only 1 Wm$^{-2}$ due to "gustiness". The model flux predictions are compared with data from SCOPE, COARE (R/V Moana Wave) and R/V Franklin, with and without capillary waves in the model. Inclusion of capillary waves increased the mean modelled fluxes of momentum (by 0.004 Nm$^{-2}$), sensible heat (by 1 Wm$^{-2}$) and latent heat (by 6 Wm$^{-2}$); and in all cases, the modelled results were closer to observation. BVW argue that the overall effect of capillary waves is three to six times that of gustiness, and is therefore much more important than convective processes.

Unfortunately, the comprehensive dataset including meteorological variables, air-sea fluxes and the various sea state parameters which could validate this algorithm are rare. Even observations of the angle between the wind and direction of wave propagation are uncommon. While the anisotropic $z_0$ aspect is qualitatively consistent with the observations of Donelan *et al.* (1997) and appears to be of reasonable magnitude, this aspect of the model has yet to be quantitatively validated.

C.  CLAYSON, FAIRALL AND CURRY (1996) FLUX ALGORITHM

The Clayson, Fairall and Curry algorithm (Clayson *et al.* 1996, CFC) is based on surface renewal theory (Brutsaert 1982) as set out in section 7.3.2.C, following the general pattern established by LKB and Fairall *et al.* (1996a). The main differences from these antecedents are: a new surface renewal time-scale parameterisation, the BWV sea state surface roughness model, derivation of the scalar roughness lengths solely from surface renewal theory, and a new skin surface temperature model.

Following Wick (1995) CFC identify Brutsaert's renewal time-scale (7.26) as a shear-driven timescale, and define a convective time-scale also:

$$t_{*_c} = Const. \left[ \frac{\nu \rho_w C_p}{\alpha g Q_N} \right]^{1/2} \tag{7.47}$$

where $\alpha$ is the thermal expansion of sea water and $Q_N$ is the sum of the turbulent and radiative fluxes. The shear-driven and convective forms are combined and the contribution of each determined by a Richardson number criterion. This composite time-scale is then used to form expressions for the interfacial Dalton and Stanton numbers after the method of Brutsaert (1975).

For $z_0$ , CFC employ the parameterisation developed by BVW, but with some differences. The capillary and gravity wave terms are simply added (not root-mean -squared) but without any weighting, and there is a clear distinction between smooth and rough flow on the same basis as BVW:

$$z_{o(rough)} = \frac{b\sigma}{u_*^2 \rho_w} + \frac{0.48}{w_a}\frac{u_*^2}{g}, \quad for\ u_* w_a > c_{p\,min}$$

$$z_{o(smooth)} = \frac{0.11\nu}{u_*} \quad , \qquad for\ u_* w_a < c_{p\,min} \tag{7.48}$$

CFC use a value of Wu's $b$ for capillary waves of 0.019. i.e. smaller even than the BVW value. Referring back to BVW (their Fig. 2), we find that this is the value found initially in their re-evaluation of Wu's data before applying the frame of reference correction. In other words, CFC adopt the simplest form of the BVW parameterisation, ignoring the features which account for anisotropic wind/wave propagation directions and frame of reference adjustment. Unlike BVW, they do not include a "gustiness" term, relying on their capillary wave parameterisation and surface renewal theory to obtain correct fluxes at low wind speeds.

The turbulent boundary layer profiles used by CFC are those of Beljaars and Holtslag (1991) for stable conditions, and Benoit (1977) for unstable conditions, with the interfacial layers of height, $h$, matched to these assuming continuity of $T$ and $q$ as before. Algebra leads to Brutsaert-like expressions for the scalar roughness lengths:

$$z_{ot} = z_o \exp\left[k\left(\frac{u_h}{u_*} - \frac{1}{Pr\,St_0}\right)\right] \quad ; \quad z_{oq} = z_o \exp\left[k\left(\frac{u_h}{u_*} - \frac{1}{ScDa_0}\right)\right] \tag{7.49}$$

where $Pr$ and $Sc$ are the turbulent Prandtl and Schmidt numbers (0.71 and 0.60 respectively), and $St_0$ and $Da_0$ the interfacial Stanton and Dalton numbers. CFC take $(u_h/u_*) = 5$ after Brutsaert (1975). They have a system of eight equations which they solve iteratively for $Da_0$, $St_0$, $u_*$, $t_*$, $q_*$, $z_0$, $z_{oT}$ and $z_{0Q}$. Because this algorithm was developed with the calculation of fluxes from satellite data in mind, they incorporate a model of the ocean cool skin (Wick *et al.* 1996) to reduce bulk SST observations to true surface skin temperature, and adjust surface humidity for the 2% reduction of vapour pressure over saline water. However, they do not correct SST for the diurnal thermocline; the data set which they use for verification (Fairall *et al.* 1996a) has sea temperature measured at 5 cm depth, so only the cool skin adjustment is needed. However, lack of a warm layer model would be of concern in the tropics particularly, with bulk water temperatures measured at customary depths on a ship's hull.

D. ZHANG AND MCPHADEN (1995)

Zhang and McPhaden (1995, ZM) studied the relationship between SST and latent heat flux in the equatorial Pacific ocean, using data from the TOGA-TAO moored array. In developing a flux algorithm for this region, they faced the same difficulties as the previous models described here, namely the need to take account of occasionally very low wind, strongly convective conditions. Their approach was to incorporate the minimum of complexity consistent with this, and we describe their model here briefly because it represents possibly the simplest of its type and is computationally economical, and because it was included in the comparison by Chang and Grossman (1999) referred to in Section 7.4.2F.

ZM employ the Kansas forms (Businger *et al.* 1971) for the stability-dependent wind, temperature and moisture profiles (7.6), and the Paulson (1970) integral expressions for the $\Psi$-functions (7.7). For the value of $\alpha$ in (7.3a) they use 16, and for $\gamma$ in (7.3b) they use a value of 7. They adopt the Smith (1988) Charnock plus smooth form for the momentum roughness length (7.14), but set the temperature and moisture roughness lengths equal at a constant $2 \times 10^{-5}$ m (Geernaert 1987).

E. BELJAARS (1994)

Beljaars (1994) has developed a parameterisation for the case of free convection in the atmosphere, for use with bulk transfer models. It is based on the idea that normal Monin-Obukhov similarity theory can be used in the surface layer without modification for free convection, except for inclusion of the convective scaling velocity, $w_*$, as an extra wind component in the bulk equation. This derives from the analysis of Godfrey and Beljaars (1991), and is given by (7.32) and (7.33) as used in the COARE algorithm.

Beljaars (1994) follows the standard development set out in Section 7.2, leading to the usual form of the bulk exchange coefficients (7.9). The "Kansas" expressions are used for the dimensionless profiles, with the Paulson (1970) integrals for the stability functions, $\psi_m$, $\psi_{t,q}$. These do not have the 1/3-power law dependence expected for free convection. However, Beljaars (1994) argues that the behaviour of the stability functions for large $-z/L$ is not too critical because vertical gradients are small in the well-mixed regime, and contribute little to the air-surface velocity, temperature or moisture difference.

The problem is simplified by writing asymptotic forms for the profile stability functions, leading to expressions for the stress and heat flux in terms of $z_0/L$, $z_{0t}/L$, $\beta w_*$ and $(t_0 - t_m)$ the temperature difference between the surface and the mixed layer; i.e. they are independent of height, $z$. Beljaars (1994) shows that the resulting heat flux transfer coefficient is strongly dependent on roughness length, indicating that the surface is still being "felt" in the free convection regime, through coupling between convective motions and the rough surface. Over a smooth surface, Beljaars (1994) adopts the classic smooth-flow form (7.12) for $z_0$, and the same expressions as BVW for the scalar roughness lengths, (7.41) from Brutsaert (1982). He compares his parameterisation with convective data taken over land by Stull (1994), and on the basis of large eddy simulation data by Sykes *et al.* (1993), estimates the empirical constant, $\beta$, to be about 1.2, close to the value measured over the western Pacific by Fairall *et al.* (1996a) during COARE.

For air-sea transfer over the ocean, Beljaars (1994) uses the Smith (1988) interpolation (7.14) for $z_0$ with a Charnock constant of 0.018, and applies the Brutsaert (1982) smooth-flow scalar roughness length parameterisation to both smooth and rough flow. His justification for this is tentative, on the grounds that empirical evidence points to an almost constant moisture transfer coefficient over the entire low to high wind speed regime (Smith 1989; DeCosmo *et al.* 1996). Approaching zero wind speed, his transfer coefficients for both heat and moisture follow quite well the increasing trend shown by the low wind data of Bradley *et al.* (1991).

F. STULL (1994)

A quite different approach from the foregoing models is the so-called convective transport theory (CTT) by Stull (1994), specifically aimed at prescribing the surface fluxes in the limit of free convection. Unlike Beljaars (1994), Fairall *et al.* (1996a), Zeng *et al.* (1998), etc., who deal with the approach to zero wind speed by introducing a *horizontal* "gustiness" velocity based on the convective scale $w_*$, Stull (1994) focuses on the role of convective plumes (thermals) in transporting heat and mass *vertically* from the surface into the mixed layer.

Like Beljaars (1994), Stull (1994) notes that a crucial factor controlling the turbulent fluxes at the surface is the *total* difference in velocity, temperature or moisture concentration (i.e. $\Delta u$, $\Delta t$ and $\Delta q$) between the surface and the atmospheric mixed layer. This total is the sum of the individual differences across the three layers discussed above, the interfacial layer, the logarithmic surface layer and the mixed layer. The lowest two layers respond fairly rapidly to changes, whereas thermal circulations are relatively slow. Stull (1994) suggests that this separation of time-scales creates a reservoir of air in the surface layer which has been modified by the surface, and that the removal of this air and its transport into the mixed layer by thermals is the bottleneck in the system. Thus, Stull (1994) argues that, apart from their role in maintaining the reservoir of air, processes in the lower two layers can be ignored, and that transport by convective plumes is the governing process.

Against this background, Stull (1994) goes on to parameterise the surface fluxes in terms of mean mixed layer variables rather than surface-layer variables. This leads to the surprising proposition that the surface fluxes should be independent of surface roughness, in contrast with the Beljaars (1994) result. Furthermore, provided the mixed layer is deep enough that variables may be defined in a mid-region well above the surface layer, Stull (1994) suggests that its depth and the shape of the surface layer profiles are irrelevant also.

Stull (1994) writes the vertical transport of an entity, $\chi$, across an interface as the product of a vertical transport velocity, $w_T$, and the concentration difference, $\overline{w'\chi'} = w_T \Delta\chi$. This is in the form of the usual bulk transport equation where vertical transport is caused by shear-driven turbulent eddies in the surface layer; i.e. $w_T$ appears in place of $C_D \Delta u$. By analogy Stull (1994) proposes that, in free convection, thermal eddies transport air aloft with a transport velocity which scales with $w_*$ :

$$w_T = C_* w_* \qquad (7.50)$$

where $C_*$ is a mixed-layer transport coefficient to be determined empirically. He therefore writes equations for the surface fluxes in the usual form, but in terms of mixed layer variables:

$$u_*^2 = C_{*D} w_* \Delta u$$
$$\overline{w't'} = C_{*H} w_* \Delta t \qquad (7.51)$$
$$\overline{w'q'} = C_{*H} w_* \Delta q$$

where $C_{*D}$ and $C_{*H}$ are mixed layer transport coefficients for momentum and scalars respectively. (To properly include all buoyancy effects, Stull (1994) works throughout with virtual potential temperature (see (7.29)), and also expresses moisture as the mixing ratio. Here we describe his formalism, but for simplicity and consistency with previous discussion, retain $t$ and $q$).

Because the fluxes appear on the RHS of (7.51) through $w_*$, Stull (1994) converts these equations to explicit form by defining a buoyancy temperature difference:

$$\Delta t_B \approx \Delta t (1 + 0.61 q_s) + 0.61 t_s \Delta q \qquad (7.52)$$

and a buoyancy velocity scale:

$$w_B \equiv \left[ \frac{g}{t} z_i \Delta t_B \right]^{1/2} \qquad (7.53)$$

which as Stull (1994) points out, unlike $w_*$ does not contain the turbulent fluxes. Finally he writes a set of equations which form the mathematical basis for the application of convective transport theory:

$$\overline{w't'}_{vs} = b_H w_B \Delta t_B$$
$$\overline{w't'}_{vs} = b_H w_B \Delta t_B$$
$$\overline{w'q'} = b_H w_B \Delta q \qquad (7.54)$$
$$u_*^{2'} = b_D w_B \Delta u$$

where $b_H (= C_{*H}^{3/2})$ and $b_D (= C_{*D} C_{*H}^{1/2})$ are simplified convective transport coefficients for scalars and momentum, respectively. These must be determined experimentally, and Stull (1994) quotes values: $b_D = (1.83 \pm 0.60) \times 10^{-3}$; $b_H = (5.0 \pm 1.9) \times 10^{-4}$ obtained from the BLX83 experiment in Oklahoma (Stull and Eloranta, 1984).

The theory is tested against the independent Koorin experiment over land in Australia (Clarke and Brook, 1979). The agreement between predicted and observed surface stress is good on average, but very scattered; the plot of kinematic heat flux has much less scatter, but a pronounced difference in slope and an offset. Stull (1994) argues that the overall agreement

between transport coefficients measured in Oklahoma and Australia confirms that neither Coriolis parameter nor Ekman layer depth are relevant for bulk transfer in free convection. For the continuity from low to high wind speed conditions, Stull (1994) proposes linear superposition of the convective transport and bulk aerodynamic formulas, suggesting that in the surface layer free convection takes over when $z/L < -3$.

Sorbjan (1997) argues that the results embodied in CTT can be obtained within the framework of Monin-Obukhov similarity theory, and suggests that the lack of dependence on surface roughness and surface layer processes could lead to errors *in situ*ations other than those under which CTT was tested. Stull (1997) disagrees, pointing out that Sorbjan's analysis is based on surface layer, rather than mixed layer equations, and that his definitions of mixed layer to surface temperature difference and of transport coefficients are not equivalent to those in CTT. Fairall *et al.* (1996a) also suggest that as the mean vector wind approaches zero, a gustiness velocity, $w_*$ , appearing in the standard bulk equation will yield a result equivalent to the Stull (1994) scaling theory. Chang and Grossman (1999) included CTT in their comparison of several algorithm's using COARE data, but needed to "tune" the coefficients of CTT for use over the tropical ocean.

## 7.5 Transfers in moderate and high winds

There is now a fairly large body of reliable momentum flux measurements at wind speeds in excess of 12 ms^{-1} (Yelland and Taylor, 1996; Yelland *et al.*, 1998; Hare *et al.*, 1999). These show that the drag coefficient increases steadily (and more or less linearly) to around 25 ms^{-1}. However, the fluxes of heat and water vapour have not yet been measured in the field for winds over 20 ms^{-1}. In fact, the most widely quoted dataset for the high wind regime, from the HEXOS experiment (DeCosmo *et al.* 1996), contains fewer than a dozen data points above 16 ms^{-1}. Furthermore, the HEXOS site was over water only 15m deep. More flux data in high winds over the open ocean are badly needed.

The evaporation of spray might be expected to modify the heat fluxes at high wind speeds. Thus Andreas (1992) and Andreas *et al.* (1995) suggested that, whereas the turbulent fluxes are proportional to wind speed, spray production should increase at roughly the third power of the wind speed. This implies that for wind speeds up to 15 m/s the spray contributes no more than 10% of the total heat flux. At 20m/s and above the spray contribution would be of similar magnitude to the surface turbulent flux. However consideration of the feedback on the parameterised surface evaporation due to changes in the mean surface humidity profiles caused by the evaporating spray was not fully included. This may substantially modify the estimated flux (Katsaros and de Leeuw, 1994, Andreas, 1994).

## 7.6 Summary of bulk algorithms

In the introduction to this chapter we outlined the traditional concept of bulk flux formulae, particularly drawing attention to the notion that many of the physical processes involved in air-sea transfer of heat or momentum became embedded within a transfer coefficient for the particular entity. The formalism commonly used to construct these transfer coefficients is given in section 7.2. The best-known algorithm employing this methodology is probably that of Large and Pond (1981,1982) who supported their analysis with some direct (covariance) flux data which in turn validated their much more extensive inertial dissipation data set. Nevertheless, while transfer coefficients were known to be a function of wind speed, height and atmospheric stability, more often than not the available test data justified use of only a constant value for the scalar fluxes, or a simple wind-speed dependant value for stress.

Such simple expressions have become inadequate for several reasons, mostly connected with the burgeoning requirements of climate research, and recognition of the sensitivity of numerical climate models to small changes in air-sea flux values, particularly when attempting to couple ocean and atmospheric GCM's. Initially, the focus was on the climatically important tropical oceans where bulk flux theory was inadequate to deal with the prevailing low winds and

strong convection. Attention was directed toward an understanding of transfer mechanisms at the surface itself, including development of surface renewal theory, and considerable experimental effort was made to obtain supporting data in this regime. Most modern bulk algorithms for the tropical regions are based on the pioneering work of Liu *et al.* (1979), and the data obtained during the 1992-93 TOGA-COARE experiment. The basis of this approach is given in section 6.3.2. In a somewhat curious twist, the exchange coefficients have now become embedded in the analysis, which is an iterative process between the fluxes and the surface roughness, and are often only calculated *post facto* for diagnostic purposes. This is indicative of the connection between stress and wave state formulated in its simple form by Charnock (1955), and now receiving closer attention.

We have described several recent bulk flux algorithms in some detail. The list is not exhaustive or even possibly up to date, because air-sea flux determination by a variety of means is a growth industry responding to the immediate needs of forecasting and climate research. Those described have in general been developed to serve some particular area of this research. Common features tend to be corrections for thermal stability, exchange processes in light winds and sophisticated representation of surface roughness lengths for velocity, temperature and humidity. Differences between algorithms tend to lie in the choice of parameterisations, for gustiness, for surface renewal parameters (timescale, thickness), and for the roughness lengths. Direct measurements of most of these parameters over the ocean are virtually non-existent. Similarly, direct covariance flux data sets against which to test the various algorithms are very limited, although some well-validated inertial dissipation measurements are available.

For research purposes, perhaps the most widely used of the modern bulk algorithms is the so-called COARE algorithm (Fairall *et al.*, 1996a), developed specifically as a common resource for COARE scientists. Originally, it adhered strictly to the LKB model as regards stability corrections and scalar roughness parameters, but gradually introduced modifications for gustiness, convection and surface roughness which were actually derived from shipboard observations during COARE. It was scaled against direct (covariance) measurements of the latent heat flux. Thus there were no arbitrary assumptions. However, from the perspective of modellers it was inefficient because of long iterative loops in the code, one of which included corrections to the measured SST for cool skin and the diurnal thermocline. At the same time, being structured around the basic physical processes involved, the results of new theory and fresh data are readily incorporated. With much additional direct flux data available in both tropics and mid-latitudes since COARE, an improved version of the "COARE" algorithm is now available, including more efficient computation.

The algorithm by Zeng *et al.* (1998) is designed to suit the needs of numerical model code, being a simplified version of the COARE algorithm. It is tuned to the same data set as the COARE algorithm for low to moderate wind speeds (the Moana Wave COARE observations by Fairall *et al.*, 1996a). However, there is very little of this data with wind speeds in excess of 12 m/s, so for higher wind speeds Zeng *et al.* (1998) extend their algorithm using the HEXOS data of DeCosmo *et al.* (1996). This is the best-known of flux data sets at stronger winds, but should be used with caution, because these are shallow water coastal measurements, and the authors show that they do not conform to open ocean exchange coefficients in the overlapping wind speed range.

The Bourassa *et al.* (1999, BVW) bulk model is notable for its attempt to relate surface roughness lengths, and hence the exchange coefficients, to various aspects of sea state, swell, gravity waves and capillary waves. They draw on, and extend, published representations of wave structure in their analysis, but adequate validating data is not yet available to test the potential of this algorithm. The Clayson *et al.* (1996) algorithm, developed to obtain surface fluxes from satellite observations, make use of the BVW sea state model, but otherwise follow the surface renewal theory and stability correction path.

Two of the algorithms which we describe depart from the conventional approach to free convection, by Fairall *et al.* (1996a) or Zeng *et al.* (1998) for example. Beljaars (1994)

approaches the problem from the perspective of the numerical modeller seeking economical solutions without violating physical reality. He argues that normal Monin-Obhukov similarity can be used in the surface layer, provided a convective scaling velocity (gustiness) is included in the bulk equation and that, in the well mixed region, the behaviour of stability functions is not too critical in any case. His analysis suggests that the surface influences the free convection regime through coupling between convective motions and the surface roughness. Stull (1994) takes a similar approach in his convective transport theory, that transport into the mixed layer by convective plumes is the dominant process, but his analysis leads to the opposite conclusion from Beljaars (1994). By parameterising the surface fluxes in terms of mixed layer, rather than surface layer variables, Stull (1994) finds that turbulent exchange is independent of surface conditions.

With such a variety of advanced bulk flux algorithms available, it is obviously tempting to intercompare their flux output using a common set of basic input data, to determine which is the "best". Using COARE and TAO mooring data, Zeng *et al.* (1998) have compared several of the algorithms described here and show that, up to around 12 m/s, the performance of the algorithms is very similar. Since they derive from essentially the same analysis as given in the above sections, the only difference will be due to the different choice of parameters or functions. As expected, these differences become more prominent at higher wind speeds, but uncertainty about the quality of the test data at these speeds makes judgement difficult. Zeng *et al.* (1998) also consider the parameterisations employed in several numerical models. They conclude that these are seriously defective, and recommend substitution with their own algorithm. As indicated in section (4.4.3B), the Zeng *et al.* (1998) algorithm is now used in the NCEP operational model, achieving some improvement. It is probably fair to comment that almost any of the modern algorithms, with reasonable roughness parameterisations and stability correction, would have considerably improved the performance of the models.

Chang and Grossman (1999) have also compared several algorithms, using the Moana Wave covariance flux measurements from COARE as reference. Adopting a particular set of criteria to constitute agreement, they find that most of the algorithms predict latent heat flux within 8% of the observed value. The predictions for sensible heat and momentum are more variable. The authors identify the departure from measured values as "a windspeed dependent bias in the model due to the surface flux parameterisation", but don't examine this in more detail. It would have been helpful to identify the sources of disagreement, as a guide to the sensitivity and relative importance of various parameters, and to the accuracy with which they need to be determined. To be constructive, any further comparisons between algorithms should consider not just the output values, but the consequences of alternative choices of parameters and internal physics.

The main shortcoming in the area of algorithm development is not so much a dearth of new parameterisations, as a supply of reliable directly measured flux data at high wind speeds and higher latitudes. Reference data from tropical regions is becoming relatively plentiful. Since TOGA-COARE, considerable additional low to moderate windspeed direct flux data has been assembled by the NOAA/ETL group, in tropical and mid-latitudes. As a result, better relationships between momentum and scalar roughness lengths than those used by LKB (1979) and Fairall *et al.* (1996a) have been established, and incorporated into the COARE algorithm. At the same time, advanced forms of the profile functions and a more accurate first estimate of the atmospheric stability have enabled convergence of the flux-roughness loop within 3 iterations, making the algorithm more attractive for numerical modelling and remote sensing applications.

## 8  RANDOM AND SAMPLING ERRORS IN FLUX FIELDS.

### 8.1  Introduction

This Chapter will consider some aspects of determining the error characteristics of flux fields.  Random errors,  and the implications for the required sampling density will be considered in Section 8.2.   Systematic errors will be only briefly discussed in Section 8.3; more discussion with respect to the parameterisation formulae was given in sections 6 and 7.  Methods of determining the systematic errors,  and error estimates for the various products are discussed in sections 9 through 11.   A potential error source for flux fields depends on the method chosen for averaging the fluxes.  The use of averages of the basic variables in the parameterisation formulae (rather than averaging individual flux estimates) was originally adopted for computational efficiency,  however it also makes fuller use of the available data in cases where all the needed basic variables are not available with each observation.   As discussed in Section 8.4,  this advantage must be weighed against the possibility of introducing biases into the flux estimates due to neglecting the correlations between the basic variables.

The problem of combining the estimates of the random and systematic errors,  to provide the overall error estimate,  will be discussed in Section 8.4.   The calculation of flux fields involves smoothing with interpolation and extrapolation of the flux estimates.  As examples,  the effects of a commonly used method,  successive correction, and the advantages of a more sophisticated method,  Kriging,  will be discussed in Section 8.5.

Although more generally applicable,  most of the discussion in sections 8.2 to 8.5 has been developed with regard to the application to ship data.  Therefore the particular sampling problems associated with satellite data will be specifically discussed in Section 8.6.

### 8.2  Random errors and sampling density

*8.2.1  Introduction*

The sampling density is an important problem with regard to the reliability of ocean-atmosphere flux fields derived from VOS and satellite observations.   With respect to individual variables,  the sampling problem can be formulated in terms of the similarity of probability density distributions of meteorological quantities, computed both from the real observations and from some kind of "ideally sampled" observations for the selected space boxes and time periods.   The latter are typically one month periods for most climatologies,  although for instance Legler (1991) studied importance of sampling for 5-day wind and temperature means.  Since the distributions of most of the directly observed quantities are not Gaussian,  or at least may be not Gaussian in particular regions,  the significance of sampling biases is regionally dependent.   Although sampling biases are usually considered with respect to temporal inhomogeneity of sampling,  for some particular regions spatial inhomogeneity of sampling may be as important as temporal.  This is especially important for VOS observations which are usually sampled along the major ship routes.  For some regions the arrangement of samples within the $n$ by $n$ degree box may seriously affect the monthly means of both the individual variables and the fluxes even though the overall number of observations may be adequate.  Morrissey and Maliekal (1995) found that a linear network,  which aligned along the major axis of the spatial correlation function,  provided standard errors in wind speed estimates three to five times higher than a random network.   This problem is serious only for spatial boxes greater than 3-4 degrees, because the ship routes form relatively wide tracks of about 100 to 200 km width.

When the fluxes of heat, moisture and momentum are computed from individual variables using strongly non-linear parameterisations, even small sampling errors in individual observations can lead to significant sampling biases in space-time averaged fluxes.  Weare and Strub (1981) studied sampling errors in the tropical surface heat fluxes, computed from VOS observations, and found eleven individual observations per month to be adequate for monthly

mean flux estimates. However in the mid and high latitudes, this limit can be several times higher due to the necessity to sample extreme conditions associated with very high sea-air fluxes. These can seriously affect monthly means. Thus, Cayan (1992a) and Legler (1991) found 50 to 100 samples per month to be required for unbiased flux computations for a 5 degree box.

Climatologies of fluxes derived from VOS observations in COADS and similar archives are characterised by adequate sampling in much of the North Atlantic and North Pacific but to be strongly affected by under sampling in the southern hemisphere. However, even in such well sampled areas as the North Atlantic, there are some regions which are poorly sampled. Such areas may also be characterised by extreme flux values of crucial importance for adequate description of regional sea-air exchange processes. A good example is the Labrador Sea, known as the source of Labrador intermediate waters which are formed by the extreme sea-air exchange processes in that limited region (LabSea Group 1998). From the 1950's to the early 1970's this region was represented by regular observations at OWS B. However, since 1973 when OWS B was stopped, only a few observations per month were available. Yet this period, the 1970's - 1990's, was characterised by several dramatic deep-convection events which are therefore poorly represented in the VOS observations.

The flux products which have become recently available from numerical weather prediction systems are regularly sampled with 6-hourly temporal resolution. These allow the sampling errors in the VOS fluxes to be estimated. Gulev *et al.* (2000) simulated the sampling frequency of COADS using the NCEP/NCAR 6-hourly fields, and found that both climate means and interannual variability patterns may be seriously affected by the poor sampling. It was found that the absolute value of the sampling error over the North Atlantic domain was within a range of $\pm$ 5 Wm$^{-2}$. Thus the meridional heat transport estimates were not seriously affected by the under sampling. However, locally the effects in such areas as the Labrador Sea were large, possibly reaching 50 to 60 Wm$^{-2}$ for climatological means.

Further assessment of the possible impact of under sampling in the VOS observations should be made using the regular instrumental observations at buoys, OWS, and other in-situ platforms. However it will be shown in the next section that, if it is the accuracy of, say, a monthly mean that is required, then that is simply determined from the variance of the calculated monthly means. It is only if natural variability is to be distinguished from variability due to sampling errors that a more sophisticated analysis is required.

*8.2.2 Errors and Variability of Monthly Mean Fields*

Monthly mean fields of the air-sea fluxes are affected by two kinds of uncertainties: systematic and random errors. In general the first influence the mean, the latter the variance of the calculated fields. The wind stress is an exception from this rule. Since the squared wind speed occurs in this parameter, random errors are not cancelled out by averaging. Consequently, they affect not only the variance, but also the mean. The principal aim is to discriminate the error variance from the true natural variability, and, of course, to determine and eliminate the systematic errors.

Random errors are completely unavoidable, but good-natured compared to systematic errors. Several statistical techniques are available to quantify them and to eliminate their mean effects at least. Random observation errors of the basic synoptic parameters, such as wind speed and temperature, propagate through the applied bulk formulae and influence the resulting flux fields. Due to random errors the true variance is increased. For long-time means, in regions with a high number of observations, the effect of random errors remains small. However, if not only the long-term mean annual cycle is considered but also the interannual variability of individual monthly means, the data density even in the central North Atlantic is not sufficient to neglect the effects of random errors.

Before discussing problems connected with variability and error variance, the different relevant variances should be clearly defined. The total temporal variance at a fixed point is:

$$\frac{1}{m-1}\sum_{k=1}^{N}\sum_{i=1}^{n_k}\left(x_i-\overline{x}\right)^2 \tag{8.1}$$

where $m$ is the total number of observations and $\overline{x}$ the total mean, $x_i$ denotes the individual values, $N$ is the number of months and $n_k$ the number of observations in the $k$-th month. Obviously, the total number $m$ can be obtained by:

$$m = \sum_{k=1}^{N} n_k \tag{8.2}$$

and monthly means $\overline{x}_k$ are defined as:

$$\overline{x}_k = \frac{1}{n_k}\sum_{i=1}^{n_k} x_i \tag{8.3}$$

The total variance can be split up into the total apparent variance and the error variance of the total mean:

$$\frac{1}{m-1}\sum_{k=1}^{N}\sum_{i=1}^{n_k}\left(x_i-\overline{x}\right)^2 = \frac{1}{m}\sum_{k=1}^{N}\sum_{i=1}^{n_k}\left(x_i-\overline{x}\right)^2 + \frac{1}{m(m-1)}\sum_{k=1}^{N}\sum_{i=1}^{n_k}\left(x_i-\overline{x}\right)^2 \tag{8.4}$$

The second righthand term in (8.4), the error variance of the total mean, is mostly very small, if the total number of observations is large enough. The first righthand term in (8.4), the total apparent variance, consists again of two parts: the apparent extra-monthly variance and the apparent intra-monthly variance:

$$\frac{1}{m}\sum_{k=1}^{N}\sum_{i=1}^{n_k}\left(x_i-\overline{x}\right)^2 = \frac{1}{m}\sum_{k=1}^{N} n_k\left(\overline{x}_k-\overline{x}\right)^2 + \frac{1}{m}\sum_{k=1}^{N}\sum_{i=1}^{n_k}\left(x_i-\overline{x}_k\right)^2 \tag{8.5}$$

The apparent extra-monthly variance gives a mean value for the interannual variability weighted by the numbers of observations per month. The intra-monthly variance gives a measure for the mean short time variability within the months. We added the expression 'apparent', because the two terms are not equal to the true variability, but both are affected by random errors, in other words, true natural variability is mixed with the error variance. In the next step we will try to separate these two kinds of variance. That will be quite simple for the extra-monthly but more difficult for the intra-monthly variance. Fortunately, we are mostly interested in those outer quantities: the monthly means and their errors and variability.

The apparent intra-monthly variance of (8.5) can be split up into:

$$\frac{1}{m}\sum_{k=1}^{N}\sum_{i=1}^{n_k}\left(x_i-\overline{x}_k\right)^2 = \frac{1}{m}\sum_{k=1}^{N}\frac{n_k}{n_k-1}\sum_{i=1}^{n_k}\left(\overline{x}_i-\overline{x}_k\right)^2 - \frac{1}{m}\sum_{k=1}^{N}\frac{n_k}{n_k(n_k-1)}\sum_{i=1}^{n_k}\left(x_i-\overline{x}_k\right)^2 \tag{8.6}$$

In order to interpret the decomposition carried out in (8.6), we have to consider the following: the mean error variance of a sample's mean is given by the variance of the sample divided by the number of independent observations. Regarding ship observations, the demand of independence is obviously fulfilled, one of the great advantages of such data sets. Thus, the error variance of an individual monthly mean is given by the inner variance of that month divided by the number of observations. A weighted average over all months gives then an estimate of the mean error variance of monthly means. The second righthand term in (8.6) just describes these errors. Subtracting this error variance from the apparent extra-monthly variance finally gives an estimate of the true natural variability.

The first righthand term in (8.6) gives the weighted average of intra-monthly variance which is still affected by observation errors. For this expression the separation of the natural

variability from errors is possible following Lindau (1995a).    Pairs of simultaneous individual observations are considered.    The idea is that natural variability increases with increasing distance, while errors are independent of separation because of their randomness.    The squared difference between both observations is plotted as a function of distance between the locations. A linear fit gives an idea of the potential value at distance zero where no natural variability but only error variance remains.    In Figure 8.1, to give an example, the mean random error of VOS observed wind speed is determined by this technique.     For zero distance a variance of 23.5 $(ms^{-1})^2$ is obtained, representing twice the error variance of merchant ships.    By repeating the same procedure with pairs of VOS-OWS  observations, the error of OWS's can be concluded. Since 11.75 $(ms^{-1})^2$ is allotted to the merchant ships, 5.4 $(ms^{-1})^2$ remain for the OWS.    But we have to keep in mind that this procedure has to be applied only when individual observations are under consideration, which is only necessary when sub-monthly processes are investigated.
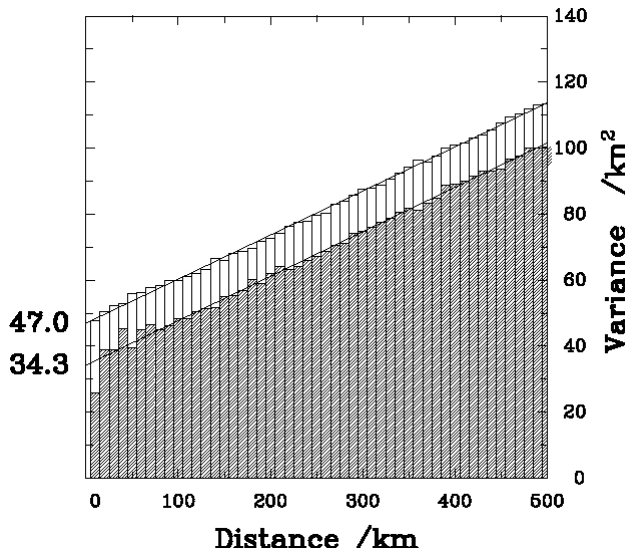


Figure  8.1 Determination of individual error variance. Mean squared wind speed differences from VOS-OWS pairs (shaded) are compared to VOS-VOS pairs (total columns).

        In contrast to the rather arduous technique to reveal the mean individual observation error,  the situation for extra-monthly errors is quite simple: the intra-monthly variance gives a measure of the error of the monthly mean.   It is not relevant whether the intra-monthly variance is caused by observation errors or natural variability.   The following consideration may help to illustrate that: even with a time series of perfect quality we are not able to derive the true average during the considered month, because of the disturbing natural variability.   The higher this variability is, the higher is the uncertainty of the mean, when a constant number of observations is available.   An additional random error of the instrument just increases the intra-monthly variance and consequently the error of the monthly mean. Thus, if we are dealing with monthly means, the error of a particular month is easy to determine: just divide the intra-monthly variance by the number of observations.   The overall effect of several months is then given by a weighted average of all such monthly errors as indicated in the second righthand term in (8.6).   As mentioned above, for the estimation of the true extra-monthly variability this variance has to be subtracted from the apparent extra-monthly variance.

        Summarising the above discussion, the total variance can be decomposed into:

$$\frac{1}{m-1}\sum_{k=1}^{N}\sum_{i=1}^{n_k}\left(x_i-\overline{x}\right)^2 \quad = \quad \frac{1}{m(m-1)}\sum_{k=1}^{N}\sum_{i=1}^{n_k}\left(x_i-\overline{x}\right)^2 \qquad (8.7)$$

$$+ \quad \frac{1}{m}\sum_{k=1}^{N}n_k\left(\overline{x}_k-\overline{x}\right)^2 \qquad (8.8)$$

$$- \; \frac{1}{m} \sum_{k=1}^{N} \frac{n_k}{n_k(n_k-1)} \sum_{i=1}^{n_k} (x_i - \bar{x}_k)^2 \qquad (8.9)$$

$$+ \; \frac{1}{m} \sum_{k=1}^{N} \frac{n_k}{n_k-1} \sum_{i=1}^{n_k} (\bar{x}_i - \bar{x}_k)^2 \qquad (8.10)$$

The four constituents are (8.7) error of the total mean, (8.8) apparent extra-monthly variance, (8.9) mean error of monthly means, (8.10) intra-monthly variance. In order to give an idea about the magnitude of these quantities, the variances of COADS derived latent heat flux for January are given in Figure 8.2 - 8.5. For these calculations only monthly 1° by 1° grid boxes with at least 2 observations can be taken into account, since errors should be definable, and 2 of such months should exist, to define the extra-monthly variance. These restrictions diminish the data base especially in the South Atlantic.

In the most parts of the Atlantic the error of the total mean is negligibly small (Figure 8.2). All other three components (Figures 8.3 - 8.5) reach their maxima in the Gulf Stream region, while the South Atlantic shows generally remarkable low variances. Comparing the different kinds of variance, it is not surprising that the intra-monthly (Figure 8.5) dominates: by averaging over a period of one month, the main part of variance will be cancelled out, so that the majority of the total amount is found inside the months and only a minor part remains for the extra-monthly variability. The prevailing of the inner variance is even increased by the effects of random errors. They are perceptible nearly entirely as an additional part of the intra-monthly variance, while only a small portion, depending on the number of observations, contributes to the error variance of monthly means. However, the intra-monthly variance is obviously not dominated by errors. Errors increase the intra-monthly variance by an amount which is equal to the mean individual observation error. In contrast to the extra-monthly case, the size of error effects does not depend on the number of observations so that a spatially homogeneous offset can be expected. Thus, the strong regional differences in intra-monthly variance are an indication for the dominance of natural variability.

However, the intra-monthly variance plays a minor role in our considerations, and is only used for the determination of the errors of our main topic, the monthly means. Their characteristics are given in Figure 8.3 and Figure 8.4. The apparent extra-monthly variance does not only reflect the true natural variability but overestimates the variance due to the included errors. These are depicted in Figure 8.4. The first striking feature is that the magnitude of the error variance is comparable to the apparent extra-monthly variance itself. Thus, the overestimation by the raw data is considerable. Subtracting the error from the apparent extra-monthly variance (not explicitly shown) reveals that the true extra-monthly variability is extremely small in the South Atlantic.

The strongest errors occur in the Gulf Stream, although this region has a remarkable high observation density. Obviously, the very strong internal variability is responsible for the high uncertainty. On the other hand, low errors are not only found in the shipping lanes but also in the South Atlantic, where an extraordinary low intra-monthly variability overcompensates the effects of sparse data coverage. Therefore, only few observations are enough to give relative accurate monthly means in that region.

One of the grid points with most observations in the central North Atlantic is considered in more detail (Figure 8.6). Error effects in such well covered regions are expected to be minimal. The latent heat flux at the selected point has a mean value of 116 Wm$^{-2}$, with a considerable extra-monthly variance. Additionally, the errors of monthly means are plotted, which depend on the intra-monthly variance and the number of observations. It becomes clear that the information about the errors is absolutely necessary, since otherwise we are not able to interpret such variability. In most months the error bar passes over the total mean line, indicating a reliability of less than 68% for a significant difference from the total mean. Total variance of the shown time series is about 1300 W$^2$m$^{-4}$. More than 60% of this is not due to

natural variability but due to errors. Remembering that such circumstances prevail in one of the best sampled regions of the world ocean, we realise the outstanding importance of errors.
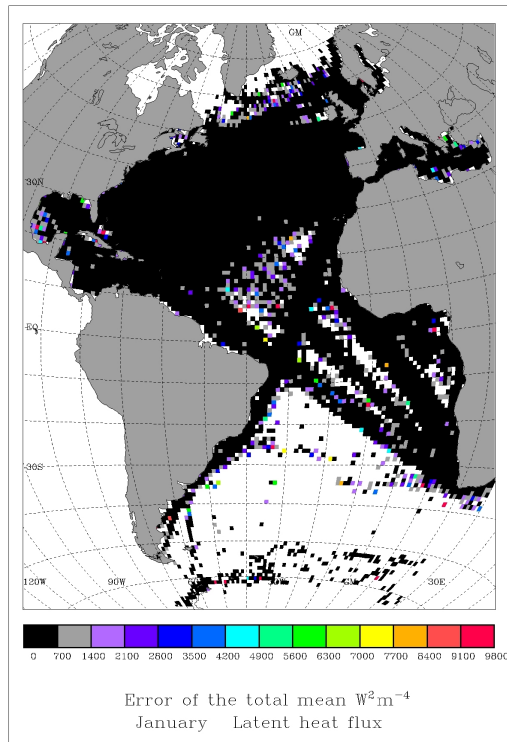


Figure 8.2 Error of the total means of LHF for January, from COADS 1940-1979.
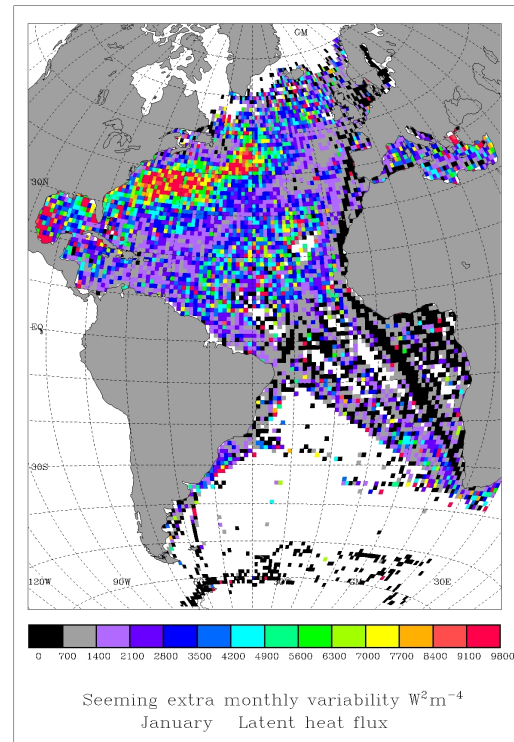


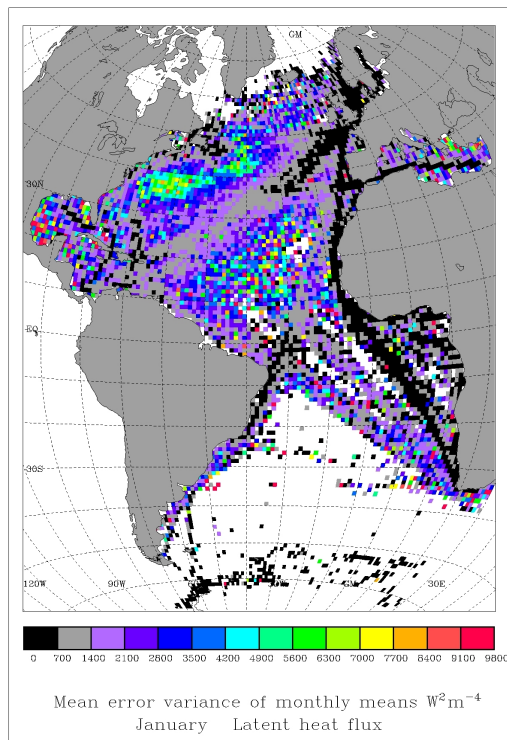Figure 8.3 As fig.8.2, but the apparent extra monthly variance
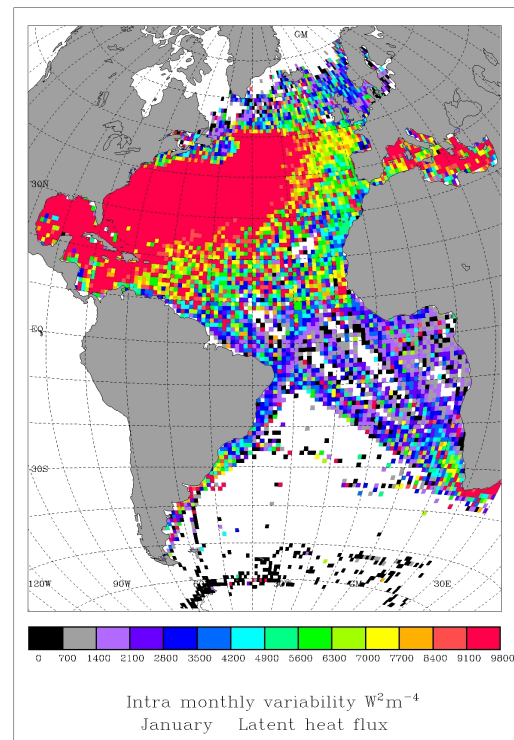


Figure 8.4. Error variance of monthly mean.



Figure 8.5 Intra monthly variance.
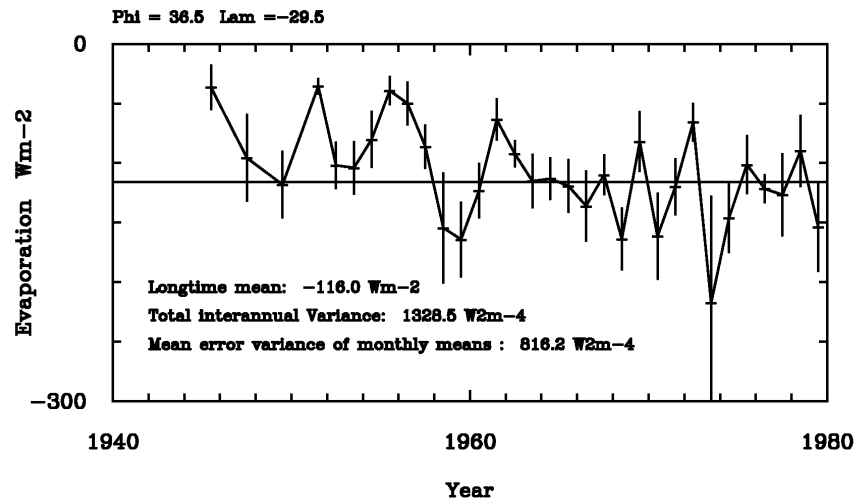
Phi = 36.5  Lam = -29.5



Figure 8.6. Example for the apparent extra variability and the error variance of monthly means for a 1° by 1° grid box in the North Atlantic (29.5° E, 36.51° N)

## 8.3 Systematic Errors

### 8.3.1 Introduction

Systematic errors occur in the measurement or estimate of the basic flux observables. They are also a fact of life within the parameterisations themselves, particularly for climate conditions that differ from those in which the parameterisation was developed. When such errors can be identified it is possible to correct their effects, but generally these errors are difficult to isolate. The key difference between systematic and random errors is that the overall systematic error is not dependent on the number of observations used to compute the flux.

### 8.3.2 Example of a parameterisation error

A possible misapplication of the Reed (1977) formula for shortwave radiation serves as an illustration for a systematic error due to parameterisation. The formula provides mean daily radiation using as astronomical input only the noon sun altitude. Obviously, such a crude parameterisation of clear sky radiation is only possible for constant latitudes. Consequently, the application of Reed's formula in high latitudes where long day lengths during summer compensate the relative low sun altitude would cause considerable systematic errors. For wind stress, to give another example, possible sources of systematic error are a mean underestimate of $C_D$ due to sea state effects or biases in the directly observed wind speed.

### 8.3.3 Determining errors in VOS reports

As an example of the determination of systematic errors in observational data consider the accuracy of data from the VOS. As for any systematic errors, determining the typical biases in the meteorological reports from merchant ships is very difficult. The accuracy depends not only on the calibration of the instruments, but their siting, the characteristics of the ship, and the way in which the observations were taken. One attempt to determine the systematic errors in ship data was the Voluntary Observing Ship Special Observing Programme - North Atlantic (VSOP-NA) project (Kent et al., 1993a). The method used was to choose a subset of 46 VOS, document the instrumentation used on each (Kent & Taylor, 1991), and ask the ships' officers to include extra information with each report. Since the ships would rarely pass close to one another, the output from an atmospheric forecast model was used as a common standard for comparison. The results were then analysed according to instrument type and exposure, ship size and nationality, and other factors. By this means relative biases could be determined. For example it was found that SST values from engine intake thermometers were biased warm compared to other methods (Kent et al. 1993a), and that daytime air temperatures were too warm due to solar heating (Kent et al. 1993b). It could be shown that the dew point

temperature was not biased by the latter error (Kent and Taylor, 1996) but, compared to aspirated psychrometer readings, the dew point was biased high when obtained from fixed thermometer screens. The VSOP-NA results suggested that correction of measured winds to allow for the height of the anemometer was advantageous. Following the VSOP-NA, later work by Kent and Taylor (1997) suggested that, for visually estimated winds, the form of the Beaufort scale devised by Lindau (1995a) gave best agreement with the anemometer winds.

A specific problem which affects VOS reports, and which can lead to errors which are systematic rather than random in nature, is errors in the reported ships' positions. About 2 to 3% of the VOS weather reports in COADS can be identified as having incorrect position information. Typically the position is incorrect by 10° or is in the wrong quadrant. Often these data exist in COADS as duplicates, one report having the correct position (Lander and Morrissey, 1987). Position errors are detected in operational forecast centres by tracking individual ships, but this is rarely done for climate studies. However position errors are potentially very serious because the ship might be falsely placed away from the shipping lanes in a data sparse region where the false report may be given undue weight. For example in January, 1984, ship reports from near Iceland appeared as a group of erroneous duplicates in the COADS data set, positioned near Antarctica.

### 8.3.4 Method of averaging fluxes

A particular problem connected with the issue of sampling, is the difference between the averaged fluxes computed from individual observations and from observations which have been previously averaged in space and time. Again this has the potential to introduce systematic errors.

The restricted computer power available in the past led to many "classical" flux fields being calculated from averaged observations rather than individual samples. Hence this problem has become known as the "sampling" versus "classical" difference in the flux fields. The present level of computer power and data availability allows fluxes to be calculated from individual observations - the sampling approach. However, reliable estimates of "sampling minus classical" differences for different flux components are still important for comparative assessments of historical data sets which are frequently only available as monthly or seasonal grids. Moreover, climate studies still use monthly averaged meteorological quantities to derive long-term series of sea-air fluxes. The problem is also important where fluxes are derived from satellite data since, in many cases, some variant of the "classical" approach must be used.

Comparisons of sampling and classical estimates of fluxes are given in many articles (e.g. Esbensen and Reynolds 1981, Hanava and Toba 1987, Ledvina *et al.* 1993, Gulev 1994, 1997b, Josey *et al.* 1995, Staneva *et al.* 1995, Zhang 1995, Esbensen and McPhaden 1996). Different authors report various "sampling minus classical" differences. Thus, for the sensible and latent heat fluxes, it is generally believed that sampling estimates are slightly higher than those computed using the classical method (by about 5 to 15 percent). Gulev (1994) and Staneva *et al.* (1995) reported larger sampling to classical ratios. Such errors will occur in regions where stronger winds are correlated with cold, dry air and large heat loss from the ocean. In contrast, Josey *et al.* (1995) found that sampling estimates for the latent flux may be smaller than classical estimates in the North East Atlantic due to negative correlations between the wind speed and humidity gradients. In this region, the stronger winds were often associated with the moist, warm air in the warm sectors of mid-latitude depressions.

The "sampling minus classical" differences will also strongly depend on the schemes used for determining the bulk transfer coefficients (Gulev, 1997b). For example, the Liu *et al.* (1979) scheme provides negative correlations between wind speed and the sensible and latent heat transfer coefficients for moderate and strong winds. The Smith (1988) parameterisation is also characterised by slightly negative correlations between wind speed and the coefficients for unstable conditions. Thus, estimates of "sampling minus classical" differences for these

schemes will be different compared to parameterisations which assume coefficient values which increase with wind speed.

*8.3.5 Further discussion*

Other examples of systematic errors in meteorological observations and their correction are described in Section 11.2.4. Systematic errors associated with parameterisations were discussed throughout Sections 5 and 6. Efforts to determine the total effect of the random and systematic errors on the total uncertainty is summarised in the next section.

## 8.4 Combining Errors

Sections 8.1-8.3 have concentrated on the quantification of random and systematic errors. To further assess confidence in our observational estimates, ultimately we need to know the combined effect on the observational uncertainty of all random and systematic errors. Gleckler and Weare (1995, 1997) attempted to formulate a strategy for combining all errors associated with VOS type flux estimates. They made use of simple sampling theory which is briefly summarised here: considering a field $F$, which is a function of $x$ and $y$, to first order the uncertainty estimate for a *single* measurement of $x$ and $y$ is:

$$\sigma_F = \sqrt{\left(\frac{\partial F}{\partial x}\right)^2 \sigma_x^2 + \left(\frac{\partial F}{\partial y}\right)^2 \sigma_y^2 + 2\rho_{xy}\left(\frac{\partial F}{\partial x}\right)\left(\frac{\partial F}{\partial y}\right)\sigma_x^2\sigma_y^2} \quad (8.10)$$

where $\sigma_x$ and $\sigma_y$ are the combined random and systematic uncertainties in $x$ and $y$, and $\rho_{xy}$ is the correlation between the error in $x$ and $y$. If $x$ and $y$ are independent, they are uncorrelated and the third term in the above equation vanishes. If they are fully dependent ($\rho_{xy}= 1$), then there is a maximum propagation of uncertainty in $\sigma_F$. In the case of anticorrelaton ($\rho_{xy} \leq 1$), or the partial derivatives with respect to $F$ are negative, the correlation term will act to reduce the uncertainty in $F$.

To estimate uncertainties from a *collection* of measurements of each observable, than the first RHS term can be expanded to:

$$\left(\frac{\partial F}{\partial x}\right)^2 \sigma_x^2 \Rightarrow \left(\frac{\partial F}{\partial x}\right)^2 \sigma_{x,xyx}^2 + \left(\frac{\partial F}{\partial x}\right)^2 \sigma_{x,ran}^2 f(N) \quad (8.11)$$

where $\sigma_{x,sys}$ and $\sigma_{x,ran}$ are respectively estimates of systematic and random uncertainties in $x$. Random uncertainties are reduced by some function of the number of available observations, $N$.

This simple treatment for the combination of uncertainties was generalised by Gleckler and Weare and applied to the same bulk parameterisations (and data) as used by Oberhuber (1988). Estimates of random and systematic errors for each basic observable and the parameterisations themselves were based on previous research, and were assumed to be constant in space and time. With the assumptions of a valid sampling theory and accurate uncertainty estimates, Gleckler and Weare were able to construct spatial maps estimating the relative importance of each uncertainty associated with the various heat flux terms. Spatial lag correlations were used to estimate the degree of spatial dependency from which random errors could be further reduced as zonal means.

Since the effort of Gleckler and Weare, several possible improvements to their method have been identified. First, there have been advancements with the parameterisations themselves in the subsequent work of da Silva *et al.* (1994) and Josey *et al.* (1999). Additionally, the estimation of random error reduction needs to be generalised to that outlined in Section 8.2.2, as Gleckler and Weare assumed temporal inhomogeneities to be nearly to be nearly Gaussian. But perhaps most importantly, significant refinements have been made to some of the uncertainty estimates used (by Gleckler and Weare) such as in the surface wind. But in fact the situation is likely to be more complex than merely updating error estimates, as Josey *et al.* (1999) have demonstrated, perhaps not surprisingly, that such errors are likely to

vary substantially in both space and time.   Thus any revisit of the method applied by Gleckler and Weare should take into account spatio-temporal variations in systematic error of basic observables and parameterisations.   Determining just what these variations are poses a significant challenge, and adds further argument to the plea for additional buoy deployments.

There has been progress in combining errors and estimating their relative importance. Quantification of the propagation of error estimates into total uncertainties should be an integral part of future flux estimates derived from VOS.   Such efforts should help to further establish confidence limits and assist us in determining how to improve them.   Clearly, further work is needed in this area.

## 8.5  Mapping errors

### 8.5.1  Introduction

Errors in flux fields may be caused by the need to smooth,  interpolate and extrapolate the data to generate global fields.   If not done correctly,  significant errors may be introduced into the analysis.   The "successive correction" method will be discussed as an example of a frequently used technique that is likely to introduce errors into a flux field.   An alternative method will then be described,  the "Kriging" technique,  which is computationally more expensive,  but which has the advantage of providing an error estimate for each part of the field.

### 8.5.2  Successive correction

Successive correction has been used in a number of studies to produce fields of geophysical variables (e.g. Barnes,  1964;  Levitus, 1982; 1994).   It has the advantage, compared to more sophisticated methods such as optimal smoothing (Kaplan *et al.* 1998), Kalman filtering, or optimal interpolation,  that it does not require information about the temporal and spatial structure of the data.   In particular, the recent surface flux climatologies of da Silva *et al.* (1994) and Josey *et al.* (1998; 1999) were compiled using this method.   Data within different radii of influence are weighted by distance and averaged in successive passes of the smoothing process.   The radii used by Levitus and da Silva were 1541, 1211, 881 and 771 km.   Josey *et al.* used 1541, 1211, 771 and 331 km, so this latter data set will contain structure on smaller scales than those of Levitus and da Silva.

Kent *et al.* (2000) have investigated the effects on a data set of smoothing by successive correction.   The resulting spatial resolution was estimated using a distribution of ship reports from a sample month.   Although the same characteristic radii were used over the whole globe, the resulting resolution was shown to be spatially variable depending on the local sampling density.   Thus in data sparse regions large month to month variability of the resolution could occur with changes in the distribution of the ship tracks.   The Josey *et al.* (1999) climatology, which was gridded at 1°,  was shown to have a typical resolution of 3°.   The mean resolution (using SST for January 1980 as an example) was 4.0 ° latitude by 5.8 ° longitude.   The maximum zonal spread of information was 50° and the maximum meridional spread was 19°. This reflected the choice of a zonal mean as the background field.   Thus  the resolution was significantly worse than the grid might suggest and information was smeared appreciable distances into data sparse areas.   An obvious example of the latter effect was the wind speed in the Southern Ocean in winter.   Since there were no data from much of the Southern Ocean, lighter winds observed further north are extrapolated southwards.   As a result the climatology shows significantly lighter winds than, for example,  were measured by satellite scatterometers in that region.

Kent *et al.* (2000) also showed that the successive correction procedure was not successful in removing all of the noise in data sparse regions.   Furthermore, the well-defined intermonthly variability in the main shipping lanes,  where there are many observations,  was degraded by the influence of poorer quality data in the surrounding regions.   This typically increased the intermonthly variability estimates in the shipping lanes by a factor of two.   In contrast,  the reduction of intermonthly variability in highly variable regions such as the Gulf

Stream by up to a factor of six, was greater than could be accounted for by noise in the individual ship reports. This reduction was due to the removal of small-scale variability by the smoothing process. Removal of coherent and persistent small-scale variability changed the temporal and spatial characteristics of the data. Kent *et al.* (2000) concluded that smoothing by successive correction, although commonly used, is poorly suited to such spatially inhomogenous data as those from the merchant ships.

Considering the impact of the successive correction smoothing on variability analysis using empirical orthogonal functions (EOF's), Kent *et al.* (2000) found little effect for the most significant modes of variability identified in the Gulf Stream region. This was because the large-scale variability occurs in the highest order modes. However, too large a fraction of the total variance explained was ascribed to these large-scale modes of variability. If raw data were used in the EOF analysis, variability with small spatial scales was more likely to be significant. Finally, little significance should be given to EOF modes with spatial scales similar to the size of gaps between shipping lanes; a distance which varies from region to region.

### 8.5.3 *Kriging of monthly means and error estimation*

#### A. INTRODUCTION

On a global scale, monthly means represent the shortest time resolution where ship observations provide reasonable results. However, even on that relative long time scale, data density begins to degrade drastically for most regions of the world ocean. In this situation the error variance of the observations begins to dominate. Therefore, monthly maps of the raw data show large unrealistic scatter which has to be eliminated. Many smoothing techniques exist, leading in each case to an acceptable appearance of the maps. But often these techniques are used in a somewhat arbitrary manner by repeating them over again until the result looks satisfactory. Clearly, we cannot be sure that such results are optimal.

It should be mentioned here, that a widely used technique for eliminating error effects, that is searching for the best bi-linear or higher order 'surface', has disadvantages. Such fitting of polynomials is used to discriminate the errors from the true natural part of the total variance. The spatial variability of the fitted 'surface' is considered to be true. Any additional variance, that is deviations of the data points from the fitted polynomial, is identified as observation error. However, polynomials of higher order are able to follow the structure of the data better and include more variance, so that the data appears to be more accurate. Which order of polynomial is appropriate is not exactly definable, so that the resulting error estimates are not entirely objective.

In Section 8.2.2 we pointed out that it is absolutely necessary to provide not only the monthly fields of air-sea fluxes but also the error estimates of each field, because in most regions of the world ocean the magnitude of error variance is comparable to the natural variability. Without knowledge of the errors the interpretation of variability is not possible.

Kriging techniques provide both optimum fields of the considered parameters together with an error map. Therefore these techniques are especially suitable for the inhomogenously distributed ship data set. In addition, it is possible to produce complete fields of values even in areas with a very low data density. Without an explicit knowledge of the errors, these regions are often left as blank areas on flux maps because the errors appear to be irresponsibly large. Kriging provides an error estimate for each point so that users may decide whether uncertain values should be omitted. Experience shows that many users would fill gappy data on their own, so that the optimal value, even if very uncertain, is better than blanks.

#### B. PRINCIPLES

In principle Kriging can be regarded as a prediction of a value $x_0$ at a location $P_0$ where no measurement has been carried out, by using information from measurements in the surrounding region, at $P_i$. That means the following expression has to be solved:

$$x_0 = \sum_{i=1}^{n} \lambda_i (x_i - \Delta x_i) \qquad (8.12)$$

where $x_0$ is the value which has to be predicted. $x_i$ denotes the available measurements and $\Delta x_i$ their errors. The task is to determine the weights $\lambda_i$. Obviously, a solution is not possible for one single case. But if a time series of $m$ measurements at each location $P_i$ is available, a reasonable requirement is that the mean squared deviation between predictions and truth is minimal:

$$\sum_{t=1}^{m} \left( x_0 - \sum_{i=1}^{n} \lambda_i (x_i - \Delta x_i) \right)^2 = \text{min} \qquad (8.13)$$

Differentiating (8.13) leads to the following expression, where, for the sake of clarity, the temporal summation is abbreviated by brackets [].:

$$
\begin{pmatrix}
[x_1 x_1] + [\Delta x_1 \Delta x_1] & [x_1 x_2] & \cdots & [x_1 x_n] \\
[x_2 x_1] & [x_2 x_2] + [\Delta x_2 \Delta x_2] & \cdots & [x_2 x_n] \\
\vdots & \vdots & \vdots & \vdots \\
[x_n x_1] & [x_n x_2] & \cdots & [x_n x_n] + [\Delta x_n \Delta x_n]
\end{pmatrix}
\bullet
\begin{pmatrix}
\lambda_1 \\
\lambda_2 \\
\vdots \\
\lambda_n
\end{pmatrix}
=
\begin{pmatrix}
[x_0 x_1] \\
[x_0 x_2] \\
\vdots \\
[x_0 x_n]
\end{pmatrix}
$$
$$(8.14)$$

Thus, a linear set of equations results, containing the covariance matrix between the data points $P_i$ with the error variances on its diagonal, and a vector giving the covariance between the predicting point $P_0$ and the locations $P_i$ where measurements are available. If these quantities are known, the solution of the above set of equations leads, via the determination of the weights $\lambda_i$, to the optimal prediction at $P_0$.

Obviously, the minimised expression in (8.13) is equal to the error of the predicted value, often called as Kriging error. Transformation of that expression leads to:

$$[x_o x_o] - 2 \sum_{i=1}^{n} \lambda_i [x_o x_i] + \sum_{i=1}^{n} \sum_{j=1}^{n} \lambda_i \lambda_j [x_i x_j] + \sum_{i=1}^{n} \lambda_i \lambda_i [x_i x_i] \qquad (8.15)$$

The first term of the transformed Kriging error denotes the variance at $P_0$. If the calculations are carried out with normalised anomalies

$$x_{\text{norm}} = \frac{x_i - \overline{x}}{\sigma_x} \qquad (8.16)$$

which is advantageous for many reasons: $[x_0 x_0]$ is equal to unity. That means if no information at all is available, the error is equal to the interannual variability. This is reasonable because without any information we cannot do more than predicting the long-time mean of this location. The error of such a crude procedure is easy to realise. If we predict for every month of a time series just the total mean, the error defined by the mean squared deviation between truth and prediction is obviously the intermonthly variance itself. This fact is represented by the first term in (8.15). A further conclusion of the above discussion is that the maximum error for monthly means is the intermonthly variability of the considered location.

The second term in expression (8.15) contains the covariances between the predicting point $P_0$ and the data points $P_i$, and represents that part of the Kriging error which can be called 'information'. Its negative sign indicates that the error decreases with increasing information. But information of the data points $P_i$ are not independent from each other, as two points in close vicinity carry more or less the same information. That is what the third term represents which we can call 'redundance'. Covariances between the data points increase the error. Obviously the fourth term describes the effects of individual errors for the data points used.

C.  NUMERICAL IMPLEMENTATION AND PRESELECTION

If a fixed number of $n$ observations is preselected, the Kriging technique is easy to apply.  By solving only a single set of linear equations (8.14) the optimum value at the predicting point is obtained.  That is of course only optimal under the condition that the preselected data points should exclusively be used.  However, the use of an additional data point $P_{n+1}$ could improve the result.  On the other hand, also omitting some data points of high individual error and redundance may lead to an improvement.  Thus, a kind of meta optimum has to be searched for.

The amount of information carried by a certain measurement does not only depend on its accuracy and its distance to the predicting point, but also on its redundancy in relation to the other points already used (8.15).  That makes an *a priori* order of rank concerning the quality of data points impossible.  Thus, beginning with the trivial prediction, the long-term mean, we have to select always that data point explaining for the moment the most variability at $P_0$.  As more and more points are included,  the Kriging error decreases.  The meta optimum is found, when no additional point is able to diminish the Kriging error under the condition of a positive weight $\lambda_{+1}$.

However, as outlined the method is arduous and time consuming.  As mentioned above a preselection of a fixed number of observations would provide only the optimum result for that specific combination, but we are searching for the meta optimum.  Nevertheless, a kind of meta preselection is necessary in any case.  Considering only the Atlantic,  on a spatial resolution of $1°$ by $1°$,  about 10,000 possible data points are involved.  Solving a huge number of 10,000 by 10,000 matrices becomes a problem even for modern computers.  On the other hand the meta preselection should not be too petty in order not to risk missing the meta optimum.  Dealing with 100 data points in the surrounding of the predicting point $P_0$ is therefore realistic.  The determination of the second data point (the first is trivial) requires solving 99 2-by-2 matrices, that of the third one 98 3-by-3 matrices, and so on.  These are still rather extensive calculations.  When arriving at,  say 58 43-by-43 matrices,  where the meta optimum may be finally found, we have to be aware that only one single monthly mean of a single parameter in one specific year at one point in the world ocean is determined.

A substantial reduction of computing time is attainable, when the potential change of the Kriging error for an additionally included data point $P_{n+1}$ is considered.  Instead of solving several matrices the potential change of Kriging can be directly computed from:

$$-2\lambda_{n+1}[x_0 x_{n+1}] \; + \; 2\lambda_{n+1}\sum_{i=1}^{n}\lambda_i[x_i x_{n+1}] \; + \; \lambda_{n+1}^2[x_{n+1}x_{n+1}] \; + \; [\Delta x_{n+1}\Delta x_{n+1}] \qquad (8.17)$$

The first two terms are giving information and redundance gain, respectively.  The last two describe natural and error variance for the potential new data point $P_{n+1}$.  The point with the highest potential Kriging error reduction is actually included, and the exact new Kriging error is obtained by solving only one single (n+1) by (n+1) matrix.  Following the above described technique, optimum monthly mean fields, always paired with their error fields, are obtained with an acceptable expenditure of time.

D.  MEANING OF THE SUM OF WEIGHTS

Spatial gradients in long-term mean fields are not treatable with correlation techniques. This becomes obvious by considering the following example.  In the extreme case two neighbouring points with different total means may well have a correlation up to 1.  In that case we would be able to predict exactly the monthly anomalies of one point from the other, but of course not the supposed difference between their long-term mean, because correlations do not contain any information about the averages at both locations.  That is the main reason for the use of anomalies instead of absolute values.

Dealing with anomalies, a constraint for the sum of weights:

$$-2\lambda_{n+1}[x_0 x_{n+1}] \quad + \quad 2\lambda_{n+1}\sum_{i=1}^{n}\lambda_i[x_i x_{n+1}] \quad + \quad \lambda_{n+1}{}^2[x_{n+1} x_{n+1}] \quad + \quad [\Delta x_{n+1}\Delta x_{n+1}]$$

(8.18)

is not necessary, moreover, it would not be useful.  To illustrate that,  the trivial case of Kriging with only one available data point may be considered.   The minimising condition of (8.13) is simplified to:

$$\sum_{t=1}^{m}\left(x_0 - \lambda_1(x_1 + \Delta x_1)\right)^2 \quad = \quad \min$$

(8.19)

with the solution:

$$\lambda_1 \quad = \quad \frac{[x_0 x_1]}{[x_1 x_1] + [\Delta x_1 \Delta x_1]}$$

(8.20)

In the denominator the total variance at $P_1$ appears, split into the natural and the error variance. The numerator shows the covariance between the predicting and the data point.   Analogue to the slope of a regression line, the entire fraction is equal to the relative variance at the predicting point, which is explained by the time series at $P_1$.   Because of the errors at $P_1$, $P_0$ is in any case not completely predictable.   Consequently, the variance at $P_0$ is underestimated, a known and unavoidable feature of regression techniques.   Thus, when Kriging techniques are applied to anomalies, the sum of weights can obviously be interpreted as the sum of explained variance.   Values less than 1 do not indicate a bias, as for absolute values, but a reduction of variance to the explainable portion, which is indeed reasonable.

E.  ESTIMATION OF THE TRUE COVARIANCE FROM REAL DATA

According to (8.14), a prerequisite for the application of the discussed Kriging technique is the knowledge of the spatial covariance matrix.   Since complete time series for all points in the world ocean, as conceived in (8.13), are obviously not available, mean covariances have to be derived.

Firstly, the covariance of two time series strongly depends on the distance between the observation places.   For many applications it is therefore sufficient to assume a constant covariance for a given distance.   However, on global scale anisotropy has to be taken into account, additionally.   Secondly, spatial covariance strongly depends on the considered time scale: the prediction of the annual anomaly at a certain location is indeed possible with measurements from a far distant station, while short-term variability is connected only over short distances.   Since we are aiming at the correlation length of monthly means, covariances should of course be calculated on the base of monthly means, which show much larger correlation lengths than individual observations representing a quasi instantaneous snap shot.

Thus, the average covariance of monthly means is calculated separately for each parameter as a function of distance and direction.   Due to the spatial averaging, the covariances of different regions are lumped together.   Therefore it is advantageous to normalise the anomalies according to (8.16).   Otherwise regions of high variability would dominate the results.   The normalisation allows to take into account adequately the information from low variability regions, such as the tropics.

An exponential fit over the covariances, which due to the normalisation are converted into correlations, conserves the directional information:

$$r = a_0 e^{-\sqrt{\frac{x^2}{a_1^2}+\frac{y^2}{a_2^2}}}$$

(8.21)

where $r$ denotes the correlation, $x$ and $y$ the zonal and meridional distances, respectively.

After the derivation of the coefficients $a_i$ in (8.21), we are able to describe the correlation as a pure function of the position. However, the coefficients $a_i$ are derived by using real observations, which are of course affected by errors. But for the intended Kriging technique information about the natural covariance on the one hand and the error variance on the other hand is needed separately. Therefore, we have to consider to which extent the observed correlation, given in (8.21), is diminished compared to the actually sought true natural correlation.

For error affected anomalies the correlation between two points is:

$$r_{err} \quad = \quad \frac{\sum\left((x_1 + \Delta x_1)(x_2 + \Delta x_2)\right)}{\sqrt{\sum(x_1 + \Delta x_1)^2 \sum(x_2 + \Delta x_2)^2}} \tag{8.22}$$

Assuming that errors $\Delta x_1$ and $\Delta x_2$ are random, the above equation can be transformed to:

$$r_{err} \quad = \quad \frac{\sum x_1 x_2}{\sqrt{\left(\sum x_1 x_1 + \sum \Delta x_1 \Delta x_1\right)\left(\sum x_2 x_2 + \sum \Delta x_2 \Delta x_2\right)}} \tag{8.23}$$

On the other hand, the true natural correlation, unaffected by errors, is:

$$r_{true} \quad = \quad \frac{\sum x_1 x_2}{\sqrt{\sum x_1 x_1 \ \sum x_2 x_2}} \tag{8.24}$$

The quotient of both is equal to:

$$\frac{r_{err}}{r_{true}} \quad = \quad \sqrt{\frac{\sum x_1 x_1 \ \sum x_2 x_2}{\left(\sum x_1 x_1 + \sum \Delta x_1 \Delta x_1\right)\left(\sum x_2 x_2 + \sum \Delta x_2 \Delta x_2\right)}} \tag{8.25}$$

which is equal to the quotient of the true variance, excluding errors, and the total variance, including errors. This becomes clearer when, for the moment, spatially homogenous variances are assumed, so that (8.25) is simplified to:

$$\frac{r_{err}}{r_{true}} \quad = \quad \frac{\sum x_1 x_1}{\sum x_1 x_1 + \sum \Delta x_1 \Delta x_1} \tag{8.26}$$

Due to errors, the observed correlation is reduced by the above given expression. Since errors do not dependent on distance, it is a reduction by a constant factor. The magnitude of this factor is given by $a_0$ in (8.21), because at distance zero the true correlation is equal to 1, so that here the observed correlation becomes equal to the reduction factor. Thus, the true correlation is obtained by a simple division of (8.21) by the factor $a_0$:

$$r = e^{-\sqrt{\frac{x^2}{a_1^2} + \frac{y^2}{a_2^2}}} \tag{8.27}$$

Besides the true spatial correlation, given in (8.27), the individual error variance of the used data points has to be known for solving the Kriging (8.14). As discussed in section 8.2.2, the error of an individual monthly mean is obtained by dividing the intra-monthly variance of that particular month by the number of available observations. For months with only a single observation the intra-monthly variance is not attainable. In order not to lose the information of such months, the error variance is assumed to be as high as the total variance at this location.

Applying the above described technique, monthly fields of the air-sea fluxes are derived. Figure 8.7 shows an example for the latent heat in January 1979, while the corresponding errors are given in Figure 8.8. In the region south of 40°S the errors are increasing up to values of 1, which is the theoretical maximum. As mentioned above, a

normalised error of 1 indicates that no information is available at all. In this case the error is equal to the interannual variability. However, since the interannual variability is extremely low in the South Atlantic, the absolute error in this region is astonishing small. Thus, we are in a lucky position. In regions as the North Atlantic, where due to high interannual variability the determination of monthly means is very difficult, many observations are available. In the South Atlantic the data base is much smaller. But both intra-monthly and extra-monthly variability are low. The first reduces the individual errors of monthly means, the second guarantees a limitation of the absolute Kriging error, even if the normalised Kriging error reaches maximum values.
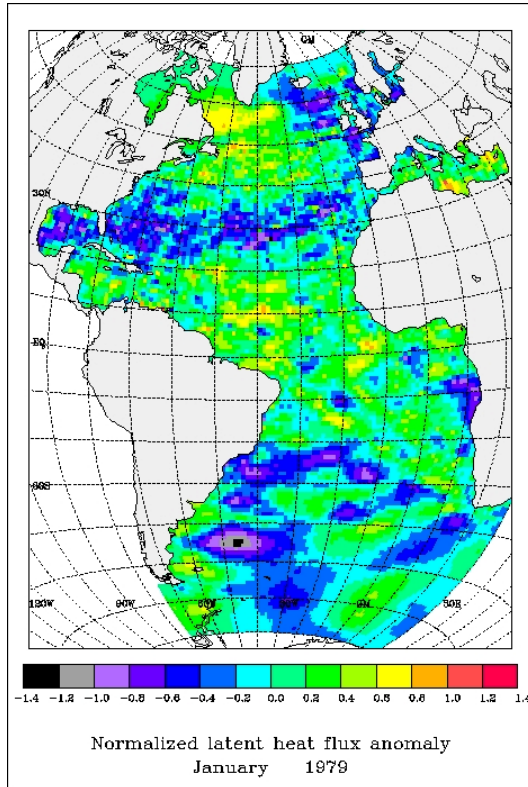


Figure 8.7 Example of a Kriging result. Values are normalised by the total standard deviation at each grid point.
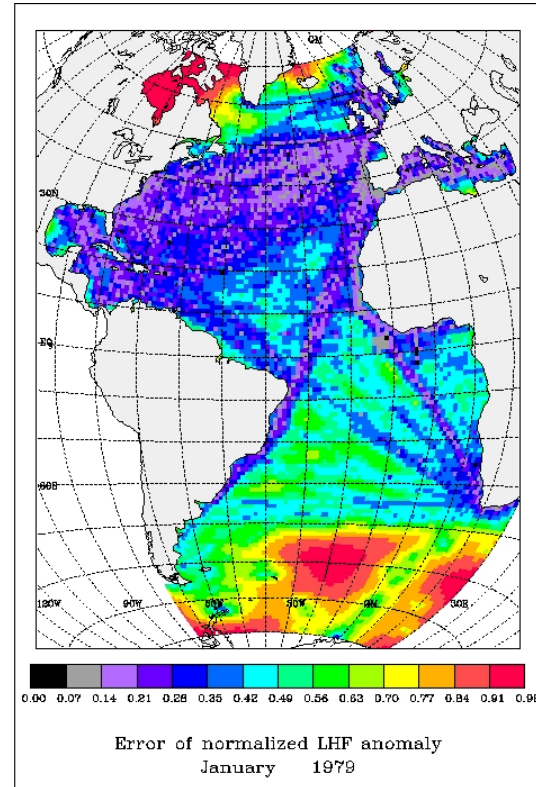


Figure 8.8. As figure 8.7, but for the Kriging error

## 8.6  Sampling problems for satellite-derived quantities

### 8.6.1 Introduction

Temporal sampling limitations of a sensor can be the most important source of both random and systematic error in longer term (i.e. monthly and longer) applications. This is especially bad for quantities like precipitation that exhibit a highly intermittent behaviour in space and time and can also have a significant diurnal cycle. The only way out of this dilemma is to combine measurements of the same kind of sensor at different orbits, or measurements from different instruments like infrared sensors on geostationary satellites and microwave sensors as done in the GPCP. Since the sampling situation is worst for precipitation the next section deals exclusively with that variable. For all other satellite-derived quantities, the sampling errors found for precipitation can be regarded as a maximum estimate.

### 8.6.2 Sampling errors for precipitation

A paper by Salby and Callaghan (1997) concentrates on the under-sampled diurnal variability using polar-orbiting measurements. They compared the time-mean behaviour of global cloud distributions to the true time-mean behaviour determined from the high-resolution

Global Cloud Imagery (GCI) according to different orbital and viewing characteristics of one and multiple platforms.  The main conclusion is that the pattern of the time-mean error closely resembles the pattern of error in the mean diurnal cycle.  This means that precessing instruments like TRMM can describe the right time-mean behaviour only as accurately as they can determine the mean diurnal cycle.  If measurements are averaged over many months to make the determination of the diurnal cycle more consistent,  the time-mean behaviour is contaminated by seasonal variations,  which is also not desirable.

Another study of satellite orbits has been performed by Shin and North (1988).  They used a stochastic model and data from the GATE I experiment to represent rainfall statistics. They stated sampling errors for a low inclination satellite at a height of 300km like TRMM of 8-12% for a monthly mean rainrate over a grid box of 5° x 5° in the tropical ocean.  This is roughly the same as what is found for instruments in a sun-synchronous orbit like the SSM/I with heights of around 750km.  It should be noticed that for a polar orbiter the maximum sampling error is located near the equator where the sampling interval is sometimes only 24h. For a precessing instrument like TRMM the sampling error increases with increasing latitude because of the uneven sampling if so called flush visits (the whole grid box is seen at one visit) are considered.  This effect is counteracted by the increasing sampling area with latitude when partial visits are considered (Shin and North, 1988).  Because there can be some doubt about the validity of GATE rainfall statistics for the whole tropical ocean,  Oki and Sumi (1994) used radar-derived rainfall maps around Japan and found for a 5° x 5° grid box a sampling error of 16% which increases at a box of 2.5° x 2.5° to 24% for the TRMM TMI swath.  The study of Soman *et al.* (1995) using data from the Darwin radar in Australia also stated high sampling errors up to 65% for sun-synchronous orbiters with a sampling interval of 24h and much lower errors (5%-10%) for non-sun-synchronous orbiters.  However, the last two studies also include data over land surfaces where the diurnal cycle of precipitation is much more distinctive,  and in the case of the Japanese data,  not only tropical convective rainfall but also midlatitude cyclones were included in the analysis.

All the above mentioned studies found that any combination of sun-synchronous with sun-synchronous or with non-sun-synchronous orbits reduces the sampling error to less than 10% if an optimal time sampling interval is chosen.  With four SSM/Is in space,  and two AMSR's to come within the next year,  it should be possible to estimate the time-mean behaviour of precipitation and all other parameters detectable at microwave frequencies with reasonable quality.  But only if all available data are used which is not the case for most existing climatologies.  Combination of microwave and infrared instruments on low orbit (300-750 km) and geostationary satellites remains attractive if an optimal coupling of methods is applied.

*8.6.3 Scatterometer Sampling Errors*

The irregular sampling from polar orbiting spacecraft leads to significant errors and loss of equivalent resolution in gridded wind fields created from remotely sensed data.  Thus, although measurements are acquired densely within swaths, the limited swath widths and spacecraft revisit times result in errors in gridded fields constructed from satellite measurements, owing to variability in the true surface field that was not measured by the satellite instrument.  The magnitudes and types of these "sampling" errors are complicated functions of the instrumental coverage (i.e., swath width and orbit) and the natural spatial and temporal variability of the true surface wind field.

Sampling errors and degraded equivalent resolution have important negative impacts on the scientific utility of remotely sensed data.  Ocean and climate models respond sensitively to wind forcing on a broad range of scales.  Modelling studies by Large *et al.* (1991) and Chin *et al.* (1997) demonstrate clearly that large-scale, low-frequency upper ocean circulation is sensitive to high-frequency, small-scale wind forcing - the large-scale circulation patterns change if the small-scale wind forcing changes.  Small-scale, high-frequency wind forcing information is thus a fundamental requirement for climate modelling and prediction,

notwithstanding the fact that the climate system variables of interest involve inherently large temporal and spatial scales.   Large *et al.* (1991) suggest that 2-3 day temporal resolution at 2 x 2 degree spatial resolution is required to properly reproduce the intra-annual streamfunction variance and barotropic Rossby wave response of the ocean in the mid and high latitude regions.   The required temporal resolution should be finer going equatorward, because the Rossby wave becomes faster.

As an attempt of determining a desirable resolution for scatterometer products,  analysis metrics have been developed by Chelton and co-workers (e.g. Greenslade *et al.*, 1997) to quantify the effective resolution of remote sensing systems and have been applied to present and planned scatterometer systems by Chelton *et al.* (1997).   The latter analysis showed that a single polar-orbiting, dual-swath scatterometer with NSCAT sampling (600 km wide swaths separated by a 329 km nadir gap) yielded an equivalent resolution of 2 x 2 degrees and nearly 20 days at 30 degree latitude.   (Resolution metrics are based on a threshold of 0.72 ms$^{-1}$ sampling-induced random component error.   Increased equivalent temporal resolution can be obtained at the expense of lower spatial resolution.   These values depend on the selected threshold value.)   In the satellite scatterometer science community, there are many efforts of constructing gridded products using different construction procedures and different temporal and spatial resolutions (e.g. Zeng and Levy, 1995;  Kutsuwada, 1998; Kubota and Yokota, 1998; Kelly *et al.*, 1999).   Continuous swath instruments (such as the one to fly on QuikSCAT and ADEOS-2) can achieve smaller spatial and temporal resolutions given the QuikSCAT orbit.

Thus,  although wind forcing information from spaceborne scatterometers has great scientific potential and utility,  no single polar-orbiting vector wind instrument can provide the data required to produce wind forcing fields with complete and proper temporal and spatial resolution for climate modelling (independent of the measurement accuracy and resolution within the satellite swath).   However, tandem missions, such as QSCAT and ADEOS-2, or possibly a SeaWinds and an ASCAT instrument,  would provide data with sufficient equivalent resolution to allow accurate climate modelling and prediction.

## 9 METHODS OF EVALUATING FLUXES AND FLUX RELATED PRODUCTS

### 9.1 Introduction

This Chapter will consider methods which can be used for verifying flux fields. Accurate flux data which can be used as a reference for verification purposes are difficult to obtain. In general there is a trade-off between accuracy and temporal and spatial coverage. Thus the most accurate flux estimates are obtained from dedicated air-sea interaction experiments which are mounted in a restricted area for a limited period, perhaps one or two months. The accuracy of these research quality flux measurements will be discussed using the TOGA-COARE experiment as a "State of the Art" example (Section 9.2.1). "Flux" buoys have been developed to obtain measurements of high enough quality such that the derived fluxes may be used for verification purposes. Such buoys have been deployed at a limited number of locations for typical periods of up to a year, occasionally longer. The data obtained is less comprehensive than that from air-sea interaction experiments but covers longer periods and more locations. The data quality (Section 9.2.2) is significantly better than that obtained from operational meteorological buoys. Research ships have been used in "opportunistic" mode to obtain time series of automated meteorological data during cruises designed for other purposes. As an example of these data, the data set obtained from the WOCE Hydrographic Programme ships will be considered (Section 9.2.3). This data set is important in that a special effort was made to assemble the data into a single data resource to which consistent quality control procedures had been applied. Such ship data can sample a wider range of geographical locations compared to the high quality buoy data; however the ships are a poorer instrument platform, and a long time series from any given area is generally not available. Finally, with regard to sources of flux reference data, the only routinely measured direct flux data is that for radiation, albeit from a limited number of locations. This will be briefly discussed in Section 9.2.4 (for more detailed discussion of direct radiation measurements see Section 5.2).

For many flux field products, suitable flux reference data are not available. In this case much can be learnt by intercomparing one product with another and this method will be used extensively in Chapters 10 and 11. In this Chapter we will consider two specific cases of such intercomparisons; the comparison with specialised products (Section 9.3.1) and comparison of the variability patterns in flux fields (Section 9.3.2). While intercomparisons allow for relative assessment of the flux field products there still remains the problem of deciding which product might more nearly represent reality. There is also the need to identify and correct for residual systematic errors in the data. A number of integral constraints are available and have variously been used for that purpose. These include the global heat and water balance (Section 9.4.1), the meridional heat and freshwater transports (Section 9.4.2), the heat and water balance of enclosed (or semi-enclosed) seas (Section 9.4.3), and ocean mixed layer budgets (Section 9.4.4).

### 9.2 Sources of reference data

*9.2.1 The accuracy of research quality measurements: experience from TOGA-COARE*

The most accurate source of basic observations for calculation of fluxes or validation of models is expected to be that obtained from ships and moorings during the small (but increasing) number of intensive air-sea measurement campaigns mounted each year in support of some particular research project (e.g. BOMEX, TOGA-COARE, SOFIA, JASMINE, etc). The instruments and methodology are usually under the supervision of scientists with particular expertise in field measurement and instrumentation. However, the harsh marine environment and limitations imposed by the platform itself, can easily degrade instrument performance relative to its calibration in the laboratory or exposure on dry land, and in unexpected ways. The state of the art for individual variables will be discussed at more length in Section 10; here we summarise the accuracy of research quality observations, as revealed by the TOGA-COARE experiment November 1992 - March 1993.

The TOGA-COARE expedition involved 15 ships, 7 aircraft and several moorings, one of which (the IMET mooring from WHOI; Hosom *et al.*, 1995) was developed specifically to obtain high quality meteorological measurements for flux calculation. Six survey ships were specially equipped for the measurement of fluxes. The cruise plans of these ships were co-ordinated to allow 2 days from the experiment total of 120 days to be dedicated to *in situ* comparison of individual instruments and, subsequently, the calculated fluxes. This was done by cruising upwind in close formation in the vicinity of the IMET buoy. Aircraft which were operational on those particular days performed repeated low-level fly-overs.

The quality of surface flux measurement achieved during TOGA-COARE is due in large measure to these field intercomparisons, carefully analysed during a series of workshops involving PI's responsible for measurements on the various platforms (Bradley and Weller, 1995a,b; 1997; Bradley et al, 1997). Instrumental faults and calibration errors were discovered which would otherwise have remained undetected. The usual procedure was to obtain "best" estimates for each variable during the intercomparison days. In some cases a particular instrument was identified as being the most reliable, on the basis of proven performance, stability of calibration, or mode of operation. Otherwise, an ensemble average was taken as the "correct" observation. At the end, bias and calibration corrections were obtained for all instruments; those with obvious calibration or other problems were recalibrated where possible.

The above effort to refine accuracy of the surface measurements was driven by the TOGA-COARE goal of no more than 10 $Wm^{-2}$ uncertainty in the total surface energy budget of the ocean (WCRP, 1990). As Fairall *et al.* (1996a) point out, this implies accuracy requirements for the individual bulk measurements, assumed independent, of about 0.2 $ms^{-1}$ for wind speed, 0.2°C for both air and sea surface temperature, and 0.2 g $kg^{-1}$ for humidity. Subsequently, Burns *et al.* (1999, 2000) have compared aircraft measurements with the surface platforms, using data from the two days and other occasions of coincidence during the experiment. Table 9.1 gives estimates by some PI's of the accuracy of their measurement following the TOGA-COARE intercomparison process, as provided to Burns *et al.* (1999, 2000). Some of these estimates appear rather optimistic; others seem conservative. Without details of how they were arrived at, and what sources of uncertainty are included, they can be regarded as a guide only, but illustrate some useful points (see also section 10).

Table 9.1 Subjective estimates (by the observers) of the accuracy of measurement on some platforms following TOGA-COARE intercomparison corrections. The last row is an estimate of what might be presently achieved under similar, tropical or subtropical, weather conditions. Accuracies in higher latitudes are likely to be worse.

| Platform | Winds $ms^{-1}$ | Air Temp.°C | Humidity g $kg^{-1}$ | Sea Temp.°C | Shortwave $Wm^{-2}$ | Longwave $Wm^{-2}$ |
|---|---|---|---|---|---|---|
| *R/V Moana Wave* | ±0.2 | ±0.2 | ±0.4 | ±0.2 | ±4 | ±2.5 |
| *R/V Wecoma* | ±0.2 | ±0.2 | ±3% | | | |
| *R/V Franklin* | ±0.2 | ±0.05 | ±0.15 | ±0.1 | ±3 | ±5 |
| IMET | ±2.5% | ±0.1 | ±0.1 | ±0.1 | ±3 | ±10 |
| ATLAS | ±0.2 | ±0.17 | ±4% | ±0.03 | | |
| Present practice | ±0.2 | ±0.1 | ±0.2 | ±0.25 (SSST) | ±3 | ±2.5 |

❍ Wind speed: all PI's considered that their wind speed measurements met the COARE goal of 0.2 $ms^{-1}$ accuracy

❍ Air temperature and humidity: on *R/V Franklin* $T_a$ (and $Q_a$) were measured with aspirated psychrometers, mounted on a boom ahead of the ship. Over land, accuracy of one or two hundredths of a degree in both wet and dry bulb temperatures can be achieved with such

instruments, but shipboard this degrades for several reasons. Other temperature/humidity measurements in the table were made with commercial sensors, comprising a Platinum resistance thermometer and moisture-sensitive polymer, basic specifications for which barely meet the COARE criterion. However, the most serious source of error (>1°C) arose from diurnal heating when the sensors were mounted in simple unaspirated screens. For this, a correction algorithm was devised (Anderson and Baumgartner, 1998). Then all air temperature measurements met the COARE goal, but not all humidities.

❍ Sea temperature: higher accuracy is possible for water temperature, using precision thermistors, because solar heating is generally negligible, the water temperature varies slowly, and because the heat capacity of water is much higher than air. During the COARE intercomparisons, night time sea temperatures agreed within 0.1°C across several platforms when the surface layer was well mixed, implying good calibration technique. However, the quoted accuracies are for sensors at various depths, and do not reflect the accuracy of skin temperature measurement (SSST); this requires extrapolation to the surface via models of the cool skin and diurnal heating (Fairall *et al.*, 1996a). The physics of the former phenomenon is well enough understood that it may be calculated to order 0.1°C. Thus the accuracy of SSST derived from the Moana Wave sensor at ~0.05m depth is probably ±0.25°C, whereas the other platforms must add the uncertainty of a mixed layer model to the quoted accuracy. With the best current instruments, direct radiometric measurement of SSST has an accuracy of about 0.2°C (Barton *et al.*, 1995).

The COARE intercomparison initiative alerted observationalists to several potential sources of error in air-sea measurement. This, together with some instrument development since COARE, might be expected to improve the accuracy of measurement of basic flux-related variables in subsequent air-sea interaction studies. The bottom line in Table 9.1 is an attempt to estimate measurement accuracy currently achievable, using equipment readily available to the investigator. A final word of caution is necessary however. TOGA COARE took place in a region of relatively benign weather. Achieving these accuracies in stormy conditions at mid to high latitudes may be significantly more difficult.

### 9.2.2 High quality buoy data

The establishment of "Flux calibration sites" for verifying the fluxes from climatologies (based on *in situ* and satellite data), and from models, was recommended by WCRP (1989). Perhaps the nearest realisation of such sites has been the series of mooring deployments undertaken by the Woods Hole group; for example, the Subduction experiment in the North Atlantic (Moyer *et al.*, 1996), the Improved Meteorological System (IMET) mooring in the west Pacific during the TOGA COARE experiment (see previous section - Weller and Anderson, 1996), and in the Arabian Sea (Weller *et al.*, 1998). Although often referred to as "flux buoys" these buoys only make direct measurements of the downward radiative fluxes. The turbulent fluxes are determined using accurate measurements of the basic variables and the bulk aerodynamic formulae.

The IMET instrumentation resulted from extensive sensor testing and development during the World Ocean Circulation Experiment (WOCE). In addition to the surface moorings, IMET has been installed on a number of the U.S. Research Vessels and is now being placed on U. S. VOS. The IMET instruments were chosen, following on laboratory and field studies, for accuracy, reliability, low power consumption, and their ability to stay in calibration during unattended operation. The actual sensors were combined with front end and digital electronics to make a module that is digitally addressable (RS- 232 or RS-485), and, importantly, retains its calibration information. The present set of IMET modules includes wind speed/direction, air temperature, sea surface temperature, relative humidity, precipitation, incoming shortwave radiation, incoming longwave radiation, and barometric pressure.

Laboratory calibrations and *in situ* calibration studies and intercomparisons have been used to assess the accuracy of the IMET sensors as installed on buoys. Figure 9.1 summarises the progress that has been achieved in reducing measurement error over a series of air-sea

interaction experiments.  However it must be remembered that the accuracy of the turbulent fluxes will also depend on the accuracy of the bulk formulae used to calculate them (Section 6).
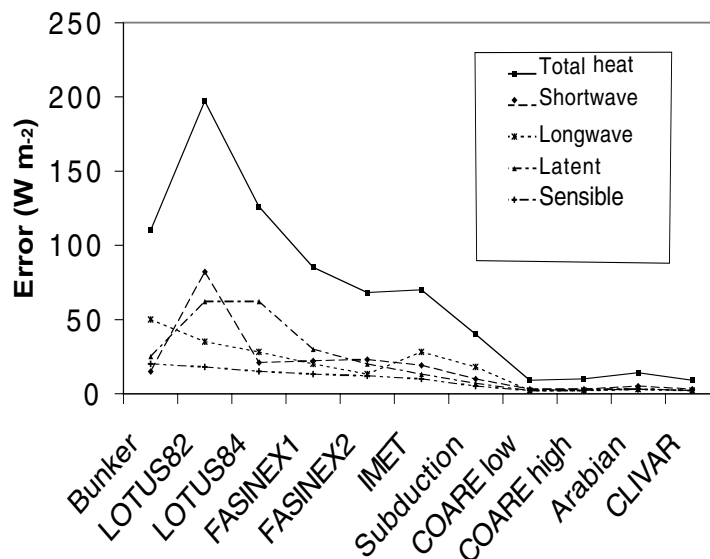


Figure 9.1.  The estimated reduction of measurement error in the components of the heat flux and net heat flux associated with surface mooring deployments during various experiments since the early 1980s.  The errors estimated in climatologies of the early 1980s, such as Bunker's, are given as a starting point (from Weller and Taylor, 1999)

Future developments of flux buoys could include the addition of instrumentation to measure the direct and diffuse solar radiation (e.g.  Reynolds, 1998) and to provide turbulent flux estimates using eddy correlation and/or inertial dissipation.

A particular cause for concern with buoy data is the accuracy of the measurements of the wind speed.  In strong winds these are believed to be biased low (Large *et al.*, 1995; Weller and Taylor, 1999; Zeng and Brown, 1998).  During the Storm Wind Study 2 experiment, SWS-2 (Dobson *et al.*, 1999; Taylor *et al.*, 1999b) 10m neutral equivalent winds were estimated using sonic anemometers on a buoy (at 4.5m) and a nearby research ship (at 17.5m).  A preliminary comparison of the measured wind speed values is shown in Figure 9.2.  On average the buoy appears to under estimate the wind by about 5%, however the data are very scattered.
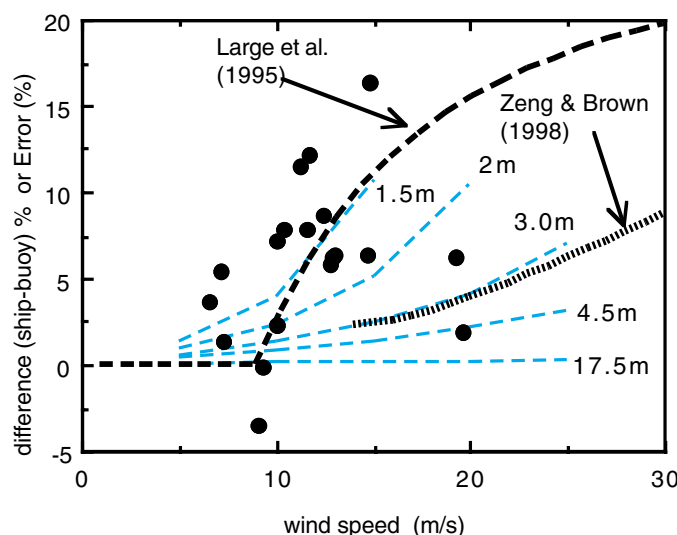


Figure 9.2.  The difference (closed circles: (ship - buoy) %) between values of the 10m neutral wind from buoy and ship data during the SWS-2 experiment for cases where the separation was less than 10 km (anemometer heights 4.5m and 17.5m respectively).  Also shown are the calculated effect of vertical movement through a logarithmic wind profiles for instruments at heights between 1.5m and 17.5m (light dashed lines); the mean error curve reported by Large *et al.* (1995) and the polynomial of Zeng and Brown (1998).  (from Taylor *et al.* 1999a)

Two possible mechanisms for the under estimate have been suggested.  First, assuming that the mean wind profile is logarithmic, an instrument being moved up and down vertically by the waves will measure an average wind which is less than the wind at the mean measurement height.  Using the observed wave height to wind relationship for SWS-2, this effect has been crudely estimated for different anemometer heights (light dashed lines on Figure 9.2).  Zeng and Brown, (1998) noted that there were a lack of high wind speed data in buoy observations used

for scatterometer calibration. They used surface air pressure data to infer a low bias for buoy winds at higher wind speeds. Their polynomial relationship (also shown on Figure 9.2) appears very similar to what might be expected due to the logarithmic averaging for a 3m anemometer height - not an unreasonable mean anemometer height for the mix of buoy data which they used.

The second mechanism is that the instrument may enter regions where the vertical wind profile is distorted due to the sheltering effect of the waves. Large *et al.* (1995) have suggested that this effect significantly biases buoy wind data for wind speeds above some threshold. Their predicted error for a 5m anemometer height is also shown on Figure 9.2, it is much greater than that predicted by Zeng and Brown (1998). The preliminary SWS-2 results shown on Figure 9.2. appear to be of similar order to the Large *et al.* (1995) prediction, however the measured friction velocity values suggested the wind error in the 20 to 25 ms$^{-1}$ region was 3% to 5% (similar to Zeng and Brown) rather than 15% or more. More work is needed before the bias in buoy wind speed measurements can be adequately quantified.

### 9.2.3 High-Quality Automated Data from ships

As mentioned previously, the IMET systems have been installed aboard numerous (six to eight) US research vessels. Additionally, similar systems are also found on other (i.e. non-US) research vessels. The WOCE Data Assembly Center (DAC) for surface meteorology, located at COAPS/Florida State University, has assembled, reviewed, and made available a sizeable record of in-situ surface meteorological data from research vessels participating in WOCE scientific cruises (approximately 1993 to present). Many of these data originate from IMET (and similar) automated systems that record and report data continuously. These data are considered to be of higher quality because of the quality of the instrumentation, complete and continuous data collection, and documentation efforts. Because these WOCE data are highly qualified, extensive quality-control reviews were undertaken and suspect data were flagged (see Smith et. al., 1996a). For the WOCE period, many of these data are from relatively poorly-sampled regions of the southern hemisphere oceans. Finally, many of these observations do not appear in the COADS nor are they reported via the GTS (implying that they are NOT included in the reanalyses or NWP products). Some of the ships do report surface meteorological values at synoptic hours, but again the data from the automated systems are not typically reported. Work is in progress to quantify the differences between simultaneous COADS and the automated system observational data.

Because of their higher-quality, uniqueness, and data coverage characteristics, these research vessel data are valuable for evaluating various flux products. As is the case for other high-quality reference data, the research vessel data allow an evaluation of flux products on much smaller (e.g. synoptic) time scales, rather than climatological or other longer-averaged quantities. The disadvantage of this approach is the limited spatial and temporal coverage (e.g. Figure 9.3). While the ships do sometimes make observations in normally under sampled regions, the research vessel database includes typically few cruises to a region, thus limiting the interpretation of the results.

The approach of implementing the automated research vessel data is straightforward, but there are many details (see Smith et. al., 2000). Automated meteorological data were reviewed and those of the best quality selected for the comparison. The observations are first height adjusted, and can be compared to gridded analysis values (nominally every 6 hours). Turbulent flux values (Smith, 1988) can then be calculated and averaged over 6-hour (or longer) periods (to match the integration period of the analysis). These values are also matched to gridded analyses (e.g. NCEP Reanalyses) for further analysis.

Note that data from other research ships and platforms may be utilised for flux evaluations. These data may not be of the same high quality as those described above, but other advantages such as longer time records and unique combinations of observations may qualify them for addressing other aspects of the flux fields under review. For example, Ocean Weather

Ship stations (see section 4.2.2) provide time series of meteorological measurements, mostly obtained by professional meteorologists, spanning about two decades in 11 sites in the mid-latitudinal North Atlantic and North Pacific with a time resolution of at least 3 hours. These data are considered to be of higher accuracy than the regular VOS observations. In addition, during the period 1981 to 1991, a considerable amount of meteorological measurements were collected in the Northwest Atlantic by six Russian sister ships (which also operated at OWS C). The data set contains about 50000 meteorological reports with temporal resolution from 1 to 3 hours (Gulev 1999). All measurements are taken by trained meteorologists using known instruments and at known observational heights. A considerable portion of the routine observations (about 30%) are accompanied by direct observations of SW and LW radiation that increases the value of this regional data set.
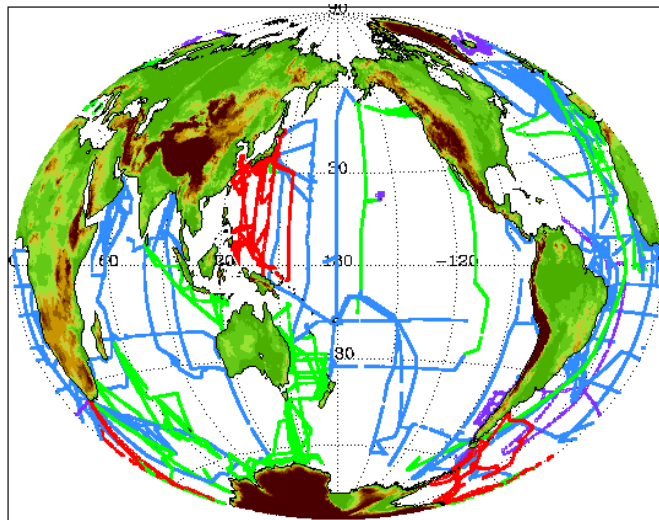


Figure 9.3 Map of positions of meteorological data obtained from research ships during the WOCE experiment for the period 1988 to 1998 as held at COAPS, FSU. The colours of the ship tracks indicate the data sampling rate:

| | |
|---|---|
| ▬ (blue) | Frequency = 1 min |
| ▬ (green) | Frequency <= 60 min |
| ▬ (red) | Frequency <= 180 min |
| ▬ (purple) | Frequency > 180 min |

*9.2.4 Data for verification of satellite products*

A.  COMPARISON OF SATELLITE PRODUCTS WITH *IN SITU* DATA

A common way to determine the quality of satellite-derived bulk parameters, fluxes, and precipitation is by comparison to different *in situ* data sources. There is always a problem of finding *in situ* data of good quality which are globally distributed. For precipitation some authors, e.g. Smith *et al.* (1998) support the opinion that the quality of *in situ* measurements is not good enough for validation or calibration of satellite methods. For turbulent fluxes it is clear that only a handful of datasets of direct flux estimates exist and are available to the community of satellite algorithm developers. The consequence is that most of the intercomparisons between satellite derived quantities rely on locally restricted datasets from scientific experiments or on the more widely distributed observations from merchant ships transmitted via the GTS. Where comparisons are made with ship data, either through individual observations or mean values, the errors inherent in the ship data must be taken into account. Since the ship data can be of doubtful quality, global *in situ* products like the da Silva *et al.* (1994) or SOC climatology (Josey *et al.* 1999) are sometimes used to avoid the problems inherent in the individual observations. However, this introduces a further problem that the comparison is very much dependent on the data analysis procedure used for the production of the *in situ* climatology.

A recurrent problem in any comparison of *in situ* and satellite products on an instantaneous time scale is the mismatch in time and space between the various measurements; point measurements are compared to field averages. The effect these two mismatches have on the result of a given comparison depends on the spatial and temporal scale of the variations in the variable considered.

B.  SOURCES OF RADIATION PRODUCTS

The direct measurement of radiation was discussed at some length in Section 5. Networks of surface measurements have been implemented for verification.  Unfortunately, to date, coverage of the sea is minimal. Available data sets include those from the Baseline Surface Radiation Network (Gilgen *et al.*, 1995), the Global Energy Balance Archive (GEBA) database of surface flux measurements (Gilgen and Ohmura, 1999), the NOAA/Climate Monitoring and Diagnostics Laboratory (CMDL) data set (Stone *et al.* 1996).  Most GEBA sites are located in the midlatitudes; a few of them are located on islands.

The CERES/ARM/GEWEX Experiment (CAGEX; Charlock and Alberta, 1996) data is available on-line at: http://snowdog.larc.nasa.gov/cagex .  CAGEX provides a space-time set of input data, calculated fluxes, and validating measurements.  With the launch of CERES, CAGEX has been extended to the ARM Tropical West Pacific (TWP) site.  ARM TWP data is expected to become a great resource for the study of radiation at the air-sea boundary.  The ARM web page is: http://www.arm.gov .  Also for CERES, work on the long-term CERES Ocean Measurement Platform for Aerosol and Radiation Evaluation (COMPARE) has begun at the Chesapeake Light, 25 km off the Virginia coast.

Otherwise satellite radiation data has been verified by comparison with other, higher quality fields.  For example, in addition to GEBA data, the GEWEX SRB files provide for verification the monthly TOA net flux by independent, higher quality measurements from the Earth Radiation Budget Experiment (ERBE; Barkstrom *et al.*, 1989) over most of the globe. Unlike the narrow-band radiometers on the ISCCP satellites, ERBE provides broadband measurements with on-board calibration for SW and LW.

## 9.3 Intercomparison of field products

### 9.3.1 Comparison to Specialised Products

Operational centres have historically had difficulty producing satisfactory wind fields over the tropical oceans (McPhaden, *et al.*, 1988).  Specialised products were developed to meet the need for near-real time tropical wind fields.  These specialised products include the much utilised Florida State University (FSU) tropical Pacific pseudo-stress product (Stricherz, *et al.*, 1997) as well as a similar product for the Indian ocean (Legler, *et al.*, 1997), and for the Atlantic the ORSTOM/IFREMER product (Servain, *et al.*, 1996).  These monthly mean fields of pseudo-stress are based on in-situ data, that is COADS (for real-time production, GTS reports are utilised; sometime later COADS-type data are utilised in a reanalysis to produce a research quality product) and extend for many years.  The Pacific and Atlantic analyses are available for 1964 to present.  The Indian Ocean analysis from 1970 to present.  The analysis methodology for these fields is largely subjective for the Pacific product, objective/subjective for the Atlantic, and objective for the Indian ocean.  Continually produced in the same way for more than a decade, these analyses have been very popular, but resolvable spatial resolution (primarily in the zonal direction) is rather coarse, and adjustments to account for observation system changes have not been considered.  Nevertheless these analyses are the longest set of consistently analysed (and highly referenced/utilised) tropical wind products available to the community.

There is value in evaluating new products such as the NCEP/NCAR (NCEPR) and ECMWF (ERA) reanalysis surface wind products in the light of these proven products.  The comparison can be based on differences of monthly pseudo-stress fields for the common analysis period, 1979-1993.  Comparison of climatological characteristics as well as anomalous features, particularly those associated with the ENSO phenomena, would be directly useful for potential users of the reanalysis winds.

### 9.3.2 Comparison of Variability patterns in different flux products

The task of intercomparison of variability patterns derived from different flux products is quite different from the intercomparison of climatologies of the mean fluxes.  Indeed, even if there is an agreement on mean values, variability patterns may not necessarily be in agreement

and vice versa. When the climatological means are removed, the comparability of flux anomalies can be considered in terms of the general level of interannual variability, characterised by standard deviations, secular tendencies, and space-time patterns of interannual variability.

Comparison of variability in different flux products with long-term time series of high quality measurements is highly desirable. The longest time series of high quality measurements (of up to four decades in length) are those from the Ocean Weather Ships (OWS's). For example, careful analysis of OWS wind records (Isemer 1995) does not support the conclusion, based on COADS data (Wu and Li 1995), that winds and evaporation exhibit significant positive trends in recent decades. The NBDC buoys provide a somewhat shorter time series of about one to two decades which nevertheless can be used for the validation of the variability reported by VOS and NWP climatologies. For some variables (e.g. winds, precipitation) comparisons against coastal and island stations may be useful. Coastal and island stations provide longer time series than those available over the sea. Bigg (1993) used coastal stations in the Tropical Atlantic to verify COADS winds and found differences in trend estimates derived from different sources. However, one has to be very careful in the extensive use of coastal and island data for comparison with VOS observations. First, these data may be influenced by different local effects, which may affect the data over the land and also over the coastal waters. Thus the comparison may be unrepresentative of the open ocean. Secondly, historical changes in observational practice may have occurred for both coastal and island data, and the effects may be of the same order of significance as inhomogeneities in the time series of ocean measurements.

When different flux products are compared to each other, they may indicate different variability patterns, and these differences may have importance for climate studies. In this context it is important to quantify the common patterns which are present in different analysed products. Recently Barnett (1999) suggested the use of so-called "common EOF's" for the intercomparison of different space-time fields. The common EOF shows the pattern of variability commonly shared by all the fields analysed and illustrates the features which can be discussed with confidence given the present state of our knowledge. Figure 9.4 shows, as an example, the first two common EOF's of the latent heat flux from the four flux products which were shown analysed separately in Figure 3.1. The first EOF accounts for 28% of the total variance and the 2nd EOF explains 12% of variance. The common normalised principal components have similar temporal behaviour and indicate quite pronounced correlation with each other. For this case, the common EOF's (Figure 9.4) show that the large-scale subpolar-subtropical dipole is present in all the flux products used and therefore can be discussed with confidence. However, although the Labrador Sea pattern is the outstanding feature of NCEP/NCAR fluxes, it does not appear in the other flux products.
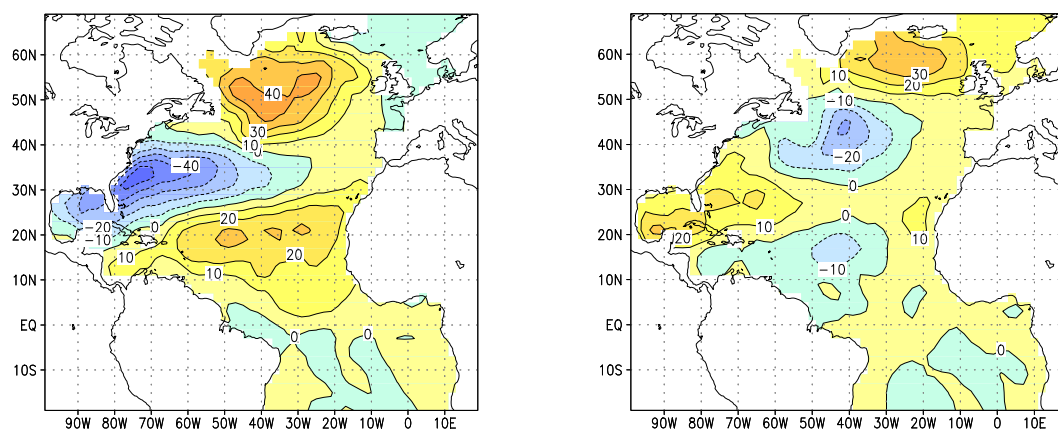


Fig. 9.4 1st two common EOF's for the latent heat flux for the analyses shown in Figure 3.1. (These were the NCEP/NCAR reanalysis; COADS ship reports; the reanalysis sampled at COADS report positions; and COADS MSTG data.)

## 9.4 Integral constraints

### 9.4.1 The global heat and water balance

An additional heat flux of 10 Wm$^{-2}$ over one year would, if stored in the top 500m of the ocean, heat that entire layer by about 0.15°C. Temperature changes on a decadal timescale are at most a few tenths of a degree (e.g. Parilla *et al.*, 1994) so the global mean heat budget must balance to better than a few Wm$^{-2}$. At present few global flux products achieve this balance, so this is a useful integral test of flux data sets. Using the global water balance as a constraint is more difficult because of the need to know river run off (section 10.9) and changes in ice amounts.

### 9.4.2 Meridional heat and water transport

A. INTRODUCTION

There is a long standing tradition to judge the reliability of global flux fields on the basis of the implied meridional heat transport (*MHT*) and meridional fresh water transport (*MFWT*). These quantities are the integrals of the zonally averaged surface heat (*H*) and water (*W*) balances in the meridional direction:

$$MHT = \int_{\varphi_0}^{\varphi} d\varphi \int Hd\lambda + H_0$$

$$MFWT = \int_{\varphi_0}^{\varphi} d\varphi \int Wd\lambda + W_0$$

(9.1)

Here $H_0$ and $W_0$ are the boundary conditions at the starting point of integration, which have to be taken from alternative estimates. For example, at approximately 70°N in the North Atlantic, the *MHT* estimate is traditionally taken from Aagaard and Greismann (1975), who give the value 0.107 PW, although Gulev (1995) and Bacon (1997) give a somewhat higher value, close to 0.3 PW. For *MFWT* the boundary condition at the north results from the fresh water flux through the Bering Strait which is estimated to be 0.78 Sv (Coachman and Aagaard 1988).

The *MHT* and *MFWT* estimates, obtained from the heat and fresh water balances at the ocean surface, may be compared to oceanographic estimates obtained from hydrographic cross-sections. These oceanographic estimates are normally considered to be of higher accuracy than can be achieved by integration of the surface fluxes. For example, typical uncertainties of *MHT* through oceanic cross-sections in the Atlantic are 0.3-0.4 PW (Hall and Bryden 1982, Rago and Rossby 1987, Molinari *et al.* 1990, Koltermann *et al.* 1999). In contrast, the uncertainty of the surface flux estimates propagates quickly into large errors in the meridionally integrated surface heat and fresh water budgets. For the Atlantic Ocean, an error in zonally averaged net heat flux of 15 Wm$^{-2}$ results in an uncertainty of *MHT* estimate of ±0.5 PW at 30°N, and up to ±1 PW at the Equator. And yet even this level of accuracy for the zonal net heat flux is a challenging target for any climatology (Gleckler and Weare 1997); the situation is even worse with regard to the fresh water flux accuracy. The same situation holds for VOS-based, remotely sensed, or reanalysis based products. Thus although *MHT* is a very important physical parameter, it has limitations with regard to determining the reliability of surface flux fields.

A better proposition is to use the oceanographic estimates of heat and freshwater fluxes through chosen hydrographic sections to determine the implied net surface flux between those sections. This value can then be compared with the mean flux derived from the climatologies. Since the latter do not need to be integrated the resulting comparison is more likely to be informative.

B. ACCURACY OF *MHT* AND *MFWT* FROM SURFACE FLUX INTEGRATION

Existing estimates of *MHT* derived from surface fluxes vary in a very wide range even in such well sampled area as the North Atlantic. Figure 9.5 summarises the sources of the

uncertainties inherent in the existing *MHT* estimates (Gulev *et al.* 2000). In order to quantify the possible range of variability of *MHT* estimates, individual LMR from the COADS Releases 1 and 1a were used for the period 1958-1997, which overlaps the NCEP/NCAR Reanalysis period. The most frequently used parameterisations for flux components and variable corrections were applied to the COADS reports. Their cross-application gave the possibility to produce an ensemble of the net flux and *MHT* estimates for the North Atlantic Ocean and to simulate the wide range of approaches used for flux computation by different authors. Of course not all of these parameterisation schemes are equally valid, so this simulation will include the worst possible combination, as might be constructed by someone with complete ignorance of the merits of the different algorithms!
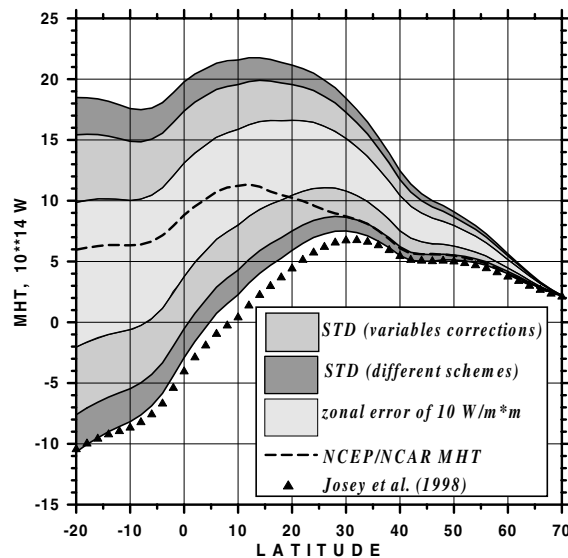


Fig 9.5. Standard deviations of *MHT* computed from the VOS data for the period 1957-1998, corresponding to the variability due to the choice of different schemes and variable corrections. *MHT* estimates derived from the NCEP/NCAR Reanalysis fluxes and from the VOS using Josey *et al.* (1998) method are also shown. The latter authors chose not to adjust their flux estimates to give global heat balance; hence the apparent bias in the *MHT* estimate.

The application of the different parameterisations and corrections to the variables may result in a ±4 PW range of *MHT* estimates at 20˚S. At 25˚N, where we have more or less consistent *MHT* estimates from oceanographic cross-sections, the range is 3 PW. The standard deviation of *MHT* estimates with different variable corrections is approximately adequate to 20 $Wm^{-2}$ zonal error in the net flux, and the standard deviation which results from the application of different schemes is somewhat greater, equivalent to about 24 to 26 $Wm^{-2}$. This is perhaps not surprising since the worst possible combination of parameterisation schemes has been included in the set. Analysis of different factors shows that the correction of winds, the choice of the equivalent Beaufort scale, and the choice of the scheme for turbulent fluxes are crucial with regard to the variations of *MHT* estimates.

With regard to the *MHT* estimates available from NWP systems, Figure 9.5 also shows values computed from the NCEP/NCAR Reanalysis fluxes for the 1958-1997 period. In terms of comparability to the oceanographic estimates, it looks like quite reasonable, giving approximately 1 PW northward transport at 25°N.

C. VARIABILITY OF *MHT* AND *MFWT*

Recent WOCE results based on sections carried out in different years (Koltermann *et al.* 1999) show that both *MHT* and *MFWT* can vary over a wide range, for example about 30% to 50% for *MHT* estimates in the mid-latitudinal North Atlantic. Thus Table 9.2 shows estimates of *MHT* and *MFWT* through three North Atlantic cross-sections for the late 1950's, early 1980's and early 1990's. Large interdecadal variability in *MHT* and *MFWT* in the North Atlantic mid latitudes is possibly suggested, with transports in the subtropics being more steady. Model simulations of the interdecadal variability (Knochel 1999) also show interannual variability of *MHT* and *MFWT*, although in a smaller range of 0.1 PW.

The variability of *MHT* and *MFWT* may explain a paradox: transoceanic hydrographic sections have been employed for some time in inverse calculations to determine the exchange of

heat between the major ocean basins (Macdonald, 1998). However, according to the method used, heat transport estimates at one individual section may differ by almost 100%, a range far greater than the error bars provided with the estimates. The WOCE observations show that in many parts of the ocean, there is a significant divergence of the meridional heat flux with large seasonal changes and weaker interannual variability. Hence, considering the "instantaneous" character of a section, a large range in heat flux estimates is to be expected. Recent attention to this issue by models and observations have not yet narrowed the range, but there is optimism that further analysis of the diverse WOCE data set will provide better estimates of the spatial and temporal variability of the meridional heat flux, and will narrow the range and produce error bars of greater significance. As an example, Ganachaud (1999) has used an inverse box model to provide estimates of the net input/output of heat over large portions of ocean basins, defined between WOCE sections with an accuracy ranging from 0.1 to 0.5 PW, which makes these estimates useful for surface flux evaluation (Figure 9.6).

Table 9.2. Meridional heat flux (Pw) and meridional fresh water transport (Sv) in the North Atlantic derived from hydrographic data at 24°N, 36°N and 43-48°N (Koltermann *et al.* 1999)

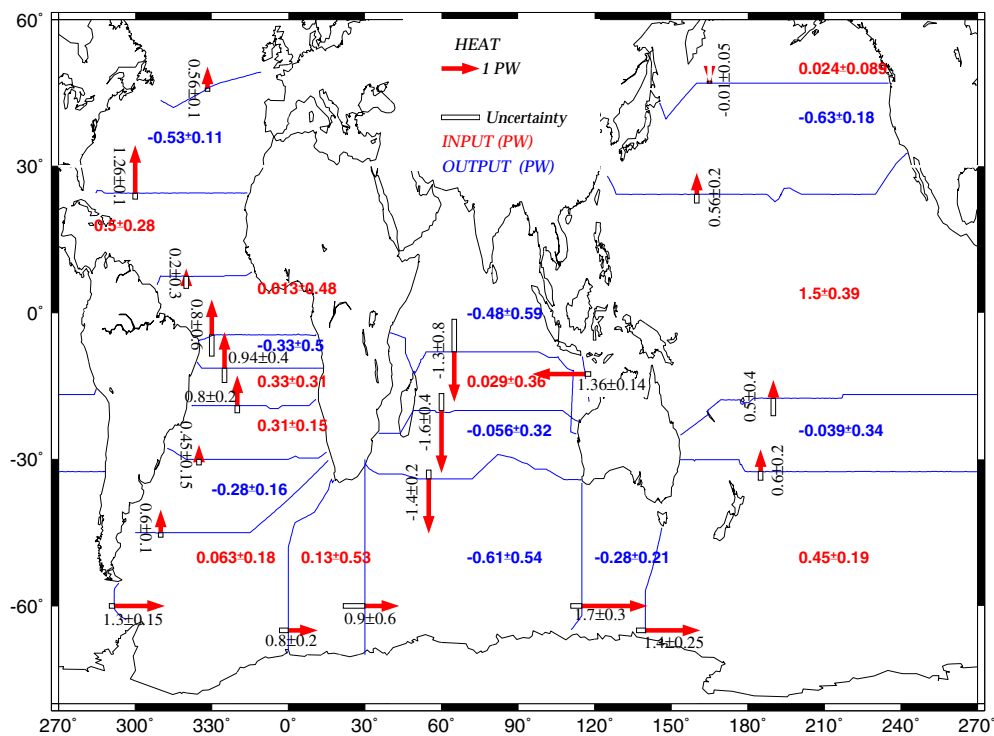| Year | LATITUDE | | | | | |
| --- | --- | --- | --- | --- | --- | --- |
| | 24° N | | 36° N | | 43-48° N | |
| | *MHT* PW | *MFWT* Sv | *MHT* PW | *MFWT* Sv | *MHT* PW | *MFWT* Sv |
| 1957-59 | 1.38 ± 0.29 | -1.19 ± 0.31 | 0.47 ± 0.24 | -0.77 ± 0.17 | 0.27 ± 0.15 | -0.87 ± 0.17 |
| 1981-82 | 1.48 ± 0.20 | -1.22 ± 0.22 | 1.29 ± 0.17 | -1.26 ± 0.13 | 0.62 ± 0.11 | -1.03 ± 0.13 |
| 1992-93 | 1.54 ± 0.19 | -1.31 ± 0.21 | 0.70 ± 0.15 | -1.14 ± 0.14 | 0.53 ± 0.12 | -1.02 ± 0.13 |



Figure 9.6. Estimates of heat transport (PW) across hydrographic sections(black labels), and net input/output of heat (PW) through the surface between sections (ocean cooling in blue, heating in red) obtained by Ganachaud (1999) with an inverse box model. Error bars are from a very careful error analysis and are independent of the model. The net heat input between two sections does not match exactly the residual of the net transport because it has been corrected for mass residuals (noise correction).

In general, the quantitative estimate of the magnitude of interannual variations in *MHT* is still under debate, although most researchers agree on the qualitative conclusion that it is variable. Therefore, reasonable comparative assessments should be done for certain years (or at

least pentads). However this approach leads to more problems with the surface balance estimates. First, the accuracy of the net flux for the selected years will be reasonably lower in comparison to the accuracy of the long-term climate mean. Second, computing *MHT* and *MFWT* for the selected years using surface heat and fresh water balances, one has to account for the interannual heat storage and fresh water storage changes. Since these changes take place in the whole ocean column (in contrast to the seasonal changes which occur primarily in the mixed layer) their accurate estimation is impossible at the present level of hydrographic data coverage. Gulev (1995) made an estimate of the possible uncertainty in *MHT* due to the heat storage changes corresponding to the decadal heating (cooling) of 0.2°C, corresponding to physically reasonable zonally integrated interdecadal temperature variations. The uncertainty obtained was 0.3 PW at 40°N and 0.5 PW at the Equator in the North Atlantic, and this uncertainty has to be coupled with the random uncertainty of the flux estimates.

D.  ADJUSTMENT OF FLUX FIELDS USING INTEGRAL CONSTRAINTS

Flux fields derived from VOS observations tend to show more heat going into the ocean than can be realistic. For example, despite carefully choosing the parameterisation schemes and applying corrections for known observation errors, the recent Josey *et al.* (1999) flux climatology suggested a net heat flux into the ocean of 30 $Wm^{-2}$. It is therefore not surprising that this climatology shows an unrealistic variation of the *MHT* (see Figure 9.3). Indeed, Figure 9.3 shows that even an error of 10 $Wm^{-2}$, which is often considered to be desirable for climate research, integrates to a significant uncertainty in the net heat flux. This problem has generally been overcome by adjusting (or tuning) the flux estimates to various oceanographic estimates of *MHT*. Based on error estimates for the different variables, reasonable ranges are determined for the transfer coefficients and other parameters. The inverse problem is then solved to adjust those parameters, within the allowed range, to give reasonable agreement between the implied *MHT* and the known oceanographic estimates. This method was used by Isemer *et al.* (1989) to tune flux estimates for the North Atlantic. Using a similar technique, da Silva *et al.* (1994) provided both unadjusted flux values, and flux values tuned to various oceanographic constraints. Earlier, Oberhuber (1988) also tuned his flux estimates in order to arrive at a reasonable *MHT* in the South Atlantic. He decreased the net shortwave and increased evaporation by imposing an arbitrary increase of the Charnock constant in his computations. Recently, Lindau (2000) also used tuning (to a number of oceanographic sections in the Atlantic) to produce *MHT* estimates based on the IFM climatology (see Section 11.2.5).

Although this approach appears very attractive, and provides the possibility of basin scale closure, there are a number of problems. Tuning does not guarantee that the individual flux components reflect reality (apart perhaps from the tuned net flux). The degree of tuning is limited by the dimensions of the domain, and, for example, tuning of fluxes for the northern North Atlantic, based on the cross-sections located north of 36°N, requires physically unreasonable changes to the variables and coefficients. The observed decadal variability of *MHT* suggests that time-dependent tuning may be required, at least for the mid latitudes. Josey *et al.* (1999) did not tune their flux estimates to the *MHT* arguing that to do so on a global scale would degrade the agreement between their flux estimates and high quality buoy observations. They argued that regionally varying flux corrections are required and that the number of oceanographic values was too few to allow adequate regional corrections to be defined. However the quality and number of such estimates is increasing and further progress on this problem should soon be possible.

In addition to matching the *MHT*, matching the *MFWT* would provide a further constraint. However there are only few VOS-based estimates of *MFWT* (e.g. Wijffels *et al.* 1992), and they have larger uncertainty than that for *MHT* due to the large errors in the precipitation.

In summary, the problem of the reliable estimation of *MHT* and especially *MFWT* from different sea-air flux fields is still open. Although there are obvious uncertainties inherent to the oceanographic estimates, we have to conclude that the accuracy of these estimates is still

significantly better than that obtained by integrating surface flux estimates. Achieving convergence between the two kinds of estimates is highly desirable. However, as measures of the reliability of flux products, the *MHT* and *MFWT* result in significant uncertainty. Nor does compatibility of the estimates of *MHT* and *MFWT* guarantee the reliability of the individual flux components. Thus, the development of flux products should be primarily based on the justification of parameterisations, variable corrections and interpolation techniques. Direct *MHT* and MWFT estimates have to serve as important and independent basin scale measures of reliability, but should not result in physically unreasonable corrections being made to fluxes or flux related parameters.

*9.4.3 Enclosed Seas Used for Flux Validations*

A.  INTRODUCTION

For the entire world ocean the net energy budget between ocean and atmosphere can be considered as balanced, since any long-term temperature changes are small compared to the inaccuracy of ship derived flux fields. However, data coverage, especially in the Southern Ocean, is too small to calculate a reliable global average. Enclosed seas give an attractive opportunity to verify ocean-atmosphere flux fields. Usually the heat and water budgets of enclosed and semi-enclosed seas are considered to be known to higher accuracy than basin-scale balances from oceanic cross-sections. The Mediterranean and the Baltic Sea, with their relatively high number of observations, are most suitable for such a purpose. Moreover, they represent rather different climate zones. If it would be possible to close the energy and water budget for these two different seas by using the same set of parameterisations, then credibility for worldwide application of those parameterisations would increase.

On the other hand, the special nature of enclosed seas, in particular the fact they are surrounded by land, means that there are a number of problems concerning the heat and fresh water budgets:

❍   river runoff becomes even more important for the smaller scale seas, and it is poorly known.

❍   many of the enclosed seas (Baltic, Caspian, Black) are characterised by continuous ice cover over a considerable part of the area and period. The number of observations in ice-covered areas is very small, and parameterisations of the flux components are poorly developed in comparison to the case of open water.

❍   consideration of budgets for enclosed seas has to account carefully for the analysis of the fluxes in the vicinity of coastlines. Local corrections are required for a number of variables in the VOS data (first of all, winds). Reanalysis and operational analysis data, especially those derived from the models with relatively coarse resolution (T62 and coarser), need to be carefully checked.

❍   the uncertainty of the estimates depends crucially on the size of the domain analysed, and increases for the large basins such as Mediterranean. On the other hand, consideration of smaller enclosed domains is difficult due to under sampling. In this sense, the use of enclosed seas is characterised by the same methical problem which is typical for the *MHT* and *MFWT* estimates.

B.  MEDITERRANEAN SEA.

Bunker *et al.* (1982) suggested the use of the Mediterranean and Red Seas as a test area for the bulk formulae. For this purpose, the parameterisations of Bunker (1976), originally used in the North Atlantic, were examined. Using individual merchant ship reports, they computed the net sea surface energy flux for the Mediterranean and the Red Sea. For the Mediterranean, a heat loss of about 5 $Wm^{-2}$ would be compatible with the measured heat import through the Strait of Gibraltar. However they found a strong surplus of energy at the surface After improving the parameterisation for longwave radiation by using climatological values of upper air humidity, in addition to surface observations, the surplus decreased from 36 to 20 $Wm^{-2}$. However, this

value was still in poor agreement with the oceanic observations.  The authors speculated that a drastic increase of the transfer coefficient $c_E$ up to values of 2 x $10^{-3}$ would be the most plausible way to achieve a near balanced state.  Similar conclusions were obtained for the Red Sea.

Gilman and Garrett (1994) also considered the energy balance of the Mediterranean Sea to detect possible inconsistencies in the bulk flux formulae.  As a starting point they used the COADS derived heat fluxes presented by Garrett *et al.* (1993) which show an imbalance of 29 $Wm^{-2}$.  Changing both short and longwave radiation, Gilman and Garrett (1994) were able to close the Mediterranean energy budget.  On the one hand, the mean longwave radiation was increased by 10 $Wm^{-2}$ compared to Bunker's results, when the formulae suggested by Bignami (see Bignami *et al.* 1995) was applied.  On the other hand, they reduced the values for the shortwave radiation by a total amount of 19 $Wm^{-2}$.  This was justified as follows: in order to take into account the effect of both anthropogenic and mineral aerosols which increase the atmospheric absorption over the Mediterranean, the transmissivity of the atmosphere was reduced by a factor of 5% for one half of the year; this weakened the solar radiation by 6 $Wm^{-2}$.  However, the major part of the shortwave reduction (13 $Wm^{-2}$) was achieved by correcting the previous misapplication of Reed's (1977) formula (5.4).  This was particularly effective because of the very low cloud amounts over the Mediterranean compared to other ocean areas.

For low cloud fractions the actual radiation $Q_{sw}$ from the Reed formula would exceed the clear sky radiation value.  Following Malevskii *et al.* (1992), a small increase over clear sky radiation may be possible due to clouds.  However, Reed recommended to neglect the cloud reduction for cloud covers less than 0.2, that means setting ($Q_{sw}/Q_{swo}$) to be not greater than 1.  A non-linear relationship between radiation and cloud cover results.  After removing this possible overestimation of shortwave radiation, Gilman and Garrett obtained a balanced energy budget for the Mediterranean.

However, Lindau *et al.* (2000) balanced the Mediterranean heat budget by using the parameterisations of Malevskii *et al.* (1992) and Bignami *et al.* (1995) for the short and longwave radiation respectively, and the corrected Beaufort scale of Lindau (1995) together with the exchange coefficients of Isemer & Hasse (1987) for the turbulent fluxes.  They found a net oceanic energy gain of only 2 $Wm^{-2}$, which is in reasonable agreement to the measurements of heat transport through the Strait of Gibraltar (MacDonald *et al.*, 1994), which imply a mean annual heat loss of 5 $Wm^{-2}$ from the sea surface.

Angelucci *et al.* (1998) analysed individual variables from the three different NWP products - the ECMWF operational analyses, NCEP operational analyses, and ECMWF Reanalysis, merged with the COADS MSTG and da Silva *et al.* (1994) cloudiness data, to compute and intercompare the heat budget of the Mediterranean Sea.  The Reed (1977), Kondo (1975) and May (1986) parameterisations for SW radiation, turbulent fluxes, and LW radiation respectively, were applied to different combinations of the data.  Angelucci *et al.* (1998) found quite a wide range of heat balance estimates, varying from -50 to 50 $Wm^{-2}$ depending on the data set used.  This range can be considered as the measure of the impact of different data on the balances examined.  Note here, that the use of VOS data would probably make this range even larger.  The closest to the Bethoux (1979) estimate of about -6 $Wm^{-2}$ was obtained using ECMWF operational analyses.  However that may have been just a function of the selection of parameterisations chosen.

Although Garrett and co-workers had checked that their balance for the heat budget was compatible with the freshwater balance, there have otherwise been few studies of the coupled error in the Mediterranean heat and fresh water balance estimates.  There are attempts to derive closed budgets from some sub-areas of Mediterranean, for instance Adriatic Sea (Maggiore *et al.* 1998), although these estimates have a more uncertain imbalance (heat outflow to the open Mediterranean) to be tuned to.

C. BALTIC SEA

Bumke *et al.* (1998) made a comprehensive study of the evaporation over the Baltic Sea on the basis of VOS data.  This included an investigation of the importance of corrections to

variables for coastal effects, and an intercomparison of several frequently used schemes for the transfer coefficients. The range of the estimates obtained was from 460 to 620 mm per year for the annual evaporation; indicating 20 to 30% uncertainty in the latent flux. This emphasised the need to carefully choose the parameterisation scheme; otherwise the uncertainty for the net flux may be of the same order as the mean flux values.

A particular problem for the Baltic Sea is the effect of sea ice. The sea ice changes the albedo of the surface and consequently the net shortwave radiation. Moreover, sea ice diminishes the effective surface temperature so that outgoing longwave radiation and the turbulent fluxes are reduced. In order to take these effects into account, the equilibrium temperature of the ice surface has to be iterated under the constraint that the four atmospheric fluxes and the conductive heat flux through the ice are in balance (Maykut & Untersteiner, 1971). If that is not possible at temperatures below 1°C, the surplus of surface energy is used for melting, which again would affect the albedo.

Using monthly mean ice charts from GISST data and applying the above scheme, the ice corrected atmospheric fluxes can be estimated. As an illustration, the mean state for the ice covered part of the Baltic Sea in the month of January is given in Figure 9.7. Averaging the individually iterated temperatures for the ice surface, a value of -6.3°C is obtained, whereas the mean reported air temperature for that month is -6.6°C. A latent heat flux of 15 $Wm^{-2}$ results. Although the sum of atmospheric fluxes cools the ice surface, melting occurs due to strong convective fluxes through the relative thin ice (of on average 24 cm). The oceanic flux at the bottom of the ice is considered to be constant at 5 $Wm^{-2}$, so that the freezing at the bottom prevails over the surface melting. For the month of January a mean ice growth of 36 cm per month results. Using this ice correction scheme together with the same flux parameterisations as in the Mediterranean, a long time mean heat loss for the Baltic Sea of 1 $Wm^{-2}$ is obtained, very close to the observed quasi-balanced state.
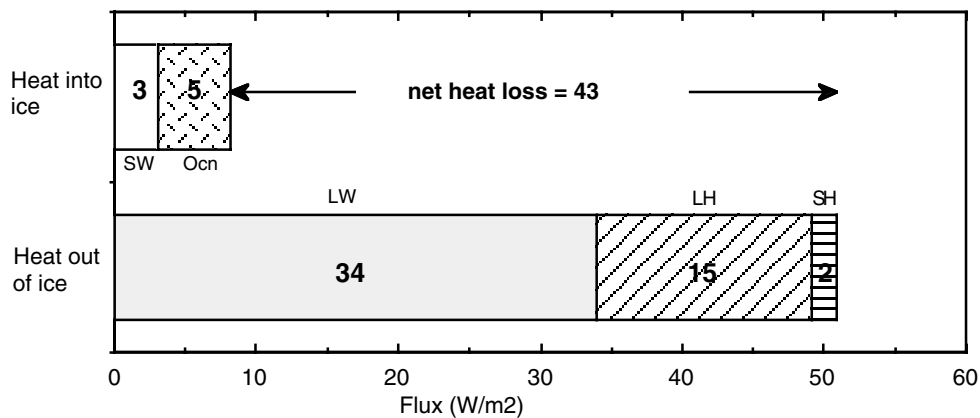


Figure 9.7 Modelled mean energy fluxes over sea ice for the Baltic Sea in January ($Wm^{-2}$). The air temperature was –6.6°C and the ice surface temperature –6.3°C. At the top ice surface the heat into the ice from shortwave radiation (SW) was 3 $Wm^{-2}$ whereas the surface cooling from longwave radiation (LW), latent heat flux (LH) and sensible heat flux (SH) totalled 51 $Wm^{-2}$. Thus the net heat loss to the atmosphere was 48 $Wm^{-2}$. This was offset by convective heat transfer upward through the ice of 53 $Wm^{-2}$. Thus melting occurred at the top surface. However since only 5 $Wm^{-2}$ heat entered the bottom of the ice from the ocean, the net heat balance for the ice was an overall cooling of 43 $Wm^{-2}$ and the ice grew downward. The mean ice thickness was 0.24m and the thickness growth rate was 0.364 m/month.

Thus the combination of parameterisations used by Lindau *et al.* (2000) provide reasonable results for both the Mediterranean and the Baltic Sea. Moreover, the meridional heat transport in the Atlantic Ocean is consistent with independent oceanographic data, giving further confidence in this choice of parameterisations. Nevertheless there are questions such as to whether the Bignami *et al.* (1995), which was developed for the Mediterranean, should be applied to open ocean areas. This will be discussed further below (Section 11.2.6).

D.  OTHER ENCLOSED SEAS

Analysis of the energy balance of the Black Sea has a long history.  The first study was done by Neumann and Roseman (1954), who used a limited data set based primarily on observations from coastal stations.  They arrived at a 36 cm per year annual imbalance in precipitation minus evaporation that constituted approximately 30 percent of the mean annual values.  Although during later decades better data were collected and more advanced parameterisations applied, progress was not too obvious.  Efimov *et al.* (1985) used probably the most complete collection of data, but found considerable underestimation of both heat and fresh water balances (e.g.  about 20 $Wm^{-2}$ for the heat) in comparison to those derived from hydrographic data.  Note that Efimov *et al.* (1985) used the Malevskii *et al.* (1992) scheme (in a previous version, which does not deviate strongly from the final version), and that this scheme, largely used in budget studies, gives relatively high values of the transfer coefficients in comparison to Large and Pond (1982) and Smith (1988).

Investigation of the balances for the Caspian sea is even less developed than for other enclosed basins.  For this, the largest lake on the globe, additional uncertainty results from the estimates of sea level changes, which are influenced by strong interannual variations and still poorly documented.  Moreover, nearly 1/3 of the Caspian Sea (its northern part) has a depth of about 1m to 5m and it is unclear to what extend the open ocean bulk parameterisations can be applied there.  In particular, the formulation for the radiative fluxes must definitely be reconsidered.  The most advanced study, of Larin and Panin (1985), showed quite large imbalances and it was pointed out that a reasonable closure requires ad-hoc adjustments of the transfer coefficients up to values which are greater than all known estimates of the coefficients.

There is a useful integral constraint on the heat and mass balance of the Arctic Ocean. Nakamura and Oort (1988) have presented polar heat balances.  For the Arctic they relate the advection of heat northward across 70°N to the surface heat balance and the top of atmosphere heat balance.  They show a net annual surface heat balance of 2 $Wm^{-2}$.  This agrees quite well with the net ice production of 0.2 m $yr^{-1}$ or an export of about 10% of the Arctic ice cover's mass each year through Fram Strait.  This freshwater export from the Arctic Ocean is crucial in determining the stability and convective potential of the Greenland Sea; a similar transport through the archipelago affects convection in the Labrador Sea.  There is no similar tidy constraint on the Antarctic ice cover, although it is true that the ice is generally formed closer to Antarctica and flows northward carrying fresh water (as ice) to melt further from Antarctica.

*9.4.4 Ocean Mixed Layer Budgets*

The overall accuracy of air-sea flux measurement can, in principle, be validated through closure of the heat (and freshwater) budgets of the ocean mixed layer.  This requires accurate measurement of the various oceanic heat (and salinity) transport processes; and in practice has never been very successful (e.g. Pollard and Thomas, 1989).  However, because of the particular care with measurement accuracy in COARE, two publications have so far appeared describing upper ocean budget closure over the 130 km square survey area (Smyth *et al.*, 1996: Feng *et al.*, 1998).  These showed that horizontal and vertical advection were major components of both the heat and salt balances, and emphasised the need to determine these components very well for the technique to be useful.  Subsequently, Godfrey *et al.* (1999) conducted a budget closure experiment in the equatorial Indian ocean specifically designed to test our ability to determine the oceanic advective components with sufficient accuracy to validate the COARE bulk flux algorithm, and the accuracy of the measured input variables.  By following a volume of water "tagged" with a drogued buoy over a 13-day period, they succeeded in closing the heat budget to within 5 $Wm^{-2}$ and freshwater to 1 mm $day^{-1}$, again finding that the advective terms were of first order.  The SEMAPHORE experiment was also designed with the aim of closing the ocean mixed layer budget (Eymard *et al.* 1996; Eymard 1998).

Final report of the
Joint WCRP/SCOR Working Group
on Air-Sea Fluxes
(SCOR Working Group 110)


INTERCOMPARISON AND VALIDATION OF
OCEAN-ATMOSPHERE ENERGY FLUX
FIELDS

by

Members of the WGASF



Edited by P.K.Taylor


Section B – Chapters 10 to 12,
References and Appendices



June 2000

## 10  BASIC VARIABLES - STATE OF THE ART

### 10.1  Introduction

In previous Chapters,  factors determining the requirements for surface flux fields have been reviewed (Chapters 2 and 3) and the available data sources have been considered (Chapter 4).  It has been shown that it is impracticable to determine the  flux fields by direct measurement (Chapter 5) and that parameterisation formulae must be used (Chapters 6 and 7). This Chapter will consider the present state of the art for determining the basic variables.  The variables considered are those used in the parameterisation formulae and also other variables which are otherwise relevant to the surface flux problem.   The evaluation of these variables has been delayed until now because the discussion of the random and sampling errors (Chapter 8), and the consideration of methods of evaluation (Chapter 9),  are relevant to fields of the basic variables as well as to the flux fields (which will be evaluated in Chapter 11).

The main property of the sea surface which is relevant to the surface fluxes is the **sea surface temperature**,  this will be considered first (Section 10.2).   Although variations of **sea surface salinity** (SSS) are not significant with regard to air-sea flux calculation, SSS is important for flux verification and for the freshwater forcing of ocean general circulation models;  it will be considered in Section 10.3.   The difference between the SST,  and the implied sea surface humidity,  compared to the **air temperature** (Section 10.4)  and **air humidity** (Section 10.5) determines the potential for transfer of heat and water vapour.   The magnitude of the transfers is determined by the **wind** (Section 10.6) which,  of course,  is also important for the momentum flux,  the wind stress.   The efficiency of the transfers of heat, water and momentum depends on the atmospheric stability,  also a function of the air-sea temperature and humidity contrasts and the wind.   It is also likely that these transfers are affected by the sea state and **waves** (Section 10.7),  which are important climatic variables in their own right.

**Cloud amount** (Section 10.8) is used in some parameterisations of the radiative fluxes and is also an important variable for the verification of NWP and climate models.  It is obtained from ship reports and satellites.  **Precipitation**  (Section 10.9) also may be estimated from ship reports;  although satellite based rainfall estimates offer better future potential.  Other variables affecting the ocean freshwater budget are **river inflow** (Section  10.10) and sea ice.   **Sea ice** (Section  10.11) is an important climate variable and the surface fluxes are significantly modified in sea ice areas.

Finally in this Chapter we will discuss a particular dataset of basic variable values, the **COADS monthly summary  trimmed groups**, MSTG  (Section 10.12).

### 10.2  Sea Surface Temperature (SST)

*10.2.1  Introduction - definition of sea surface temperature*

Sea surface temperature is the basic ocean variable which influences the magnitude of the surface turbulent fluxes and also the upward flux of longwave radiation.  The state of our present knowledge of SST fields was examined at a recent GCOS workshop (Arkin, 1999);  the following sections have made considerable use of the conclusions of that workshop.

First we must consider the definition of sea surface temperature.   The sea surface skin temperature (SSST) is the temperature that physically determines the surface heat fluxes.   It may be measured radiometrically from ships and other *in situ* platforms, and by satellite-borne radiometers provided the atmospheric effects are properly corrected.   The cooling due to sensible and latent heat fluxes and the longwave emission occurs at the skin,  whereas the shortwave heating is distributed over a greater depth.   Thus,  most of the time,  the SSST is colder than the water just beneath the skin,  typically by a few tenths ˚C.   This difference increases with increased surface cooling and decreases with increasing wind speed.   However

occasions can exist (for example with advection of warm, moist air over a colder sea producing low cloud or fog) when the SSST may be warmer than the water directly below.

If there is a significant net heat flux from the ocean to the atmosphere then the water below the skin will be well mixed and *in situ* measurements will record a temperature, normally reported as the SST,  which will be warmer than the skin temperature.  For traditional bulk formulae (Section 7.2)  the transfer coefficients have been determined with respect to this bulk SST,  so for application of these formulae, this would be the more appropriate temperature to use.   The bulk temperature also has the advantage of varying relatively slowly with time; thus bulk temperature observations may be composited over several days.   Indeed, most traditional SST products are, in effect, fields of estimated bulk SST.

However there are problems with defining SST as being the bulk value.   Newer forms of the bulk formulae (Section 7.3.2) use transfer coefficients derived from surface renewal theory.   For these the skin temperature is the appropriate value.   Also,  under daytime light wind conditions (less than, say, 3 ms$^{-1}$) a diurnal warm layer may form below the surface skin. Sea temperatures in this warm layer may be a few degrees C higher than in the bulk of the ocean mixed layer.   Since the layer may not be well mixed and in any case is shallow (say one or two metres),   the numerical value of a bulk temperature measurement beneath the surface skin will vary with the measurement depth.   The COARE bulk algorithm (Fairall *et al.*, 1996a – see Section 7.4.1) incorporates models of both the cool skin and warm layer, and so can estimate SSST from a bulk measurement at known depth.   For determination of precise fields of SST or SSST the use of such models would appear to be the way forward particularly if flux estimates are required with high time resolution in tropical regions.

Fortunately,  the offset of the surface skin temperature should not be considered too serious a problem for mean flux determination.   Averaged over 70 days during COARE, taking account of the cool skin increased heat input to the ocean by about 11 Wm$^{-2}$, while the warm layer decreased it by about 4 Wm$^{-2}$ (although the effect can be up to 50 Wm$^{-2}$ at midday – see Fairall *et al.*, 1996b).   Over much of the mid-latitude and high latitude ocean,  assuming a surface skin offset of about 0.3˚C would probably be adequate.   Since this is also the order of accuracy of radiometric measurements (see below),  a large programme of operational *in situ* radiometric SST measurements is not justified;  although research campaigns to improve our knowledge of the skin effect may still be encouraged.

*10.2.2  in situ SST measurements*

A.  HIGH QUALITY IN-SITU MEASUREMENTS

The accurate measurement of sea surface skin temperature (SSST) is a matter of wide importance in climate-related research and simulation,  particularly for tropical regions.   The TOGA program specified an accuracy of ±0.3°C for SSST over a 2 x 2 degree region (WCRP 1985) as a target for validation of space-borne radiometers.   An error of 0.3°C changes sensible and latent heat fluxes calculated with a bulk algorithm by 2 Wm$^{-2}$ and 10 Wm$^{-2}$ respectively, for typical climatic conditions in the tropics (winds 3-4 ms$^{-1}$, air and sea temperatures around 30°C, 75% humidity).   However, it would cause an error of only 1.8 Wm$^{-2}$ in the calculation of longwave exitance, which is still more accurate than direct pyrgeometer measurement at sea (see Section 5.2.3 ).

In response to this specification, the past few years have seen development of several high-resolution infrared radiometers (Smith *et al.*, 1996c).   Barton *et al.* (1995)  describe validation of the Along Track Scanning Radiometer (ATSR) on ERS-1 during several cruises of *R/V Franklin*.   High-resolution, self-calibrating infrared radiometers were mounted on the ship to measure SSST, using narrow spectral bands similar to the 11 and 12 μm channels of the ATSR.   Barton *et al.* (1995) quote the absolute accuracy of their instrument as 0.1°C,  and the SSST measurement as accurate to 0.2°C,  after correction for reflected sky radiation and surface emissivity (see below).  They conclude from their validation results that ATSR can provide SSST within its design accuracy of 0.3°C, and foresee an improvement to 0.2°C.

Measurements of SST from a high-quality commercial CTD, well-calibrated and mounted on a mooring, SeaSoar or hydrographic rosette are extremely accurate, in the order of a few thousands °C (see for example Table 1 of Hosom *et al.*, 1995).   This degree of precision, achieved by using a highly stable platinum resistance thermometer (PRT), is usually far greater than necessary when calculating heat and moisture fluxes from a bulk algorithm.  The main value of such accurate (and usually costly) measurement of sea temperature is in the determination of small vertical gradients, conversion of conductivity to salinity, and cross-calibrating alternative sensors which may be more convenient for continuous deployment. These would include lower quality PRT systems (accuracy 0.01°C) or thermistors which are nowadays available with accuracies of 0.05°C to 0.2°C (depending on cost).   These figures represent the basic accuracy of an SST measurement, when the sensor is deployed clear of the ship or on a mooring.   When used in a research vessel's thermosalinograph, two other uncertainties arise; possible changes in the water temperature through contact with the ship's hull or (depending on the sensor arrangement) *en route* from intake to sensor, and uncertainty about the original depth of the water entering the intake.

The latter is of importance when using a model of the mixed layer to obtain SSST as noted above.   There are few estimates of the accuracy of SSST obtained in this way; comparison with a high-quality infrared radiometer (of the type discussed above) is required. During COARE, measurements from the *R/V Franklin's* thermosalinograph, taking water effectively from 1m depth, were extrapolated to the surface using the COARE bulk algorithm. Comparison against an early version of the Barton *et al.* (1995) IR radiometer showed an average bias of –0.11°C with rms deviation of 0.47°C, for a 10-day period during which 3 days experienced diurnal surface warming greater than 3°C.  It is impossible to apportion sources of error between the model and the radiometer, but we note that the correction for reflected sky radiation was fixed at the average value of 0.4°C, not measured continuously.  Depending on sky conditions and atmospheric water vapour content,  this correction can vary from close to zero to at least 1°C;  i.e. coincident observations (sky temperature or atmospheric soundings) needed to make this correction are essential if the final estimates of SSST are to be within the specified accuracy.

It is possible that improvements in infrared radiometers for industrial purposes may make them more readily available and affordable for use on ships, particularly enabling simultaneous seaward and skyward observation.  Donlon *et al.* (1998) describe tests at sea of one such radiometer (spectral response 8-12 μm, beam half-angle 4.3°, cost ~US$600) by four separate research groups,  with excellent results.   Comparison against an 0.1°C accurate radiometer, of the type described above, showed a bias of only 0.1°C with rms 0.08°C.  With appropriate protection from the marine environment, such an instrument could be used widely in an SST validation program.

B. VOS

Ship SST data are obtained mostly from Engine Room Intake (ERI) thermometers or (about 1/3 of the modern data) from SST buckets.   A small but increasing number of ships use hull contact sensors which, if carefully calibrated, appear to give the most consistent SST data (Kent *et al.*, 1993a; Emery *et al.*, 1997).   Although the VOS are asked to report temperatures in tenths °C, many reports are given to half or whole degrees, probably reflecting the confidence the ship's officers have in the accuracy of the reading.   At the OOPC/AOPC Workshop (Arkin, 1999), Taylor *et al.* (1999c) presented results that suggested that, compared to hull contact sensors, ERI SST data were warmer under most conditions, on average by 0.35C although there was significant scatter about this typical value.   Individual ships using ERI readings had mean biases between -0.5°C (too cold) and +2.3°C (too warm).  Bucket measurements were found only to be biased compared to hull values during sunny daytime conditions when they gave on average SST values about 0.3°C warmer.   This is more likely due to the buckets heating on deck prior to use rather than to near surface ocean heating.   However, at the same meeting, Parker presented data that showed different characteristic biases between the observing

methods.   A plot of the zonal averages of "bucket" minus "non-bucket" SST values for the period 1975 to 1981 indicated the non-bucket values to be 0.1 to 0.2°C warmer except in the high latitude northern hemisphere (Folland *et al.*, 1993).   A more detailed study of the regional comparisons on which the zonal averages were based suggested that the buckets were biased cold in some high ocean to atmosphere heat flux areas.

Kent *et al.* (1999) found that the rms errors for a single VOS SST observation were typically between 1°C to 2°C.   The median rms error was 1.4°C and the mean rms error 1.5°C. The highest values,  up to 3°C occurred in high latitude coastal regions,  and higher values occurred in the Gulf Stream and Kuroshio regions than in other areas at the same latitude. However it is possible that in these cases the error was being overestimated due to the effect of varying SST values on very short spatial scales.

A historic reconstruction of the global SST time series (Folland and Parker, 1995) assumed that SST data were, on average, biased cold in 1860 by about 0.1°C with this bias increasing to 0.4°C in 1940 due to the increased use of canvas (rather than wood) buckets.  It was then assumed that wartime conditions resulted in a wholesale switch to ERI SST data; those buckets used after that time were assumed to be of insulated construction.   Thus, no correction is applied for the period 1942 to the present.   Comparisons of the trend in the corrected SST with night time marine air temperatures and temperatures over land implied that these adjustments were successful.   However the differences between present day bucket and ERI measurements suggests that further evaluation is necessary.

C.  BUOY DATA

**Drifting buoys** provide data away from shipping lanes and are used for adjusting the satellite calibration.   However,  the SST Workshop (Arkin, 1999) suggested that we do not have sufficient knowledge of the characteristics of the various different types of drifting buoys with respect to SST measurement.   The type of each drifting buoy should be known and the calibration details fully documented.  This is not presently the case.  Thus the accuracy of buoy data varies but it is usually better than 0.5°C,  significantly better than the ship data (Reynolds, 1999).

The most useful **moored  buoys** are those in the open ocean, for example the JMA buoys and the TAO and PIRATA arrays.   Unfortunately many moored buoys are deployed near coasts where high SST gradients are likely.    They are of limited value for satellite data verification and are not routinely used for satellite calibration adjustments.

Research buoys designed to allow flux determination (such as the IMET system) are important for verification of SST analyses and climatological SST data sets (Taylor *et al.*, 1999c,d).   Carefully calibrated sensors may be deployed at various depths in radiation shields (e.g. Weller *et al.*, 1998).   Since these buoys are limited in number and deployment duration, perhaps their best use is as a "withheld" data source which has not been used in, or had a significant impact on, the various SST analyses.

*10.2.3  Remote sensing of SST*

Infrared radiometers carried by satellites provide the potential for SSST measurement over the global ocean on a regular repeat basis.   Unfortunately,  at any time significant areas of the ocean are cloud covered and data from different over-passes must be composited. Atmospheric water vapour, aerosols, and clouds have all the potential to significantly bias the data unless adequate correction procedures are implemented.  Reliable cloud clearance remains a problem, as does the effect of sub-pixel cloudiness.   The measurements rely upon a small number of sensors with the possibility of changes in sensor characteristics between satellites.

Accurate operational SST retrievals from the AVHRR carried on the NOAA series of polar orbiting satellites have been available since late 1981 (Reynolds, 1999).   The error budget for the AVHRR is dominated by the instrument calibration accuracy and atmospheric transmission effects.   Thus the instrument must be calibrated against drifting buoys and the

calibration accuracy continually verified.  Walton *et al.* (1998) reviewed the algorithms used which are different depending on whether it is day or night.   They found that the daytime rms accuracy (compared to drifting buoy data) had improved from 0.8°C in 1989 to 0.5°C in 1998, whereas the night time rms had remained constant at about 0.5°C.   The bias was normally between -0.2°C to +0.4°C.   However large errors can occur due to changes in atmospheric aerosol loading.  For example the eruption of Mount Pinatubo resulted in a regional cold bias of order 2°C over much of a two year period.   Explicit water vapour corrections using SSM/I derived vertically integrated water vapour content (or "precipitable water") have been tested and shown to be successful (Emery *et al.*, 1994);  however they have not been implemented operationally.

Compared to the AVHRR,  the Along-Track Scanning Radiometer (ATSR) has improved sensor stability and built-in calibration systems.  However there have been problems in ensuring that clouds do not contaminate the data.   For cloud-free pixels,  Simpson *et al.* (1998) compared ATSR and drifting buoy data and found a mean difference (ATSR - buoy) of -0.24°C ±0.51°C (standard deviation);  similar to what might be expected given the typical skin-bulk difference.  Merchant and Harris (1999) used the TOGA TAO array buoys for verification and found the mean and standard deviation of the differences to be -0.16°C and ±0.37°C respectively.   Using the TAO data to calculate a skin temperature they obtained an even closer match:  +0.07°C ±0.27°C.   They concluded that about 5% of the ATSR retrievals had errors which they attributed to residual cloud contamination.  For the uncontaminated data they suggested a standard deviation of ±0.19°C.   Examining retrievals for the period when the atmospheric aerosol loading due to Mount Pinatubo was decreasing,  they found no significant trend in the error (0.00 ±0.16°C/year),  suggesting that the retrieval scheme was robust to aerosol effects.  With regard to the cloud contamination problem,  Jones *et al.* (1996a,b) also suggested that 4.65% of the data was cloud contaminated and suggested a scheme for removing the residual cloud pixels.

Thus the ATSR appears capable of achieving accuracies which are significantly better than can be achieved with ship data,  and apparently better than the drifting buoy data. However the sampling is limited by the 500km wide swath.  If the ATSR retrieval algorithms are confirmed to be "aerosol proof" then this instrument may be best used both as a source of SST data and as a source of calibration data for the wider swath AVHRR instrument.

*10.2.4  SST analyses*

Reynolds (1999) has summarised intercomparisons of different available climate scale SST analyses,  both by Hurrell and Trenberth (2000) and as reported at the Ocean Observing Panel for Climate SST Workshop (Arkin 1999).   These analyses (Table 10.1) typically have temporal resolutions from weekly to monthly and spatial resolutions from 1° to 5°.   It was found that differences among the analyses were smaller within the tropics compared to other areas.   Monthly rms differences between analyses were in the range 0.2°C to 0.5°C between about 40°S and 60°N except in coastal areas.   Analyses which did not use satellite data had differences greater than 1°C south of 40°S.   The largest differences occurred north of 60°N due to uncertainties near and within the Arctic sea ice. This was because different schemes are used to determine SST from ice cover or concentration,  and different ice cover analyses exist.   It was stressed that the use of satellite data (AVHRR) without bias correction has the potential to introduce large errors into the analysis.

## 10.3  Sea Surface Salinity (SSS)

*10.3.1  Introduction*

The sea surface salinity (SSS) is an ocean variable which enters the calculation of the fluxes only by reducing the saturation water vapour pressure (SVP) over sea water compared to fresh water.  This is normally accounted for by assuming a relative humidity of 98% for the air in direct contact with the sea surface.  Since the variability of SSS is not sufficient to cause significant variations in SVP (except in regions such as river estuaries) the SSS does not

explicitly enter the air-sea flux formulae.   However it is well correlated to the freshwater flux, and is essential for an accurate verification of freshwater flux estimates.   Furthermore, it has been until now the most important component of the freshwater forcing of ocean general circulation models.


Table 10.1  Summary of different climate scale SST analyses (adapted from Reynolds, 1999). The columns show the period available,  the spatial resolution,  whether satellite data is used ("Yes","No") or used with additional bias correction ("Corr.") and whether ice data is used to define SST's in high latitudes.  N.B. some parameters may vary between different releases of some analyses.

| Analysis | Period | Res'n | Sat. | Ice | Reference |
|---|---|---|---|---|---|
| BMRC | Jul-93 on | 1° | Corr. | Yes | (quoted by Reynolds, 1999) |
| UKMO GISST | 1871 on | 1° | Corr. | Yes | Rayner *et al.* (1996) |
| JMA | 1982 on | 2° | No | No | (quoted by Reynolds, 1999) |
| LDEO | 1856 on | 5° | No | No | Kaplan *et al.* (1998) |
| UK MOHSST | 1856 on | 5° | No | No | Parker *et al.* (1994) |
| NCEP EOF | 1950-1998 | 2° | No | No | Smith *et al.* (1996b) |
| NCEP OI | Nov-81 on | 1° | Corr. | Yes | Reynolds & Smith (1994) |
| NRL | 1979 on | 0.25˚ | Yes | Yes | (quoted by Reynolds, 1999) |
| NOAA/NASA AVHRR Pathfinder | 1985 on | 0.18˚ | Yes | Yes | Brown *et al.* (1993) |


### 10.3.2  In situ measurement of SSS

        In-situ measurements of sea surface salinity are far less numerous than in-situ measurements of sea surface temperature.  One major reason is the technology which is far heavier, more expensive and less reliable for conductivity than for temperature sensors. Conductivity sensors were added to disposable instruments (XCTD) only 15 years ago, and still most VOS lines are, mainly for cost reasons,  limited to the routine acquisition of SST.  In consequence, our knowledge of the surface salinity has been largely established from a compilation of the available hydrographic sections (Levitus *et al.*, 1994).  At present,  if an accurate climatological estimate for the annual mean sea surface salinity is required for the global ocean, the present data set presents severe deficiencies in large regions of the ocean (mainly in the southern hemisphere in winter conditions).  As a result, our knowledge of the climatological seasonal cycle at a global scale is still largely inaccurate, and investigation of the inter-annual variability has to be restricted to a very few well sampled oceanographic regions of limited area.   The situation is expected to improve in a near future, driven by the emerging needs of operational oceanography and the rapid development of a global ocean observing system.   With respect to salinity, the ARGO programme with its large number of profiling floats is expected to be a major contribution.

### 10.3.3  Remote sensing of SSS

        Despite the crucial role sea surface salinity plays in determining the ocean circulation and in understanding the water cycle up to the present it has not been monitored from space. Levitus *et al.* (1994) showed that the number of *in situ* sea surface salinity observations reached a peak in the late 1960's and has significantly decreased in the following decades.  This, and the relatively poor geographical distribution of *in situ* salinity measurements over the world oceans, could be significantly improved by measurements from space.  In early papers, Klein and Swift (1977) and Swift and McIntosh (1983) gave a detailed description of the physical basis of how, and at which frequencies,  it would be possible to obtain sea surface salinity from space.   A recent paper on remote sensing of sea surface salinity by Lagerloef *et al.* (1995) recycled this idea with the aim of proposing a salinity mission to NASA.

Basically, the ocean radiometric brightness temperature $T_B$ is related to the sea surface temperature $T_S$ and the emissivity $\varepsilon$:

$$T_B = \varepsilon(T_S, S, \nu, \theta_i, pol)T_S \qquad\qquad (10.1)$$

The emissivity is a function of sea surface temperature, salinity, frequency, incidence angle, and polarisation. The dependence on salinity is expressed through the dielectric constant which is governed by electrical conductivity and frequency. The conductivity itself is a function of salinity and temperature. Other effects on salinity, not covered by (10.1) but which must be allowed for in a retrieval of sea surface salinity, are wind, foam, and rain, and their impact on the surface within the field of view of the radiometer. Additionally, for an accurate computation of a signal measured at satellite altitude (10.1) has to be extended by the upward and downward components of atmospheric emission, and the transmitted and reflected part of the galactic space emission.

Lagerloef *et al.* (1995) stated that frequencies of 1.4 and 2.65 GHz seem to be the best choice to retrieve salinity since the variation of brightness temperature due to salinity is at its maximum at these frequencies. Another argument is that the relation between $T_B$ and $T_S$ and salinity differs at these two frequencies which should allow a simultaneous retrieval of salinity and $T_S$. However, the brightness temperature variation at 1.4 GHz is not greater than ~5 K under open ocean conditions (see Fig.2 in Lagerloef *et al.*, 1995) which is small compared to the dynamic ranges of ~100K caused by variations in water vapour or rain for the SSM/I channels. Another problem to consider is that the wind speed, or better the surface stress, must be known at the same time and location where the salinity will be retrieved. However, Lagerloef *et al.* (1995) showed that it is possible to measure salinity with the airborne 1.4 GHz Electrically Scanning Thinned Array Radiometer (ESTAR). They monitored the sea surface salinity in a transect from seaward of the Gulf Stream to Cape Hatteras. The large salinity changes from coastal to off-shore waters are clearly seen and are in agreement with frontal features noted in sea surface temperature maps.

Sea surface salinity is used in the air-sea flux problem for the relaxation of ocean general circulation models forced by the changing fresh water flux on the surface (Barnier *et al.* 1995), and for the correction of humidity variables. The latter does not require the salinity more accurately than 1 psu. Ocean model simulations require at least 0.1 psu accuracy for monthly averaged salinity and it can be expected that the increase of model resolution will require even higher accuracy for the reliable simulation of ocean circulation. Although this accuracy is problematic for the potential satellite techniques, it is also hardly attainable from the traditional alternative sources of the salinity data (in-situ STD, XBT and MBT measurements), except for well sampled ocean regions such as the North Atlantic and northwest Pacific. Thus, progress in the future is likely to be achieved by better instrumentation and by combining *in situ* and remote sensing information.

A new study on critical requirements for ocean salinity retrieval by Drange *et al.* (1999) addresses this issue in the light of the optimised and threshold requirements for GODAE. Thus to describe and quantify many important ocean processes, the accuracy target for sea surface salinity should be 0.1 psu over a distance of 100 or 200 km for a time period of 10 days. Several retrieval simulations revealed the following results:

❍  Measurements of horizontally and vertically polarised brightness temperatures at 1.4 GHz are needed to obtain reasonable retrievals.

❍  Accurate retrieval of salinity requires small or no bias in the measurement of the brightness temperature. This has implications on the engineering design and calibration of a passive microwave salinity sensor.

❍  If wind speed fields with accuracy better than 0.5 ms$^{-1}$ and sea surface temperature fields with accuracy better that 0.5K can be obtained, then the error in the retrieved

salinity will be lower than 0.4 psu. This is not unrealistic because the accuracy concerns averages over $(200\,\mathrm{km})^2$ and 10 days.

❍   The time scale of mesoscale changes in the ocean is such that a simultaneous measurement of SST should not be necessary.

❍   Polar and subpolar waters are extremely sensitive to changes in sea surface salinity. Those regions will require retrieval accuracies around 0.01 psu to be fully useful. Since the accuracy of remotely sensed salinity decreases with decreasing sea surface temperature, it will be very difficult to obtain reliable salinity measurements at high latitudes from space.

The study concluded that the simulations have shown that the GODAE requirements can be closely met; however some aspects of the problem were not tackled in this study e.g. geometrical effects inherent to a certain radiometer or the effects of rainfall in modifying the surface roughness. The Drange *et al.* (1999) study is related to an activity initialised by a group of European and American scientists. They proposed to the European Space Agency (ESA) a satellite mission called the Soil Moisture and Ocean Salinity (SMOS) Satellite ( http://www-sv.cict.fr/cesbio/smos/ ) which consists of an L-band (1.4 GHz) 2D interferometric radiometer that should be able to detect soil moisture over land and sea surface salinity over oceans. The mission has been selected for further study during the next two years. The satellite launch is planned for the year 2004.

## 10.4  Air Temperature

### 10.4.1  In situ air temperature measurement

A.  HIGH QUALITY IN-SITU MEASUREMENTS

Instruments used for measurement of the basic variables at sea are often different from those used routinely over land. This is because of the increased demands on ruggedness, waterproofing, and, in the case of those intended for use on buoys, power consumption and long-term unattended operation. For atmospheric temperature and humidity, the most accurate instrument in regular use is the psychrometer (wet and dry bulb thermometer) whose measurements are based on well-established thermodynamic theory. The most critical requirements to attain its potential accuracy are adequate ventilation of air past the sensing elements (3 - 4 ms$^{-1}$ flow rate), to ensure the full wet bulb depression, and adequate shielding from solar radiation. This usually means a double shield with the space between also ventilated. Basic accuracy depends on the type of sensing element used; for the familiar sling and Assman psychrometers this is the precision of the particular mercury-in-glass thermometer, 0.1°C at best.

For automatic recording, 0.01°C is not difficult to achieve in principle using platinum resistance thermometers, although in practice environmental sources of error appear, particularly when the instrument is used at sea (salt spray, signal interference, etc). In TOGA-COARE the use of aspirated psychrometers aboard *R/V Franklin* revealed the inadequacy of temperature sensors on other platforms which were enclosed in radiation screens without forced aspiration (Bradley and Weller, 1995a, b). Temperature errors during daytime could be well over 1˚C due to solar heating (Anderson and Baumgartner, 1998). Aboard many research vessels and moorings, air temperature is measured with PRT's or precision thermistors, often integral with a commercial temperature/RH instrument (see Section 10.5.1); quoted accuracies are between 0.1˚C and 0.25˚C (Hosom *et al.*, 1995; Freitag *et al.*, 1994; Burns *et al.*, 2000).

B.  VOS DATA - THE VSOP-NA PROJECT

It has been known for a long time that temperature measurements on board merchant ships have considerable systematic errors. Their consequences on heat flux calculations had been discussed by Dietrich (1950). Kent *et al.* (1999) found that, while a typical RMS air temperature error for a single temperature observation from VOS was about 1.4°C, there were a

significant number of higher error values representing high latitude coastal regions with mean air temperatures of 10°C or lower.   This may indicate a failure to remove spatial variability from the error estimate (for example in the Gulf Stream and Kuroshio areas)  or it may be that errors in air temperature observations are greater in cold conditions.    For example, psychrometers may not be exposed outside the wheelhouse for a long enough period.

The exposure of thermometer screens on the VOS selected for the VSOP-NA project (Kent et al. 1993a) varied from good (e.g. screens hung on stanchions on the outboard rails of either bridge wing) to very bad (e.g. "the screen is made of brown varnished wood and fitted to the side of the wheelhouse in the 'porch' of the bridge wing on the port side").   The effect on the temperature readings is illustrated in Figure 10.1.   This shows the mean difference between the VOS air temperature observations and an atmospheric forecast model for sensor exposure classed as "good", "medium", or "poor".   The left part of this figure shows night data plotted against cloud cover and the right part shows day time observations plotted against the solar radiation.  The latter was calculated from the ships' position and the reported cloud cover.   At night the better exposed sensor recorded lower temperatures than the model,  suggesting a possible bias in the model.  The poorly exposed sensors were about 0.5°C warm.   During the day all the sensors showed increasingly warm readings with increasing solar radiation.   For the better exposed sensors this bias was up to 2°C;  for the poorly exposed sensors the mean bias reached over 4°C.
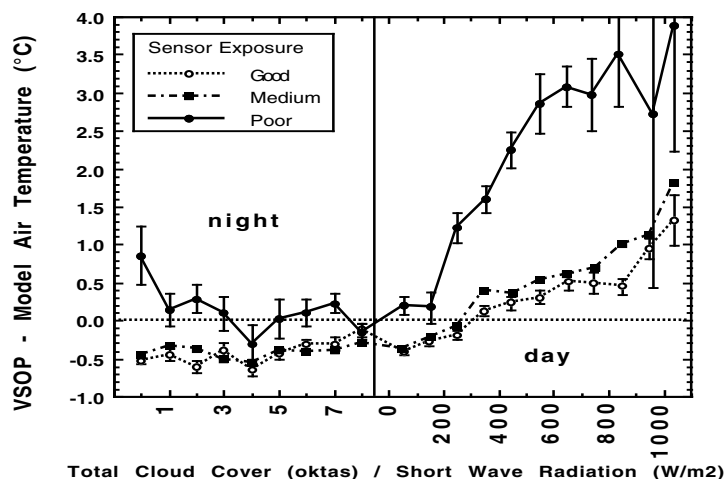


Figure 10.1.  The effect of different instrument exposure on air temperature observations.  Night time data are plotted against total cloud cover,  day time data are plotted against the calculated incoming solar radiation.  See text for discussion. (from Kent et al. 1991)

Data obtained from hand held psychrometers showed solar heating effects similar to the better exposed screens suggesting that the bias represents a heat island effect caused by the ship.  The bias in data from better exposed sensors (which constituted the majority of the observations) was found to depend both on the solar heating and the relative wind speed and a correction scheme was devised (Kent et al., 1993b).

C.  VOS - COMPARISON WITH WEATHER SHIPS

The important values for sensible and latent heat fluxes are the small differences between air temperature $T_a$ and wet bulb temperature $T_w$, respectively, compared to the sea surface temperature $T_s$.   To quantify the systematic errors in these quantities, Lindau (2000) has compared temperature measurements of Ocean Weather Ships,  on the assumption that they are correct,  with reports of merchant ships in the vicinity of the OWS.   Data were available from 15 Stations, 11 in the North Atlantic and 4 in the North Pacific, operating during different periods between 1945 and 1989 (see Section 4.2.2).   Simultaneous merchant ship observations within a radius of 300 km were extracted from COADS.   In this way,  700,000 pairs of observations were obtained.   To avoid errors due to an unsymmetrical distribution of merchant ships around the OWS,  data were interpolated on a two-dimensional linear field for each month and each station.

The air temperature measured on merchant ships was higher than OWS reports for all stations, except OWS M (Figure 10.2).   The mean difference $(T_a(VOS) - T_a(OWS))$ varied considerably from - 0.00°C at OWS M to 0.69°C at OWS P.   Because no relation to climate zones was obvious, the difference was averaged over all stations giving an overestimation of 0.259°C.  The comparison of wet bulb temperatures yielded similar results. $T_w$ was generally overestimated by merchant ships,  the mean bias was 0.235°C (Figure 10.3).   For the calculated specific humidity (or dew point ) of the air to be unaffected by the temperature error, $T_w$ needs to change by an amount which depends on the air temperature  (Hoeber, 1995; Kent and Taylor, 1996) but which is about half the air temperature error.  Thus compared to the weather ship data, the ship wet bulb values were too warm, but only by about 0.1°C.  For SST,  averaging the results from all stations, Lindau (2000) found a negligible bias (0.005°C) between merchant ships and OWS measured $T_s$ (Figure 10.4).
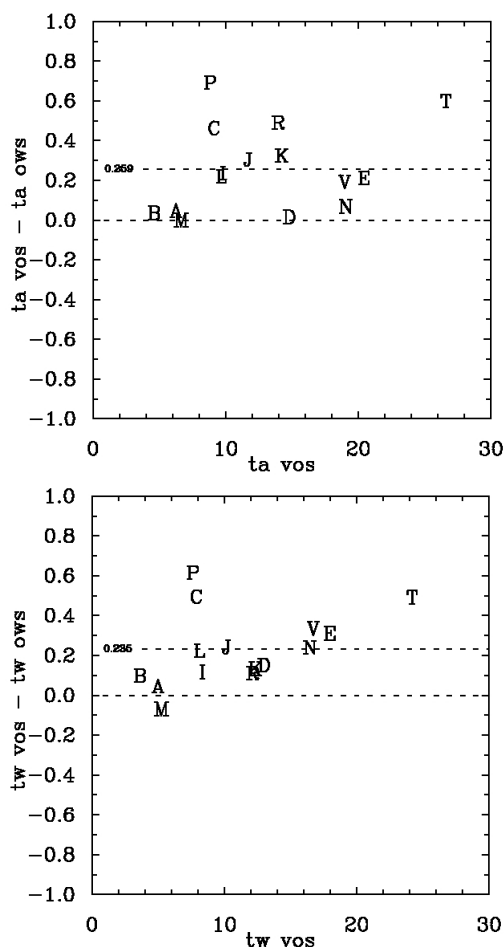


Figure 10.2  The mean difference of air temperature measurements (Merchant ships minus Ocean Weather Ships) at Atlantic OWS's A, B, C, D, E, I, J,K, L, M, R, and Pacific OWS's P, N, T, V. The dashed line shows the mean of all stations.
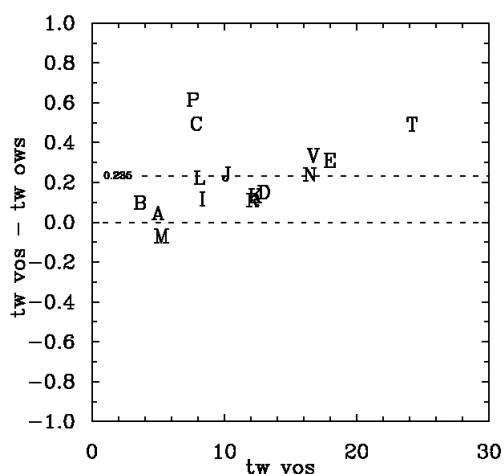


Figure 10.3.  As Figure 10.2 but for wet bulb temperature.
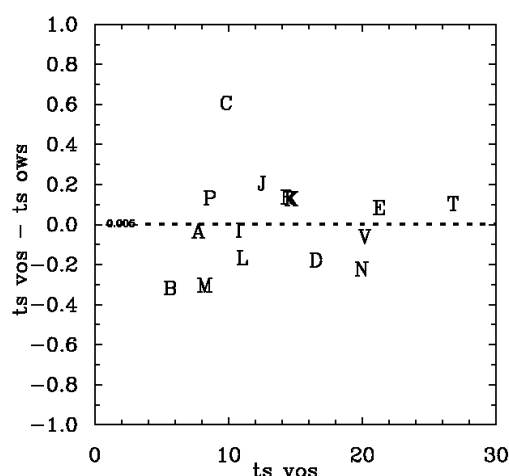


Figure 10.4.  As Fig 10.2 but for sea surface temperature.

However,  the important quantities for determining heat fluxes are mainly the errors for the air-sea temperature differences.  Thus, merchant ships were reporting a too warm atmosphere,  and one which contained too much water vapour.   As the values at sea surface were fairly well determined, the vertical temperature and humidity gradients were too small, so that the sensible and latent heat fluxes would be underestimated.   Thus the estimated temperature biases in the merchant ship observations found by Lindau (2000) were:

$$\Delta T_a = 0.259°C \qquad\qquad \Delta T_w = 0.235°C \qquad\qquad \Delta T_s = 0.005°C$$

This is in contrast to Kent *et al.* (1993a), who found higher over-estimations for all three temperatures reported by VOS.   If not only air and wet bulb temperature should be overestimated by a comparable bias,  but also the SST,  much of the overall error effect on

fluxes would be compensated.   Thus the mean correction suggested above is not beyond question.

### 10.4.2  Surface air temperature from the satellite SSM/I sensor

The near-surface air temperature $T_a$ enters the bulk formula for sensible and latent heat fluxes in different ways.   It is needed directly to determine the air-sea temperature difference in the computation of sensible heat flux.    But it is also involved in the computation of exchange coefficients, air density, and latent heat of evaporation for both turbulent heat fluxes.   Because there is no means to directly obtain the air temperature from the satellite measurements currently used for heat flux estimation,  some indirect methods of varying accuracy have been developed.

A very simple method is to assume slightly unstable conditions at any location at any time and set $T_a = T_S - 1$, where $T_S$ is the sea surface temperature.   The results of Wells and King-Hele (1990) show that most of the observed air-sea temperature differences in the tropical oceans are of the order of 1°C.   However if,  instead of the assumed unstable conditions, stable conditions occur,  the exchange coefficient for latent heat flux will be underestimated at low wind speeds by ~50% (Schulz *et al.* 1997).   Another simple method is to compute $T_a$ from the retrieved air specific humidity (see Section 10.5.2) assuming a constant relative humidity, e.g. 80% (Liu, 1988),  or using a climatological relative humidity.   This might be accurate enough to compute the exchange coefficients but seems to be too rough an estimate to determine the sensible heat flux.

A more sophisticated approach using a relationship between $T_S$ and the Bowen ratio at long time scales (compared to the synoptic time scale) has been undertaken by Konda *et al.* (1996).   This work is based on the previous work of Hicks and Hess (1977) who established this relationship from experimental data.  Their aim was the reconstruction of sea surface skin temperature (rather that the bulk temperature measured by ships) in order to compute long term averages of the turbulent fluxes more correctly.    Adapted from Konda *et al.* (1996) the turbulent heat fluxes can be written as:

$$H = -\rho c_p K_H \left( \frac{\partial T_a}{\partial z} \right); \quad E = -\rho L K_E \left( \frac{\partial q}{\partial z} \right) \tag{10.2}$$

where $\rho$ is the air density, $L$ is the latent heat of evaporation, $c_P$ is the specific heat at constant pressure, $K_H$ and $K_E$ are the diffusivity coefficients of heat and humidity, $T_a$ is air temperature, and $q$ specific humidity. Assuming that $K_H = K_E$ we obtain for the Bowen ratio:

$$\beta = \frac{H}{E} = \frac{c_p}{L} \frac{\partial T_a}{\partial q} \tag{10.3}$$

If one uses the bulk formulae for the fluxes (for example, (7.8)) the Bowen ratio reads:

$$\beta = \frac{c_p C_H (T_0 - T_z)}{L C_E (q_0 - q_z)} \tag{10.4}$$

where $C_H$ and $C_E$ are the bulk transfer coefficients and the indices *0* and *z* denote values at the sea surface and at the reference level over the surface, respectively. (10.3) and (10.4) together give:

$$\left. \frac{L}{c_p} \frac{\partial q}{\partial T_a} \right|_{T=T_z} = \frac{L C_E (q_0 - q_z)}{c_p C_H (T_0 - T_z)} \tag{10.5}$$

If $q$ is written as $\alpha q_S(T)$  with $\alpha$ relative humidity and $q_S(T)$ denoting the saturation humidity function (10.5) can be written as:

$$\frac{C_E(q_0 - q_z)}{C_H(T_0 - T_z)} = \frac{q_z}{q_S(T_z)} \left.\frac{\partial q_S(T_z)}{\partial T}\right|_{T=T_z} + q_S(T_z)\left.\frac{\partial \alpha}{\partial T}\right|_{T=T_z} \tag{10.6}$$

The second term on the right hand side of (10.6) has been neglected by Konda *et al.* (1996) because it is much smaller than the first term and it is not directly determinable from satellite or buoy measurements.

Using the empirical relationship between total precipitable water, obtained from SSM/I measurements and near-surface humidity established by Liu (1986), and AVHRR multichannel sea surface temperatures adjusted to skin temperatures, $T_a$ can be computed from (10.6). The error of a monthly mean satellite-derived air temperature is then approximately $-0.3° \pm 3.1°C$ as found by comparison to TOGA TAO buoys and buoys of the Japan Meteorological Agency. This accuracy is not high enough to study sensible heat fluxes on a monthly scale, but can be useful for analysing interannual variations. Improvements to this technique by using further developments of the retrieval schemes for $T_S$ and $q$ have not been explored. However, comparison with the approach based on the assumption of a constant relative humidity show that the Konda *et al.* (1996) method is better in bias and rms error.

A recent paper by Jones *et al.* (1999) tried to invert monthly means of $T_a$ from SSM/I measurements of total precipitable water, $W$, and sea surface temperature, $T_S$, analysis from NCEP using neural network techniques. The network was trained with data extracted from the Surface Marine Data provided by da Silva *et al.* (1994). The neural network was used in a sort of double loop where in the first round the network was trained only with $W$ and $T_S$ and in the second round the bias between the algorithm's outcome and the truth data set was used as an third input parameter for the network. From this procedure it was not surprising that the global mean bias between the $T_a$ produced by the network and the da Silva data set was negligible. The global rms was stated to be $0.72 \pm 0.38°C$ which is much lower than the results obtained with the Konda *et al.* (1996) method or the method of Jourdan and Gautier (1995) who obtained a global rms error of $2.6 \pm 1.4°C$ from a polynomial fit between $W$ and $T_a$. However, a criticism is that the da Silva *et al.* (1994) data set was regarded as ground truth. Given the large differences between *in situ* climatologies found by Josey *et al.* (1999), compared to independent high quality buoy measurements, this may not be appropriate. Since the satellite-derived data sets are expected to improve on the *in situ* climatologies, a real challenge for verification would be to compare with the independent long term buoy data sets like that of the Subduction experiment (Moyer and Weller, 1997).

## 10.5 Humidity

### 10.5.1 In situ humidity measurement

A. HIGH QUALITY IN-SITU MEASUREMENTS

The wet and dry bulb psychrometer is the traditional meteorological instrument for the routine measurement of temperature and humidity. In general, however, psychrometers are not suitable for continuous routine measurement of atmospheric humidity at sea in stand-alone or automatic mode because of their need for attention (e.g. washing salt from the wick, replenishing the water reservoir). Dewpoint hygrometers are also based on sound thermodynamic theory, measuring the temperature at which a film of dew forms on a cooled mirror, but are generally too complex to serve as operational instruments. Their main use in air-sea studies is as a reference standard; accuracy of $0.2°C$ in dewpoint is readily achievable (corresponding to $0.2\text{gkg}^{-1}$ at about $22°C$).

Nowadays, thin-film polymers which absorb or desorb water as the relative humidity changes are the most common humidity sensors, and recent developments have greatly improved their accuracy and stability of calibration. The polymer usually forms the dielectric of a capacitance in a circuit which provides an electrical output proportional to relative humidity. Conversion to mixing ratio, specific or absolute humidity requires the temperature of

the air surrounding the dielectric.   Provided this temperature is obtained from a co-located PRT or thermistor, errors in humidity measurement are less severe than those of temperature,  water vapour  being  a  conservative  quantity.      However,  for  accurate  measurement  these temperature/RH sensors should be shielded from solar radiation in a double screen with forced ventilation in the same way as a psychrometer.   At very high humidity,  or if the polymer becomes physically wet,  the humidity measurement can become unrealistic (greater than 100% relative humidity).    Earlier versions of these sensors often failed to recover from this,  but recent models seem to have largely overcome the problem and recover,  although sometimes only after several hours.

More sophisticated instruments which measure humidity fields (e.g. Raman lidar) are described by Post *et al.* (1998).  Most of these are still at prototype stage, and are unlikely to impact the routine measurement of humidity for flux calculation for many years.

## B. VOS HUMIDITY DATA

In assessing the accuracy of VOS observations, Kent *et al.* (1999) examined the random errors in specific humidity because that is the humidity variable that is used in calculating the latent heat flux.   However they found that the errors in specific humidity reflected the variation of saturation vapour pressure with temperature.    Higher errors occurred in tropical regions where the air is warm.   The humidity variable reported by the ships is dew point temperature. Errors for dew point tended to be about 2°C in colder regions and somewhat less, between 1°C and 2°C in warmer regions (Figure 10.5)
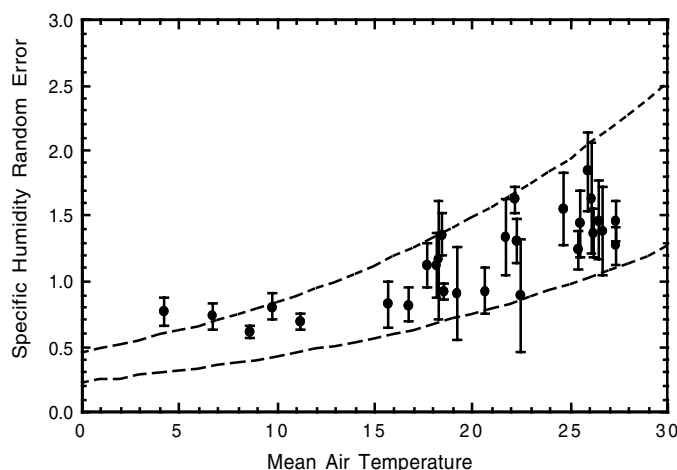


Figure 10.5. Random observational error in specific humidity ($gkg^{-1}$) as a function of mean air temperature (°C). The upper line is the error in specific humidity arising from a 2°C error in dew point temperature and the lower that from a 1°C error in dew point. A relative humidity of 80% has been assumed in the calculation. (from Kent *et al.* 1999)

The VSOP-NA results (Kent *et al.* 1993a) showed that psychrometers produced lower (and therefore presumably more accurate) dew point readings compared to screens.   Since the ship may often be a source of heat but is rarely a significant source of water vapour,  shipboard humidity readings may be of better quality than the temperature data (see for example Kent & Taylor, 1996).   The humidity data is vital for determining the latent heat flux which, over much of the ocean, represents the major loss of heat to the atmosphere and which tends to dominate the interannual variability of the fluxes.   However humidity is at present not reported by a large number of the VOS.    Equipping those ships with wet and dry bulb psychrometers and encouraging them to report humidity observations would represent a major improvement to the VOS data set.

### 10.5.2 *Remote sensing of near surface humidity*

## A. INTRODUCTION

Because the interaction of the radiation field with water vapour at a distinct level is not measurable,  all methods for determining the near-surface humidity make use of a vertically integrated water vapour content (obtained from a passive microwave instrument such as the SSM/I) as a predictor for the near-surface specific humidity, *q* , required for the bulk approach.

The correlation between both quantities depends heavily on the time scale considered. At any given time, Schlüssel (1989) showed that the total precipitable water, $W$, is only weakly correlated to $q$. He computed the correlation coefficients between adjacent atmospheric layers and atmospheric layers separated by a distance of 50 hPa or more. Vertical profiles of the correlation coefficient were larger than 0.9 for adjacent layers and values larger than 0.8 for layers with a separation distance of 50 hPa. However, the correlation profile always exhibited a significant minimum near the mean height of the atmospheric boundary layer whenever the distance between the layers was larger than 50 hPa. This indicates a decoupling of the moisture in the boundary layer from that in the free troposphere. Liu (1990) found similar results when he examined vertical variance profiles of semi-daily and daily radiosonde ascents for two tropical stations and one station in mid-latitudes. All three variance profiles showed a maximum at approximately 800 hPa caused by varying atmospheric boundary layer height and a varying contrast with the water vapour content above the boundary layer. The variance maximum as well as the correlation minimum are much less distinct if monthly averages are considered. This is the reason why Liu and Niiler (1984) had success in establishing the polynomial relationship between monthly averages of $q$ and $W$.

B. THE LIU AND NIILER (1984) ALGORITHM

The method of Liu and Niiler (1984) determines the monthly marine surface-layer humidity with a simple polynomial regression of $q$ versus $W$. The relation was found by examining radiosonde data from 11 mid-ocean island stations and weather ships scattered over the Atlantic and the Pacific ocean. The accuracy stated for the global regression formula was 0.8 gkg$^{-1}$ (Liu, 1986) and 1 gkg$^{-1}$ (Liu *et al.*, 1991) depending on the validation data source. This simple formula can be used with any retrieval algorithm which determines $W$, for example that of Schlüssel and Emery (1990):

$$W = k_0 + k_1 \ln(280 - T_v^{22}) + k_2 (\ln(280 - T_v^{22}) - T_v^{37}) \qquad (10.7)$$

which has as accuracy of 1.5 kgm$^{-2}$ for instantaneous SSM/I measurements. Upper indices on temperature denote the SSM/I channel and the lower index stands for the polarisation. Some scientists have tried to also use this method for the production of daily values of $q$ but, as may be expected from the previous discussion, this reduces the accuracy in $q$ so much that the result becomes more or less useless.

C. THE SCHULZ *ET AL.* (1997) ALGORITHM

Because of the inability of Liu's method to determine $q$ for individual situations, Schulz *et al.* (1993) developed a new method that first derives the integrated water vapour content of the atmospheric boundary layer $w_B$ (using a somewhat artificial height of 500 m) and then deduces $q$ with a simple linear regression from $w_B$. Schulz *et al.* (1993) showed that $w_B$ can be independently retrieved from $W$ and that the correlation between $q$ and $w_B$ is much higher than that with $W$. Schlüssel *et al.* (1995) improved this technique slightly by obtaining the specific humidity directly from the brightness temperatures, thus avoiding the error propagation that occurs in the two-step method. The standard error for this globally valid retrieval was stated to be 1.1 g kg$^{-1}$ for an instantaneous SSM/I measurement. Comprehensive comparisons have been made by Schlüssel (1995) and Schulz *et al.* (1997), using data from merchant ships, OWS and scientific experiments. They confirmed the global validity of this method and found rms errors not much higher than the stated retrieval error. A large portion of the error was due to the mismatch of the measurements in time and space as shown by Wentz (1997). However, a problem was found over tropical oceans where a systematic overestimation of $q$ occurred if the mid-tropospheric humidity was high. Schulz *et al.* (1997) reported that the correlation between the surface $q$ and the water vapour content in the lowest 500 m of the atmosphere was much lower than that for extratropical atmospheres. A reason might be that a 500m layer does not represent the boundary layer depth in a case of convective activity and high mid-tropospheric humidity very well.

D. THE CHOU *ET AL.* (1995) EOF METHOD

Recently, an alternative approach has been reported by Chou *et al.* (1995b; 1997). They estimated $q$ from the total water vapour content $W$ and $w_B$, retrieved with the algorithms

of Wentz (1989) for *W* and Schulz *et al.* (1993) for $w_B$, using an EOF (empirical orthogonal function) method with different EOF's for six classes of *W*.   The accuracy attained for *q* was not much different from the Schulz *et al.* (1993) method since the weights for $w_B$ in the EOF analysis were two orders of magnitude larger than those for *W*.   Some corrections were introduced for dry and wet biases occurring respectively at the low and high end of the humidity spectrum.   At the low end,  Chou *et al.* (1997) only used *W*  within the EOF analysis to correct for an underestimation of *q* during wintertime over extratropical oceans.   The other correction concerned a positive humidity bias during summer in regions where warm air moves over a colder ocean surface.   In that case they constrained the surface air humidity to the saturation humidity at sea surface temperature.   A side effect of this was that,  in each case with an overestimated $w_B$ ,  a positive bias will be automatically corrected.

E.  THE JONES *ET AL.* (1999) NEURAL NETWORK APPROACH

As for the near-surface air temperature (see section 10.4.2) Jones *et al.* (1999) used a neural network to obtain monthly averages of *q*.   Input to the neural network were *W* and sea-surface temperature extracted from the Surface Marine Data provided by da Silva *et al.* (1994), and the monthly averages of SSM/I brightness temperatures on a 1˚ x 1˚ grid.   Since the bias between satellite derived *q* and *in situ* data is incorporated in a second loop of the neural network, again it is not amazing that this method showed no bias when compared to the da Silva dataset.   The global rms error stated was 0.77 g kg$^{-1}$ with smaller errors in the North Atlantic and in the North Pacific (0.6 g kg$^{-1}$) and larger errors in the southern Indian, Pacific, and Atlantic Oceans (1.2 g kg$^{-1}$) reflecting the small observation density in the da Silva dataset in those regions.   This method was only compared to that of Liu (1986) and showed the expected improvement.   Comparisons to Chou's and Schulz's methods and to independent *in situ* measurements are needed to evaluate this method more carefully.

## 10.6  Wind

### 10.6.1 Introduction

Accurate wind data are important because wind stress increases roughly as (wind speed)$^{2.7}$ and mixed layer deepening with (wind speed)$^4$ while accurate high resolution wind fields are crucial for accurate wave modelling.   Furthermore, the scalar fluxes calculated using a bulk flux algorithm are directly proportional to the wind speed and the wind stress is an important factor in determining the atmospheric stability.   Thus any error in wind speed will result in errors in  the latent and sensible heat fluxes.

Concerning the wind stress, a correction has to applied because observation errors, even if random, would cause a systematic bias.   There are two opposite effects: the first is an overestimation of the wind stress due to errors in the wind speed by the factor

$$1+ \frac{\overline{\Delta W \Delta W}}{\overline{WW}}$$

(10.8)

where the second term denotes the relative error variance (Figure 10.6).   The second effect is an underestimation of the true wind stress due to errors in wind direction by the factor $\overline{\cos \Delta d}$ where $\Delta d$ denotes errors in wind direction (Figure 10.7).   The errors decrease the steadiness of reported wind fields and lead consequently to a lower mean wind stress.   As discussed in Section 8.2 the errors can be determined by comparing pairs of simultaneous wind reports as a function of the distance between the ships (Lindau, 1995a).   Considering both the speed and steadiness error,  the latter dominates in most wind climates, so that the stress may be underestimated by 5% to 10%.

Wind data are available both from *in situ* observations and by remote sensing.   With regard to *in situ* data (Section 10.6.2)  it will be argued that even the available "high quality" data is likely to contain biases. This is important since these data have been used to verify the routine wind data and also to develop and validate remote sensing algorithms. The routine wind

observations available from the VOS are obtained either from anemometer readings or by visual estimate.  Each technique will be shown to have advantages and disadvantages.   Remotely sensed wind data is available from active radar instruments (scatterometer and altimeter) and passive microwave radiometers.  There have been four scatterometer missions during the 1990s that provided wind vector information.  The passive microwave SSM/I instrument can also provide wind speed information.  Compared to these instruments the altimeter derived data is limited to wind speed values along the sub-satellite track.  However it should be noted that there has been a sequence of altimeter missions over a number of years, allowing these data to be used as a useful climatological data set for both significant wave height (e.g. Cotton and Carter 1994b) and wind speed.
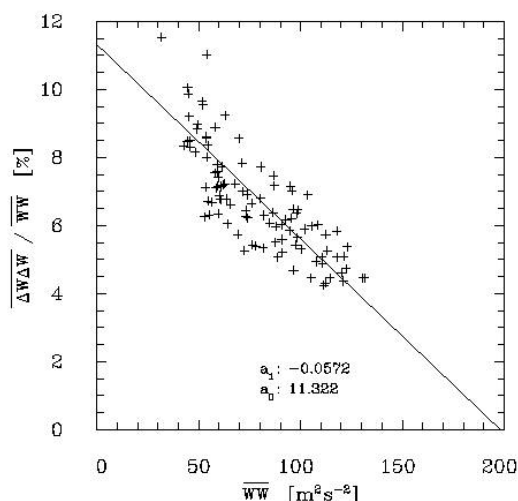


Figure 10.6 Relative overestimation of the wind stress as a function of squared wind speed. Individual crosses depict monthly 5° by 10° averages in the North Atlantic. A linear fit was applied, to be used for the correction.
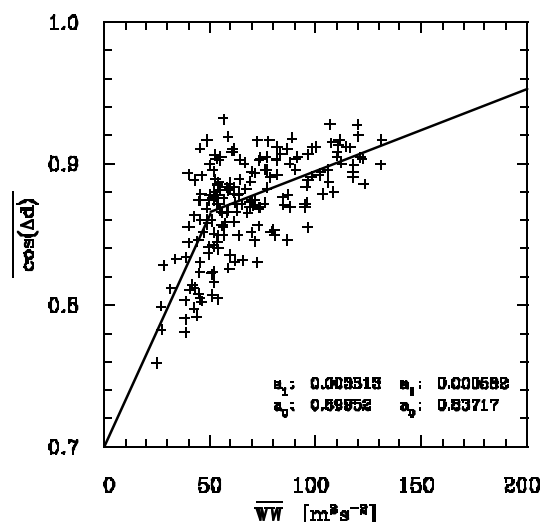
Figure 10.7 Relative error of the wind direction as a function of squared wind speed $\overline{WW}$.  Individual crosses depict monthly 5° x 10° averages.

### 10.6.2  In situ wind data

A.  HIGH QUALITY IN-SITU MEASUREMENTS

The accuracy of ship and buoy winds has recently been discussed by Taylor *et al.* (1999a),  who stress that accurate measurement of wind over the ocean is difficult.   It might be expected that the best data sources would be anemometer measurements from ocean weather ships (OWS),  research ships, or meteorological buoys.   However there are biases in each of these data types.   For example, examining data from the period 1992 to 1994,  Taylor *et al.* (1995) showed that the wind observations from OWS Cumulus were not properly corrected for ship motion when the ship was drifting or hove to.   This resulted in errors of up to 1.5 ms$^{-1}$. Isemer (1995) has attempted to evaluate the ocean weather ship wind data more generally.   As for any other ship,  the wind data from OWS and research ships are in error due to the air flow distortion caused by the ship (Yelland *et al.*, 1998);  errors of order 10% are quite possible.   As discussed in Section 9.2.2,  wind speeds from meteorological buoys are believed to be biased low in strong winds (Large *et al.*, 1995; Weller and Taylor, 1999; Zeng and Brown, 1998). Two possible causes are the vertical movement of the buoy through a non-linear near surface wind profile,  and the distortion of that profile due to the effect of high waves; again errors of order 10% may be possible.

It is often overlooked that the appropriate wind speed for use in bulk flux algorithms is relative to the ocean surface (see Equation (7.8)).  In many cases currents are a small fraction of the wind speed, and the contribution to error in ($u_z$ - $u_o$) also small,  but this is not always so.  Also,  for light winds with a stable ocean surface layer,  the wind-driven current can be a significant correction (Kudryavtsev and Soloviev, 1990).   This introduces another source of uncertainty, because the surface velocity is very seldom measured.  There are two ways in which conversion from relative to true wind can take some account of the surface velocity;  by combining the ship motion in earth coordinates (e.g. from GPS) with currents from the ship's ADCP; or by using the Döppler-log/gyro which provides the ship's motion through the water. Both methods incur additional sources of instrumental error, and furthermore the measured currents are at considerable depth (of order 10m) where the locally induced wind drift will be very small.   Thus we can assume that,  for the bulk formulae,  the wind induced surface drift has been accounted for in the determination of the transfer coefficient.   However any ocean current,  other than that locally induced by the wind,  should be taken into account.

## B.  VOS - ANEMOMETER WINDS

For the VOS data,  Kent *et al.* (1999)  found that a typical root mean square (RMS) error for a single wind speed observation is about 2.2 ms$^{-1}$.  However this was after instrumental observations had been corrected for the height of the anemometer above the sea surface (using the WMO47 data) and visual observations corrected using the Lindau (1995a) version of the Beaufort scale.   For the observations as reported,  the errors were about 15% greater - about 2.5 ms$^{-1}$.   This demonstrates that, despite the varying effects of air flow distortion around the ship, correcting the data for anemometer height does reduce the errors.   The RMS wind speed errors appeared to be lower than average in tropical regions,  however no significant dependence on wind speed was found.

The VOS in the VSOP-NA project (Kent *et al.* 1993a) reported the anemometer estimated, relative wind speed in addition to the calculated true wind speed.   Kent *et al.*, (1991) showed that a major cause of error was the calculation of the true wind speed.   Only 50% of the reported winds were within 1 ms$^{-1}$ of the correct value,  30% of the reports were more than 2.5 ms$^{-1}$ incorrect.  For wind direction,  only 70% were within ±10° of the correct direction and 13% were outside ±50°.   These are large,  needless errors which significantly degrade the quality of anemometer winds.   A similar conclusion was reached by Gulev (1999). Preliminary results from a questionnaire distributed to 300 ships' officers showed that only 27% of them used the correct method to compute true wind.   The problem is not confined to VOS observations.   A majority of the wind data sets obtained from research ships during the World Ocean Circulation Experiment showed errors in obtaining true wind values (Smith *et al.*, 1999).

Taylor *et al.* (1995) reanalyzed the VSOP-NA results for wind speed.  They found that, having corrected OWS *Cumulus* data for ship motion and corrected the VOS data for anemometer height,  there appeared to be agreement between the OWS and VOS data for winds below 10 ms$^{-1}$.  For higher wind speeds the VOS winds were biased high - by about 1.5ms$^{-1}$ to 2 ms$^{-1}$ at 20 ms$^{-1}$ wind speed.   If this bias is real, the reasons might include mis-reading of the anemometer dial (gust values rather than mean winds being reported) and air flow distortion. The use of computational fluid dynamics (CFD) to analyse the air flow over typical VOS shapes shows that there is a plume of accelerated air above the wheelhouse top (Taylor et al. 1999a). The shape of this plume depends on the geometry of the ship's accommodation block.   An anemometer mounted above the wheelhouse may be below, in, or above the plume maximum depending on how high and how far aft it is mounted.   Below the plume the wind will be significantly underestimated,  in or above the plume an overestimate will occur.

## C.  VOS - VISUAL WINDS

Kent and Taylor (1997) reviewed the various Beaufort Equivalent Scales and found that that of Lindau (1995a) was most effective at giving similar wind speed distributions for both anemometer estimated and visual monthly mean wind data.   They also confirmed Lindau's suggestion that the characteristic biases of the earlier Beaufort scales could be explained by the

statistical method by which they were derived.   It should be noted that the Lindau scale is more similar to the WMO1100 scale used for the observations  (and also to the "UWM" scale used by da Silva *et al.* (1994)) compared to the so called "scientific scale" recommended by CMMIV (Table 10.2, see also WMO, 1970).  Derivation of an accurate scale is not simple so the method will be briefly described.

The Lindau (1995a) scale was derived by comparing wind speed measurements from Atlantic OWS with visual estimates from passing merchant ships (VOS).   To ensure a true comparison two conditions had to be fulfilled: the error variance and the natural variability must to be equal in both data sets.   Lindau averaged over four individual OWS observations but over six VOS observations to compensate for their different accuracy.   The OWS data were averaged over 24 hours and calculated for the VOS data for each location and each season the radius that contained the same variability as for one day.   The new scale was derived from these averages by the method of cumulative frequencies, which treats the variances of both data sets in a symmetric manner.  As a result,  the new scale (Table 10.2) was able to reproduce the OWS wind speed without systematic errors in either the average or in the variance.

Table 10.2. New 10m-equivalent values compared to the WMO Code 1100. N gives the number of data pairs, which consists of daily means for OWS measurements and spatial means for Voluntary Observing  Ships (VOS).

| Bft | 0 | 1 | 2 | 3 | 4 | 5 | 6 | 7 | 8 | 9 | 10 | 11 | 12 |
|-----|-----|-----|------|------|-------|-------|------|------|------|------|------|------|------|
| WMO | 0.0 | 1.7 | 4.7 | 8.4 | 13.0 | 18.3 | 23.9 | 30.2 | 36.8 | 44.0 | 51.4 | 59.4 | 67.7 |
| New | 0.0 | 2.3 | 5.2 | 8.9 | 13.9 | 18.9 | 23.5 | 28.3 | 33.5 | 39.2 | 45.5 | 52.7 | 61.1 |
| N | 6 | 378 | 2287 | 8441 | 17197 | 11598 | 8870 | 4655 | 2068 | 597 | 122 | 15 | 1 |

The definition of the Beaufort scale has changed during time (as have the characteristics of the ships from which the estimate is made).  A time dependent equivalent scale may therefore be necessary.   Lindau (1995b) checked North Atlantic wind observations of the last hundred years against simultaneous individual pressure differences between the reporting ships. Assuming a constant relationship between wind speed and pressure gradient throughout the years a time dependent scale was obtained (Figure 10.8) .   Applying this scale to COADS the apparent positive trend in wind speed since 1945 was removed.

D.  RELIABILITY OF COADS MONTHLY WINDS

The reliability of the COADS Release 1a 2-degree monthly winds has been tested by comparison with instrumental measurements in the North-West Atlantic for the period 1981-1991 (Gulev, 1999).   The instrumental data set contained anemometer measurements of high homogeneity and quality,  taken by six research sister-ships with known anemometer heights in the North West Atlantic.   Care was taken to process the instrumental data to provide compatibility with the COADS winds.   In particular,  the error variances for monthly averages of wind speed were tested to allow a two-way regression comparison.   The results showed an overestimation of the COADS winds in the low ranges and underestimation of the strong and moderate winds.   Such a relationship is different from those obtained in the other validation studies (e.g. Lindau, 1995b; Kent and Taylor, 1997);  indeed,  application of alternative Beaufort scales did not remove the bias,  but made it even more pronounced.   Thus,  the conclusion of Gulev (1999) was that the disagreement resulted mainly from errors in the anemometer measurements in COADS,  primarily from the incorrect evaluation of the true wind (Section 10.6.2B).   Taylor *et al.* (1999a) suggested that airflow effects, for the class of research ship used,  may also have contributed to the differences. In either case a possible conclusion is that Beaufort estimates may well be less biased in the COADS than anemometer measurements. Similar arguments to these are used to justify the continuing preference of a number of meteorological agencies for visually estimated winds rather than anemometer readings.
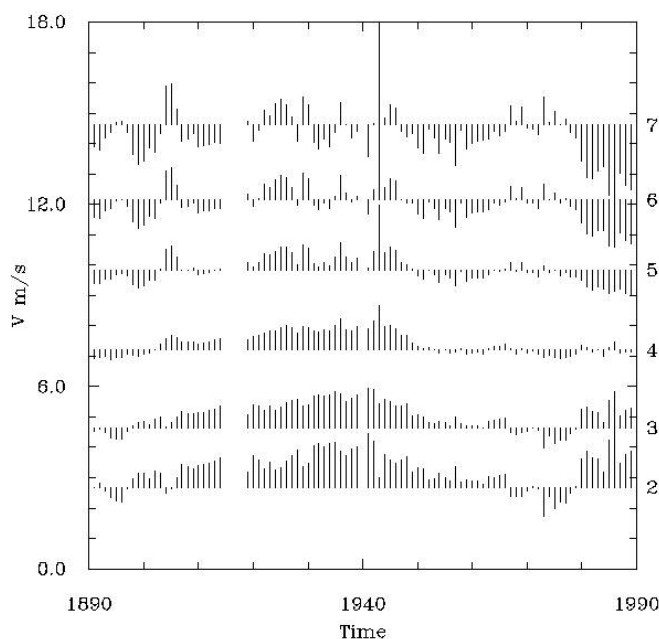
Figure 10.8 Time dependent equivalent scale illustrated by the temporal evolution of Beaufort forces 2 to 7.

### 10.6.3  Remote sensing of surface wind

A. SCATTEROMETRIC SURFACE WIND VECTORS

Wind vector estimates from scatterometers are based on empirical relationships ("model functions") relating backscattered energy to wind speed at 10m under neutral conditions. Geophysical validation over a wide range of wind speeds has been difficult due to a) the difficulty in acquiring suitable in-situ observations and b) the inherent incompatibility between scatterometer measurements and buoy observations (Freilich and Dunbar, 1999). However the model functions have improved over time with the introduction of more sophisticated techniques and also as more scatterometer and high-quality *in situ* data become available to test the full parameter space of the backscatter-wind relationship. Scatterometer data are available from numerous sources (each using a different model function). Thus it is important to note the particular version and source of scatterometer data.

The fundamental scatterometer design results in multiple possible wind directions (so-called ambiguities) from which the most likely solution is determined. This ambiguity selection process is fairly accurate; for regions with rms wind speed greater than 4 ms$^{-1}$, the NSCAT ambiguity removal skill is conservatively estimated to be 95% (Gonzales and Long, 1999). The sampling characteristics (number and width of data swaths, data coverage) of the scatterometer data govern the ability to estimate synoptic fields of winds. This issue was addressed more fully in Section 8.6.3.

The accuracy of the scatterometers is relatively excellent compared to errors for winds from VOS. Validation of the CERSAT ERS-1/2 scatterometer wind retrievals found an systematic underestimation of nearly 0.75 m s$^{-1}$ and an RMS error of ~1.3 m s$^{-1}$ (Graber et. al., 1996). Directional biases and RMS errors were ~7° and ~22° respectively. Other comparisons further explore such dependencies as wind direction on incidence angle (e.g. Ebuchi and Graber, 1998) and validation in coastal seas (Kent et. al., 1998).

Evaluation of the 25-km NSCAT instrument winds has been much more comprehensive. Compared to high-quality ship winds (Bourassa et. al., 1997), the NSCAT winds had RMS differences for speed and direction of 1.8 m s$^{-1}$ and 14°. When compared to buoys, the bias was -0.3 m s$^{-1}$ and RMS error ~1.3 m s$^{-1}$ (Freilich and Dunbar, 1999). Other validations are available and include a wide range of approaches, including gridded product evaluation through direct comparisons to other products (e.g. Atlas et. al., 1999); comparison of

ocean models forced by various products (e.g. Verschell et. al, 1999); and comparisons for use in air-sea carbon exchange (e.g. Boutin et. al., 1999).

Some numerical weather prediction (NWP) centres have been incorporating scatterometer data into their operational surface wind analyses. For example, since January 1996, ERS scatterometer winds have been assimilated in the operational ECMWF analysis. This will likely continue as the QuikSCAT data systems include the operational distribution of QuikSCAT data by NOAA.

B. PASSIVE MICROWAVE SURFACE WIND SPEEDS FROM SSM/I

**Introduction:** Thermal radiation emitted by the sea surface at millimetre frequencies is strongly modified by wind induced sea surface roughness and partial foam coverage. The classical description of the emissivity of a foam covered rough ocean surface as a function of frequency $\nu$, incident angle $\theta_i$, and polarization $P$ is:

$$\varepsilon(\nu,\theta_i,P;u,C_f) = (1 - C_f)\varepsilon(\nu,\theta_i,P;u) + C_f\varepsilon_f(\nu,\theta_i,P) \qquad (10.9)$$

where $C_f$ is the fractional foam coverage, $\varepsilon_{rw}$ is the emissivity of a wind roughened surface, and $\varepsilon_f$ is the emissivity of foam. In the algorithm development history different theoretical and empirical models have been used to relate $C_f$, $\varepsilon_{rw}$, and $\varepsilon_f$ to the physical state variables of the sea surface and to the wind field above. In the material that follows four types of wind speed algorithms for the SSM/I are described. These are the modified D-Matrix approach by Goodberlet and Swift (1989), the radiation transport model and regression based algorithm of Schlüssel and Luthardt (1991), neural network algorithms by Stogryn *et al.* (1994) and Krasnopolsky *et al.* (1995), and the wind speed part of the SSM/I all weather algorithm by Wentz (1997) and Wentz and Spencer (1998). The selection of these four algorithms does not cover all the available wind speed algorithms but it gives a description of different methodologies and a brief survey of the history of algorithm development.

The original **D-Matrix algorithm** as given in Lo (1983) computes the wind speed at a reference level of 19.5m from a linear combination of SSM/I brightness temperatures. It uses 11 sets of coefficients representing particular seasons and latitude bands. Goodberlet and Swift (1989) found that the original D-Matrix algorithm did not meet the accuracy criteria of 2 ms$^{-1}$ when results obtained from SSM/I measurements were compared to NOAA buoys. Additionally, they found a low bias at high wind speeds and zonal discontinuities due to the coefficient scheme used. They developed an alternative new D-Matrix algorithm from SSM/I brightness temperatures and buoy wind speeds using linear regression analysis that met the 2 ms$^{-1}$ criterion for all seasons and latitude bands. Since this algorithm works only for rain free cases, the D-Matrix algorithm uses a rain flag system to discard affected measurements. Such an algorithm is quite robust but doesn't point the way to future improvements since it is purely statistical; no information on the influence on the measurements of the surface emissivities given in (10.8), or of the atmospheric part of the signal, can be quantified. Goodberlet and Swift (1992) improved their algorithm with a nonlinear version that should account for water-laden atmospheres. As stated by Krasnopolsky *et al.* (1995) this retrieval has a singularity at $\Delta_{37} = 30.7$ K which may fall within the useful range of brightness temperatures.

The **Schlüssel and Luthardt (1991) algorithm** is based on studying theoretically the radiative transport within the SSM/I channels for a large set of oceanic/atmospheric situations with respect to wind speed. The retrieval formula is derived by multivariate regression analysis from the simulated synthetic measurements. It derives the wind speed mainly from the brightness temperature difference between horizontally and vertically polarised components at the same frequency so it is, like the Goodberlet and Swift (1989) algorithm, a linear combination of SSM/I channels. The theoretical accuracy for the globally valid passive wind speed retrieval is stated to be 1.4 ms$^{-1}$ under conditions where the satellite measurements are not affected by heavy rain.

This retrieval was evaluated by Schlüssel and Luthardt (1991) by comparing satellite derived wind speeds with objectively analysed *in situ* wind speeds over the North Sea (Luthardt, 1985) during the period July 1987 to June 1988. They obtained a standard error of 1.9 ms$^{-1}$ with a small bias of 0.2 ms$^{-1}$. Schulz (1993a) compared 3403 globally distributed buoy and ship measurements with retrieved wind speeds during the period July 1987 to September 1987 and found a standard error of 2.1 ms$^{-1}$ with the same bias as for the North Sea. The systematic error was only significant at wind speeds above 15 ms$^{-1}$ and could have been caused by an insufficient parameterisation of the emissivity of the ocean surface at high wind speeds. This is difficult to prove since there are only a few measurements during high wind speeds and moreover still fewer measurements of the emissivity in the microwave region under those conditions. However, this comparison revealed also that this algorithm produces a high bias of 0.81 ms$^{-1}$ at latitudes between 20°N and the equator, showing that the retrieval scheme is sensitive to liquid water in the atmosphere.

Consequently, Schlüssel (1995) modified the algorithm to allow more liquid water in the atmosphere during the radiative transport simulations and also determined new coefficients for the algorithm (using the same channels) if light rain was present. The choice of retrieval was decided using a rain flag system similar to Goodberlet and Swift (1989). The accuracy for the light rain retrieval was determined to be 1.6 ms$^{-1}$.

**Neural network approaches** are alternative empirical methods to derive wind speed from passive microwave brightness temperatures which have become popular during the last five years. Neural networks can be advantageous if:

❍    nonlinearities occur in the transfer function, from brightness temperature to the sought geophysical parameter, that vary over the range of measurement space.

❍    there is no a priori knowledge with regard to an analytical representation of the transfer function.

Stogryn *et al.* (1994) and Krasnopolsky *et al.* (1995) have developed neural network retrieval schemes that outperform all of the previously described algorithms. The biases and rms errors as stated by Krasnopolsky *et al.* (1995) were 0.05 ms$^{-1}$ and around 1.6 ms$^{-1}$, respectively, when compared to buoy measurements in their test data set. Krasnopolsky *et al.* (1995) introduced a new rain flag system that was based on liquid water content and which recovered 40% of measurements rejected by the Goodberlet rain flag system.

However, these algorithms can have limitations because:

❍    the training data sets must include enough low and high wind speed cases. Otherwise a high bias at low wind speed and a low bias at high wind speed occurs and the variance of the wind speed distribution is too low.

❍    neural networks are more sensitive to sensor-dependent systematic errors (like calibration). For example, Krasnopolsky *et al.* (1995) trained their network for the DMSP F8 satellite and when they apply their coefficients to data of the F11 satellite they obtain a bias of -0.9 ms$^{-1}$ and a rms error of 1.85 ms$^{-1}$ although the brightness temperature differences between F8 and F11 were only ~1K for all channels. This effect can be diminished by computing coefficients for each satellite but it should be kept in mind if neural networks are blindly applied.

With respect to equation (10.8), the same arguments hold as for the empirical regression algorithms if we ask for physical explanations of the change of surface emissivity with wind speed. As for any empirical algorithm, they may give good estimates of wind speed but little can be learnt about the physics. This could be changed if the neural network were not trained on buoy-satellite match ups but rather used in conjunction with radiative transfer models thus giving more control over the situations considered.

The **Wentz (1997) all weather algorithm** represented a more physical approach in retrieving the wind speed from SSM/I measurements in rain free situations. Wind speed was

retrieved,   along with columnar water vapour and columnar cloud liquid water,   using a nonlinear optimisation method.    The wind-induced emissivity of the sea surface was parameterised by a two scale theory (Wu and Fung, 1972; Wentz, 1975) which was based on a knowledge of the root mean square slope of the large gravity waves,  the standard deviation of the small irregularities,  and the correlation length of the small surface structures.   In practice, Wentz (1997) expressed the wind-induced emissivity as a monotonic function of wind speed which consisted of two linear segments connected by a quadratic spline such that the function and the first derivatives in wind speed were continuous.   The coefficients for this model were derived from collocated buoy and SSM/I observations.

Wentz (1997) also investigated the role of wind direction on the retrieval accuracy and found that errors of approximately 3 ms$^{-1}$ could occur,  especially if the radiometer looked in the upwind direction.   He developed a correction of this effect which brought the error down to 0.5 ms$^{-1}$.    Additionally,  he claimed that the information on wind direction inherent to the SSM/I measurements can be retrieved if the signal to noise ratio can be enhanced by building averages over large scales and long times.

Importantly,  Wentz (1997) also gave an error estimation that resolved the error budget in terms of model errors,  wind direction errors,  radiometer noise,  sampling mismatch between satellite and buoys,   and other errors that could not be resolved.   This enabled him to subtract the sampling mismatch error from the total observed error.   For his own retrieval he ended up with a small systematic error of 0.3 ms$^{-1}$ and an rms accuracy of 0.9 ms$^{-1}$ ;  significantly better that all previous algorithms.

In a new all weather algorithm (Wentz and Spencer, 1998) the retrieval methods are extended to rain cases.   With respect to wind speed,  this simply consists of discarding the retrieval and filling in values from neighbouring pixels,  or using a monthly climatological value derived from SSM/I.   This algorithm has been used to compute a 10 year time series of wind speed from the chain of SSM/I sensors which is,   together with other atmospheric variables,  available via the internet under http://www.ssmi.com.

## 10.7  Waves

Wave information is currently available from measurements on buoys and other in-situ platforms, VOS observations, satellite measurements (altimeter and SAR), and from model experiments.

Wave recorders at NDBC and JMA buoys, light vessels, and OWS's provide measurements of significant wave height with continuity of records from several months to nearly two decades.   These are relatively high quality data which can be used for validation of other products, but their spatial coverage is poor, since most of the buoys located in offshore regions are in the subtropical northwest Atlantic, mid-latitudinal northeast Pacific and equatorial Pacific.   Long-term observations from shipborne wave recorders (SBWR's) are available in a number of locations in the northeast midlatitudinal Atlantic, particularly at OWS L and Seven Stones Light Vessel.   These two records (with a continuity of 12 to 20 years) were used to identify secular changes in significant wave height (SWH) by Bacon and Carter (1991, 1993). However, it is unclear to what degree the records from NDBC buoys and SBWR's are consistent.   There are some specific biases in both buoy and ship records and these have not yet been quantified.

Reports containing visual wave observations appear in COADS in the early 1960's, and for later years the contribution of reports with wave observations exceeds 40%.   These visual VOS observations were used to produce "Ocean Wave Statistics" (Hogben and Lumb 1967) and "Global Wave Statistics" (Hogben *et al.* 1986), which contain statistical distributions based on limited visual wave data from 50 and 104 areas of the World Ocean respectively.   These have been widely used by sailors and naval engineers.   Gulev and Hasse (1998) brought the visual

wave observations from COADS reports up to date,  producing a North Atlantic wave climatology on a 5° grid for the period 1964-1993.  They derived heights, periods and directions for wind sea and swell.   SWH was derived using a combined approach of Barratt (1991) where SWH is assumed to be the square root of the sum of squares of sea and swell heights for the cases when sea and swell directions are within a certain directional sector  (found to be equal to 30° (Gulev and Hasse 1998));  for other cases it is taken as higher of the two components. Relatively good agreement was obtained for the resulting SWH in comparison to *in situ* observations from NDBC buoys and OWS measurements.   Some known biases in the COADS observations include the overestimation of very small seas and swell  (which results from the coding of all waves smaller than 0.5 m with the unique code figure "1"), general underestimation of both sea and swell periods by approximately 0.1 to 0.4 seconds, and large overestimation of swell periods for 1968-1969 due to a change in swell period codes in 1968 which was not implemented simultaneously by all observers.

The only observation-based wave height climatologies available at present are derived from the altimeters flying on board GEOSAT, ERS-1/2 and TOPEX/POSEIDON.   Products derived from the ERS-1 and ERS-2 scatterometers are still under development.    First assessments showed that the algorithms used to retrieve $H_s$ from the scatterometer severely underestimated wind sea, but gave very reasonable estimates of swell (Bauer and Heimbach 1999).   Due to the limited sampling, altimeter derived wave climatologies are only available as monthly means.   Cotton and Carter (1994a) calibrated these monthly means against co-located buoy measurements.   They found the accuracy of the calibrated data to be better than 18 cm. This made it possible to combine time series from different missions and construct a global climatology which has continuity over about 12 years (starting in 1985) with some gaps in early 1990's.   Bauer and Staabs (1998) compared the statistical properties of altimeter derived $H_s$ with those of measurements from OWS and in general found good agreement.   They also, however, observed that the algorithm used before 1994 to retrieve Hs from the ERS-1 altimeter produced an unrealistic high frequency of occurrence of Hs = 2m, a deficiency that had already been noted by Cotton and Carter (1994a).

By now,  wave models driven by winds from NWP systems can produce long-term climatologies of waves (hindcasts) covering global ocean or individual ocean basins for periods of several decades.   These wave products are not fully independent, because they are largely affected by the wind forcing used.   Sterl et al. (1998) produced a 15 year climatology of waves by driving the WAM wave model with the ERA winds (see also Section 2.4 of this report). While the patterns of Hs thus obtained compared favourably with those derived from altimeter measurements, the absolute wave heights were generally found to be too low.   As the most probable reason the authors identified the limited resolution of ERA,  stressing once more the importance of the wind input for the modelling of waves.   OceanWeather Inc. performed a number of 40-yr (1958-1997) wave hindcasts using the ODGP-2 1G fully discrete spectral wave model and ODGP 3G wave model with a grid resolution of 2.5° longitude and 1.25° latitude (1G) and 1.25° x 0.625° (3G) (Cox and Swail 2000).   These hindcasts were driven by the NCEP/NCAR 10m winds.   Time resolution of this product is 6 hours, and all major wave parameters, such as significant wave height, sea and swell heights are available.   Details of the OceanWeather Inc. wave hindcasts were described in Cox and Swail (2000).

Recently Young and Holland (1996) and Young (1999) produced a combined wave product based on satellite remote sensing and NWP wave outputs.   This global scale wave climatology covers a 10-year period from 1986 to 1995 and has 2° spatial resolution for monthly means of significant wave height and period.   Data from ERS, GEOSAT and TOPEX/POSEIDON,  as well as from the ECMWF operational system (WAM),  were used to produce the climatology.   Analysis of the global fields of Young (1999) shows that this product still requires comprehensive validation efforts.

**10.8 Cloudiness**

*10.8.1 Introduction*

Comprehensive, ocean-basin scale observations of clouds are based on either (1) synoptic reports or (2) satellite data. Some ship campaigns have also used intensive passive and active remote sensing systems (e.g. ceilometers and cloud radars) for a more precise characterisation of cloudiness in a restricted region.

*10.8.2 In situ cloud data*

Considering the VOS observations, the main problem is the quality of the cloud reports returned by the relatively untrained observers. There have been hardly any studies of the quality of the reports. With regard to these data, Warren et al. (1988) remains the standard reference climatology. Ship synoptic reports were obtained from the "SPOT" archive of the Fleet Numerical Oceanography Center (FNOC) and Release 1 of the COADS for 1930-1979. The painstaking work on this atlas yielded gridded monthly and seasonal cloud cover, cloud type amounts, frequencies of occurrence, cloud base heights, harmonic analyses of annual and diurnal cycles, and interannual variability and trends. Warren (personal communication) notes that since 1988, the analysis methods have been improved; moonlight data is now included. Work on a new atlas will cover the 44 years 1952-1995. A digital forms of the atlas is available. The main problem is the degree of reliability that can be ascribed to visual cloud observations made by observers with little relevant training and whose view of the sky is in many cases obscured.

Information on cloud base height and cloud overlap from synoptic atlases are sometimes used as a cross check on satellite-based retrievals of parameters, such as surface downwelling LW (e.g. Gupta et al., 1999).

*10.8.3 Remote sensing of cloud data*

ISCCP has combined geostationary and polar orbiting satellite data to produce a geographically comprehensive cloud record. The ISCCP second generation "D2" data is available for July 1983 – December 1998. ISCCP is an officially reviewed WCRP product, and CD ROM's of ISCCP clouds are issued by the NASA Langley DAAC. ISCCP cloud retrievals are based primarily on two imaging channels, the reflected SW and LW in the emission window. For polar latitudes only, a third channel at 3.5 micron is also used. Pixel resolution is nominally 4 km. The pixels are sampled every 30 km and 3 hours (yielding the advanced research product "DX", which is internal to ISCCP). The main ISCCP D product is gridded in 280 by 280 km equivalent areas. Sunsynchronous NOAA satellites equipped with the AVHRR are used at high latitudes. Low latitude retrievals are based on geostationary data. The requirement to produce comprehensive coverage has resulted in the application of fairly rudimentary, but ingenious, algorithms in ISCCP. Calibration of ISSCP has resulted in a improved record from the radiometers on operational satellites (Brest et al., 1997), but good calibration remains a challenge for ISCCP (for example, Klein and Hartmann 1993). ISCCP calibration is sufficient to identify the geographical patterns of interannual variability, such as that due to ENSO. However, no presently operational cloud imager is considered to have the stability to confidently identify a small secular change in global mean cover. That includes the VIRS imager on TRMM, which is used by CERES to process coarser resolution broadband data. The CERES broadband radiometers are, however, sufficiently stable to identify changes in global mean radiation (in Wm-2 rather than per cent cloud cover) to within 0.2%.

*10.8.4 Combined products*

Another source of cloud observations is the United States Air Force Real-Time Nephanalysis (RTNEPH, Hamill et al. (1992)). It is operationally produced 8 times daily on Northern and Southern Hemisphere polar stereographic grids (horizontal resolution 47.625 km at 60o latitude). Data sources are primarily the infrared and visible channels on the DMSP satellites, with some information from NOAA polar orbiters. Surface observations are used to a

significant extent when available, and a manual bogus procedure is used during each analysis cycle. The RTNEPH data set consists of total clouds and up to four distinct cloud layers. Each grid point contains cloud coverage, geopotential height of the cloud layer bases and tops, time of observation, and diagnostic information.

The analysis system makes assumptions to estimate the magnitude of lower cloud obscured by higher clouds. There are rarely more than two distinct cloud layers. Hamill et al. (1992) note that the intent is to maximise the probability of cloud detection; therefore both clear and overcast conditions tend to be overestimated. The IR retrieval is a one-channel algorithm; therefore, if there is no visible channel or surface data available, the analysis tends to miss warm low stratus and high thin cirrus or to place the cirrus too low in the atmosphere. There are plans to improve the algorithm by using multi-spectral satellite techniques. Masutani et al. (1999) have compared several estimates of clouds, including ISCCP and RTNEPH.

## 10.9 Precipitation

### 10.9.1 Surface-based precipitation data

A. HIGH QUALITY IN SITU PRECIPITATION MEASUREMENTS

The advantages and disadvantages of different methods of high quality precipitation measurements has been discussed at some length in Section 5.4 which dealt with the direct measurement of precipitation as a flux. It must be recognised that the number of in-situ precipitation measurements over the whole world ocean is still probably no more than several thousand samples. Also, there is no possibility of covering much more than a few percent of the ocean with radar measurements. Therefore these measurements (be they from mechanical or optical gauges, disdrometers, or radar) are better considered as a means of verifying satellite measurements and NWP products rather than the basis for the creation of a precipitation atlas. However, the development of accurate and reliable raingauges, and their introduction into operational use would provide a sharp increase in the number of open ocean samples within a few years.

Despite the progress which has been achieved in precipitation measurement, there are some problems which are still unresolved. In particular, wintertime solid precipitation in mid- and high latitudinal regions is still poorly determined, and it is unclear at the moment how this can be best overcome. Should the existing gauges be improved or completely new instruments developed specifically to measure solid precipitation?

B. RADAR MEASUREMENT OF PRECIPITATION

Radar meteorology has a long history of application to precipitation measurement, and to the study of atmospheric dynamics from fields of backscatter intensity and Doppler velocity. Its strength is the ability to display spatial patterns of rainfall within some hundreds of kilometres surrounding the radar position. Unfortunately, radar-derived rainfall measurement cannot be regarded as direct; to make the observed returns quantitative a number of error-prone steps are involved. The fundamental problem is determination of the relationship between radar reflectivity, $Z$ ($mm^6 m^{-3}$), and rainfall rate, $R$ ($mm\ hr^{-1}$), which has to be established empirically for each situation. The traditional form is:

$$Z = aR^b \qquad\qquad (10.10)$$

where the constants a and b fall within rather broad bounds, a being typically a few hundred while b ranges between about 1.2 and 1.8 (Battan, 1973)[1]. Z - R relationships have rather an extensive literature; see for example the discussions by Austin (1987) and Sauvageot (1994). The accuracy of measurement therefore depends on a number of factors; the radar calibration, signal attenuation due to the rain along the radar path and water on the radome, the vertical

---

[1] Radar meteorologists usually quote the reflected signal in *dbZ* where

$Z(dbZ) = 10.\log10\ Z\ (mm^6 m^{-3})$

structure of the precipitating system, and knowledge of the scan volume geometry.  The latter presents a particular challenge when the radar is mounted on a ship, because of the motion. Finally, it is usual practice to adjust the radar Z - R relationship to whatever in-situ gauge array may be under the radar beam (Steiner and Houze, 1997).  Clearly, this presents difficulties over the open ocean, and often leads to dependence on the nearest island-mounted gauge where the rainfall may not be representative.

A recent use of radars for measuring precipitation at sea occurred during COARE when C-band Doppler radars were deployed simultaneously on two ships for a total period of 90 days. Each radar antenna was stabilised, using the combination of an Inertial Navigation Unit (INU) and the Global Positioning System (GPS) to calculate all instantaneous components of ship motion and their time derivatives so that the antenna appeared to be fixed to a horizontal plane. The pointing accuracy was estimated to be 0.1 degrees.  The COARE radar rainfall data have undergone close scrutiny in the light of the initial disagreements with shipborne *in situ* rain gauges (see Section 10.9.4E), and are well documented (Rutledge et al., 1993; Short et al., 1997; Petersen et al., 1999).  Several sources of error were discovered, and improvements made to the signal processing and data analysis.  These included careful recalibration of the system, corrections for range attenuation and gain, and separate *Z - R* relationships for convective and stratiform rainfall.  Tokay and Short (1996) showed that, for the same reflectivity, stratiform rain rates are about half those of convective precipitation because stratiform produces more large raindrops than convective rainfall due to aggregation, and fewer small to medium drops. Tropical stratiform falls from a layer of melting aggregates, which cause the well-known radar "bright band",  a region of enhanced reflectivity just below the zero degree isotherm.  Short *et al.* (1997) give reflectivity $Z = 323R^{1.43}$ for stratiform and $Z = 120R^{1.43}$ for convective rainfall. For monthly rainfall, however, Steiner and Houze (1997) question the value of using separate relationships for convective and stratiform rainfall.

COARE demonstrated that the combination of high-quality Doppler radar with precise pointing and stabilisation has application in both oceanographic and meteorological studies associated with precipitating systems over the ocean.  Research vessels (e.g. the US *R/V Ronald H. Brown* and the Japanese *R/V Mirai*) are beginning to install such systems as part of the ship's inventory of equipment, but it is clear from the above that it is far from being a system for general use.  At the same time, Lebedev and Tomczak (1999) have described a method of recording and analysing the raw reflectivities from a ship's navigational radar with a view to its possible use to measure open ocean precipitation routinely from research vessels and ships of opportunity.

A novel use of Doppler wind profilers for precipitation profile measurements was also introduced during COARE.  The NOAA Aeronomy Laboratory has developed UHF wind profiler technology for tropical dynamics and climate research (Carter *et al.* 1995).  The profilers, originally intended for the measurement of lower tropospheric winds in the tropics, have now been applied to precipitation research (Gage *et al.* 1994, 1996; Ecklund *et al.* 1995; Williams *et al.* 1995, 1999).  The UHF profilers are sensitive to hydrometeors and provide a highly-resolved time-height cross section of precipitating cloud systems.  A unique precipitation data set was collected using UHF profilers at Integrated Sounder System (ISS) sites during COARE. Preliminary studies show reasonable agreement between profiler and scanning radars in the statistical partitioning of tropical precipitation.  The profiler uses the vertical structure of hydrometeor echoes, their Doppler velocity, and spectral width, as well as their temporal continuity in determining precipitation type (Williams *et al.* 1995).  Since COARE, a network of wind profilers has been maintained operationally, particularly in the western Pacific region, to observe precipitating cloud systems. Profiler data at Darwin have also been analysed for rainfall (Cifelli *et al.* 1996; Ecklund *et al.* 1997).

C.  VOS PRECIPITATION ESTIMATES

Precipitation is not measured on ships but is determined from the "present weather" descriptions reported in the ships' weather observations (Tucker, 1961).  Weather codes which

indicate that precipitation is occurring are modelled by formulae which describe the precipitation rate based on the contribution from three continuous rain categories:  light, moderate, or heavy.  The relationship between these categories,  and the rain rate which they represent, was found empirically.   On a global basis accuracy of any "present-weather" based precipitation estimate is not likely to be high.   Dorman and Bourke (1978) adapted Tucker's scheme for tropical regions by taking temperature into account.   Lindau (2000) proposed a simple rain algorithm, which needs as input the reported weather code and specific humidity. The algorithm was derived by using wind-corrected rain measurements of German lightships. With weather code and specific humidity they were able to explain more than 70% of the intermonthly variance.   It has been used to determine evaporation minus precipitation on a global basis.

### 10.9.2  Precipitation by ocean freshwater budgets

An integral method of rainfall determination involves calculating ocean budgets from surveys of temperature and salinity in space and time over the ocean mixed layer.  Typically, T/S profiles are obtained over an area of ocean from an array of moorings, or from ships making CTD casts at frequent stations along the cruise track or with a towed CTD (e.g. mounted on a SeaSoar).  It is necessary to analyse heat and freshwater fluxes in three dimensions, because advective components have been found to be of first order.  The closure of freshwater budgets during COARE by Feng et al. (1998), Smyth et al. (1996) and in the Indian ocean by Godfrey et al. (1999) are examples of the successful integration over space and time of the patchy rainfall pattern, indicating that with proper care the ocean can be its own rain gauge.

### 10.9.3  Satellite remote sensing of precipitation

A. INTRODUCTION

This section describes the existing global estimates of precipitation obtained from satellites that might be used for model evaluation or creation of freshwater flux data sets.  The order in which the different products are described should not be considered as a ranking of data sets.   The major problem facing satellite estimates of precipitation is the lack of alternative fields for validation.   Early attempts at validation have been restricted to comparisons with climatologies obtained from ship present weather reports which also suffer from large uncertainties (Jaeger, 1976; Legates and Willmott, 1990).   However in recent years three Algorithm Intercomparison Projects (AIP) have been sponsored by the GPCP.   In addition, the NASA WetNet project has also sponsored three projects called Precipitation Intercomparison Projects (PIP).   The aims and results of both types of project are discussed below (Section 10.9.4).

B. GPCP

Global climatological fields of monthly mean precipitation over both ocean and land, derived from a combination of satellite and terrestrial observations made over the period July 1987 to March 1998,  have recently been produced within the Global Precipitation Climatology Project, GPCP (Huffman et al., 1997).  The data are provided on 2.5˚ x 2.5˚ latitude-longitude grids.  The values were obtained using a combination of passive microwave and infrared techniques.   The infrared techniques rely on a correlation between cloud top brightness temperatures and rain rate and are more appropriate for use with deep convective systems. Used within 40˚ of the equator, they exploit the frequent sampling afforded by geostationary satellites.   The microwave technique detects the radiative effects of hydrometeors and has a stronger correlation with surface rainfall.   It relies on sensors on polar orbiting satellites (to obtain adequate spatial resolution) and hence has a relatively low sampling rate,  as long as only one satellite is in use, but can be employed to higher latitudes in the GPCP analysis.   A future version of GPCP will deliver a daily precipitation map on a 1˚ x 1˚ grid.

C. CMAP

The CPC Merged Analysis of Precipitation, CMAP (Xie and Arkin, 1997),  consist of a 17 year period,  from 1979 to 1995,  of gridded global (ocean and land) monthly precipitation

fields with a resolution of 2.5˚ x 2.5˚ in latitude and longitude.   Merged into this dataset are a variety of satellite measurements, gauge observations, and NCEP-NCAR reanalysis.   Thus its value for evaluating models is somewhat reduced.   However,  it might be a very useful dataset for climate analysis and hydrological research.   Many of the data sources used are the same as for the GPCP dataset.  In particular, the Geostationary Precipitation Index, GPI (derived from infrared data of geostationary satellites) and the SSM/I-derived components - like the Ferraro *et al.* (1994, 1996) dataset described below.   Thus differences between CMAP and GPCP remained small over tropical and subtropical oceans.   Over extratropical oceans significant differences have been found.   These were caused by the additional use of MSU data (Spencer, 1993) and the Outgoing Longwave Radiation (OLR) based Precipitation Index (OPI) (Xie and Arkin, 1998).

D.  PURE MICROWAVE-DERIVED PRODUCTS

In addition to the merged datasets described above,  some of the microwave algorithms established for the SSM/I have also been used to derive global precipitation climatologies. Two of these are the Ferraro *et al.* (1994) and the Bauer and Schlüssel (1993) algorithms. Those datasets have a higher spatial and temporal resolution,  typically 1˚ x 1˚ in latitude and longitude and one to five days.   An obvious deficiency of these datasets is that they were constructed from data from only one SSM/I at a time;  this enhanced the sampling error significantly.    The sampling error could be strongly reduced if all available SSM/I measurements were to be used (at least two sensors have been in space simultaneously since 1992).

For the construction of freshwater flux fields (like HOAPS) from SSM/I data it might be essential to use SSM/I only algorithms since it is important that the precipitation is not sampled in a different manner than the evaporation.

*10.9.4  Intercomparison projects*

A.  INTRODUCTION

The following conclusions from the recent intercomparison projects on rainfall measurements from space are mostly adapted from two important papers by Ebert and Manton (1998) and Smith *et al.* (1998) that gave a comprehensive overview of the results of the AIP-3 and PIP-2 projects.   The AIP and PIP projects had the common objective of improving satellite algorithms.  The goal of the AIP projects was to validate different satellite algorithms against ground based gauges and radar estimates,  which were treated as truth in terms of bias and rms error.    The underlying idea was to calibrate satellite algorithms with ground based measurements and merge them together as was done in the GPCP dataset described above. Thus the AIP's were focussed on regional areas with different atmospheric conditions.   AIP-1 was conducted over Japan and surrounding waters using data from June to August 1989,  AIP-2 was located over the British Isles and surrounding waters using data during February to April, 1991.   AIP-3 attracted the largest number of algorithms (57) for a comparison over the radar covered area of the TOGA COARE experiment domain during November 1992 - February 1993.   The philosophy of the PIP's was quite different from the AIP's since they rejected the notion that ground data are representative enough to serve as a final calibration standard (Smith *et al.*, 1998).    The PIP's were directed at establishing a passive microwave algorithm that incorporated the best features of all existing algorithms.   While PIP-1 and PIP-3 were focussed on monthly rain accumulations over global grids,  PIP-2 was dedicated to instantaneous rain rate estimates.  The aim was to understand the systematic differences between the algorithms, when applied to globally distributed test cases,  rather than to use the differences from ground based measurements as an indication of the uncertainty.

Results from all these intercomparison studies are now in the literature with the exception of PIP-3.  AIP-1 results are described in Arkin and Xie (1994),  and in more detailed in Lee *et al.* (1991).   AIP-2 results are published in Allam *et al.* (1993) and Liberti (1995).  The results of PIP-1 are documented in a special issue of *Remote Sensing Reviews*.   Since AIP-3

(Ebert, 1996; Ebert and Manton, 1998) and PIP-2 (Smith *et al.*1998) contain the newest findings their conclusions are summarised below.

B.  AIP-3 CONCLUSIONS

Comparisons of satellite algorithms using GMS VIS/IR, AVHRR, and SSM/I data (on instantaneous and monthly time scales) to Doppler radar data (sampled every 10 minutes and mapped to a 0.5˚ grid) revealed that:

❍     Over the whole TOGA COARE experiment the median value of the ratio of satellite estimated to radar-derived rain rates was 1.3,  with considerable variations for single phases of the experiment.  No categorical differences in bias between algorithms were found.

❍     Infrared, visible/infrared, and mixed infrared/microwave algorithms exhibited slightly higher correlations at monthly time scales than did estimates based on AVHRR or SSM/I alone.   But the difference in correlation was too small to be statistically significant due to the small number of quasi-monthly samples.

❍     On an instantaneous time scale,  the SSM/I algorithms outperformed all other algorithms having a statistically significant, higher correlation to the radar data.  The success of the SSM/I algorithms was related to their ability to distinguish raining from non-raining areas.

❍     The coupled infrared/SSM/I algorithms did not perform better than infrared alone algorithms because for these the best SSM/I algorithms were not used.

❍     Results from NWP models showed similar biases and rms errors as the satellite algorithms but exhibited much lower correlations because they can not resolve the raining and non raining areas.

C.  PIP-2 CONCLUSIONS

PIP-2 examined a number of globally distributed case studies and intercompared the algorithm results in various ways:  to one another,  to algorithm category composites (algorithms were divided in categories by their solution method, channel input, and screening approach),  to the overall algorithm composite,  and to ground-based data.   From this the main conclusions drawn were:

❍     Passive microwave rainfall algorithms applied to SSM/I data performed credibly.  The biases and rms errors found corresponded reasonably to the AIP-3 results.  Nevertheless, it was stated that the differences between algorithms were not larger that the uncertainty in the validation data.   PIP-2 gave evidence that ground-based gauge data from reputable sources were not reliable as a calibration standard for instantaneous rain rates.

❍     The results of the intercomparison were strongly dependent on the algorithms' decision as to where it was raining and where it was not.   This was most important at low rain rates.   Thus algorithm developers were requested to seek a common rain/no rain threshold and a common rain screening method for determining the area of rainfall.   In the future, rain screening should deserve more attention than the conversion of brightness temperatures into rain rates.

❍     Despite the first conclusion it was concluded that,  before a calibration model is developed,  intercomparison projects like AIP and PIP are useful to improve algorithms.

❍     The final,  somewhat contentious,  conclusion stated that the point has been reached where ground validation data are no longer effective in determining the precision of satellite algorithms.   As an alternative validation strategy,  a comprehensive calibration model should be developed consisting of the most complete radiative transfer model together with a detailed microphysical model.

D.  BEST ESTIMATE

In the light of the findings of all the AIP's and PIP's it is difficult to say which climatological dataset might be the best estimate.   All strategies to build long term datasets can be defended on scientific grounds.   However, the user of these datasets must be cautious with regard to the purpose for which the dataset will be used.   For example, it might not be meaningful to use a dataset which contained reanalyses data to verify the reanalyses.   It would be helpful if each dataset were accompanied by error maps giving the size of the systematic and the random errors.   For instance,  products derived from one satellite only,  like the pure passive microwave datasets,  would have an error map that gave an estimation of the sampling error as the most important systematic component.

Another conclusion that can be drawn from the intercomparison projects is that not only should the quality of satellite estimates be improved but also the status of routinely gained surface based measurements.   This is considered important,  despite the PIP-2 conclusions, because the development of a calibration model as suggested by PIP-2 is not easy and will be a long-term project.   A first step in this direction is the attempt to archive high quality ground radar data for comparison with measurements of the TRMM sensors.   With this sensor package a new era of remote sensing of rain has recently begun with infrared, passive and active microwave instruments specially dedicated to measure rain on the same platform. Thus, for the first time,  synergistic algorithms can be developed.

E.  COARE MEASUREMENT RECONCILIATION

As mentioned above (Section 10.9.1B),  serious disagreements between various estimates of rainfall during COARE led to intensive study into the reasons, and reappraisal of instruments and methods.   When all instrumental corrections had been made to the various rainfall methods, the IOP-average disagreement was reduced but still too large. Ciesielski and Johnson (1999; see also Bradley and Weller 1997, p.17; Bradley *et al.* 1997) resolved the situation through analysis of atmospheric heat and moisture budgets.  This technique, described by Yanai *et al.* (1973), makes use of atmospheric soundings of temperature and humidity obtained over space and time, to determine the "apparent heat source" (known as Q1) and the "apparent moisture sink" (Q2) of a volume of the atmosphere.  Being an integral method, it overcomes small-scale variability.  An extensive array of sounding sites was distributed over the COARE domain, within which the budgets for specific regions were determined using the interpolation technique of Nuss and Titley (1994).

Ciesielski and Johnson (1999) determined the IFA-averaged rainfall rate for the IOP to be 8.2 mm/day compared to a radar estimate of 4.8 mm/day (because of compensating effects, correcting the soundings for the humidity bias described in section 6.3.3 increased the budget estimate by only 2.5% to 8.4 mm/day).   However, when their budgets are computed just over the radar area (which covers about one-third of the  IFA) and for the same 101 days that the radar was operational, their rainfall rate is 5.2 mm/day, which is much closer to that of the radar.  For these same 101 days but over the entire IFA, their budget estimate is 7.3 mm/day. These results indicate that (a) the radars were situated in a relatively dry region of the IFA, and (b) the 101-day radar exposure was from a relatively dry period of the IOP.  They serve as a reminder that, for meaningful comparisons of quantities as variable as rainfall, sample regions and periods must be strictly coincident.

## 10.10  River Inflow

River runoff perceptibly lowers the salinity of the ocean.   It might be thought that the consequences on the buoyancy would be very local in comparison to the size of ocean basins. However salinity anomalies of fluvial origin may be advected rather far by ocean currents.   For example, the impact of major rivers like the Amazon, the Congo or the Saint-Laurent on the surface salinity of the Atlantic ocean are perceptible several hundred of kilometres away from the mouth of the rivers (Figure 10.9).   The inflow of freshwater from the rivers is of extreme importance in the global freshwater balance of the ocean.   This balance is the result of the loss

of water by evaporation, the gain of freshwater by precipitation, and coastal river runoff. The contribution of rivers to this balance was estimated at 1.26 Sv (1 Sv=$10^6$ m$^3$/s) by Baumgartner and Reichel (1975), nearly 10% of the contribution of precipitation. Neglecting this contribution would increase the average salinity of the upper Atlantic ocean (first 50 m) by 1.5 psu after 10 years.

Global river runoff data are available from the International Hydrography Program (IHP) which published a Global River Discharge Catalogue (Vorosmarty *et al.*, 1996), and from the Global Runoff Data Centre (GRDC). IHP data available in reports published by UNESCO, are a selection of monthly discharges at 949 stations over six continents (Africa, Asia, North America, South America, Europe and Australia/Oceania). Several stations may exist for the same river, and only 219 stations are listed as corresponding to a direct discharge into an ocean basin. These reports do not include runoff from the Arctic and Antarctic regions. The length of the records from which climatic monthly means can be estimated varies from 1 to 100 years, the average length being 19.3 years. A great disparity exits between continents, Europe and North America presenting the longest records. These data do not include the inflow of freshwater into oceans due to underground water.
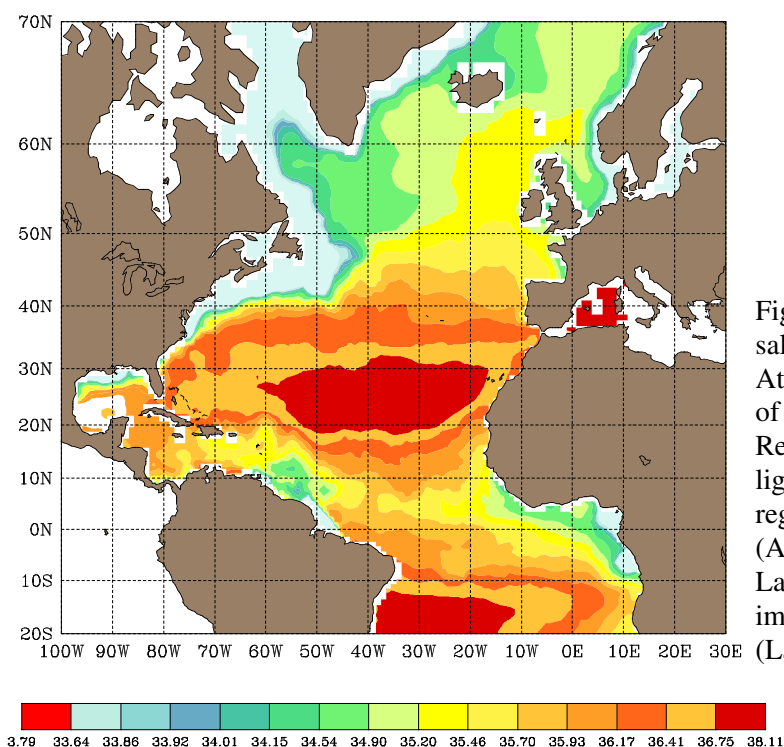


Figure 10.9. Mean sea surface salinity (PSU) in the North Atlantic from the climatic atlas of Reynaud *et al.* (1998). Regions of low salinity are in light grey and correspond to regions near the major rivers (Amazon, Congo, Saint-Laurent) and regions of important sea-ice melt (Labrador Sea).

| | | | | | | | | | | | | | | |
|---|---|---|---|---|---|---|---|---|---|---|---|---|---|---|
| 3.79 | 33.64 | 33.86 | 33.92 | 34.01 | 34.15 | 34.54 | 34.90 | 35.20 | 35.46 | 35.70 | 35.93 | 36.17 | 36.41 | 36.75 | 38.11 |

Using the IHP data set, Boukthir *et al.* (2000) have computed a monthly mean climatology of the direct contribution of rivers to the freshwater flow into the ocean. In their analysis, these authors excluded the contribution of rivers for which flow does not exceed 800 m$^3$/s for at least one single month in the year, and they also neglected rivers for which no continuous records at least 24 month long were found. Thus their calculation used 145 stations for 109 river mouths. For the major rivers, the discharge computed by Boukthir *et al.* (2000) agreed very well with the analysis of Hagemann and Dümenil (1996) who used data from GRDC for the purpose of model validation. The cumulative runoff for all the rivers considered by Boukthir *et al.* (2000) sums to 0.57 Sv. A previous comparable estimate based on former UNESCO reports published in 1969 is that of Baumgartner and Reichel (1975) who found 0.73 Sv, a value significantly larger, but which includes all rivers for which records were available (even with very small discharge), and also includes the contribution of regions beyond the polar circles which they estimated from other sources. Note that in the analysis of Baumgartner and Reichel (1975), the direct contribution of river discharge accounts for only 60% of the total

freshwater runoff which is 1.26 Sv.   They obtained this latter value from a global hydrological balance calculation and part of the runoff was estimated as a residual.

GRDC data are in the form of daily and monthly discharge data for several thousand stations for more than 2,800 rivers.   However, many stations are far from the mouth of the rivers, and many,  being quite recent,  do not yet have records long enough for climatological estimates.   If one is interested in long time series, GRDC and IHP likely provide, at present, very similar information.

Therefore,  the data set gathering carried out by the IHP and more recently by the GRDC are initiatives that deserve great support.   However a considerable amount of work is still necessary to reach an accurate estimate of the amount of water which reaches the ocean.   In particular, the contribution of underground waters and small streams cannot be measured and has still to be estimated, often as a residual of the global budget.   Furthermore, it is likely that human activities, with increase damming and irrigation,  have significantly reduced the river discharge reaching the ocean in the last twenty years (by 50% for the Nile River for example). It is therefore important to encourage the type of studies which permit synthesis of the information contained in these huge data sets in terms of freshwater flux to the ocean,  and which quantify recent changes.

## 10.11  Sea Ice

*10.11.1  Sea ice amount*
Sea ice concentration and extent data are extracted from satellites routinely.  The first multichannel instrument, SMMR, the Scanning Multichannel Microwave Radiometer, was launched in 1978 on SeaSat and Nimbus 7.  Shortly before the demise of the latter in 1987, a new series was launched: the Special Sensor Microwave/Imager, SMM/I; this series continues flying today (see Section 4.3.2).  A single-channel instrument  the Electronically Scanning Microwave Radiometer, ESMR, flew on Nimbus 5 from 1973 to 1976;  its best application is in defining ice extent.

The multichannel sensor resolution varies between 12 and 150 km,  smaller for higher frequencies.  Data products are produced at 12 and 25 km grid spacings, which are ideal for a large-scale geophysical view.  Coverage is excellent: global except poleward of 84° latitude for SMMR and 87° for SSM/I.  Because the atmosphere is fairly transparent at their frequencies, microwave sensors are "all-weather" providing data in darkness and through clouds.

Over sea ice the microwave signals are usually interpreted as concentrations of all ice and of only multiyear ice.  The 15% concentration contour is usually taken as the ice edge. Estimates of the uncertainties in these quantities vary: ice extent, ±12 km; ice concentration, ±6%, with possible biases of similar magnitude; and multiyear concentration, ±20%, again with biases of similar size.

Data sets are available through the National Snow and Ice Data Center (http://www-nsidc.colorado.edu) for October 1978 to the present, for total, first-year and multiyear ice concentrations.   They are on a 25 x 25 km grid, daily and monthly, for both hemispheres.   The passive microwave record is presented in three atlases: Gloersen *et al.* (1992), Parkinson *et al.* (1987), and Zwally *et al.* (1983).

*10.11.2  Flux-related variables over ice*

Air surface temperature in the Arctic is available from buoys and land stations.   The rms error is 2.5˚C (Rigor *et al.*, 2000).   In the Antarctic, with far fewer observations, the best source is reanalyses, and the rms error of these is likely 3 to 5˚C.

In polar regions, the default source of surface winds is NCEP and ECMWF reanalysis data sets.  The extreme stability of the planetary boundary layer in winter is an important component for an accurate estimation of surface winds,  but stable PBL's are not handled well in these numerical weather prediction models.  Some ice models estimate surface winds from

surface pressure fields and do not treat the varying stability in the planetary boundary layer, producing errors up to 50% in speed and 30 degrees in direction.   In the Arctic surface winds from reanalysis (or operational model) surface pressure and TOVS-Polar Pathfinder drag coefficients and turning angles have errors of ±4 ms$^{-1}$ in speed and ±5 degrees in direction.   In the Antarctic there are no TOVS-Polar Pathfinder products and there are many fewer pressure data than in the Arctic.

Arctic cloud fraction data sets are available individually from TOVS and AVHRR, from the ISCCP project,  and both the NCEP and ECMWF reanalyses.  The intercomparison of radiation data by Rothrock and Zhang (1997) shows quite large discrepancies,  both in the annual cycle and in five-year means, which vary from a low of 44% for NCEP to a high of 70% for ECMWF.   A comparison of TOVS-Polar Pathfinder and AVHRR-derived cloud fractions from the ISCCP project (Schweiger *et al.*, 1999) shows reasonable correlations between TOVS-derived cloud fractions and  surface observations from Russian drifting stations at time scales of greater than 3 days.  Mean monthly cloud fractions from TOVS-Polar Pathfinder for the area north of 80˚ agree within 15% with a climatology based on meteorological surface observations (Hahn *et al.*, 1995).   Arctic cloud fractions from the ISCCP project (D-series) are do not appear to capture properly the annual cycle and actually show lower cloud fractions during summer than during  winter in disagreement with climatologies.

Comparisons of cloud fractions from TOVS-Polar Pathfinder, AVHRR-CASPR, and surface observations (which include standard meteorological reports) as well as a sophisticated cloud lidar/radar system during SHEBA paint a more complicated picture.  Meteorological reports (such as those from the north polar drifting stations) appear to under report clouds by as much as 30% during winter compared with lidar/radar.   Lidar/radar observations also show a better agreement with TOVS- and AVHRR-derived cloud fractions during  winter.   Based on SHEBA data the annual cycle of cloudiness in the Arctic appears much less pronounced than previously thought.

Over the Arctic Ocean, precipitation has been estimated from 1979 to present from TOVS.   The procedure uses TOVS moisture profiles and NCEP reanalysis wind profiles and computes the moisture flux convergence, which equals P-E (precipitation - evaporation) at the surface.  Evaporation, E, is computed independently from TOVS-derived surface winds and vertical moisture gradients, satellite ice concentration data, and different transfer coefficients for the ice-covered portion and the open water portion.   Adding E to P-E gives the precipitation P (Groves, 1999).   Monthly precipitation fields are computed as the sum of net precipitation and evaporation.   These fields are completely independent of any parameterised precipitation processes and can serve as good tests of such parameterisations in models.  Daily fields are available;  monthly data are believed to have an accuracy of about ±1 mm/month.

## 10.12  COADS Monthly Summary Trimmed Groups (MSTG) Variables.

The most extensive collection of the basic individual variables presently available is the Comprehensive Ocean-Atmosphere Data Set (COADS),  which beside the collection of individual observations (known as long marine reports - LMR),  also provides monthly summaries (MSTG) which contain basic monthly statistics, computed by the COADS community (Woodruff *et al.* 1998).  These MSTG data have been widely used by climate researchers and so will be considered here as a special example of the basic variable data sets. The MSTG statistics are available at ftp://ftp.cdc.noaa.gov/Datasets/coads1a.enh (coads1b.enh) for the 1a and 1b releases respectively (see below).

At present,  the available MSTG statistics are based on the very latest update of COADS which was specially reprocessed in support of the NCEP/NCAR Reanalysis project. The time period covered by this new update is from 1950 to 1995 (with extension to 1997 expected in early 2000).   The data set for the period 1980-1995 is known as COADS Release 1a, and MSTG statistics for 1950-1979 belong to COADS Release 1b.   Monthly statistics for 2˚ and 1˚ boxes were computed for SST,  air temperature,  specific humidity,  relative humidity,

scalar wind speed and its north and east components,  sea level pressure and total cloud cover. Additionally, MSTG includes pseudo flux variables computed on the basis of individual observations,  for example products of temperature and humidity differences with scalar wind. These can be used,  together with the fluxes derived from the COADS based climatologies (e.g. da Silva *et al.* 1994, Josey *et al.* 1999),  for pilot studies and comparative assessments. COADS MSTG normally provides, as the basic statistics for each variable,  monthly means, monthly standard deviations, and the number of observations.   Additionally information is available about the mean day of the month, mean coordinates, and the fraction of observations in daylight.   Pre-processing of the individual reports used for computation of the COADS MSTG included different quality control procedures and duplicate checks (Woodruff *et al.* 1998).   Trimming in Releases 1a and 1b was performed using both $4.5\sigma$ and $3.5\sigma$ level limits, which correspond to the so-called "enhanced" and "standard" MSTG products respectively. Use of the $4.5\sigma$ limits is recommended because of the possible impact of trimming procedure based on $3.5\sigma$ limits on some very pronounced anomalies,  in particular those associated with El Niño events (Wolter 1997).

In general, the MSTG products are of use for different multidisciplinary studies dealing with sea-air flux fields.   Of course,  the MSTG products still contain the so-called "known" biases in COADS.   In particular, visual wind speed estimates in MSTG are based on the WMO1100 scale, no corrections for measurement height were applied, and there were no corrections of biases in SST and humidity.   Use of MSTG pseudo-flux products can only partly avoid the averaging effects caused by the "sampling-to-classical" biases in the flux computations (see Section 8.3.4).   Thus, one has to be careful when using MSTG products for climate research and especially for budget studies.   For example,  artifacts in the MSTG winds can lead to very pronounced biases, both climatological and time dependent (Ward 1992, Ward and Hoskins 1996, Isemer 1995, Gulev 1999).   However, the MSTG data also have some important advantages for the climate studies.   First, they are easily available to the flux users from the CDC FTP server.   Second, with respect to the advanced climatologies (da Silva *et al.* 1994, Josey *et al.* 1999) they have better sampling in some very poorly sampled areas, which are nevertheless crucially important from the viewpoint of flux variability.   Indeed, in some regions of the Labrador Sea, GIN Sea, and Southern Ocean, the sampling density in MSTG is several times greater than the sampling density provided by the flux climatologies.   That is because the latter only use reports which contain values for all the basic variables.   However it is not immediately obvious whether biases connected with undersampling (which is the cost of the better variable processing and flux computations) are smaller than those inherent in MSTG. Taking into account that in the future COADS Releases, for instance Release 2,  expected in 2001,  many of variable corrections can be included in the new updates of MSTG, this product will continue to have an important future for climate research.

## 11. EVALUATION OF FLUX PRODUCTS

### 11.1 Introduction

In this Chapter we will attempt to evaluate a number of the flux products. These will include climatologies based on *in situ* data (Section 11.2), in particular the UWM (da Silva *et al.* 1994), SOC (Josey *et al.* 1999) and IfM (Lindau, 2000) climatologies. Satellite based products (Section 11.3) will include an evaluation of the HOAPS (Schulz *et al.* 1997) surface fluxes and a number of radiative flux products of US and Japanese origin. The Residual method (Trenberth and Solomon, 1994), which used top of the atmosphere satellite measurements together with model derived flux divergences, will also be considered in this section. The fluxes from the reanalysis projects will be discussed in Section 11.4 for ERA15 (Gibson *et al.* 1997), GEOS1 (Schubert *et al.* 1995), NCEP1 (Kalnay *et al.* 1996; Kistler *et al.*, 2000), and NCEP2 (Kanamitsu *et al.* 2000). We have not attempted to evaluate operational models, however the situation for these will be summarised in Section 11.5. The state of our knowledge for fluxes over sea ice will be discussed in Section 11.6. Sea State and Waves will be considered in section 11.7. Finally 11.8 will provide an illustration of the difficulty of providing a comparative evaluation of the flux products.

Comparison of the various flux products is not easy. Wherever possible, the comparisons must be done for the same time period, however in some cases the products do not overlap. In particular high quality *in situ* data is only available for limited periods and areas. Variables such as temperature, humidity and winds should be compared at the same height. However only time-mean values are normally available, and it is not possible to accurately convert a 2m mean value to 10m or vice versa. Nevertheless it will be shown that there are differences between the various flux products which are significantly greater than would be introduced by the differences in specification for the variables compared.

### 11.2 Flux Products Based on *in situ* Data

*11.2.1 Introduction*

The differences between the various flux climatologies are due to several factors: whether "sampling" or "classical" flux calculation was used, what wind scale was used to interpret the visually observed winds, what other corrections (if any) were applied to the observations, the formula used for each of the radiative flux components, the formula used for each of the turbulent flux components, and other factors such as the smoothing algorithm, grid scale, and time period of the data set used. Climatologies of the heat fluxes produced prior to 1990 include the North Atlantic flux maps of Bunker (1976) and Isemer and Hasse (1987 and Isemer *et al.* 1989), and the global climatologies of Esbensen and Kushnir (1981), Hsiung (1986), and Oberhuber (1988). More recent climatologies are those of da Silva *et al.* (1994), Josey *et al.* (1999), and Lindau (2000). The characteristics of these various studies is shown in Table 11.2.1.

The characteristics of the selected pre-1990 studies will first be summarised (based on the comparison of sensible and latent heat fluxes by Kent and Taylor, 1995). The post 1990 studies will then be described in more detail before a comparative assessment is presented.

*11.2.2 Pre-1990 flux studies*

A. BUNKER (1976)

Bunker calculated the wind stress and sensible and latent heat fluxes from individual ship reports using transfer coefficients tabulated as a function of air-sea temperature difference and wind speed. These were based on his review of experimental studies between 1957 and 1974. Based on the results from BOMEX (Holland *et al.*, 1972), Bunker increased the transfer coefficients by 10% compared to the experimental values to allow for the difference between merchant ship data and research platforms. This he assumed accounted for the effects of the ship on the local environment as well as the anemometer being generally higher than 10m

height.   He assumed that the transfer coefficient for sensible heat was equal to that for latent heat.   Fluxes were not calculated if all the necessary parameters were not present for a given ship report.  The fluxes were averaged by 10° square, month and year.   Annual and monthly averages for subdivisions of the 10° squares,  called gerrymanders,  were presented.  The number and shape of the gerrymanders depended on the number of observations in the region, with an attempt being made to enclose homogeneous water masses.

Table 11.2.1 - Characteristics of  climatological studies of the air-sea heat fluxes.   The table shows the area and time period covered,  the spatial resolution,  the origin of the sensible and latent heat bulk formula coefficients,  implied Beaufort wind scale,  and whether the fluxes were calculated from the individual samples ("yes") or the means of the observations ("no").  IH87 calculated their flux values using mean values but then applied a correction.

| Study | Area Period | Grid Scale | Short Wave | Long Wave | Sens/Lat Ht | Wind scale | Sample |
|---|---|---|---|---|---|---|---|
| Bunker 1976 | N Atl. 41-72 | 1°x 1°(coast) 2°x 5° (ocean) | Budyko 1963 | Budyko 1963 | Bunker | WMO 1100 | yes |
| Esbensen & Kushnir 1981 | Globe 46-79 | 4° x 5 ° | Budyko 1963 | Berliand & Berliand1952 | Liu *et al.* 1979 | WMO 1100 | no |
| Hsiung 1986 | Globe 46-79 | 5 °x 5 ° | Reed type | Budyko 1963 | Bunker | WMO 1100 | no |
| Isemer & Hasse 1987 (IH87) | N Atl. 41-72 | 1°x 1° | Reed 1977 | Budyko 1974 | Bunker (modified) | Kaufeld 1981 | no + adj. |
| Oberhuber 1988 | Globe 50-79 | 2° x 2 ° | Zillman '72 / Reed | Berliand & Berliand 1952 | Large & Pond '82 (modified) | WMO 1100 | no |
| da Silva *et al.* (1994) | Globe 45-89 | 1° x 1 ° | Reed type | Rosati & Miyakoda 88 | Large & Pond 1982 | da Silva *et al.* 1995 | yes |
| Josey *et al.* (1999) | Globe 80-93 | 1° x 1 ° | Reed 1977 | Clark  1974 | Smith 1988 | Lindau 1995a | yes |
| Lindau (2000) | N.Atl. 40-79 | 1° x 1 ° | Malevskii et al. 1992 | Bignami *et al.* 1995 | Isemer & Hasse 1987 | Lindau 1995a | yes |

B.  ESBENSEN AND KUSHNIR (1981)

        Esbensen and Kushnir used 5° x 5° monthly mean climatological parameters.   These values were transformed onto a 4° latitude by 5° longitude grid using a Gaussian space averaging technique designed to uniformly suppress features with wavelengths shorter than about 1600 km.   The data are therefore both presented on a large scale grid and also have very large spatial filtering applied.   Additional smoothing was applied in low data density areas. The fluxes were calculated with the skin temperature version of the Liu *et al.* (1979) transfer coefficients (Section 7.3.2) although the observed bulk temperature of the ocean surface was used.   This increased the calculated fluxes slightly.  For the North Atlantic, Kent and Taylor (1995) estimated an increase of 3Wm$^{-2}$  and 7Wm$^{-2}$  for sensible and latent flux respectively.

C.  HSIUNG (1986)

        Hsiung produced a 5° x 5° global flux product using the Bunker transfer coefficients applied to monthly means of the basic meteorological variables.   Bunker had stated that his coefficients were determined from data averaged over short time periods and should not be used with monthly means of the bulk variables. However Hsiung justified her choice by summarising studies which compared the "classical" and "sampling" methods (see Section 8.3.4).

D.  ISEMER AND HASSE (1985, 1987)

        The atlas of Isemer and Hasse (1987) contains two distinct sets of flux maps,  those calculated using Bunkers original parameterisations (see above),  and also fluxes calculated

using revised parameterisations which had been adjusted using an inverse technique based on a heat budget study.   Isemer and Hasse used the monthly mean averages of the basic variables (Isemer & Hasse, 1985) for each of the gerrymanders as calculated by Bunker (1976).  They attempted to update the parameterisations used by Bunker in several ways.  To account for more recent open ocean determinations of the transfer coefficients,  they reduced that for sensible heat by 17% and latent heat by 13%.  They used an approximate conversion to the Kaufeld (1981) wind scale.  Although applied to the mean values,  the correction was weighted according to the frequency distribution of wind speeds as calculated by Bunker.   Thus they assumed that,  for the period up to 1972 used by Bunker,  all wind speeds were visual estimates.  Stability effects were calculated using virtual temperature, rather than temperature, resulting in a more unstable density stratification and larger fluxes particularly in moist areas such as the tropics.

The Isemer and Hasse study therefore has fluxes calculated using the 'classical' method but with corrections applied in order to approximate fluxes calculated using the 'sampling' method.   To attempt to correct their flux values for any errors so introduced,  Isemer and Hasse adjusted their calculated fluxes for each gerrymander by the ratio of [(Bunkers original results) / (fluxes calculated using the monthly mean values with Bunkers original parameterisations)].

The second set of flux maps presented by Isemer and Hasse (1987) were adjusted  using inverse analysis with the oceanographic constraint of 1 PW of heat transport across 25°N (Hall and Bryden, 1982).   The parameters included in the inverse analysis were the atmospheric transmission factor and cloud cover coefficient for short-wave radiation,   cloud cover exponent in the infrared formula, the transfer coefficients, and the air-sea differences in temperature and dewpoint.   The uncertainties in the variables were estimated and the additional constraint applied that the sum of the changes in the variables normalised by the estimated uncertainty of each variable was an rms minimum.   The adjustments added just over 16 Wm$^{-2}$  to the net heat flux.   The main changes were due to a increase of 5.7% in $C_E$  ($C_H$ by 4.4%)  and an addition of -0.07°C to the air-sea and dewpoint-sea temperature differences.    Isemer *et al.* (1989) confirmed these changes using a selection of different constraints.

### E.  OBERHUBER (1988)

Oberhuber used the COADS data set of filtered monthly means of hourly values averaged onto a 2° x 2° grid as prepared by Wright (1988).   Although he stated that the transfer coefficients used were from Large and Pond (1982),  it would appear that this only applied to the corrections to neutral stability.  The neutral transfer coefficients were calculated using the Charnock (1955) relationship (see Section 7.3.2) with the Charnock parameter taken initially as 0.0064.  However he found that he needed approximately another 20Wm$^{-2}$  heat loss from the ocean to agree with estimates of the meridional heat transport.  He therefore increased the Charnock parameter to 0.032.   He suggested that this was necessary to allow for the use of mean,  rather than instantaneous values,  in the bulk formulae, in other words, to correct for his use of the "classical method".  However,  this seems unlikely to be the case (Section 8.3.4). The transfer coefficients for sensible and latent heat were calculated assuming constant roughness lengths for temperature and humidity.   Since the Charnock formula predicts that $z_o$ increases with wind speed,  this implies that all the transfer coefficients increase with wind speed.   Oberhuber (1988) also used a constant albedo of 0.06 rather than the varying albedo used in other studies.

### F.  OTHER CLIMATOLOGIES

<u>Hellerman</u> and <u>Rosenstein</u> (1983)

This wind stress climatology is still in widespread use for forcing models or comparing wind stress products. However the drag coefficient used was essentially that of Bunker (1976) which resulted in wind stress values some 20 to 30% higher than those computed by, for example, Harrison (1989) using the more realistic Large and Pond (1982) coefficients (see Section 11.2.6F). Josey *et al.* (2000) found a similar difference in comparison to the SOC climatology (Josey *et al.* 1999) except at high latitudes where differences were ascribed to the different periods of the climatologies.  In contrast, Böning et al. (1991) found that differences

from the Isemer & Hasse (1987) climatology were dominated by the visual wind correction used by the latter authors.

Hastenrath and Lamb (1977, 1978, 1979)

Hastenrath and Lamb (1977) produced a climatic atlas of the Tropical Atlantic and Eastern Pacific Oceans which was the basis of the heat budget study of Hastenrath and Lamb (1978).  Similarly a  climatic atlas of the Indian Ocean was used for the heat budget study of Hastenrath and Lamb, (1980).  Hastenrath (1980) considered the heat budget of the tropical oceans more generally.  These studies have not been discussed in detail here since they were limited to the tropical ocean,  a region for which significantly more data has become available in recent years.

*11.2.3  UWM/COADS*

A. INTRODUCTION

The UWM/COADS climatology (da Silva et al. 1994 - http://www.cdc.noaa.gov /coads/uwm.shtml.) was the result of a collaboration between researchers at the Department of Geosciences of the University of Wisconsin--Milwaukee (UWM) and the Ocean Climate Laboratory (OCL) at the National Oceanographic Data Center (NODC).   The aim was to extend the COADS data set to include "true" flux values in addition to the "pseudo" flux values contained in the COADS monthly means.  Objective, global analyses of observed and derived surface marine parameters were based on individual observations found in the Comprehensive Ocean-Atmosphere Data Set (COADS) Release 1 complemented by an interim release for the 1980's.  Results of the analyses are presented in Atlas of Surface Marine Data 1994, a five volume series depicting 45-year seasonal climatologies (1945 - 89), anomalies, and standard deviations of various quantities which characterise the surface marine climate (da Silva 1994). In-depth documentation of the data set is found in Volume 1.   Besides describing all parameterisations, calculations, and analysis methods used in creating the data set, this volume discusses possible biases the COADS data may contain and explains the bias corrections employed.   Also discussed are the constraining of heat and fresh water fluxes by oceanographic transport estimates (see below), sampling and fair weather biases, surface layer formulation, equations for astronomical calculations (e.g., altitude of the sun), and NetCDF data access software.  Volumes 2 through 5 represent a graphical representation of the data set.   These consist mainly of seasonal contour plots of climatology, standard deviation, and anomalies of the analysed quantities organised according to parameter type.  Volume 2 contains directly observed quantities, Volume 3 contains heat and momentum fluxes.  Fresh water fluxes can be found in Volume 4, and Volume 5 has an assortment of miscellaneous derived quantities.  The more recent Volume 6 contains the Heat Flux Sensivity to Sea Surface Temperature.

B. DERIVATION

The analyses presented in the Atlas of Surface Marine Data 1994 were derived from the individual observations found in Compressed Marine Reports--Product 5 (CMR-5) of COADS Release 1 (Slutz *et al.* 1985, Woodruff *et al.* 1987)  for years 1945 through 1989.  The transfer coefficients used were from Large and Pond (1981,1982) except that $C_{D10n}$ was modified for wind speeds below 3 ms$^{-1}$ following Trenberth *et al.* (1989).  The visual winds were adjusted as discussed by da Silva *et al.* (1995).   Following Hahn *et al.* (1995),  cloudiness observations were rejected if they were made under dark sky conditions (calculated from the phase and altitude of the moon and the altitude of the sun).   Present weather observations were adjusted for an error in the version of COADS used by da Silva *et al.* (1994) so that clear weather observations were not assumed to be missing.  No other corrections were made to the data for observational errors.   Precipitation estimates are based on Present Weather reports using the algorithm of Tucker (1961) with a variant of Dorman and Bourke's (1978) corrections.

Mean climatological fluxes were calculated by averaging the 45 years of COADS data into 1˚ x 1˚ grid cells and then applying the successive correction technique described by Levitus (1982) (Section 8.5.2) with radii of influence equal to 1541 km, 1211 km, 881 km, and 771 km on successive passes.  Below 40˚S only the first two passes were used.   By calculating

a complete array of atmospheric forcing parameters, and by using the same grid and analysis scheme as in Conkright *et al.* (1994) and Levitus *et al.* (1994), the UWM/COADS data set was intended to be used as a complement to the surface and subsurface marine analyses found in Conkright *et al.* (1994) and Levitus *et al.* (1994a,b,c).

C. FLUX TUNING

da Silva *et al.* (1994) found that their fluxes indicated a global imbalance of about 30 Wm$^{-2}$ . For the period 1981 to 1992, White (2000) found the smaller imbalance of 23 Wm$^{-2}$; the difference may have been partly due to different methods of taking ice covered regions into account. Whereas the individual flux components, evaporation and precipitation provided in UWM/COADS were not tuned or constrained, the net heat flux, buoyancy flux, and (E-P) fields were presented, with the requirement that there should be no net, global heat transport through 65°S and that the equivalent freshwater transport should be 0.06 Sv. The main factors were about a 10% decrease of SW radiation and a 14% increase in latent heat flux. To balance the freshwater budget, precipitation was increased by about 12%. However da Silva *et al.* (1994) stressed that these values were only an example and that it was to be expected that other users would need to apply different constraints. To that end sensitivity fields associated with each of the tuning parameters were presented. Thus users may specify their own values for the error estimates for the observed quantities and hence calculate new fields of constrained fluxes.

D. VERIFICATION

The UWM/COADS flux fields have been compared to other climatologies (see for example 11.2.4E) and have been extensively compared with results from models, both reanalysis (see Section 11.4) and operational.

*11.2.4 SOC*

A. CONCEPT

The Southampton Oceanography Centre (SOC) flux climatology (Josey *et al.* 1999 - http://www.soc.soton.ac.uk/JRD/MET/fluxclimatology.html ) was based on the methods used by Kent and Taylor (1995) for the "best estimated fluxes" which they used to compare previous North Atlantic flux fields. The idea was that, if the observations could be corrected for systematic error, then the correct flux values would be calculated using the best estimates of the transfer coefficients derived from air-sea interaction experiments without any adjustment of those coefficients. The error correction was based on the results of the VSOP-NA experiment which identified relative biases due to different instrumentation types (see Section 8.3.3). In order to apply the VSOP-NA corrections, additional information was needed. This was obtained from the International List of Selected, Supplementary and Auxiliary Ships ("WMO 47", e.g. WMO, 1990) which is published regularly by the World Meteorological Organisation (WMO). The details of the instrumentation carried on most of the 7000 plus Voluntary Observing Ships include the method of SST, air temperature and humidity measurement, and whether the ship carried an anemometer and, if so, the anemometer height. These meta-data were merged onto the COADS release 1A data set using the ship's call sign on a report by report basis. The success rate in matching the COADS and WMO47 data increased with time as the information contained in WMO47 became more comprehensive (Figure 11.2.1). Because many ship reports from years earlier than 1980 have not been archived with valid call signs, this method limited the range of years for which the SOC climatology could be calculated.

The observations were corrected for biases in SST data from engine room intake thermometers, in daytime air temperatures errors due to solar heating, and in dew point temperatures from fixed thermometer screens. In addition measured winds were corrected for the anemometer height taking into account the atmospheric stability. Visual winds were adjusted to the Lindau (1995a) scale. The impact of the various data corrections on the calculated net ocean to atmosphere heat flux varied from area to area and season to season being generally being within the range ±15 Wm$^{-2}$. Fluxes were decreased in the northern oceans in winter (mainly due to the wind and sea temperature corrections) and increased in the tropical oceans (mainly due to the temperature and humidity corrections (Josey *et al.*, 1999). These

corrections for ship observation error were smaller than might have been expected, partly because some flux errors cancel.
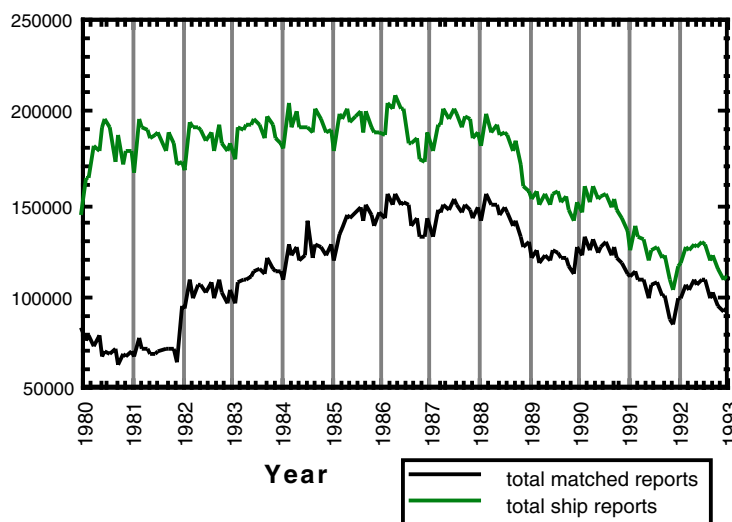


Figure 11.2.1 A time series of the number of reports used in the SOC climatology for which matching WMO47 data was available. The top (grey) line shows the monthly number of reports from ships. The lower line shows the number of these ship reports matched (adapted from Taylor *et al.* 1999f).

### B. VERIFICATION OF HEAT FLUXES

Despite these corrections, the SOC climatology was similar to other studies in that it showed a net heat flux into the ocean of about 30 $Wm^{-2}$ . On a year to year basis this imbalance was remarkably consistent with a standard deviation of $\pm 7 Wm^{-2}$ (implying a standard error on the 14 year mean imbalance of $< 1 Wm^{-2}$ ). However, based on comparisons with high quality buoy data, Josey *et al.* (1999) did not attempt to correct their fluxes to produce a balanced product. Figure 11.2.2 shows the difference between the SOC and buoy values for the Subduction experiment (Moyer and Weller, 1997), FASINEX (Weller *et al.* 1995), TOGA COARE (Weller and Anderson 1996) and the Arabian Sea (Weller *et al.* 1998). For the radiative fluxes (Figure 11.2.2a) the comparison varied from site to site, particularly for the SW flux. At a number of sites the SW and LW differences were of opposite sign as might be expected if the cloud amount was in error. Site to site variation also occurred for the turbulent fluxes (Figure 11.2.2b). The largest difference was for FASINEX where the climatology underestimated the total turbulent cooling by about 50 $Wm^{-2}$ due to the sea being colder, and the atmosphere moister, in the SOC climatology compared to the buoys. For the net heat flux (Figure 11.2.2c), adjusting the fluxes to achieve a global heat balance (following da Silva *et al.* 1994) did not generally improve the agreement with the buoy values. Furthermore the two sites where significant improvement occurred were characterised by significantly different biases. For FASINEX the improvement was due to increasing the SOC latent heat flux (by 13%) whereas for TOGA this worsened the turbulent flux comparison. At that site the improvement came through reducing the SOC SW heating values (by 8%). Thus Josey *et al.* (1999) argued that regionally varying corrections were required, a conclusion which was supported by comparisons with flux values derived from ocean heat transport data.

### C. TROPICAL HEAT FLUXES

The comparisons with the TOGA COARE buoy were considered in more detail by Taylor *et al.* (1999e). The SOC climatological fluxes predicted about 23 $Wm^{-2}$ greater net heat flux into the ocean compared to the buoy. For the specific months of the buoy deployment, the SOC values over estimated the shortwave heating by about 24 $Wm^{-2}$ and under estimated the longwave cooling by about 8 $Wm^{-2}$, thus causing the over estimate of the ocean warming. The shortwave difference could be accounted for if the cloudiness had been under-estimated by about 1 octa (true value 6.2 octas). In contrast, the SOC turbulent flux values slightly over estimated the magnitude of the turbulent fluxes (by about 8 $Wm^{-2}$ ). This was surprising; it was expected that the sensible and latent heat fluxes would be under estimated in the SOC climatology under the low wind conditions of the TOGA-COARE area, since constant transfer

coefficients for sensible and latent heat were used, the Smith 1980 drag coefficient ($C_{D10n}$) was (unjustifiably) extrapolated to zero ms$^{-1}$, the merchant ship data were unlikely to have detected any diurnal warm layer, and no gustiness factor was implemented.

(a)



(b)



(c)
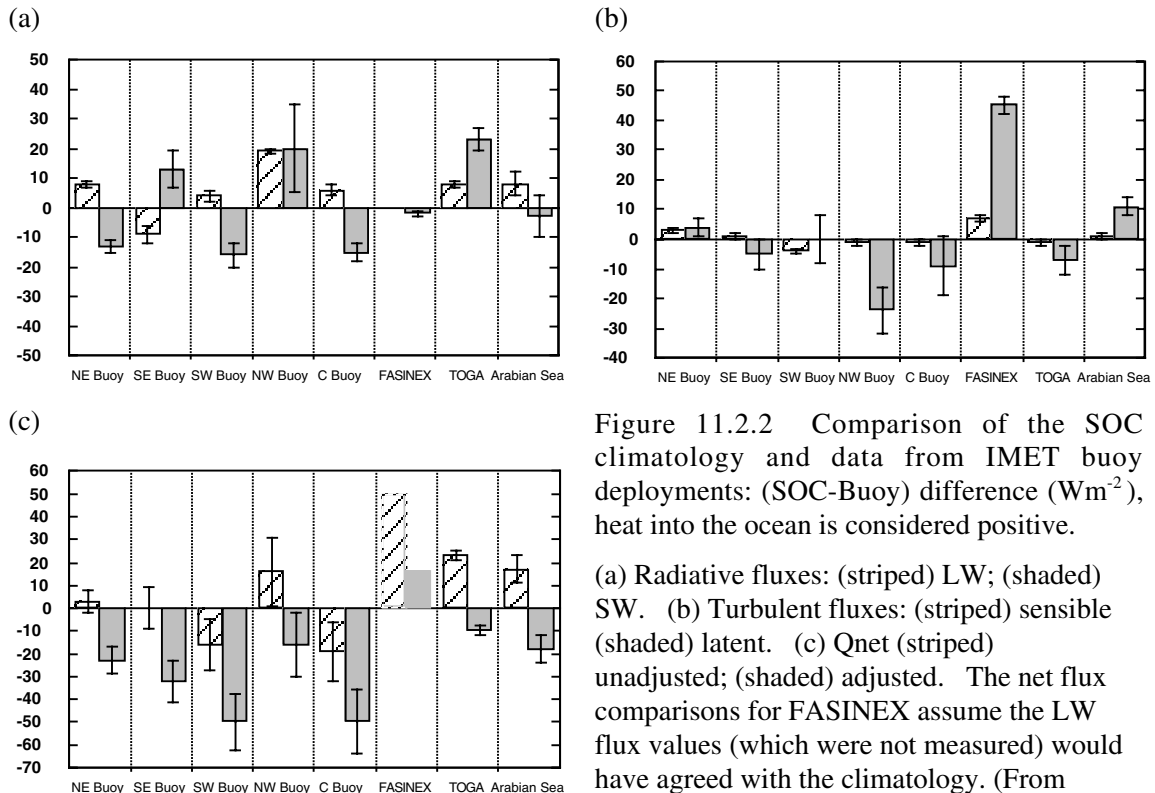


Figure 11.2.2   Comparison of the SOC climatology and data from IMET buoy deployments: (SOC-Buoy) difference (Wm$^{-2}$), heat into the ocean is considered positive.

(a) Radiative fluxes: (striped) LW; (shaded) SW.   (b) Turbulent fluxes: (striped) sensible (shaded) latent.   (c) Qnet (striped) unadjusted; (shaded) adjusted.   The net flux comparisons for FASINEX assume the LW flux values (which were not measured) would have agreed with the climatology. (From Josey *et al.* 1999).

Taylor *et al.* (1999e) showed that the over estimate of the turbulent fluxes was, in fact, due to the extrapolation of the Smith (1980) formulae for $C_{D10n}$. Using a $C_{D10n}$ formula with increased drag at low wind speeds (Yelland and Taylor,1996) reduced the calculated flux significantly. The reason was that the original $C_{D10n}$ formula had resulted in small values for the friction velocity at low wind speeds, very unstable values for the stability parameter ($z/L$), and therefore large values for $C_E$ . The use of a larger $C_{D10n}$ gave less unstable conditions and therefore smaller transfer coefficients for sensible and latent heat. These effects were only significant below about 5ms$^{-1}$ and therefore would not be not important for much of the world's ocean. Bearing in mind that the behaviour of $C_{D10n}$ at low wind speeds is not well known (Section 7.3.2), this example serves to emphasise just how difficult it is to obtain reliable flux estimates in low wind speed tropical regions using ship data.

No correction for this bias in the TOGA COARE area has been applied in the SOC climatology. While it might be considered at least a partial source of the apparent global heat imbalance, it is not clear whether the problem is confined to the highly convective regions of the west Pacific warm pool and the relatively narrow ITCZ, of whether it is applicable to the tropical ocean in general.

D. VERIFICATION OF WIND STRESS

Josey *et al.* (2000) have verified the SOC wind stress climatology against the IMET buoy deployments. A comparison of the mean wind stress components for each buoy deployment is shown in Figure 11.2.3. The wind stresses were generally in good agreement. The only consistent difference was for the Arabian Sea were the SOC stress values were greater than those from the buoy during the latter part of the deployment. Noting that prior to the replacement of the anemometer there had beeen good agreement, Josey et al. (2000) suggested that a poor anemometer calibration might have been the cause. Although higher mean stress

components were observed at the Subduction site compared to the Arabian sea, this was due to the greater consistency of the wind velocity. Good agreement was found at that site.
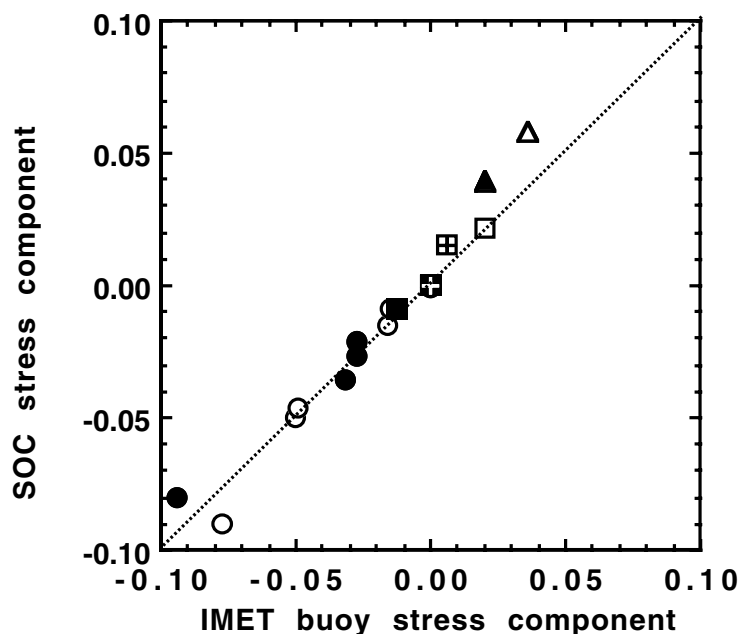


Figure 11.2.3 Comparison of the mean wind stress values between the SOC climatology and the IMET buoy deployments. Open (closed) symbols represent the eastward (northward) component. Circles: Subduction buoys (Moyer and Weller, 1997); Squares: TOGA COARE (Weller and Anderson 1996); Triangles: Arabian Sea (Weller *et al.* 1998); Squares with cross: FASINEX experiment (Weller *et al.* 1995). The line of agreement is shown (data from Josey *et al.* 2000)

E. COMPARISON WITH UWM/COADS

Josey *et al.* (1999) discussed differences between the SOC and unconstrained UWM/COADS climatologies. These may have resulted from the effects of those observational bias corrections included in the SOC analysis but not in UWM/COADS, the use of different parameterisation formulae, the difference in the time periods sampled, and the different scales used in the objective analysis. The main variations were found to occur in the sensible and latent heat flux fields. The radiative flux fields were typically in agreement to within 10 $Wm^{-2}$. The major differences in the latent heat flux occurred over the Gulf Stream and the sub-tropical North Pacific. In UWM/COADS, the Gulf Stream region of strong latent heat loss was broader and appeared to be displaced further south than in the SOC analysis. This resulted in adjacent bands of positive and negative heat flux difference. The narrower region of strong heat loss found in the SOC analysis may have been due to the choice of a smaller objective analysis scale relative to that used for UWM/COADS. Similar behaviour was seen over the Kuroshio although the differences were smaller in magnitude. Over a broad area in the sub-tropical central North Pacific, the UWM/COADS heat loss was stronger by up to 30 $Wm^{-2}$. It is unlikely that this feature was a result of the ship corrections as these only resulted in differences of order 5-10 $Wm^{-2}$ in this region. It may have been due to the different periods used to generate the two climatologies; either because of changes in the instrumentation used by ships in this area , or to an actual climatic change.

Differences between the two climatologies were also seen in the sensible heat flux field for which the UWM/COADS analysis had losses of order 10-20 $Wm^{-2}$ greater in the annual mean over the Gulf Stream and Kuroshio and localised areas of the high latitude North Atlantic and North Pacific. In contrast, the effect of the ship corrections used by Josey *et al.* (1999) was typically less than 5 $Wm^{-2}$. The difference in objective analysis scales may again have been partly responsible. The net heat flux difference field was dominated by the effects of the differences in the latent and sensible heat fluxes. Typically the difference was within ±15 $Wm^{-2}$, although regions of stronger heat loss in the UWM/COADS fields over the Gulf Stream and sub-tropical central North Pacific were up to 50 $Wm^{-2}$. However despite these regional differences the global heat imbalance for the SOC and unconstrained UWM/COADS climatologies were remarkably similar; around 20 to 30 $Wm^{-2}$ excess heat into the ocean.

*11.2.5  IFM*

A.  DERIVATION

The Institut für Meereskunde (IfM) surface fluxes and flux related parameters (Lindau, 2000 - http://www.ifm.uni-kiel.de/me/research/Projekte/WGASF ) were derived from the Comprehensive Ocean Atmosphere Data Set (COADS).   This raw data set contains several million individual ship observations from the world ocean since about 1850.   However the computations were restricted spatially to the Atlantic Ocean and temporally to the period 1940 to 1979, where the best data coverage was available.   This was necessary, since the intention was not so much to describe the longtime climate of the Atlantic but rather to provide data for studies on climate variability.   Consequently, the IfM data set contains not only the mean annual cycle but also the year to year variations of several climate relevant parameters on a nominal spatial grid of 1˚ by 1˚.  To attain such resolution the appropriate statistical treatment of the raw data plays an important role.

Since the observations were concentrated along narrow ship routes a kriging technique was used to obtain completely covered fields.   For this aim correlation lengths depending on the geographical direction were derived for all considered parameters.   Using the information on intra-monthly variance the accuracy of individual monthly means was derived and taken into account in the further calculations.   In contrast to ordinary kriging,  Lindau did not prescribe a fixed radius of influence, but searched by iteration for that combination of grid points which gave the lowest errors at the prediction point.   This minimum was reached when the potential increase of redundancy and error variability was higher than the information gain from any additional grid point.   In that way Lindau produced twin fields: each monthly mean map is accompanied by a map giving an estimation of the error variance.

These pairs of maps show the anomaly and its error not as absolute values, but normalised by the observed standard deviation of the longtime monthly time series at each location.   For the renormalisation, two maps are available for each calendar month and parameter; these give the standard deviation and longtime mean.   Lindau decided to leave the fields in that form (as they were originally computed), because although the kriging technique used is also applicable for the absolute values, it is optimal only for normalised anomalies.

In deriving the IfM fluxes, much effort was spent in correcting the known biases in wind speed, which is an essential parameter not only for the wind stress but also for the turbulent heat fluxes.   Since the majority of marine wind observations in the Atlantic during this period were Beaufort estimates, a correct equivalent scale was of fundamental importance. Wind measurements from Ocean Weather Stations (OWS's) carried out in the 1960's give a good opportunity for calibrating an equivalent scale.   However, there are good reasons for assuming a possible drift in the relationship between the reported Beaufort force and true wind speed since definition of the Beaufort scale and observation practice gradually changed during the times.   Consequently, Lindau used a time-dependent equivalent scale, derived firstly for the 1960's when measurements from OWS's were available, and expanded to other decades by using the spatial pressure differences between the reporting ships (see Section 10.6.2C)

An additional correction was applied to the wind stress calculations, because due to the quadratic dependence of the stress on wind speed, observation errors, even if random, cause a systematic bias (Section 10.6.1).   In addition, COADS temperature measurements of air, sea surface and dew point were compared to the OWS's in the Atlantic and Pacific, in order to remove systematic errors in the turbulent heat fluxes.

B.  MERIDIONAL HEAT TRANSPORT

Considering longterm averages and neglecting decadal changes of the mean ocean temperature, any net heat loss at the sea surface has to be compensated by an oceanic heat transport into this region. These horizontal transports are sufficiently well determined from oceanographic sections to serve as an independent constraint for the computed net air-sea heat

flux. As the Atlantic is laterally enclosed only the meridional heat transport (MHT) contribute to a heat exchange with other oceans. The heat transport across 65°N (where the northern boundary of the Atlantic may be defined) is small. According to Gulev & Tichonov (1989) the net heat loss into the Arctic Ocean is equal to 0.275 PW, whereas Aargaard & Greisman (1975) estimated a smaller value of 0.098 PW. The integration of the net air-sea heat flux from 65°N southward, yields, according to (9.1), the MHT as function of latitude.

Beginning with 0.098 PW at 65°N, Lindau(2000) found a maximum northward heat transport of 1.09 PW at 23°N (fig.11.2.4) while an energy rate of 0.78 PW crossed the equator. Southward of 10°S the MHT remained at a nearly constant northward flow of about 0.5 PW, because the heat budget in this region is approximately balanced. The vertical bars in figure 11.2.4 give the oceanographic estimate of Bryden & Hall (1980) for 25°N, that of Wunsch (1984) for the equator, that of Speer *et al.* (1996) for 11°S and that of Holfort (1994) for 30°S. Since Lindau's results were in good agreement with these independent estimates no additional adjustment of parameterisations was considered necessary.
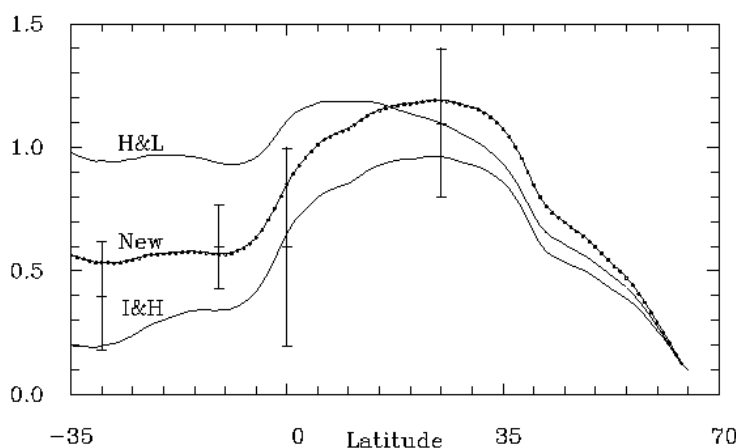


Fig.11.2.4: Atlantic meridional heat transport (PW) compared to the results of I & H: Isemer & Hasse (1987) and H & L: Hastenrath & Lamb (1978). These authors used different data bases. For comparability, their parameterisations have been applied to COADS. Results of oceanographic sections are indicated at the relevant latitude together with their error bars: 30° S: Holfort (1994), 11°S: Speer & al. (1996), 0°: Wunsch (1984), 25°N: Bryden & Hall (1980).

C. GLOBAL PRECIPITATION PRODUCT

For the derivation of the Lindau (2000) precipitation algorithm the weather and humidity observations of 24 years from four light vessels in the German Bight were calibrated against the wind corrected daily rain measurements carried out aboard these ships. In a second step the quality of the resulting rain algorithm was checked by its application on independent COADS data. For monthly means a correlation of 0.85 is obtained, for the climatic annual cycle even one of 0.96.

A comparison with SSM/I derived rain (Ferraro & Marks,1995) showed an acceptable agreement in the global distribution and mean oceanic precipitation for January 1988. Applying this algorithm for the entire period 1980 to 1993, 81% of the world ocean is covered with data and a mean annual precipitation of about 1300 mm results (Figure 11.2.5). Comparison with evaporation shows an imbalance of -298 mm, which can be explained by the water export on the continents and low data coverage of the Southern Ocean where rain prevails.

*11.2.6 Comparative assessment*

A. INTRODUCTION

In this section we will compare the characteristics of the various studies described above in order to determine the strengths and weaknesses of each. As we have already noted, the differences between the various flux climatologies are due to a number of factors: whether "sampling" or "classical" flux calculation was used, what wind scale was used to interpret the visually observed winds, what other corrections (if any) were applied to the observations, the

formula used for each of the radiative flux components, the formula used for each of the turbulent flux components, and other factors such as the smoothing algorithm, grid scale, and time period of the data set used.
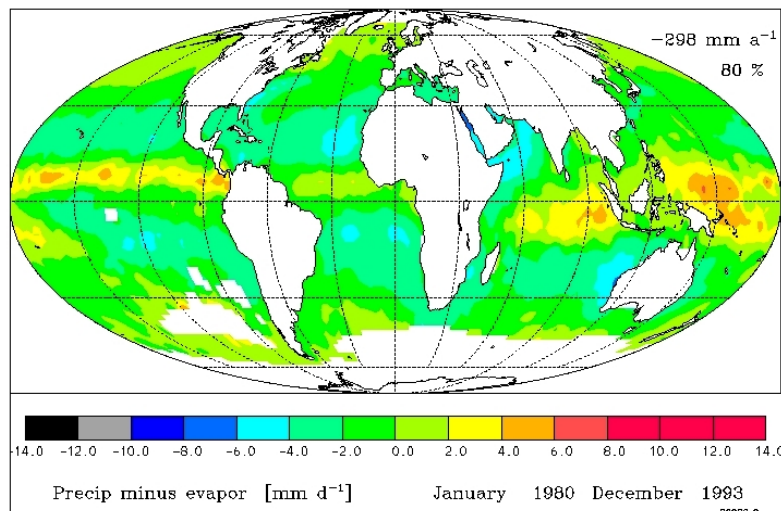


Figure 11.2.5
Precipitation minus evaporation derived by Lindau (2000) for the period 1980 to 1993 from COADS.

### B. "SAMPLING" OR "CLASSICAL"

Apart from the major effort of Bunker (1976) and co-workers, the restricted computing resources available resulted in all the pre-1990 climatologies being calculated from mean values - the "classical" method. Because correlations of the basic variables are neglected, use of the classical formula is likely to have introduced a bias of order ±5% to ±15% which varies from one climatological region to another and even with the flux parameterisation used (Section 8.3.4). Isemer and Hasse (1987) attempted to correct for this on the basis of the Bunker (1976) calculations. Each of the more recent climatologies has been calculated using the "sampling" method. This is to be preferred, at least where observations are plentiful; thus we favour the post-1990 studies. However it should be noted that the sampling method has the disadvantage of requiring all the basic variables needed for flux calculation to be available with each observation. This reduces the number of available data significantly and may increase the noise in many areas. It also makes it more difficult to combine data sets; for example to calculate a flux product based on remotely sensed and *in situ* data. Thus there are cases where climatologies based on the "classical" method still may be preferred.

### C. VISUAL WIND SCALE

The wind scale defined by WMO for visual wind observations is known as "WMO1100" (WMO, 1970). The different variations on this "Beaufort" scale were discussed in Section (10.6.2.C). We emphasise that, not only did Lindau (1995a) devise a scale which produced good agreement between visual and anemometer winds, he also demonstrated that the differences in the older scales were due to the method used in their derivation. Kent and Taylor (1997) confirmed Lindau's results with respect to the VOS. Independently da Silva *et al.* (1974) produced their own version of the Beaufort scale (da Silva *et al.* 1995). Fortunately this scale and that of Lindau (1995a) are not very dissimilar to WMO 1100. Thus the only climatology listed in Table 11.2.1 which used a significantly different Beaufort scale was that of Isemer and Hasse (1987). That study has effectively been replaced by that of Lindau (2000).

### D. OTHER OBSERVATION CORRECTIONS

With the exception of Esbensen and Kushnir (1981), most of the pre-1990 studies used increased transfer coefficients to allow for some degree of observational error assumed to characterise the data sets. This was either done initially (e.g. Bunker, 1974) or after some form of inverse analysis (e.g. Isemer and Hasse, 1987, Oberhuber, 1988). The results of recent investigations into VOS observational errors were too late to be incorporated in the UWM (da Silva *et al.* 1994) study (although they are mentioned in the documentation). The more recent

studies at SOC (Josey *et al.* 1999) and IfM (Lindau, 2000) have applied explicit corrections to the data (see sections 11.2.4, 11.2.5.).   Taking the SOC corrections as an example, the effect on the heat fluxes varied region by region.   In general the heat loss was increased but generally by less than 10 $Wm^{-2}$ .   On a global mean basis the SOC values agreed closely with the unadjusted UWM values to within a few $Wm^{-2}$  in the flux components and the net flux,  a somewhat surprising result.   Compared to the SOC fluxes,  the temperature corrections suggested by Lindau would have increased the ocean cooling,  probably by around 10 $Wm^{-2}$ or less.   The main difference between the SOC and IfM is likely to be due to the different transfer coefficient schemes (see below).

E. RADIATIVE FLUX FORMULAE

For shortwave flux, Bunker (1976) and Esbensen and Kushnir (1981) used the Budyko (1963) shortwave parameterisation.  Dobson and Smith (1988) considered this formula to be questionable. Most other studies have used some variation on the Reed (1977) algorithm which was recommended by the comparative studies of Frouin *et al.*, (1988) and Dobson and Smith (1988).   The latter found a site dependant long term bias of -1 to +12 $Wm^{-2}$  and a monthly mean rms error of about 8 $Wm^{-2}$ .   We should note that,  using comparisons with data from several air-sea interaction experiments,  Katsaros (1990) found this formula to be biased high by about 20 $Wm^{-2}$.   The comparison between SOC and buoy values (Figure 11.2.2) does not support this,  however it may be that the instrumentation is at the limit of its accuracy (Section 5.5.2).   The IfM study (Lindau, 2000)  used the Malevskii *et al.* (1992) algorithm which has been found to be less biased in comparison to the Reed formula,  at least in mid latitudes (Niekamp, 1992).

In a comparative study of algorithms for estimating longwave radiation Katsaros (1990) found little difference between the models compared.   In general the biases were less than 10 $Wm^{-2}$ and the rms scatter was significantly less than for the shortwave parameterisations.   Of those tested,  Josey *et al.* (1997) evaluated two of the better performing algorithms,  that of Clark (1974) which was based on the earlier Berliand and Berliand (1952) formula and that of Bunker (1976) which was based on Efimova (1961).   In comparison against pyrgeometer measurements from several cruises they found that the Clark algorithm performed better and hence chose it for calculating the SOC climatology.   In contrast they found that the Bignami *et al.* (1995) formula underestimated the downward longwave flux by around 25 $Wm^{-2}$ .   This fitted with the Schiano *et al.* (1993) observations in the western Mediterranean that almost all the formulae they tested over estimated the downward LW flux by 25 to 40 $Wm^{-2}$.   It was based on those results that Bignami *et al.* (1995) had developed their algorithm.  Garrett *et al.* (1993) suggested that this greater radiational cooling was needed to balance the heat budget of the Mediterranean and Gilman and Garrett (1994) suggested that the difference was due to the different atmospheric properties over this land locked sea.   Thus the use of the Bignami formula for the IfM LW flux over the Atlantic may not be an appropriate choice.   It will give significantly greater cooling compared to the formulae used for the UWM or SOC studies.   In comparison to the buoy data (Figure 11.2.2a) the SOC values showed too little cooling but only by about 6 $Wm^{-2}$  (standard error $\pm$ 3$Wm^{-2}$ )

F. TURBULENT FLUX FORMULAE

The studies evaluated here all used the "traditional" bulk formulae (Section 7.2) and differences caused by variations in the algorithms are likely to be small compared to those due to different choices of transfer coefficient.   Since latent heat is usually the dominant flux we will discuss here the choice of $C_{E10n}$ and note that the discussion for $C_{H10n}$ would be very similar.

The transfer coefficient for latent heat as used in the different studies is shown in Figure 11.2.6.  There is clearly a significant difference between the relationship assumed by Bunker (1976) and that recommended in the review of Smith (1989) (1.2 $\pm$ 0.1) or the observations of DeCosmo *et al.* (1996)  (1.12 $\pm$ 0.24).   Ignoring any error in the ship data,  at first sight it would appear that the SOC climatology which uses the Smith (1989) value should be more accurate than the IfM climatology which uses the original Isemer and Hasse version of $C_{E10n}$.

However it is interesting to note that most of the coefficients that have been adjusted to satisfy some form of oceanographic constraint (global heat balance or meridional heat transport) have similar values at typical midlatitude wind speeds of about 10 ms$^{-1}$. Thus the Oberhuber (1988), adjusted Isemer and Hasse (1997), and constrained da Silva (1994), all have 1000 x $C_{E10n}$ between 1.3 and 1.4 in that wind speed range. So too does Lindau (2000) whose $C_{E10n}$ values were based on the unadjusted Isemer and Hasse (1997). While such values are high compared to Smith (1989) or DeCosmo *et al.* (1996) they are not outside the range of possibility. At wind speeds higher than about 12 ms$^{-1}$ there is very little data on the behaviour of $C_{E10n}$ with wind speed. DeCosmo *et al.* could not rule out a tendency for $C_{E10n}$ to increase with wind speed and recent determinations of $C_{E10n}$ by Dupuis *et al.* (1999) actually indicated an increase of $C_{E10n}$ with wind speed similar to that assumed by Lindau (2000).

The lower $C_{E10n}$ values used in the SOC climatology were justified by Josey *et al.* (1999) mainly on the grounds that the fluxes calculated were in reasonable agreement with the IMET buoy values. However the IMET fluxes were calculated using the version 2.5 (or earlier) of the TOGA COARE algorithm (Section 7.4.1). That algorithm uses a constant Charnock parameter of 0.011 with the result that the values of $C_{E10n}$ and $C_{H10n}$ tend to <u>decrease</u> with increasing wind speed. Using a Charnock parameter which increases with wind speed as observed (Yelland *et al.* 1998, Hare *et al.* 1999) results in more constant values of $C_{E10n}$ and $C_{H10n}$ (version 2.6 of the TOGA COARE algorithm).
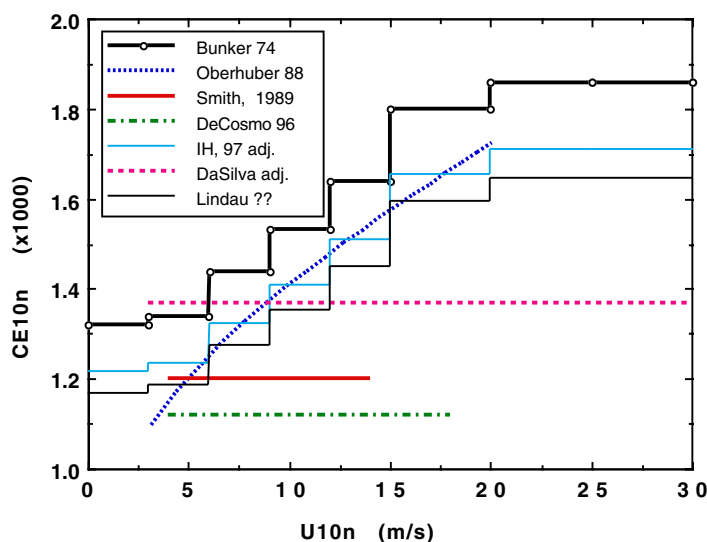


Figure 11.2.6. The transfer coefficient for latent heat as used in different studies plotted as a function of the 10m neutral wind speed.

The conclusion is that, despite all the various air-sea interaction experiments, our knowledge of the magnitude of the transfer coefficients is still by no means adequate. New fast response instruments are beginning to become available for use at sea and their use to determine $C_{E10n}$ and $C_{H10n}$, particularly at wind speeds above 10 ms$^{-1}$, is to be strongly encouraged.

With regard to the drag coefficient, $C_{D10n}$, the present state of our knowledge is somewhat better. One might allow that there is a dispute with regard to the magnitude of $C_{D10n}$ at wind speed above, say 15 ms$^{-1}$ (e.g. Janssen, 1999, 2000; Taylor & Yelland, 2000b), and evidence that swell can alter $C_{D10n}$ at lower wind speeds (say below 5 ms$^{-1}$) (Donelan et al, 1997; Rieder and Smith, 1998). However there is a growing body of evidence for the wind speed range 5 to 15 ms$^{-1}$ that supports the lower $C_{D10n}$ values suggested by the observations of Smith (1980), Large and Pond (1982), and Yelland *et al.* (1998). Thus the higher $C_{D10n}$ values (Figure 11.2.7) used by Hellerman and Rosenstein (1983) or Oberhuber (1988) are not supported by the majority of the observations. It follows that the wind stress values contained in the latter climatologies will be significantly too high for most wind speeds. However, in poorly sampled regions like the Southern Ocean the stresses contained in almost all *in situ* climatologies are believed to be severely underestimated, particularly in winter.
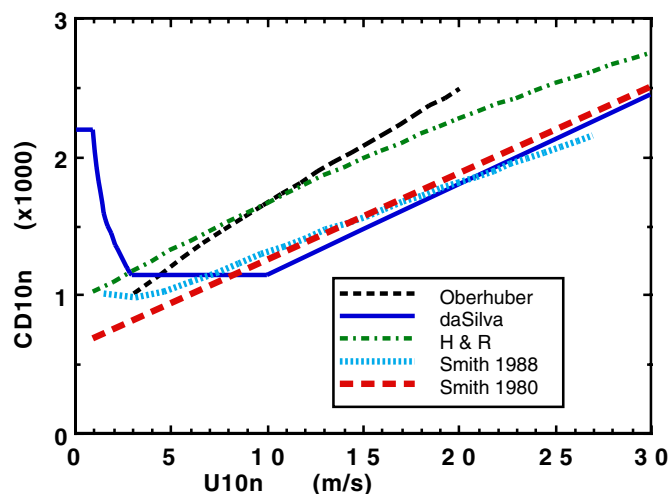
Figure 11.2.7 The drag coefficient $C_{D10n}$ as used in different studies plotted as a function of the 10m neutral wind speed.

G. SMOOTHING ALGORITHM

    The disadvantages of the successive correction technique as used for UWM/COADS and the SOC climatology has been discussed in Section 8.5.2, and the advantages of the kringing method (used for the IFM fluxes) in Section 8.5.3. The disadvantage of kriging is that it is computationally expensive and, at this time, global flux fields have not been computed using this technique. However, with increasing computer power, there is no doubt that future global flux climatologies will be based on improved analysis methods such as kriging, reduced space optimal analysis (Kaplan *et al.* 1997, 1998), or other techniques.

H. CONCLUSION

    Much effort has been invested to ensure that each new release of COADS has a more nearly complete collection of the historical data. For that reason alone, the newer climatologies are to be preferred to those calculated in the past. With regard to the parameterisations used for the heat fluxes one might have hoped to categorically state that the new climatologies are superior to previous studies. However, at present we can only state that we believe that to be the case. For wind stress the case is more definite. There is strong evidence that climatologies such as Hellerman and Rosenstein (1983) or Oberhuber (1988) have over estimated the wind stress in most ocean regions. Thus, for wind stress the newer climatologies are to be preferred. However the poor *in situ* sampling in the southern hemisphere, and particularly in the Southern Ocean, suggests that the lengthening data set of satellite derived wind data is a promising alternative.

    Of the recent global *in situ* climatologies it is hard to choose between the UWM/COADS and SOC products. The SOC product has been found to be in marginally better agreement with buoy measurements than the <u>unconstrained</u> UWM/COADS product (e.g. Weller *et al.* 1998). Thus the SOC fluxes may be preferred for regional studies. However if global net heat flux must be in balance (e.g. for forcing models) then the <u>constrained</u> UWM/COADS product must be preferred even though comparisons with buoy data are significantly worse for that product (Weller *et al.* 1998, Josey *et al.* 1999). Compared to the SOC climatology the UWM/COADS covers a significantly longer period. Extension of the SOC fields back in time is hindered by the lack of metadata for applying the ship corrections. However, perhaps the greatest strength of the UWM/COADS climatology is the provision of sensitivity fields so that users can apply their own error estimates and oceanographic constraints. It is recommended that more use be made of that facility.

    For the Atlantic Ocean, the IFM product has the advantage of a good mapping technique, good error estimates, and providing a realistic meridional heat transport. While the latter has been attained through the use of radiation parameterisations and transfer coefficients which have allowed balanced budgets to be obtained for the Baltic and Mediterranean Seas, these are not, at present, the generally accepted choices for open ocean

regions.  This is the newest product and further verification is desirable and doubtless will be forthcoming.

Finally we emphasise again that there is still a need for many more measurements of the transfer coefficients,  particularly in open ocean moderate to high wind conditions. Whenever possible such determinations should be made using both the eddy correlation and the inertial dissipation methods.   Both methods are likely to have systematic errors when used on ships.  However the nature of those errors is different for the two techniques.  A large data set of consistent transfer coefficient estimates obtained using the two methods by several research groups working from various ships would give confidence that the systematic errors had properly been accounted for.

## 11.3  Flux Products Based on Satellite Data

### 11.3.1  Introduction

The next section will evaluate a recent satellite based flux product, HOAPS,  which represents one of the first attempts to use satellite data to produce fields of all the surface fluxes except SW radiation.   Satellite radiation products will be discussed separately in Section 11.3.3 amd 11.3.4 for US and Japanese products respectively.   Finally Section 11.3.5 will briefly consider fluxes produced using the Residual Method, a combination of satellite measurements and model calculations.

For development of flux climatologies from satellite data the consistency of data over time is of paramount importance for the flux field producer.   As an example we will consider the SSM/I sensor.   This has been flown on several DMSP platforms (see Section 4.3.3) and has been widely used to construct long time series of flux fields and flux related variables. Differences between the same sensor on different platforms in different orbits can cause differences in zonal monthly averages.   For example,  for wind speed differences of approximately 1 ms$^{-1}$ can occur (Jost *et al.*, 1999).  Colton and Poe (1999) conducted a study of sensor-to-sensor differences for six DMSP platforms starting in 1987 and ending in 1997. Their  paper  summarises  the  prelaunch  and  postlaunch  performances  found  through comprehensive calibration/validation activities.   Besides several sensor-specific components two major results of this study were:

❍     The remarkable stability of the SSM/I sensor provided the opportunity to quantify the incremental brightness temperature differences to which the SSM/I's can be intercalibrated.   The so called "noise floor" has been determined using distribution functions constructed from the brightness temperatures.   The noise floor is estimated to be 0.25-0.35K for the five low-frequency channels and 0.45K for the 85 GHz channels.

❍     The interpretation of sensor to sensor differences based solely on monthly averaged brightness  temperatures is not recommended for multi-year time series but can be sufficient for limited periods because regressions between different SSM/I are relatively stable.

From these results it is suggested that flux producers should focus not only on high accuracy of the retrievals but also on constructing consistent time series of satellite data.

### 11.3.2  Evaluation of HOAPS

A. INTRODUCTION

The **H**amburg **O**cean **A**tmosphere **P**arameters and Fluxes from **S**atellite Data (**HOAPS**)  dataset (Schulz and Jost, 2000) is solely based on the use of infrared and microwave satellite data within retrievals developed with the aid of radiative transfer theory. A time period of 10.5 years (July 1987 - December 1996) is freely available for use by other scientific groups[1], and this will be extended in the future.  It contains the following variables:

---

[1]  from http://sop.dkrz.de/HOAPS

evaporation [mm h$^{-1}$], rain rate [mm h$^{-1}$], *E-P* [mm h$^{-1}$], near surface air humidity [g kg$^{-1}$], 0.98 ∗ specific saturation humidity at sea surface temperature [g kg$^{-1}$], wind speed [m s$^{-1}$], latent heat flux [W m$^{-2}$], sensible heat flux [W m$^{-2}$], and longwave net radiation [W m$^{-2}$]. The following subsections describe the methodology used to derive the fields and give a summary of attempts to verify the product through a comprehensive intercomparison with a range of observation types,  from merchant ship observations to data from high quality IMET buoys.

B.  METHODOLOGY

The evaporation at the sea surface is parameterised using a bulk approach as described in Chapter 6.  The wind speed *u* and the atmospheric specific humidity $q_l$ are determined from SSM/I measurements using the retrieval of Schlüssel and Luthardt (1991) as described in Section 10.6.2 and the method of Schlüssel *et al.* (1995) for $q_l$ as described in Section 10.5.2.

The saturation specific humidity at the sea surface is essentially a function of the sea surface temperature.  Since continuous handling of large data sets like the AVHRR raw data requires large amounts of computer and man power,  it was decided to use the NOAA/NASA Oceans Pathfinder Sea Surface Temperature product (see Table 10.1).  These products are available as daily fields with a spatial resolution of (9 km)$^2$ at best.

Because all the needed variables can not be inverted from the available satellite measurements, some empirical assumptions have to be incorporated into the computations. The most important one is an assumption about the atmospheric stability, needed to compute the transfer coefficient for latent and sensible heat.  For use in the scheme of Smith (1988),  it is assumed that the atmosphere has a relative humidity of 80% at any time and any place. With that assumption the missing air temperature can be computed from the measured $q_l$.  The errors in the transfer coefficient that occur if this assumption is wrong are between 2% at high wind speeds and strong unstable conditions,  and 50% at low wind speeds and strongly stable conditions (Schulz *et al.*, 1997).  Other assumptions concerning the surface pressure or air density are not of great importance.

Measurements of rainfall at the sea surface with radiometers in space have been the topic of many studies in recent years.  In an early stage of the preparation of the climatology it was decided to use the rain algorithm of Bauer and Schlüssel (1993) which delivers an instantaneous rain rate.  This algorithm has been successfully tested within the Precipitation Intercomparison Project (PIP) and the Algorithm Intercomparison Projects (AIP) described in Section 10.9.4.

In addition to the variables needed for computing *E-P* the radiative longwave net flux and the sensible heat flux have been included in the climatology.  The longwave net flux is computed by a scheme described in Schlüssel *et al.* (1995) (see Section 6.4.2) and the sensible heat flux is determined using the air temperature derived under the assumption of 80% relative humidity.

The rain retrieval is applied first because all other retrievals can only be applied in rain free or light rain cases.  If the derived rain rate is below a certain level the other retrievals are applied to instantaneous SSM/I measurements to obtain the basic state variables *u* and $q_l$. Within the bulk approach,  *u* and $q_l$ are combined for each instant whereas the instantaneous *u* has been combined with the mapped weekly averaged $q_S$ computed from the Pathfinder SST. The latter is bilinearly interpolated to the location of the SSM/I pixel.  Weekly averages must be used for  $q_S$ because of the cloud cover problem.  After applying the retrieval algorithms, all the fluxes are computed on this quasi-instantaneous basis using the bulk approach of Smith (1988).

The derived, quasi-instantaneous fluxes are mapped to grids with three different resolutions: 0.5°, 1.0°, and 2.5° .  The time averaging is then performed on the maps and the fields are stored as daily, pentad, monthly, yearly, and climatological fields.

C. LIMITATIONS

Obviously, the present satellite-derived climatology has limitations just as any climatology has. Since large parts of the climatology are based on measurements from only one SSM/I at a time, a serious sampling error can be expected, particularly for precipitation. A case study with data obtained during the TOGA COARE campaign showed that the sampling error for grid resolutions of 2° by 3° and a sampling time of 3 weeks can be as high as 30% if only one satellite overpass per day were available. If data from two SSM/I's were used this error is diminished to less than 4%. So a recomputation of the time series using all the available satellite data is a major task for the future.

Another systematic error that has not yet been fully explored is caused by the use of radiometers on different platforms (AVHRR on NOAA and SSM/I on DMSP). It is expected that this error is rather small because the sea surface temperature obtained from the AVHRR data is a relatively inert quantity compared to the atmospheric variables obtained from SSM/I measurements. But this argument holds only if the measurement of the sea surface temperature is not hampered for weeks by persistent cloudiness or by long periods of darkness over polar regions. For the latter case the sea surface temperature could be biased due to the more difficult cloud detection using infrared data.

Additionally, the climatology is limited by the fact that the river runoff into the ocean is not implemented. The observed monthly averages of runoff for several rivers are available (Dümenil *et al.*, 1993) and there would be in principle no obstacle to use them to check the long term mean of the *E-P* fields.

D. VERIFICATION OF FLUXES

Introduction

The HOAPS data set has been evaluated using a two way validation strategy. As a first step, each retrieval algorithm used has been validated with *in situ* data from different sources such as scientific experiments or data from the GTS. These intercomparisons focussed mostly on the quality of the instantaneous retrievals, with the exception of using a sample of GTS data to compare on a monthly time scale but with very coarse spatial resolution. The second step focused more on comparisons of the gridded HOAPS dataset to long term buoy measurements like the Subduction Experiment (Moyer and Weller, 1997) and on comparisons to global climatologies derived from *in situ* data, namely that of the Southampton Oceanography Centre (SOC - Josey *et al.* 1999) and of the University of Wisconsin-Milwaukee (UWM - da Silva 1994). Some of these intercomparisons using different types of *in situ* data are briefly described below.

Globally distributed comparisons to GTS data

Schulz *et al.* (1997) described intercomparisons of satellite-derived wind speed, near-surface air humidity, and latent heat flux with ship data taken from the GTS during a period from July to September 1987. Table 11.3.1 gives bias and standard deviation between both datasets.

Table 11.3.1 Bias and standard deviation for an intercomparison of satellite-derived wind speed, near-surface air humidity, and latent heat flux with GTS data at two different time scales. N denotes the number of match ups for the instantaneous time scale and the number of 2° x 2° grid boxes at the monthly time scale, respectively.

| Temporal scale | $N$ | $u$ (ms$^{-1}$) | | $q_l$ (gkg$^{-1}$) | | $Q_{lat}$ (Wm$^{-2}$) | |
|---|---|---|---|---|---|---|---|
| | | bias | σ | bias | σ | bias | σ |
| instantaneous | 11108 | 0.2 | 2.1 | 0.06 | 1.6 | 3 | 50 |
| monthly average | 136 | -0.05 | 1.3 | 0.08 | 1.1 | 0.5 | 20 |

The bias of 3 Wm$^{-2}$ in latent heat flux was mostly caused by systematic higher latent heat flux estimates from the satellite south of 40˚S,  where only very few *in situ* observations contribute to the comparison.   All standard deviations must be interpreted with respect to errors in both the satellite retrieval and the ship measurements.   As shown by Wentz (1997) for wind speed the mismatch of the ship point measurement and an instantaneous SSM/I pixel can be the largest component in the error budget.   If we conservatively assume that at least 10% of the obtained standard deviation is caused by the mismatch and distribute the remaining error equally then the accuracy for an instantaneous estimate of latent heat flux is approximately 30 Wm$^{-2}$.   This was a great improvement compared to older techniques like that of Crewell *et al.* (1991) applied to SMMR measurements over the North Atlantic. Although they only derived the near-surface humidity from the satellite,  and took the wind speed and sea-surface temperature from *in situ* measurements,  a much larger standard deviation (73 Wm$^{-2}$ compared to 50 Wm$^{-2}$) was obtained.   So from this intercomparison it can be concluded that the retrieval of low-level water vapour content and the use of AVHRR derived sea surface temperature considerably improved the satellite derived fluxes.

Table 11.3.1 also shows values for the bias and standard deviation for monthly averages of $u$, $q_l$, and latent heat flux $<Q_{lat}>$. The numbers in the table were gained from a comparison on a grid with a 2˚ x 2˚ resolution.   Such a coarse resolution was necessary because the ship measurements were widely scattered over the ocean.   Another limiting condition was that to obtain a representative monthly mean each grid box must be covered with *in situ* measurements on at least 25 observation days.   As a result of this the number of boxes was decreased to only 136, which indicates that all the numbers should be interpreted carefully.   To estimate the error of the satellite-derived latent heat flux Schulz *et al.* (1997) computed the noise of the ship data for the 136 bins by randomly dividing the *in situ* data in each bin in two subsets and taking the standard deviation between the subsets as noise. Applying this procedure the error of the satellite-derived flux has been estimated to be ~15 Wm$^{-2}$.   This error estimate fits very well in the upper and lower bound error estimation of Chou *et al.* (1995b) and is slightly higher than that stated by Schlüssel *et al.* (1995).   The larger error could be caused by the fact that many of the grid boxes are located in coastal areas where $q_l$ (which contributes most to the error in $<Q_{lat}>$) is much sensitive to the land-ocean contrast (Liu *et al.*, 1992).   However compared to earlier attempts to derive $<Q_{lat}>$ from satellite data this was an significant improvement because phenomena such as physically unrealistic downward fluxes in the mid- and high-latitude North Pacific and North Atlantic Oceans during summer were eliminated.   Such problems were found by Esbensen *et al.* (1993) who compared COADS data with satellite data obtained using Liu's (1986) method.

Comparisons to weather ship data

Schulz *et al.* (1997) also compared HOAPS to data from the weathership M for a one year (August 1987 - August 1988) time series using the "instantaneous" values. The aim was to check that the retrieval schemes for wind speed, air humidity, and sea surface temperature worked well over the seasonal cycle.   The results of this comparison showed two major things.   Firstly,  most differences between the *in situ* and satellite-derived quantities were much smaller than in the comparison with unfiltered GTS data.   For both wind speed and air humidity,  no bias and standard deviations of 2.0 ms$^{-1}$ and 0.97 gkg$^{-1}$ respectively were obtained for the whole time series.   Whereas the deviation for speed is similar to the comparison above the value for humidity is strongly decreased. This indicates that only high quality *in situ* data are really useful for the assessment of retrieval errors. The second finding concerns the chosen sea surface temperature dataset which was in this case the MCSST (Multi Channel Sea Surface Temperature) described in McClain (1981).   The surface saturation humidity showed a systematic under-estimation during July, August, and October 1987 and also during the first three months in 1988.   This resulted in a mean under-estimation of the sea surface saturation humidity of 0.5 gkg$^{-1}$.   This bias was caused by extensive periods of cloud cover and/or darkness that led to a shift toward a nighttime bias in the day/night observation ratio.   Cloud detection is more difficult during nighttime than during daytime since a combination of tests using the three infrared channels of the AVHRR

is required, rather than simple reflectance tests. So less measurements, and a deteriorated cloud detection, can lead to a significant cold bias in the sea surface temperature. However, this problem has been recognised and producers of newer datasets (e.g. the Oceans Pathfinder Sea Surface Temperature dataset) are aware of such problems.

Comparisons to scientific experiment data

Comparisons to data sets gained during scientific experiments have mostly the aim of showing that the satellite algorithms are able to describe the local temporal variability of energy fluxes and flux related variables. HOAPS retrievals have been compared to data gained during TOGA COARE (Bradley and Weller, 1997) and CEPEX as well as during ARKTIS'93 (Brümmer *et al.*, 1993). Both intercomparisons represent regions with rather extreme climates. The ARKTIS'93 experiment was conducted in February and March 1993 in the northern part of the Norwegian Sea. The *in situ* measurements were taken by standard instruments aboard the German research vessel Valdivia. The major result was that in most cases the measurements of the bulk parameters and the parameterised fluxes were in good agreement. The exception was some cases relating to situations where the ship was too close to the coastline. The errors found were comparable to the weathership M exercise. Another result was that the wind speed algorithm was not able to reproduce high wind speeds (around 20 ms$^{-1}$). The same result was found in tests of other algorithms (Goodberlet *et al.*, 1989 and Stogryn *et al.*, 1994). This problem, inherent with most of the existing wind speed retrievals, can be caused by insufficient accuracy of the emissivity parameterisation during high wind speed events. However, a slightly surprising result was that the retrievals of wind speed and humidity gave good results even in the case when the ships instrumentation recorded light rain of up to 2 mmh$^{-1}$.

The TOGA COARE and CEPEX field phases took place in purely tropical environment. For both experiments, data from the US research vessel Vickers have been used to make intercomparisons to the retrieval schemes. It was found that precipitable water (both total and of the 500 m bottom layer) and the surface wind speed were retrieved excellently by the SSM/I during both experiment phases. Errors were not larger than in other regions of the world oceans. However, the retrieval for near-surface air-humidity showed a systematic overestimation of 1-2 gkg$^{-1}$ during a 12 day period in February 1993. The failure was in some way connected to the vertical structure of the water vapour distribution, since during that period the radiosonde data exhibited very high water vapour loadings in the upper troposphere with relative humidities higher than 90%. When the tropospheric humidity was lower the retrieval worked quite well. The reason for this malfunction is not yet fully clarified. On one hand it can be argued that the high water vapour loading leads to a signal saturation effect so that any variation below this thick water vapour layer can not be detected well. Against this is that the 500m integrated water vapour was retrieved quite well during this phase. On the other hand there was a considerable decrease of correlation between the integrated water vapour amounts and the near-surface air humidity (which is almost constant); thus the assumed linear relationship might not be valid in the Western Pacific warm pool. Whether this behaviour of the humidity retrieval is typical for tropical oceans can't be answered definitely because the CEPEX data (which were recorded along 2° south and north of the equator) showed that the retrieval worked well shortly after the ship left the warm pool area. Additional comparisons to data from the TAO buoy array in the equatorial Pacific and data from the Pilot Research Moored Array in the Tropical Atlantic (PIRATA) are necessary. However these datasets lack the information on vertical atmospheric humidity structure which might be essential for resolving possible retrieval errors.

Comparisons in enclosed seas

Because of the rather coarse spatial resolution of microwave radiometers, only two intercomparison studies over the North Sea region have been conducted. Objectively analysed and gridded fields with a spatial resolution of (42 km)$^2$ and a time resolution of 3 hours have been used as *in situ* data (Luthardt, 1985). The first study (Schlüssel, and Luthardt, 1991) was mostly aimed at validating the wind speed retrieval. The second study,

by Schulz (1993b),  examined one case study over the North Sea and compared air-humidity and sea surface temperature, wind speed, and latent heat flux.   Concerning wind speed both studies found that the wind speed is recovered by the SSM/I with an accuracy of 2ms$^{-1}$ in the inner areas of the North Sea but that the accuracy decreases approaching coastal waters due to the field of view of the antenna including signals from land surfaces.   For sea surface temperature it was found that the *in situ* measurements were not able to reproduce the fine scale structure obtained from the AVHRR data and that *in situ* measurements were positively biased by approximately 1K.   This can be explained by the possible existence of a cool skin at the surface,  and the well known overestimation of the temperature at cooling water intakes on ships.   With respect to air-humidity the same results as in the global comparison have mostly been found.   The parameterised latent heat flux in this case study shown in Figure 11.3.1 exhibited generally a good agreement but some hot spots of high differences between satellite and *in situ* data occur in regions where the coverage of *in situ* measurements was low. It should be noticed that the quality of the *in situ* temperature and humidity fields is not as good as the wind fields because the fields couldn't be adjusted by a geostrophic constraint. Hence, the observation density plays a greater role in the comparison of the thermodynamic components.
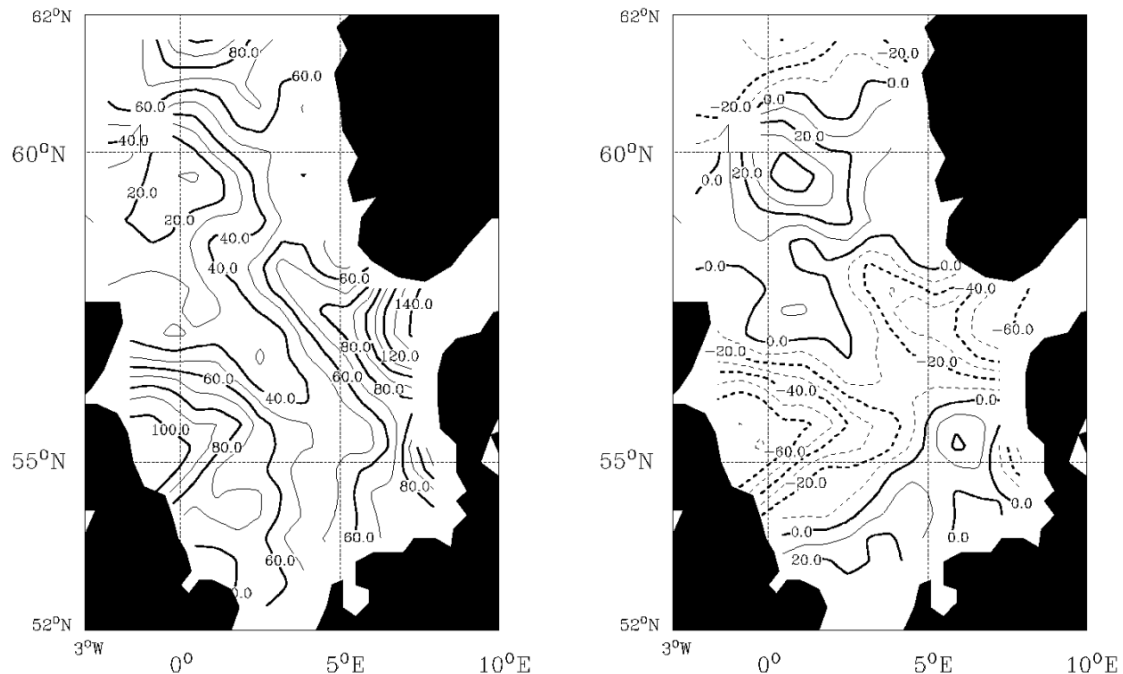


Figure 11.3.1: Distribution of latent heat flux on 3. August 1987 in Wm$^{-2}$ (left), and differences between *in situ* latent heat flux at 6:00 a.m. and those derived from satellite data in Wm$^{-2}$ (right). The contour interval is 10 Wm$^{-2}$, negative isolines are dashed.

Comparisons to global *in situ* climatologies

        To establish differences between HOAPS and climatologies derived from *in situ* measurements comparisons have been made with the SOC climatology described by Josey *et al.* (1999) and the UWM climatology described by da Silva (1994).   Since the findings are very similar for both *in situ* climatologies the following discussion is restricted to the SOC climatology.   Because HOAPS and SOC do not cover the same time period,  only a five and a half year climatology from July 1987 to December 1993 was considered to ensure that phenomena like El Niño were,  or were not, included in both.   Figures 11.3.2 to 11.3.4 show the global climatological mean distributions of evaporation *E*, precipitation *P*, and *E-P* from (a) HOAPS, (b) SOC, and (c) the difference (HOAPS - SOC).

In the evaporation distribution (Figure 11.3.2),  it can clearly be seen that the differences are smallest in the North Atlantic where the in situ data density is at its maximum. A positive outcome of the comparison is that the Gulf Stream is located at the same position in both datasets, which is by no means a matter of course.   Also, only small differences are observed in the strength of the evaporation over the Gulf Stream which are most significant during winter.

Large zonal homogeneously distributed biases occur over the tropical oceans and the whole southern hemisphere.   The differences in the tropics are manifested by a negative bias of about -1.5 ms-1 in wind speed and a positive bias of about 1.5 gkg-1 in air-humidity.   A possible explanation for the bias in air humidity may be the malfunctioning of the satellite algorithm,  as found in the comparisons with the COARE data.  However that would assume that the atmospheric conditions in the warm pool could be considered to be typical for tropical oceans in general.   This is contradicted by the results from the  CEPEX comparison which cover a much larger tropical area.   The wind speed bias is not yet explained;  all comparisons of wind speed retrievals to tropical experiment data show no bias of the magnitude although the number of comparisons is rather small.   It should be kept in mind that the observation density of the in situ measurements is quite low in the tropics (see Figure 2 in Josey et al., 1999) so that wind speed and air-humidity values may be influenced by subtropical conditions resulting in higher wind speed and lower humidity values compared to HOAPS.   This would also partly explain the zonally homogeneous distribution of these biases.

In the southern oceans, HOAPS shows a higher evaporation than SOC which is expressed by a zonal homogeneous positive bias in wind speed of  about 2 ms-1 whereas the bias in air-humidity is negative in the range of -0.5 to -4 gkg-1 with maximum differences found to the south of South Africa.   These southern ocean biases are surely caused by undersampling in the in situ climatology with the result that the analysed values are strongly influenced by measurements from better sampled regions further north.

Considering precipitation,  it is obvious that in situ precipitation estimates can only be useful where the spatial observation density is high because precipitation has a very intermittent spatial structure.   Figure 11.3.3 shows that the precipitation pattern,  in the southern hemisphere at least,  appears to be unrealistic for SOC but reasonable for HOAPS.   Due to the small observation density the analysis of in situ data tends to create clusters of high precipitation in the South Pacific and Indian Ocean with rainfall that is higher than that in HOAPS by a factor of 2 to 3.   Whereas HOAPS shows large areas to the west of the continents with minimum rainfall of less than 0.5 mmd-1,  those areas are much smaller in the SOC dataset.   But even in the well sampled North Atlantic,  substantial differences occur over the Gulf Stream region and to a lesser extent over the Kuroshio in the North Pacific during winter time (Figure 11.3.3). Rainfall amounts in HOAPS are as high as in the ITCZ which seems to be not unrealistic if the independent estimates from the TRMM Precipitation Radar (Kidd, 1999, *pers. comm.*) over the southern part of the Gulf Stream are considered.   So the reason for the  difference may lay  in the  method  of Tucker (1961) for estimating rainfall from actual weather observations which has an upper limit of 8.13 mm/(3 hours).   For tropical precipitation was found that this scheme underestimated rainfall seriously and an empirical temperature dependent correction was developed by Dorman and Bourke (1978).   Because this correction does not take effect over the Gulf Stream,  in situ climatologies may underestimate rainfall there.   An examination of SSM/I rainfall estimations for single orbits during the winter months of 1992, 1993 and 1997 shows that SSM/I derived rain rates are on average twice as large as the maximum possible in situ rain rate of 2.7 mmh-1. In addition,  the work of Tucker (1961) showed that the observation frequency of weather codes related to this maximum is rather low.

The differences in the precipitation fields have large implications for the freshwater budget, E-P , which is shown in Figure 11.3.4.   Whereas the satellite-derived field is characterised by a quite thin ITCZ and a somewhat broader SPCZ where the ocean is provided with an precipitation excess of about 6 mmd-1,   on average the ITCZ covers a much broader area in the in situ climatology.  The patterns in the  northern  hemisphere are characterised by
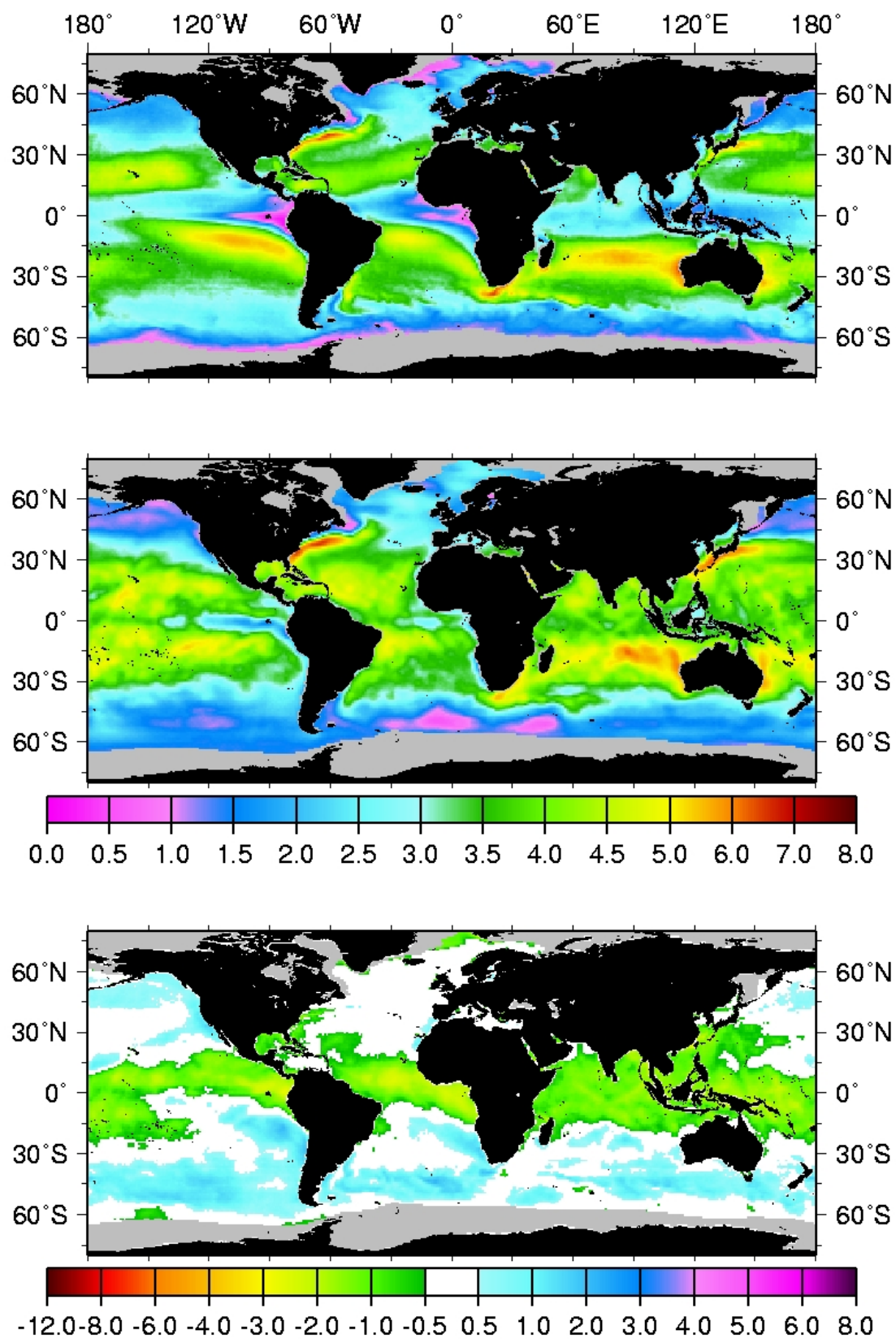
Figure 11.3.2 Comparison of evaporation (mm/day) from (top) HOAPS, (middle) SOC, (bottom) HOAPS-SOC difference.
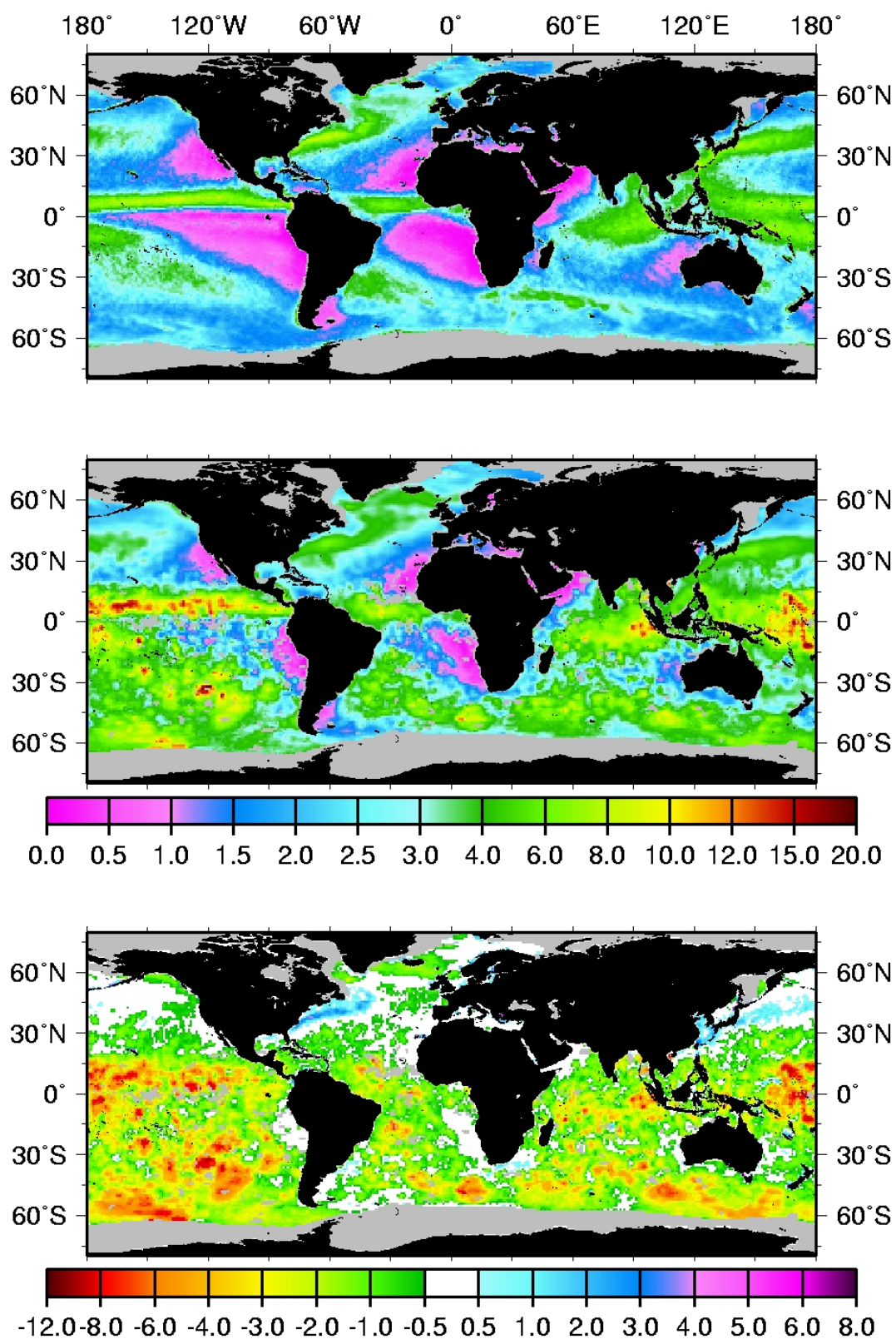
Figure 11.3.3 Comparison of precipitation (mm/day) from (top) HOAPS, (middle) SOC, (bottom) HOAPS-SOC difference.
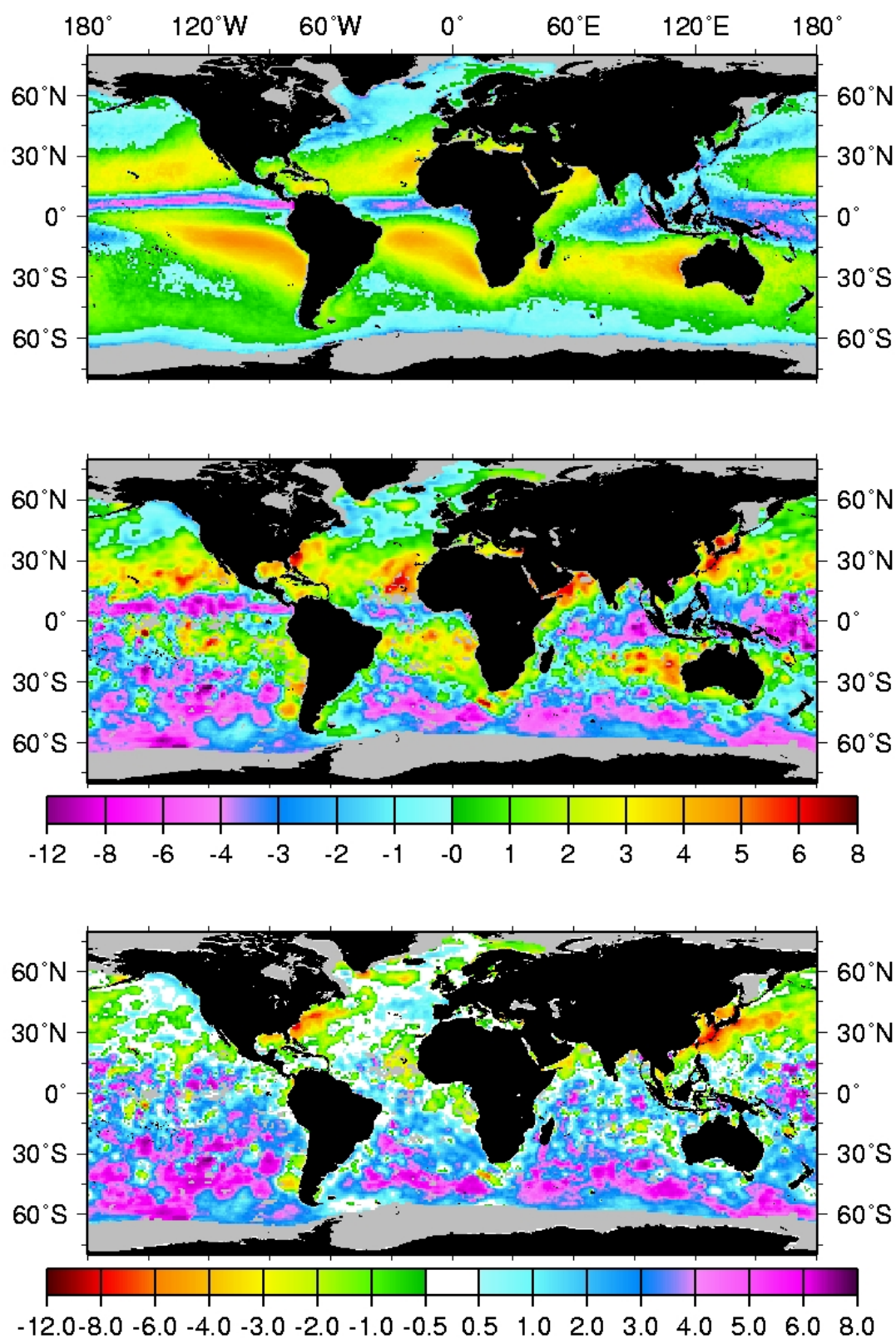
Figure 11.3.4 Comparison of (E-P) (mm/day) from (top) HOAPS, (middle) SOC,  (bottom) HOAPS-SOC difference.

evaporation excess in the trade wind belts and precipitation excess along the North Atlantic and North Pacific storm tracks in both climatologies.   Because of the differences in the precipitation fields, the largest differences (even in sign of E-P )  exist over southern parts of the warm currents.   Over the southern hemisphere both climatologies show very different patterns with the SOC pattern very intermittent due to the structure of the precipitation field.   The satellite-derived E-P values show a more realistic pattern with a slightly larger evaporation excess in the trade wind belts compared to the northern hemisphere,  and slight freshening near the Antarctic ice margin.   Here the SOC climatology shows values up to 8 mmd-1 compared to a maximum of 2 mmd-1 in the HOAPS climatology.

Comparison to the Subduction Experiment buoys

        Because climatologies can not serve as a validation dataset for each other, independent ground truth must be used for deeper analysis of the errors.   Josey et al. (1999) have used the data from the Subduction Experiment described by Moyer and Weller (1997) for verification. The same task has been repeated for the HOAPS climatology.   Unfortunately, buoy arrays with very high quality measurements are not available at many locations in the oceans so that this comparison can only serve as a tool to identify possible regional biases in either climatology.

        A time series of monthly mean values from the Subduction buoys was compared with 1˚ x 1˚ field data from the HOAPS dataset.   The time series at all buoys agreed fairly well with correlation coefficients greater than 0.95 for all basic state variables and a slightly lesser correlation for the derived fluxes.   The variability of the bulk parameters within one month was almost of equal size for both datasets for all months during the two year period.   That implies that,  even with only two satellite overpasses per day,  it appears to be feasible to represent the intra-monthly variability of basic state variables - at least in the Subduction area.   However, positive biases were found for wind speed at both northern buoys over the whole buoy deployment period.   The reason for this bias can only be found through a comparison of the wind speed spectra derived from simultaneously measured buoy and SSM/I data.   A possible reason could be an underestimation of the wind speed at the buoy,  because the sensors were installed at a height of 2 to 3m so that the instruments may be in the wave trough region during high wind speed events (Section 9.2.2).   Negative biases were found for sea surface temperature at both southern moorings during the first year of the deployment period.   The suggestion that this bias was caused by aerosols from the Mt Pinatubo eruption,  with subsequent deterioration of the cloud screening in the AVHRR dataset,  seems to be unrealistic because this feature should be found at all buoy sites.   Estimates of specific air humidity are almost bias free at all moorings during the deployment period.

        The averages and mean differences between HOAPS and all five Subduction buoys are summarised in Table 11.3.2.   The positive bias in wind speed resulted in an overestimation of sensible and latent heat flux at the North East and the Centre buoy whereas the negative biases in sea surface temperature cause a negative bias in latent heat flux at both southern buoys. Although the bias for sensible heat flux equalled zero at three of the five buoys,  this should only be taken as an indication that crude assumptions,  like a constant relative humidity of say 80%,  may be sufficient to determine a climatological mean value (rather than the annual cycle which appears somewhat exaggerated in the HOAPS dataset).   Estimates of longwave net flux are not generally biased low or high.   Because of the dependence of the downwelling radiation on actual cloud cover,  differences in satellite and buoy estimates can be caused by satellite resolution effects.   The satellite instrument can't resolve the cloud spatial and time scales because of its coarse spatial resolution - only 30 - 70 km and only two measurements per day per satellite.   All the more surprising is that the mean differences in net longwave fluxes between HOAPS and the buoys are not much larger than differences between buoy data and the SOC climatology.

        Comparison of the mean differences between the HOAPS dataset and the Subduction buoy measurements,  for all fluxes and basic state variables, with the findings summarised in the study done by Josey et al. (1999) reveals that the satellite dataset appears to be competitive with the in situ product even in this not too badly sampled region.

Table 11.3.1 Mean heat fluxes and differences for the Subduction experiment buoy array.

| Location | Source | Qsens Wm$^{-2}$ | Qlat Wm$^{-2}$ | u ms$^{-1}$ | qS gkg$^{-1}$ | qL gkg$^{-1}$ | QLW Wm$^{-2}$ |
|---|---|---|---|---|---|---|---|
| NE Buoy, N=23 | HOAPS | 14 ± 9 | 102±24 | 6.7±1.2 | 15.2±2.4 | 11.2±2.0 | 74±12 |
| (33° N, 22° W) | Buoy | 9±4 | 97±20 | 5.5±0.6 | 15.2±2.4 | 11.1±2.0 | 66±8 |
|  | HOAPS-Buoy | 5±9 | 5±21 | 1.2±0.8 | 0±0.3 | 0.1±0.7 | 8±10 |
| SE Buoy, N=14 | HOAPS | 7±21 | 95±53 | 7.3±0.7 | 15.9±1.4 | 12.5±2.1 | 84±26 |
| (18° N, 22° W) | Buoy | 7±3 | 103±25 | 7.3±0.8 | 16.6±1.5 | 13.0±1.6 | 47±16 |
|  | HOAPS-Buoy | 0±20 | −8±33 | 0±0.6 | −0.8±0.6 | −0.5±1.0 | 37±13 |
| SW Buoy, N=14 | HOAPS | 5±15 | 101±43 | 6.9±0.9 | 18.1±1.3 | 14.1±1.9 | 60±16 |
| (18° N, 34° W) | Buoy | 5±3 | 129±25 | 6.6±0.5 | 18.6±1.4 | 13.7±1.8 | 60±11 |
|  | HOAPS-Buoy | 0±13 | −28±28 | 0.3±0.7 | −0.6±0.6 | 0.4±0.8 | 0±11 |
| NW Buoy, N=13 | HOAPS | 7±8 | 86±23 | 6.5±1.5 | 15.9±2.7 | 12.3±2.5 | 66±13 |
| (33° N, 34° W) | Buoy | 7±3 | 84±20 | 5.1±1.1 | 16.0±2.9 | 12.0±2.2 | 76±9 |
|  | HOAPS-Buoy | 0±7 | 2±22. | 1.4±0.6 | −0.1±0.3 | 0.3±0.5 | −10±9 |
| C Buoy, N=18 | HOAPS | 16±10 | 116±27 | 6.5±0.8 | 16.6±1.7 | 12.1±1.8 | 76±12 |
| (25.5° N, 29° W) | Buoy | 7±3 | 107±18 | 5.7±0.8 | 16.8±1.8 | 12.2±1.8 | 66±13 |
|  | HOAPS-Buoy | 9±8 | 9±18 | 0.7±0.5 | −0.2±0.3 | −0.1±0.6 | 11±13 |

*11.3.3  US satellite radiation products*

A. INTRODUCTION

The evaluation of US produced satellite-based global products for surface radiative fluxes is described here.  Japanese radiation products will be described in the next section. Networks of surface measurements have been used for validation, but coverage of the sea is minimal.  Surface measurements and satellite-based retrievals are improving; they are indeed useful for many ocean modeling studies.  However,  intensive, local scale studies have uncovered significant problems in both the measurement and theoretical computation of surface SW flux.  The surface SW insolation retrieved by the satellite-based programs and computed by radiative transfer theory generally exceeds measured values; the discrepancies between measurement and theory are significant and unresolved.  It should also be noted that none of the LW algorithms described below yet accounts for corrections to SST due to the cool skin (~0.3 K) discussed in Section 10.2.1.

The CERES/ARM/GEWEX Experiment (CAGEX; Charlock and Alberta, 1996) illustrates SRB issues for both SW and LW CAGEX provides a space-time set of input data, calculated fluxes, and validating measurements.  Following the launch of CERES,  CAGEX is being extended to the ARM Tropical West Pacific (TWP) site.  ARM TWP data is expected to become an important resource for the study of radiation at the air-sea boundary.  The ARM web page is:  http://www.arm.gov/

B. GEWEX SRB

Version 1

The first version of global products by the GEWEX Surface Radiation Budget (SRB) Project (Whitlock *et al.*, 1995) have been in use for a few years. Access is through the NASA

Langley Distributed Active Archive Center (DAAC) with the web address: http://eosweb.larc.nasa.gov/

The GEWEX SRB is an official project of the WCRP, and it is formally reviewed by the WCRP WG on Radiative Fluxes. The GEWEX SRB uses ISCCP (operational satellite; Rossow *et al.*, 1991) data and covers 1985-1988, a period for which the adjusted ISCCP calibration was fairly stable. GEWEX SRB presently issues SW products only. Daily and monthly-averaged insolation is available in the 280 by 280 km equivalent area grid system from the primary algorithm by Pinker and Laszlo (1992); and monthly retrievals from a backup algorithm due to Staylor (see Darnell *et al.*, 1992); both algorithms are based on radiative transfer physics. In addition to the surface SW insolation (downwelling), the Pinker algorithm produces the surface upwelling flux, the surface net flux, the surface albedo, and the top-of-the atmosphere (TOA) net flux.

For validation, the GEWEX SRB files provide:

(1) monthly TOA net flux by independent, higher quality measurements from the Earth Radiation Budget Experiment (ERBE; Barkstrom *et al.*, 1989) over most of the globe. Unlike the narrowband radiometers on the ISCCP satellites, ERBE provides broadband measurements with on-board calibration for SW and LW.

(2) measured monthly-averaged surface insolation for a small fraction of the land mass as compiled by the Global Energy Balance Archive (GEBA; Gilgen and Ohmura, 1999). Most GEBA sites are located in the midlatitudes; a few of the GEBA surface sites are located on islands (note earlier remarks on pyranometer accuracy and GEBA in Section 5.2.2). October 1985 was a fortuitous month in that the monthly mean bias of the Pinker algorithm relative to midlatitude GEBA obaervations was only 2.7 Wm-2.

The estimated global and monthly averaged bias for GEWEX SRB insolation is about 15 $Wm^{-2}$; that is, the retrieved global insolation for a 24-hour day is probably too large by 15 $Wm^{-2}$; most GCM's produce even larger values for surface insolation. The estimated rms error for monthly mean GEWEX SRB insolation in a 280 by 280 km grid box is 20-25 $Wm^{-2}$; a figure indicated smaller values for European GEBA sites in October 1985. Errors are smaller over the midlatitudes and larger over the tropics. The largest errors are found in regions with extensive biomass burning. We do not know if the errors in surface insolation are larger (or smaller) over sea. At the TOA, there is not a significant land versus sea bias in the GEWEX SRB when compared to ERBE TOA measurements. The ERBE global mean uncertainty for SW is 5-7 $Wm^{-2}$; this estimate for ERBE uncertainty is based on the imbalance of ERBE TOA SW and LW observations. The bias in GEWEX SRB surface insolation appears to be due to an atmosphere that absorbs more SW than is predicted by radiative transfer theory. The estimated error for the GEBA surface insolation measurements is 3%; this error may have a significant systematic component.

Version 2

A new Version 2 of the GEWEX SRB will be issued in early 2001 (p.w.stackhouse@larc.nasa.gov). An improved Pinker algorithm will be used for SW. A 2/4 stream version of the Fu and Liou (1993) algorithm will be used in the LW. The new Version 2 will provide a higher spatial resolution of 1 by 1 degree; time spacing will be 3-hourly, daily average, monthly-hourly (i.e., the monthly mean flux from 0200-0300 UTC, etc.), and monthly average; covering July 1983 to at least June 1995.

GEWEX SRB Version 2 will be based on ISCCP DX (pixel scale) data, rather than the ISCCP C1 (280 by 280 km equivalent area gridboxes; 2.5 by 2.5 degree at the equator; number of gridboxes changing with latitude) used now; this will provide a true enhancement of spatial resolution, as opposed to a simple interpolation of C1 to 1 by 1 degree (a few such interpolations are circulating at present). The pixels in both ISCCP DX and C1 are sampled at the same ~30 km spacing, however; unlike ERBE and CERES (whose pixels are almost

contiguous), the pixels in ISCCP samples are quite separated;  the sampling produces spatial noise in a gridbox product.

Both ERBE and ISCCP are liable to large instantaneous errors of up to 50 $Wm^{-2}$ because of uncertainty in angular distribution models (ADMs) used to invert from directional radiance (W/sr - energy per unit solid angle measured by a scanning satellite radiometer) to directionally-integrated flux ($Wm^{-2}$ irradiance - energy per unit area).  ADM errors are reduced enormously by averaging, but they may be the source of the present 5-7 $Wm^{-2}$ imbalance between SW and LW in the ERBE record.

C.  LANGLEY SRB

Darnell *et al.* (1996) and Gupta et al (1999)  have released an 8-year CD-ROM "Langley SRB Dataset" for monthly-mean downwelling and upwelling, shortwave and longwave fluxes.   Monthly, 280 by 280 km retrievals are available from : http://eosweb.larc.nasa.gov/PRODOCS/srb/table_srb.html .

The "Staylor" SW (Darnell *et al.*, 1992) and the Gupta *et al.* (1992) LW algorithms are used  together with the ISCCP C1 cloud products (Rossow and Schiffer, 1991) that provide information on clouds, the atmosphere and the surface,  and the ERBE top-of-atmosphere shortwave and longwave fluxes (Barkstrom *et al.*, 1989).   Accuracy with the Staylor SW algorithm is comparable to that with the Pinker SW.  The Pinker algorithm was selected (over the Staylor algorithm) for official GEWEX SRB processing because, with more comprehensive physics,  Pinker produces a TOA flux which may be compared with ERBE.   The Gupta downwards LW flux was larger than BSRN measurements at the mean of 7 sites for 3 months in 1992  by 5 $Wm^{-2}$; the rms error was 20 $Wm^{-2}$.   In comparison with the GEBA database of surface flux measurements (Gilgen and Ohmura, 1999), the NOAA/Climate Monitoring and Diagnostics Laboratory (CMDL) dataset, and the CSIRO, Australia, dataset,   the overall uncertainty in monthly mean downwelling fluxes was estimated to be about ± 15 $Wm^{-2}$ for both shortwave and longwave.

For October 1985, the surface net SW flux (absorption by the surface; global mean 160.6 $Wm^{-2}$) is larger than the surface net LW flux (negative value denotes cooling; global mean -46.6 $Wm^{-2}$) and dominates the geographical pattern of surface net total (SW+LW) flux (global mean 114 $Wm^{-2}$) over the ocean.   The interannual variability for 8 Octobers showed that the net SW (global mean standard deviation 10.2 $Wm^{-2}$) dominates the net LW (global mean standard deviation 6.22 $Wm^{-2}$) in setting the pattern of the surface net total interannual variability (global mean standard deviation 11 $Wm^{-2}$).   Patterns of interannual variability are strongest over the tropical oceans.  For an individual gridbox, the interannual variability is smaller than the error in the satellite retrieved value for a given month.  Satellite retrievals do, however, demonstrate skill in identifying the geographical patterns in interannual variability. A regional analysis of interannual variability in the SW SRB demonstrated that the interannual variability retrieved by satellites represents the pattern and maginitude of interannual variability in the GEBA ground measurements quite well (Alberta *et al.*, 1994).

D.  CERES RADIATION DATA

The ADM problem (see section 11.3.3B) is approached by sophisticated Rotating Azimuth Plane Scanning (RAPS) in CERES (Wielicki and Barkstrom, 1991).   The first launches of CERES were in November 1997 on TRMM (tropical and midlatitude coverage) and in December, 1999 on Terra (formerly EOS-AM1 - global coverage).   SRB retrievals will be validated and released 2-3 years after launch.   Gridded products (1x1 degree) will eventually be available 3-hourly, daily, and monthly.   Instantaneous SRB at the individual "footprints" of the broadband CERES scanner will typically have diameters of 10-50 km.  The goal of the CERES SRB is to reduce the error in the GEWEX SRB by a factor of two.   CERES has extensive documentation  of  its  algorithms  and  validation  activities  at  http://asd-www.larc.nasa.gov/ceres/ASDceres.html .

A verification facility (CERES Ocean Validation  Experiment COVE) has been established at the Chesapeake Light, 25 km off the Virginia coast.  Measurements of shortwave spectral radiances reflected by the sea surface are obtained using a southward facing Spectrophotometer. The measurements are intended to  improve classic formulations of ocean bi-directional reflectance and albedo.  The radiance scans are complemented by collocated, continuous, long-term  observations of surface radiation and aerosols  and meteorology, wind waves, and sea swell.  COVE measures broadband fluxes, both upwelling and downwelling, and participates in the BSRN.

### E.  BISHOP SHORTWAVE RADIATION PRODUCT

Bishop *et al.* (1997) have produced a global dataset of daily-mean downwelling shortwave fluxes at the surface covering an eight year period (July 1983 -- June 1991) at 2.5° latitude-longitude resolution.   This dataset is available by request from Dr. James K.B. Bishop (e-mail: jkbishop@lnl.gov) or from the archives at the National Center of Atmospheric Research in Boulder, Colorado (dataset reference = DS741.0 SURFACE SOLAR IRRADIANCE BY BISHOP).

These fluxes are calculated by applying an approximate radiative transfer method (Bishop and Rossow, 1991) to the ISCCP C1 cloud products (Rossow and Schiffer, 1991) that provide information on clouds, the atmosphere and the surface.   The Bishop  *et al.* (1997) method uses the cloud properties retrieved from the narrowband satellite radiances (also based on a radiative transfer model) as input into a calculation of the fluxes that explicitly accounts for multiple scattering in and between clouds and the surface: it was tested by comparison to a full radiative transfer model using the same input data.   The results were further verified by comparison with the GEBA database of surface flux measurements over land (Gilgen and Ohmura, 1999) and an extensive number of buoy-based measurements from a series of ocean experiments.  Overall uncertainty is estimated to be about $\pm$ 25 $Wm^{-2}$ rms for daily-mean values, due mostly to cloud sampling errors, and $\pm$ 15 $Wm^{-2}$ for monthly mean values, due mostly to calibration and aerosol optical thickness errors.

A new global product of daily mean surface solar irradiance is now being produced with a spatial resolution of 0.5° latitude-longitude based on the revised ISCCP cloud products (Rossow and Schiffer, 1999). This dataset is complete for a couple of years; more information about this dataset can be found at ( http://www.giss.nasa.gov/data/seawifs/ ).

### F.  BREON  SURFACE NET SHORTWAVE FLUX AND ALBEDO

Breon *et al.* (1994) have produced a global dataset of monthly-mean surface net shortwave and albedo covering a two-year period (1985-1986) at 2.5° latitude-longitude resolution.   These surface quantities are determined from ERBE (Barkstrom *et al.*, 1989) monthly-mean full-sky and clear-sky albedos, together with the top-of-atmosphere solar irradiance, by removing the atmospheric and surface scattering and absorption effects using results pre-calculated with a radiative transfer model developed by Tanre *et al.* (1990). This method is conceptually similar to that proposed by Li *et al.* (1993).  The results were evaluated by comparison with surface shortwave fluxes determined from narrowband satellite radiances by Gautier (1988).   The estimated uncertainty of the monthly-mean values is +15 $Wm^{-2}$ bias and $\pm$14 $Wm^{-2}$ rms. This dataset may be obtained by contacting the authors.

### G.  NASA GODDARD INSTITUTE FOR SPACE STUDIES

Rossow *et al.* (1995) have produced a global dataset of downwelling and upwelling, shortwave and longwave fluxes at the top-of-atmosphere, in-atmosphere, and at the surface covering an four year period (April 1986 -- January 1989, every third month) with a 3-hr time resolution and a 2.5° latitude-longitude spatial resolution.   More information about this dataset and sample statistics can be found at ( http://isccp.giss.nasa.gov/flux.html ) and the whole dataset can be obtained by sending a request to Dr. Yuanchong Zhang, NASA Goddard Institute for Space Studies, 2880 Broadway, New York, NY 10025, USA.

The analysis approach follows that proposed by Rossow *et al.* (1989) and Rossow and Lacis (1990).   The fluxes are calculated by applying a full radiative transfer model from the GISS climate GCM (Zhang, *et al.*, 1995) to the ISCCP C1 cloud products (Rossow and Schiffer, 1991).   This model treats the full spectral dependence of absorption and scattering by atmospheric gases, including all radiatively important trace species, six different types of aerosol, clouds and the surface.   The results were verified by comparison with the ERBE top-of-atmosphere fluxes (Barkstrom *et al.*, 1989), the GEBA database of surface flux measurements (Gilgen and Ohmura, 1999), several other specific surface site measurements and/or field experiment datasets, and by comparison with other satellite analyses.   Overall uncertainty is estimated to be $\pm10$-15 $Wm^{-2}$ for monthly-mean top-of-atmosphere fluxes and $\pm15$-25 $Wm^{-2}$ for monthly-mean surface fluxes.

A new global radiation flux product covering the period from July 1983 through to present is planned, based on application of an improved radiative transfer model applied to the new ISCCP D-series cloud products (Rossow and Schiffer, 1999).   The model improvements include a refined treatment of cloud scattering dependence on cloud optical thicknesses and particle sizes, including for non-spherical ice cloud particles, extension of the aerosol properties to include two size ranges for each of six types, refinement of the spectral representation of longwave absorption and the water vapor continuum, and improved specification of surface albedos and emissivities.   Input quantities have been improved by including both ice and liquid water clouds, a revised aerosol optical thickness climatology to include more absorbing species, a revised atmospheric temperature and humidity dataset,  and treating cloud type dependence and layer structure more completely.   The new product will report, every 3 hr at 2.5˚ latitude-longitude resolution, the cloudy and clear, upwelling and downwelling, shortwave and longwave fluxes at five levels: surface, 680 mb, 440 mb, 100 mb and top-of-atmosphere. Cloud-type dependence will also be reported.   Production of this new product is expected to begin early in 2000 and to be available from Dr. Yuanchong Zhang (see above).

H.  SUMMARY - US SATELLITE RADIATION PRODUCTS

Figure 11.3.5 shows the climatological zonal mean net surface shortwave radiation from seven different products discussed in this Section.  In the low latitudes the satellite products suggest that substantially more radiation reaches the surface compared to the VOS estimates and reanalyses.   Throughout the low latitudes, the flux in both reanalysis is substantially smaller, as pointed out in Section 11.4 a likely result of cloud cover problems in the models. Discounting the reanalysis, the spread among the estimates is still on the order of 25 $Wm^{-2}$ in the zonal mean.

*11.3.4  Japan surface shortwave and longwave products*

A.  KIZU (1999) SW FLUXES

Kizu(1999) has produced surface shortwave radiation fluxes covering from October 1992 to September 1993 with monthly and 1.0° x 1.0° latitude-longitude resolution.   The spatial coverage is from 80°E to160°W and from 60°N to 60°S.  He used the 3-hourly Visible and Infrared Histogram Data from GMS/VISSR with 0.25° latitude-longitude spatial resolution as a primary data source, and additionally monthly precipitable water from SSM/I (Wentz,1994), monthly total ozone amount from TOMS/Nimbus7, and seasonal climatology of tropospheric aerosol from NOAA/AVHRR (Husar et al, 1997).   Long-term degradation of the VISSR instruments was corrected by Kizu(2000).   A simple parameterization model by Iqbal (1983) was used to formulate fundamental radiative transfer processes in the atmosphere, and the five-daily GMS imagery data was used to estimate the cloud albedo.   The methodology was described in detail in Kizu(1995).   Based on comparison with routine ground measurements of insolation,  mainly in Japan and Australia, the statistical errors of daily and monthly mean
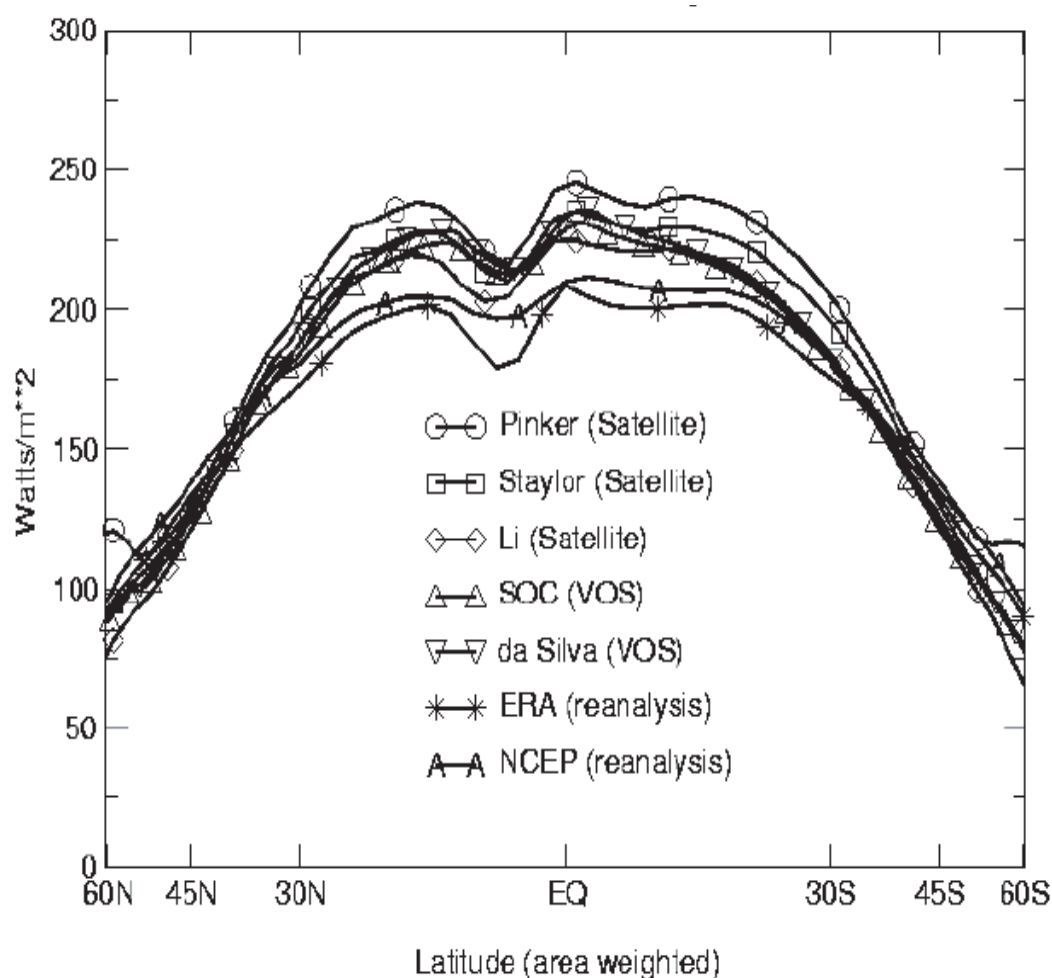
Figure 11.3.5 The climatological zonal mean net surface shortwave radiation from three satellite products, two VOS based products, and two reanalysis products.

values were estimated to be less than 20% and 10%, respectively. The validation procedure is continuing by collecting other available in-situ measurements on both land and sea, and the products will soon be extended over 11 years from March 1987 to September 1999.

B. IWASAKA(1999) LW FLUXES

Iwasaka(1999), using the narrow band model proposed by Goody(1964), has estimated monthly products of surface longwave radiation flux in each 1.0° x 1.0° latitude-longitude grid over the western Pacific and eastern Indian Oceans (80°E-160°W, 60°S-60°N). The primary data source was Infrared Radiation (IR) Histogram Data derive from Geostationary Meteorological Satellite (GMS-4), and additionally Multi-channel Sea Surface Temperature (MCSST) data derived from NOAA/AVHRR data and climatological SST data derived from COADS were used. The narrow band radiation model proposed by Goody (1964) was used to calculate atmospheric absorption and emission between the cloud bottom and sea surface. This model covers the $H_2O$ continuum, the $CO_2$ 15 micrometer and the $H_2O$ 6.3 micrometer bands. The parameters in the model were given by Rogers and Walshaw (1966), Goldman and Kyle (1968) and Roberts et al .(1976). The spectral range of 0-2200 cm^{-1} was divided into 23 narrow bands to calculate the radiation flux.

Construction procedures were as follows.  First, in order to detect cloud coverage in each pixel, a pseudo sea surface temperature was computed from IR Histogram data and compared with the MCSST data.  A pixel where the difference between the pseudo SST and MCSST exceeded 3.0K was assumed to be cloud-covered.  Next, the height of cloud base was determined under the assumption of constant cloud thickness and the cloud base temperature was calculated from NCEP reanalyses data.  The downward longwave radiation value was calculated from black body radiation theory using the assumption of the emissivity = 0.9 at the cloud base.  Atmospheric absorption and emission between the cloud base and sea surface were assessed by a narrow band radiation model.  On the other hand, in a cloud free area downward radiation was calculated in a layer below 300 hPa level determined by the NCEP data.  Upward longwave radiation was calculated from the black body theory using the sea surface emissivity of 0.984 based on Konda *et al.*(1994).  Downward longwave radiation values observed at Kwajalein Island were used to compare with the estimated values in this data set.  The results revealed that the estimates had a tendency to be over-estimated in cloudy conditions and under-estimated in a cloud-free conditions.  The bias and random error were both 10-20 W m$^{-2}$ for monthly mean product.  These data sets will be available on the Internet  in the near future at http://dtsv.scc.u-tokai.ac.jp/.

### 11.3.5  Residual method
During the last 20 years various estimates of oceanic meridional heat transport have been made by combining satellite and atmospheric data.  These 'residual method' calculations have provided meridional transport profiles which have been compared to estimates derived from hydrographic transects as well as those implied by net heat flux climatologies derived from COADS.  One disadvantage of this method is that only the net surface heating is computed.  On the other hand, the only other means to date of estimating the net surface heating on a large scale has been via COADS type climatologies or reanalysis, and there are clearly large uncertainties in both.  Thus the residual method has the potential to be a valuable means of estimating the total surface energy balance of the global ocean.

Subtracting atmospheric flux divergence from the net radiation at the top of the atmosphere, Trenberth and Solomon (1994) were the first to rigorously apply a residual method to estimate surface net heating locally.  Making use of ERBE radiation data and ECWMF analysis for a single year (1988),  Trenberth and Solomon derived the spatial distribution of the annual mean net surface heat flux for the global oceans.  Keith (1995) applied similar methods with four years of ERBE data (1995-1988) and combination of ECMWF and NMC analysis.

One significant problem encountered in these studies was large imbalances over land (up to $\pm$ 100 W/m$^{-2}$) in the annual mean net heat flux.  Both studies suggest that these imbalances were due to problems associated with orographic effects in the atmospheric models, and Trenberth and Solomon estimated errors to be on the order of 30Wm$^{-2}$, on the order of the global imbalances in the SOC and unadjusted da Silva climatologies.  Trenberth and Solomon corrected for these land imbalances by applying an atmospheric mass correction and also solved a Poisson equation with the constraint of no heat flux normal to continental boundaries.  Since both studies, examination of the ECMWF model has revealed that land surface imbalances were largely attributed to a non adiabatic condition at lowest level of the land surface model, which has since been rectified.

A map of the annual mean Trenberth and Solomon estimate of annual mean net heat flux is shown in Figure (11.8.2) along with estimates from the SOC and da Silva climatologies, and the ERA and NCEP reanalysis climatologies.  There are many encouraging similarities with other estimates.  The noise is likely attributable to the fact that there is no geophysical consistency between the satellite and analysis.

## 11.4  Evaluation of the Reanalysis Products

### 11.4.1  Introduction

Reanalysis has provided a long, consistent record of the interchange of momentum, energy and moisture between the earth's surface and the atmosphere.  This record presents the best opportunity to date to evaluate the accuracy of air-sea fluxes from atmospheric data assimilation systems.  There is no "ground truth" for most of these fluxes, since they are not directly measured over most of the globe and must be estimated indirectly from observations and sometimes significantly tuned to ensure net energy balance.  In this section we compare surface energy fluxes, winds, wind stress and precipitation from the four reanalyses to each other and to independent estimates and review other work evaluating the reanalyses.

### 11.4.2  Comparisons to in-situ observations

Zeng *et al.* (1998) used TOGA COARE ship data and TAO moored buoy data to compare six different bulk aerodynamic algorithms, including the ones used in the ERA15, GEOS1 and NCEP reanalyses.  They found that the ERA15 algorithm gave slightly better fits to roughness lengths than the GEOS1 and NCEP1 algorithm and that the GEOS1 algorithm gave slightly better fits to momentum and latent heat fluxes using TOGA COARE data.  The equation for roughness length for heat in the NCEP1 and NCEP2 algorithm appeared to be inappropriate under strong wind conditions and to overestimate latent heat flux.  None of the reanalysis algorithms considered the vapour pressure reduction of 2% over salt water versus fresh water, which has a significant impact on latent heat flux under strong winds.

Smull and McPhaden (1998) found that annual mean NCEP1 surface winds were weaker and less divergent (more zonal) than those observed by the TOGA-TAO moorings in the tropical Pacific.  Directional differences of 20-30° were common, although locally these were as much as 90° near the ITCZ.  Magnitudes differed by about 1-2 ms$^{-1}$ in the annual mean, but by as much as 5-6 ms$^{-1}$ locally in monthly means.  In the western Pacific NCEP1 tended to be too easterly.  ERA-15 displayed broadly similar biases, but had 10-20% smaller differences with the TAO observations, and performed well at intra-seasonal time scales.  Bony *et al.* (1997) examined the NCEP1 and GEOS1 reanalyses in the tropics and concluded that NCEP1 overestimated evaporation in regions of subsidence.

Shinoda *et al.* (1999) compared NCEP1 surface fluxes in the tropical warm pool of the western Pacific and Indian Ocean to surface fluxes estimated from mooring data during TOGA COARE and to independent gridded estimates.  The independent estimates were based on operational wind and surface pressure analyses and satellite observations of rainfall, short wave radiation, and outgoing long wave radiation.  Stress and latent heat flux that depend primarily on surface wind variations agreed better than surface short wave radiation and precipitation that depend largely on fluctuations in convection.  The intra-seasonal (periods of 25-100 days) variance of short wave radiation and precipitation in NCEP1 was about half that estimated from in-situ observations and satellite observations.  NCEP1 stress and latent heat variations associated with the Madden-Julian oscillation (MJO) agreed well in magnitude and phasing with the independent estimates; NCEP1's composite short wave radiation and precipitation for the MJO agreed in phase but had less than half the amplitude of the satellite-based estimates.

Klinker (1997) compared latent and sensible heat flux from ERA15 to the TOGA COARE IMET buoy at 156E and 1°45'S and found that ERA15's latent heat flux had a 17 Wm$^{-2}$ (16.5%) positive bias.  ERA15 represented major events with strong latent heat fluxes well, reflecting good analyses of wind speed, but produced too much latent heat flux during low wind speed periods.  ERA15 had a drier boundary layer than later versions of the ECMWF model.  ERA15's sensible heat flux failed to increase during convective events, as the IMET buoy's

sensible heat flux did, and had a negative bias compared to the buoy.  ERA15's precipitation did not agree well with the precipitation observed at the IMET buoy.  Planton *et al.* (2000) found that ERA15, compared to *in situ* observations and independent climatologies, underestimated net short wave and overestimated latent heat flux in the tropics and overestimated net long wave in mid-latitudes.

Smith *et al.* (1999) compared NCEP1 near-surface meteorological and air-sea flux fields to high-quality observations collected by numerous international research vessels during the World Ocean Circulation Experiment (WOCE).  These observations were all recorded continuously by automated systems, thus enabling the data to undergo a higher level of quality control.  The data covers a wide range of conditions over the world's oceans, but do not typically repeatedly sample the same region.  The data are first height adjusted to reference levels of the reanalysis using Smith (1988).  Air-sea fluxes are then calculated, again using Smith (1988).  All meteorological and air-sea fluxes are then compared to co-located reanalysis values.  The RMS differences varied with latitude.  They found that the reanalysis atmospheric pressure values are too weak, most notably in the tropical regions.  Additionally, pressure extremes were underestimated. The winds are underestimated at all latitudes.  Air temperatures and humidity agree better and indicate no clear pattern of differences over varying parts of the globe.  For the fluxes, the reanalysis wind stresses matched the wind results, i.e. stresses were underestimated at all latitudes.  NCEP1's sensible and latent heat fluxes were surprisingly too large.  The RMS differences increased with latitude, but the biases in sensible heat flux were fairly uniform (5 W M$^{-2}$).  Reanalysis latent heat flux was too large (~10-30 W M$^{-2}$).  The bias is largest in the Northern Hemisphere, especially in the 20-40°N band.  Use of the Smith (1988) algorithm on NCEP1 near-surface fields led to considerably better agreement for latent and sensible heat fluxes with ship-based fluxes.

Renfrew *et al.* (2000) compared meteorological surface observations taken aboard the R/V Knorr during the Labrador Sea Deep Convection Experiment from Feb. 6 to Mar. 13, 1997 to operational analyses by ECMWF and reanalyses by NCEP1.  (The ECMWF operational system used in 1997 was very similar to the system used in ERA15.)  They found that the analyses reproduced the observed surface layer well, with ECMWF performing somewhat better, perhaps due to its higher resolution.  They did find discrepancies in sea surface temperature, due to the scarcity of satellite determined SSTs and the crude sea ice mask used in the models, and in relative humidity, where ECMWF was 10% higher than observed and NCEP1 25%.  The reanalyses did not include a marginal ice zone.

Renfrew *et al.* (2000) also calculated bulk estimates of surface momentum and heat fluxes from the ship observations, using the bulk flux algorithm of Smith (1988) with neutral exchange coefficients updated to those of DeCosmo *et al.* (1996).  They compared these fluxes to fluxes from ECMWF and NCEP1.  The time series of heat fluxes had correlations above 0.9; however, ECMWF had up to 30% more sensible and latent heat flux and NCEP1 up to 100% more sensible and 50% more latent heat flux during high heat flux events.  Averaged over the entire cruise, ECMWF's heat fluxes were 15% stronger than the estimate from the Knorr, within an estimated uncertainty of 15% in exchange coefficients (Garratt, 1992).  NCEP1 overestimated the mean sensible and latent heat fluxes by 50% and 30%.  Discrepancies in momentum fluxes between the reanalyses and the Knorr reflected mainly discrepancies in the 10-meter wind.  Renfrew *et al.* (2000) found that recalculating fluxes from model surface-layer data with the Smith/DeCosmo algorithm dramatically reduced the disagreement in fluxes.  They found that the roughness length formula used by NCEP1 (and NCEP2 as well) overestimated heat fluxes in cases of large air-sea temperature differences and high wind speed.  Zeng *et al.* (1998)'s bulk formula, a simplification of the TOGA-COARE algorithm (Fairall *et al.*, 1996a), was introduced in the NCEP operational model in Jan. 1998 and appears to correct these problems.

Josey (2000) compared surface fluxes from NCEP1 and ERA15 to those determined from five meteorological research buoys deployed in the north-east Atlantic between 18N-33N and 34W-22W during the Subduction Experiment between June 1991 and June 1993. The buoys used radiometers to measure radiative fluxes, while the COARE flux algorithm (Fairall *et al.*, 1996) determined sensible and latent heat fluxes from one minute mean meteorological measurements. Josey (2000) found that ERA15 and NCEP1 overestimated the mean evaporation for the buoy by 16 and 11 $Wm^{-2}$, underestimated net short wave by 14 and 22 $Wm^{-2}$, and underestimated the net downward heat flux into the ocean by 32 and 35 $Wm^{-2}$. Fields from the SOC flux dataset based on ship reports (Josey *et al.*, 1998) displayed better agreement with the estimates from the buoys.

Josey (2000) also calculated the implied ocean heat transport from ERA15 and NCEP1 climatologies for 1980-93 and found reasonable agreement with independent hydrographic estimates. Trenberth (1998) examined the heat budget of the atmosphere and ocean in the NCEP1 reanalysis. He adjusted the NCEP1 surface heat flux south of 30S to achieve balance in the surface energy budget over the ocean; the resulting ocean heat transports were consistent with independent estimates.

Trenberth *et al.* (2000a) calculated surface fluxes from the ERA15 and NCEP1 reanalyses using the residual method. A comparison of these derived surface fluxes with the surface fluxes calculated directly in the reanalyses and with the UWM COADS-based estimates found that all the estimates showed the same broad scale features. The reanalyses' surface fluxes agreed very well with the COADS estimates over the northern extratropical oceans, but all three were biased and were not suitable for determining ocean heat transports. The paper found "…no useful common signal in the tropics". The derived surface fluxes from the residual method were found to produce more reasonable ocean heat transports. The results implied that "…clouds are a primary source of problems in the models' fluxes, both at the surface and the TOA".

Trenberth *et al.* (2000b) compared troposphere temperatures measured by a satellite microwave sounder (MSU) to analyzed temperatures from the ERA15 and NCEP1 reanalyses. The NCEP and MSU temperatures agree fairly well. The ERA reanalyses has two discontinuities in the tropics in late 1986 and early 1989 and also displays "... further spurious interannual variability", indicating too much month to month tropical variability in the ERA15 reanalysis and reflecting at least partly problems with biases in satellite radiances.

Curry *et al.* (1999) compared satellite-derived surface fluxes to ERA15 over the tropical ocean for TOGA COARE. The satellite-derived stress showed short-lived, high-wind events that ERA15 did not. They also found that ERA15 surface net short wave flux exceeded the satellite-derived estimate during cloudy periods and was less during clear conditions. Daily values of latent heat flux and wind stress were substantially correlated; daily values of surface radiative fluxes had low correlations.

Wild (2000) compared radiative fluxes from the NCEP1, ERA15 and GEOS1 reanalyses to collocated observations of surface radiation over land (including island stations) from the Global Energy Balance Archive and satellite observations of top of the atmosphere (TOA) radiation from the Earth Radiation Budget Experiment. NCEP1 and GEOS1 overestimate the downward solar radiation at the surface due to a lack of absorption in the atmosphere, especially at low latitudes and even in cloud-free regions; ERA15 shows good agreement with observations. All the reanalyses underestimate aerosol absorption and show little difference in vertically integrated water vapour. NCEP1's excessive downward solar radiation is offset by too high surface albedo. Wild *et al.* (1998) found that ERA15 underestimated the downward long wave flux at the surface by 5-10 $Wm^{-2}$ compared to surface observations.

*11.4.3  Polar regions*

        At the 2nd International Conference on Reanalyses in 1999, a number of papers identified shortcomings in the reanalyses in the polar regions, including overly simplistic representations of sea-ice, albedo parameterisation, treatment of snow cover and clouds in polar regions.  The shortage of data over Antarctica in the earlier years of the reanalyses compromises the reliability of trends or changes in the reanalyses.  Data assimilation systems often have problems assimilating isolated observations, since drifts in the "first guess" forecast in the absence of data can cause isolated observations to be rejected.

        In NCEP1 summertime precipitation in the Arctic is unrealistic, there is insufficient cloud cover, solar radiative fluxes are too large and distortions in the moisture fields are evident. In ERA15 there is a marked two-metre temperature bias and wrong topographic heights over Greenland and Antarctica, with particular consequences notable as a result of an error in the elevation of the Vostok station.  In ERA40 a full range of ice concentrations will be represented and perhaps variable ice thickness.  An improved blended ice/sea surface temperature field will be used, sea-ice thermal characteristics will be better treated, there will be a refined treatment of snow cover and much more accurate topographic data sets will be used together with the innate advantage of higher resolution in representing topography.  NCEP2 corrected the valley snow problem and other mistakes in NCEP1, has more recent physical parameterisations than NCEP1 and has a better treatment of soil moisture that uses observed precipitation (Kanamitsu et al. , 2000).

*11.4.4  Ocean surface energy balance*

        Da Silva *et al.* (1994) (University of Wisconsin at Milwaukee (UWM)) carefully calculated oceanic heat fluxes from several decades of carefully corrected COADS (Comprehensive Ocean-Atmosphere Data Set) ship observations.  The result did not produce a reasonable global heat balance, reflecting at least in part the scarcity of COADS data over much of the ocean outside the mid-latitude Northern Hemisphere.  Other COADS-based air-sea flux estimates, such as the climatology calculated by the Southampton Oceanography Centre (Josey *et al.*, 1998, 1999), display similar biases.  To obtain a reasonable heat balance, da Silva *et al.* (1994) mathematically tuned the fluxes, effectively increasing the evaporation by 15% and decreasing the net short wave (NSW) by approximately 7% globally.  They changed the sensible heat and net long wave (NLW) much less.  The tuning was applied uniformly over the globe and not predominately where ship reports are least abundant.

Table 11.4.1: Global mean ocean surface energy balance in Wm[-2] estimated from COADS data by da Silva *et al.* (1994) (without tuning), from the four reanalyses and from satellite-based estimates (SRB)

|                | UWM   | ERA15 | GEOS1 | NCEP1 | NCEP2 | SRB   |
|----------------|-------|-------|-------|-------|-------|-------|
| Sensible heat  | 10.1  | 9.8   | 10.5  | 10.9  | 5.4   |       |
| Latent heat    | 88    | 103.4 | 79.5  | 92.7  | 104   |       |
| Net short-wave | 170.4 | 160.5 | 197.8 | 165.9 | 167.2 | 173.4 |
| Net long-wave  | 49.2  | 50.5  | 68.0  | 56.4  | 50.6  | 41.9  |
| Net heat flux  | 23.3  | -3.7  | 40.0  | 5.8   | 7.2   |       |

        Table 11.4.1 shows global mean components of the ocean surface energy balance for the four reanalyses for 1981-92.  It also displays da Silva *et al.* (1994)'s untuned air-sea fluxes

averaged over 1981-92 (UWM) and satellite-based estimates of surface NSW by Darnell *et al.* (1992) and net long-wave radiation (NLW) by Gupta *et al.* (1992) averaged over July 1983-June 1991. These satellite-based estimates from the Langley Surface Radiation Budget (SRB) Project (see section 11.3.3C) are derived from satellite observations of TOA radiation, International Satellite Cloud Climatology Project (ISCCP) cloud estimates and radiative transfer codes.

The ERA15 fluxes shown are from twice-daily 12-24 hr forecasts; GEOS1, NCEP1 and NCEP2 fluxes are from the four times daily 0-6 hr forecasts used as the first guess or background field in the analysis cycle. The ERA15 hydrological cycle intensifies ("spins up") between the 0-6 hr and 12-24 hr forecasts; the global hydrological cycle and surface energy budget are in better balance in the 12-24 hr ERA15 forecasts than in the 0-6 hr forecasts. The system used in the NCEP1 reanalysis appears to have less global "spin-up" than ERA15. ECMWF recommends the use of 12-24 hr fluxes from ERA15.

ERA15's and NCEP2's global evaporation disagree the most with the untuned UWM estimate, but agree the best with the tuned estimate; NCEP2 has the least sensible heat flux. For NSW, the UWM untuned estimate displays the best agreement with the satellite estimate; GEOS1 displays considerable higher radiative fluxes than the other estimates. NCEP1, NCEP2 and ERA15 are nearly in balance over the global ocean; GEOS1 and untuned UWM produce a substantial net heat flux (NHF) into the ocean.

Kiehl and Trenberth (1997) found that climatological estimates of global mean surface NSW and NLW varied by 20 $Wm^{-2}$. Estimates of global mean surface sensible and latent heat varied by 11 $Wm^{-2}$. Section 11.3.3 implies that the SRB surface NSW may have a positive bias. Satellite-based estimates of surface NLW display more qualitative disagreement with each other than do satellite-based estimates of surface NSW (White, 1996a). Gupta *et al.* (1992)'s global mean estimate for NLW is lower than most of the estimates. The global mean net surface radiation implied by Darnell *et al.* (1992)'s and Gupta (1992)'s estimates is larger than most estimates examined by Kiehl and Trenberth (1997) and would require substantially higher sensible and/or latent heat fluxes for balance than those found in UWM and the reanalyses.

*11.4.5 Evaporation*

Figure 11.4.1 displays the zonal mean latent heat flux over the ocean averaged over 1981-92. Both the original UWM and the tuned UWM estimates are shown. The GEOS1 reanalysis has the lowest evaporation of all, while ERA15 shows good agreement with the tuned UWM estimate and NCEP1 lies between the original and tuned UWM estimate. NCEP2 has the highest evaporation in the subtropics. The large differences between the original and tuned UWM estimates indicate a significant uncertainty in the UWM estimate (and in COADS-based estimates in general). Significant differences between UWM and the reanalyses can be seen near the North Pole. The reanalyses show more evaporation in late spring and early summer and less the rest of the year. In the polar regions ship reports are more abundant during summer than winter, perhaps biasing the UWM estimates. The reanalysis estimates over the oceans used here include fluxes over sea ice as well as over the open ocean.

Figure 11.4.2(a) shows the geographical distribution of the original UWM estimate of latent heat flux. ERA15 (Figure 11.4.2(b)) shows more evaporation nearly everywhere, with maximum differences in the northern subtropical oceans and slightly south of the equator, particularly in the southern winter, in the mid-Pacific and western Atlantic. All the reanalyses evaporate less than UWM in the Far East equatorial Pacific. GEOS1 (Figure 11.4.2(c)) has less evaporation over the Gulf Stream and Kuroshio, especially in the fall and early winter, and in the eastern tropical Pacific. All four reanalyses display more evaporation than UWM near 60S. NCEP1 (Figure 11.4.2(d)) has more evaporation in the subtropics but generally less along the equator. Like ERA15, NCEP2 (Figure 11.4.2(e)) shows more evaporation than UWM nearly

everywhere.  ERA15, NCEP1 and NCEP2 appear to have a more tightly defined Gulf Stream than UWM, perhaps reflecting differences in spatial resolution and smoothing.

Figure 11.4.3 shows the temporal correlation of UWM's monthly mean evaporation with evaporation from NCEP1 for the years 1981-92.  Correlations are highest where ship reports (Figure 11.4.4) are most abundant (such as over the Northern Hemisphere oceans between 20 and 60N, and off the western coast of Africa).  Correlations are near zero or negative near the poles.  Low correlations tend to occur in regions of few ship reports, but can also occur in regions of low variability such as the South Atlantic.
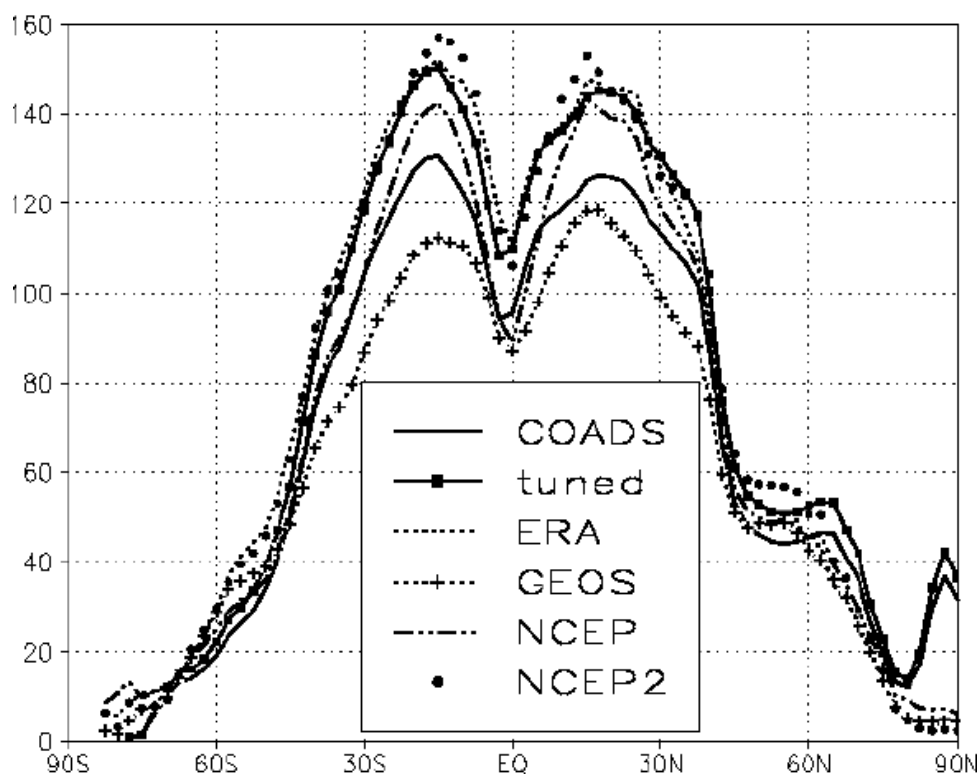


Figure 11.4.1 Zonal mean latent heat flux over the oceans for 1981-92 in Wm$^{-2}$.

Figure 11.4.5 compares the zonal averaged correlations with UWM estimates of evaporation for all four reanalyses for monthly mean values for 1981-92 (Figure 11.4.5(a)), for the monthly mean annual cycles averaged over 1981-92 (Figure 11.4.5(b)) and for monthly anomalies from their own climatologies for 1981-92 (Figure 11.4.5(c)).  The reanalyses all show very similar levels and patterns of agreement with UWM.  ERA15's climatology shows the best correlation with the UWM estimate, while NCEP1 and NCEP2's anomalies agree more with UWM than do ERA15 or GEOS1.  GEOS1 shows somewhat less agreement with UWM than the other three reanalyses.  In Figure 11.4.5(b) correlations are much higher in the lower latitudes of the Southern Hemisphere than in Figure 11.4.5(a) or Figure 11.4.5(c), exceeding 0.6 from 65N to 40S.  Correlations of anomalies in Figure 11.4.5(c) exceed 0.6 only from 25N to 55N.  NCEP2's correlations with UWM are slightly higher than NCEP1 for the climatological annual cycle and slightly lower than NCEP1 for anomalies.

Fig.
11.4.2(a).
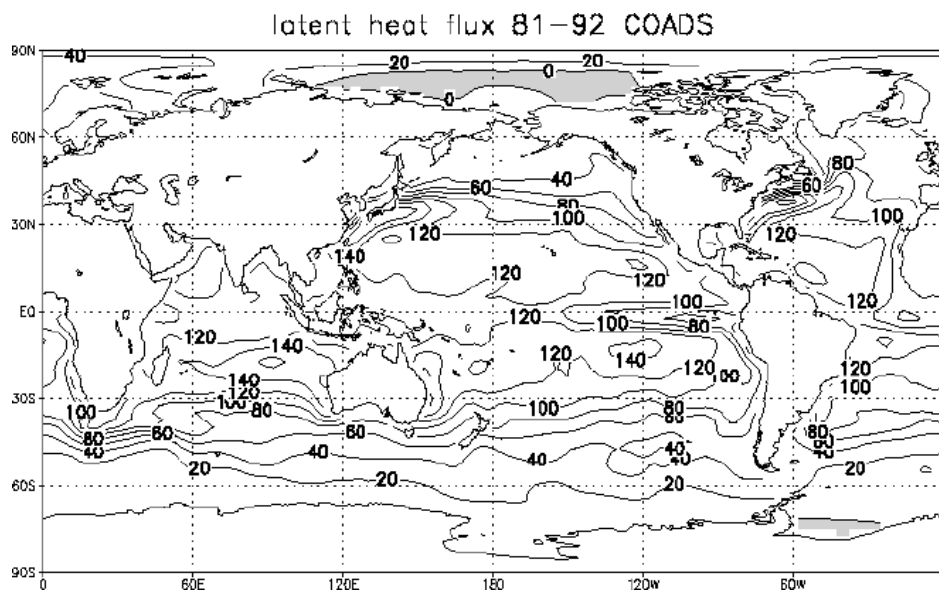
Fig.
11.4.2(b).
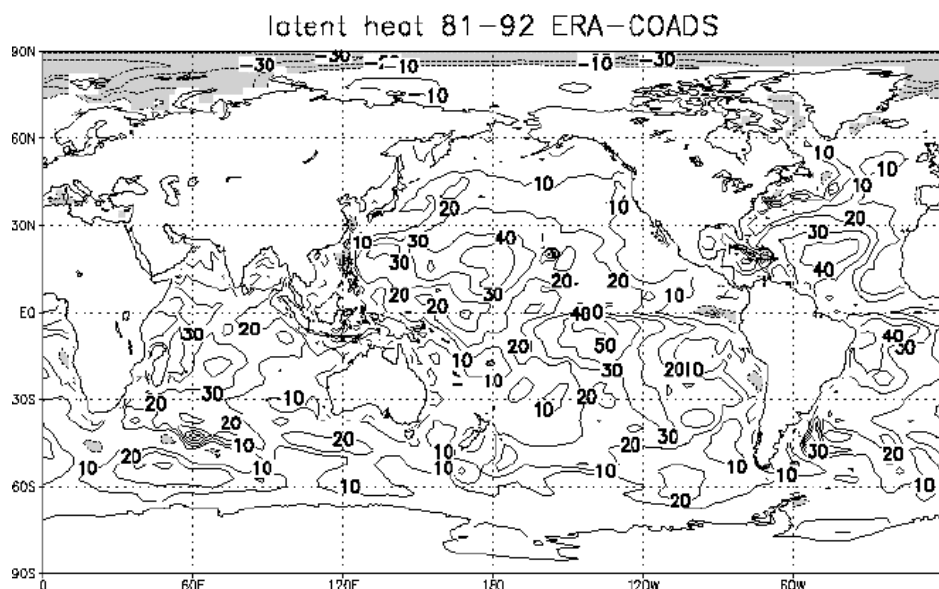
Figure 11.4.2:   (a) Latent heat flux from the original COADS estimate (UWM) by da Silva *et al.* (1994) averaged over 1981-92.  Contour interval 20 Wm$^{-2}$, negative values shaded

(b) Difference in latent heat flux ERA15 minus UWM averaged over 1981-92. Contour interval 10 Wm$^{-2}$, zero omitted, negative values shaded.

(c) As (b) but for GEOS1 minus UWM.

(d) As (b) but for NCEP1 minus UWM.

(e) As (b) but for NCEP2 minus UWM.

latent heat 81-92 GEOS-COADS

Fig.
11.4.2(c).



latent heat 81-92 NCEP-COADS

Fig.
11.4.2(d).



latent heat 81-92 NCEP2-COADS
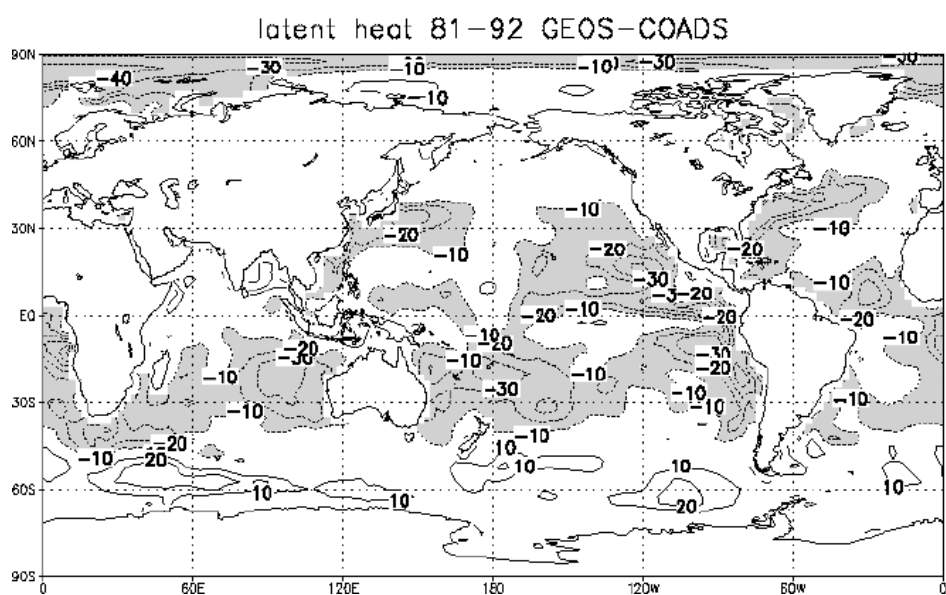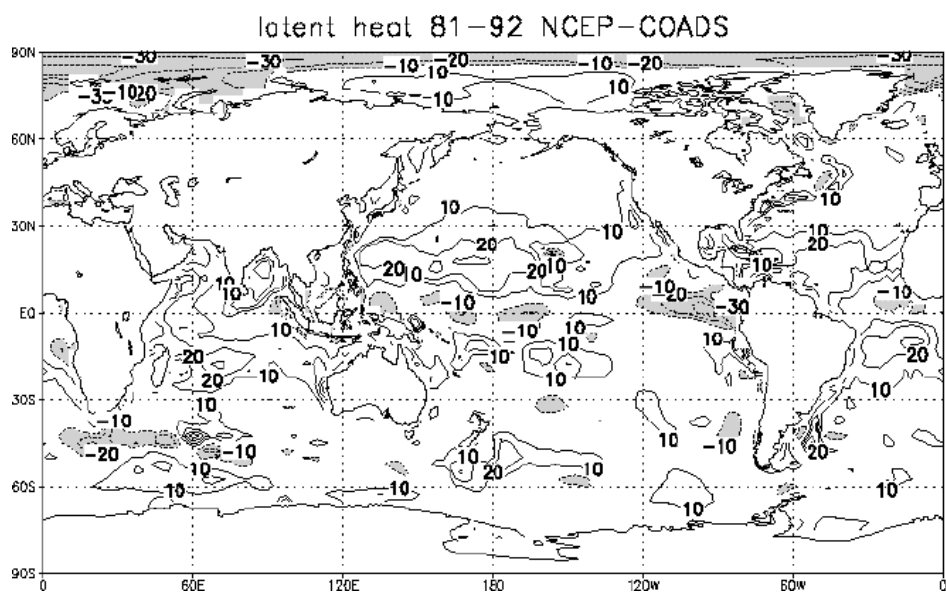
Fig.
11.4.2(e).
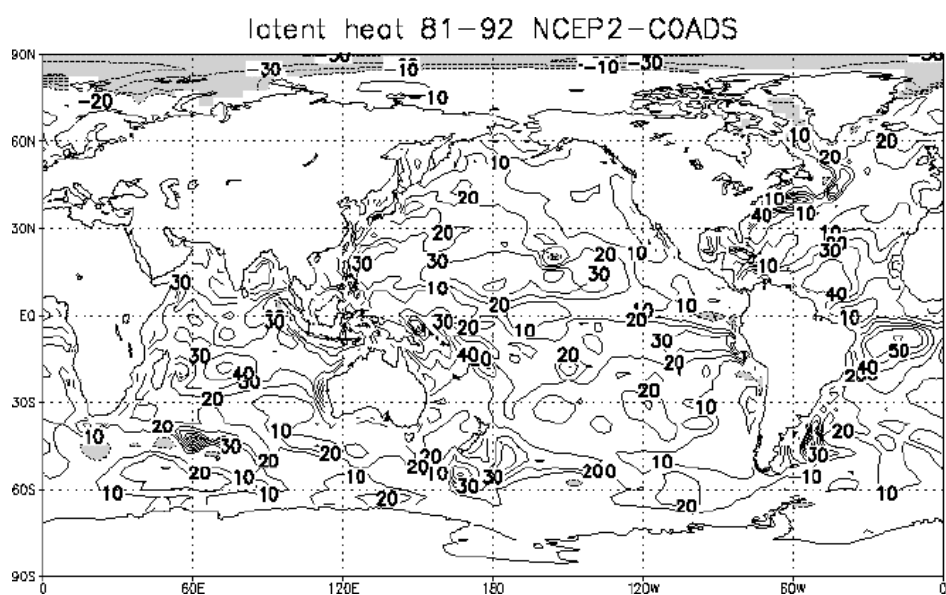
The reanalyses include other sources of data over the ocean than ship reports and can interpolate and extrapolate other sources of data from land, from other levels in the atmosphere and from previous analyses. Operational forecasts display considerable skill in the Southern Hemisphere, indicating that modern data assimilation systems produce accurate daily analyses of the Southern Hemisphere. Anomalies in evaporation from the four reanalyses correlate well with each other over the oceans except near the poles and the equator. The differences in correlations between COADS data rich and data poor regions evident in Figure 11.4.3 is not nearly so evident in correlations of the reanalyses with each other or with independent estimates of fluxes and precipitation based on satellite data (see below). This suggests that the asymmetry in correlation is due to the relative lack of ship observations outside 20-60N and suggests that the usefulness of COADS in defining inter annual variability may be largely limited to the Northern Hemisphere mid-latitudes and a few other regions. Figure 11.4.5(b) implies, however, that COADS estimates of evaporation are useful in defining the climatological annual cycle in the lower latitudes of the Southern Hemisphere.
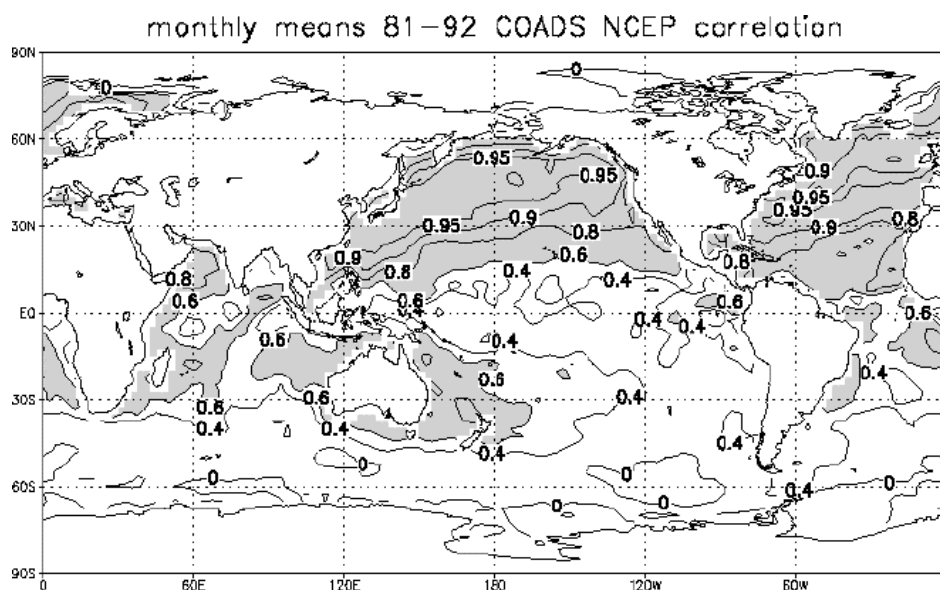


Figure 11.4.3    Correlation of monthly mean evaporation from UWM and from NCEP1 for 1981-92. Contours 0, .4, .6, .8, .9, and .95. Values over 0.6 are shaded.
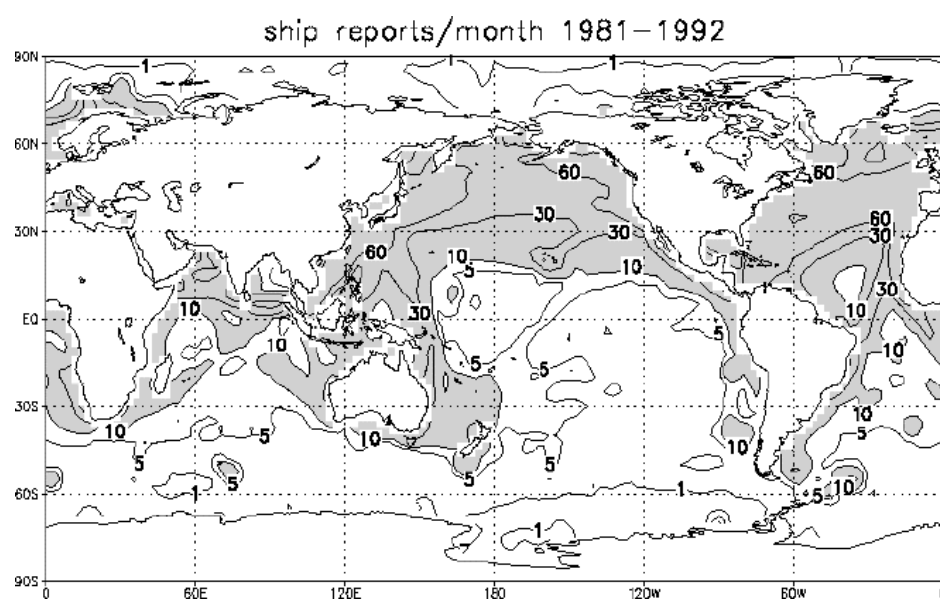


Figure 11.4.4    Average number of ship reports available to NCEP1/month/2.5° box for 1981-92. A nine-point smoother was applied to the field. Values over 10 are shaded.

Figure 11.4.5(a).
Zonal mean correlation between the reanalyses and UWM of mean latent heat flux over the oceans for individual months during the period 1981-92.
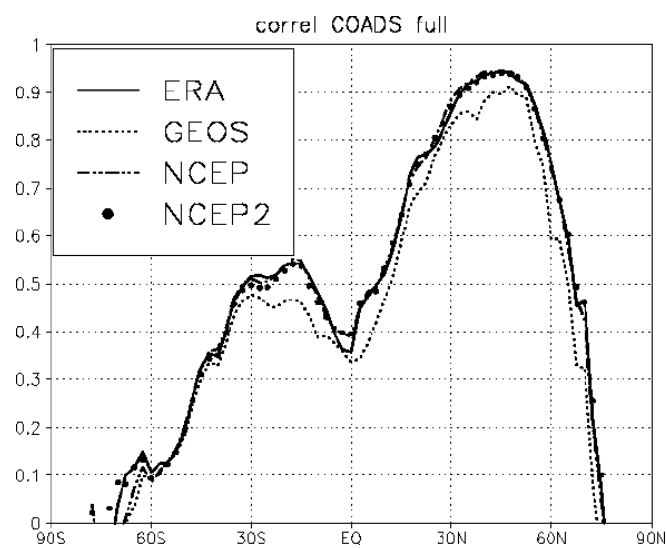


Figure 11.4.5(b).
As in (a), but for climatological monthly means averaged over 1981-92.
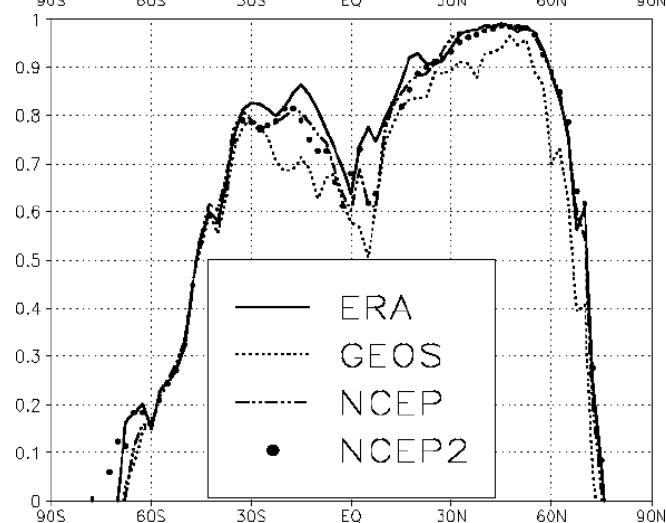


Figure 11.4.5(c).
As in (a), but for monthly mean anomalies from each estimate's climatology for 1981-92.
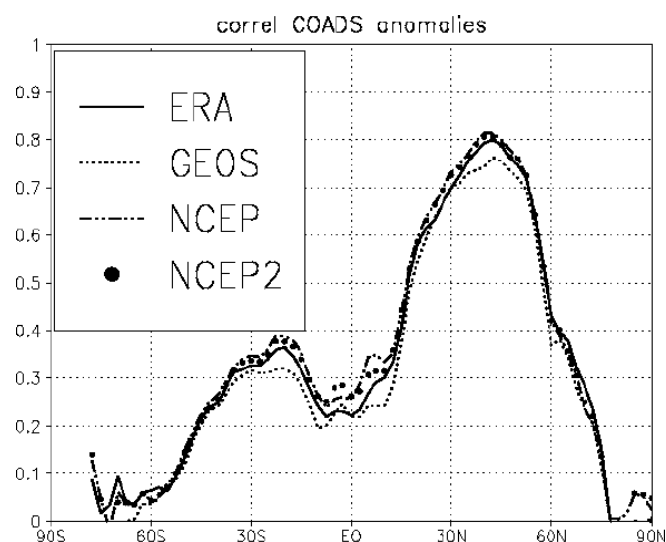
Figure 11.4.6 shows the root-mean-square (RMS) differences between the reanalyses and UWM for monthly mean values (Figure 11.4.6(a)), for the monthly mean annual cycle averaged over 1981-92 (Figure 11.4.6(b)) and for monthly anomalies from the climatology (Figure 11.4.6(c)). The RMS differences in Figure 11.4.6(a) exceed 20 Wm$^{-2}$ except between

30 and 60N where ship reports are most abundant and near Antarctica where evaporation is low. NCEP2 has the largest RMS differences from UWM, reflecting the largest month-to-month variability (nearly 30% more than UWM between 20 and 60N) (see Figure 11.4.7 below). GEOS1's anomalies are the least different from UWM estimates, reflecting lower month–to–month variability than the other reanalyses, while NCEP1's annual cycle generally is least different from UWM. GEOS1 has the weakest annual cycle and the weakest anomalies of the four reanalyses, and a weaker annual cycle than UWM (10% weaker between 20 and 60N). ERA15, NCEP1 and NCEP2 generally have a stronger annual cycle than UWM and their anomalies tend to be larger than UWM in the Northern Hemisphere mid-latitudes. Note that the largest differences in the anomalies occur in the Southern Hemisphere mid-latitudes and are twice as large as differences in the Northern Hemisphere mid-latitudes.

Figure 11.4.6a.
Zonal mean root-mean square (RMS) difference in monthly mean latent heat flux over the oceans between the reanalyses and UWM for 1981-92 in Wm$^{-2}$.
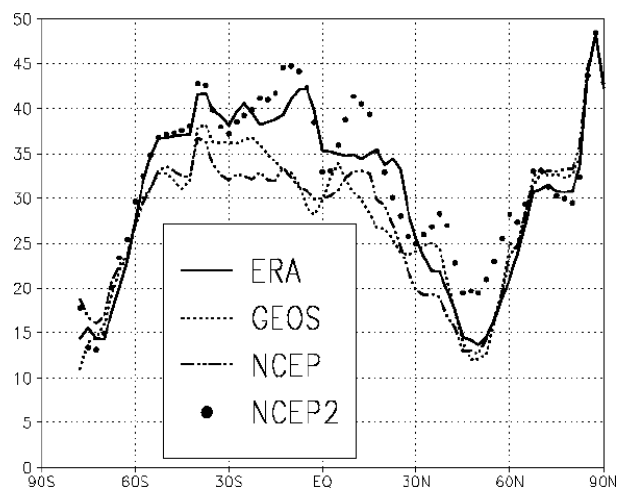
Figure 11.4.6b)
As in (a), but for climatological monthly means averaged over 1981-92.
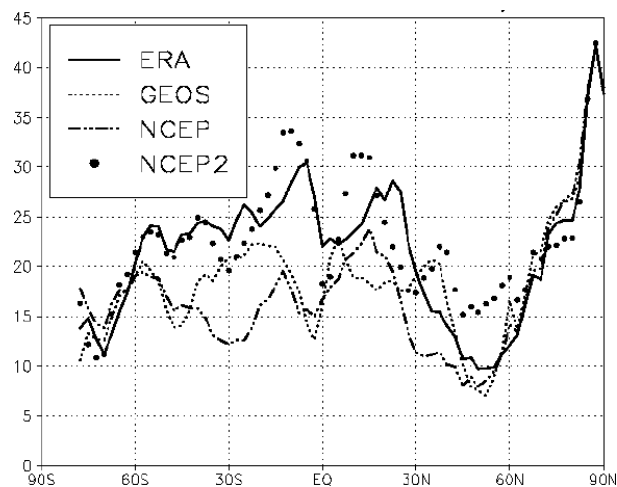
Figure 11.4.6c.   As in a), but for monthly mean anomalies from each estimate's 1981-92 climatology.
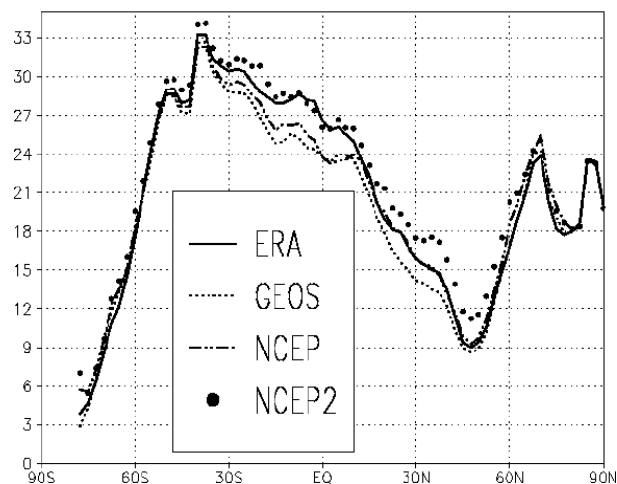
Figure 11.4.7(a) compares the standard deviation averaged over 20-60N of monthly evaporation from UWM and the reanalyses for the period 1981-92. NCEP2 has the largest month-to-month variability while GEOS1 has the lowest variability of the reanalyses. The RMS difference averaged over 20-60N of the reanalyses from UWM is shown in Figure 11.4.7(b). By this measure NCEP2 is most different from UWM and GEOS1's anomalies are closest to UWM. However, if one normalises the RMS difference of a reanalysis from UWM by dividing it by the standard deviation of evaporation in that reanalysis, as is shown in Figure 11.4.7(c), GEOS1 now appears the most different from UWM. NCEP1 shows the least normalised difference from UWM.

Figure 11.4.7(a)

Standard deviation averaged over 20-60N of monthly mean latent heat release over the ocean in Wm$^{-2}$. Full values calculated from monthly means for 1981-92, annual from climatological monthly mean annual cycles averaged over 1981-92, and anomalies from departures of monthly means from the climatological annual cycle.
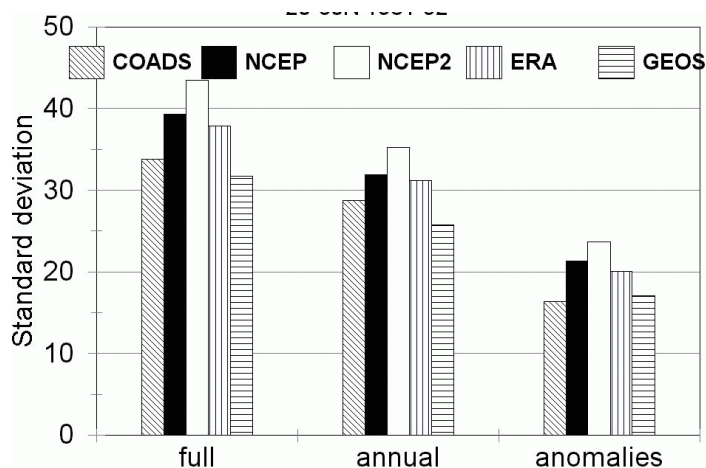


Figure 11.4.7(b)

RMS difference averaged over 20-60N of monthly mean latent heat in the reanalyses from UWM in Wm$^{-2}$.
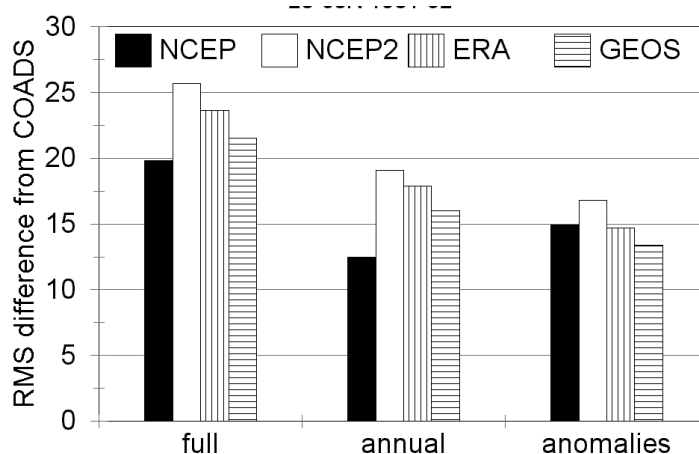


Figure 11.4.7(c)

Ratio of the RMS difference from UWM to the standard deviation for each of the reanalyses.
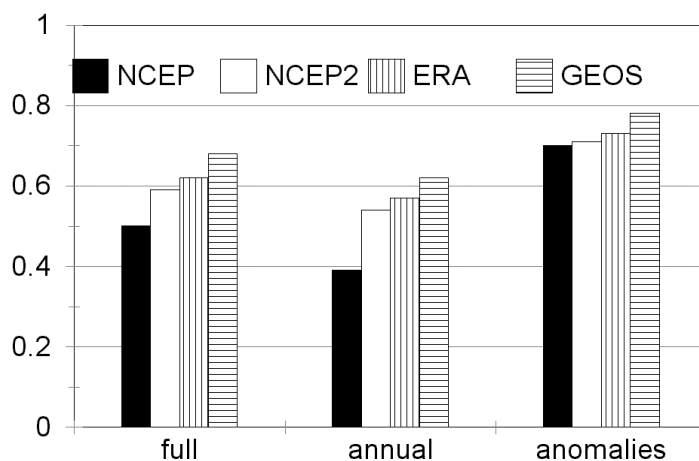
Figures 11.4.8(a) and 11.4.8(b) compare anomalies in evaporation from the four reanalyses over the Gulf Stream (a data-rich area) and the central equatorial Pacific (a data-poor area). Figure 11.4.8(a) shows that anomalies in the four reanalyses show very good agreement with each other over the Gulf Stream, even though GEOS1 (Figure 11.4.2(c)) has less mean evaporation there than the other reanalyses (Figures 11.4.2 (b), (d), (e)). Over the central equatorial Pacific anomalies from the four reanalyses (Figure 11.4.8(b)) show less agreement than over the Gulf Stream. ERA15 displays significantly lower evaporation in Figure 11.4.8(b) after 1986 than before, a pattern not evident in the other reanalyses. A similar discontinuity has been observed in other fields in the ERA15 reanalysis (Stendel and Arpe, 1997). This may reflect an interaction between the ERA15 analysis/forecast system and TOVS radiances in response to a sudden, large change in the MSU channels in November 1986 (Fiorino, 2000). ERA15 was the only reanalysis that used satellite radiances rather than temperature soundings derived from satellite radiances.



Figure 11.4.8 (a):
Time series of latent heat flux anomalies (Wm$^{-2}$) from the four reanalyses for 1981-92 for a Gulf Stream Region: 35-40N, 65-60W.
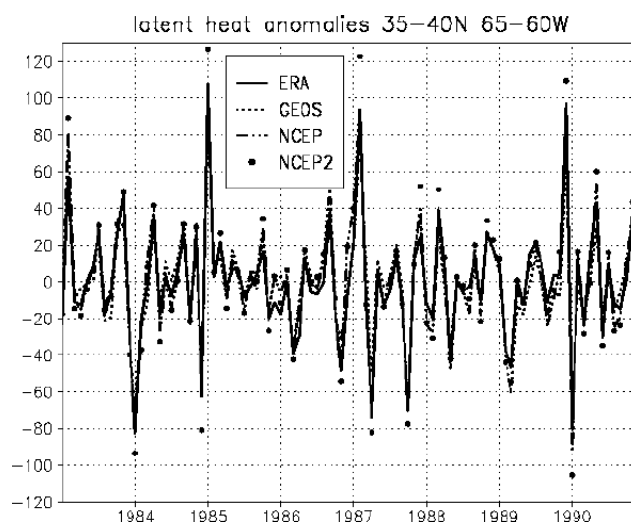


Figure 11.4.8 (b):
As (a) but for the central equatorial Pacific: 2.5S-2.5N, 177.5E-177.5W.
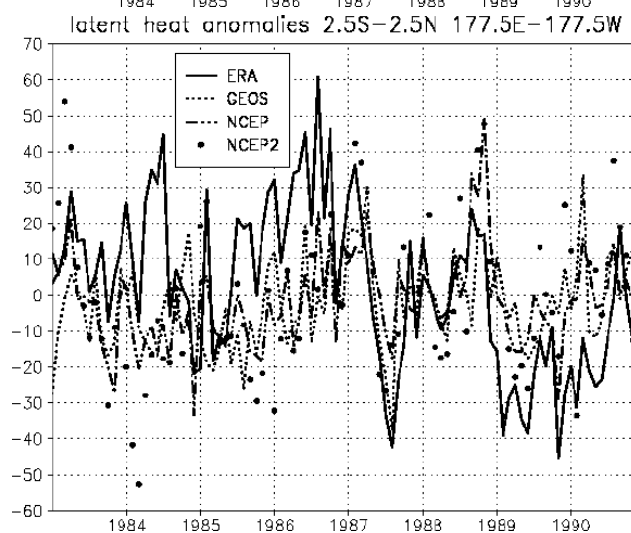
### 11.4.6  Sensible heat flux

Figure 11.4.9 compares the zonal mean sensible heat flux over the ocean from UWM and the four reanalyses for the years 1981-92. The reanalyses are quite different from UWM over the poles, but agree with UWM fairly well in the best-sampled region between 30 and 60N. Near the North Pole UWM shows a substantial upward sensible heat flux except in summer while the reanalyses show downward fluxes most of the year. NCEP1 has the strongest sensible

heat flux. ERA15, GEOS1 and NCEP1 have more sensible heat flux than UWM near 60S, particularly in winter, and less than UWM nearer Antarctica where GEOS-1 and NCEP1 show sensible heat fluxes into the ocean. NCEP2 has the least upward sensible heat flux and has the strongest downward flux in higher latitudes.



Figure 11.4.9. Zonal mean sensible heat flux over the oceans for 1981-92 in Wm$^{-2}$.
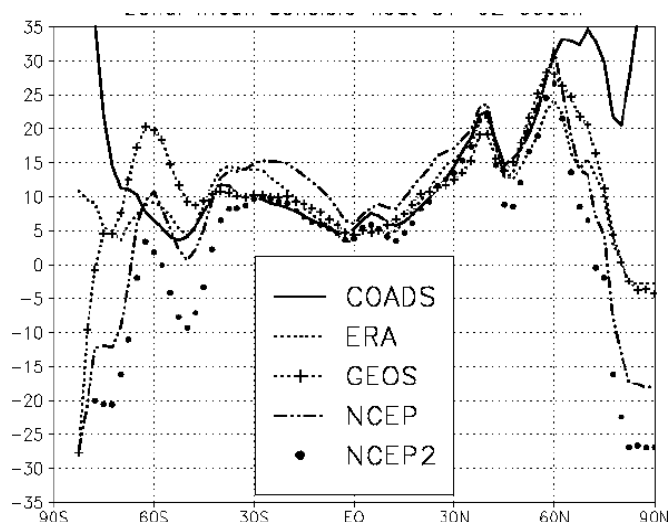
The 12-year mean regional distribution of sensible heat flux from UWM is shown in Figure 11.4.10a. ERA15 (Figure 11.4.10b) and especially GEOS1 (Figure 11.4.10c) have less upward sensible heat flux than UWM over the Kuroshio and Gulf Stream (especially in late fall and winter), where NCEP1 (Figure11.4.10d) has more than UWM as well as more upward flux in the subtropical oceans. NCEP1 has somewhat more sensible heat flux into the ocean in the northern mid-latitudes in summer than UWM. ERA15, GEOS1 and NCEP1 exceed UWM estimates in the eastern subtropical oceans. Large differences appear near Antarctica and in the Arctic Ocean. NCEP2 (Figure 11.4.10e) has more upward sensible heat flux than UWM over the Gulf Stream and near Japan, but less than UWM elsewhere in the North Pacific and in the Southern Hemisphere mid-latitudes.

Zonally averaged correlations of sensible heat from the reanalyses with UWM estimates (not shown) display similar patterns and values to Figure 11.4.5. The reanalyses display less agreement with UWM in the tropics than for evaporation, reflecting small values of sensible heat flux in the tropics. GEOS1 displays less agreement with UWM than the other reanalyses do. ERA15 and NCEP2 tend to show the best agreement with UWM, slightly better than NCEP1.

Figure 11.4.11 shows the root-mean-square (RMS) differences between the reanalyses and UWM for monthly mean values (Figure 11.4.11a) and for monthly anomalies from the climatology (Figure 11.4.11b). ERA15 generally shows the smallest differences from UWM. NCEP2 has the largest RMS differences, reflecting the largest month-to-month variability. Differences in the climatologies between the reanalyses and UWM are less than 10 Wm$^{-2}$ between 50N and 50S. The largest differences between UWM and the reanalyses occur near 60° in both hemispheres, where sensible heat fluxes exhibit considerable variability. However, sensible heat fluxes also exhibit more variability between 30 and 45N than elsewhere outside the polar regions and display relatively small differences there, indicating, as do the correlations, better agreement between UWM and the reanalyses there than elsewhere. GEOS1 shows the least variability in sensible heat flux of the five estimates; NCEP1 and NCEP2 display more variability than the UWM estimate between 20 and 60N. ERA15's climatological annual cycle displays the least normalised RMS difference from UWM between 20 and 60N, where NCEP1's anomalies have the smallest normalised RMS difference from UWM anomalies. NCEP2 displays slightly larger normalised RMS differences than NCEP1 or ERA; GEOS1 has the largest.

Figure
11.4.10(a)



sensible heat flux 81—92 COADS

Figure
11.4.10(b)



sensible heat 81—92 ERA-COADS

Figure
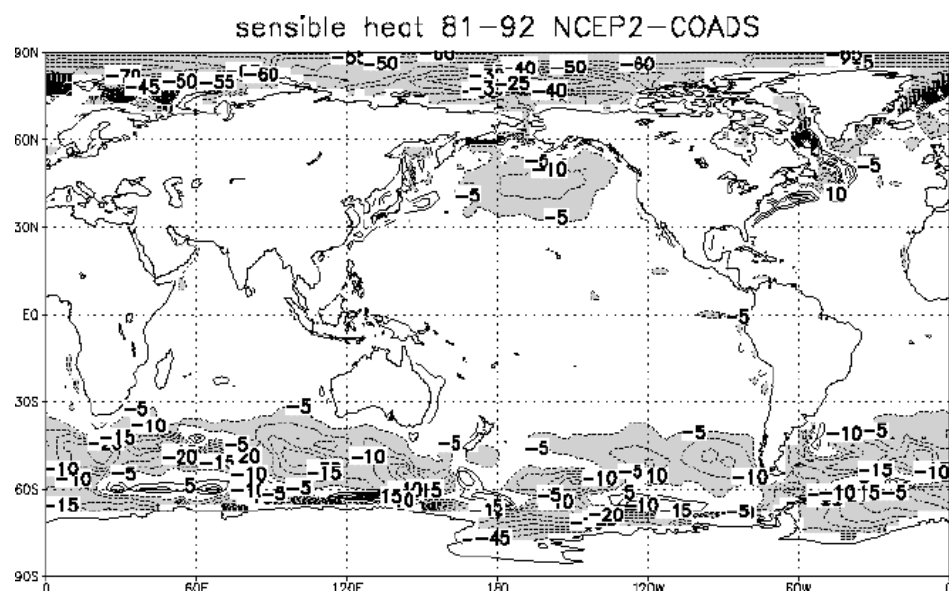11.4.10(c)



sensible heat 81—92 GEOS-COADS
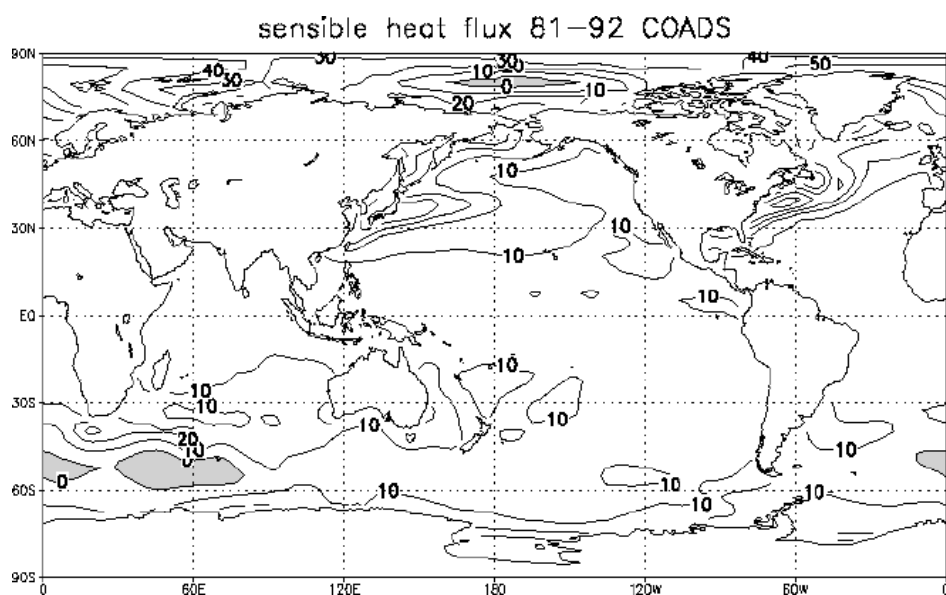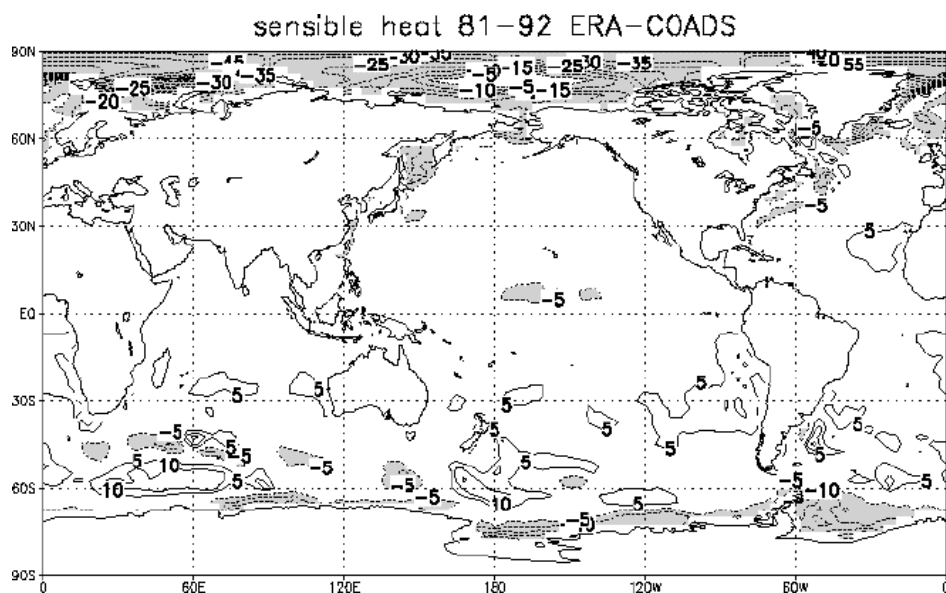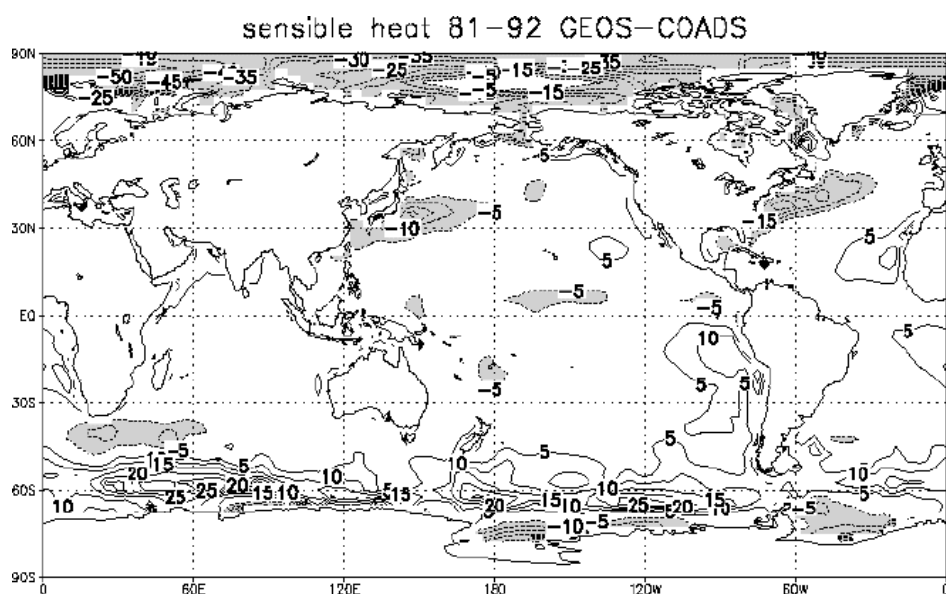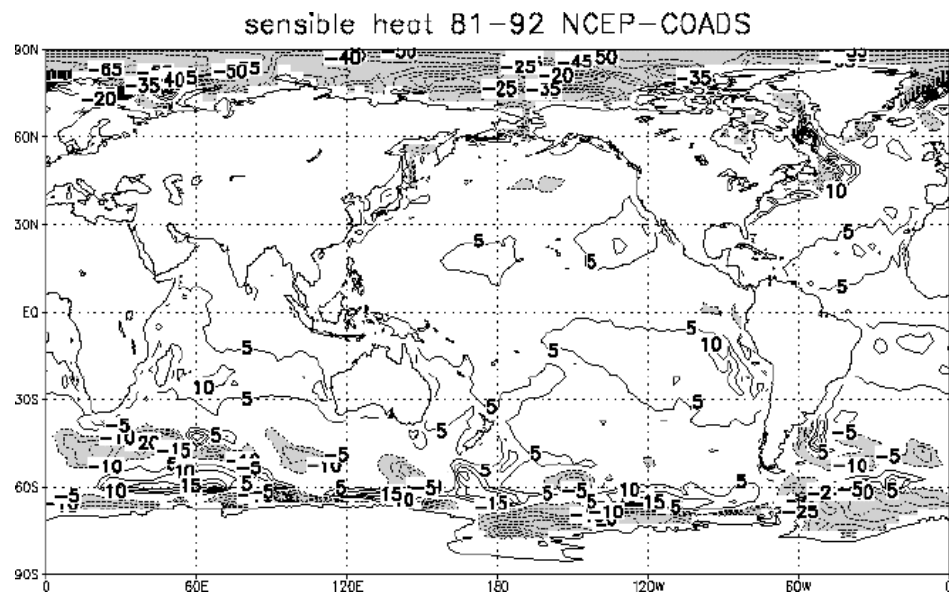
Figure
11.4.10(d)



Figure
11.4.10(e)



Figure 11.4.10:  (a) Sensible heat flux (Wm$^{-2}$) from UWM averaged over 1981-92, negative
              values shaded.
              (b) Difference in sensible heat flux ERA15 minus UWM.  Contour interval
              5Wm$^{-2}$, zero omitted, negative values shaded.
              (c) As (b) but for GEOS1 minus UWM.
              (d) As (b) but for NCEP minus UWM.
              (e) As (b) but for NCEP2 minus UWM.

### 11.4.7  Net short-wave

        Here both UWM and reanalysis estimates of surface net short-wave (NSW) radiation
are compared to Darnell *et al.* (1992)'s satellite-based (SRB) estimates of NSW. The ERA15
reanalysis used a prognostic cloud parameterisation tuned to ISCCP clouds, the clouds used in
calculating the SRB estimate of surface NSW. The NCEP reanalyses used a diagnostic cloud

scheme tuned to Air Force nephanalyses, which produce lower cloud amounts than ISCCP estimates.

It has been suggested that satellite estimates of surface NSW may be more reliable than other global estimates of surface NSW, although satellite estimates of surface NSW can differ substantially from point surface measurements of NSW (White, 1996a). Figure 11.4.12 shows the zonal mean surface NSW over ocean for July 1983-June 1991 from the four reanalyses, the untuned UWM estimate by da Silva *et al.* (1994) and SRB.



Figure 11.4.11(a)
 RMS differences in monthly mean sensible heat flux over the oceans between the reanalyses and UWM for 1981-92 in Wm$^{-2}$.
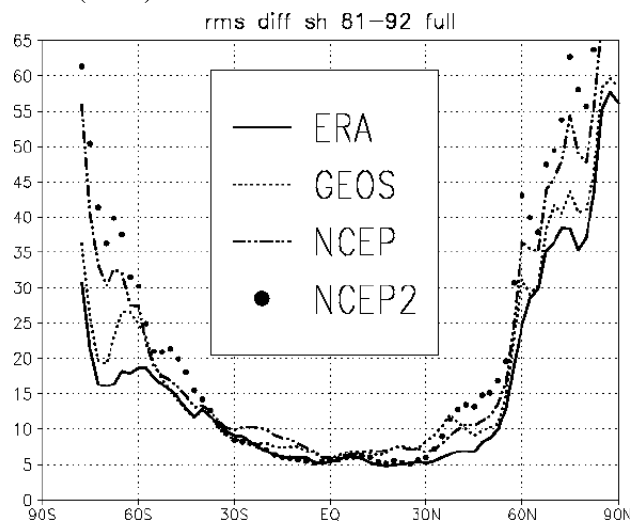


Figure 11.4.11(b) As in a) but for monthly mean anomalies
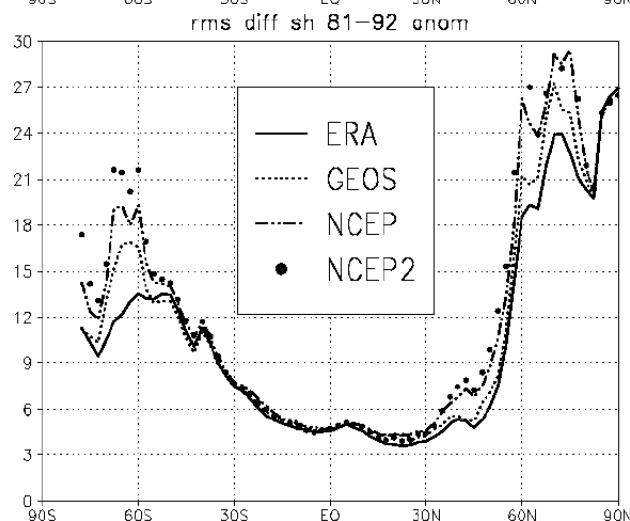


Figure 11.4.12 Zonal mean surface net short wave radiation over the oceans for 1981-92 in Wm$^{-2}$.
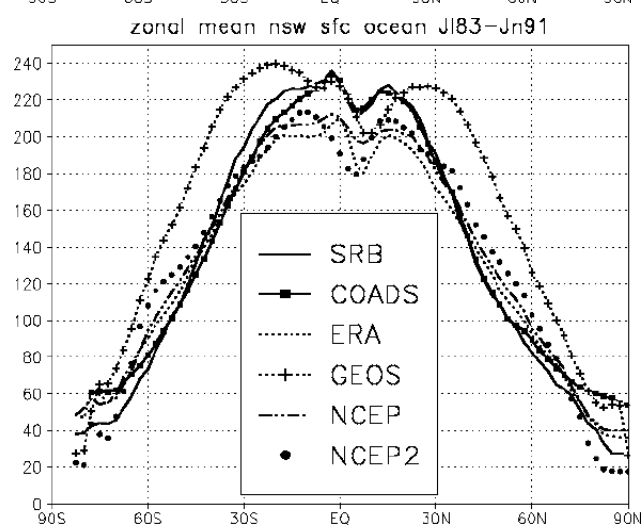
Figure 11.4.13(a) shows the regional distribution of SRB NSW. GEOS1 (Figure 11.4.13(d)) has considerable more NSW than SRB poleward of 30$^o$ and in the eastern subtropical oceans, but less in the western tropical Pacific. GEOS1 has very strong NSW in the eastern subtropical oceans where other estimates show relative minimums due to the presence of low-level stratus clouds. NCEP1 (Figure 11.4.13(e)), NCEP2 (Figure 11.4.13(f)) and ERA15 (Figure 11.4.13(c)) have less in the tropics and more in higher latitudes than SRB; NCEP2 and ERA15 appear to have slightly larger biases than NCEP1 in the tropics and NCEP2 has a larger positive bias in higher latitudes than NCEP1 or ERA15. UWM (Figure 11.4.13(b)) shows the best agreement with SRB in the tropics, in spite of the simplicity of the UWM parameterisation of NSW. In higher latitudes UWM and the reanalyses tend to have more NSW in summer than the SRB estimate. The time-mean differences of the reanalyses' TOA NSW from the Earth Radiation Budget Experiment (ERBE) satellite estimate are similar to their differences from the SRB estimate of surface NSW. Since satellites observe TOA NSW directly, this similarity lends credence to the reliability of the SRB estimate of surface NSW.

The time-mean NSW from ERA15 (Figure 11.4.14(c)) and GEOS1 (Figure 11.4.14(d)) shows no evidence of the influence of low-level stratus clouds on the surface NSW in regions such as the ocean off Baja California in the Northern Hemisphere summer; NCEP1's NSW (Figure 11.4.14(e)) does show the influence of low-level stratus cloud. Over the rest of the Pacific NCEP1 and ERA15 clearly underestimate surface NSW; GEOS1 overestimates surface NSW. NCEP2 (Figure 11.4.14(f)) displays less evidence of stratus clouds off Baja California than NCEP1, but does display higher NSW than NCEP1 or ERA15 (although still less than SRB) elsewhere in the Pacific. NCEP2 changed the parameterisation of low-level stratus clouds to require a higher relative humidity threshold than in NCEP1. The UWM summertime surface NSW (Figure 11.4.14(b)) resembles SRB (Figure 11.4.14(a)) much more than the reanalyses do.

NCEP1's surface NSW benefited from offsetting mistakes. Its ocean surface albedo was too high, and it had too much downward short wave radiation at the surface (Wild, 2000). Its cloud albedo was too high and it had fewer clouds than other reanalyses. NCEP2 corrected the ocean surface albedo and had more cloudiness. Figure 11.4.15 displays the global mean downward surface short wave for January and July averaged over 8 years. ERA15 and NCEP2 agree with the SRB estimate; NCEP1 is 10% high.

The annual cycle in surface NSW (calculated over 1984-90) in the reanalyses is well correlated with the SRB estimate (Figure 11.4.16(a)), exceeding 0.9 outside the tropics where NSW has a small annual cycle. The anomaly correlations of the reanalyses with SRB (Figure 11.4.16(b)) (calculated over July 1983-June 1991) are much lower with only UWM anomalies showing a correlation greater than 0.6 in the Northern Hemisphere. GEOS1's correlations are lower than the other reanalyses; NCEP2's correlations with SRB are higher than GEOS1 but lower than ERA15 or NCEP1. UWM NSW anomalies agree the best with SRB anomalies from the North Pole to 20S, but show much less agreement south of 30S. Correlation of TOA NSW from the reanalyses with ERBE TOA NSW yields similar levels of agreement to Figure 11.4.16.

The UWM estimates show the smallest RMS differences from SRB for the full monthly means (Figure 11.4.17(a)) and the climatologies and between 15N and 50N for the anomalies (Figure 11.4.17(b)). UWM is most different from SRB near the North Pole and for anomalies in much of the Southern Hemisphere. In mid-latitudes GEOS1 shows the largest differences from SRB in the full monthly means and in the climatologies, reflecting a larger bias and a stronger annual cycle. NCEP1 tends to be closer to SRB than ERA15 and has less variability than SRB. ERA15 has considerably more variability in monthly anomalies in the tropics than does SRB. NCEP2's anomalies are the most different from SRB, reflecting a greater month-to-month variability than the other estimates; in mid-latitudes the normalised RMS difference of NCEP2 anomalies from SRB anomalies is the least of the reanalyses. For most latitudes the RMS differences of the reanalyses from SRB are more than 20 Wm$^{-2}$ for the full monthly means and more than 10 Wm$^{-2}$ for the anomalies.
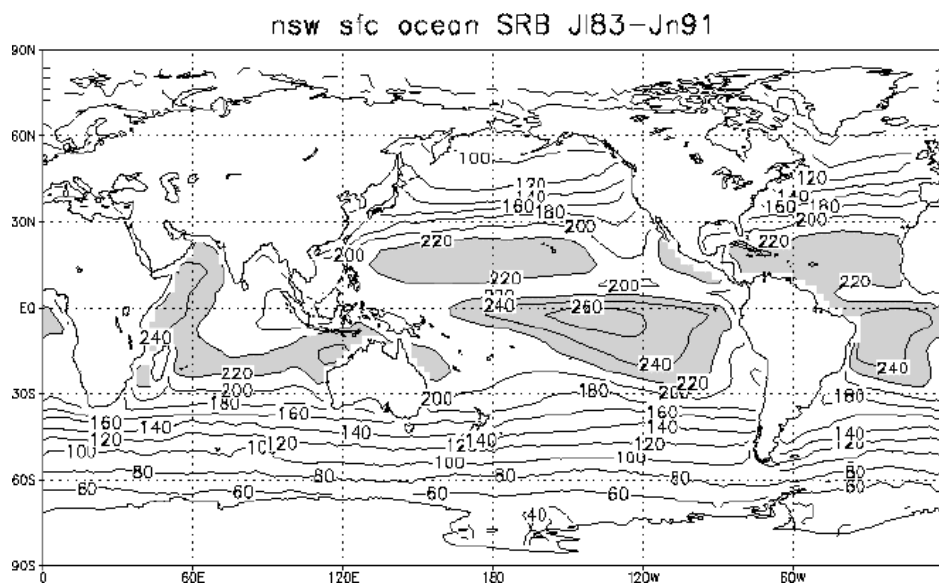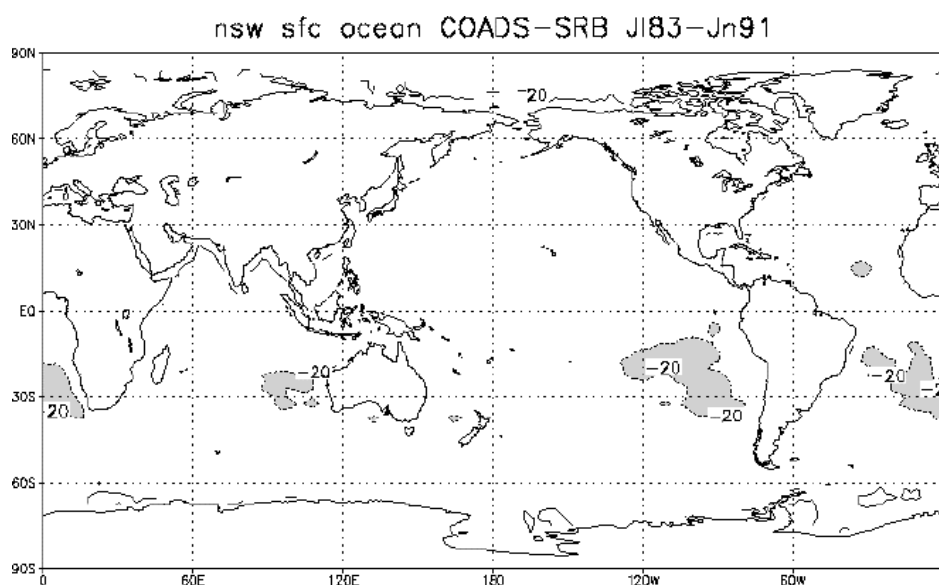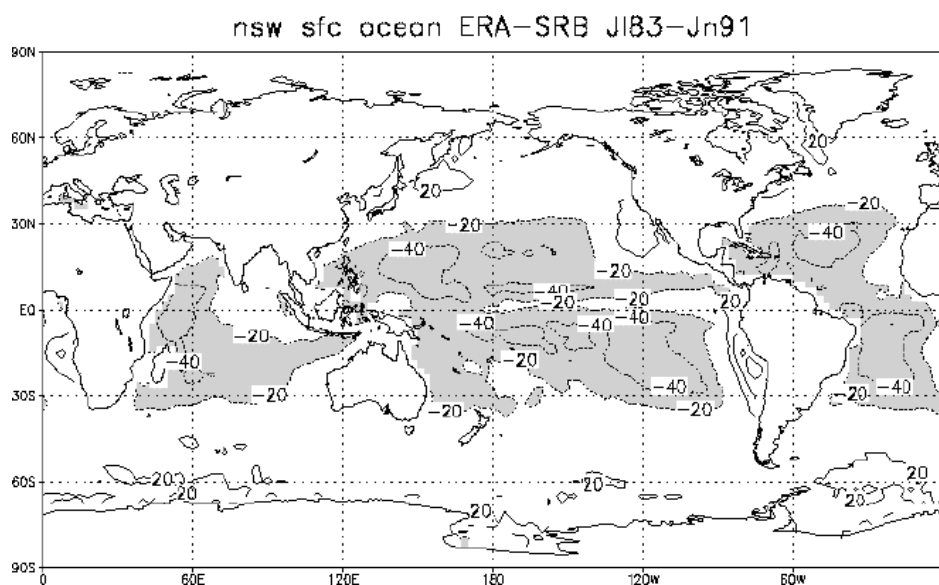
Figure
11.4.13(a)

nsw sfc ocean SRB Jl83-Jn91

Figure
11.4.13(b)

nsw sfc ocean COADS-SRB Jl83-Jn91

Figure
11.4.13(c)

nsw sfc ocean ERA-SRB Jl83-Jn91

Figure
11.4.13(d)

nsw sfc ocean GEOS-SRB Jl83-Jn91

Figure
11.4.13(e)

nsw sfc ocean NCEP-SRB Jl83-Jn91

Figure
11.4.13(f)

nsw sfc ocean NCEP2-SRB Jl83-Jn91
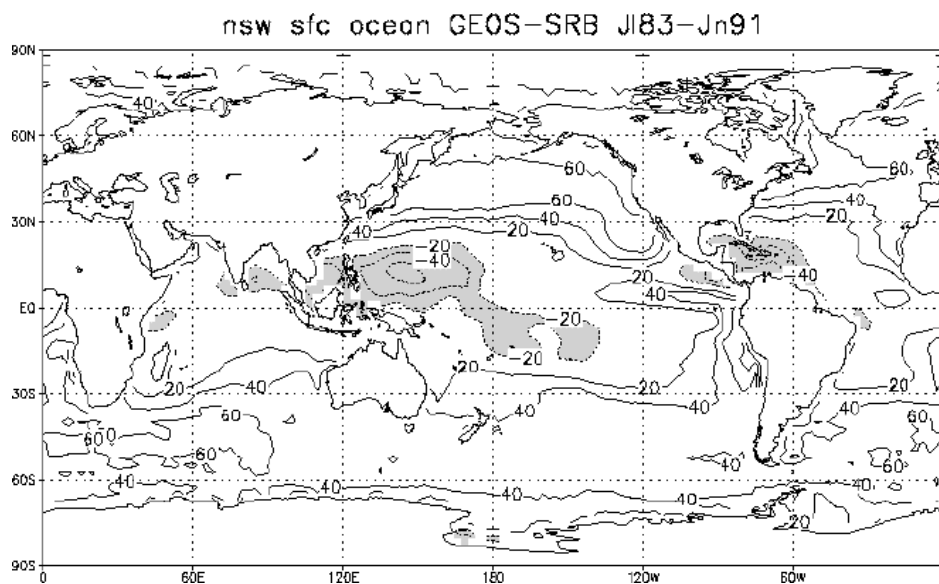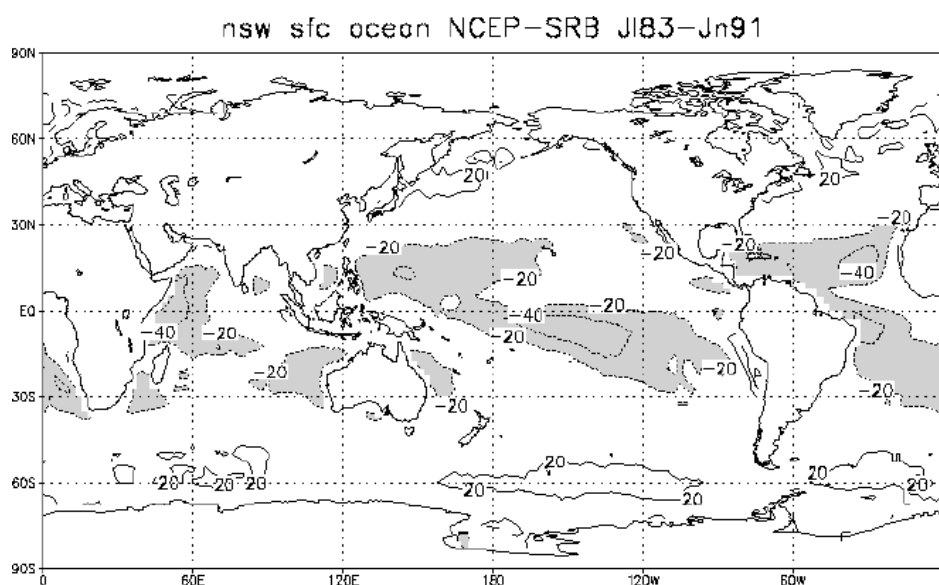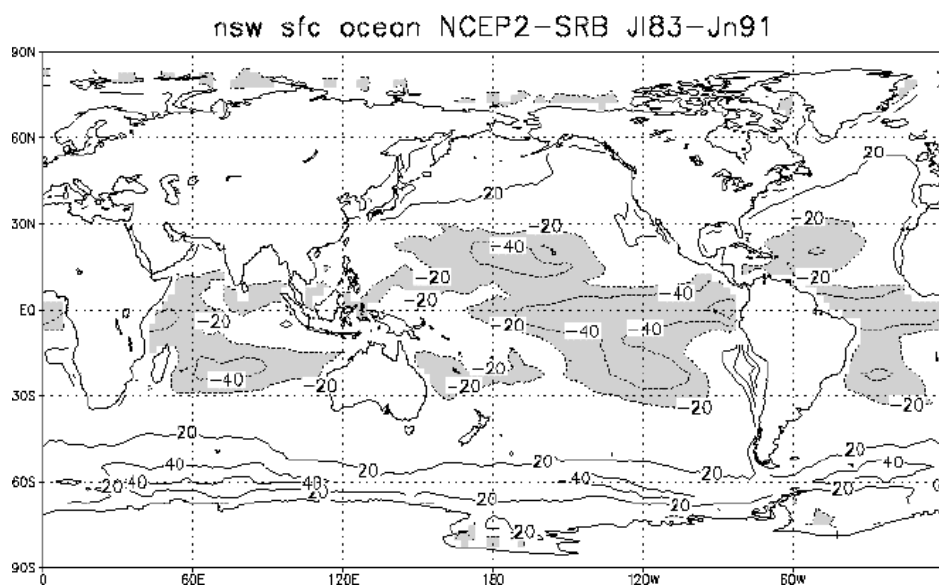
Figure 11.4.13:   (a) Surface NSW radiation from the SRB satellite estimate averaged over July
1983-June 1991.  Contour interval 20 Wm$^{-2}$. Values over 220Wm$^{-2}$ shaded.
(b) Difference in surface NSW UWM minus SRB.  Contour interval 20 Wm$^{-2}$ ;
zero omitted, negative values shaded.
(c) As (b) but for ERA15-SRB.
(d) As (b), but for GEOS minus SRB.
(e) As (b) but for NCEP1 minus SRB.
(f) As (b) but for NCEP2 minus SRB.

Figure
11.4.14(a)
SRB
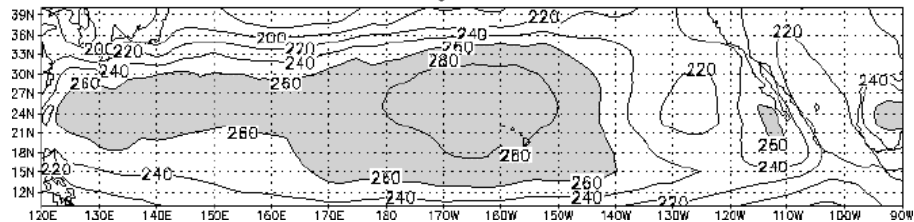
Figure
11.4.14(b)
UWM/
COADS
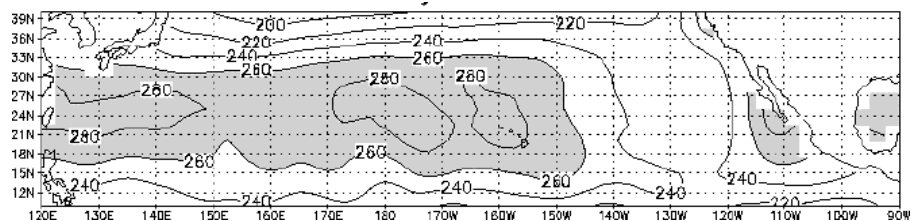
Figure
11.4.14(c)
ERA
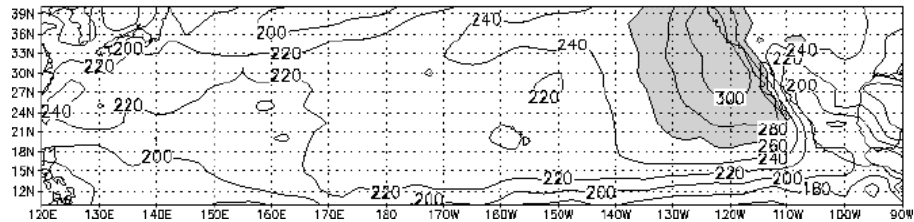
Figure
11.4.14(d)
GEOS
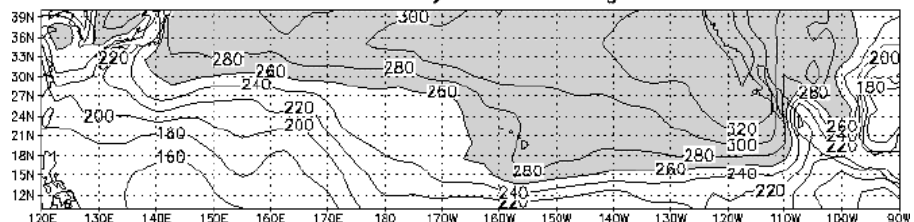
Figure
11.4.14(e)
NCEP
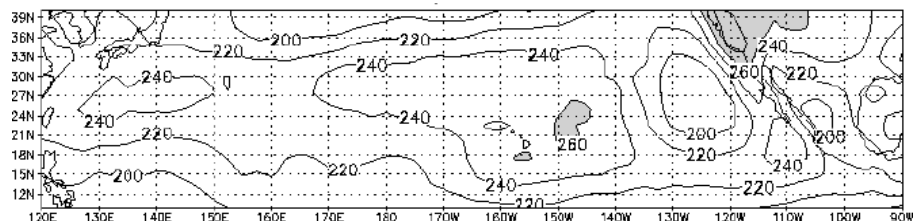
Figure
11.4.14(f)
NCEP2
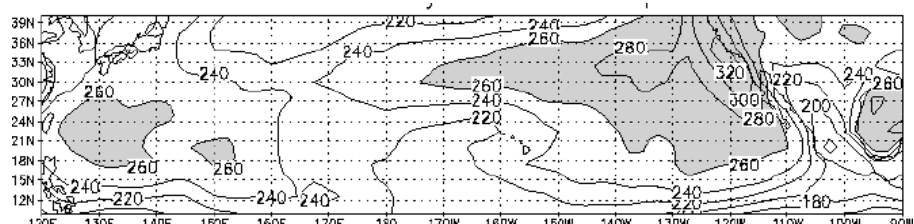


Figure 11.4.14.  Surface NSW radiation from different sources averaged over July 1983-1990.
Contour interval 20 Wm$^{-2}$. Values over 260 Wm$^{-2}$ are shaded.
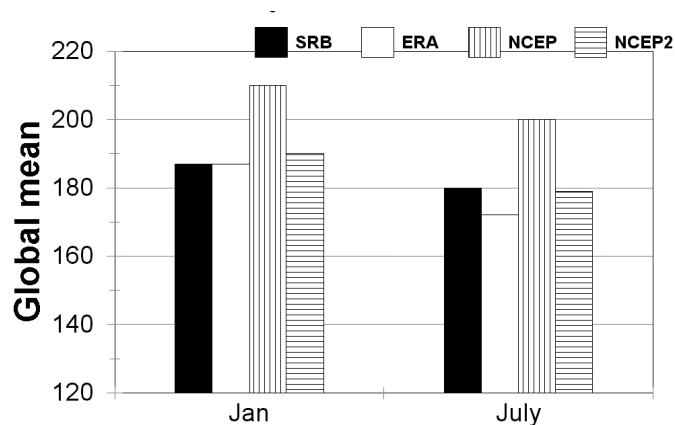
Figure 11.4.15 Global mean downward short wave radiation at the surface from SRB and from ERA, NCEP1 and NCEP2 reanalyses for Jan. 1984-91 and July 1983-90 in Wm$^{-2}$.

Figure 11.4.16 (a) Zonal mean correlation of monthly mean climatological surface NSW over the oceans of the reanalyses and UWM with SRB for the annual cycle averaged over 1984-90.
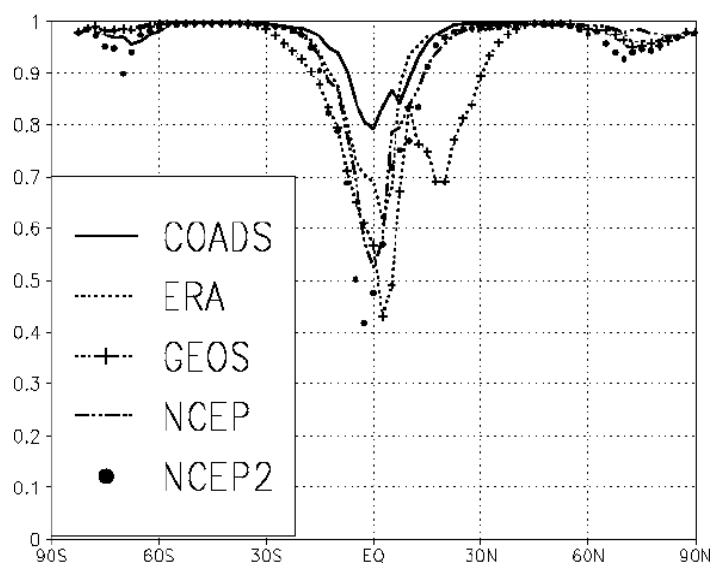


Figure 11.4.16 (b) Zonal mean correlation of monthly mean anomalies in NSW over the oceans of the reanalyses and UWM with SRB for July 1983-June 1991. The anomalies are from each estimate's climatology for 1984-90.
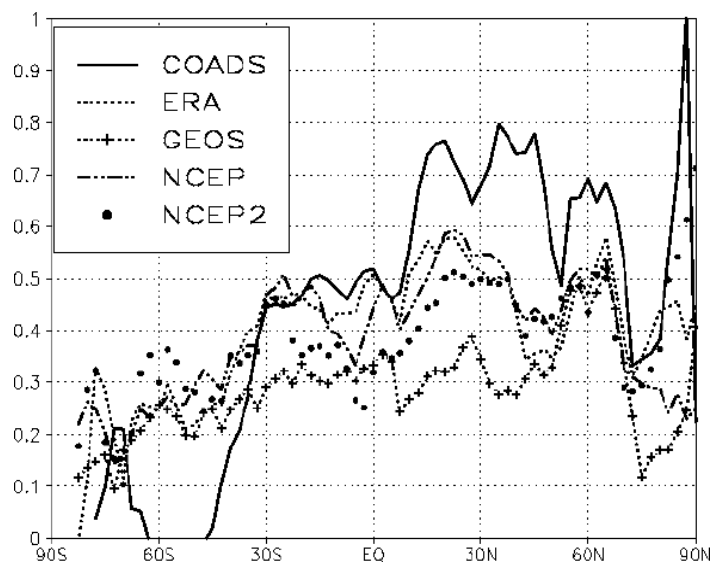
Figure 11.4.17 (a) RMS differences in monthly mean surface NSW over the oceans of the reanalyses and UWM from SRB for July 1983-June 1991 in Wm$^{-2}$.
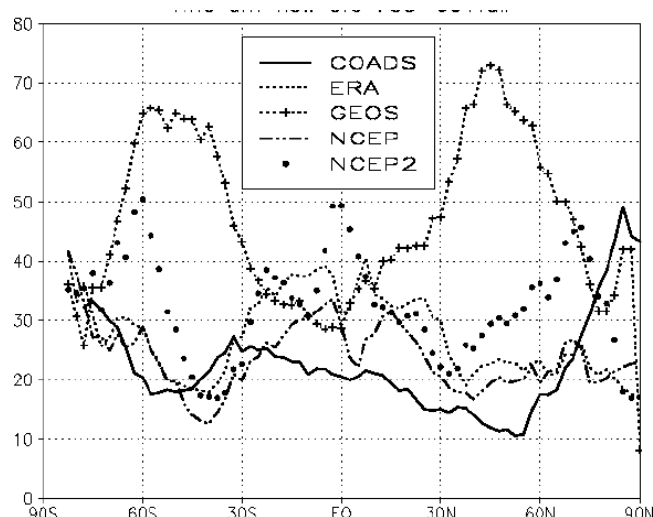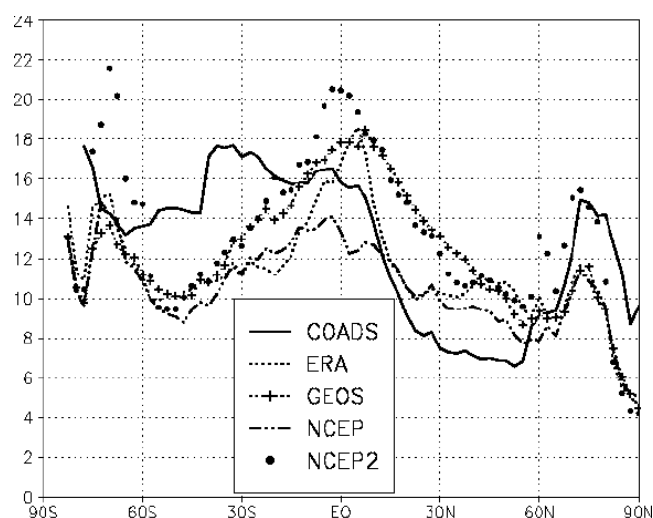


Figure 11.4.17 (b) As (a) but for anomalies.



### 11.4.8 Net long-wave

The zonal mean surface net long-wave (NLW) radiation over the ocean is shown in Figure 11.4.18. Figure 11.4.19(a) shows the regional distribution of the satellite estimate (SRB) of NLW (Gupta *et al.*, 1992). The SRB estimate is lower than the other estimates. UWM (Figure 11.4.19(b)) agrees the best with SRB, showing, as do the reanalyses, the largest differences from SRB in the eastern subtropical oceans. GEOS1 (Figure 11.4.19(d)) shows the highest NLW and the largest differences from SRB. ERA15 (Figure 11.4.19(c)) shows larger differences from SRB in the eastern subtropical oceans than NCEP1 (Figure 11.4.19(e)), but has smaller differences elsewhere. NCEP2 (Figure 11.4.19(f)) is generally closer to the SRB estimate than NCEP1. The large differences of GEOS1, ERA15 and NCEP2 from the SRB estimate in the eastern subtropical oceans may reflect problems in their treatment of low-level stratus clouds.

Figure 11.4.20(a) displays the zonally averaged correlations of the mean annual cycles in NLW averaged over 1984-1990 from UWM and the reanalyses with SRB over the oceans. Figure 11.4.20(b) displays the zonal mean correlations of the anomalies for July 1983-June 1991 from the climatologies averaged over 1984-90. The correlations of the climatologies with SRB are less in mid-latitudes than for other components of the surface energy balance; NCEP2's annual cycle shows the least agreement with SRB. The anomaly correlations are less than 0.6 at all latitudes for the reanalyses and nearly all latitudes for UWM. NCEP1's NLW anomalies agree the best with SRB of the four reanalyses; GEOS1 displays the worst agreement.

Figure 11.4.18

Zonal mean surface NLW radiation over the oceans for 1981-92 in Wm$^{-2}$.



zonal mean nlw sfc ocean Jl83−Jn91
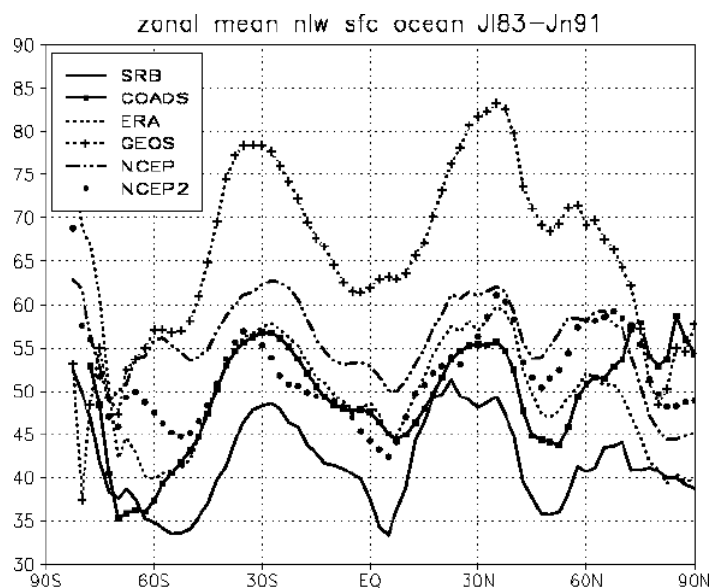
RMS differences with the SRB estimate are shown in Figure 11.4.21(a) for the full monthly means and in Figure 11.4.21(b) for the monthly anomalies. GEOS1 is clearly the most different from the SRB estimate and has considerably more variability than the SRB estimate outside the tropics. ERA15's and UWM's mean annual cycles are different from SRB by about 11 Wm$^{-2}$, while NCEP2's annual cycle is closer to SRB than NCEP1. NCEP1's anomalies are closest to SRB's except in the northern mid-latitudes where UWM is less than 6 Wm$^{-2}$ different from SRB. The SRB estimate displays the most variability in the tropics and the least outside the tropics.

Figure 11.4.19:   (a) Surface NLW from SRB averaged over July 1983-June 1991. Contour
*(Next page:)*          interval 10  Wm$^{-2}$.  Values greater than 40  Wm$^{-2}$ shaded.
                (b) Surface NLW UWM minus SRB. Contour interval 10 Wm$^{-2}$; zero omitted,
                    negative values shaded.
                (c) As (b) but for ERA minus SRB.
                (d) As (b) but for GEOS minus SRB.
                (e) As (b) but for NCEP1 minus SRB.
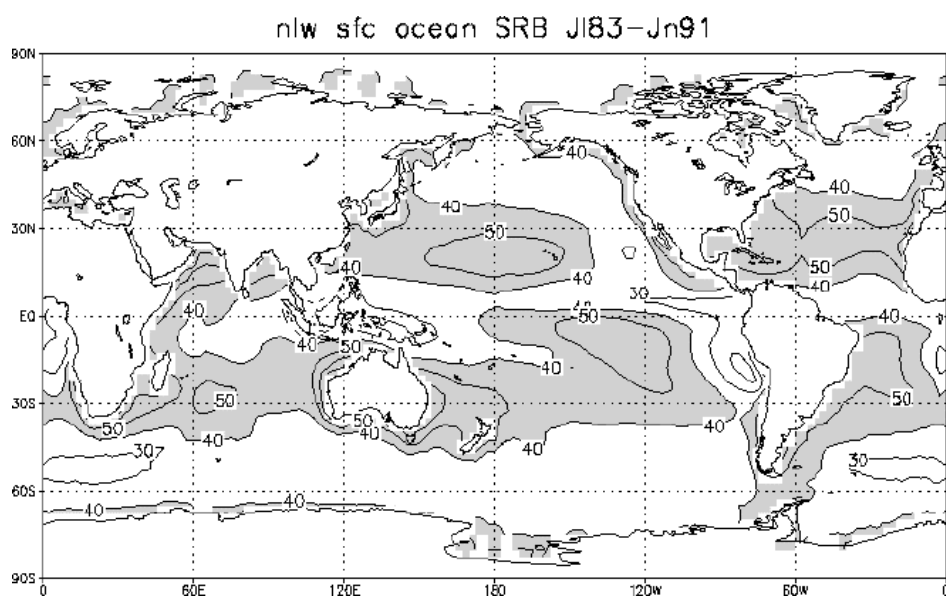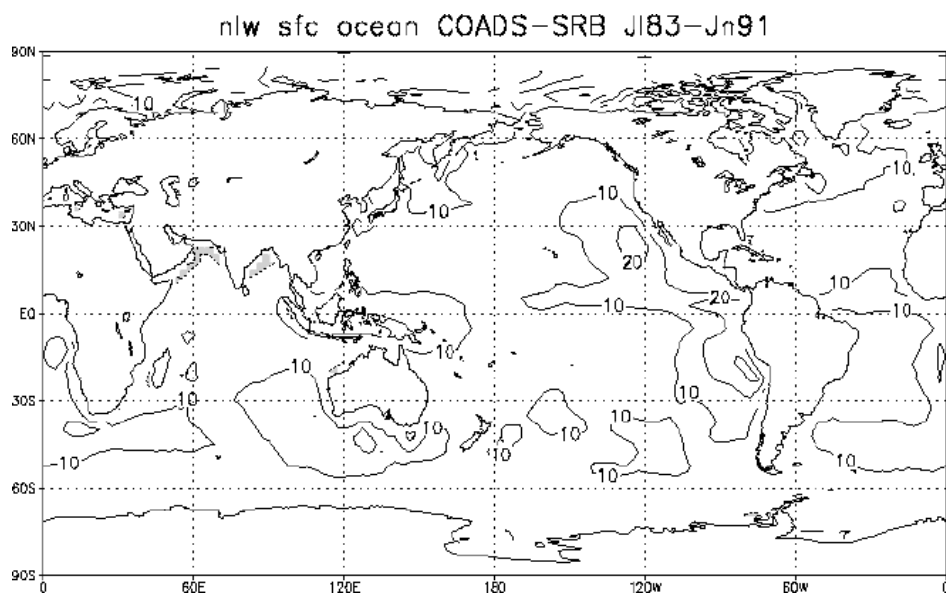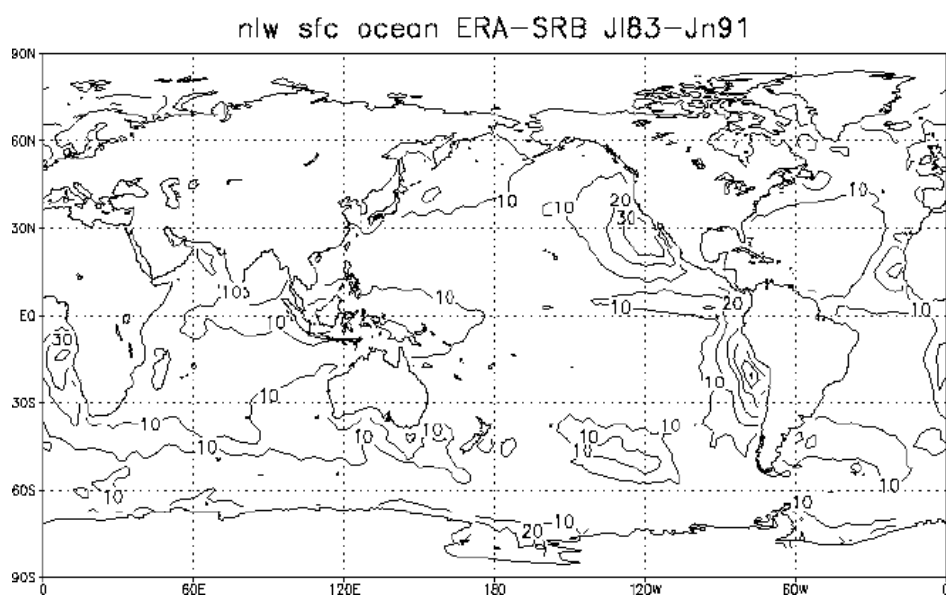                (f) As (b) but for NCEP2 minus SRB.

Figure
11.4.19(a)

nlw sfc ocean SRB Jl83–Jn91

Figure
11.4.19(b)

nlw sfc ocean COADS–SRB Jl83–Jn91

Figure
11.4.19(c)

nlw sfc ocean ERA–SRB Jl83–Jn91

Figure
11.4.19(d)



nlw sfc ocean GEOS-SRB Jl83-Jn91

Figure
11.4.19(e)



nlw sfc ocean NCEP-SRB Jl83-Jn91

Figure
11.4.19(f)



nlw sfc ocean NCEP2-SRB Jl83-Jn91
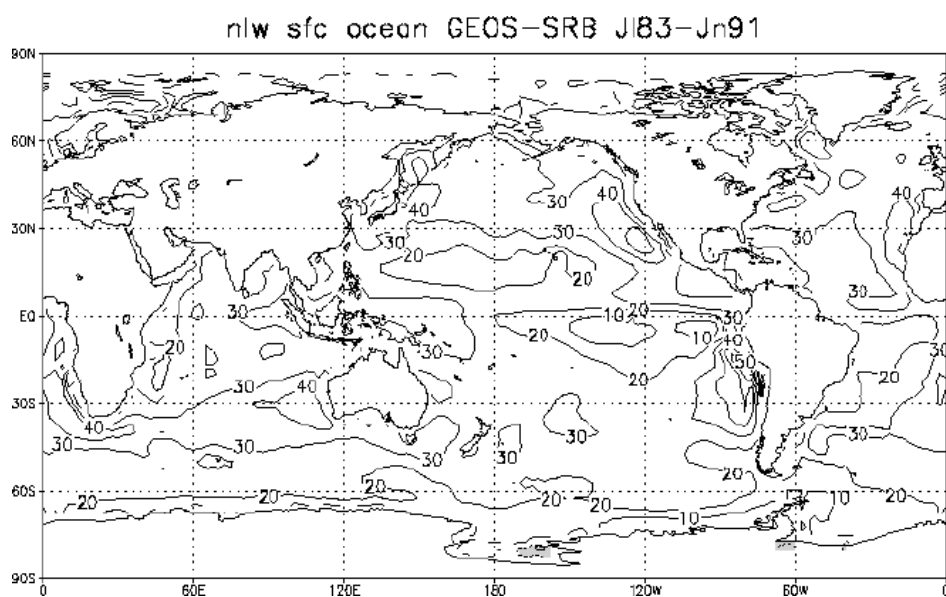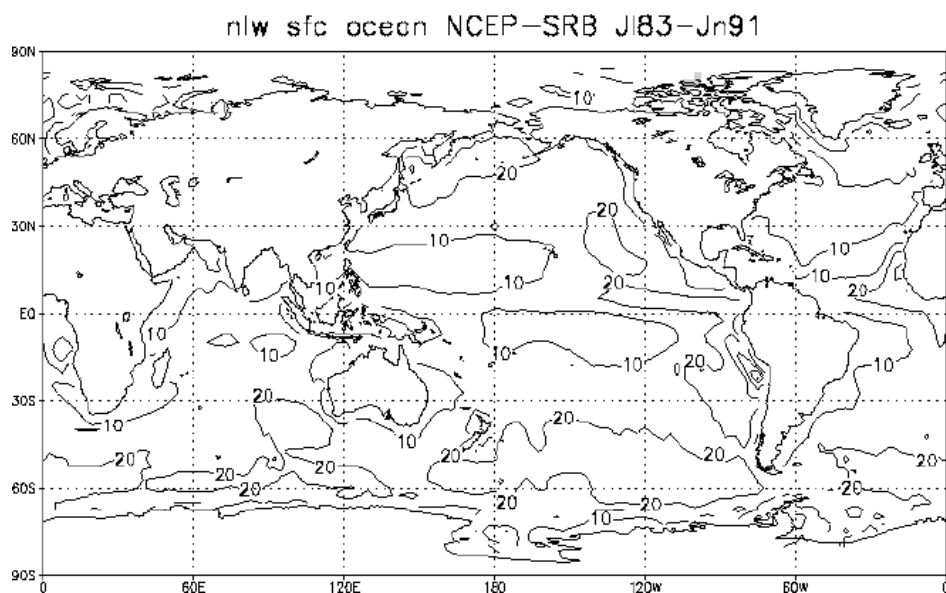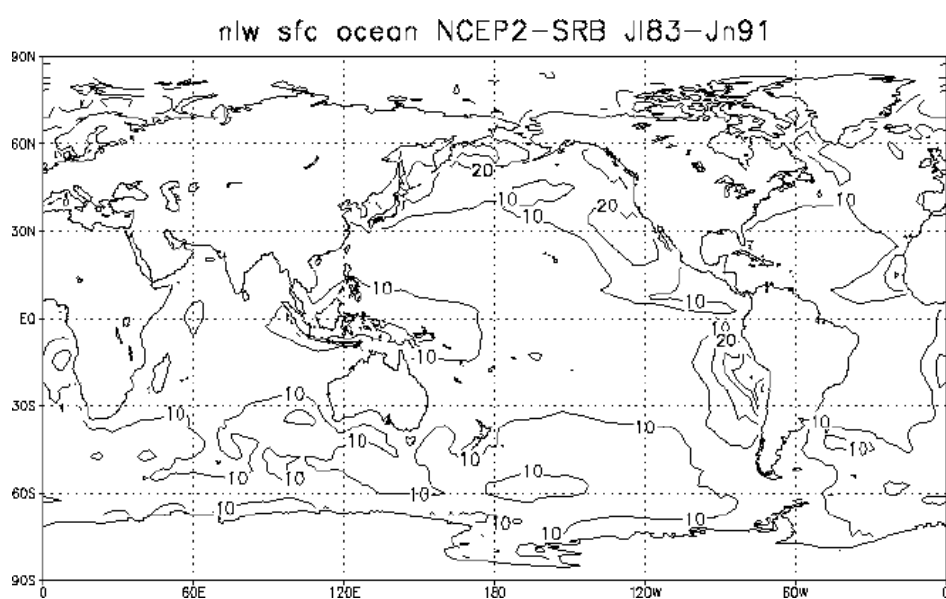
Figure 11.4.20 (a) Zonal mean correlation of monthly mean climatological surface NLW over the oceans of the reanalyses and UWM with SRB for the annual cycle averaged over 1984-90.
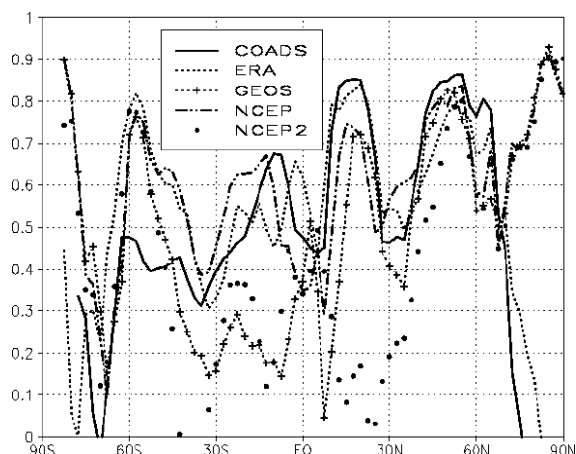


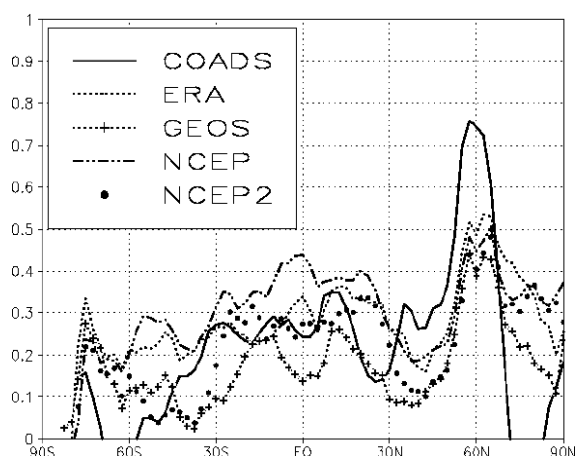Figure 11.4.20 (b) As (a) but for anomalies for July 1983-June 1991 from each estimate's climatology for 1984-90.



Figure 11.4.21(a) RMS differences in monthly mean surface NLW over the ocean of the reanalyses and COADS from SRB for July 1983-June 1991 in Wm$^{-2}$.
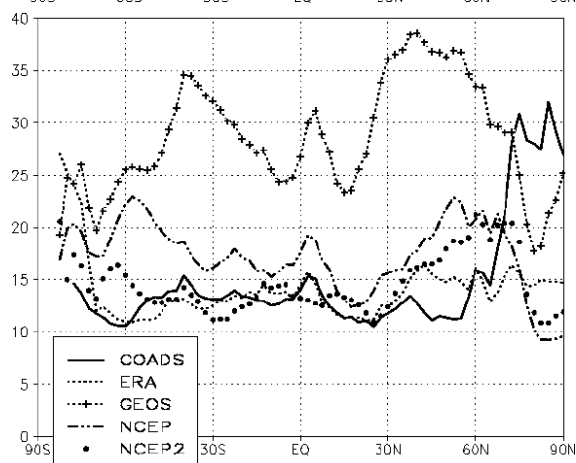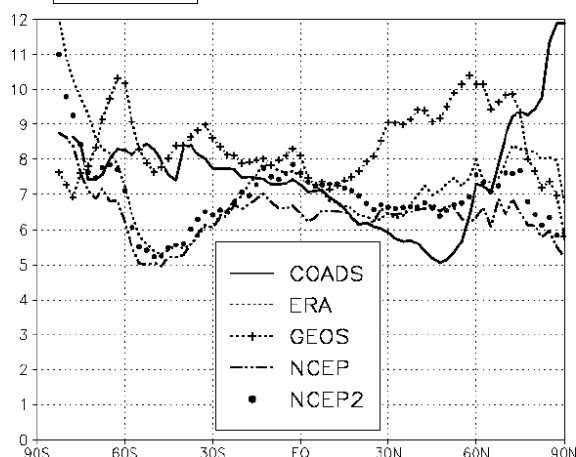


Figure 11.4.21(b) As (a) but for anomalies for July 1983-June 1991 from each estimate's climatology for 1984-90.

*11.4.9  Net heat flux*

　　Figure 11.4.22 shows the zonal mean NHF into the ocean averaged over 1981-92.  The untuned UWM estimate (da Silva *et al.*, 1994) is predominately into the ocean; GEOS1 has an even stronger downward net heat flux.  The tuned UWM estimate, NCEP1, NCEP2 and ERA15 show a more balanced distribution of fluxes into the ocean near the equator and fluxes out of the ocean in the subtropics.  The UWM estimates show much more NHF into the atmosphere near the North Pole.  Near 45° in either hemisphere NCEP1 and ERA15 show NHF into the ocean, in better agreement with the untuned UWM estimate than the tuned.  NCEP2 shows more NHF into the ocean near 45S than ERA15, NCEP1 or UWM.  NCEP1, NCEP2 and ERA15 show good agreement with the untuned UWM estimate between 40N and 60N, where ship observations are most abundant, but are close to the tuned COADS estimate in the tropics.  The reanalyses show more NHF into the oceans in the Southern Hemisphere mid-latitudes in summer and more NHF into the atmosphere near 60S in winter than the tuned UWM estimate.  Da Silva and White (1995) found that replacing the NCEP1 estimate of surface net short-wave with an estimate based on satellite data (Pinker *et al.*, 1995) improved the time-mean global oceanic heat balance.

　　The tuned UWM estimate of the 12-year mean net heat flux, shown in Figure 11.4.23(a), shows strong heat flux into the ocean in the eastern equatorial Pacific and intense upward heat flux over the Kuroshio and Gulf Stream and south of Africa.  The original UWM estimate (Figure 11.4.23(b)) shows broad areas where it is more than 40 Wm$^{-2}$ different from the tuned estimate.  All four reanalyses show large positive differences from the tuned UWM estimate south of Africa and in the Far East equatorial Pacific and Atlantic. ERA15 (Figure 11.4.23(c)) has less downward/more upward net heat flux than UWM over much of the tropical oceans; NCEP1 (Figure 11.4.23(e)) has less upward heat flux in the mid-latitudes.  GEOS1 (Figure 11.4.23(d)) has more downward/less upward net heat flux nearly everywhere.  ERA15 (Figure 11.4.23(c)) and GEOS1 (Figure 11.4.23(d)) show bigger differences in the eastern subtropical Pacific than NCEP1 (Figure 11.4.23(e)) does, perhaps reflecting differences in the treatment of stratus clouds.　 NCEP2's differences from UWM tuned (Figure 11.4.23(f)) resemble NCEP1's differences, but are larger in the eastern subtropical oceans where low-level stratus clouds are important and between 30 and 60S.



Figure 11.4.22.  Zonal mean net heat flux into the ocean averaged over 1981-92 from COADS and the four reanalyses.  Positive values denote a flux from the atmosphere into the ocean.
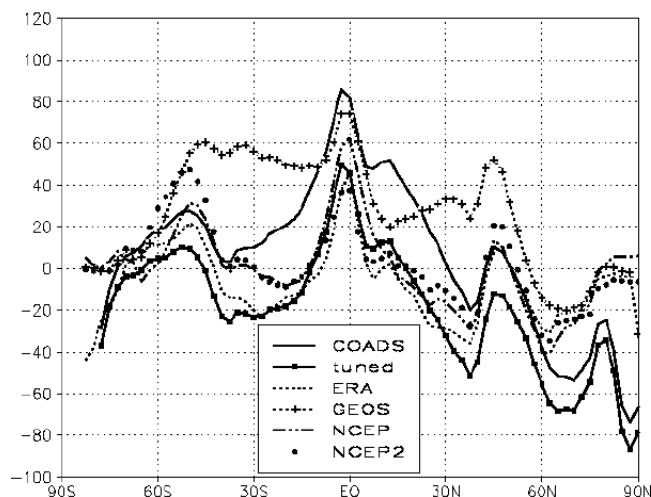
Figure 11.4.23:　(a) Surface net heat flux into the ocean from the tuned UWM estimate
*(next page)*　　　averaged over 1981-92.  Contour interval 25 Wm$^{-2}$.  Shaded areas indicate
　　　　　　　(negative) upward heat flux.
　　　　　(b) The effect of tuning on UWM (untuned minus tuned).  Contour interval 20
　　　　　　　Wm$^{-2}$; zero omitted, negative values shaded.
　　　　　(c) As (b) but for the difference in net heat flux for ERA minus UWM tuned.
　　　　　(d) As (c) but for GEOS minus UWM tuned.
　　　　　(e) As (c) but for NCEP1 minus UWM tuned.
　　　　　(f) As (c) but for NCEP2 minus UWM tuned.

Figure
11.4.23(a)
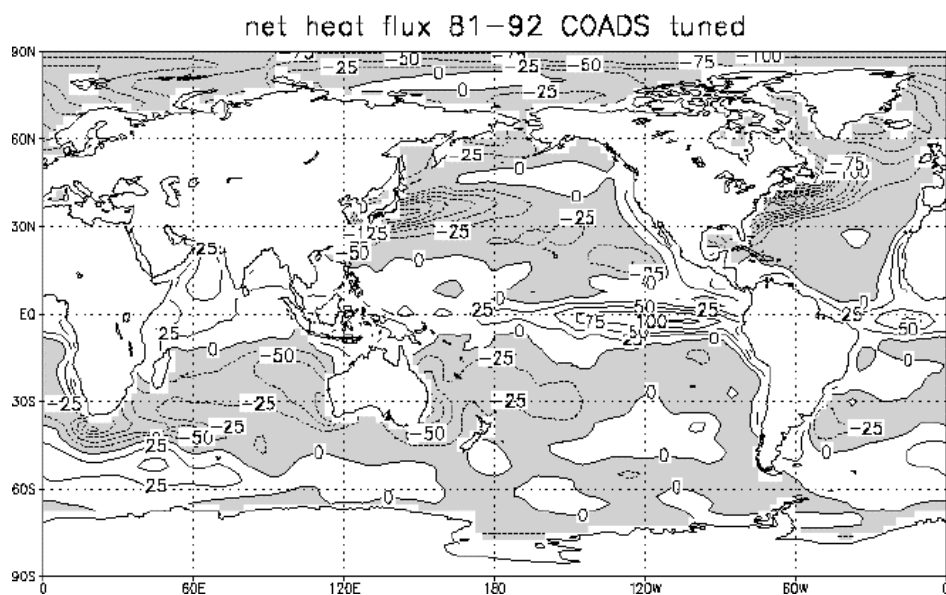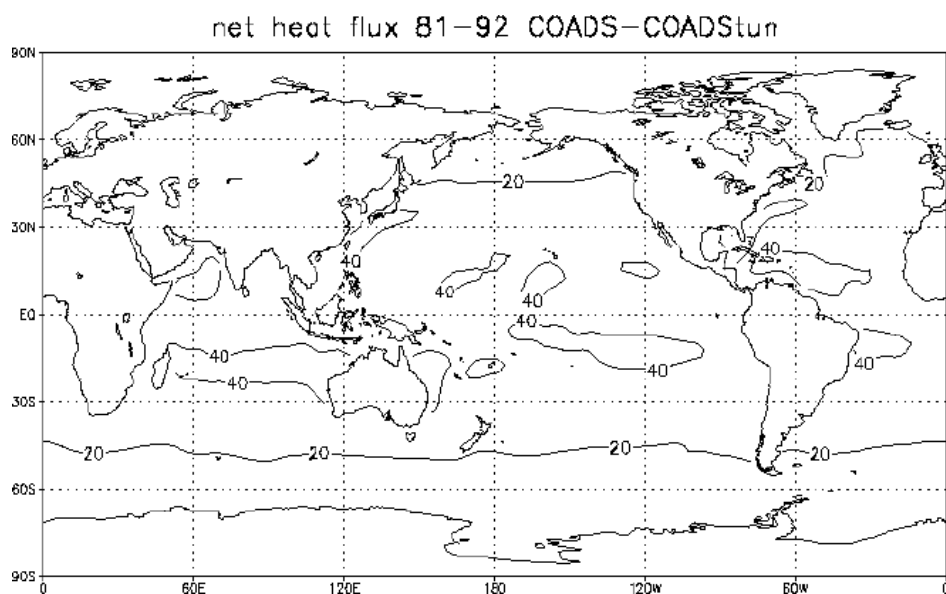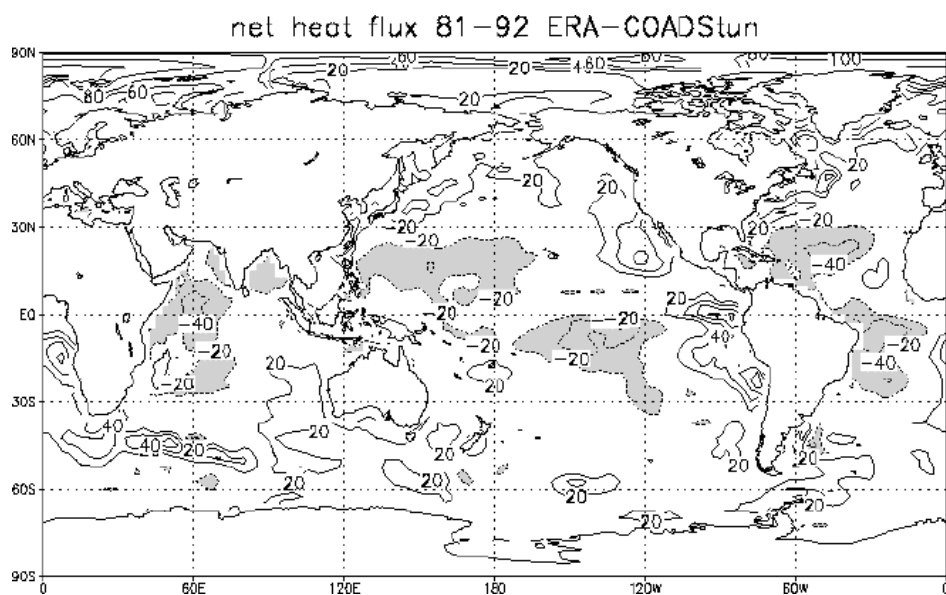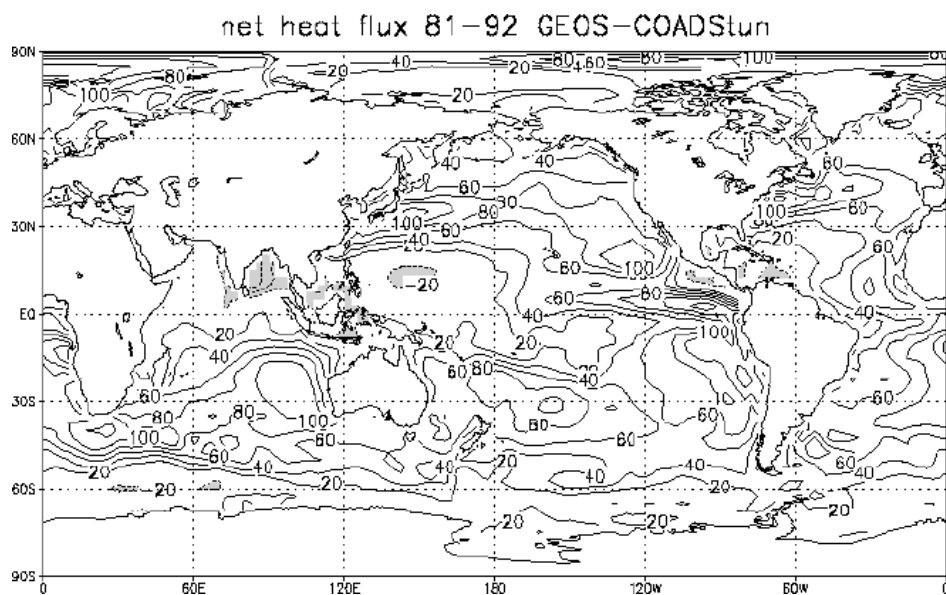


net heat flux 81-92 COADS tuned

Figure
11.4.23(b)



net heat flux 81-92 COADS-COADStun

Figure
11.4.23(c)



net heat flux 81-92 ERA-COADStun

Figure
11.4.23(d)

net heat flux 81-92 GEOS-COADStun



Figure
11.4.23(e)

net heat flux 81-92 NCEP-COADStun



Figure
11.4.23(f)

net heat flux 81-92 NCEP2-COADStun
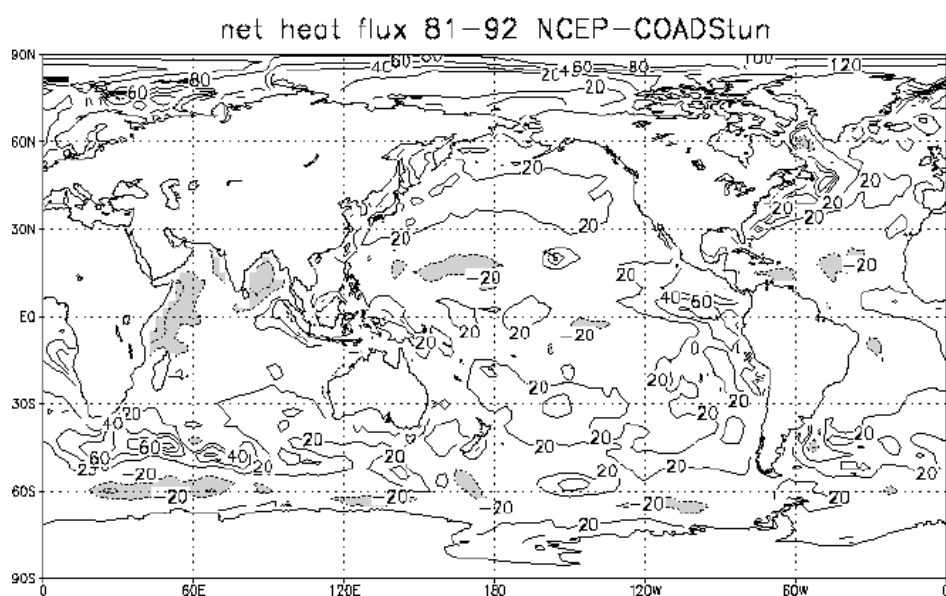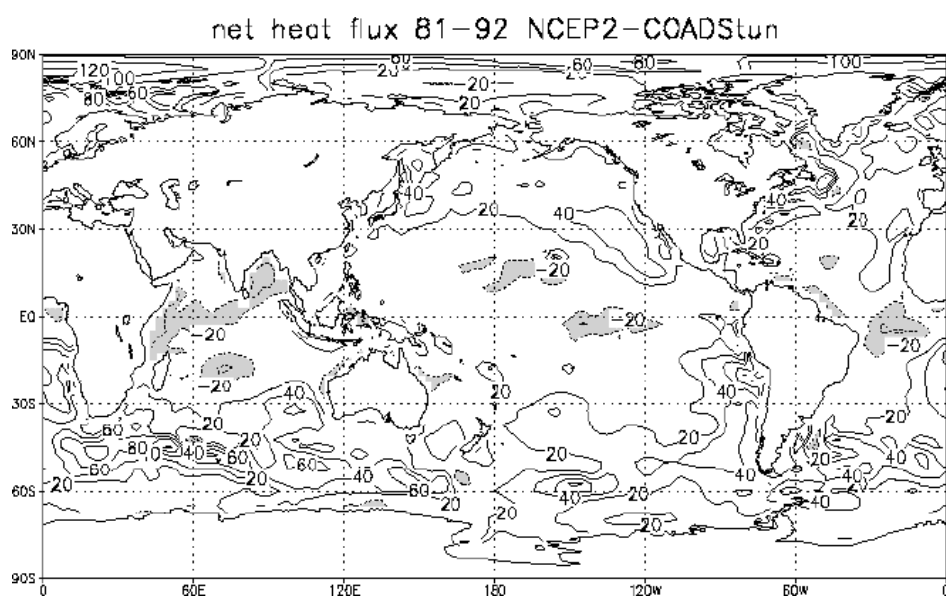
The zonal averaged correlations of the mean annual cycles in NHF of the reanalyses with the tuned UWM estimate resemble the correlations of the mean annual cycles in NSW (Figure 11.4.16(a)).  Very high correlations near 1.0 are seen in mid-latitudes, reflecting the great variation with season of the net heat flux outside the tropics; near the equator the correlations drop to 0.3(GEOS1) to 0.6 (ERA15).  The correlations of anomalies in NHF are very similar to the correlations for latent heat (Figure 11.4.5(c)), with correlations above .6 only in the northern mid-latitudes.  Correlations for NHF are virtually the same for NCEP1, NCEP2 and ERA15 and a little lower for GEOS1.  ERA15's annual cycle in these fields tends to agree slightly more with UWM than NCEP1's or NCEP2's; NCEP1's and NCEP2's anomalies tend to agree slightly more with UWM than ERA15's.

Figure 11.4.24 (a): RMS differences in monthly mean NHF over the oceans of the reanalyses from tuned UWM for 1981-92. (left bottom)
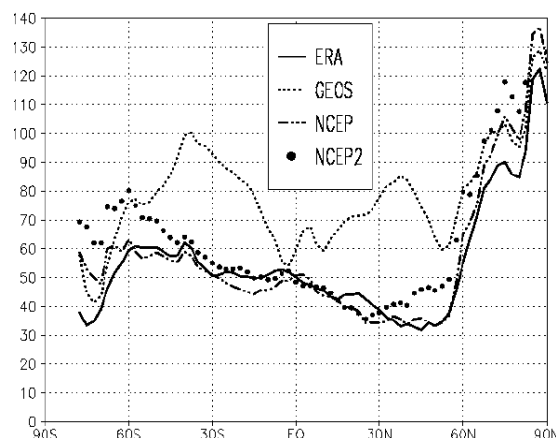


Figure 11.4.24 (b) As in 24a, but for the climatological annual cycle averaged over 1981-92. (above)
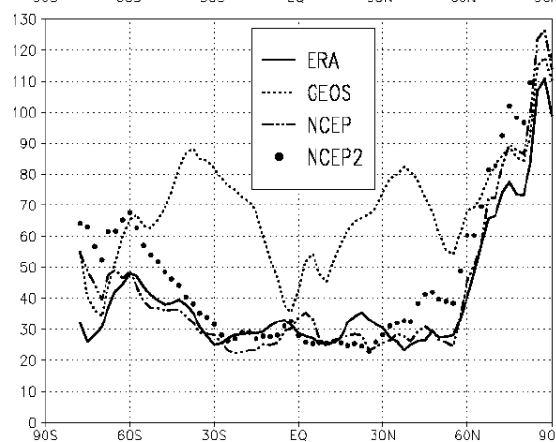


Figure 11.4.24 (c) As in 24a, but for anomalies from the climatological annual cycle.
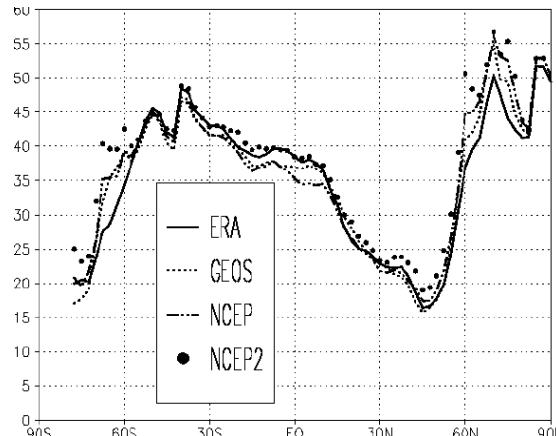


The climatological annual cycles in NHF in the reanalyses have RMS differences from the tuned UWM estimate of more than 20 $Wm^{-2}$ at all latitudes (Figure 11.4.24(b)) and the full monthly means are more than 30 $Wm^{-2}$ different (Figure 11.4.24(a)) at all latitudes.  Anomalies in NHF (Figure24(c)) are more than 15 $Wm^{-2}$ different at all latitudes.  GEOS1's climatology is

much more different from the tuned estimate than the other reanalyses; NCEP2's climatology is more different from UWM than NCEP1 or ERA15. Anomalies from all four reanalyses show very similar RMS differences from UWM; NCEP2's anomalies are slightly more different from UWM than the other reanalyses and display more month-to-month variability. GEOS1 has the largest normalised RMS differences from UWM between 20 and 60N.

### 11.4.10 Evaluating the NCEP1 reanalysis by forcing an ocean model

Fluxes from NCEP1 and ERA15 reanalyses are now widely used to force ocean circulation models at global and basin scale. At present, the mean biases in model solutions make it difficult to assess the quality of the climatological mean of these fluxes. However, model solutions have shown in several cases a seasonal to interannual variability which compares qualitatively well with ocean observations. For example, Figure 11.4.25 shows variations of the maximum mixed layer depth in March in the Labrador Sea during the period 1958-1997, simulated with a 1° primitive equation ocean model forced with fluxes from NCEP1 (from Knochel, 1999). This parameter shows a significant decadal variability. This variability appears consistent with noticeable oceanic events observed in this region. These include weak convection periods between 1962 and 1972 (related to the Great Salinity Anomaly, GSA, (Dickson *et al.*, 1988)) and between 1976 to 1982 (related to the lesser GSA (Lazier, 1997)) and particularly active convection periods in 1972-76 (McCartney *et al.*, 1997), and in the early nineties (1990- 1995), as described by Dickson *et al.* (1996).

This indicates that the low frequency variability found in the reanalysis fluxes could make sense and should be useful to understand climate change over recent times (the last 40-50 years). These results, which however remain qualitative, indicate that the inter-annual variability described in the reanalysis products make sense.

Figure 11.4.25 Variations of the maximum mixed layer depth in March in the Labrador Sea during the period 1958-1997, simulated with a 1° primitive equation ocean model forced with fluxes from NCEP1 (from Knochel, 1999).
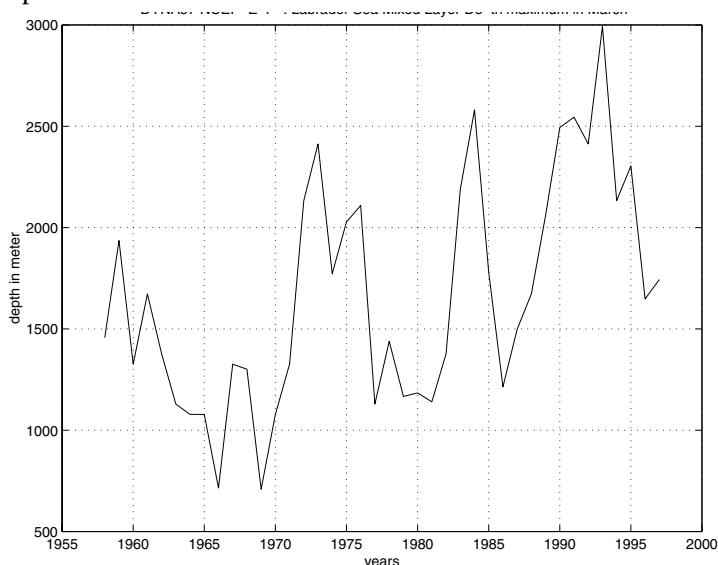


### 11.4.11 Winds

A. COMPARISON OF THE NCEP WINDS WITH INSTRUMENTAL MEASUREMENTS AT OWS

In order to compare surface winds from the NCEP1 Reanalysis with instrumental measurements for the 1980s and 1990s, Zolina and Gulev (1998) used observations at four mid-latitude ocean weather ships (OWS) in the North Atlantic: C, L, M, and R. These observations are individual three hourly anemometer observations taken at known anemometer heights by professional observers. Additionally, wind data from the SECTIONS Programme (Gulev, 1994) were used. These data were collected by six sister-ships that also operated at OWS C from 1975 to 1990. All wind measurements from OWS and SECTIONS were adjusted to 10-m

height and neutral stability. For the comparison NCEP1 data at the nearest grid point of the Gaussian grid to the measurement location were used.

In general, instrumental wind speed in the North Atlantic mid-latitudes has been found to be somewhat higher than NCEP1 winds. Annual mean intercepts for the OWS data vary within the range of 0.1 to 0.35 ms$^{-1}$; the largest deviations of about 0.7 ms$^{-1}$ are obtained for the SECTIONS data. Note that OWS data were assimilated in the NCEP1 Reanalysis; therefore, the intercomparison is not independent. However, only 25% of the SECTIONS measurements were included in the COADS archives and assimilated in the NCEP1 reanalysis. This explains the larger differences obtained for this data sub-set.

The largest overestimation was observed for the winter months for the SECTIONS data and all OWS, except for the OWS L. In summer the instrumental measurements of the winds were less than the reanalysis winds by 0.1 to 0.3 ms$^{-1}$. Estimation of the regression slopes gave values varying from 0.88 to 0.97, demonstrating a general tendency of overestimating low winds and underestimating moderate and high winds in NCEP1. Since the assimilation of the COADS winds in NCEP1 should provide in general an opposite tendency due to the usage of WMO1100 scale in COADS, this bias can be explained by the impact of the NCEP1 model on the wind fields. Separate analysis of the wind components shows that zonal components in the reanalysed products and instrumental measurements are in better agreement than meridional components.

B. ERA15 AND NCEP1 REANALYSIS TROPICAL WIND EVALUATIONS

Monthly mean surface wind products from the NCEP1 and ERA15 reanalysis projects over the tropical regions have been compared to specialised products from Florida State University (FSU) and Centre ORSTOM/IFREMER (see section 9.3.1). Monthly mean fields from the reanalyses for the common period 1979-1993 were first constructed. For comparison purposes, the daily or 4-time per day NCEP1 and ERA15 10-m winds were first adjusted to 20-m height (nominal reference height for FSU products) using the BVW parameterisation scheme, and monthly mean fields of pseudo-stress were produced. NCEP1 and ERA15 products were then interpolated to the same spatial grids as the specialised products to allow direct comparisons. Comparisons of the respective climatologies of the pseudo-stress fields, the divergence and curl as well as the variations of these fields resulted in a number of conclusions and Figures 11.4.26 and 11.4.27.

Comparisons of the climatological reanalysis products to the FSU and ORSTOM climatologies indicate the Indian Ocean is much more comparable than the Pacific or Atlantic. During the Indian Ocean southwest monsoon, the ERA15 winds are strongest in the northern basins, followed by FSU and then NCEP1. The NCEP1 has the strongest trades in the southern third of all tropical regions. This strength is in sympathy with the strength of the trades (i.e. even stronger during trade maximum during June–December). Model spin-up problems near island stations, particularly in ERA15, results in relatively large gradients in the pseudo-stress vector fields. Not only does this impact the pseudo-stress vectors, but also the kinematic fields – especially the curl where numerous large bipolar patterns are co-located adjacent to many islands. The NCEP1 Inter-tropical Convergence Zones (ITCZ) in the eastern Pacific and western Atlantic are poorly resolved during July-December, i.e. when the southerly trades are maximum and the ITCZ is also strongest and at its maximal northern location. The NCEP1 ITCZ is too broad (north south) and too weak. This seems to be linked to the presence of anomalous weak cross-equatorial southerlies. Not only are the NCEP1 southerlies weak, but in the equatorial region (0° to 5°S), particularly during January-June, the easterlies are notably weaker (up to 5 m s$^{-1}$) than the other analyses. Comparisons of the pseudo-stress anomalies highlight the outlier nature of the NCEP1 fields in the tropics. These comparative results vary over time. For example, Pacific east west winds along the equator for all three analyses correlate much better during ENSO events than at any other time. Additionally, NCEP1 winds correlate better with FSU during 1988-1991 and the ERA equatorial easterlies are stronger than FSU only for the 1979-1986 period, but afterwards, the FSU easterlies are stronger.
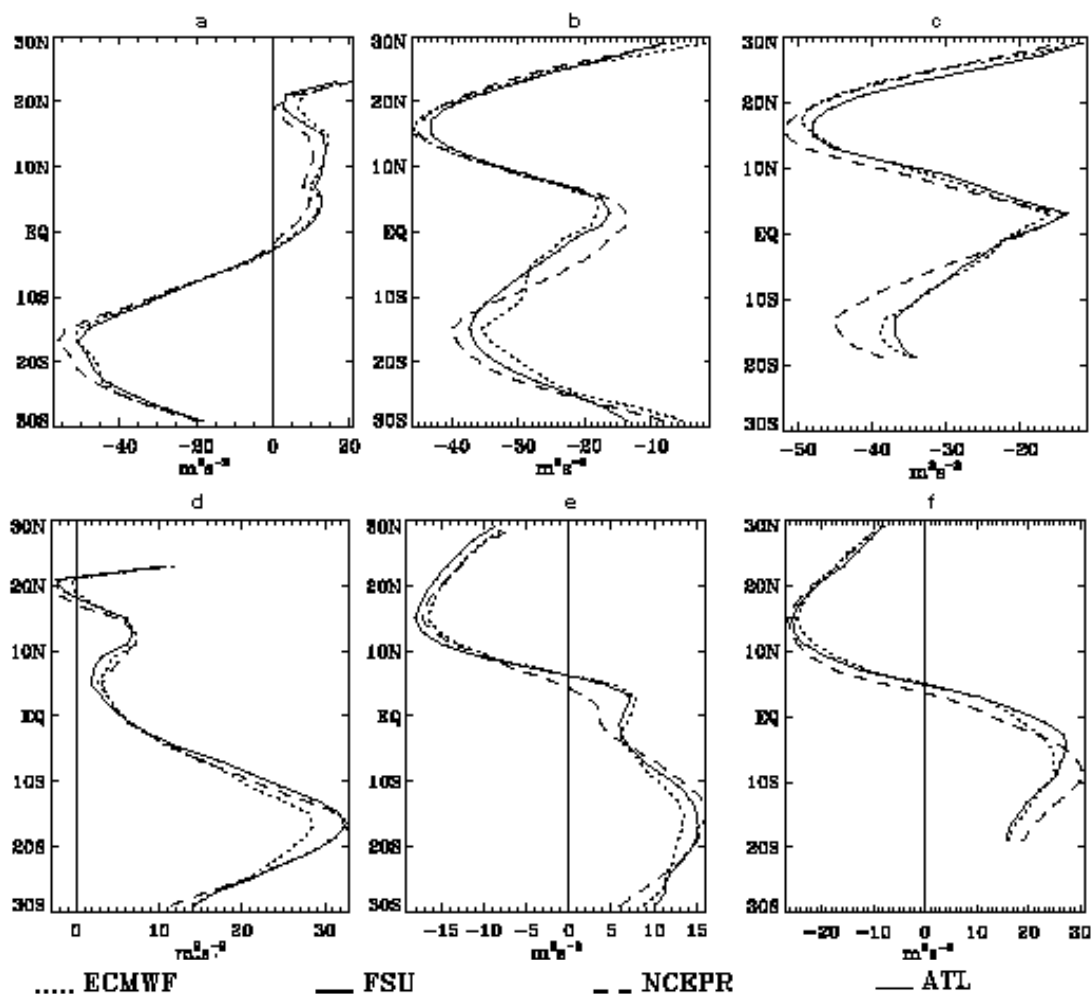
Figure 11.4.26 Zonal mean climatological pseudo-stress components for FSU, ORSTOM (ATL) and (height adjusted) ERA15, NCEP1 reanalysis products: (a) east-west component for the Indian Ocean region (30°E-120°E); (b) east-west component for the Pacific Ocean region (120°E-70°W); (c) east-west component for the Atlantic Ocean region (60°W-15°E); (d) north-south component for the Indian Ocean; (e) north-south component for the Pacific Ocean region; and (f) north-south component for the Atlantic Ocean region.
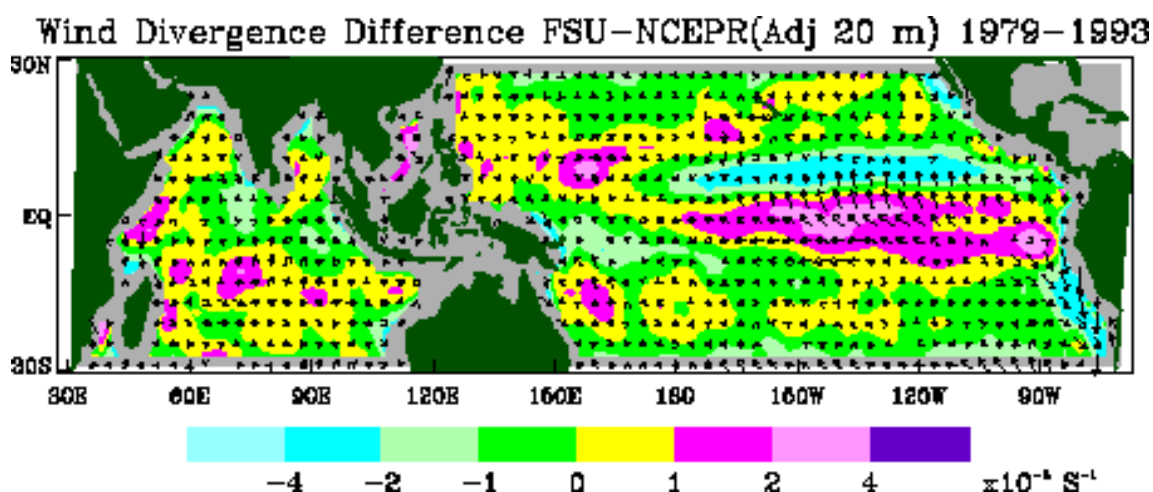


Figure 11.4.27 Difference (FSU-NCEP1) of FSU and (height adjusted) NCEP1 climatological pseudo-stress vectors for the period 1979-1993 with colours indicating magnitude of the difference of the wind divergence fields. Areas with no vectors are areas where FSU and reanalyses do not overlap.

Other approaches to flux product evaluation include the use of ocean models and independent validation. For example, recent work by Hackert *et al.* (2000) compares ocean model simulations for the 1997-1998 ENSO event forced with NCEP reanalysis, satellite-based winds, and other wind products. They found that the satellite wind products perform best overall, but add that each wind product has its own respective strengths and weakness with regards to simulating observed SST, subsurface temperatures, and sea level anomalies.

### 11.4.12 Zonal surface stress

Zonal surface stress is compared to the UWM COADS-based estimates. Zonally averaged values over the ocean (Figure 11.4.28(a)) are similar, except in the Southern Hemisphere mid-latitudes where the reanalyses differ in magnitude from each other, but are all stronger than UWM in a region of few ship reports. UWM's weak values near 50S may reflect interpolation from lower latitudes in the Southern Hemisphere where the zonal stress is less. ERA15 and NCEP2 tend to have stronger maxima than the others, GEOS1 tends to be the weakest.

Figure 11.4.28(b) compares zonal surface stress along the equator from the four reanalyses and from UWM averaged over 1981-92. ERA15 appears somewhat stronger than UWM while NCEP1 is too weak in the Pacific. Comparisons to observations of surface winds in the east Pacific also indicate that NCEP1 near-surface winds are too weak (White, 1996b). GEOS1 and NCEP2's zonal surface stresses are closer in magnitude to UWM in the east Pacific, but shift the maximum value to the east.



Figure 11.4.28 (a) Zonally averaged zonal surface stress over the ocean averaged over 1981-92 from UWM and the reanalyses (right) in Nm$^{-2}$.
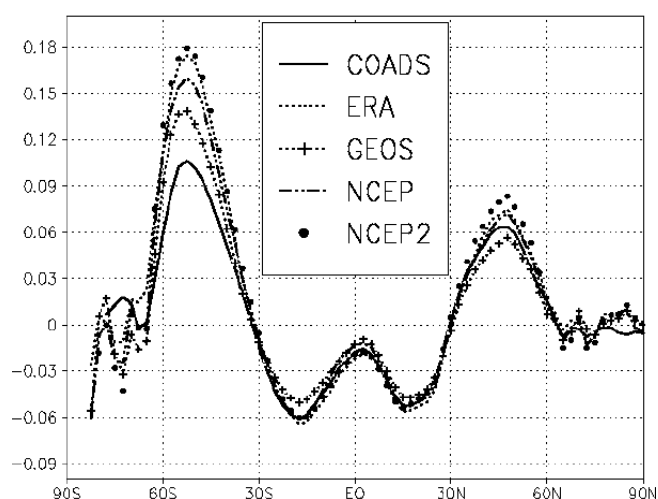


Figure 11.4.28 (b) As (a) but for zonal surface stress along the equator.
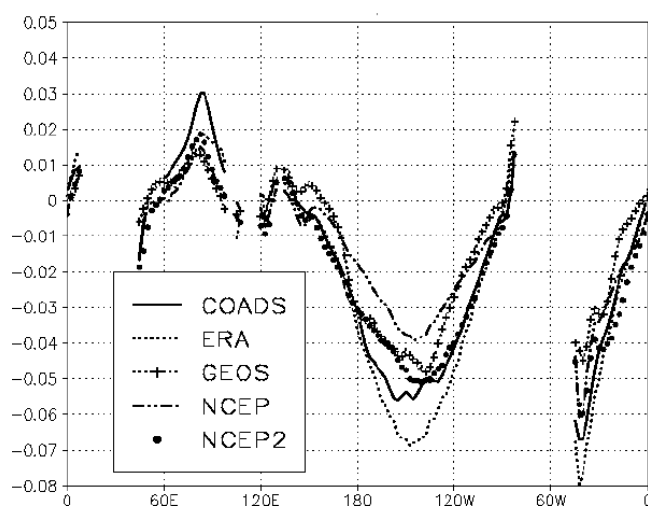
Figure 11.4.29(a) displays the mean zonal surface stress from UWM for 1981-92. ERA15 (Figure 11.4.29(b)) displays stronger westerly stresses in mid-latitudes and stronger easterly stress in the tropics than UWM. GEOS1 (Figure 11.4.29(c)) displays weaker stresses than UWM except south of 30S. NCEP1 (Figure 11.4.29(d)) displays the weakest easterly stress in the central equatorial Pacific, but stronger stresses than UWM elsewhere. NCEP2 (Figure 11.4.29(e)) agrees better with UWM than NCEP1 does in the equatorial Pacific and has the strongest stresses in mid-latitudes.

Figure
11.4.29(a)
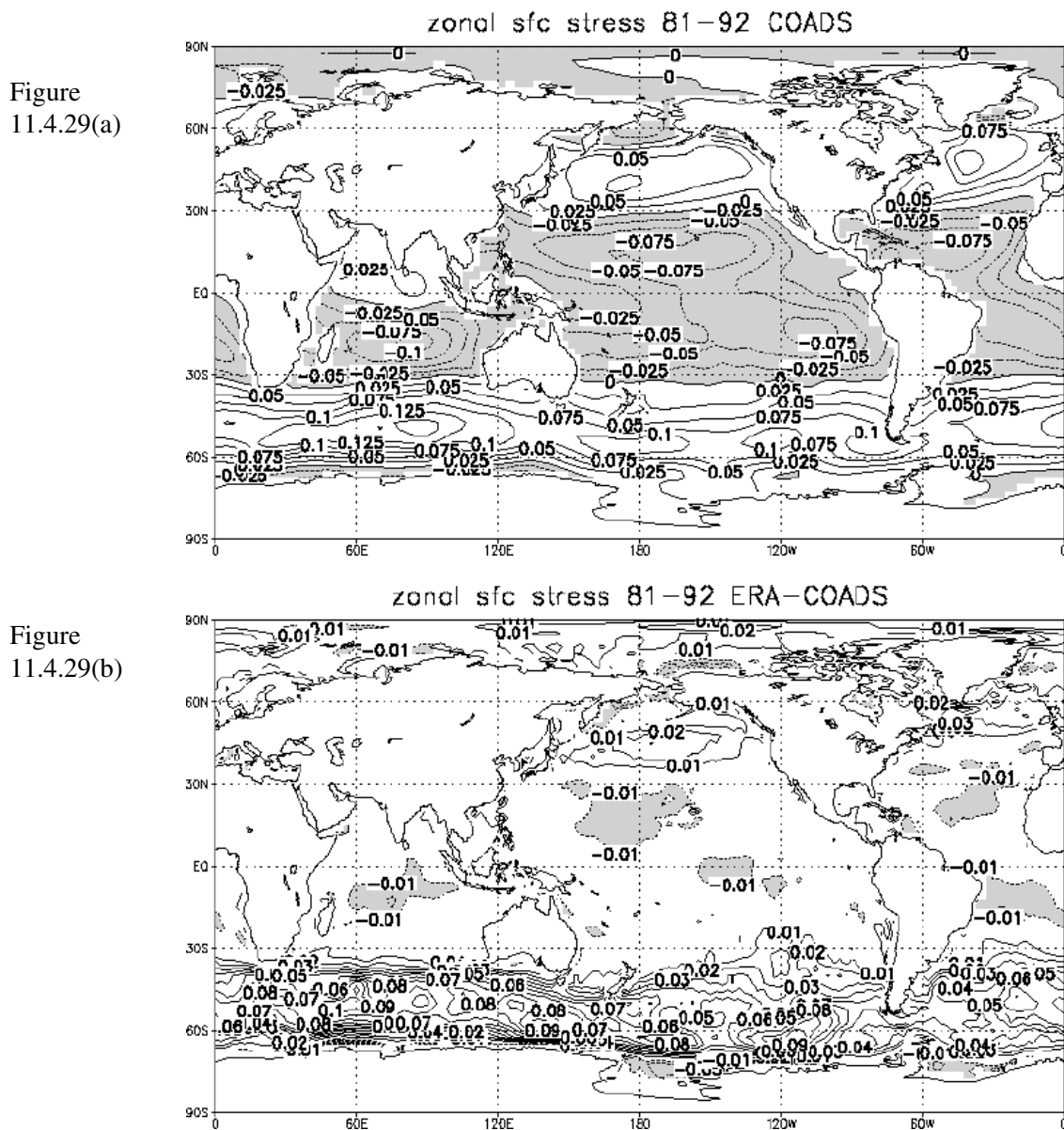


Figure
11.4.29(b)



Figure 11.4.29:    (a) Zonal surface stress from UWM for 1981-92. Contour interval 0.025 Nm$^{-2}$, easterly stress shaded.
(b) Difference in zonal surface stress ERA12 minus UWM. Contour interval 0.01 Nm$^{-2}$, zero omitted, negative (more easterly) values shaded.
(c) As (b) but for GEOS minus UWM.
(d) As (b) but for NCEP1 minus UWM
(e) As (b) but for NCEP2 minus UWM.

Figure
11.4.29(c)



zonal sfc stress 81-92 GEOS-COADS

Figure
11.4.29(d)



zonal sfc stress 81-92 NCEP-COADS

Figure
11.4.29(e)



zonal sfc stress 81-92 NCEP2-COADS
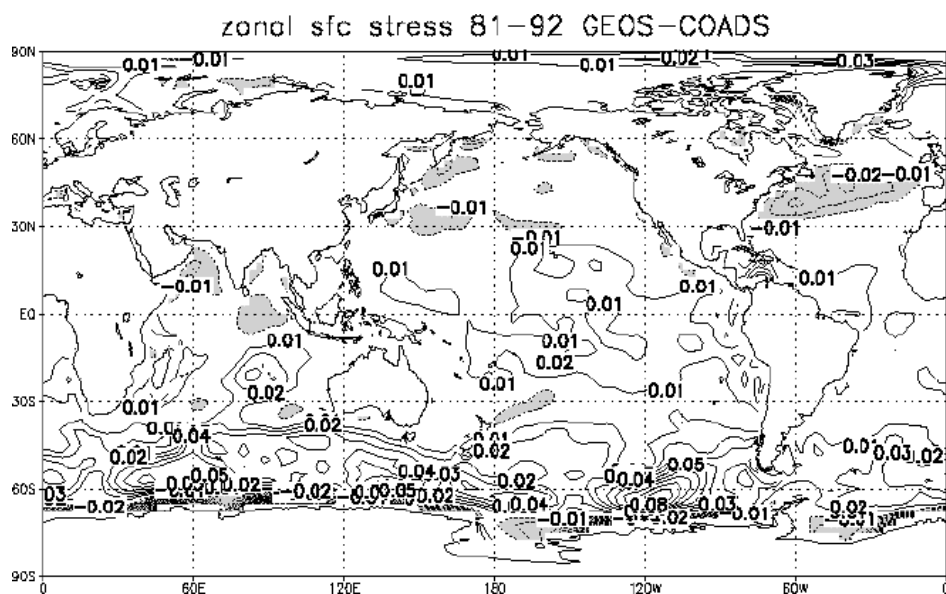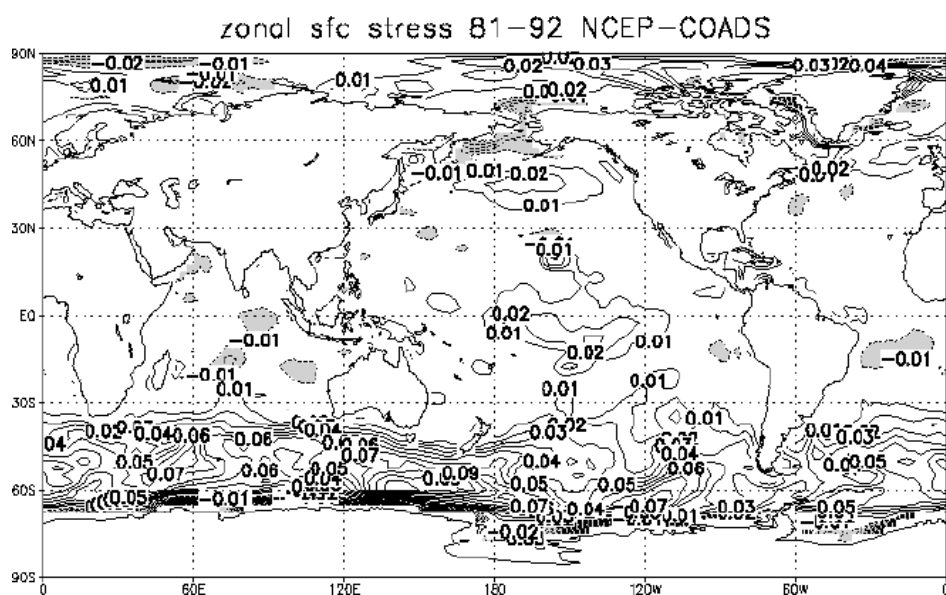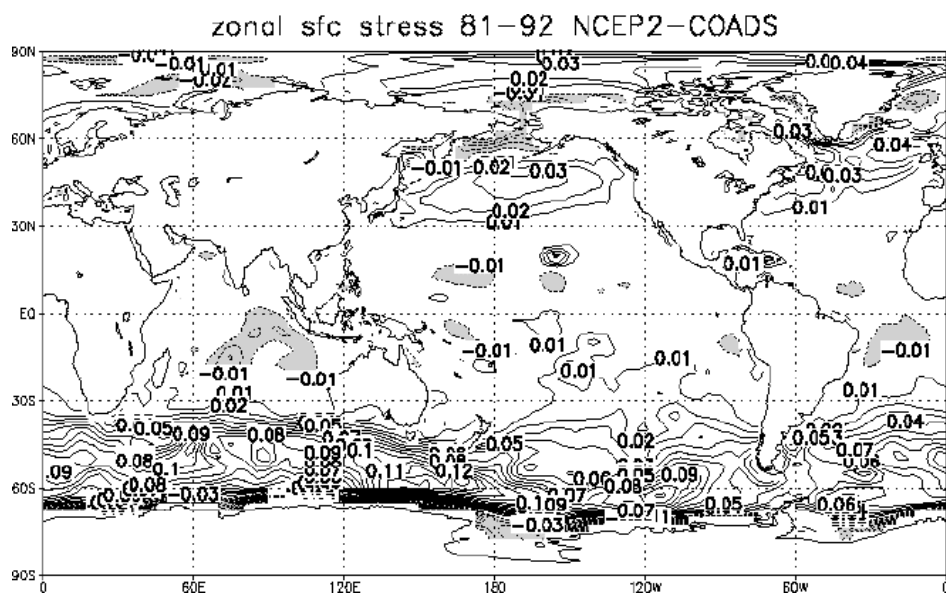
Figure 11.4.30(a) displays the zonal mean correlations of the annual cycles in zonal surface stress in the reanalyses with the annual cycle in the UWM estimate from da Silva *et al.* (1994). The annual cycles are from monthly mean values averaged over 1981-92. All three reanalyses show correlations above 0.6 from 65N to 40S.

The correlations of monthly mean anomalies from the climatologies are shown in Figure 11.4.30(b). The pattern is similar to that seen for latent heat flux (see Figure 11.4.5(c)); however, correlations are somewhat higher in Figure 11.4.30(b), particularly in the tropics. Correlations for zonal surface stress are virtually the same for NCEP1 and ERA15 and slightly lower for GEOS1. ERA15's annual cycle agrees slightly more with UWM than NCEP1's in the tropics but not in mid-latitudes; NCEP1's anomalies agree slightly more with UWM than ERA15's except in the Southern Hemisphere mid-latitudes. NCEP2 displays slightly less agreement with UWM than NCEP1, but more agreement than GEOS1. Anomalies from the reanalyses correlate well with each other over the oceans except near Antarctica; correlations between the reanalyses are lower near the equator than in mid-latitudes.



Figure 11.4.30(a) Zonal mean correlations of monthly mean climatological zonal surface stress over the reanalyses and UWM for the monthly mean annual cycle averaged over 1981-92.
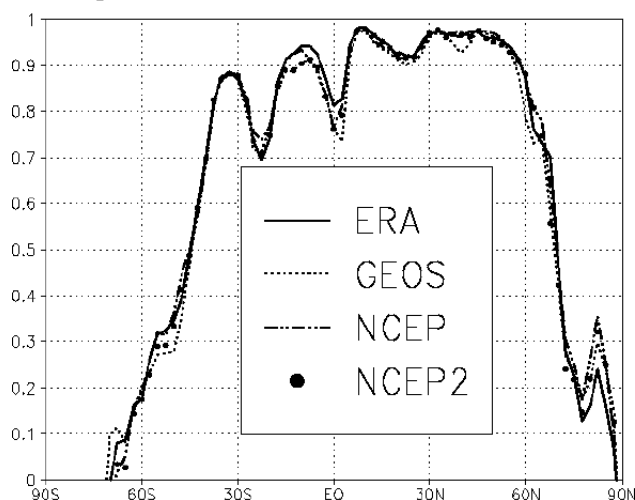
Figure 11.4.30(b) As (a) but for anomalies from each estimate's climatology for 1981-92.
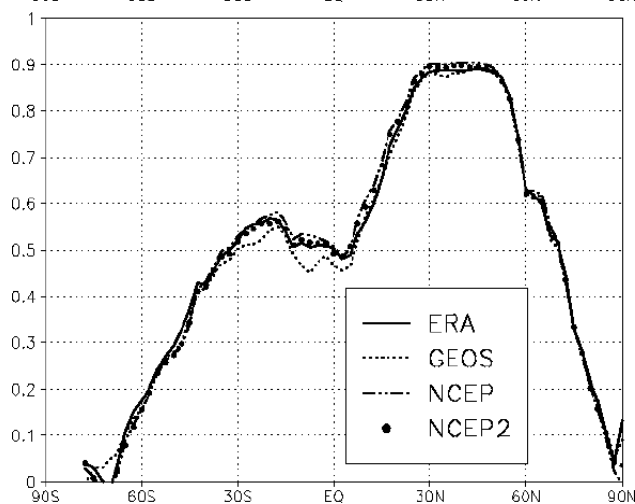
Zonal mean RMS differences between the four reanalyses' zonal surface stress and UWM are shown in Figure 11.4.31(a) for the full monthly means and in Figure 11.4.31(b) for the monthly mean anomalies. NCEP2 displays the largest RMS differences from UWM in higher latitudes, reflecting at least in part the largest variability in both the annual cycle and in anomalies. GEOS1 shows less RMS difference from UWM than other reanalyses, reflecting at least in part the lowest variability and the weakest stress of all the estimates. ERA15 and NCEP1 are more variable in the northern mid-latitudes than UWM. Between 20 and 60N, NCEP1 has the smallest normalised RMS differences from UWM and GEOS1 the largest.

Figure 11.4.31(a) RMS difference in
monthly mean zonal surface stress over the
oceans between the reanalyses and UWM
for 1981-92 in Nm$^{-2}$.



Figure 11.4.31(b) As (a) but for anomalies
from each estimate's climatological annual
cycle in Nm$^{-2}$.
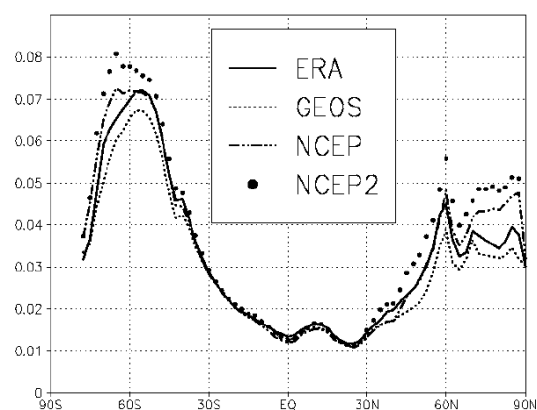


## 11.4.13  Meridional surface stress

The zonal mean meridional surface stress over the ocean averaged over 1981-92 is
shown in Figure 11.4.32.  GEOS1 has weaker northward stress in the Southern Hemisphere
tropics than UWM, particularly in the Southern Hemisphere winter; all the reanalyses have
weaker southward stress in the Northern Hemisphere tropics, especially in the Northern
Hemisphere winter.  In mid-latitudes in both hemispheres the reanalyses all have stronger
poleward stresses than UWM.

Figure 11.4.32 Zonally averaged
meridional surface stress over
the ocean averaged over
1981-92 from UWM and the
reanalyses in  Nm$^{-2}$.
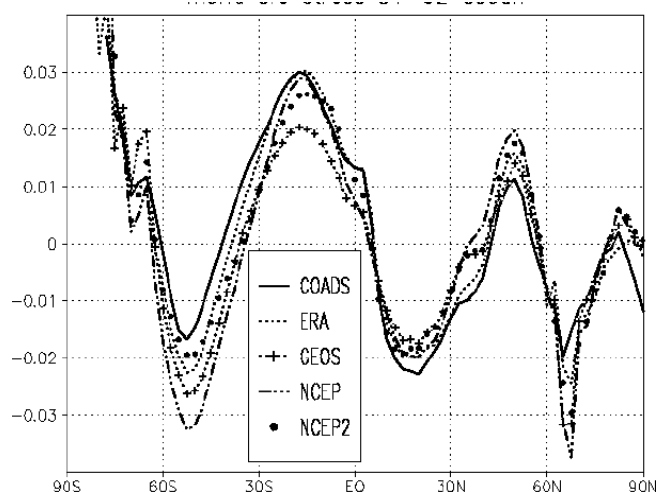


Figure 11.4.33(a) shows the annual mean meridional surface stress for 1981-92 from
UWM.   In the east tropical Pacific, a strong northward stress can be seen at the equator and a
strong southward stress near 15N.  ERA15 (Figure 11.4.33(b)) shows a similar, but slightly
weaker pattern; GEOS1 (Figure 11.4.33(c)) and NCEP1 (Figure 11.4.33(d)) are significantly

Figure
11.4.33(a)



merid sfc stress 81-92 COADS

Figure
11.4.33(b)



merid sfc stress 81-92 ERA-COADS

Figure
11.4.33(c)



merid sfc stress 81-92 GEOS-COADS

Figure
11.4.33(d)



merid sfc stress 81-92 NCEP-COADS

Figure
11.4.33(e)



merid sfc stress 81-92 NCEP2-COADS
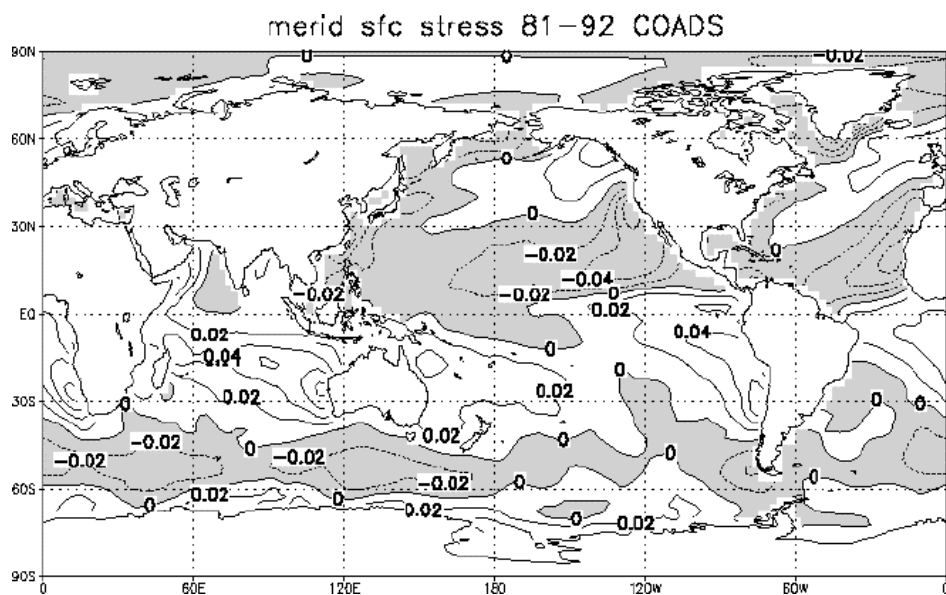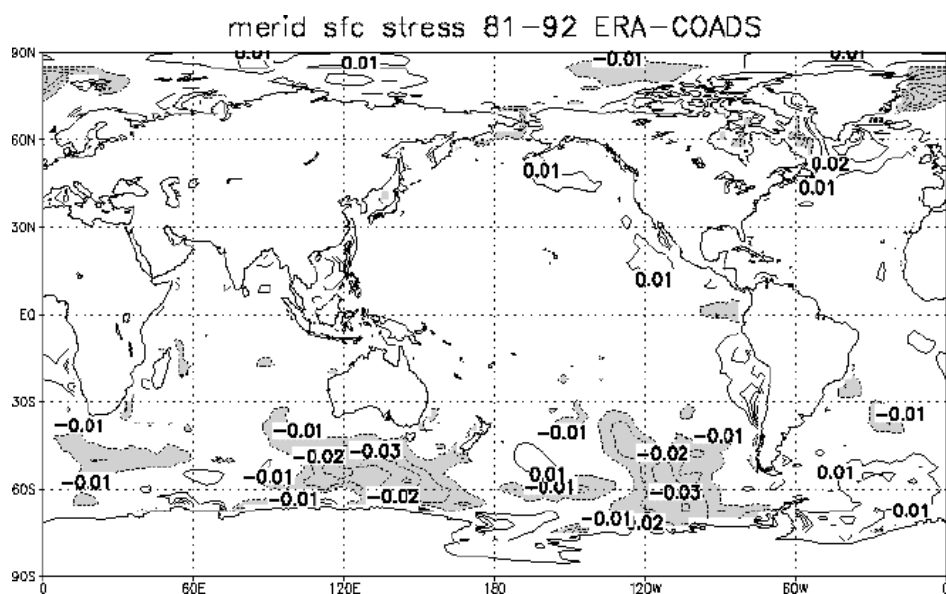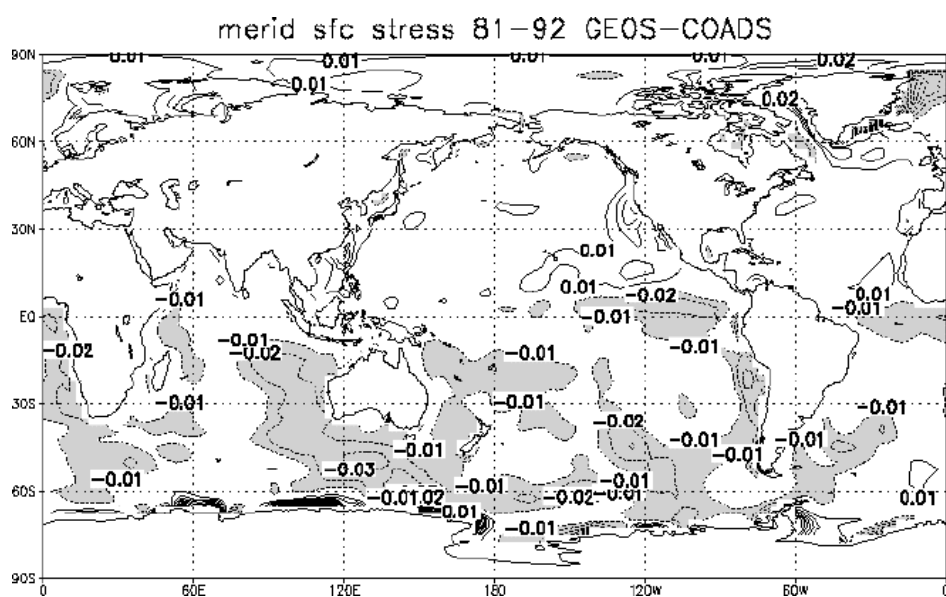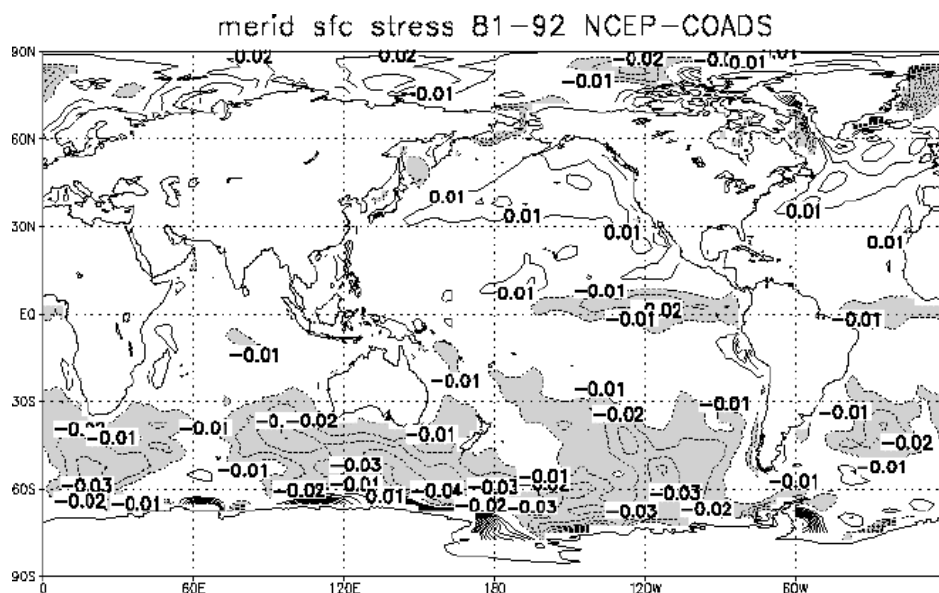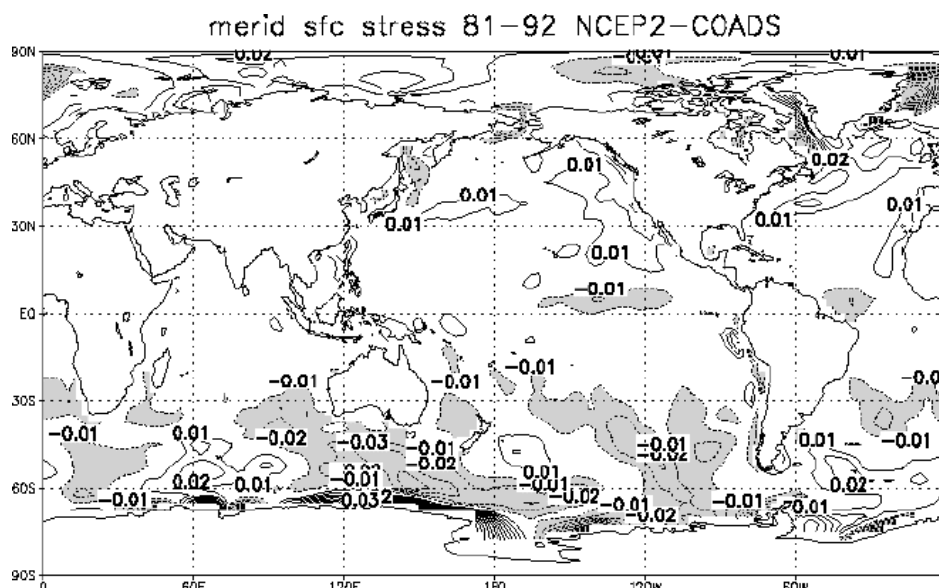
Figure 11.4.33:   (a) Meridional surface stress from UWM based on COADS.  Contour interval
                       0.02 Nm$^{-2}$, northerly stress shaded.
                   (b) Difference in meridional surface stress ERA minus COADS.  Contour
                       interval 0.01 Nm$^{-2}$, zero omitted, negative values shaded.
                   (c) As (b) but for GEOS minus UWM.
                   (d) As (b) but for NCEP1 minus COADS.
                   (e) As (b) but for NCEP2 minus COADS.

weaker than UWM in the eastern tropical Pacific and in the tropical Atlantic.  NCEP2 (Figure
11.4.33(e)) shows smaller mean differences from UWM than NCEP1, especially along the
equator.  All the reanalyses show significant differences from UWM south of 30S.

Zonal mean correlations between UWM and the reanalyses for meridional surface stress
are similar to, but somewhat lower than, the correlations for zonal surface stress (Figure
11.4.30).  The annual cycles in the reanalyses agree quite well (0.9 or higher) with UWM
between 55N and 15S; the correlation of the reanalyses' anomalies with UWM anomalies
exceeds 0.8 from 25N to 55N.  NCEP1's annual cycle has the worst agreement with UWM
between 20 and 60N and ERA15's agrees the best; GEOS1 has the worst agreement elsewhere.
GEOS1's anomalies agree the worst with UWM; NCEP1's anomalies tend to agree the best.

NCEP2's annual cycle is slightly better correlated with UWM than NCEP1; its anomalies are slightly worse.

Zonal mean RMS differences between the three reanalyses' meridional surface stress and UWM are shown in Figure 11.4.34(a) for the full monthly means and in Figure 11.4.34(b) for the monthly mean anomalies. Even though GEOS1 displays the least variability of the four estimates, ERA15's annual cycle is the least different from UWM. The anomalies in GEOS1 are the least different from UWM in high latitudes and have the lowest month-to-month variability. NCEP2 tends to show the largest differences from UWM in high latitudes and has the largest month-to-month variability. GEOS1 has the largest normalised RMS differences from UWM between 20 and 60N; ERA15 has the least.

Figure 11.4.34(a) RMS differences in monthly mean meridional surface stress over the oceans between the reanalyses and UWM for 1981-92 in Nm$^{-2}$.
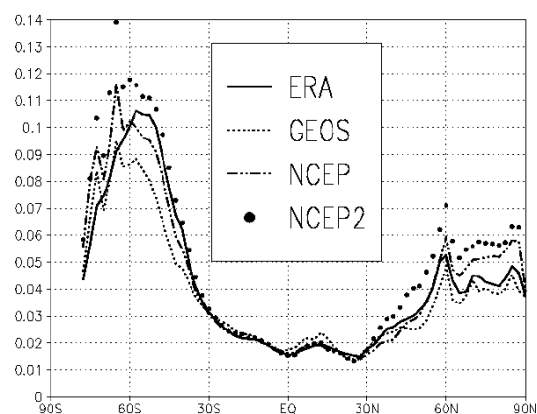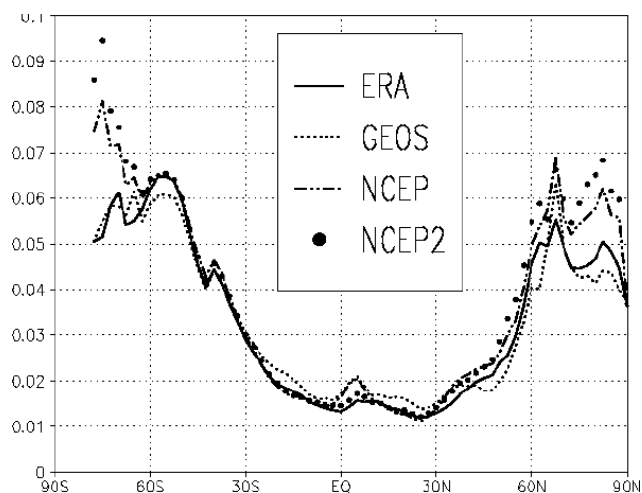


Figure 11.4.34(b) As (a) but for anomalies from each estimate's climatological annual cycle in Nm$^{-2}$.
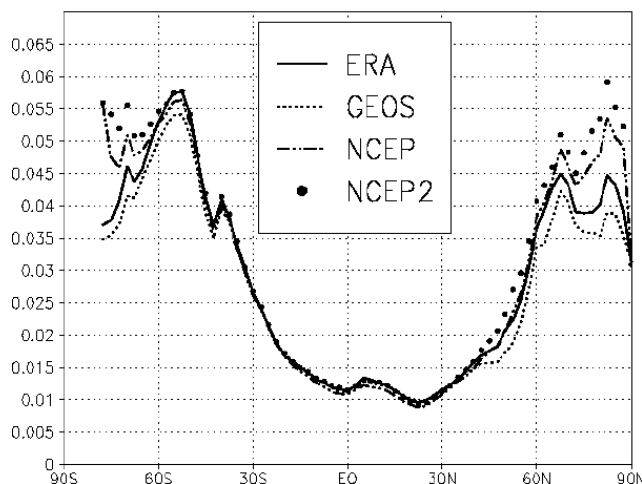


*11.4.14  Precipitation*

Stendel and Arpe (1997) evaluated the hydrological cycle in the ERA15, NCEP1 and GEOS1 reanalyses. Trenberth and Guillemot (1998) examined atmospheric moisture and the hydrological cycle in the NCEP1 reanalysis and compared NCEP1 precipitation to CMAP precipitation. Janowiak *et al.* (1998) compared GPCP precipitation with precipitation from the NCEP1 reanalyses. Arpe *et al.* (2000) examined the hydrological cycle in the reanalyses and concluded, "There is not one reanalysis which is superior in all respects and a new evaluation of the reanalyses has to be made before each application."

Table 1 compares mean precipitation estimates averaged over different oceanic regions from the reanalyses with two independent estimates by Xie and Arkin (1996, 1997) (CMAP) and by the Global Precipitation Climatology Project (GPCP) (World Climate Research Programme, 1990; Huffman *et al.*, 1997). The two independent estimates are based on satellite estimates of precipitation over the ocean. In mid-latitudes ERA15 and NCEP2 agree the best

with the independent estimates; NCEP1 and GEOS1 are less.  In the tropics and over the whole region between 50S and 45N NCEP2 and ERA15 exceed the independent estimates, while NCEP1 and GEOS1 are close to the independent estimates.

Table 1 Mean precipitation in mm/day over different regions of the ocean averaged over 1988-92 for the four reanalyses and two independent estimates derived from satellites over the ocean.

|  | 50S-45N | 20-50S | 20S-20N | 20-45N |
|---|---|---|---|---|
| CMAP | 3.33 | 2.55 | 4.13 | 2.75 |
| GPCP | 3.1 | 2.64 | 3.54 | 2.84 |
| ERA15 | 3.79 | 2.47 | 5.13 | 2.8 |
| GEOS1 | 3.05 | 1.88 | 4.2 | 2.29 |
| NCEP1 | 3.15 | 2.13 | 4.12 | 2.54 |
| NCEP2 | 3.7 | 2.64 | 4.8 | 2.84 |

Figure 11.4.35   Zonal mean precipitation over the oceans averaged over 1988-92 from the reanalyses, CMAP (Xie-Arkin) and GPCP in mm/day.
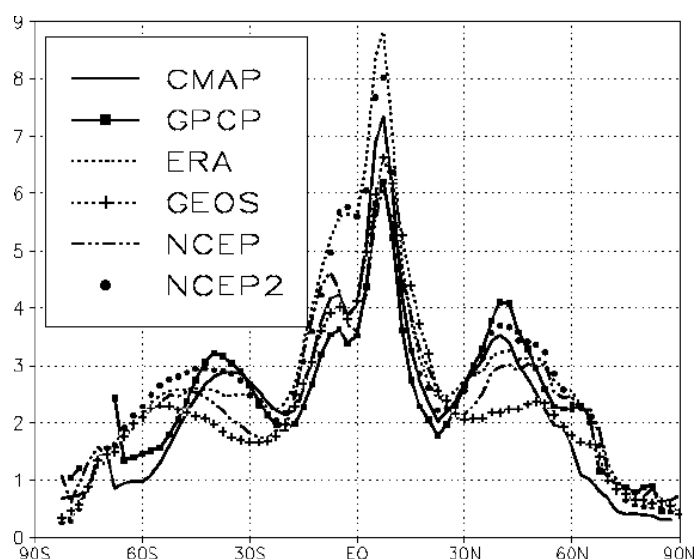


Figure 11.4.35 compares zonal mean precipitation over the ocean from the four reanalyses with CMAP and GPCP for the years 1988-92.  Over the ocean ERA15 and NCEP2 clearly have the most rainfall in the tropics, where the two independent estimates disagree with each other by as much as 1 mm/day.  GEOS1 lies between the two independent estimates while NCEP1 agrees with the lower independent estimate (GPCP).  CMAP uses similar data sets to GPCP; however, CMAP uses rainfall measurements from tropical atolls to calibrate satellite rainfall estimates over the tropical oceans and GPCP does not.  The mid-latitude maxima in precipitation are further poleward in the reanalyses than in the satellite-based estimate.  NCEP2 has more precipitation in mid-latitudes than the other reanalyses.

Figure 11.4.36 compares the standard deviation of rainfall from the three reanalyses and from CMAP over the ocean for the full monthly means (Figure 11.4.36(a)), the annual cycle averaged over 1988-92 (Figure 11.4.36(b)) and monthly mean anomalies for 1988-92 from the annual cycle (Figure 11.4.36(c)).  The results suggest that the ERA15 and NCEP2 reanalyses overestimate variability and NCEP1 and GEOS1 underestimate variability over the tropical oceans. All four reanalyses and GPCP have larger precipitation anomalies at higher latitudes than CMAP.  NCEP2 has the strongest variability in mid-latitudes.

Figure 11.4.36(a) Zonal mean standard deviation of monthly mean precipitation over the oceans for 1988-92 in mm/day.



Figure 11.4.36(b) As (a) but for monthly mean climatology averaged over 1988-92.
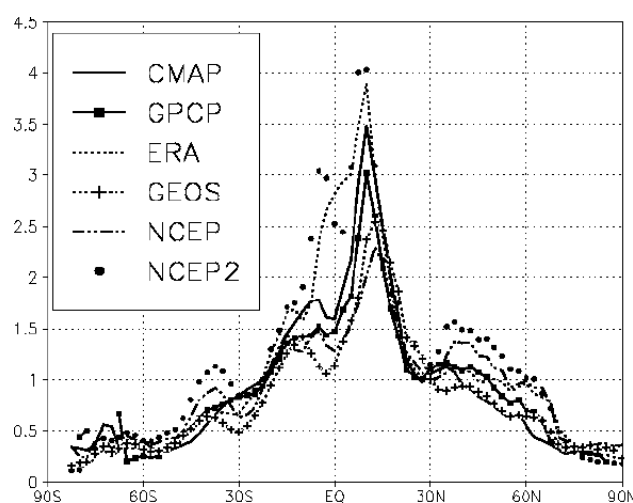


Figure 11.4.36(c) As (a) but for monthly anomalies for 1988-92 from the monthly mean climatology.
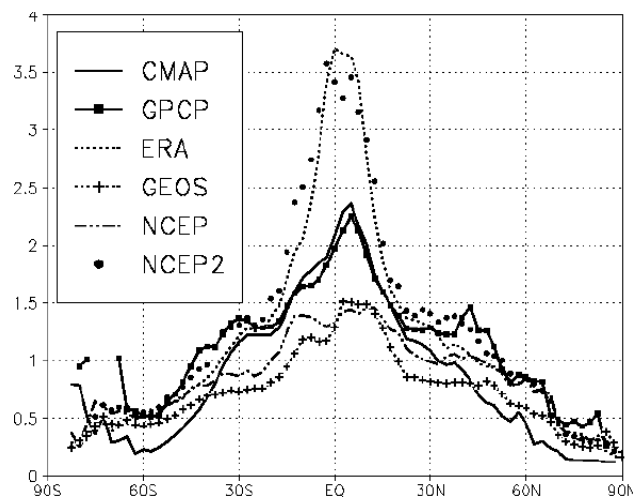


Figure 11.4.37(a) shows the five-year mean precipitation estimate from CMAP. GPCP (Figure 11.4.37(b)) has less rain in the tropics and more near 45° in both hemispheres. The two independent estimates based on satellite estimates differ by more than 1 mm/day over much of the tropical ocean. ERA15 (Figure 11.4.37(c)) has more intense tropical convergence zones than CMAP, less precipitation near 30S and 45N and more near 60N and 60S. GEOS1 (Figure 11.4.37(d)) shows less rain in the east Pacific and Atlantic ITCZ and in the South Pacific and South Atlantic convergence zones, but more precipitation than CMAP north of the equator in the western Pacific and Caribbean. It has the least precipitation over the northern mid-latitude storm tracks. NCEP1 (Figure 11.4.37(e)) also has weaker convergence zones than CMAP.

Figure
11.4.37(a)

precipitation 1988-92 CMAP

Figure
11.4.37(b)

precip 1988-92 GPCP-CMAP

Figure
11.4.37(c)

precip 1988-92 ERA-CMAP

Figure
11.4.37(d)

precip 1988-92 GEOS-CMAP

Figure
11.4.37(e)

precip 1988-92 NCEP-CMAP

Figure
11.4.37(f)

precip 1988-92 NCEP2-CMAP
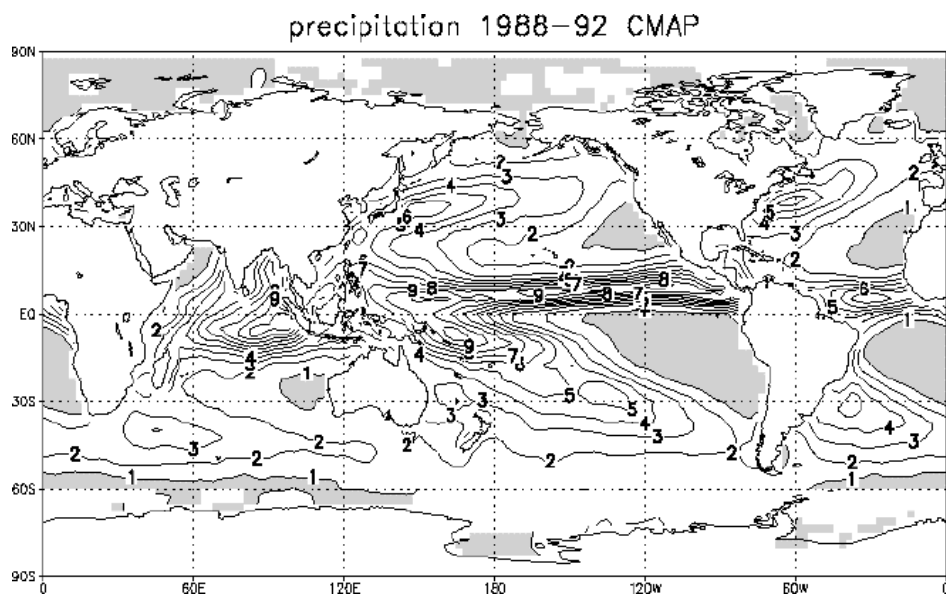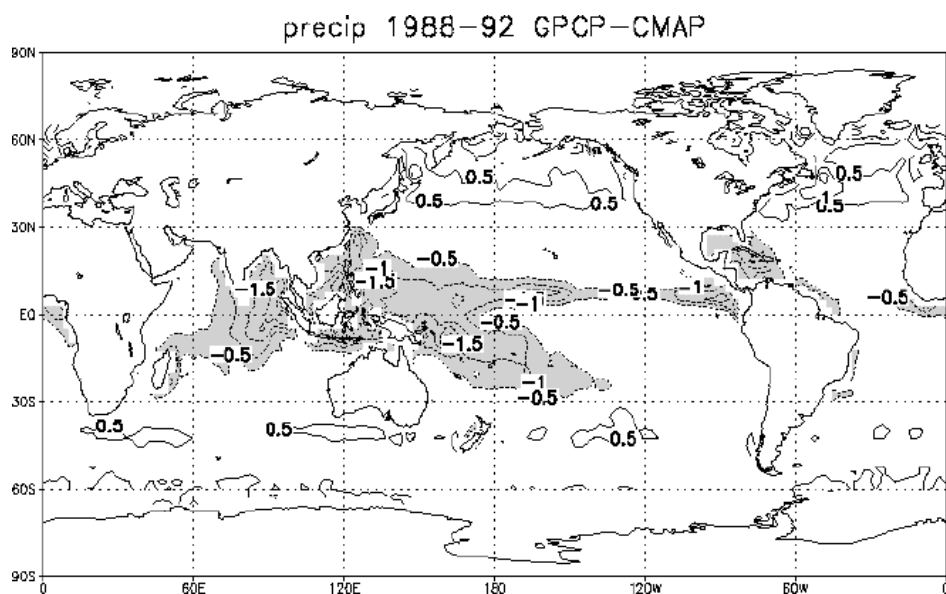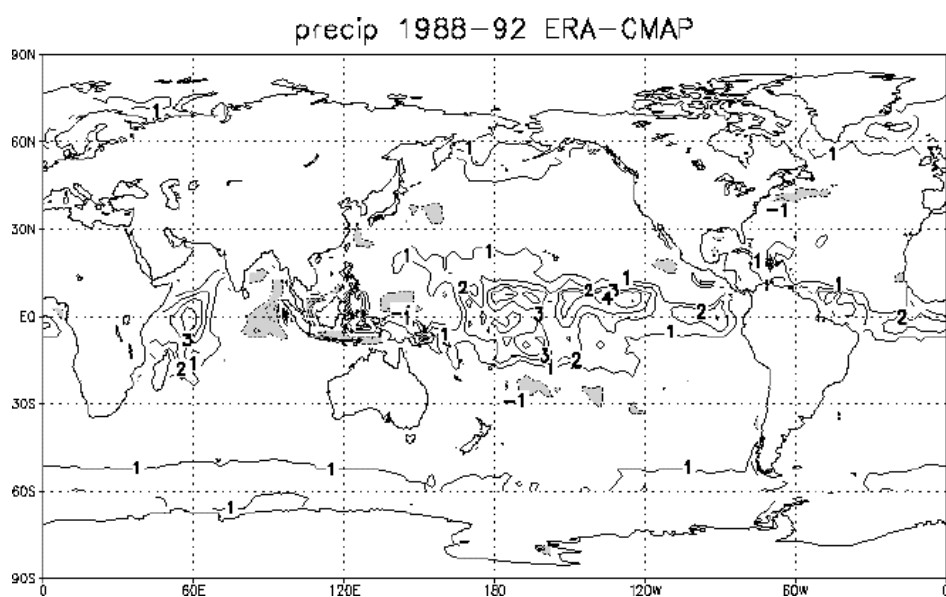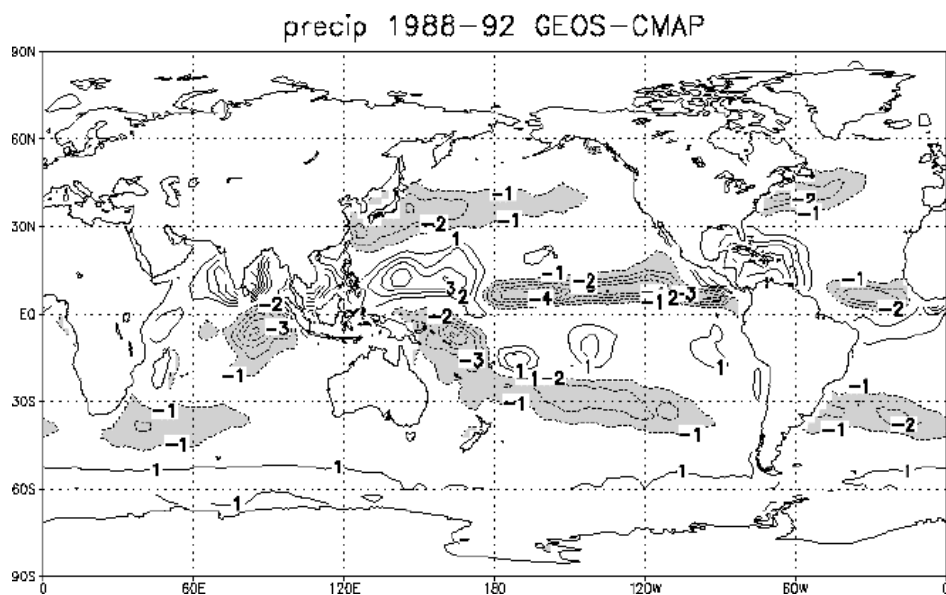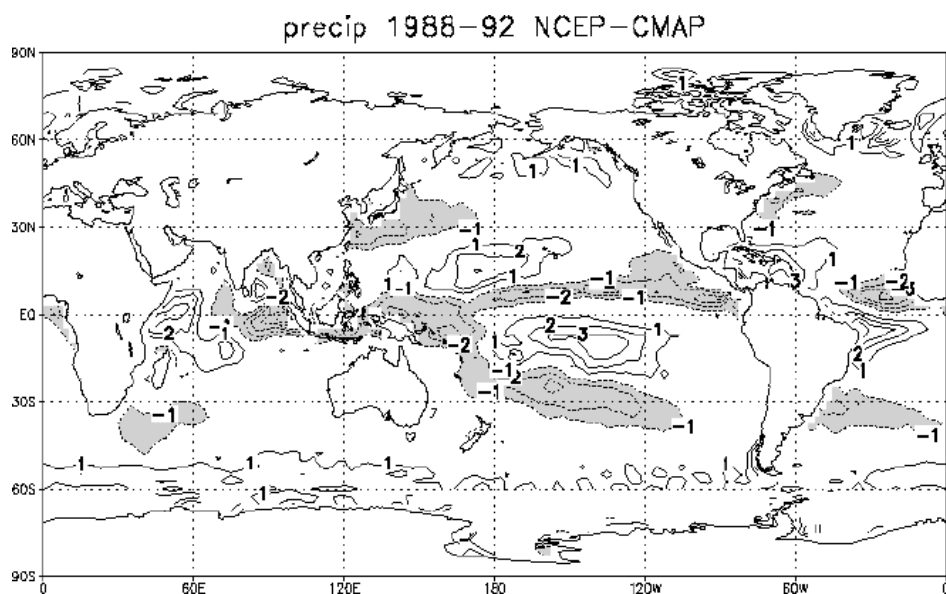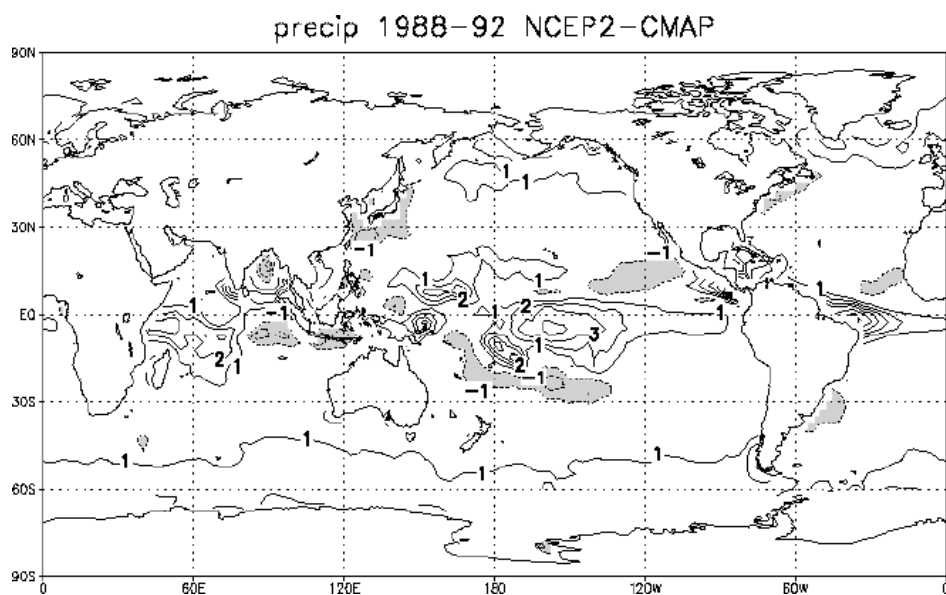
Figure 11.4.37:  (a) Mean precipitation from CMAP (Xie-Arkin) for 1988-92.  Contour interval
1 mm/day. Values less than 1 mm/day shaded.
(b) Difference in precipitation GPCP minus CMAP.  Contour interval 0.5
mm/day, zero omitted, negative values shaded.
(c) Difference in precipitation ERA15 minus CMAP.  Contour interval 1
mm/month, zero omitted, negative values shaded.
(d) As (c) but for GEOS1 minus CMAP.
(e) As (c) but for NCEP1 minus CMAP.
(f) As (c) but for NCEP2 minus CMAP.

NCEP1 (Figure 11.4.37(e)) and NCEP2 (Figure 11.4.37(f)) have more rain than CMAP off northeast Brazil and in the east Pacific dry zone between the ITCZ and the South Pacific convergence zone.  In all the reanalyses the South Pacific Convergence Zone tends to have an east-west orientation rather than a northwest-southeast orientation.  NCEP2 clearly has more rainfall over the tropical oceans than NCEP1 and the independent estimates.  ERA15, GEOS1 and NCEP1 have less rain than CMAP in the mid-latitude storm tracks, as can be seen to the east of Japan and the United States, and more precipitation further poleward.

Zonal mean correlations of oceanic precipitation estimated by CMAP with GPCP and the ERA15, GEOS1 and NCEP1 reanalyses are shown in Figure 11.4.38(a) for the annual cycle averaged over 1988-92 and in Figure 11.4.38(b) for anomalies from the annual cycle.  The regional patterns of correlations in the reanalyses are similar to each other.  Low correlations appear over the east Pacific and Atlantic ITCZ's and other convective regions.  The reanalyses also show high correlations along the equator in the Pacific and lower correlations to the north and south.  Over the oceans the reanalyses all show high correlations near 30° and low correlations at higher latitudes in both hemispheres.  ERA15 has the highest correlations, while GEOS1 is somewhat lower than NCEP1 over the ocean. NCEP2 is better correlated with CMAP estimates than NCEP1 in mid-latitudes, especially for the climatological annual cycle.

Figure 11.4.38(a) Zonal mean correlation of climatological precipitation over the oceans for the reanalyses and GPCP with CMAP (Xie-Arkin) for the monthly mean annual cycle averaged over 1988-92.
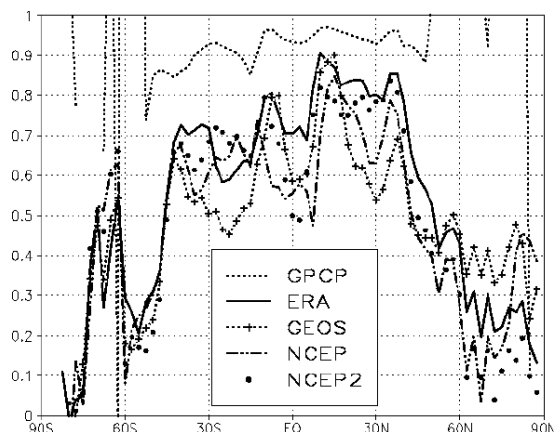
Figure 11.4.38(b)  As (a) but for monthly anomalies for 1988-92 from the climatological annual cycle.
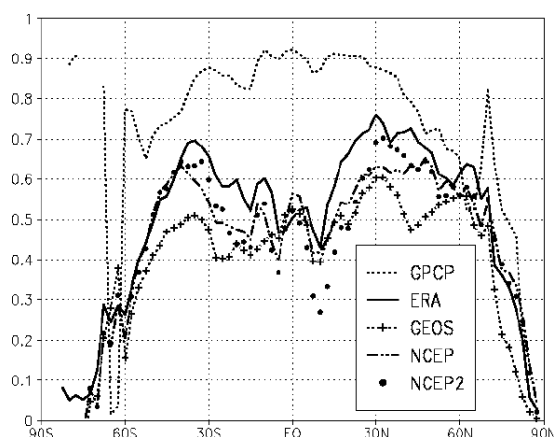
Precipitation in CMAP and GPCP is derived from raingauges over land and by empirical techniques from satellite observations over the oceans. The regional pattern of correlation of precipitation anomalies in GPCP and in CMAP is similar to the regional pattern of correlation between CMAP and reanalysis precipitation anomalies. (However, the correlations between GPCP and CMAP exceed 0.80 in most regions and are considerably higher than the correlations between the reanalysis and CMAP.) This similarity of pattern suggests that a secondary part of the spatial variation in correlation between the reanalyses and CMAP, such as lower correlations at higher latitudes, may reflect uncertainty in the CMAP estimate of precipitation.

RMS differences from the monthly means of CMAP are shown in Figure 11.4.39(a) for the monthly means for 1988-92, in Figure 11.4.39(b) for the annual cycle averaged over 1988-92, and in Figure 11.4.39(c) for the anomalies from the annual cycle. Of the reanalyses, ERA15 has the lowest RMS difference over the extratropical oceans. NCEP2 and ERA15 have the largest RMS difference over the tropics where they display considerably more month-to-month variability than CMAP or the other reanalyses. NCEP2 tends to have the largest RMS difference from CMAP outside the tropics, reflecting greater month-to-month variability in precipitation than other reanalyses and CMAP. GEOS1 tends to have the largest normalised RMS difference from CMAP and ERA15 the least. NCEP2's normalised RMS difference from CMAP is significantly less than NCEP1's.

Also shown in Figures 11.4.38 and 11.4.39 are correlations and RMS differences between monthly means for GPCP and for CMAP, as a measure of the uncertainty in CMAP estimates of precipitation. Since GPCP and CMAP use similar methods of estimating precipitation, they should be regarded as a lower estimate of the uncertainty in CMAP. Correlations between CMAP and GPCP anomalies are considerably higher than the correlations between CMAP and the reanalyses, but are lower over the extra-tropical oceans than in the tropics. RMS differences between GPCP and CMAP anomalies are as large in higher latitudes as the RMS differences between CMAP and reanalysis anomalies and are not negligible in the tropics. Satellite estimates of precipitation are often developed and "tuned" for the tropical oceans. In addition certain satellite estimates use the cloud-top temperature as a proxy for rainfall rate; this method does not work well far from the equator. Thus satellite estimates may not be as applicable to the extra-tropical oceans as they are to the tropical oceans. This suggests that significant uncertainties remain in the independent estimates of precipitation, perhaps more so in the magnitude than in the pattern of precipitation, and that a secondary part of the differences between the reanalyses' precipitation and satellite estimates of precipitation reflects uncertainty in the satellite estimates over the oceans.

Figure 11.4.39(a) RMS differences in monthly mean precipitation over the oceans between the reanalyses and GPCP and CMAP for 1988-92 in mm/month.
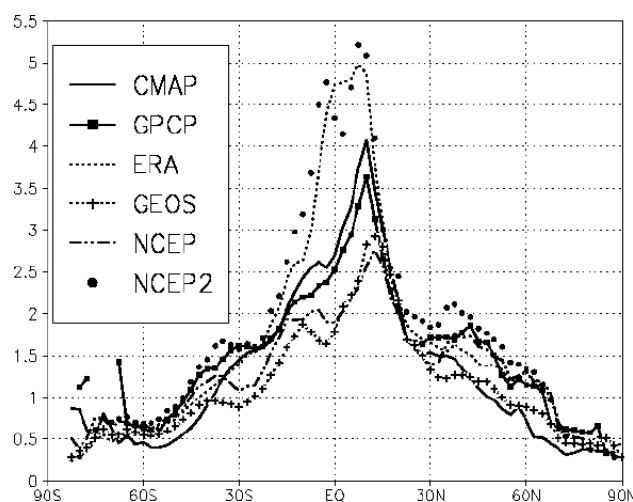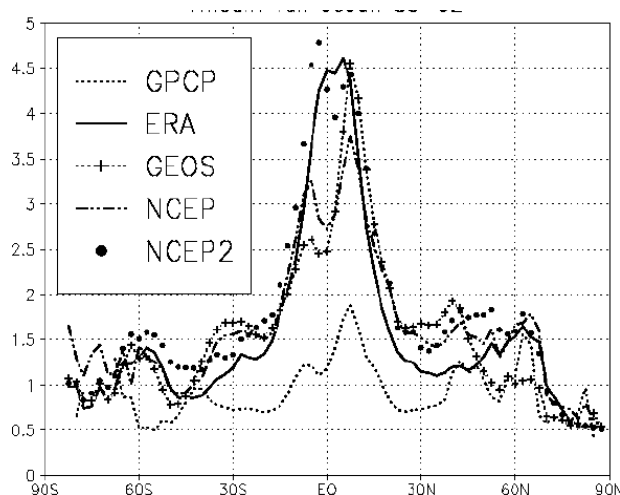
Figure 11.4.39(b) As (a) but for climatological monthly means averaged over 1988-92.
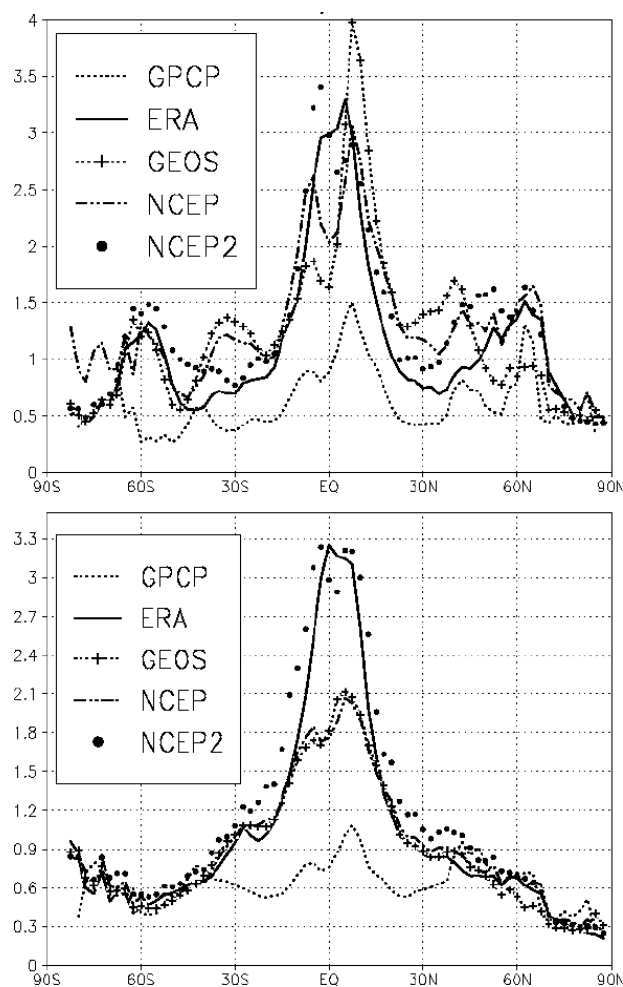


Figure 11.4.39(c) As (a) but for anomalies for 1988-92 from the climatology.



*11.4.15 Conclusions*

　　　An enormous effort has gone into the careful calculation of surface fluxes from COADS data. The best COADS estimates of surface fluxes, however, are still far from a global mean energy balance (Josey *et al.*, 1999) and it is not at all clear that the imbalance is solely due to the scarcity of ship observations over large regions of the oceans. The adjustments commonly made to achieve balance include a large reduction in surface net short wave radiation. The original UWM NSW actually agrees well with the satellite-based SRB estimate; however, the SRB estimate may have a positive bias. The SRB satellite estimate of NLW also appears questionable. The global mean SRB NLW appears to be quite different in magnitude than other estimates and the net surface radiation resulting from the SRB NSW and NLW implies a need for considerably larger sensible and latent heat fluxes than the estimates examined here. This study has shown significant time-mean differences between the reanalyses and independent estimates and has not resolved which is correct.

　　　Surface fluxes from the NCEP1, NCEP2 and ERA15 reanalyses generally show very similar levels of agreement with UWM and SRB estimates; in many cases fluxes from GEOS1 show lower correlations with independent estimates. The annual cycle in ERA15 tends to agree slightly better with independent estimates than NCEP1's annual cycle; NCEP1's anomalies agree slightly more in general with independent estimates than ERA15's anomalies. NCEP1 appears to underestimate variability over the tropical oceans; NCEP2 and ERA15 appear to overestimate variability in the tropics. NCEP2 has more upward latent heat flux and less upward sensible heat flux than NCEP1; this may reflect a change in the boundary layer formulation. NCEP2's sensible heat flux is less than the other estimates. NCEP2 appears to have fewer stratus clouds and worse short wave radiation in the eastern subtropical oceans than NCEP1, but corrects two problems in NCEP1: too much downward short wave radiation at the surface and too high ocean surface albedo. NCEP2 tends to have the largest month-to-month

variability of the reanalyses; GEOS1 tends to have the least.

The climatologies from the reanalyses show good agreement with the UWM climatology in the mid-latitudes of both hemispheres; flux anomalies from the reanalyses show good agreement with UWM anomalies in the Northern Hemisphere mid-latitudes. The results suggest that UWM is useful for defining month to month variability in fluxes in the northern mid-latitudes and a few other regions but may be useful in defining climatological fields in the Southern Hemisphere north of 40S.

The reanalyses appear to have large biases in surface NSW. GEOS1 in particular appears to have quite different surface radiation than the other estimates examined here. This suggests that cloudiness needs to be improved in the reanalyses. Whether these biases reflect primarily problems in the parameterisation of cloudiness or problems in the parameterisation of the hydrological cycle is not clear. A major problem in the reanalyses appears to be the treatment of low-level stratus clouds, particularly in the ERA15, GEOS1 and NCEP2 reanalyses.

Comparisons with in-situ measurements have revealed differences in sensible and latent heat flux due to differences in flux algorithms; the NCEP algorithm is deficient at high wind speeds where it yields too much latent heat flux. This problem has been corrected in the operational NCEP model, but not the NCEP2 reanalysis. While the ERA15 algorithm appears to perform better over the Labrador Sea, it and NCEP2 gives even more evaporation globally than NCEP1 and display no more agreement in general with UWM estimates. It should be noted that fluxes in NWP analysis/forecast systems reflect the entire physics package and the analysed near-surface meteorological fields and not just the flux algorithms. One major question to which the answer is not clear is the magnitude of the hydrological cycle.

Surface stresses from the NCEP1 and ERA15 reanalyses generally show very similar levels of agreement with da Silva *et al.* (1994) COADS-based surface stresses; GEOS1 stresses show slightly less agreement with UWM. The annual cycle in ERA15 agrees slightly better with UWM than the NCEP1 annual cycle; the NCEP1 anomalies agree slightly more with COADS than the ERA15 anomalies. Time-mean stresses from NCEP2 show less difference from COADS than do NCEP1 stresses. NCEP2's stronger tropical surface stress appears to be more realistic than NCEP1, perhaps reflecting stronger tropical precipitation than in NCEP1. The stronger tropical precipitation in NCEP2 may not be more realistic in magnitude than NCEP1.

The reanalyses appear to have large biases in precipitation. ERA15 appears to be somewhat better in depicting monthly precipitation patterns than NCEP1 or GEOS1; NCEP1 may be somewhat better than GEOS1 over the oceans. NCEP2 appears more correlated than NCEP1 with independent estimates outside the tropics and has less normalised RMS difference from CMAP in the tropics as well as mid-latitudes. ERA15 and NCEP2 exceed the independent estimates over the tropical oceans. NCEP1 underestimates variability over the tropical oceans; ERA15 overestimates variability in the tropics and NCEP2 appears to overestimate it nearly everywhere.

A major uncertainty is the true magnitude of precipitation over the ocean. Smith *et al.* (1999) found the NCEP1 reanalysis evaporation exceeded estimates derived from ship observations using the Smith (1988) algorithm by 20 Wm$^{-2}$. (Both NCEP2 and ERA15 have more oceanic evaporation and more precipitation than NCEP1.) This implies that global precipitation from the NCEP1 reanalysis should also be too high; comparisons with independent estimates shown above suggest that NCEP1 precipitation is not too high over the oceans but that NCEP2 and ERA are. Comparisons with CMAP and GPCP over land suggest that all the reanalyses are too high over land by 0.43 to 0.7 mm/day between 50S and 45N and by 0.8 to 1.19 mm/day between 20S and 20N. This suggests that too high evaporation over the ocean in the NCEP1 reanalysis (and other reanalyses as well) may be associated with too much precipitation over land. In that case the excessive evaporation could be due to errors in the NWP systems' parameterisation of convection as well as errors in their parameterisation of evaporation over the oceans.

## 11.5  Flux Products from Operational NWP Model's

Because operational NWP models are constantly evolving,  the Working Group on Air-Sea Fluxes decided that flux products from these models could not be evaluated for this report. Rather they requested the Working Group on Numerical Modelling (WGNE) to consider this problem.   Here we summarise the present position.

The increasing interest in seasonal forecasting has resulted in a much greater need for improved surface fluxes.  Additionally, analysis and reanalysis offer some of the best hope for improved estimates of large-scale fluxes.   The WGNE has identified the need for an infrastructure to assist NWP centres in the evaluation and intercomparison of analysed surface fluxes.   Previous studies (e.g., White, 1995) have studied ocean surface fluxes from single versions of several operational models.   NWP fluxes have been found to be within the range of differences found with COADS-type climatologies,  although cloudiness has been identified as a major source of uncertainty.   Significant differences from each other and satellite estimates in net surface short wave and OLR suggest important variations in cloud-radiative effects.   While valuable, these "snapshot" studies have not enabled operational centres to monitor how derived fluxes vary with their evolving systems.

In response to the urging of the WGNE, Peter Gleckler (PCMDI) and Jan Polcher (LMD) have agreed to reinvigorate the study of NWP surface fluxes.   There are several components to the planned study, the first being a reworking of White (1995) with recent operational data.   The project extends previous efforts in two ways.   First, fluxes over ocean and land are to be evaluated.   Although different in many ways (e.g. the types of observational data available), the study of ocean and land surface fluxes will be coordinated to optimise the efforts involved.   The second difference from earlier efforts, and more ambitious aspect of this project,  amounts to a pilot study.   The objective of this exploratory initiative is to examine the feasibility of developing an operational system to evaluate and intercompare NWP surface fluxes.

Following the data and metadata standards established for AMIP, centres have begun to contribute 6 hourly fluxes for 1999 at different spin-up intervals.   An update to the White (1995) study is expected within one year,  and by the 16th Session of the WGNE (Nov 2000) experience should be sufficient to evaluate the usefulness and practicality of establishing an operational flux evaluation system.

Examples from the AMIP2 comparison for the period 1998 - 1999 are shown in Figures 11.5.1 and 11.5.2.  For latent heat flux (Figure 11.5.1) the results from the operational models tended to have a similar magnitude or be greater than the ERA15 reanalysis.  In comparison the NCEP1 latent heat fluxes were somewhat less and the unadjusted COADS based fluxes, significantly less.  In contrast for the net surface SW flux (Figure 11.5.2) the reanalyses have relatively low values and the COADS based estimates are similar to or less than the satellite estimates.  The operational models span the whole range of the other estimates.  However the majority are similar to or even greater than the satellite based estimates.

## 11.6  Evaluation of Fluxes in Sea-Ice Covered Areas

### 11.6.1  Cloud and surface radiative flux data sets in the Arctic

A review of downwelling radiative fluxes from models, satellites, and reanalyses shows large discrepancies among the various estimates of over 50 $Wm^{-2}$  in monthly means and over 30 $Wm^{-2}$ for 5-year means in reanalysis flux fields (Rothrock and Zhang, 1997). Large discrepancies are traceable to different estimates of the cloud fraction, shown in Figure 11.6.1. The ISCCP satellite data set show an annual cycle out of phase with the Huschke cloud climatology, which shows the accepted higher cloud fractions in summer.  The two numerical weather prediction models show little annual cycle; NCEP is uniformly low and ECMWF is uniformly high.   Five-year mean cloud amounts vary over a huge range from a low of 44 % for

NCEP reanalysis to 70 % for ECMWF forecast data.  A similar range is seen in 5-year monthly means.
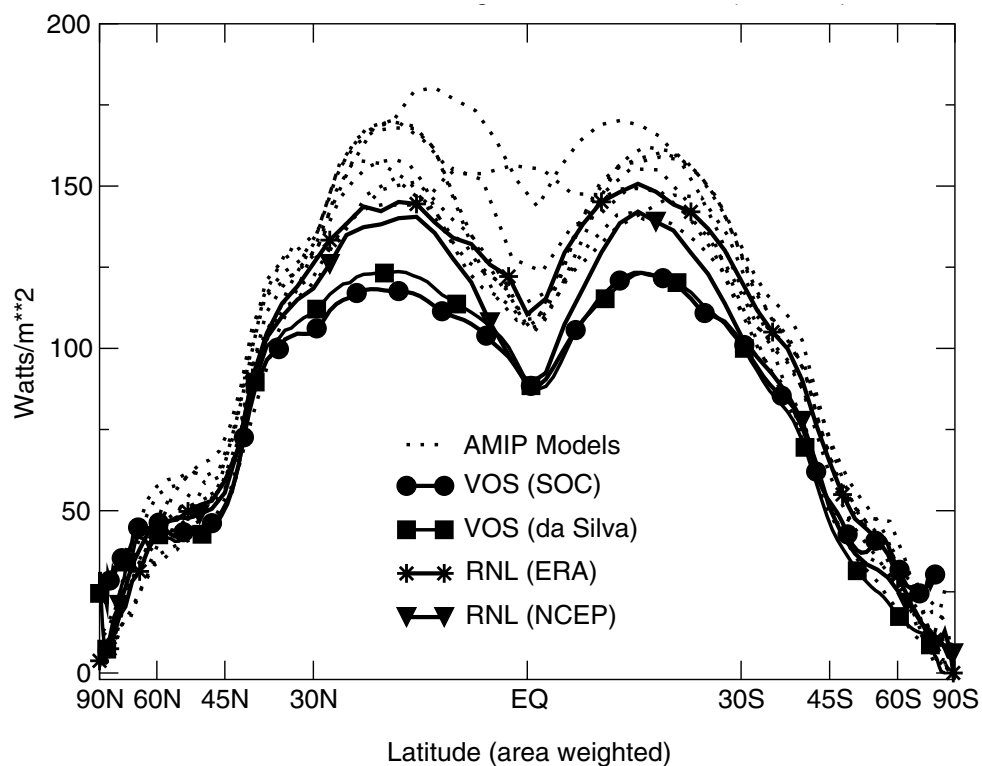


Figure 11.5.1 Zonal averages of the Global Ocean latent heat flux from reanalyses, observations (COADS)  and AMIP2 (1998-99)
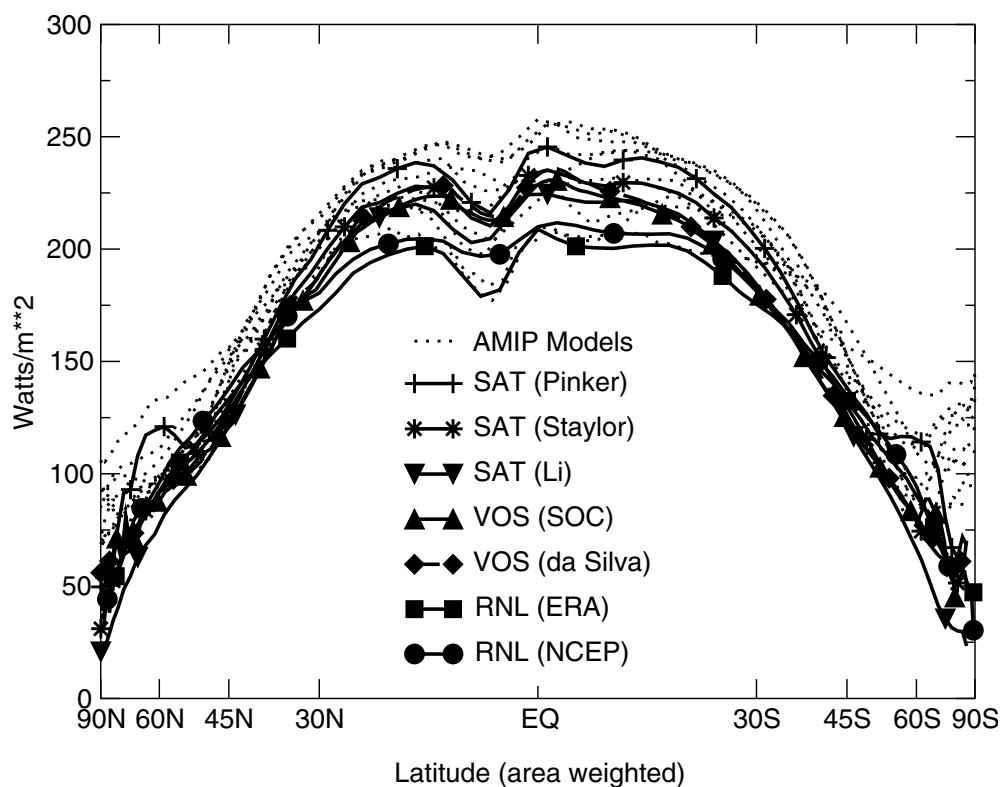


Figure 11.5.2 Zonal averages of the Global Ocean net SW flux from reanalyses, observations (COADS and satellites) and AMIP2 (1998-99)
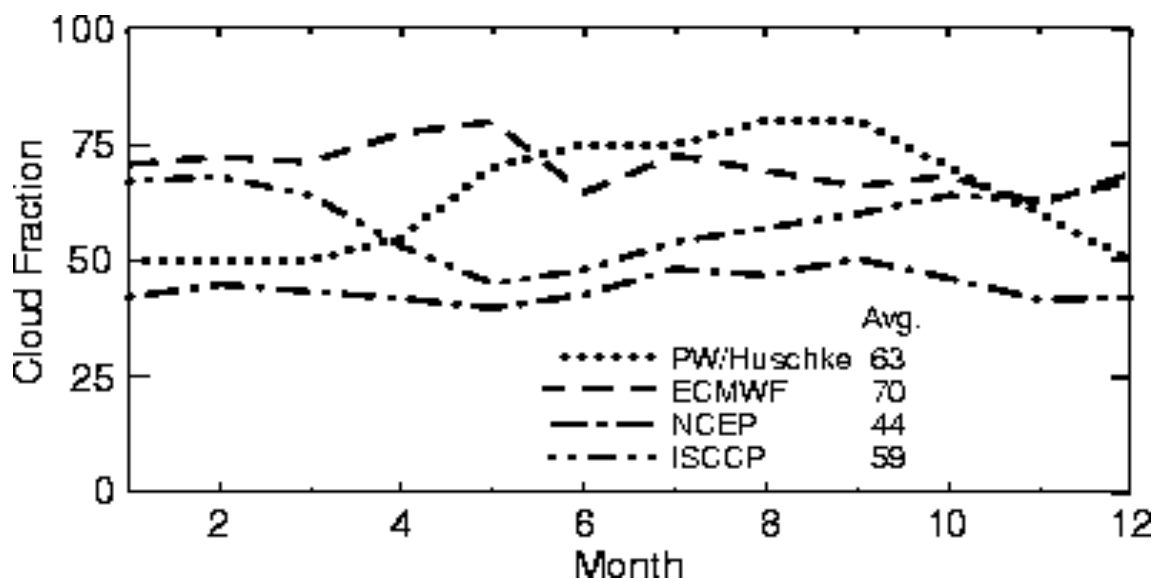
Figure 11.6.1 Cloud fraction in percent from four data sources. Huschke's is a spatially uniform climatology; the others have been averaged over the Arctic Ocean and over the five years from 1986-1990.

The mean annual cycle of downward shortwave and longwave for five data sets is shown in Figure 11.6.2. We tend to look on the observations of Marshunova as the best estimate; the annual average downward shortwave from Marshunova is 100 Wm$^{-2}$. The extreme estimates of downward shortwave are from the two numerical weather prediction analyses: NCEP is high in every month (because of its low cloud fraction), with an annual average of 128 Wm$^{-2}$, and ECMWF is low through May, with an annual average of 80 Wm$^{-2}$. The ISCCP satellite-derived data set is in good agreement with Marshunova's climatology. Although satellite-derived data sets have low cloud amounts in summer, they have compensating high cloud optical depth and low surface albedo that tend to keep the downward shortwave from being overestimated.

The annual average downward longwave from Marshunova is 224 W m$^{-2}$ (Figure 11.6.2b). Other means vary from 198 for NCEP to 231 for the PW parametric estimates. Most estimates are above those of Marshunova by 10 to 20 W m$^{-2}$ in winter and below by 20 W m$^{-2}$ in summer and fall. The low summer cloud amounts in the ISCCP data show up here as low estimates of summer downward longwave.

Biases of 10 W m$^{-2}$ in downwelling fluxes correspond to rather large errors (10 to 30%) in ice thickness. The large discrepancies among radiative flux data sets should be understood better before choosing any of them as the "standard" against which to test or with which to force sea ice or climate models.

### 11.6.2 Precipitation in the Arctic

Two recent studies have examined the quality of both the precipitation and evaporation fields and the atmospheric flux convergence (P-E) in NCEP and ERA reanalyses (Cullather and Bromwich., 2000; Serreze and Hurst, 2000). In the central Arctic (north of 75°N), the spatial patterns of precipitation are in rough agreement with observations, although both data sets tend to underestimate precipitation over the Atlantic side. The mean annual values of precipitation are overestimated by NCEP and underestimated by ERA, each by about 20%. NCEP precipitation has its maximum a month earlier than the observed August peak, whereas ERA has its maximum a month after the observed peak. NCEP fields have spectral noise that has been removed in later versions (see note at proof in Cullather *et al.*, 1999).

*11.6.3  Need for more assessment*

Broader reviews of the polar surface flux literature and further intercomparisons and evaluations of flux and flux-related data sets, many of which are quite new, are sorely needed, especially for the Antarctic.
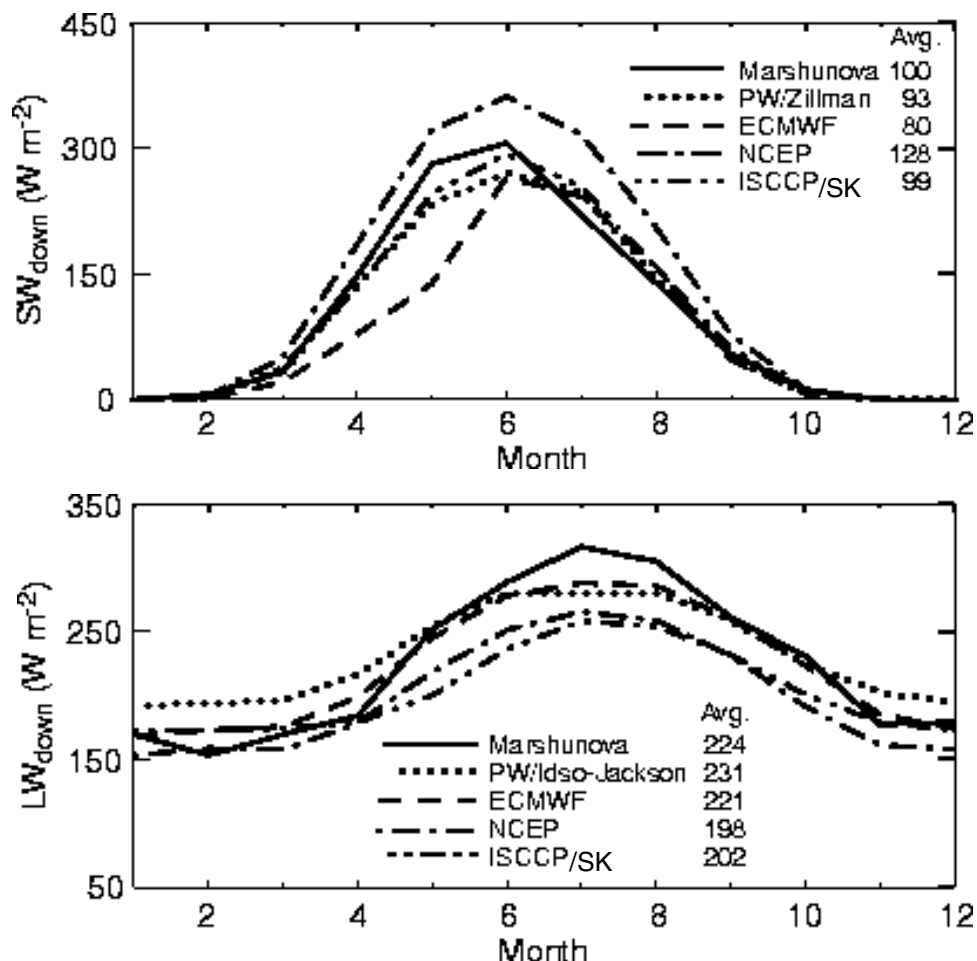


Figure 11.6.2a  (top) Downwelling shortwave fluxes from five data sources.  These are five-year monthly means for the Arctic Ocean.

(b ) As (a) but for the downwelling longwave flux.

## 11.7  Evaluation of Waves

*11.7.1 Visual wave observations*

Evaluation of different wave products have been performed on the basis of intercomparison with *in situ* measurements at buoys and the other *in situ* platforms,  with observations at OWS's (which are expected to have somewhat better accuracy compared to routine visual estimates from merchant ships), and by intercomparison of different products one to each other.

Visual VOS observations may be biased due to the poor separation of sea and swell in the VOS reports.   Some young swells can be reported as seas, and it is also possible that observations of developed seas propagate into the swell domain.   Gulev and Hasse (1999) checked joint probability distributions of visual wave height and wind speed against JONSWAP curves for known wind durations and found that at least the wind sea was well defined in visual

observations.   Estimation of the observational accuracy of visual VOS wave observation (Gulev and Hasse 1999) shows that the day minus night difference in visual wave estimates is not as large as in wind observations.   In the North Atlantic it lies within the range several centimetres to 0.2 m and does not have any pronounced spatial pattern.

The main question for evaluation of wave heights obtained from VOS, is a way of determining significant wave height from the separately reported sea and swell components. Wilkerson and Earle (1990) intercompared visual wave observations at merchant ships with measurements at NDBC buoys in the subtropical Atlantic, tropical and mid-latitudinal Pacific. They selected visual observations within a radius of 25 to 100 km around the buoys location and found that least biased estimate of significant wave height ($H_s$) resulted from taking the higher of the sea and swell heights. They also found a random observational error of several tens centimetres in significant wave height, and large errors for the period estimates.   Gulev and Hasse (1998) intercompared visual wave observations with measurements at buoys, OWS L, and Seven Stones Light Vessel in the North Atlantic.   They found that an estimate of $H_s$ computed following Hogben (1988):

$$H_S = (h_w^2 + h_s^2)^{1/2}$$                                      (11.7.1)

where $h_w$ and $h_s$ are wind sea and swell heights respectively, over estimated the observed $H_s$ in the majority of cases at each site by several tens of centimetres (mean bias of 0.27m).  However, there has been a tendency for frequent under estimation especially in mid latitudes of using the $H_s$ estimate of Wilkerson and Earle (1990) - the higher of the two estimates.   The best method was found to be a combined estimate,  similar to that recommended by Barratt (1991). Equation (11.7.1) is used when sea and swell are within the same 30° directional sector (Barratt had suggested 45˚),  in all other cases the higher of the two components is used.  This combined estimate gave mean "buoy minus VOS" differences of -0.03m and -0.07m respectively.

Visual estimates of wave periods were found to be systematically underestimated in VOS observations.  The peak of the wave period distribution may be 1 or 2 seconds less for VOS observations compared to instruments.  However the mean difference for the wave periods is somewhat less.   Wilkerson and Earle (1990) reported about 0.2 s buoy minus VOS differences.  Gulev and Hasse (1998) found a mean departure of about 0.26 s with 0.1 to 0.6 s standard deviation.   Dacunha *et al.* (1984) and Hogben (1988) reported larger systematic biases for wave periods for the Cobb seamount in the North Pacific.    In order to correct these biases several methods were developed.  Ochi (1978) and Dacunha *et al.* (1984) recommended to fit joint probability distributions of wave heights and periods to the observed ones, giving the possibility to obtain corrected mean periods.  Gulev and Hasse (1998) developed a method for the correction of individual observations of periods which has an accuracy of 0.12 s.

*11.7.2 Altimeter wave data*

Extensive evaluation of altimeter measurements has been undertaken by Cotton and Carter (1994b) who used NDBC buoy measurements to calibrate altimeter wave height estimates, which then were used by Sterl *et al.* (1998) to assess the quality of their WAM wave model.  They found that in general high waves were under, and low waves overestimated.  For the periods of overlap of buoy measurements with the altimeter measurements,  Cotton and Carter (1994b) applied regression analysis which helped to remove biases between the three *Ku*-band altimeters of GEOSAT, TOPEX/POSEIDON and ERS-1/2.  Thus it was possible to merge the three altimetric products and to create a data set with continuity over about 12 years.  Laing and Reid (1999) performed an evaluation of altimetric significant wave height in the South Pacific using a limited collection of visual data around New Zealand.  They found that $H_s$ derived using (11.7.1) under-predicted altimeter measurements by approximately 0.2 m for all ranges.  It is unclear whether this bias has a regional nature or results from the considerable undersampling by the VOS observations in the South Pacific.

A pilot study by Gulev *et al.* (1998) performed a triple intercomparison of significant wave height derived from visual observations, the WAM model,  and altimeters. Climatological

spatial patterns of significant wave height in all three products were found to be consistent, although the differences between the VOS wave data, altimeter measurements and the model hindcast were not negligible;  the nature of the biases still has to be precisely studied.  The smallest "VOS minus WAM" and "VOS minus altimeter" differences were found in mid latitudes,  where the differences were of opposite sign: VOS waves overestimated the model hindcast by 0.1 to 0.3 m and underestimated the altimeter $H_s$ by approximately 0.1-0.2 m.  In the tropics,  where the waves and winds are smaller, VOS wave height was higher than those taken from WAM,  or the altimeter,  by 0.3 to 0.7 m.   An alternative interpretation is that the WAM $H_s$ and the altimeter data fit better to each other in low latitudes,  and show the largest disagreement in mid latitudes where the "altimeter minus WAM" biases are from 0.3 to 0.5 m. Of the three sets of comparisons, the VOS and altimeter SWH show least scatter, whilst the largest scatter is obtained for the "VOS-WAM" comparison.

Two long-term 40 year wave hindcasts of OceanWeather Inc. (Cox and Swail 1999) were evaluated using in-situ and altimeter measurements (Cox *et al.* 1999).  In-situ comparison was based on the NDBC buoy 44138 measurements and a number of platform measurements. This comparison showed that the highest waves are usually under-predicted in the model simulations, and alternatively, smaller waves tended to be over-predicted.  Comparison with satellites was done for four regions: Southern Hemisphere, Northern Hemisphere, Tropics, and Global.  Charts of differences show pronounced overestimation of hindcasted waves in mid latitudes, and slight underestimation in the tropics.  The best agreement has been found in the North Atlantic Ocean.

## 11.8  Summary

Here we briefly review some this Chapter's results for the heat flux fields to illustrate the difficulty of determining the "best" product.  Figure 11.8.1 summarises results for the global heat balance that were also presented in Table 11.4.1.   For each flux component, and for the net flux,  the difference is shown between the fluxes from the various analyses (ERA15, GEOS1, NCEP1,  and  NCEP2)  and  the  UWM/COADS  climatology.   Figure 11.8.1a shows the comparison with the unconstrained UWM product and Figure 11.8.2b shows the difference from the tuned values of da Silva *et al.* (1994).  On the latter plot the net heat flux values displayed assume that, for the period considered,  the tuned UWM/COADS product had an exact heat balance.   It is clear the GEOS1 product is far from a global balance and inspection of Figure 11.8.1 in general shows this product to be an "outlier" so this product can be assumed to be incorrect with regard to the surface fluxes.   The other reanalysis products (and the tuned UWM fluxes, which are not shown) all have a global balance within 10 Wm$^{-2}$.

However,  achieving global balance does not guarantee that the regional variation of the fluxes,  or the partitioning between components will be similar from one data set to another. Thus Figure 11.8.2 shows the net heat flux for the VOS estimates, reanalysis, and the residual calculation described in Section 11.3.5.  The two reanalyses shown at the top of the figure are clearly more similar one to another than the two COADS based flux fields (middle plots). However, this is mainly due to the fact that the COADS products have not been adjusted for the global mean heat imbalance, which for both exceed 20 Wm$^{-2}$.   The lower left hand "tuned" estimate of da Silva is more similar to the reanalysis than either uncorrected VOS estimate.

Despite the noisiness of the residual method plot,  it also shows similarities to the other plots particularly in regions of excessive heating or cooling such as the western boundary currents, eastern Indian Ocean and the western tropical Pacific.  However more careful inspection shows that there are significant differences between the different data sets shown in Figure 11.8.2.   These are particularly marked in the Indian Ocean. For example the  Residual method suggests ocean heating north of Madagascar of a magnitude more similar to the untuned COADS products than to the tuned product;  this is not shown by the reanalyses.  On the other hand the ocean cooling west of Australia is more similar to the tuned COADS fluxes.  This cooling is seen in the NCEP reanalysis but is displaced westward in the ERA results.  Note that

the time period differs for each of these climatologies, but this unlikely to have been a major cause of the large systematic differences which are evident.

That there should be regional variations in the differences between the various net heat flux estimates is not surprising given the likely biases in the individual flux components. If these biases could be understood and corrected the need to tune the COADS would be removed. However we presently do not have that understanding. For example almost all schemes to "correct" the COADS data require the net surface SW to be decreased. However satellite estimates of net SW show more ocean heating compared to the untuned COADS values, not less (Figure 11.8.3). It is possible that this is caused by a bias in the satellite derived values. However, tuning the COADS values for net SW results in greater disagreement with both satellite and reanalysis estimates (compare Figure 11.8.1 (a) and (b)).
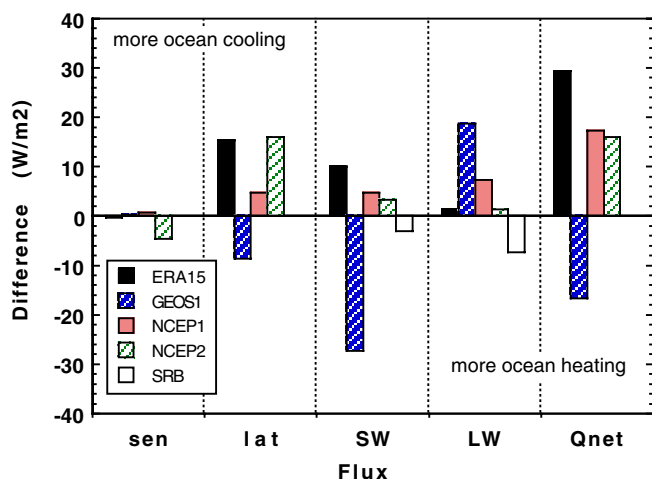


Figure 11.8.1 a. Global mean difference between different flux data sets and the unadjusted UWM/COADS climatology for each flux component and for the net flux. The SRB data are satellite estimates of net SW by Darnell *et al.* (1992) and net LW by Gupta *et al.* (1992) averaged over July 1983-June 1991.
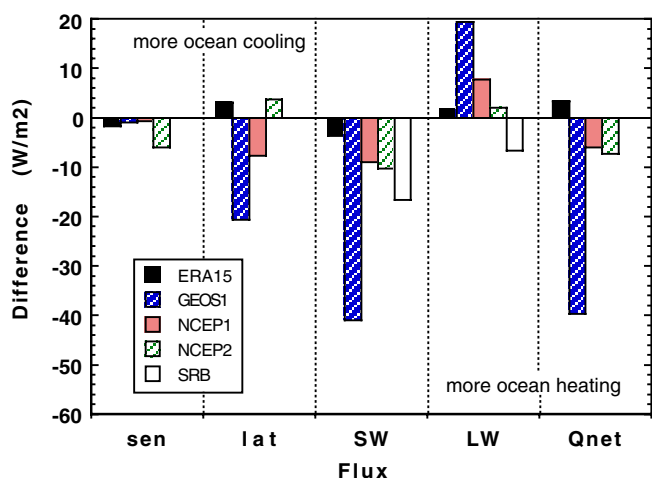


Figure 11.8.1 b. As (a) but for the global mean difference from the tuned UWM/COADS climatology. For the net flux the global balance is shown..

Tuning also increases the latent heat (or evaporative) flux (Figure 11.8.4). The untuned VOS estimates (SOC and da Silva) compare qualitatively quite well, as do the climatologies derived from reanalyses. However, in the sub tropical western ocean basins, there is much more evaporation in the reanalysis than in the VOS estimates. Thus it might seem that there is scope for increasing the VOS flux values. However it would be difficult to justify a large enough adjustment to the latent flux to balance the budget if, on the basis of the satellite data, the net SW flux were not adjusted. Figure 11.8.4 also shows two other flux maps. The ERA 0 to 6 hour map illustrates (in comparison to the 12 to 24 hour map) how the spin up process in the early forecast hours affects the hydrological cycle. The satellite derived estimate (HOAPS) falls into yet another category. In the tropics this estimate is significantly lower than either the VOS or reanalyses, but elsewhere they are all comparable in magnitude - although the patterns vary. It would appear that further verification and development of the satellite product is required, particularly in the tropics.
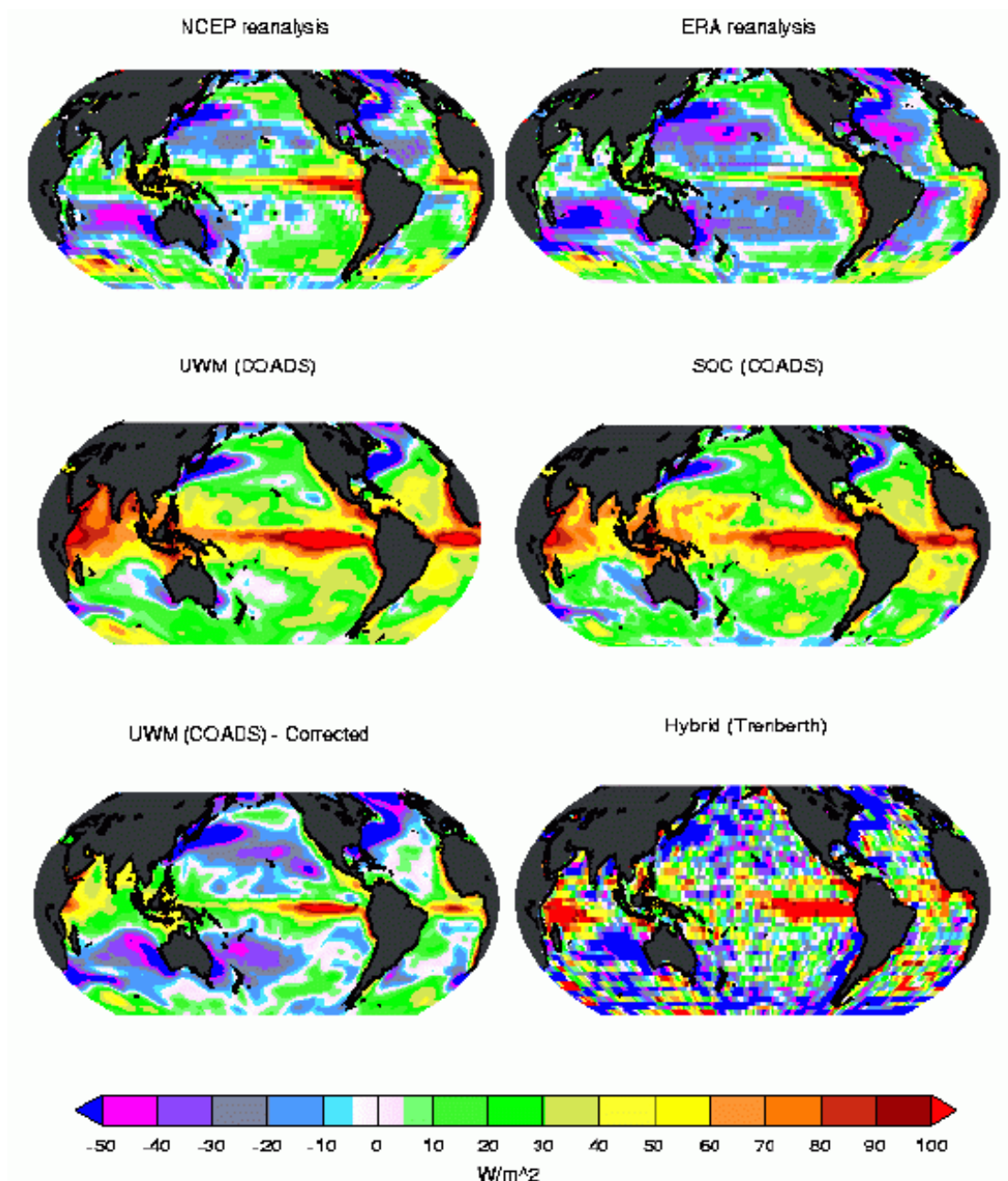
Figure 11.8.2  The annual mean climatology of six estimates of surface net heat flux.  Shown are values from the NCEP reanalysis (top left), the ERA15 reanalysis (top right), the untuned UWM/COADS climatology (middle left),  the SOC climatology (middle right),  the tuned UWM/COADS climatology (bottom left), and the Residual method (Trenberth and Solomon, 1994) (bottom right).

In summary,  while there are encouraging similarities between the various estimates there are also large differences.   The discrepancies are often most obvious in the low latitudes but they are not restricted to those regions.  Winter/summer maps of either the latent heat or surface net shortwave clarify that the differences are relative, i.e., wherever the fluxes are large, so are the differences with the other flux estimates.  This is indicative of relative systematic errors.  The maps certainly do not tell the whole tale of the challenges associated with ocean surface flux estimates.  But they do give a glimpse of the difficulty.  Each class of estimates has its own strengths and weaknesses, and the errors associated with them are complex and

extremely difficult to quantify.  Clearly, further analysis is needed in this area before we can get a better grasp of the relative quality of the estimates.
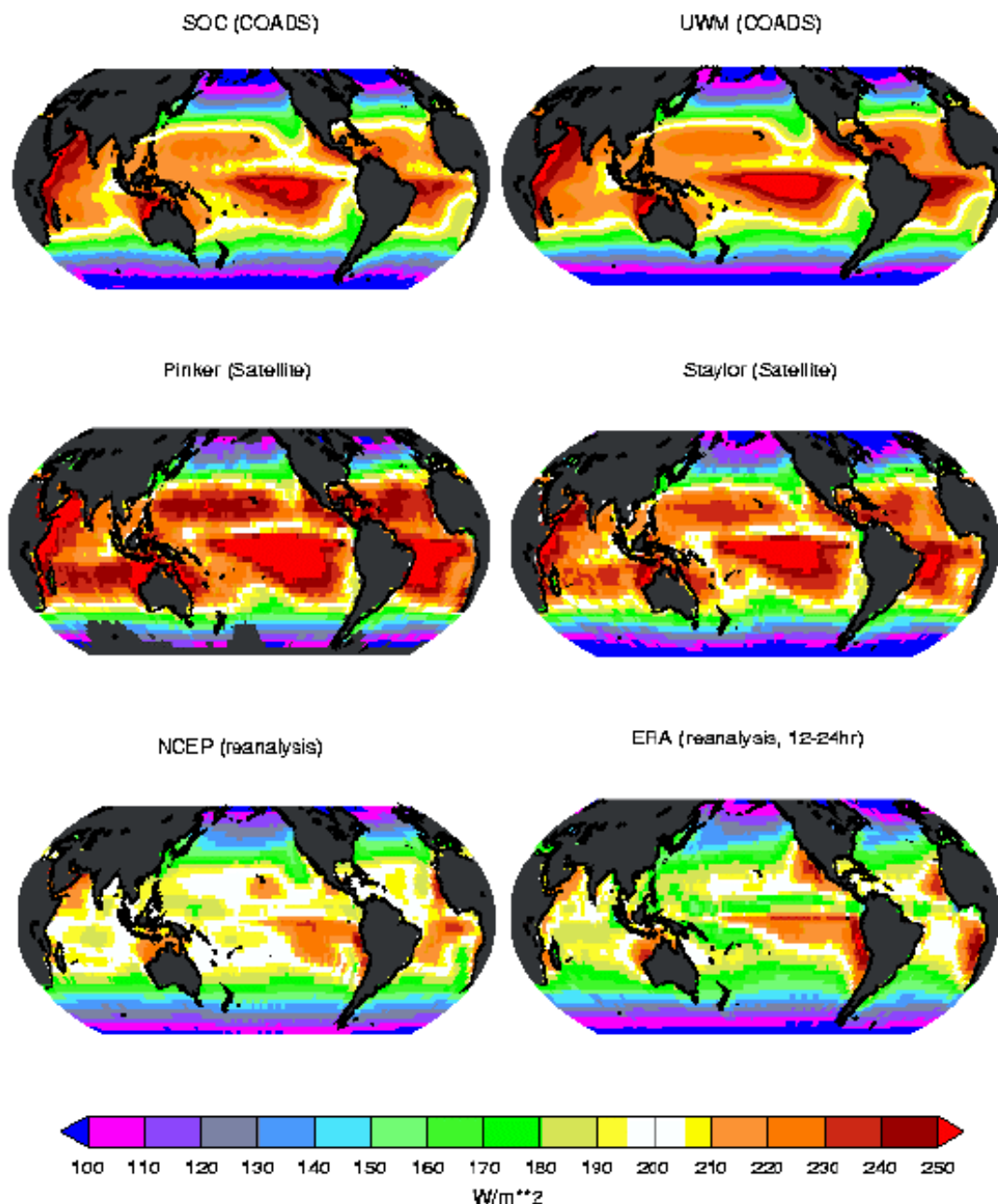


Figure 11.8.3  The annual mean climatology of six estimates of surface net SW flux.  Shown are values from the SOC climatology (top left), the untuned UWM/COADS climatology (top right), the Pinker satellite algorithm (middle left),  the Staylor satellite algorithm (middle right),  the NCEP reanalysis (bottom left), and the ERA15 reanalysis (bottom right).

Finally the limited evaluation presented here allows the relative merits of the COADS, model, and satellite products to be considered.   COADS based climatologies have given us much information about the marine climate.  However comparison with the model data suggests that, as might be expected, such products perform best where there is adequate sampling.  Thus the COADS climatologies can define both the mean climate and interannual variability of monthly means in regions such as the North Atlantic but, at best, can only describe the mean

climatology for Southern Hemisphere regions.   For the Southern Ocean in winter they may be badly biased.   To obtain a global heat balance they  must be tuned.   Flux fields  from the

SOC (COADS)                                        UWM (COADS)

ERA (reanalysis, 12-24hr)                          NCEP (reanalysis)

ERA (reanalysis, 0-6hr)                            HOAPS (Satellite)

| 0 | 10 | 20 | 30 | 40 | 50 | 60 | 70 | 80 | 90 | 100 | 110 | 120 | 130 | 140 | 150 |

W/m**2
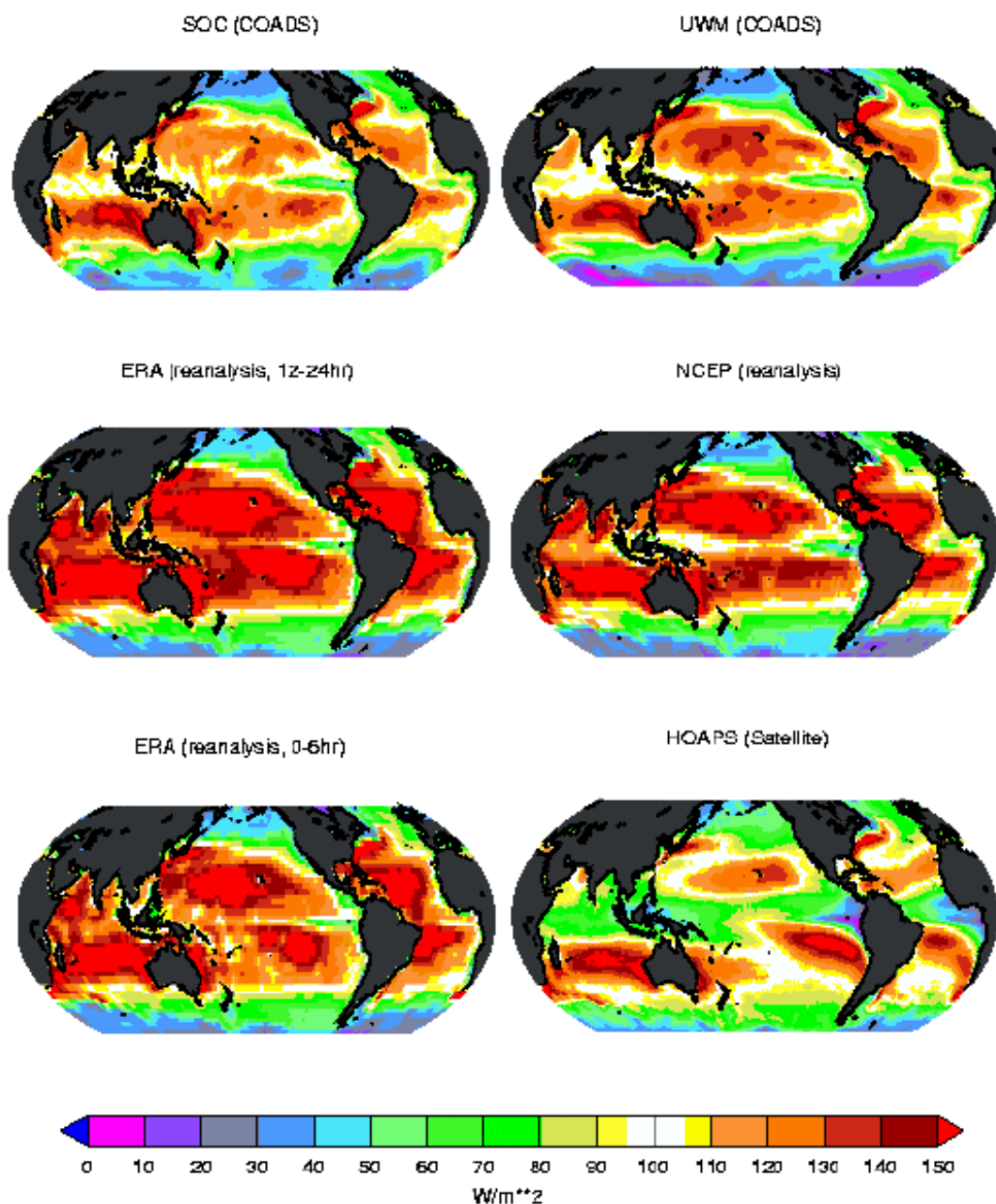
Figure 11.8.4  The annual mean climatology of six estimates of surface latent heat flux.  Shown are values from the SOC climatology (top left), the untuned UWM/COADS climatology (top right),   the 12 to 24 hour estimate from the ERA15 reanalysis  (middle left),   the NCEP reanalysis (middle right),   the 0 to 6 hour estimate from the ERA15 reanalysis   (bottom left), and the HOAPS satellite product (bottom right).

 reanalyses are expected to be of more unifom quality from region to region and they typically exhibit a smaller global heat imbalance.   However comparisons with satellite fluxes,  or even the COADS fluxes,  suggests that the magnitude and distribution of the radiative fluxes is significantly in error;  shortwave heating in particular.   Similarly,  if the comparisons with buoy data can be trusted,  the latent heat flux is over estimated in many regions.

Finally, although the satellite surface SW flux estimates appear realistic there are still significant differences between products and there may be an overall bias.   In comparison satellite longwave surface flux estimates are less reliable.   A more direct use of the satellite flux data is to define the top of the atmosphere fluxes for use in models or in the Residual flux method.  The latter technique offers a method of defining the surface heat flux independent of the bulk formulae and could be used as an important constraint on fluxes produced by other methods.   With regard to the turbulent fluxes,  we have evaluated one satellite based product, HOAPS,  which attempts to determine the surface latent heat flux from satellite data.  While this product shows promise there is clearly a need for improvement, particularly in the tropics.

In short,  there is presently no one flux climatology which does not exhibit significant errors in one region or another in each of the various flux components.

## 12. CONCLUSIONS

### 12.1. Introduction

Air-sea interactions play a pivotal role in regulating the Earth's climate, and there are now urgent requirements in climate and oceanographic research for quality estimates of large scale air-sea fluxes of heat, momentum and fresh water. In recent years there has been substantial progress in our knowledge of ocean surface fluxes. Research has helped us to better understand and correct the historical record of merchant ship observations, and field experiments have led to refined formulae for estimating fluxes. Surface fluxes derived from satellites are becoming increasingly promising. Weather forecasting and data assimilation systems have been used to create a consistent record of the recent past atmospheric state from which surface fluxes are derived. And yet despite these advancements, the air-sea flux problem is extremely difficult, and in many ways remains unsolved. Whether derived from in-situ data, satellites, or analysis systems, the deficiencies are complex and difficult to quantify. The optimal product will depend on the application and often will not be easy to identify. The overall thrust of this Working Group, guided by the terms of reference, has been to present a coherent picture of the state-of-the-art of our present understanding.

### 12.2. Summary

The requirements for "well qualified" air-sea flux information are both wide ranging and compelling. As discussed in Chapter 2, they include climate change and diagnostic studies; sea-ice modelling; atmospheric and oceanic synoptic-scale case studies; shelf and coastal seas studies; oceanic, climate, and earth observing systems; biogenic cycles, etc. The diverse nature of the requirements makes considering them all impractical. Thus this report focuses on the most common requirements and considers only those products that are non real-time, large-scale, readily-available to the scientific community, and documented.

One facet of the flux requirements is particularly interesting. As discussed in preceding chapters, the absolute accuracies of air-sea flux products still do not meet the desired standards. However, as demonstrated in Chapter 3, when one considers the requirements for exploring the spatial and temporal characteristics of the flux variability, requirements are identified that are new and different from those applicable to the mean, climatological fluxes. This topic of flux variability is largely unexplored in this report, but is important for many studies and thus is a likely candidate for attention in the future.

The sources of data used to construct flux products were discussed in Chapter 4. Broadly speaking, there are three primary sources: *in situ*, remotely-sensed, and model products. Each of these sources has unique characteristics, which translate into advantages or disadvantages for estimating fluxes. *In situ* data have been widely used; however, biases traceable to the observing techniques, as well as the restricted spatial coverage, limit their applicability. Satellites provide global coverage and hold great promise to deliver quality data, but they have not been able to estimate net fluxes except within very limited domains. Finally there are model products that synthesise several sources of observations and data using short-range forecasting systems to produce gridded fluxes. These need to be continually verified to identify regional and systematic biases. Other techniques for flux estimation, based on residual and assimilation approaches, have had relatively little application in the past but are expected to be utilised more in future.

Direct measurements of the air-sea fluxes (Chapter 5) are relatively few and therefore large scale fields cannot be constructed based solely on these measurements. However, they are important for developing, calibrating, and verifying the parameterisation formulae used to indirectly estimate fluxes from the basic variables. Thus the accuracy of the direct measurements will ultimately limit the accuracy of the parameterised estimates. The quality of the direct measurements is related both to instrument design and to our understanding of the

underlying physics. Carefully designed experimental campaigns can increase the accuracy achieved.

Without direct measurements, air-sea fluxes are often parameterised using formulae based on the basic meteorological observations. Radiative fluxes are particularly difficult to parameterise (Chapter 6). The shortwave (SW) flux parameterisation has traditionally been based on visual observations of cloud amount. Because this method is fairly imprecise, and moreover due to the limited set of verifying direct measurements, accurate determination of SW through this type of parameterisation will continue to present a challenge. A similar situation exists for longwave (LW) radiation. Other approaches to parameterising radiative fluxes are based on satellite determined top-of-the-atmosphere radiation, coupled with radiative transfer models to bring these values to the surface. For SW the situation is promising. However for both SW and LW, difficulties in correctly modelling the presence of clouds and aerosols limits the accuracy. New techniques to estimate LW from combinations of satellite information may hold promise, but they have not been fully evaluated. The range of surface albedo for the ocean and also sea ice over a wide variety of conditions continues to be investigated.

For turbulent fluxes, parameterisations have been developed which are based largely on measurements of basic variables such as wind speed, temperatures, and humidity (Chapter 7). These "bulk formulae" are the most commonly used technique to estimate air-sea fluxes. The formulae are dependent typically on wind speed measured at some height, and the difference in values of appropriate basic variables between some height and the sea surface. There have been a number of bulk algorithms published in the literature. Newer bulk formulae (for example the TOGA COARE algorithm) are improved to the extent that they incorporate treatments of specific physical processes, such as the warm surface layer, and wind gustiness. Many questions remain as to the accuracy and/or applicability of these formulae in regimes where relatively few direct measurements have been made. This is particularly true of moderate to high wind regimes; in effect winds greater than 10 ms$^{-1}$. Additionally, the role of ocean waves in modulating the turbulent flux estimates remains an open question.

In the early chapters, we considered the errors when estimating individual air-sea flux values. In Chapter 8, we discuss limitations on the accuracy of flux fields due to the synthesis of these errors. Both theoretical approaches and practical examples of quantifying random, systematic, and sampling errors, indicate that it is possible to estimate these cumulative errors. Additionally, for many applications, the requirement is for gridded flux fields that are complete both in space and over some significant time period. The non-uniform sampling of the in-situ and remotely-sensed fluxes necessitates an analysis method to fill in the gaps. Such techniques alter the error budgets of the flux fields. For example, depending on the particular choice of method and averaging period, it is not unusual for sampling errors in remotely-sensed data to be dominant compared to systematic biases. What is most important, but rarely satisfied, is for all flux products to include error estimates. Preferably these error estimates should consider as many contributing factors as possible. Although good error values are often difficult to calculate, they are extremely valuable in a) establishing confidence limits; b) assessing improvements; and c) fulfilling many of the requirements described in chapter 2.

There are a wide variety of flux products available to the scientific community. These products span a very large range of characteristics in terms of, for example, temporal and spatial coverage, grid spacing, input data, and parameterisations. Evaluation of all such products would be a very large and continuous effort. We have attempted to concentrate only on those products with basin to global coverage, which are easily accessible to the community, and well documented. The determination of the "best product(s)" for specific applications is very difficult due to the problem specific characteristics. Instead we focus on objective evaluations of the strengths and weaknesses of the selected products. For objective evaluation we have used the following methods:

❍       comparisons to reference data sets (i.e. to direct flux measurements or those from high-quality sources);

❍        intercomparisons with similar products;

❍        integral constraints of heat and water balance and transports;

❍        enclosed basin budgets;

❍        other indirect flux estimates.

As discussed in Chapter 9,  each evaluation methodology has its own inherent advantages and limitations.

For many of the flux estimates the accuracy is limited by the accuracy of the basic variables that are used in the parameterisation formulae.  The state of the art with regards to observing or estimating these basic variables was considered in Chapter 10.  Each variable and measurement method has its unique characteristics that must be carefully considered in determining the usefulness of the data for flux estimation or for verification.

The chosen flux products were evaluated in Chapter 11 including a first detailed global comparison of the various reanalyses.  The following conclusions are based on the results of that evaluation.  The conclusions are grouped according to the requirements for the several types of activities which were described in Chapter 2.

## 12.3. Meeting the Needs

### 12.3.1. Budget studies

Budget studies of the ocean surface energy and water balance of the ocean are often used as an evaluation method for the data sets rather than to derive values of the budget.   On longer time and space scales the energy budget can be regarded as balanced,  at least in comparison to the uncertainties in the available estimates of net energy flux at the sea surface. Proper evaluation of budget studies requires error estimates,  both for the individual flux components and for the net flux.

All flux products presently available (VOS-based, satellite, re-analyses) are imbalanced, that is the fluxes of heat and moisture do not meet known geophysical constraints.  Imbalances of the net heat flux are within several tens $Wm^{-2}$.  VOS - based climatologies tend to underestimate net ocean heat loss, and this underestimation varies from 20 to 30 $Wm^{-2}$.  Poor sampling,  insufficient information to correct variables in the appropriate way, and uncertainties in many parameterisations,  are considered to be reasons for these imbalances.  In this situation, an assessment of the reliability of the VOS flux fields has to be considered with respect to the specific application for which the flux product is going to be used  (for example forcing ocean models, analysis of interannual variations in sea-air fluxes, basin-scale budgets).   For some purposes,  flux fields adjusted to give a balanced heat budget may be preferred;  however there is evidence that the available tuned flux fields may have significant regional errors.

Most reanalyses are much better balanced than the VOS-based flux products, they achieve imbalances within ±10 $Wm^{-2}$.  Possible reasons are a more adequate description of the fluxes in poorly sampled areas (e.g. the South Pacific),  and more data types being taken into account as assimilation input.  However, despite the more realistic global balances derived from reanalyses products,  individual flux components are characterised by strong biases.  This suggests that some sort of tuning, explicit or implicit in the model formulation, may be responsible.

For both reanalyses and VOS-based flux climatologies,  the reliability of the fresh water budgets is even worse than for the net heat flux.   This reflects a lack of direct measurement of precipitation over the oceans. Precipitation in NWP systems is sensitive to changes in physical parameterisations and to "spin-up".  In this sense satellite observations (e.g. SSM/I and TRMM), which already are providing evaporation minus precipitation estimates over an extending, continuous period,  are extremely valuable.  To produce a freshwater budget,  it is

necessary to consider not only the direct exchange between ocean and atmosphere but also the river runoff from land surfaces.

Meridional heat and fresh water transport estimates still remain very uncertain when computed from the VOS - based fluxes. Re-analyses flux products (which are better balanced) provide more plausible estimates at least for MHT. Comprehensive verification of MHT and MFWT estimates derived from surface balances against oceanographic estimates at hydrographic sections should, of necessity, take into account the interannual variability of the ocean interior. Time-dependent estimates of MHT and MFWT require knowledge of the long-term storage terms for the ocean, which are nevertheless smaller than the errors in flux products.

## 12.3.2. Climate variability studies

The variability of ocean-atmosphere fluxes on climate time scales is still poorly known. Up to the present, the basic meteorological variables (e.g. SST, pressure, winds) have more frequently and effectively been used for describing the coupled modes of the ocean atmosphere system. On the one hand, the errors and uncertainties inherent in the mean climatological flux fields, particularly those connected with parameterisation errors, do not seriously affect the accuracy of the climate anomalies of the fluxes. On the other hand, the time dependent biases present in various flux products create considerable problems for the analysis of variability with any confidence. These biases result from historical changes in observational techniques and sampling frequency (for the VOS data), from changes in the model configuration (for operational models), and changes in the assimilation input (for both operational NWP and reanalysis systems). In this context, satellite data will be extremely valuable for climate change studies once a climatologically significant length of record has been achieved. Even so, the continuity of the satellite data can suffer from changes in satellites and from instrument drift. At present the SSM/I and AVHRR provide a continuity of flux time series reaching nearly 15 years, the ERS -1 and ERS-2 missions approach 10 years continuity. For sea ice, long time series (up to 22 years) are available from SMMR and SSM/I. All these data can be used for studying short-period variability, for example the interannual variability of monthly mean values.

The quickest progress in the application of flux time series can be expected with regard to mid-latitudinal variability on interannual to decadal time scales (associated with the NAO, PNA and NPO patterns). This is due to the large magnitude of the anomalies to be characterised (up to 50 $Wm^{-2}$), relatively high sampling frequency, and the dominance of the turbulent fluxes in forming the net flux anomalies. Reanalyses flux products better resolve variability in poorly sampled areas, but they have still to be verified. Climate variability in tropical atmosphere-ocean fluxes is largely influenced by the anomalies of the radiative fluxes and precipitation. Both are poorly resolved in the VOS and re-analysis products; precipitation anomalies in particular. Fortunately the weaker synoptic and meso-scale variability in the tropics reduces the sampling requirements compared to mid latitudes. The Atlantic subtropical dipole, Pacific tropical variability, and monsoon intensity variations are the main phenomena which have to be described in terms of surface flux anomalies. Further improvement of the short wave radiation and precipitation from future reanalyses will aid progress.

Reliability of interdecadal to secular changes derived from the ocean-atmosphere flux fields is considerably worse than that for interannual to decadal scale variability. Beside the crucial importance of time-dependent biases, the reliable time series of the ocean-atmosphere fluxes is still restricted to at most several decades. The possible extension of the flux time series, at least for a few locations, is very important.

Empirical and model studies of oceanographic decadal variability require estimates of the climate variability for the basin scale heat and fresh water budgets, as well as quantitative estimates of the climate variations in MHT and MFWT. Although the uncertainty is large, estimates for selected latitudinal belts, bounded by the pre-WOCE and WOCE sections in the Atlantic ocean, can be made on the basis of VOS, NWP and satellite products.

### 12.3.3. Climate models

The accuracy of available surface flux estimates limits their value for evaluation of climate models.  Despite this, it is useful to compare both atmospheric and coupled ocean-atmosphere models with available climatologies, because these models are known to have substantial systematic errors in their representation of surface fluxes.  Errors in both coupled and uncoupled climate models manifest themselves differently and independent evaluation of these models is complementary.

Evaluation of coupled model variability is becoming increasing important, and as noted in this report, in some respects our knowledge of variability is more accurate than estimates of the mean climate.  Further improvements are anticipated with, for example, improvements in satellite based estimates.

Improved accuracy of mean climatologies remains the greatest need for climate model evaluation.  It is no coincidence that this is a daunting task and is central to the 'surface flux problem' identified in this report.  There are many parallels between observational and model deficiencies as they are generally reliant on the same techniques and theory. There has been encouraging progress with the problem of climate drift in coupled model simulations, but further advancements may be limited by our deficient understanding of the mean surface energy balance.  There is substantial model-to-model scatter in simulated basin-scale means.  In some cases observational estimates help reveal serious model biases, but in others the disparity between the climatologies is such that model errors cannot be identified.

As efforts to improve climatologies continue, additional measures can be taken to evaluate models with available products.  More emphasis could be given to the basic observables described in this report such as surface air temperature, humidity and wind speed. This requires careful vertical interpolation, but it is nevertheless helpful given the uncertainties in flux estimates.  Additionally, as noted throughout this report, comparison of large scale flux estimates with reference sites (e.g., 'flux buoys') is proving increasingly useful.  Following this strategy with climate simulations could yield an important advancement in model evaluation.

### 12.3.4. Ocean general circulation models

The wind field produced by satellite-borne scatterometers is the component which by far matches best the requirements for forcing ocean general circulation models.  Its high spatial and temporal resolution allows an accurate estimate of the stress vector and its curl,  which is the dominant forcing for the ocean gyres.  One problem is the short length of the record, but the situation is continuously improving.   The continuity in the long term is now assured with an operational scatterometer program being set-up jointly by ESA and EUMETSAT.  NWP forecasts also benefit from scatterometer winds, and, in turn,  operational wind products from NWP centres are challenging scatterometer winds as an alternative forcing for ocean models.

Other satellite products have a large potential for improvement and they may be considered the best practicable alternative to NWP products for forcing ocean circulation models in the future.  The greatest expectations concern the radiation fluxes.  With the increasing use of geo-stationary satellites in combination with orbiting platforms, the space and time resolution could approach the important scales of oceanic turbulence (a few tens of kilometres, and a few hours).  Progress in the estimation of turbulent fluxes and precipitation is slower, and these scales do not seem attainable in the very near future for these variables, however there are possibilities for improvements.

The long records of NCEP/NCAR and ECMWF re-analyses, their fairly high space-time resolution, and the reasonable degree of consistency between the various components of the forcing (momentum, heat and freshwater), make them extremely valuable to define a complete forcing function for ocean GCM's. The recent availability of these products is largely responsible for the rapid development of ocean variability studies in relation to climate change in recent times.  These products are unique for that purpose, and it is essential that re-analyses be pursued and continuously improved.

Although covering a similar period, COADS derived flux climatologies have severe deficiencies in the Southern Hemisphere. In such regions they can not compete with NWP re-analysed products for defining the ocean forcing. However, in particularly well sampled regions, such as the North Atlantic and the North Pacific, they remain valuable products that should be used, for example, to force basin scale ocean models in studies investigating model sensitivity to air-sea fluxes or to changes in flux parameterisations. In those regions the COADS SW fluxes are generally superior to the present reanalysis products, and the LW and sensible heat fluxes superior to satellite based products.

It is likely that the most accurate air-sea flux estimates may come from a combination of various products in which the contribution of NWP and satellite products will be dominant. It remains the case that for ocean general circulation models, the consistency of fluxes from various space-borne sensors will have to be verified and this will be an additional constraint that the combined products will have to satisfy. Acknowledging that future combined flux estimates will have a higher accuracy, such products would appear to be the best choice for the operational or pre-operational oceanographic systems under development (GODAE, Mercator, etc.).

### 12.3.5. Wave modelling

Wave models require forcing at a high spatial and temporal resolution. In particular, the required temporal resolution of ~3 hours can at present only be met by numerical products. While reanalysis products have the advantage of being quasi-homogenous in time, their limited spatial and temporal resolution may be regarded as a disadvantage. However, the planned ERA-40 reanalysis will include a wave model forced at the atmospheric model's timestep, so time resolution will not be a problem in that case.

### 12.3.6. Sea-ice modelling

For sea-ice modelling, our knowledge of net surface heat flux in polar regions has proven adequate to determine a realistic annual cycle of the global sea-ice cover. However, this mean cycle is undoubtedly maintained by surface heat flux components with offsetting errors easily as large as 50 $Wm^{-2}$. A principal focus of ice-ocean modellers now is to understand interannual variability; this objective seems desirable now that we are acquiring multidecadal satellite and submarine records of ice extent and ice thickness with which to document interannual ice variability. So the new direction is to drive sea-ice models with flux and flux-related data sets that are not simply climatologies, but which incorporate interannual variability. If this new understanding is to be pursued, it will require a higher level of accuracy in our data on the radiative forcing of the ice surface; the present 50 W $m^{-2}$ uncertainty and lack of data on interannual variability of snowfall will not suffice. Are greater polar cloud fractions enhancing downward longwave radiation at the expense of downward shortwave? Are air temperature variations changing the turbulent fluxes? Is enhanced snowfall insulating the ice from the cold winter air temperatures and reducing ice thickness? These questions cannot be answered with our present uncertainties both in surface heat flux components and in precipitation. The errors in reanalysis and satellite-derived surface flux fields must be better characterised and then reduced by more thorough comparisons amongst themselves and with *in situ* observations. Surface wind fields from NWP models and reanalyses are in general satisfactory, but are subject to errors in magnitude and direction during winter when the planetary boundary layer is stable; PBL formulations need to be examined for their applicability in polar conditions.

### 12.3.7. NWP and data assimilation

The reanalyses provide consistent, complete global fields of near-surface meteorology and surface fluxes over many years. Even when reanalysis fields have time-mean biases, their variability can still be quite realistic. Many scientists from a wide range of disciplines have studied the reanalyses, providing valuable feedback to the data assimilation and modelling groups producing the reanalyses. The reanalyses are the most evaluated of all the flux products. It needs to be remembered, however, that the reanalyses are only interpolations of the input

observational data that have many gaps in space and time. Physical parameterisations are especially important in regions of little or no data; differences between reanalyses can highlight what fields in what regions are uncertain. The reanalyses so far have provided fields every six hours; many surface flux users desire them at least every three hours.

The GEOS-1 reanalysis was the first extensive reanalysis produced; its surface radiation fluxes are larger than other estimates. The GEOS data assimilation system has developed substantially since the reanalysis was conducted. The NCEP-1 reanalysis covers the longest period and is the most widely distributed and studied reanalysis. NCEP-1 made many fields available on the Internet and CD-ROM's. It has the most realistic oceanic low-level stratus clouds of the various reanalyses to date. At the time of writing, NCEP-2 is shorter than NCEP-1. It corrected mistakes in NCEP-1 and used improved short wave radiation and boundary layer parameterisations. Its precipitation patterns, downward short wave radiation at the surface, and equatorial wind stress appear superior to NCEP-1, but its sensible heat flux over the oceans is lower than other estimates. It has not been widely distributed and studied, but is available on the Internet. ERA-15 is the highest resolution reanalysis now available. It appears to produce the most realistic precipitation patterns of the four reanalyses and has more realistic surface downward short wave radiation than NCEP-1 and GEOS. It has not been as widely available as the NCEP-1 reanalysis. The ERA-40 reanalysis is beginning; first results should be available during 2000. The reanalyses differ not only in time-mean fields but in the magnitude of month-to-month variability in surface fluxes. GEOS has the smallest variability in general, NCEP-2 tends to have the largest.

The reanalyses' fields of sensible and latent heat and wind stress show generally good agreement with COADS in the regions where ship reports adequately sample the atmosphere. The magnitude of latent heat flux varies significantly (by 24 $Wm^{-2}$ in the global mean), reflecting differences in the complete model physics packages as well as (if not more than) in the flux algorithms. The exact magnitude of oceanic evaporation appears uncertain, reflecting uncertainty in our knowledge of the strength of the hydrological cycle. Comparisons with fluxes from ship observations and buoys suggest that NCEP-1, NCEP-2 and ERA-15 evaporation may be too large in many areas.

Comparison with the reanalyses suggests that the COADS data base appears adequate to give useful information on the interannual variability of the monthly means in the mid-latitude North Pacific and North Atlantic and in parts of the South Atlantic. Over much of the tropics and the Southern Hemisphere (north of 40S) it appears adequate to give useful information on a long-term monthly mean climatology.

The reanalyses all appear to have substantial errors in surface radiation fields, reflecting problems in clouds and clear sky radiation. NCEP-1 has offsetting errors in its radiation fields. A major shortcoming for ERA-15, GEOS-1 and NCEP-2 appears to be a lack of low-level stratus clouds over the eastern subtropical oceans. SRB short wave radiation appears to have more realistic patterns than the reanalyses, but may well have a positive bias. Radiative transfer models in general appear to give too much downward short-wave radiation at the surface compared to actual measurements. Since surface long wave radiation is quite sensitive to atmospheric humidity profiles (that are not well-determined globally) and in particular to cloud base height, it is more uncertain than surface short wave.

There are significant differences between the hydrological cycles of the reanalyses. The magnitude of precipitation appears uncertain and varies widely in the estimates examined here. Twelve-year mean tropical precipitation over the ocean varies from 3.54 mm/day to 5.13 mm/day. The difference between NCEP-1 and NCEP-2 in precipitation indicates that data assimilation systems' estimates of the hydrological cycle are quite sensitive to changes in the physical parameterisations. Satellite estimates of precipitation are generally more uncertain in high latitudes than in the tropics. All the reanalyses have problems with the time-mean pattern of precipitation. Comparisons to CMAP and GPCP over land implies too much precipitation in all the reanalyses. This may be linked to too much evaporation over the ocean.

        Reanalyses were produced with unchanging data assimilation systems, but the available observations change with time.  ERA-15 has discontinuities in several fields at the end of 1986 associated with the use of satellite radiances.  NCEP-1 has discontinuities calling into question long-term trends.  Before 1979 the observational network needs to be considered in assessing the reliability of reanalysis.  During the period 1948-79 the observation network became more global with time; these changes in coverage affect the NCEP-1 reanalysis.  The end of 1978 marked the beginning of the modern satellite era.  In recent years the number of satellite observations have increased while observations from the surface have decreased; the consequences of this needs to be assessed.

## 12.4. Perspectives

        Because of the length of time needed to do a lengthy reanalysis, fluxes from global operational NWP systems will much of the time be based on more developed, more complex, and hopefully better physical parameterisations and therefore will be worth evaluating in addition to reanalysis results.  Such evaluations would benefit future reanalyses as well as weather forecasting.  We applaud WGNE's plans to archive and evaluate the fluxes from a number of global NWP systems.

        *In situ* observations and field experiments provide a very valuable check on near-surface meteorology and flux estimates from both satellites and data assimilation.  These need to be performed in a wide variety of locations and climates.  Successful field experiments require years of analysing and processing the data once the field experiment is actually carried out.  Funding agencies need to be willing to fund such work for an extended period.  Uncertainty estimates need to be provided in the resulting data sets.  In data assimilation analysis/forecast systems,  all the physical parameterisations influence each other;  adjusting one physical parameterisation to fit one independent estimate or one field experiment too precisely may distort other physical fields,  or the same physical field in other locations.

        Study of the TOGA COARE experiment has increased our knowledge of air-sea fluxes and improved our ability to measure them, partly because of a willingness to devote several years to analysing and processing the data after the actual field experiment.  It is not clear that the knowledge gained has been completely absorbed yet by the data assimilation/NWP community.  The data assimilation/NWP community has paid much attention recently to the assimilation of new satellite data; increased attention also needs to be paid to the development and implementation of improved physical parameterisations. Indeed improved physical parameterisations are needed to take full advantage of new satellite measurements of moisture and the hydrological cycle.  Funding needs to be provided for such work and to provide opportunities for people from the TOGA COARE community to work with operational data assimilation/modelling groups in the interest of improving future reanalyses as well as weather forecasting.

        The NCEP-1 Reanalysis is continuing as a climate data assimilation system analysing current data.  In the future,  reanalysis and climate data assimilation may diverge from data assimilation for NWP.  Such an independent system would be free from the time constraints on operational NWP and could have a much longer data cutoff time.  It could also have more complex physics, enabling it to process all observations and eliminating any need for separate retrievals of satellite data for any field.  Thus satellite and data assimilation estimates of surface fluxes might be merged within a single consistent system using as complete as necessary physical parameterisations.

        Satellite products have been demonstrated to have great potential to improve the overall situation especially concerning coverage, time sampling, and data consistency.  In addition, the time period covered by satellite data is approaching a length where such data become useful for climate variability studies (at least on the interannual scale).  However up to now it was not possible to construct a product that included the four relevant energy fluxes and the freshwater flux.  This was of high importance given the requirements of the data user

community.  Thus the following recommendations concerning the future use of satellite data can be drawn.  Firstly, to approach at least a climatological net flux estimate from satellite data alone,  projects must be established on the combination of different sensors.  Future satellite missions should follow the strategy of the TRMM satellite,  where instruments for measuring radiative fluxes, basic variables for heat flux estimation, and precipitation have been installed on one platform.  Secondly, to take full advantage of the satellite data there is a definite need for flux reference sites.  These should deliver highly accurate measurements of all the  heat fluxes for both error estimation and long term calibration.  This is particularly important for the construction of long time series from similar sensors on different satellite platforms.  Thirdly, the use of satellite data in conjunction with in situ data products should be carefully evaluated to establish a data set that takes full advantage of each data source and which is independent from the models.  Finally,  within mission related programs,  international and national funding agencies should more strongly support activities targeted on the use of the data for generation or continuation of user friendly flux products.

The report has shown that all existing flux estimates have deficiencies and that they are only suitable for some of the described applications.  Nevertheless, despite the various problems with the range of flux products that were reviewed in this report, it is evident that the products are complementary rather than being in competition, and that the ensemble of air-sea flux estimates that they represent cover the time and space scales relevant to present ocean science studies.

## 12.5. Specific Recommendations

The main conclusions from the Working Group's endeavours appear throughout the body of this report.  They have been summarised in the preceding sections of this Chapter which includes a number of recommendations.   At its final meeting, the Working Group also adopted the following specific recommendations:

❍   Reanalyses should be performed every 5-10 years by more than one centre; adequate resources should be provided to the reanalysis efforts to improve their surface fluxes, to carry out and evaluate the reanalyses and to ensure that they are easily available to the entire scientific community.  Surface fields should  be output every 3 hours .

❍   Evaluation of the fluxes from global operational NWP systems will benefit future reanalyses as well as provide critical guidance and product uncertainty estimates to users of these flux products. The WGNE's plans to archive and evaluate the fluxes from a number of global NWP systems should therefore be supported.

❍   A network of high quality flux reference platforms (combination of long-term moorings and ships) should be established to deliver highly accurate values of stress and all components of the air-sea heat fluxes for, inter alia, verification of flux estimates from satellites and models, and the long term calibration of satellite sensors.

❍   There is continuing need to compare and assess the quality of fluxes derived from various sources, and to evaluate the parameterisations used.  Encouragement should be given to efforts to enhance the reliability of momentum, net heat and freshwater fluxes by combining the best estimates from these various sources.

❍   Support should be provided for the continuing assembly of flux and flux-related data sets (in particular Voluntary Observing Ship-based collections such as COADS and other historical data).   Continued efforts are needed to remove non-stationary observational biases in historical data.  Basic meteorological variables should be included as well as uncertainties, error estimates and adequate documentation for all flux data sets.  A catalogue of flux data sets should be maintained on the Internet.

❍ Research and field experiments are needed to improve boundary layer parameterisations and bulk formulae, especially in regions where our physical understanding is poor. Adequate resources for complete analysis of the resulting data are necessary to realise the full benefits of the field experiments.

# REFERENCE

Aagaard, K., and P.Greismann, 1975: Toward new mass and heat budgets for the Arctic Ocean. *J.Geophys. Res.*, **80**, 3821-3827.

Alados-Arboledas, L., J. Vida and J.I.Jimenez, 1988: Effects of solar radiation on the performance of pyrgeometers with silicon domes. *J. Atmos. Oceanic Technol.*, **5**, 666-670

Alberta, T. L., and T. P. Charlock, 1999: A comprehensive resource for the investigation of short-wave fluxes in clear conditions: CAGEX Version 3. *Proc. AMS Tenth Conf. on Atmospheric Radiation*, Madison WI (June 28 – July 2, 1999), 279-282.

Alberta, T. L., T. P. Charlock, C. H. Whitlock, F. G. Rose, R. DiPasquale, R. Pinker, W. F. Staylor, and S. Gupta, 1994: Climate observations with GEWEX Surface Radiation Budget Project data. *Proc. AMS Eighth Conf. on Atmospheric Radiation*, Nashville TN (January 23-28, 1994), 22-24.

Albrecht, B.A., M.Poellot and S.K.Cox, 1974: Pyrgeometer measurements from aircraft. *Rev. Sci. Instrum.*, **45**, 33-38.

Alexander, M.A., and J.D.Scott, 1997: Surface flux variability over the North Pacific and North Atlantic Oceans. *J.Climate*, **10**, 2963-2977.

Allam, R., G. Holpin, P. Jackson, and G.-L. Liberti, 1993: Second Algorithm Intercomparison Project of the Global Precipitation Climatology Project: AIP-2. *pre-Workshop Report,* 133 pp. [Available from Satellite Image Applications Group, UKMO, Bracknell, Berkshire, United Kingdom.]

Anderson, S.P., and M.F.Baumgartner, 1998: Radiative heating errors in naturally ventilated air temperature measurements made from buoys. *J. Atmos. Oceanic Technol.,* **15**, 157-173.

Andreas, E.L., 1992: Sea spray and the turbulent air-sea heat fluxes. *J. Geophys. Res.*, **97**, 11,429-11,441.

Andreas, E.L., 1994: Reply (to Katsaros and de Leeuw, 1994). *J. Geophys. Res.*, **99**, 14,354-14,350.

Andreas, E.L., J.B. Edson, E.C. Monohan, M.P. Rouault, and S.D. Smith, 1995: The spray contrbution to net evaporation from the sea: a review of recent progress. *Boundary-Layer Meteor.*, **72**, 3-52.

Angelucci, M.G., N.Pinardi, and S.Castellari, 1998: Air-Sea fluxes from operational analyses fields: intercomparison between ECMWF and NCEP analyses over the Mediterranean area. *Phys. Chem. Earth* , **23**, 5/6, 569-574.

Arkin, P. A. and P. Xie, 1994: The global precipitation climatology project: First Algorithm Intercomarison Project. *Bull. Amer. Meteor. Soc.*, **75**, 401-419.

Arkin, P. A., 1999 (Ed.) : *Report of the OOPC/AOPC Workshop on Global Sea Surface Temperature Data Sets.* (Palisades, N.Y., USA, 2-4 November 1998). Report GCOS-57, GOOS-79, WMO/TD 978, WMO.

Arpe, K. and E. Klinker, 1986: Systematic errors of the ECMWF operational forecasting model in mid-latitudes. *Quart. J. R. Met. Soc.*, **112**, 181-202.

Arpe, K., 1989: Impact of changes in the ECMWF analysis-forecasting scheme on the systematic error of the model. *Ten years of medium-range weather forecasting*, ECMWF Seminar 4-8 Sept. 1989, ECMWF, Reading, England, 69-114.

Arpe, K., 1991: The hydrological cycle in the ECMWF short-range forecasts. *Dynamics of Atmospheres and Oceans,* **16**, 33-59.

Arpe, K., C. Klepp and A. Rhodin, 2000: Differences in the hydrological cycles from different reanalyses – which one shall we believe?. *Proc. Conf.2ⁿᵈ Intl. Conf. on Reanalyses*, Reading, England, 23-27 Aug. 1999. WCRP-109 (WMO/TD 985) WMO, 193 - 196.

Atlas, R., & co-authors, 1999: Geophsical valiation of NSCAT winds using atmospheric data and analyses. *J. Geophys. Res*, **104**, 11405-11424.

Austin, P.M., 1987: Relation between measured radar reflectivity and surface rainfall. *Mon. Wea. Rev.*, **115**, 1053-1070.

Axys, 1996: Meteorological and Oceanographic *Measurements from Canadian Weather Buoys.* (draft), Axys Environmental Consulting Ltd., Sidney, B.C., Canada, 35 pp. + Apps.

Bacon, S. 1997: Circulation and Fluxes in the North Atlantic between Greenland and Ireland *J. Phys. Oceanogr.* **27** (7) 1420–1435.

Bacon, S. and D.J.T. Carter, 1991: Wave climate changes in the North Atlantic and North Sea, *Int. J. Climatol.* **11**, 545-558

Bacon, S. and D.J.T. Carter, 1993: A connection between mean wave height and atmospheric pressure gradient in the North Atlantic, *Int. J. Climatol.* **13**, 423-436

Bane, J.M., and K.E. Osgood, 1989: Wintertime air-sea interaction processes across the Gulfstream. *J. Geophys. Res.*, **94**, 10755-10772.

Barkstrom, B.E., E.Harrison, G.Smith, R.Green, J.Kibler, R.Cess & ERBE Science Team, 1989: Earth Radiation Budget Experiment (ERBE) archival and April 1985 results. *Bull.Amer.Meteor.Soc.*, **70**, 1254-1262.

Barnes, S. L., 1964: A Technique for Maximising Details in Numerical Weather Map Analysis. *Journal of Applied Meteor.*, **3**, 396 - 409.

Barnett, T.P., 1999: Comparison of near surface air temperature Variability in 11 coupled global climate models. *J.Climate,* **12**, 511-518.

Barnier, B., 1998. Forcing the ocean. *Ocean Modeling and Parameterization*, E.P. Chassignet and J. Verron Eds., Kluwer Academic Publishers, The Netherlands, 45-80.

Barnier, B., L. Siefridt, and P. M. Marchesiello, 1995: Thermal forcing for a global ocean circulation model using a three-year climatology of ECMWF analyses. *J. Marine Systems*, **6**, 363 - 380.

Barrat, M.J., 1991: Waves in the North East Atlantic. *UK Dept. of Energy Report* OT190545, HMSO, London

Barton, I.J., A.J.Prata and R.P.Cechet, 1995: Validation of the ATSR in Australian waters. *J. Atmos. Oceanic Technol.*, **12**, 290-300.

Battan, L.J., 1973: *Radar Observations of the Atmosphere.* University of Chicago Press, 324pp.

Bauer, E., and C. Staabs, 1998: Statistical properties of global significant wave heights and their use for validation. *J. Geophys. Res.* **103**, 1153-1166

Bauer, E., and P. Heimbach, 1999: Annual validation of significant wave heights from ERS-1 Synthetic Aperture Radar Wave Mode Spectra using TOPEX/POSEIDON and ERS-1 altimeter data. *J. Geophys. Res.* **104**, 13345 - 13357.

Bauer, P. and P. Schlüssel, 1993: Rainfall, total water, ice water and water-vapour over sea from polarized microwave simulations and SSM/I data, *J. Geophys. Res.* **98**, 20737- 20759.

Baumgartner, A., and Reichel, E., 1975. *The World Water Balance.* Elsevier, New-York, 179pp.

Beljaars, A.C.M. and A.A.M. Holtslag, 1991: On flux parameterization over land surfaces for atmospheric models. *J. Appl. Meteor.*, **30**, 327-341

Beljaars, A.C.M., 1994: The parameterization of surface fluxes in large-scale models under free convection. *Quart. J. Roy. Meteor. Soc.*, **121**, 255-270.

Beljaars, A.C.M., 1997: Air-sea interaction in the ECMWF model. *Seminar on Atmosphere-surface Interaction*, 8-12 Sept. 1997, ECMWF, Reading, UK, 33-52.

Benoit, R., 1977: On the integral of the surface layer profile-gradient functions. *J.Appl.Meteor.*,**16**,859-860

Berliand, M. E. and T. G. Berliand, 1952: Determining the net long-wave radiation of the Earth with consideration of the effect of cloudiness., *Isv. Akad. Nauk. SSSR Ser. Geofiz.*

Best, A.C. 1950: The size distribution of raindrops, *Quart. J. Roy. Meteor. Soc.* **76**, 16 – 36.

Bethoux, J.P., 1979: Budgets of the Mediterranean Sea: their dependence on the local climate and on the characteristicas of the Atlantic water. *Oceanol. Acta*, **2**, 157-163.

Betts, A. K., S.-Y. Hong and H.-L. Pan, 1996: Comparison of NCEP-NCAR reanalysis with 1987 FIFE data. *Mon. Wea. Rev.*, **124**, 1480-1498.

Bigg, G.R., 1993: Comparison of Coastal wind and pressure trends over the tropical Atlantic: 1946-1987. *Int. J. Climatol.*, **13**, 411-421.

Bignami, F., S.Marullo, R.Santoleri & M.E. Schiano, 1995: Longwave radiation budget in the Mediterranean Sea. *J. Geophys. Res.*, **100**, 2501-2514.

Bishop, J.K.B., and W.B. Rossow, 1991: Spatial and temporal variability of global surface solar irradiance. *J. Geophys. Res.*, **96**, 16,839-16,858.

Bishop, J.K.B., W.B. Rossow and E.G. Dutton, 1997: Surface solar irradiance from the International Satellite Cloud Climatology Project 1983 - 1991. *J. Geophys. Res.*, **102**, 6883-6910.

Blanc, T. V., 1987: Accuracy of bulk-method-determined flux, stability, and sea surface roughness. *J. Geophys. Res.*, **92**, 3867-3876.

Blanc, T.V., 1985: Variation of bulk-derived surface flux, stability and roughness results due to the use of different transfer coefficient schemes. *J. Phys. Oceanog.*, **15**, 650-669.

Bloom, S., L.L. Takacs, A. M. da Silva, and D. Ledvina, 1996: Data assimilation using incremental analysis updates. *Mon. Wea. Rev.*, **124**, 1256-1271.

Böning, C. W., R. Döscher, and H.-J. Isemer, 1991: Monthly mean wind stress and Sverdrup transport in the North Atlantic: A comparison of the Hellerman-Rosenstein and Isemer-Hasse climatologies. *J. Phys. Oceanogr.*, **21**, 221-229.

Bony, S., Y. Sud, K. M. Lau, J. Susskind, and S. Saha, 1997: Comparison and satellite assessment of NASA/DAO and NCEP-NCAR reanalyses over tropical ocean: Atmospheric hydrology and radiation. *J. Climate*, **10**, 1441-1462.

Boukthir M., Barnier B., K. Béranger and E. Garnier, 2000. A monthly mean climatology of river runoff into Oceans *(in preparation)*.

Bourassa, M. A., M. H. Freilich, D. M. Legler, W. T. Liu, and J. J. O'Brien, 1997: Wind observations from new satellite and research vessels agree. *EOS Trans. Amer. Geophys. Soc.*, **78**, 597-602.

Bourassa, M.A., D.G. Vincent and W.L.Wood, 1999: A flux parameterization including the effects of capillary waves and sea state. *J. Atmos. Sci.*, **56**, 1123-1139.

Boutin, J., J. Etcheto, M. Rafizadeh, and D. C. E. Bakker, 1999: Comparison of NSCAT, ERS 2 active microwave instrument, special sensor microwave imager, and Carbon Interface Ocean Atmosphere buoy wind speed: consequences for the air-sea CO2 exchange coefficient. *J. Geophys. Res.*, **104**, 11375-11392.

Boville, B.A. & P.R.Gent, 1998: The NCAR Climate Sysems Model, Version one. *J. Climate*, **11**, 1115 - 1130.

Bowker, D. E., R. E. Davis, D. L. Myrick, K. Stacy, and W. T. Jones, 1985: *Spectral Reflectances of Natural Targets for Use in Remote Sensing Studies*. NASA Reference Publication 1139, 191 pp.

Bradley, E.F. and Weller, R.A. (editors) 1995b: *Third Workshop of the TOGA COARE Air Sea Interaction (Flux) Working Group.* Univ. of Hawaii, Honolulu, USA, 2 4 August 1995. (TOGA COARE International Project Office, UCAR, Boulder, USA), 34 pp.

Bradley, E.F. and Weller, R.A. (editors), 1997: *Fourth Workshop of the TOGA COARE Air–Sea Interaction (Flux) Working Group.* WHOI, Mass., USA, 9-11 October 1996. (TOGA COARE International Project Office, UCAR, Boulder, USA, 61pp.

Bradley, E.F. and Weller, R.A. (eds.), 1995a: *Joint Workshop of the TOGA COARE Flux and Atmospheric Working Groups.* Boulder, Colorado, USA, 11 13 July 1995. (TOGA COARE International Project Office, UCAR, Boulder, USA), 35 pp.

Bradley, E.F., C.W. Fairall and J.E. Hare, 2000: An old and improved bulk algorithm for air-sea fluxes: COARE2.6a. *Proc. 14th Symp. Boundary Layer and Turbulence*, Aspen, 7-11 August, Amer. Meteor. Soc.

Bradley, E.F., M. Moncrieff and Weller, R.A. (editors), 1997: *Joint Workshop of the TOGA COARE Flux and Oceans Working Groups, and the GEWEX Cloud Systems Study Working group 4.* NCAR, Boulder CO, 14-16 May, NCAR/MMM, UCAR, Boulder, 61pp.

Bradley, E.F., P.A. Coppin and J.S. Godfrey, 1991: Measurements of sensible and latent heat fluxes in the western equatorial Pacific ocean. *J. Geophys. Res.*, **96**, Suppl. 3375-3389.

Bradley, S.G. and C.D. Stow, 1974: The measurement of charge and size of raindrops: Part 1. The disdrometer. *J. Appl, Meteor..*, **13**, 114-130.

Breon, F-M., R. Frouin and C. Gautier, 1994: Global shortwave energy budget at the Earth's surface from ERBE measurements. *J. Climate*, **7**, 309-324.

Brest C. L., Rossow W. B., Roiter M. D. 1997: Update of radiance calibrations for ISCCP *J. Atmos. Oceanic Tech.* **14**: (5) 1091-1109.

Brown, J.W., O.B. Brown, and R.H. Evans, 1993: Calibration of AVHRR Infrared channels: a new approach to non-linear correction, *J. Geophys Res.*, **98**, 18257 - 18268.

Brümmer, B., 1993: ARKTIS 1993 - Report on the field phase with examples of measurements. *Berichte aus dem Zentrum für Meeres- und Klimaforschung, Reihe A: Meteorologie*, **11**. [from Univ. Hamburg Meteorol-ogisches Inst., Bundesstraße 55, Hamburg, Germany].

Brutsaert, W. A., 1975: A theory for local evaporation (or heat transfer) from rough and smooth surfaces at ground level. *Water Resour. Res.,* **11**, 543-550.

Brutsaert, W. A., 1982: *Evaporation into the atmosphere.* Reidel, Dordrecht, 299 pp.

Bryden H.L. & M.M.Hall, 1980: Heat tranport by currents across 25° N in the Atlantic Ocean. *Science*, **207**, 884-886.

Budyko, M. I., 1963: Atlas of heat balance of the world., *Glabnaia Geofiz. Observ*.

Budyko, M. I., 1974: *Climate and Life.* Academic Press, New York.

Bumke, K., U.Karger, L.Hasse, and K.-P.NIekamp, 1998: Evaporation over the Baltic Sea as an example of a semi-enclosed sea. *Contr.Atmosph.Phys*., **71**, 249-261.

Bunker, A.,F., 1976: A computation of surface energy flux and annual cycle of the North Atlantic Ocean, *Mon. Weather Rev.*, **104**, 1122-1140.

Bunker, A.F., H.Charnock and R.A.Goldsmith, 1982: A note on the heat balance of the Mediterranean and the Red Seas. *J. Marine Res.* **40**, Supplement, 73-84.

Bunker, A.F.,1982: Trends of variations and energy fluxes over the Atlantic Ocean from 1948 to 1972. *Mon. Wea. Rev.*, **104**, 1122-1140.

Burns, S.P., & co-authors 2000: Comparisons of aircraft, ship and buoy radiation and SST measurements from TOGA-COARE. *J. Geophys. Res.*, *submitted*

Burns, S.P., & co-authors, 1999: Comparisons of aircraft, ship and buoy meteorological measurements from TOGA-COARE. *J.Geophys.Res.*, **104**(D24) 30853-30883.

Busch, N.E., 1972: On the mechanics of atmospheric turbulence. in "*Workshop on Micrometeor.*", D.A. Haugen (Ed.), Amer. Meteor. Soc., Boston, MA, 1-61.

Bush, B.C., F. P. J. Valero, A. S. Simpson, L. Bignone, 2000: Characterization of thermal effects in pyranometers: A data correction algorithm for improved measurement of surface insolation. *J. Atmos. Oceanic Technol.* **17** (2) 165-175.

Businger, J.A., J.C.Wyngaard, Y. Izumi and E.F.Bradley, 1971: Flux-profile relationships in the atmospheric surface layer. *J. Atmos. Sci.*, **28**, 181-189.

Caldwell, D.R. and W.P. Elliott, 1971: Surface stresses produced by rainfall. *J. Phys. Oceanog.*, **1** 145-148.

Caplan, P. M., and G. H. White, 1989: Performance of the National Meteorological Center's Medium-Range Model. *Wea. and Fcst*., **4**, 391-400.

Cardone, J.S., J.G. Greenwood and M.A.Cane, 1990: On trends in historical marine wind data. *J.Climate,* **3,** 113-127.

Cardone, V.J., H.C. Graber, R.E. Jensen, S. Hasselmann, M.J. Caruso, 1995: In search of the true surface wind field in SWADE IOP-1: Ocean wave modelling perspective. *Global Atmos. Ocean System*, **3**, 107-150.

Carslaw, H.S. and J.C. Jaeger, 1959: *Conduction of heat in solids.* Oxford University Press, London, 510 pp.

Carter, D.A., K. S. Gage, W. L. Ecklund, W. M. Angevine, P. E. Johnston, A. C. Riddle, J. Wilson and C.R. Williams, 1995: Developments in lower tropospheric wind profiling at the NOAA Aeronomy Laboratory. *Radio Sci.*, **30**, 977-1001.

Cayan, D., 1992a: Latent and sensible heat flux anomalies over the Northern Oceans: The connection to monthly atmospheric circulation. *J.Climate*, 5, 354-369.

Cayan, D.,1992b: Variability of latent and sensible heat fluxes estimated using bulk formulae. *Atmosphere-Ocean*, **30** (1), 1-42.

Cayan, D.,1992c: Latent and sensible heat flux anomalies over the Northern Oceans: Driving the sea surface temperature. *J.Phys.Oceanogr*, **22**, 859-881.

Cess, R. D., & co-authors, 1995: Absorption of solar radiation by clouds: Observations versus models. *Science*, **267**, 496-499.

Chang, H.-R. and R.L. Grossman, 1999: Evaluation of bulk surface flux algorithms for light wind conditions using data from the Coupled Ocean-Atmosphere Response experiment (COARE). *Quart. J. Roy. Meteor. Soc.*, **125**, 1551-1588.

Charlock, T. P., F. G. Rose, and T. L. Alberta, 1999: An observational study of cloud forcing to the atmospheric absorption of SW over Kansas and Oklahoma for January-August 1998. *Proc. AMS Tenth Conf. on Atmospheric Radiation*, Madison WI (June 28 – July 2, 1999), 262-265.

Charlock, T. P., F. G. Rose, T. L. Alberta, and G. D. Considine, 1998: Comparison of computed and measured cloudy-sky shortwave (SW) in the ARM Enhanced Shortwave Experiment (ARESE). *Proc. ARM Science Team Meeting*, Tuscon, AZ, March 23-27, 1998 (available at the URL www.arm.gov).

Charlock, T., & co-authors,, 1997: CERES Algorithm Theoretical Basis Document. Compute Surface and Atmospheric Fluxes (Subsystem 5.0). Release 2. NASA Langley Research Center. 51 pp.

Charlock, T., and T. Alberta, 1996: The CERES/ARM/GEWEX Experiment (CERES) for the retrieval of radiative fluxes with satellite data. *Bull. Amer. Meteor. Soc.*, **77**, 2673-2683. (see also http://www-cagex.larc.nasa.gov/cagex/cagex.html )

Charnock, H., 1955: Wind stress on a water surface. *Quart. J. Roy. Meteor. Soc.,* **81**, 639-640.

Chelton, D.B., M.H. Freilich, and M.G. Schlax, 1997: Sampling errors in wind fields constructed from single and multiple scatterometer datasets. (Poster presentation at NSCAT Science Working Team Meeting, Maui, HI, 10-14 November 1997).

Chin, T.M., R.F. Milliff, and W.G. Large, 1998: Basin-scale, high-wavenumber sea surface wind fields from a multiresolution analysis of scatterometer data. *J. Atmos. Ocean. Tech.*, **15**, 741-763.

Chinman, R., & co-authors, 1995: *Summary report of the TOGA-COARE International Data Workshop.* Toulouse, France, 2-11 August 1994. (TOGA COARE International Project Office, UCAR, Boulder, USA)

Chou, M.-D., 1992: A solar radiation model for use in climate studies. *J. Atmos. Sci.*, **49**, 762-772.

Chou, M.-D., and W. Zhao, 1997: Estimation and model validation of surface solar radiation and cloud radiative forcing using TOGA COARE measurements. *J. Climate*, **10**, 610-620.

Chou, M-D., A. Arking, J. Otterman, and W. L. Ridgway, 1995a: The effect of clouds on atmospheric absorpion of solar radiation.*Geophys.Res.Lett*.,**22**,1885-1888.

Chou, S.-H., C.-L.Shie, R.M.Atlas, and J.Ardizzone, 1997: Air-sea fluxes retrieved from special sensor microwave imager data. *J. Geophys. Res.*, **102**, 12705-12726.

Chou, S.-H., R. M. Atlas, C.-L. Shie, and J. Ardizzone, 1995b: Estimates of surface humidity and latent heat fluxes over oceans from SSM/I data. *Mon. Wea. Rev.*, **123**, 2405-2425.

Ciesielski, P.E. and R.H. Johnson, 1999: Precipitation estimates for the COARE intensive observing period. *Proc. Conf. on the TOGA Coupled Ocean-Atmosphere Response Experiment (COARE98), Boulder CO, 7-14 July 1998,* WCRP-107, WMO, Geneva, 193-194.

Cifelli, R., S.A. Rutledge, D. J. Boccippio, and T. Matejka, 1996: Horizontal divergence and vertical velocity retrievals from Doppler radar and wind profiler observations. *J. Atmos. Oceanic Tech.*, **13**, 948-966.

Clark, N.E., R. M.Eber, J.A.Renner and J.F.T.Saur, 1974: *Heat exchange between ocean and atmosphere in the eastern North Pacific for 196 -71.* NOAA Tech. Rep. NMFS SSRF-682, U.S.Dept.Commerce, Wash., D.C.

Clarke, R.H. and R.R. Brook, 1979: *The Koorin expedition, atmospheric boundary layer data over tropical savannah land.* Bureau of Meteor., Australian Govt. Pub. Service, Canberra, 359 pp.

Clayson, C. A., C. W. Fairall, and J. A. Curry, 1996: Evaluation of turbulent fluxes at the ocean surface using surface renewal theory. *J. Geophys. Res.*, **101**, 28503 - 28513.

Clough, S.A., 1995: The water vapor continuum and its role in remote sensing, in *Optical Remote Sensing of the Atmosphere*, **2**, *OSA Tech. Dig. Ser.*, 76-78, Opt. Soc. of Amer., Washington, D.C.

Clough, S.A., M.J. Iacono and J.-L. Moncet, 1992: Line-by-line calculations of atmospheric fluxes and cooling rates: application to water vapor. *J. Geophys. Res.,* **97**, 15761-15785.

Coachman, L.K., and K.Aagaard, 1988: Transports through Bering Strait: Annual and Interannual variability. *J.Geophys. Res.*, **93**, 15535-15539.

Cole, H.L. and E.R. Miller, 1999: Correction and re-calculation of humidity data from TOGA-COARE radiosondes, and development of humidity correction algorithms for global radiosonde data. *Proc. of COARE98, A Conference On The TOGA Coupled Ocean-Atmosphere Response Experiment, Boulder, Colorado, USA, 7-14 July 1998*. WCRP-107, WMO/TD 940, WMO, Geneva.

Colton, M. C. and G. A. Poe, 1999: Intersensor Calibration of DMSP SSM/I's: F-8 to F-14, 1987-1997. *IEEE Transactions on Geoscience and Remote Sensing*, **37**, 418-439.

Conkright, M. E., S. Levitus, and T. P. Boyer, 1994: *World Ocean Atlas 1994, Volume 1: Nutrients.* NOAA Atlas NESDIS 1, U.S. Dept. Commerce, NOAA/NESDIS.

Cotton, P. D. and D. J. T. Carter, 1994b: Interannual variability in global wave climate from satellite data. *SPIE*, **2319**, 174 - 180.

Cotton, P.D., and D.J.T. Carter, 1994a: Cross calibration of TOPEX, ERS-1, and Geosat wave heights. *J. Geophys. Res. 99*, 25025-25033.

Covey, C. and co-authors, 2000: *The Seasonal Cycle in Coupled Ocean-Atmosphere General Circulation Models,* PCMDI Report 51, Lawrence Livermore National Laboratory, Livermore, CA (May 2000 - originally released February 1999).

Cox, A. T. and V. R. Swail, 2000: A global wave hindcast over the period 1958 – 1997: validation and comate assessment, *J. Geophys. Res. (Oceans) – submitted.*

Cox, A. T., V. J. Cardone, and V.R. Swail, 1999: On the use of *in situ* and satellite wave measurements for the evaluation of wave hindcasts. in *CLIMAR 99, WMO Workshop on Advances in Marine Climatology*, Vancouver, 8 - 15 Sept. 1999, 130 – 138.

Cox, M. D., and K. Bryan, 1984. A numerical model of the ventilated thermocline. *J.Phys.Oceanogr.*,**14**, 674-687.

Crewell, S, E. Ruprecht, and C. Simmer, 1991: latent heat flux over the North Atlantic ocean-a case study. *J. Appl. Met.*, **30**, 1627 - 1635.

Crosby,J.D., 1994: Precipitation measurement on ocean-going platforms. *Proc. MTS-94 Conf. and exposition on Oceanogr. Instrumentation,* 7-9 Sept., Wash., D.C.

Cullather, R.I., and Bromwich, D.H., 2000: The atmospheric hydrologic cycle over the Arctic basin from reanalyses. Part I: Comparison with observations and previous studies *J. Climate* **13** (5) 923-937.

Curry, J. A., & co-authors, 1999: High-resolution satellite derived dataset of the surface fluxes of heat, freshwater and momentum for the TOGA COARE IOP. *Bull. Amer. Meteor. Soc.*, **80**, 2059-2080.

Curry, J.A., W.B. Rossow, D. Randall and J.L. Schramm, 1996: Overview of Arctic cloud and radiation characteristics. *J. Climate*, **9**, 1731-1764.

da Silva, A. and G. White, 1995: A comparison of surface marine fluxes from GEOS-1/DAS and NMC reanalyses. *Proc. of the Workshop on the GEOS-1 Five-Year Assimilation,* NASA Tech. Memo. 104606, Vol. 7, GSFC., Greenbelt, MD, 129-136.

da Silva, A. M., C. C. Young and S. Levitus, 1994: *Atlas of Surface Marine Data 1994,* NOAA Atlas NESDIS 6. (6 Volumes) Available from: U.S Dept. Commerce, NODC, User Services Branch, NOAA/NESDIS E/OC21, Washington D.C, 20233, USA.
Vol. 1: Algorithms and Procedures.
Vol. 2: Anomalies of Directly Observed Quantities.
Vol. 3: Anomalies of Heat and Momentum Fluxes.
Vol. 4: Anomalies of Fresh Water Fluxes.
Vol. 5: Anomalies of Miscellaneous Derived Quantities.
Vol. 6: Heat Flux Sensivity to SST.

da Silva, A. M., C.C.Young and S. Levitus, 1995: Towards a revised Beaufort equivalent scale. Internat. *COADS Winds Workshop*, Kiel, Germany, 31 May - 2 June 1994, NOAA/ERL, 270 - 286.

da Silva, A., and G. White, 1996: Intercomparison of surface marine fluxes from GEOS-1/DAS and NCEP/NCAR reanalyses. *WCRP Workshop on Air-Sea Flux Fields for Forcing Ocean Models and Validating GCMs,* Reading, England, 24-27 Oct. 1995, WMO/TD-762, WMO, Geneva, 19-24.

Dacunha, N.M.C., N. Hogben, and K.S. Andrews, 1984: Wave climate synthesis worldwide, *Proc. Internat. Symp. on Wave and Wind Climate Worldwide*, Roy. Inst. Naval Architects, London, 1-11.

Darnell, W. L., W. F. Staylor, N. A. Ritchey, S. K. Gupta, and A. C. Wilber, 1996: Surface radiation budget: A longterm global dataset of shortwave and longwave fluxes. *Eos, Trans. Amer. Geophys Union*, February.

Darnell, W.L., W.F. Staylor, S.K. Gupta, N.A. Ritchey, and A.C. Wilber, 1992: Seasonal variation of surface radiation budget derived from International Satellite Cloud Climatology Project C1 Data. *J. Geophys. Res.,* **97**, 15741-15760.

Deacon, E. L., 1988: The streamwise Kolmogoroff constant. *Boundary-Layer Meteor.*, **42**, 9 - 17.

Deardorff, J.W.,1970: Convective velocity and temperature scales for the unstable planetary boundary layer and for Rayleigh convection. *J.Atmos.Sci.*,**27**,1211-1213.

DeCosmo, J., K. B. Katsaros, S. D. Smith, R. J. Anderson, W. A. Oost, K. Bumke and H. Chadwick, 1996: Air-sea exchange of water vapor and sensible heat: The Humidity Exchange Over the Sea (HEXOS) results. *J. Geophys. Res.,* **101**, 12001-12016.

Dedieu,G., P.Y.Deschamps and Y.H.Kerr, 1987: Satellite estimation of solar irradiance at the surface of the Earth and of surface albedo using a physical model applied to METEOSAT data. *J. Climate Appl. Meteor.*, **26**, 79-87.

DeLuisi, J., 1991: *Second Workshop on Implementation of the Baseline Surface Radiation Network.* WCRP-64, WMO/TD 453, WMO, Geneva.

Derber, J. C., D. F. Parrish and S. J. Lord, 1991: The new global operational analysis system at the National Meteorological Center. *Wea. Forecasting*, **6**, 538-547.

Dickey, T. D., D. V. Manov, R. A. Weller and D. A. Siegel, 1994: Determination of longwave heat flux at the air-sea interface using measurements from buoy platforms. *J. Atmos. & Oceanic Tech.*, **11**, 1057 - 1078.

Dickson, R. R., Lazier, J., Meincke, J., Rhines, P., and Swift, J., 1996. Long term coordinated changes in the convective activity of the North Atlantic. *Decadal Climate variability*, Anderson D. L. T., and Willebrand, J., Eds., Springer-Verlag, 211-262.

Dickson,R.R., Meincke,J.,Malmberg,A.,& Lee,A.J., 1988. The Great Salinity Anomaly in the northern North Atlantic 1968-1982. *Prog Oceanogr.*,**20**,103-151.

Dietrich, G., 1950: Über systematische Fehler in den beobachteten Wasser- und Lufttemperaturen auf dem Meere und ihre Auswirkungen auf die Bestimmung des Wärmeumsatzes zwischen Ozean und Atmosphäre. *Deutsche Hydrogr. Zeitschr.* **3**, 314-324.

Dobson, F. W., R. J. Anderson, P. K. Taylor and M. J. Yelland, 1999: Storm Wind Study II: Open Ocean Wind and Sea State Measurements. in *Proc Symp. On the Wind-driven Air-sea Interface* (Ed. M.L. Banner), Univ. of New South Wales, Sydney, 11-15 January 1999, 295 - 296.

Dobson, F., and S. Smith, 1988: Bulk model of solar radiation at sea. *Quart.J. Roy. Meteor. Soc.*, **114**, 165-182.

Donelan, M. A., 1982: The Dependence of the Aerodynamic Drag Coefficient on Wave Parameters. *First Internat. Conf. on Meteor. and Air-Sea Interaction of the Coastal Zone*, Amer.Meteor.Soc., Boston, 381-387.

Donelan, M.A., F.W. Dobson, S.D. Smith and R.J. Anderson, 1993: On the dependence of sea surface roughness on wave development. *J. Phys. Oceanog.*, **23**, 2143-2149.

Donelan, M.A., W.M. Drennan and K.B. Katsaros, 1997: The air-sea momentum flux in conditions of wind sea and swell. *J. Phys. Oceanog.*, **27**, 2087-2099.

Donlon, C. J., S. J. Keogh, D. J. Baldwin, I. S. Robinson, I. Ridley, T. Sheasby, I. J. Barton, E. F. Bradley, T. J. Nightingale and W. Emery, 1998: Solid-state radiometer measurements of sea surface skin temperature. *J. Atmos. Oceanic Tech.*, **15**, 775-787.

Dorman, C. E. and R. H. Bourke, 1978: A temperature correction for Tucker's ocean rainfall estimates. *Quart. J. Roy. Meteor. Soc.*, **104**, 765 - 773.

Drange, H., P. Schlüssel, and M. Srokosz, 1999: *Study of critical requirements for ocean salinity retrieval using a low frequency microwave radiometer,* Final report of ESA contract No. 13224/98/NL/MV, [available: http://www.nrsc.no/gcrieber/rwin.html ].

Dümenil, L., K. Isele, H.-J. Liebscher, U.Schröder, M. Schumacher and K. Wilke, 1993: *Discharge data from 50 selected rivers for GCM validation,* Max-Planck-Institut für Meteorologie, Tech. Rep., 100, Hamburg.

Dupuis, H., P.K.Taylor, A Weill and K.B.Katsaros 1997: Inertial dissipation method applied to derive fluxes over the ocean during the SOFIA/ASTEX and SEMAPHORE experiments in low to moderate windspeeds. *J. Geophys. Res.* **102,** 21115-21129.

Dupuis,H., C.Guérin, A.Weill, and D.Hauser, 1999: Heat Flux estimates by the inertial dissipation method during the FETCH experiment. *Proc Symp. On the Wind-driven Air-sea Interface* (Ed. M.L.Banner), Univ. New South Wales, Sydney, 11-15 Jan., 297 - 304.

Dutton, E.G, 1993: An extended comparison between LOWTRAN7 computed and observed broadband thermal irradiances: global extreme and intermediate surface conditions. *J.Atmos.OceanicTech.*,**10**,326-336.

Ebert, E. E. and J. M. Manton, 1998: Performance of satellite rainfall estimation algorithms during TOGA COARE. *J. Atmos. Sci.*, **55**, 1537 - 1557.

Ebert, E.E. 1996: *Results of the 3rd algorithm intercomparison project (AIP-3) of the Global Precipitation Climatology Project (GPCP).* BMRC Report No. 55, 199 pp., BMRC, GPO Box 1289K, Melbourne, Vic., Australia 3001.

Ebert, E.E. and J.A. Curry, 1993: An intermediate one-dimensional thermodynamic sea-ice model for investigating ice-atmosphere interactions. *J. Geophys. Res.*, **98**, 10085-10109.

Ebisuzaki, W. and R. Kistler, 2000: An examination of a data-constrained assimilation. *Proc. Conf. 2nd Intl. Conf. on Reanalyses*, Reading, England, 23-27 Aug. 1999. WCRP-109 (WMO/TD 985) WMO, 14 - 17.

Ebisuzaki, W., M. Chelliah, and R. Kistler, 1998: NCEP/NCAR Reanalysis: Caveats. *Proc. 1st WCRP Intl. Conf. on Reanalyses.* 27-31 Oct. 1997, Silver Spring, MD, USA, WCRP-104, WMO/TD-876. WMO, Geneva, 81-84.

Ebuchi, N., and H. C. Graber, 1998: Directivity of wind vectors derived from the ERS-1/SMI scatterometer. *J. Geophys. Res.*, **103**, 7787-7797.

Ecklund, W. L., C. R. Williams, P. E. Johnston, and K. S. Gage, 1997: Profiler observations of deep convective clouds in MCTEX. *Proc. 22nd Conf. on Hurricanes and Tropical Meteor.*, 19-23 May, Fort Collins, CO, Amer. Meteor. Soc., Boston, MA.

Ecklund, W.L., P. E. Johnston, J. M. Warnock, W.L. Clark, and K. S. Gage, 1995: An S-Band profiler for tropical precipitating cloud studies. *Proc. 27th conference on Radar Meteor.*, 335-336, Oct., Vail, CO, Amer. Meteor. Soc., Boston, MA.

Edson, J. B. and C. W. Fairall, 1998: Similarity relationships in the Marine Atmospheric surface layer for terms in the TKE and scalar variance budgets. *J. Atmos. Sci.*, **55**, 2311 - 2328.

Edson, J.B., A. A. Hinton, K. E. Prada, J.E. Hare, and C.W. Fairall, 1998: Direct covariance flux estimates

from moving platforms at sea. *J. Atmos. Oceanic Tech.*, **15**, 547-562.

Edson, J.B., C.W.Fairall, P.G.Mestayer and S.E.Larsen, 1991: A study of the inertial-dissipation method for computing air-sea fluxes. *J. Geophys. Res.*, **96**, 10689-10711.

Efimov, V.V., N.A. Timofeev, I.V. Kurzeevsky and E.N. Sychov, 1985: The estimate of the coefficients of the heat and moisture transfer between the ocean and atmosphere. *Phys. Atmos. Ocean, Izvestia Academy Sciences of the USSR*, **21**, (7), 735-743.

Efimova, N.A., 1961: On methods of calculating monthly values of net longwave radiation (in Russian), *Meteor. Gidrol.*, **10**, 28 – 33.

Ellingson, R. G., and Y. Fouquart, 1991: The intercomp-arison of radiation codes in climate models (ICRCCM): An overview. *J. Geophys. Res.*, **96**, 8926-8929.

Ellingson, R.G., J. Ellis and S. Fels, 1991: The intercomp-arison of radiation codes used in climate models: long wave results. *J. Geophys. Res.*, **96**, 8929-8963.

Emery, W. J., K. Cherkauer, B. Shannon and R. W. Reynolds, 1997: Hull-mounted sea surface temperatures from ships of opportunity. *J. Atmos. & Oceanic Tech.*, **14**(5), 1237-1251.

Emery, W., Y. Yu, and G.Wick, 1994: Correcting infrared satellite estimates of sea surface temperature for atmospheric water vapor attenuation, *J. Geophys Res.*, **99**, 5219 - 5236.

Esbensen, S. K. and Y. Kushnir, 1981: The heat budget of the global ocean: An atlas based on estimates from surface marine observations., *Climatic Research Institute Report No 29*, Oregon State University.

Esbensen, S.K. and R.W. Reynolds, 1981: Estimating monthly averaged air-sea transfers of heat and momentum using the bulk aerodynamic method. *J. Phys. Oceanogr.*, **11**, 457-465.

Esbensen, S.K., and M.J. McPhaden, 1996: Enhancement of tropical ocean vaporation and sensible heat flux by atmospheric mesoscale systems. *J.Climate*, **9**, 2307-2325.

Esbenson, S. K., D. B. Chelton, D. Vickers, and J. Sun, 1993: An analysis of errors in SSM/I evaporation estimates over the global Ocean. *J. Geophys. Res.*, **98**, 7081-7101.

Evans, K. F., 1998: The spherical harmonic discrete ordinate method for three-dimensional atmospheric radiative transfer. J. Atmos. Sci., 55, 429-446.

Eymard, L., 1998: Introduction: The SEMAPHORE experiment. *J. Geophys. Res.*, **103**, 25,005-25,008

Eymard, L., S. Planton, P. Durand, and Co-authors, 1996: Study of the air-sea interactions at the mesoscale: The SEMAPHORE experiment. *Ann. Geophysicae*, **14**, 986-1015.

Ezraty, R., and A. Cavanié, 1999: Intercomparison of backscatter maps over Arctic sea ice from NSCAT and the ERS scatterometer, *J. Geophys. Res.*, **104**, 11,471-11,483.

Fairall, C. W., E. F. Bradley, J. S. Godfrey, G. A. Wick, J. B. Edson, and G. S. Young, 1996b: Cool skin and warm layer effects on sea surface temperature. *J. Geophys. Res.*, **101**, 1295-1308.

Fairall, C. W., P. O. G. Persson, E. F. Bradley, R. E. Payne, and S. Anderson, 1998: A new look at calibration and use of Eppley Precision Infrared radiometers: Part I theory and application. *J. Atmos. Oceanic Tech.*, **15**, 1230-1243.

Fairall, C.W., A.A. Grachev, A.J. Bedard, and R.T. Nishiyama 1996c: *Wind, wave, stress, and surface roughness relationships from turbulence measurements made on R/P FLIP in the SCOPE experiment.* NOAA Tech. Memo ERL ETL-268, 37pp.

Fairall, C.W., A.B. White, J.B. Edson, and J.E. Hare, 1997: Integrated shipboard measurements of the marine boundary layer. *J. Atmos. Oceanic Tech.,* **14**, 338-359.

Fairall, C.W., and S.E. Larsen, 1986: Inertial dissipation methods and turbulent fluxes at the air ocean interface. Bound.-Layer Meteor., 34, 287-301.

Fairall, C.W., E.F. Bradley, D.P. Rogers, J.B. Edson, and G.S. Young, 1996a: Bulk parameterization of air-sea fluxes for the Tropical Ocean-Global Atmosphere Coupled-Ocean Atmosphere Response Experiment. *J. Geophys. Res.*, **101**, 3747-3764.

Fairall, C.W., J.B. Edson, S.E.Larsen and P.G.Mestayer, 1990: Inertial-dissipation air-sea flux measurements: a prototype system using real-time computations. *J. Atmos. Oceanic Tech.,* **7**, 425-453.

Fels, S. B., and M. D. Schwarzkopf, 1975: The simplified exchange approximation: A new method for radiative transfer calculations. *J. Atmos. Sci.*, **37**, 2265-2297.

Feng, Ming, P. Hacker, and R. Lukas, 1998: Upper ocean heat and salt balances in response to a westerly wind burst in the western equatorial Pacific during TOGA COARE. *J. Geophys. Res.,***103**, 10289-10311.

Ferraro R.R., F. Weng, N.C.Grody, and A.Basist, 1996: An eight-year (1987-1994) time series of rainfall, clouds, water vapor, snow cover, and sea ice derived from SSM/I measurements. *Bull.Amer.Met.Soc.*, **77**, 891-905.

Ferraro, R. R., and Marks, G. F., 1995: The development of SSM/I rain-rate retrieval algorithms using ground-based radar measurements, *J.Atmos.Oceanic Tech.* **12**, 755-770.

Ferraro, R. R., N. C. Grody, D. Forsyth, R. Carey, A. Basist, J. Janowiak, F. Weng, G. F. Marks, and R. Yanamandra, 1994: Microwave measurements produce global climatic, hydrologic data. *Eos, Trans. Amer. Geophys. Union*, **75**, 337 - 343.

Fiorino, M., 2000: The impact of observing system changes on the climate-scale variability and temperature in the ECMWF and NCEP reanalyses. *Proc. Conf. 2ⁿᵈ Intl. Conf. on Reanalyses*, Reading, England, 23-27 Aug. 1999. WCRP-109 (WMO/TD 985) WMO, 65 - 68.

Folland, C. K. and D. E. Parker, 1995: Correction Of Instrumental Biases In Historical Sea-Surface Temperature Data. *Quart. J. Roy. Meteor. Soc.*, **121**(522), 319 - 367.

Folland, C. K., R. W. Reynolds, M. Gordon and D. E. Parker, 1993: A study of six operational sea surface temperature analyses. *J. Climate.*, **6**(1), 96 - 113.

Folland,C.K., 1988: Numerical models of the raingauge exposure problem, field experiments and an improved collector design. *Quart. J. Roy. Meteor. Soc.*, **114**, 1485-1516.

Freilich, M. H., and R. S. Dunbar, 1999: The accuracy of the NSCAT 1 vector winds: Comparisons with National Data Buoy Center buoys. *J. Geophys. Res*, **104**, 11231-11246.

Freitag, H.P., Y. Feng, L.J. Mangum, M.J. McPhaden, J. Neander, and L.D. Stratton, 1994: *Calibration procedures and instrumental accuracy estimates of TAO temperature, relative humidity and radiation measurements.* Tech. Report No. 1589,

NOAA/Pacific Marine Environmental Lab., Seattle WA. (see also http://www.pmel.noaa.gov/toga-tao/caldoc/cal.html).

Frenzen, P. and C. A. Vogel, 1992: The turbulent Kinetic Energy budget in the atmospheric surface layer: a review and an experimental reexamination in the field. *Boundary-Layer Meteor.*, **60**, 49 - 76.

Friehe C.A., & co-authors, 1991: Air-sea fluxes and surface layer turbulence around a sea surface temperature front, *J. Geophys. Res.*, **96**, 8593-8609.

Friehe, C.A. and K.B. Schmitt, 1976: Parameterization of air-sea interface fluxes of sensible heat and moisture by the bulk aerodynamic formulas. *J. Phys. Oceanog.*, **6**, 801-809.

Friehe, C.A., 1991: Air-sea fluxes and surface layer turbulence around a sea surface temperature front. *J.Geophys. Res.*, **96**, 8593-8609.

Frouin, R., C. Gautier, and J. J. Mocrette, 1988: Downward longwave irradiance at the oceans surface from satellite data: methodology and *in situ* validation, *J. Geophys. Res.*, **93**, 597-619.

Fu, Q., and K.-N. Liou, 1993: Parameterization of the radiative properties of cirrus clouds. *J. Atmos. Sci.*, **50**, 2008-2025.

Fujitani, T., 1985: Method of turbulent flux measurement on a ship by using a stable platform system. *J. Meteor. Soc. Japan*, **36**, 157-170.

Gage, K. S., C. R. Williams and W. L. Ecklund, 1996: Application of the 915 MHz profiler for diagnosing and classifying tropical precipitating cloud systems. *Meteor. and Atmospheric Physics*, **59**, 141-151.

Gage, K. S., C. R. Williams, and W. L. Ecklund, 1994: UHF wind profilers: a new tool for diagnosing tropical precipitating cloud systems. *Bull. Amer. Meteor. Soc.*, **73**, 2289-2294.

Ganachaud A., 1999: *Large Scale Oceanic Circulation and Fluxes of Freshwater, Heat, Nutrients and Oxygen*. Ph.D. Thesis, Department of Earth, Atmospheric and Planetary Sciences, Massachusetts Institute of Technology, Cambridge, USA, 267 pp.

Gardashov, R. G., K. S. Shifrin, J. K. Zolotova, 1988: Emissivity, thermal albedo and effective emissivity of the sea at different wind speeds. *Oceanologica Acta*, **11**, 121 - 124.

Garnier, E., B. Barnier, K. Béranger, and L. Siefridt, 1998: Global ocean thermohaline forcing from 15 years of ECMWF reanalysis Proc. of the 1st International Conf. on Reanalyses, October 27-31, Silver-Spring WCRP-104 (WMO/TD 876) WMO, Geneva, 57 - 60.

Garratt, J. R., 1977: Review of drag coefficients over oceans and continents. *Mon.Weather Rev.*,**105**,915-929.

Garratt, J. R., 1992: *The atmospheric boundary layer*. Cambridge University Press, New York, 316 pp.

Garrett, C., R. Outerbridge, and K. Thompson, 1993: Interannual variability in Mediterranean heat and buoyancy fluxes. *J.Clim.*, **6**, 900-910.

Gaspar, P., Y. Gregoris, and J. M. Lefevre, 1990: A simple kinetic energy model for simulations of the oceanic vertical mixing: tests at station Papa and Long-Term Upper Ocean Study site, *J. Geophys. Res.*, **95**, 16,179-16,193.

Gautier, C., 1988: Surface solar irradiance in the central Pacific during Tropic Heat: Comparison between *in situ* measurements and satellite estimates. *J. Climate*, **1**, 600-608.

Gautier, C., G. Diak and S. Masse, 1980: A simple physical model to estimate incident solar radiation at the surface from GOES satellite data. *J. Appl. Meteor.*, **19**, 1005-1012.

Geernaert, G.L., 1987: On the importance of the drag coefficient in air-sea interactions. *Dyn. Atmos. Oceans*, **11**, 19-38.

Geernaert, G.L., 1990: Bulk parameterizations for the wind stress and heat fluxes. In S*urface Waves and Fluxes*, vol. 1, G.L. Geernaert and W.J. Plant (eds.), 91-172, Kluwer, Dordrecht.

Gibson, J. K., P. Kallberg, S. Uppala, A. Noumura, A. Hernandez, and E. Serrano, 1997: *ERA Description*. ECMWF Re-Analysis Project Report Series, 1. ECMWF, Reading, UK, 77 pp.

Gilgen, H., and A. Ohmura, 1999: The Global Energy Balance Archive. *Bull.Amer.Meteor.Soc.*, **80**, 831-850.

Gilgen, H., C. H. Whitlock, F. Koch, G. Mueller, A. Ohmura, D. Steiger, and R. Wheeler, 1995: *Technical Plan for Baseline Surface Radiation Network (BSRN) Data Manangement.* WCRP, WMO TD-No. 443, WMO Geneva.

Gilhousen et al., 1990 Gilhousen, D.B.,1998: Improved Real-Time Quality Control of NDBC Measurements. *Preprints of the 10th Symp. on Meteorological Observations and Instrumentation,* Phoenix, AZ 363-366 (available from NDBC, Building 1100Stennis Space Center, MS 39529, USA).

Gilman C. and C. Garrett, 1994: Heat flux parameterization for the Mediterranean Sea: The role of atmospheric aerosols and constraints from the water budget. *J.Geophys.Res.*, **99**, 5119-5134.

Gleckler, P. J. and B. C. Weare, 1995: *Uncertainties in global ocean surface heat flux climatologies derived from ship observations.* PCMDI Rep. 26, Lawrence Livermore National Lab., Livermore, Ca., 39 pp.

Gleckler, P. J., & co-authors, 1994: *Cloud-radiative effects on implied oceanic energy transports as simulated by atmospheric general circaulation models.* PCMDI Report 15, Lawrence Livermore National Laboratory, Livermore, CA., 13 pp.

Gleckler, P., and B.Weare, 1997: Uncertainties in global ocean surface heat flux climatologies derived from ship observations. *J.Climate*, **10**, 2764-2781.

Gloersen, P., Campbell, W.J., Cavalieri, D.J., Comiso, J.C., Parkinson, C.L., Zwally, H.J., 1992: *Arctic and Antarctic Sea Ice, 1978-1987: Satellite Passive Microwave Observations and Analysis*, NASA SP-511, Washington, D.C.

Godfrey, J.S., and Beljaars, 1991: On the turbulent fluxes of buoyancy, heat and moisture at the air-sea interface at low wind speeds. *J. Geophys. Res.* **96**, 22043-22048.

Godfrey, J.S., E.F. Bradley, P.A. Coppin, L. Pender, T.J. McDougall, E.W. Schulz, and I. Helmond, 1999: Measurements of upper ocean heat and freshwater budgets near a drifting buoy in the equatorial Indian ocean. *J. Geophys. Res.* **104**, 13269-13302.

Godfrey, J.S., M. Nunez, E.F. Bradley, P.A. Coppin and E.J. Lindstrom, 1991: On the net surface heat flux into the western equatorial Pacific. *J. Geophys. Res.*, **96**, suppl., 3391-3400.

Goldman, A., and T. G. Kyle, 1968: A comparison between statistical model and line calculation with application to the 9.6 micro-meter ozone and the 2.7 micro-meter water vapor bands. *Applied Optics*, **3,** 203-208.

Gonzales, A. E., and D. G. Long, 1999: An assessment of NSCAT ambiguity removal. *J. Geophys. Res.*, **104**, 11449-11457.

Goodberlet, M. A. and C. T. Swift, 1989: Remote sensing of ocean surafce winds with the Special Sensor Micro-wave/Imager. *J. Geophys. Res.*, **94**, 14547 - 14555.

Goodberlet, M. A. and C. T. Swift, 1992: Improved retrievals from the DMSP wind speed algorithm under adverse weather conditions. *IEEE Trans. Geosci. Remote Sens.*, **30**, 1076 - 1077.

Goodberlet, M. A., C. T. Swift, and J. C. Wilkerson, 1989: Remote sensing of oceans surface winds with the Special Sensor Microwave/Imager. *J. Geophys. Res.*, **94**, 14547- 14555.

Goody, R. M., 1964: *Atmospheric Radiations I. Theoretical Basis.* Oxford University Press, 436pp

Gordon, C., Cooper C., Senior C.A., Banks H., Gregory J.M., Johns T.C., Mitchell J.F.B., Wood R.A. 2000: The simulation of SST, sea ice extents and ocean heat transports in a version of the Hadley Centre coupled model without flux adjustments, *Climate Dynamics* **16**: (2-3) 147-168.

Gosnell, R., C.W. Fairall and P.J. Webster, 1995: The sensible heat of rainfall in the tropical ocean. *J. Geophys. Res.*, **100**, 18437-18442.

Graber, H. C., N. Ebuchi, and R. Vakkayil, 1996: *Evaluation Of ERS-1 Scatterometer Winds With Wind & Wave Ocean Buoy Obervations.* Technical Report, RSMAS 96-003, 1996/05/01, RSMAS/University of Miami, Miami, FL, 78pp.

Graber, H.C., R.E. Jensen, V.J. Cardone, 1995: Sensitivity of wave model predictions on spatial and temporal resolution of the wind field. *4th Intern. Workshop on Wave Hindcasting and Forecasting,* Banff, Alberta, October 16-20, 1995, 146-158.

Grachev, A. A., C. W. Fairall and S. E. Larsen, 1998: On the determination of the neutral drag coefficient in the convective boundary layer. *Boundary-Layer Meteor.*, **86**, 257 - 278.

Grachev, A. A., C. W. Fairall, and E. F. Bradley, 2000: Convective profile constants revisited. *Boundary Layer Meteor.*, **94** (3), 495 - 515

Grachev, A.A. and C.W. Fairall, 1997: Dependence of the Monin-Obukhov stability parameter on the bulk Richardson number over the ocean. *J. Appl. Meteor.*, **36**, 406-414.

Greenslade, D.J.M., D.B. Chelton, and M.G. Schlax, 1997: The midlatitude resolution capability of sea level fields constructed from single and multiple satellite altimeter datasets. *J. Atmos. Ocean. Tech.,* **14**, 849-870.

Grell, G. A., 1993: Prognostic evaluation of assumptions used by cumulus parameterizations. *Mon. Wea. Rev.*, **121**, 654-787.

Grossklaus, M., K. Uhlig and L. Hasse, 1998: An optical disdrometer for use in high wind speeds. *J. Atmos. Oceanic Tech.*, **15**, 1051-1059.

Groves, D.G., 1999: A new moisture budget of the Arctic atmosphere derived from 19 years of daily TOVS satellite moisture retrievals and NCEP reanalysis winds, *Proc. 5th AMS Conf. on Polar Meteor. and Oceanogr.*, Dallas, TX, 107-112.

Guest, P.S., 1998: Surface longwave radiation conditions in the eastern Weddell sea during winter. *J. Geophys. Res.,* **103**, 30761-30771.

Guichard, F., D. Parsons, and E. Miller, 2000: Thermodynamical and radiative impact of the correction of sounding humidity bias in the tropics. *J. Climate, in press.*

Gulev S.K. & V.A.Tichonov, 1989: Interannual variations of the ocean heat balance and meridional heat transport. *Atmosphere-Ocean-Space*, **7**, 332-341.

Gulev, S. K. and L. Hasse, 1998: North Atlantic wind waves and wind stress fields from voluntary observing ship data. *J. Phys. Oceanogr.*, **28**, 1107 - 1130.

Gulev, S.K. and J. Tonkacheev, 1996: Investigation of the Ocean-Atmosphere Interaction in the North Atlantic mid-latitude Frontal Zone. In: *The Air-Sea Interface*, Editors: M.Donelan, W.Hui and W. Plant, RSMAS, Miami, 535-542.

Gulev, S.K., 1994: Influence of space-time averaging on the ocean-atmosphere exchange estimates in the North Atlantic mid-latitudes. *J.Phys.Oceanogr.*, **24**, 1236-1255.

Gulev, S.K., 1995: Long-term variability of sea-air heat transfer in the North Atlantic Ocean. *Int.J.Climatol.*, **15**, 825-852.

Gulev, S.K., 1997a: Climate variability of the intensity of synoptic processes in the North Atlantic midlatitudes. *J.Climate*, **10**, 574-592.

Gulev, S.K., 1997b: Climatologically significant effects of space-time averaging in the North Atlantic sea-air heat flux fields. *J.Climate*, **10**, 2743-2763.

Gulev, S.K., 1999: Comparison of COADS Release 1a winds with instrumental measurements in the North-West Atlantic. *J.Atmos.Oceanic Technology*, **16**, 133-145

Gulev, S.K., and Hasse, L. 1999: Changes of wind waves in the North Atlantic over the last 30 years, *Int. J. Climatology* **19** (10) 1091-1117.

Gulev, S.K., D. Cotton, A. Sterl, 1998: Intercomparison of the North Atlantic wave climatology from Voluntary Observing Ships, Satellite Data and Modelling. *Phys. Chem. Earth* **23**, 587-592.

Gulev, S.K., T.Jung, and E.Ruprecht, 2000: Intercomparison of the ocean-atmosphere heat fluxes from the voluntary observing ship data and numerical weather prediction system. *J.Phys. Oceanogr.*, (submitted).

Gupta, S.K, W.L. Darnell and A.C. Wilber, 1992: A parameterization for longwave surface radiation from satellite data: Recent improvements. *J. Appl. Meteor.*, **31**, 1361-1367.

Gupta, S.K., N.A. Ritchey, A.C. Wilber, C.H. Whitlock, G.G. Gibson and P.H. Stackhouse, 1999: A climatology of surface radiation budget derived from satellite data. *J. Climate*, **12**, 2691-2710.

Hack, J.J. 1998: Analysis of the improvement in implied meridional ocean energy transport as simulated by the NCAR CCM3 *J. Climate* **11**: (6) 1237-1244.

Hackert, E. C., A. J. Busalacchi, and R. Murtugudde, 2000: A wind comparison study using an ocean general circulation model for the 1997-1998 El Niño. *J. Geophys. Res.*, *submitted.*

Haeffelin, M., S. Kato, A. M. Smith, K. Rutledge, T. Charlock, and J. R. Mahan, 2000: Determination of the thermal offset of the Eppley Precision Spectral Pyranometer. *Submitted to Appl. Opt.*

Hagemann S. and Dümenil, L., 1996: Development of a parameterisation of lateral discharge for the global scale, MPI Report No. 219, 34pp.

Hahn, C.J, S.G. Warren, and J. London, 1995: The effect of moonlight on observations of cloud cover at night, and applications to cloud climatology. *J. Climate*, **8** (5) part 2, 1429-1446.

Häkkinen, S., 1993. An Arctic source for the Great Salinity Anomaly: A simulation of the Arctic ice

ocean system for 1955-1975. *J. Geophys. Res.*, **98**, 16397-16410.

Hall, M.M., and H.L.Bryden, 1982: Direct estimates and mechanisms of ocean heat transport. *Deep-Sea Res.*, **35**, 1441-1450.

Halliwell, G.R., and P. Cornillon, 1990: Large-scale SST variability in the Western North Atlantic sutropical convergence zone during FAZINEX. Part II: Upper ocean heat budget and frontogenesys. *J.Phys. Oceanogr.*, **20**, 223-234.

Hamill, T. M., R. P. d'Entremont and J. T. Bunting, 1992: A description of the Air Force real-time nephananalysis model. *Wea. and Fcst.*, **7**, 288-306.

Han, Y. J., 1984: A numerical world ocean general circulation model. Part II. A baroclinic experiment. *Dyn. Atmos. Oceans*, **8**, 141-172.

Hanava, K., and Y.Toba, 1987: Critical examination of estimation methods of long-term mean air-sea heat and momentum transfers. *Ocean-Air Inter.*, **1**, 79-93.

Hanen, J. E., M. Sato, A. Lacis, R. Ruedy, I. Tegen, and E. Matthews, 1998: Climate forcings in the Industrial era. *Proc. Natl. Acad. Sci.,* **95**, 12753-12758.

Haney, R. L., 1971: Surface thermal boundary condition for ocean circulation models, *J. Phys. Oceanogr.*, **1**, 145-167.

Hare, J. E., P. O. G. Persson, C. W. Fairall and J. B. Edson, 1999: Behaviour of Charnock's relationship for high wind conditions. *Preprint vol.: 13th Conf. on Boundary Layers and Turbulence*, Dallas, Texas, 10-15 January, 1999, Amer. Meteor. Soc., Boston, MA.

Harrison, D. E., 1989: On climatological monthly mean wind stress and wind stress curl fields over the world ocean. *J. Climate*, **2**, 57-70.

Harshvardhan, R. Davies, D. A. Randall, and T. G. Corsetti, 1987: A fast radiation parameterization for atmospheric circulation models. *J. Geophys. Res.*, **92**, 1009-1016.

Hasse, L., M. Grossklaus, K. Uhlig and P. Timm, 1998: A ship rain gauge for use in high winds. *J. Atmos. Oceanic Tech.*, **15**, 380-386.

Hastenrath, S. and P. J. Lamb, 1977: *Climatic atlas of the Tropical Atlantic and Eastern Pacific Oceans*, University of Wisconsin Press, 105 pp.

Hastenrath, S. and P. J. Lamb, 1978: *Heat budget atlas of the Tropical Atlantic and Eastern Pacific oceans*, The University of Wisconsin Press, Madison, WI., 90 pp.

Hastenrath, S. and P. J. Lamb, 1979: *Climatic atlas of the Indian Ocean: Part 1 Surface climate and atmospheric circulation*, The University of Wisconsin Press, Madison, WI., 19pp + 97 charts.

Hastenrath, S. and P. J. Lamb, 1980: On the heat budget of the hydrosphere and atmosphere in the Indian Ocean, *J. Phys. Oceanogr.* **10**, 694 - 708.

Hastenrath, S., 1980: Heat budget of the tropical ocean and atmosphere. *J. Phys. Oceanogr.* **10**, 159 - 170.

Heberden, W., 1769: Of the quantities of rain which appear to fall, at different heights, over the same spot of ground. *Phil. Trans. Roy. Soc.*, **59**, 359.

Heckley, W.A., 1985: Systematic errors of the ECMWF operational forecasting model in tropical regions. *Quart. J. Roy. Meteor. Soc.*, **111**, 709-738.

Hellerman, S. and M. Rosenstein, 1983: Normal monthly wind stress over the world ocean with error estimates. *J. Phys. Oceanogr.*, **13**, 1093 - 1104.

Hendon, H., and T. Shinoda, 1999: Assessment of warm pool surface fluxes from NCEP reanalyses. *COARE-98: Proc. Conf. TOGA coupled Ocean-Atmosphere Response Experiment (COARE),* Boulder, CO. 7-14 July 1988. WCRP-107, WMO/TD-940. WMO, Geneva, 255.

Henjes, K., 1998: Justification of the inertial dissipation technique in anisotropic mean flow. *Boundary-Layer Meteor.*, **88**, 161-180.

Hicks, B. B. and G. D. Hess, 1977: On the Bowen ratio and surface temperature at sea. *J. Phys. Oceanog.*, **7**, 141 - 145.

Higgins, R. W., Y.-P. Yao, M. Chelliah, W. Ebisuzaki, J. E. Janowiak, C. R. Ropelewski and R. E. Kistler, 1996: *Intercomparison of the NCEP/NCAR and the NASA/DAO reanalyses (1985-1993).* NCEP/Climate Prediction Center ATLAS No. 2. U.S. Dept. of Commerce, Washington, D.C., 169 pp. - see also http://yao.ncep.noaa.gov:2000/atlas_2/toc_1.html

Hilmer R., Harder M., Lemke P. 1998: Sea ice transport: a highly variable link between Arctic and North Atlantic, *Geophys. Res. Lett.* **25**: (17) 3359-3362.

Hnilo, J. J., B. D. Santer, J. S. Boyle, K. E. Taylor, and C. Doutriaux, 2000: Research activities at the program for climate model diagnostics and intercomparion. *presented at 2ⁿᵈ Intl. Conf. on Reanalyses*, Reading, England, 23-27 Aug. 1999. (see http://wesley.wwb.noaa.gov/reanalysis2/kana/hnilo1.pdf )

Hoeber, H., 1995: Comment on "Correction of Marine Air Temperature Observations for Solar Radiation Effects". *J. Atmos. & Oceanic Tech.*, **12**, 197 - 198.

Hogben, N. and F.E. Lumb, 1967: *Ocean Wave Statistics*, Ministry of Technology, HMSO, London, 263 pp.

Hogben, N., 1988: Experience from compilation of Global Wave Statistics, *Ocean Eng.*, **15**, 1-31.

Hogben, N., N. Dacunha and G. Oliver, 1986: *Global Wave Statistics*, Unwin Brothers, London, 661pp.

Holfort J., 1994: Grossräumige Zirkulation und meridionale Transporte im Südatlantik. *Berichte aus dem Institut für Meereskunde an der Christian-Albrechts-Universität*, Kiel, **260**, 96 pp.

Holland, J. Z., 1972: Comparative evaluation of some BOMEX measurements of sea surface evaporation, energy flux and stress. *J. Phys. Oceanogr.*, **2**, 476-486.

Hollinger, J. P., R. Lo, G. Poe, R. Savage, and J. Pierce, 1987: *Special Sensor Microwave/Imager user's guide.* Naval Research Laboratory, Washington, D.C., 177 pp.

Holtslag, A. A. M., E. I. F. de Bruijn, and H.-L. Pan, 1990: A high resolution air mass transformation model for short range weather forecasting. *Mon. Weath. Rev*, **118**, 1561 – 1575.

Hong, S.-Y., and H.-L. Pan, 1996: Nonlocal boundary layer vertical diffusion in a medium-range forecast model. *Mon. Wea. Rev.*, **124**, 2322-2339.

Hosom, D.S., R.A. Weller, R.E. Payne, and K.E. Prada, 1995: The IMET(Improved Meteor.) ship and buoy systems. *J. Atmos. Oceanic Technol.,* **12**, 527-540.

Hsiung, J., 1986: Mean surface energy fluxes over the global ocean. *J. Geophys. Res.*, **91**(C9), 10585-10606.

Hu, Yongxiang, 2000: *Personal communication.*

Huffman, G. J., & co-authors, 1997: The Global Precipitation Climatology Project (GPCP) combined precipitation dataset. *Bull. American Met. Soc.*, **78**, 5 - 20.

Hurrell, J. W. and K. E. Trenberth, 2000: Global sea surface temperature analyses: multiple problems and their implications for climate analysis, modeling, and reanalysis. *Bull. Am. Meteor. Soc.*, (in press).

Husar,R.B., J.M. Prospero and L.L.Stowe, 1997: Characterization of tropospheric aerosols over the oceans with the NOAA advanced very high resolution radiometer optical thickness operational product. *J. Geophy. Res.,* **102(D14),** 16889-16909.

Illingworth, A.J., and C.J. Stevens, 1987: An optical disdrometer for the measurement of raindrop size spectra in windy conditions. *J. Atmos. Oceanic Tech.,* **4**, 411-421.

Inamdar, A. K., and V. Ramanathan, 1997: Estimation of Longwave Surface Radiation Budget from CERES (Subsystem 4.6.2). Earth Observing System (EOS) CERES Algorithm Theoretical Basis Document (ATBD), Release 2.2, June 1997, 19 pp. + apps.

Iqbal,M., 1983: *An introduction to solar radiation.* Academic Press, 390pp.

Isemer, H.J. & L.Hasse, 1987: *The Bunker climate atlas of the North Atlantic Ocean. Volume 2: Air-sea interactions.* Springer Verlag, Berlin, 252 pp.

Isemer, H.-J., 1994: *On the homogeneity of Surface Wind Speed records from Ocean Weather Stations*, Institut für Meereskunde, Kiel, Germany, 43 pp. + figs.

Isemer, H.-J., 1995: Trends in marine surface wind speed: Ocean Weather Stations versus Voluntary Observing Ships. *Proc. Internat. COADS Winds Workshop*, Kiel, Germany, 1994. Ed. H.Diaz and H.-J.Isemer, NOAA-ERL, IFM (Kiel), 68-84.

Isemer, H.-J., and L. Hasse, 1985: *The Bunker Climate Atlas of the North Atlantic Ocean.* Vol. 1, *Observations*, Springer Verlag, Berlin, 218 pp.

Isemer, H.-J., J.Willebrand, and L.Hasse, 1989: Fine adjustment of large-scale air-sea energy flux parameterizations by direct estimates of ocean heat transport. *J.Climate*, **2**, 1163-1184.

Iwasaka, N., 1999: Estimation of longwave radiation flux at sea surface based on satellite measurements. *Rep. of Sci. Res. on Priority Areas (No.08241111) of Better Understanding of Water and Energy Cycles by Satellites (BUWECS)*, Japanese Ministry of Education, Science, Sports and Culture, 11-19. (in Japanese).

Iwasaka, N., and J.M.Wallace, 1995: Large-scale air-sea interaction in the Northern hemisphere from a view point of variations of surface heat flux by SVD analysis. *J.Met.Soc.Japan,* **73,** 781-794.

Jabouille, P., J. L. Redelsperger, and J. P. Lafore, 1995: Modification of surface fluxes by atmospheric convection in the TOGA COARE region. *Mon. Wea. Rev.*, **124**, 816-837.

Jaeger, L., 1976: Monatskarten des Niederschlags für die ganze Erde. *Berichte des Deutschen Wetterdienstes*, Offenbach, 33 pp. and plates.

Jakob, C., 1994: The impact of the new cloud scheme on ECMWF's Integrated Forecast Scheme (IFS). *Proc. ECMWF/GEWEX Workshop on Modelling, Validation and Assimilation of Clouds, ECMWF, Nov. 1994.* ECMWF, Reading, UK.

Janowiak, J.E., A. Gruber, C. R. Kondragunta, R. E. Livezey, and G. J. Huffman, 1998: A comparison of the NCEP/NCAR reanalysis precipitation and the GPCP raingauge-satellite combined data set with observational error considerations. *J. Climate*, **11**, 2960-2979.

Janssen, J. A. M., 1997: Does wind stress depend on sea-state or not? - a statistical error analysis of HEXMAX data. *Boundary-Layer Meteor.*, **83**, 479-503.

Janssen, P. A. E. M., 1999: On the effect of ocean waves on the kinetic energy balance and consequences for

the inertial dissipation technique. *J. Phys. Oceanogr.*, **29**(3), 530 - 534.

Janssen, P. A. E. M., and P. Viterbo, 1996: Ocean waves and the atmospheric climate. *J. Climate,* **9**, 1269-1287.

Janssen, P.A.E.M., 2000: Ocean waves do affect the kinetic energy balance. *J. Phys. Oceanogr., submitted.*

Janssen, P.A.E.M., G.J. Komen, W.J.P. de Voogt, 1984: An operational coupled hybrid wave prediction model, *J. Geophys. Res.*, **89**, 3635-3654.

Jevons, W.S., 1861: On the deficiency of rain in an elevated rain-gauge, as caused by wind. *Phil. Mag.*, **22**, 421-433.

Jones, C., P. Peterson and C. Gautier, 1999: A new method for deriving ocean surface specific humidity and air temperature: an artificial neural network approach. *J. Appl. Met.*, **38**: (8) 1229-1245.

Jones, C.S., D.M.Legler, and J.J.O'Brien, 1995: Variability of surface fluxes over the Indian Ocean: 1960-1989. *Global Atmos.Ocean Syst.*, **3**, 249-272.

Jones, M. S., M. A. Saunders and T. H. Guymer, 1996a: Global remnant cloud contamination in the along-track scanning radiometer data: Source and removal. *J. Geophys. Res.*, **101**, 12141-12147.

Jones, M. S., M. A. Saunders and T. H. Guymer, 1996b: Reducing cloud contamination in ATSR averaged sea surface temperature data. *J. Atmos. & Oceanic Tech.*, **13**, 492 - 506.

Josey, S. A., 2000: A comparison of surface heat fluxes in the subduction region of the North-East Atlantic from the ECMWF and NCEP/NCAR reanalyses with moored buoy measurements. *J. Climate. (accepted).*

Josey, S. A., D. Oakley and R. W. Pascal, 1997: On estimating the atmospheric longwave flux at the ocean surface from ship meteorological reports. *J. Geophys. Res.*, **102**(C13), 27961 - 27972.

Josey, S. A., E. C. Kent and P. K. Taylor, 1998: *The Southampton Oceanography Centre (SOC) Ocean-Atmosphere Heat, Momentum and Freshwater Flux Atlas.* Report No. 6, Southampton Oceanography Centre, Southampton, United Kingdom, 30 pp + figs.

Josey, S. A., E. C. Kent and P. K. Taylor, 2000: On the wind stress forcing of the ocean in the SOC and Hellerman and Rosenstein climatologies. *J.Phys.Oceanogr. (submitted).*

Josey, S. A., E. C. Kent, and P. K. Taylor, 1999: New insights into the ocean heat budget closure problem from analysis of the SOC air-sea flux climatology. *J. Clim.*, **12**, 2856-2880.

Josey, S., E.C.Kent, and P.K.Taylor, 1995: Seasonal variations between sampling and classical mean turbulent heat flux estimates in the Eastern North Atlantic. *Ann. Geophys.* **13**, 1054-1064.

Joss, J., and A. Waldvogel, 1967: A raindrop spectrometer with automatic readout. *Pure Appl. Geophys.*, **68**, 240-246.

Jost, V., J. Schulz, and S. Bakan, 1999: Remote Sensing of the Global Energy and Water Cycle. Vol. II, *Proc. OceanObs 99 Conf.*, St. Raphael, France, 18-22 Oct., CNES.

Jourdan, G. and C. Gautier, 1995: Comparison between global latent heat flux computed from multisensor (SSM/I and AVHRR) and from *in situ* data. *J. Atmos. Oceanic Technol.*, **12**, 46 - 72.

Kader, B. A. and A. M. Yaglom, 1990: Mean fields and fluctuation moments in unstably stratified turbulent boundary layers. *J. Fluid Mech.*, **212** 637 – 662.

Kallberg, P., 1997: *Aspects of the Re-analysed Climate*. ECMWF Re-Analysis Project Report Series, 2. ECMWF, Reading, UK, 89 pp.

Kalnay, E., & co-authors, 1996: The NCEP/NCAR 40-year reanalysis project. *Bull. Amer. Meteor. Soc., 77*, 437-471.

Kalnay, E., 1999: Atmospheric models for weather prediction and climate simulations. *Global Energy and Water Cycles*, K. A. Browning and R. J. Gurney, eds., Cambridge University Press, Cambridge, UK, 30-32.

Kalnay, E., S. J. Lord and R. D. McPherson, 1998: Maturity of operational numerical weather prediction: Medium range. *Bull. Amer. Meteor. Soc.*, *79*, 2753-2769.

Kanamitsu, M., 1989: Description of the NMC global data assimilation and forecasting system. *Wea. and Forecasting*, *4*, 335-342.

Kanamitsu, M., W. Ebisuzaki, J. Woolen, J. Potter, and M. Fiorion, 2000 An overview of NCEP/DOE Reanalysis-2. *Proc. Conf.2ⁿᵈ Intl. Conf. on Reanalyses*, Reading, England, 23-27 Aug. 1999. WCRP-109 (WMO/TD 985) WMO, Geneva, 1 - 4.

Kaplan, A., M. Cane, Y. Kushnir, A. Clement, M. Blumenthal and B. Rajagopalan, 1998: Analyses of Global Sea Surface Temperature, 1856 - 1991. *J. Geophys. Res.*, *103*, (C9) 18567 - 18589.

Kaplan, A., Y. Kushnir, M. Cane and M. Blumenthal, 1997: Reduced space optimal analysis for historical datasets: 136 years of Atlantic sea surface temperatures.Analyses of Global Sea Surface Temperature, 1856 - 1991. *J. Geophys. Res.*, *102*, 27835 – 27860.

Kato, S., T. P. Ackerman, E. E. Clothiaux, J. H. Mather, G. R. Mace, M. Wesley, F. Murcray, and J. Michalsky, 1997: Uncertainties in modeled and measured clear-sky surface shortwave irradiances. *J. Geophys. Res.*, *102*, 25,881-25,898.

Katsaros, K.B. 1990: Parameterization schemes and models for estimating the surface radiation budget. In G.L.Geernaert and W.J.plant (eds.), *Surface waves and Fluxes, Volume II*, 339-368, Kluwer.

Katsaros, K.B. and G. de Leeuw, 1994: Comment on "Sea spray and the turbulent air-sea heat fluxes" by Edgar L. Andreas. *J. Geophys. Res.*, *99*, 14.339-14,343.

Katsaros, K.B. and J.E. DeVault, 1986: On irradiance measurement errors at sea due to tilt of radiometers. *J. Atmos. Oceanic Tech.*, *3*, 740-745.

Katsaros, K.B., L.A. McMurdie, R.J. Lind and J.E. DeVault, 1985: Albedo of a water surface, spectral variation,effects of atmospheric transmittance, sun angle, and wind speed. *J. Geophys. Res.*, *90*, 7313-7321.

Kaufeld, L., 1981: The development of a new Beaufort equivalent scale. *Meteor. Rundsch.*, *34*, 17-23.

Keith, D.A., 1995: Meridional energy transport: Uncertainty in zonal means. *Tellus*, *47A*, 30-44.

Kelly, K.A., S.Dickinson and Z. Yu, 1999: NSCAT tropical wind stress maps: Implications for improving ocean modeling. *J.Geophys. Res.*, *104*, 11291-11310.

Kent, E. C. and P. K. Taylor, 1991: *Ships observing marine climate: a catalogue of the Voluntary Observing Ships Participating in the VSOP-NA*. Marine Meteor. and Related Oceanographic Activities 25, WMO, Geneva, 123 pp.

Kent, E. C. and P. K. Taylor, 1995: A comparison of sensible and latent heat flux estimates for the North Atlantic ocean. *J. Phys. Oceanogr.*, *25*, 1530 - 1549.

Kent, E. C. and P. K. Taylor, 1996: Accuracy of humidity measurements on ships: consideration of solar radiation effects. *J. Atmos. & Oceanic Tech.*, *13*, 1317 - 1321.

Kent, E. C. and P. K. Taylor, 1997: Choice of a Beaufort Equivalent Scale. *J. Atmos. & Oceanic Tech.*, *14*, 228 - 242.

Kent, E. C., P. G. Challenor and P. K. Taylor, 1999: A Statistical Determination of the Random Observational Errors Present in Voluntary Observing Ships Meteorological Reports. *J. Atmos. & Oceanic Tech.*, *16*, 905-914.

Kent, E. C., P. K. Taylor and P. G. Challenor, 2000: The Characteristics of a Sea Surface Temperature Dataset Smoothed by Successive Correction. *J. Climate*, *13* (11), 1845 – 1857.

Kent, E. C., P. K. Taylor, and P. Challenor, 1998: A Comparison of Ship and Scatterometer-Derived Wind Speed Data in Open ocean and coastal areas. *Int. J. Remote Sensing*, *19*, 3361-3381.

Kent, E. C., P. K. Taylor, B. S. Truscott and J. A. Hopkins, 1993a: The accuracy of Voluntary Observing Ship's Meteorological Observations. *J. Atmos. & Oceanic Tech.*, *10*, 591 - 608.

Kent, E. C., R. J. Tiddy and P. K. Taylor, 1993b: Correction of marine daytime air temperature observations for radiation effects. *J. Atmos. & Oceanic Tech.*, *10*, 900 - 906.

Kessler, E., 1969: On the distribution and continuity of water substance in atmospheric circulations. *Met. Monographs*, *10*, (32). Amer. Meteor. Soc., Boston, MA, 84 pp.

Key, R.K., R.A. Silcox and R.S. Stone, 1996: Evaluation of surface radiative flux parameterizations for use in sea ice models. *J. Geophys. Res.,* *101*, 3839-3849.

Kiehl, J. T., and K. E. Trenberth, 1997: Earth's annual global mean energy budget. *Bull. Amer. Meteor. Soc.*, *78*, 197-208.

Killworth, P. D., A. D. Smeed, and A. J. Nurser, 2000: The effects on ocean models of relaxation towards observations at the surface. *J. Phys. Oceanogr.*, *30* (1) 160-174.

Kistler, R., & co-authors, 2000: The NCEP/NCAR 50-year reanalysis. Submitted to *Bullet. of the Amer. Meteor. Soc.* (Prelim. version: http://sgi62.wwb.noaa.gov:8080 /DISTRIBUTION/wd23gw/close/reanl2.htm. ).

Kizu, S., 2000: Degradation of VISSR visible radiometers aboard three GMS-series satellites from 1987 to 1999. (To be submitted to *Int'l J. Remote Sensing*).

Kizu,S., 1995: A study on thermal response of ocean surface layer to solar radiation using sateliite remote sensing. *Doc. Thesis, Tohoku University*, 100pp.

Kizu,S., 1999: Estimation of surface shortwave radiation over the western Pacific based on satellite measurements. *Rep. of Sci. Res. on Priority Areas (No.08241111) of Better Understanding of Water and Energy Cycles by Satellites (BUWECS) by the Japanese Ministry of Education, Science, Sports and Culture,* 1-10. (in Japanese).

Klein S.A., and D.L. Hartmann 1993: Spurious Changes in the ISCCP Dataset *Geophys Res Lett* *20* (6) 455 – 458.

Klein, L. A. and C. T. Swift, 1977: An improved model for the dielectric constant of sea water at microwave frequencies. *IEEE Trans. Antennas and Propag.*, *25*, 104 - 111.

Klinker, E. and P. D. Sardeshmukh, 1987: The diagnosis of systematic error in numerical weather prediction models. *Proc. Workshop on Diabatic Heating*, 30 Nov.-2 Dec. 1987, ECMWF. ECMWF, Reading, UK,, 209-244.

Klinker, E., 1997: Diagnosis of the ECMWF model performance over the tropical oceans. *Seminar on Atmosphere-surface Interaction*, 8-12 Sept. 1997, ECMWF. ECMWF, Reading, UK, 53-66.

Klinker, E., A. Y. Hou and G. H. White, 1999: The legacy of COARE for global weather forecasting and re-analysis. *COARE-98: Proc. Conf. on the TOGA Coupled Ocean-Atmosphere Response Experiment (COARE)*, Boulder, CO. 7-14 July 1988, WCRP-107, WMO/TD 940, WMO, Geneva, 95-104.

Kneizys, F.X. & co-authors, 1988: *Users guide to LOWTRAN7.* AFGL-TR-88-0177, Air Force Geophysics Laboratory, Hanscom AFB, MA, 137pp.

Knochel, H., 1999. Développement et validation d'un modèle numérique de circulation océanique à coordonnée sigma pour l'étude climatique de l'Atlantique Nord. Thèse de l'Université Joseph Fourier, Grenoble, France.

Koltermann, K.P., A.V.Sokov, V.P.Tereschenkov, S.A.Dobroliubov, K.Lorbacher, A.Sy, 1999: Decadal changes in the thermohaline circulation of the North Atlantic. *Deep-Sea Res II*, **46**, 109-138.

Komen, G., P. A. E. M. Janssen, V. Makin and W. Oost, 1998: On the sea state dependence of the Charnock parameter. *Global Atmos.Ocean Syst.*, **5**, 367 - 388.

Komen, G.J., L. Cavaleri, M. Donelan, K. Hasselmann, S. Hasselmann, P.A.E.M. Janssen, 1994: *Dynamics and Modelling of Ocean Waves,* Cambridge Univ. Press, New York, 532 pp.

Konda, M, Imasato, N., and A. Shibata, 1996: A new method to determine near-sea surface temperature by using satellite data. *J. Geophys. Res.*, **101**, 14349 - 14360.

Konda, M., N. Imasato, K. Nishi and T. Toda, 1994: Measurement of the sea surface emissivity. *J. Oceanogr.*, **50,** 17-30.

Kondo, J., 1975: Air-sea bulk transfer coefficients in diabatic conditions. *Bound-Layer Met.*, **9** ,91-112.

Koschmeider, H., 1934: Methods and results of definite rain measurements. *Mon. Wea. Rev.*, **62**, 5-7.

Krasnopolsky, V. M., L. C. Breaker, and W. H. Gemmill, 1995: A neural network as a nonlinear transfer function model for retrieving surface wind speeds from the special sensor microwave imager. *J. Geophys. Res.*, **100**, 11033 - 11045.

Kraus, E. and J.A. Businger, 1994: *Atmosphere-Ocean Interaction* (2nd. Edition), Oxford University Press, New York, 362 pp.

Kropfli R.A. and S.F. Clifford, 1994: The San Clemente Ocean Probing Experiment: A study of air-sea interaction with remote and in-situ sensors, *Proceedings IGARSS '94*, Pasadena CA, IEEE, pp 2407-2409.

Kubota, M and H. Yokota, 1998: Construction of surface wind stress fields with high temporal resolution by using the ERS-1 scatterometer data. *J. Oceanogr.*, **54**, 247-256.

Kubota, M. 1999: Introduction of Japanese Ocean Flux Data Sets with Use of Remote Sensing Observations (J-OFURO), *Proc. Internat. Symp. on Remote Sensing,* Kangnung, Korea, 231-236.

Kudryavtsev, V.N. and A.V. Soloviev, 1990: Slippery near-surface layer of the ocean arising due to daytime solar heating. *J. Phys. Ocean.*, **20**, 617-628.

Kummerow, C., W. Barnes, and T. Kozu, 1998: The tropical measuring mission (TRMM) sensor package. *J. Atmos. Sci.*, **55**, 809 - 817.

Kuroda, Y., Y. Amitani, K. Sono and A. Shoji, 1999: On-line Oceanographic Data System for Moored Buoys - TRITON Buoy Data Stream-. *http://www.jamstec.go.jp/jamstec/TRITON*

Kurtyka, J.C., 1953: *Precipitation measurements study.* Report of Investigation No. 20, State Water Survey, Illinois.

Kushnir, Y., 1999: Europe's winter perspectives. *Nature*, **398**, 289-291.

Kutsuwada, K., 1998: Impact of wind/wind-stress field in the North Pacific constructed by ADEOS/NSCAT data, *J. Oceanogr.*, **5**, 443-456.

Kwok, R., and D.A. Rothrock, 1999: Variability of Fram Strait ice flux and North Atlantic oscilliation, *J. Geophys. Res.*, **104**, 5,177-5,190.

LabSea Group, 1998: The Labrador Sea Deep convection Experiment. *Bull Amer. Met. Soc.*, **79**, 2033-2058.

Lacis, A. A., and J. E. Hansen, 1974: A parameterization for the absorption of solar radiation in the Earth's atmosphere. *J. Atmos. Sci.,* **31**, 118-133.

Lagerloef, G. S. E., C. T. Swift, and D. M. Le Vine, 1995: Sea surface salinity: The next remote sensing challenge. *Oceanography*, **8**, 44 - 50.

Laing, A. K. and S. J. Reid, 1999: Evidence of mesoscale lows off the west coast of New Zealand. *Weather Forecast* **14** (3) 369-383.

Lander, M. A. and M. L. Morrissey, 1987: Unexpected duplicate ship reports in the Comprehensive Ocean-Atmosphere Dataset (COADS). *Trop.Ocean-Atmospher Newsletter*, **38**, 13 - 14.

Large, W. G., 1979: *The turbulent fluxes of momentum and sensible heat over the sea during moderate to strong winds.*, Ph.D. thesis, University of British Columbia, 180 pp.

Large, W. G., G. Danabasoglu, S. C. Doney, and J. C. McWilliams, 1997. Sensitivity to surface forcing and boundary layer mixing in a global ocean model: Annual-mean climatology. *J. Phys. Oceanogr.*, **27**, 2418-2447.

Large, W. G., J. Morzel and G. B. Crawford, 1995: Accounting for Surface Wave Distortion of the Marine Wind Profile in Low-Level Ocean Storms Wind Measurements. *J. Phys. Oceanogr.*, **25**, 2959 - 2971.

Large, W.G and S. Pond, 1981: Open ocean momentum flux measurements in moderate to strong winds. *J. Phys. Oceanog.*, **11**, 324-336.

Large, W.G. and S. Pond, 1982: Sensible and latent heat flux measurements over the ocean. *J. Phys. Oceanog.*, **12**, 464-482.

Large, W.G., W.R. Holland, and J.C. Evans, 1991: Quasi-geostrophic ocean response to real wind forcing: The effects of temporal smoothing. *J. Phys. Oceanogr.*,**21**, 998-1017.

Larin, D.A. and G.N.Panin, 1985: The correlation between meteorological parameters influence on the calculations of evaporation and heat exchange over the Caspian Sea. *Water Res.*, **5**, 68-75.

Lazier, J. N. R., 1980: Oceanic conditions at Weather Station Bravo, 1960-1974. *Atmosphere-Ocean*, **18**, 227 - 238.

Lazier, J. R., 1997. The salinity decrease in the Labrador Sea over the past thirty years. In *Decade to century time scales of natural climate variability*, (Irvine C.A.S. Editor), National Academy Press.

Lebedev, I., and Tomczak, M., 1999: Rainfall measure-
ments with navigational radar. *J. Geophys. Res.*, **104**,
13697 - 13708.

Ledvina, D.L., G.S.Young, R.A.Miller, and C.W.Fairall:
1993: The effect of averaging on bulk estimates of
heat and momentum fluxes for the tropical Western
Pacific Ocean. *J.Geophys.Res.*, **98**, 20211-20217.

Lee, T. H., J. E. Janowiak, and P. A. Arkin, 1991: *Atlas
of Products from the Algorithm Intercomparison
Project 1: Japan and Surrounding Oceanic regions.*
UCAR, 131 pp.

Legates, D. R. and C. J. Willmott, 1990: Mean seasonal
and spatial variability in gauge corrected global
precipitation. *Int. J. Climatol.*, **10**, 111 - 127.

Legler, D. M., J. N. Stricherz, and J. J. O'Brien, 1997:
*TOGA Pseudo-Stress Atlas 1985-1994: III Indian
Ocean.* COAPS Report 97-3, COAPS/Florida State
University, Tallahassee, FL  32306-3041, 163 pp.

Legler, D., 1991: Errors in five-day mean surface wind
and temperature conditions due to inadequate
sampling. *J.Atmos.Oceanic.Technol.*, **8**, 705-712.

Levitus, S. et al., 1994: *World Ocean Atlas 1994* (4
Volumes)  NOAA Atlas NESDIS 4, U.S. Department
of Commerce, Washington, D.C., 117 pp.  Available
from:  U.S Department of Commerce,  NODC,  User
Services Branch,  NOAA/NESDIS E/OC21,
Washington D.C,  20233,  USA.
Vol. 1: (Conkright, M. E., S. Levitus, and T. P.
Boyer) Nutrients.
Vol. 2: (Levitus, S. and T. P. Boyer) Oxygen.
Vol. 3: (Levitus, S., R. Burgett and T. P. Boyer)
Salinity.
Vol. 4: (Levitus, S. and T. P. Boyer) Temperature.

Levitus, S., 1982: *Climatological Atlas of the World
Ocean.* U S Government Printing Department,
NOAA Professional Paper No. 13, Washington D.C.,
173 pp.

Li, Z., and H. Leighton, 1993:  Global climatologies of
solar radiation budgets at the surface and in the
atmosphere from 5 years of ERBE data. *J. Geophys.
Res.*, **98**, 4919-4930.

Li, Z., H.G. Leighton, K. Masuda and T. Takashima,
1993: Estimation of SW flux absorbed at the surface
from TOA reflected flux. *J. Climate*, **6**, 317-330.

Liberti, G. L., 1995: Review of SSM/I based algorithms
submitted for the GPCP-AIP/2. *Microwave
Radiometry and Remote Sensing of the Environment.*
D. Solimini, Ed., VSP Press., 297 - 306.

Lind, R.J, and K.B. Katsaros, 1986: Radiation
measurements and model results from R/V
*Oceanographer* during STREX 1980. *J. Geophys.
Res.*, **91**, 13308-13314.

Lind, R.J., K.B. Katsaros and M. Gube, 1984: Radiation
budget components and their parameterization in
JASIN. *Quart. J. Roy. Meteor. Soc.*, **110**, 1061-1071.

Lindau R., 2000: *Climate Atlas of the Atlantic Ocean
derived from the Comprehensive Ocean Atmosphere
Data Set,* Springer Verlag Berlin, 488pp.

Lindau, R., 1995a: A new Beaufort equivalent scale.
*Internat. COADS Winds Workshop*, Kiel, Germany,
31 May - 2 June 1994, Environmental Research
Labs., NOAA, Boulder, Colorado, 232 - 252. (also at
http://www.cdc.noaa.gov/coads/kiel/ )

Lindau, R., 1995b: Time dependent calibration of marine
Beaufort estimates using individual pressure
differences. *Internat. COADS Winds Workshop*, Kiel,
Germany, 31 May - 2 June 1994, Environmental
Research Labs., NOAA, Boulder, Colorado, 253 –
269. (also at http://www.cdc.noaa.gov/coads/kiel/ )

Lindau, R., H.-J.Isemer and L.Hasse,1990: Towards
time-dependent calibration of historical wind
observations at sea. *Trop.Ocean-Atmos.Newslett.*, **54**,
7-12.

Lindsay, R.W. and D.A. Rothrock, 1994: Arctic sea ice
albedo from AVHRR. *J. Climate,* **7**, 1737-1749.

Liou, K. N., 1992:  Radiation and Cloud Processes in the
Atmosphere.  Oxford University Press, 487 pp.

Liu, Q., C. Simmer, and E. Ruprecht, 1997: Estimating
longwave net radiation at sea surface from the
Special Sensor Microwave/Imager (SSM/I). *J. Appl.
Met.*, **36**, 919-930.

Liu, W. T., 1986: Statistical relation between monthly
mean precipitable water and surface-level humidity
over global oceans. *Mon. Wea. Rev.*, **114**, 1591-1602.

Liu, W. T., 1988: Moisture and latent heat fluxes
variabilities on the Tropical Pacific derived from
satellite data. *J. Geophys. Res.*, **93**, 6749 - 6760.

Liu, W. T., 1990: Remote sensing of surface turbulence
heat flux. *Surface Waves and Fluxes*, G. L. Geernaert
and W. J. Plant, Eds., Kluwer Academic Publishers,
Dordrecht, 293-309.

Liu, W. T., and P. P. Niiler, 1984: Determination of
monthly mean humidity in the atmospheric surface
layer over ocean from satellite data. *J. Phys.
Oceanogr.*, **14**, 1452-1457.

Liu, W. T., W. Tang, and F. J. Wentz, 1992: Precipitable
water and surface humidity over global oceans from
Special Sensor Microwave Imager and European
Center for Medium Weather Forecasts. *J. Geophys.
Res.*, **97**, 2251-2264.

Liu, W. T., W. Tang, and P. P. Niiler, 1991: Humidity
profiles over the ocean. *J. Climate*, **4**, 1023 - 1034.

Liu, W.T. and J.A. Businger, 1975: Temperature profile
in the molecular sublayer near the interface of a fluid
in turbulent motion.  *Geophys. Res Lett.*, **2**, 403-404.

Liu, W.T., K.B.Katsaros and J.A.Businger 1979.  Bulk
parameterization of the air-sea exchange of heat and
water vapour including the molecular constraints at
the interface.  *J. Atmos. Sci.*, **36**, 1722-1735.

Lo, R. C. A., 1983: A comprehensive description of the
mission sensor microwave imager SSM/I
environmental parameter extraction algorithm. *NRL
Memo. Rep. 5199*, 48 pp., Nav. Res. Lab.,
Washington, D.C.

Louis, J.F., 1979: A parametric model of vertical eddy
fluxes in the atmosphere. *Boundary-Layer Meteor.*,
1**7**, 187-202.

Lumb, F. E. , 1964: The influence of cloud on hourly
amount of total solar radiation at the sea surface.
*Quart. J. Roy. Meterol.  Soc.*, 90, 43-56.

Luthardt, H., 1985: Estimation of mesoscale surface
fields of meteorological parameters in the North Sea
area from routine measurements. *Beitr. Phys. Atmos.*,
**58**, 255 - 272.

Macdonald A. M., 1998: The global ocean circulation: a
hydrographic estimate and regional analysis.
*Progress in Oceanography*, **41**, 281-382.

Macdonald, A. M.,  and C. Wunsch, 1996: An estimate of
global ocean circulation and heat fluxes. *Nature*, **382**
(6590) 436-439.

MacDonald, A., J.Candela & H.L. Bryden, 1994: An
estimate of the net heat transport through the Strait of
Gibraltar. *Coastal Estuarine Stud.* **46**, edit. P.E.
Violette, AGU, Wash. DC.

MacWhorter, M.A., and R.A. Weller, 1991: Error in
measurements of incoming shortwave radiation made
from ships and buoys. *J. Atmos. Oceanic Tech.*, **8**,
108-117.

Magiorre, A., M.Zavaterelli, M.G.Angelucci, and N.Pinardi 1998: Surface heat and water fluxes in the Adriatic Sea: seasonal and interannual variability. *Phys. Chem. Earth* , **23**, 5/6, 561-567.

Malevskii S.P., G.V.Girduk & B.Egorov, 1992: Radiation balance of the ocean surface, *Hydrometeoizdat*, Leningrad, 148 pp.

Marshall, J. S. and W.M. Palmer, 1948: The distribution of raindrops with size, *J. Meteor.* **5**, 165 – 166.

Masutani, M., K. A. Campana, and S. J. Lord, 1999: Note of cloud cover of the ECMWF nature run used for OSSE/NPOESS project. *NCEP Office Note 427.* NCEP, 4700 Silver Hill Rd., Mail Stop 9910, Washington, DC 202330-9910, 19 pp + figs.

May, P. W. 1986: *A brief explanation of Mediterranean heat and momentum flux calculations*, NORDA code 322, NSTL, MS 39529.

Maykut, G.A., and N. Untersteiner, 1971: Some results from a time-dependent thermodynamic model of sea ice, *J. Geophys. Res.,* **76**, 1550-1575.

McCartney, M.S., R.G. Curry, and H.F. Bezdek, 1997.:The interdecadal warming and cooling of Labrador Sea Water. *ACCP notes,* **IV**(1), 1-11

McClain, E. P., 1981: Multiple atmospheric window techniques for satellite-derived sea surface temperatures. *Oceanography from Space*, J. Gower, Ed., Plenum, 73 - 85.

McPhaden, M. J., A. J. Busalacchi, and J. Picaut, 1988: Observations and wind-forced model simulations of the mean seasonal cycle in tropical Pacific sea surface topography. *J. Geophys. Res.*, **93**, 8131-8146.

Medwin, H., J.A. Nystuen, P.W. Jacobus, D.E. Snyder, and L.H. Oswald, 1992: The anatomy of underwater noise. *J. Acoust. Soc. Amer.*, **92**, 1613-1623.

Mehta, V., 1998: Variability of the tropical ocean surface temperatures at decadal-multidecadal time scales. Part I. Atlantic Ocean. *J. Climate*, **11**, 2351-2375.

Melville, W.K., 1977: Wind stress and roughness length over breaking waves. *J. Phys. Oceanog.*, **7**, 702-710.

Merchant, C. J. and A. R. Harris, 1999: Toward the elimination of bias in satellite retrievals of sea surface temperature 2. Comparison with *in situ* measurements. *J. Geophys. Res.*, **104**, 23579 - 23590.

Michalsky, J., M. Rubes, T. Stoffel, M. Wesely, M. Splitt, and J. DeLuisi, 1997: Optimal measurement of surface shortwave irradiance using current instrumentation - The ARM experience. *Ninth AMS Conf. on Atmospheric Radiation.* Long Beach, CA. Amer. Meteor. Soc., Boston, MA, J5-J9.

Miller, D.K., and K.B. Katsaros, 1992: Satellite derived surface latent heat fluxes in a rapidly intensifying marine cyclone. *Mon. Wea.Rev.*, **120**, 1093-1107.

Minnis, P., W. L. Smith, Jr., D. P. Garber, J. K. Ayers, and D., R., Doelling, 1995: *Cloud properties derived from GOES-7 for spring 1994 ARM intensive observing period using Version 1.0.0 of ARM satellite data analysis program.* NASA reference publication 1366, 58 pp.

Miskolczi, F., 1994: Modeling of downward surface longwave flux density for global change applic-ations and comparison with pyrgeometer measure-ments. *J. Atmos. Oceanic Tech.*, **11**, 608-612.

Miyakoda, K., and J. Sirutis, 1996: *Manual of the E-physics.* Available from Geophysical Fluid Dynamics Laboratory, Princeton University, P. O. Box 308, Princeton, NJ 08542.

Mlawer, E. J., S. J. Taubman, P. D. Brown, M. J. Iacono, and S. A. Clough, 1997: Radiative transfer for inhomogeneous atmospheres: RRTM, a validated correlated-k model for the longwave. *J. Geophys. Res.*, **102**, 16663-16682.

Molinari R. L., E. Johns, and J. F. Festa, 1990: The annual cycle of meridional heat flux in the Atlantic Ocean at 26.5N. *J.Phys. Oceanogr*, **20**, 476-482.

Moll, W.J.M., 1923: A thermopile for measuring radiation. *Proc. Phys. Soc. (London),* **35**, 257-260.

Monahan E.C., and I.G. O'Muircheartaigh, 1987: Comments on "Albedos and glitter patterns of a wind-roughened sea surface". *J. Phys. Oceanogr.*, **17**, 549-550.

Moorthi, S., and M. J. Suarez, 1992: Relaxed Arakawa Schubert: A parameterization of moist convection for general circulation models. *Mon. Wea. Rev.*, **120**, 978-1002.

Morcrette, J.-J., 1991: Radiation and cloud radiative properties in the European Centre for Medium-Range Weather Forecasts forecasting system. *J. Geoph. Res.*, **96**, 9121-9132.

Morrissey, M.L., and J.A. Maliekal, 1995: Standard error estimation of COADS monthly mean winds. *Proc. Internat. COADS Winds Workshop,* Kiel, Germany, 1994. Ed. H.Diaz and H.-J.Isemer, NOAA-ERL, IFM (Kiel), 165-170.

Moyer, K. A., and R. A. Weller, 1997: Observations of surface forcing from the subduction experiment: a comparison with global model products and climat-ological datasets. *J. Climate*, **10**, 2725-2742.

Moyer, K. A., S. P. Anderson and R. A. Weller, 1996: Observations of surface forcing from the subduction experiment and TOGA COARE: a comparison with global model products and climatology. *Proc. WCRP Workshop on Air-Sea flux fields for forcing ocean models and validation of GCM's*, ECMWF, Reading, 24 - 27 October 1995, WCRP-95 (WMO/TD 762), WCRP, Geneva, 69 - 74.

Mueller, C.C. and E.H. Kidder, 1972: Rain gage catch variation due to airflow disturbances around a standard rain gage. *Water Resources Research*, **8**, 1077-1082.

Nakamura, N., and A. Oort, 1988. Atmospheric heat budgets of the polar regions*, J. Geophys. Res.,* **93**, 9510-9524.

Neiman P.J., Shapiro M.A., Donall E.G., Kreitzberg C.W. 1990: Diabatic Modification Of An Extra-tropical Marine Cyclone Warm Sector By Cold Underlying Water *Mon. Weath.Rev.* **118**: (8) 1576-1590.

Neumann, J., and N. Roseman, 1954: The Black Sea: energy balance and evaporation. *Trans. Amer. Geophys. Union*, **35**, 767-774.

Niekamp, K.-P., 1992: Untersuchung zur Gute der Parametrisierung von Malevskii-Malevich zur Bestimmung der solaren Einstrahlung an der Ozeanoberflache. Diploma Msc, Institut für Meereskunde, Kiel, 108 pp.

Nordeng, T.E., 1991: On the wave age dependent drag coefficient and roughness length at sea. *J. Geophys. Res.*, **96**, 7167-7174.

Nuss, W.A., and D.W. Titley, 1994: Use of multiquadratic interpolation for meteorological objective analysis. *Mon. Wea. Rev.*, **122**, 1611-1631.

Nystuen, J.A., 1996: Acoustical rainfall analysis: Rainfall drop size distribution using the underwater sound field. J. Atmos. Oceanic Tech., 13, 74-84.

Nystuen, J.A., 1999: "Listening to raindrops", Solstice 10, No. 2, http://www.imagenet.org .

Nystuen, J.A., J. R. Proni, P. G. Black and J. C. Wilkerson, 1996: A comparison of automatic rain gauges. *J. Atmos. Oceanic Tech.*, **13**, 62-73.

Nystuen, J.A., M.J. McPhaden, and H.P. Freitag, 2000: Surface measurements of precipitation from an ocean mooring: The Underwater Acoustic Log from the South China Sea. *J. Applied Meteor.*, (in press.).

Oberhuber, J. M., 1988: An atlas based on the COADS data set: the budgets of heat, buoyancy and turbulent kinetic energy at the surface of the Global Ocean. Rep*., Max-Plank-Institut fur Meteorologie*, No. 15, Hamburg, Germany, 100 pp.

Ochi, M.K., 1978: Wave statistics for the design of ships and offshore structures, *Proceedings SNAME*, November 1978, New York, NY.

Oki, R. and A. Sumi, 1994: Sampling simulation of TRMM rainfall estimation using radar-AMeDAS composites. *J. Appl. Met.*, **33**, 1597 - 1608.

Olbrük, G., 1979: Precipitation measurements at sea. Marine meteorological and related oceanographical activities. Rep. 1, WMO, Geneva, 39 pp.

Oost, W. A., 1998: The KNMI HEXMAX stress data - a revisit. *Boundary-Layer Meteor.*, **86**, 447 - 468.

Paltridge, G.W. and C.M.R Platt, 1976: *Radiative Processes in Meteor. and Climatology*, 318pp., Elsevier, New York.

Pan, H. -L. and W. -S. Wu, 1995: *Implementing a mass flux convection parameterization package for the NMC medium-range forecast model.* NMC Office Note 409, 40 pp.  Available from NCEP, 5200 Auth Road, Washington, DC 20233.

Pan, H. -L., 1999: Parameterization of subgrid-scale processes. *Global Energy and Water Cycles,* K.A. Browning and R. J. Gurney, ed., Cambridge University Press, Cambridge, England, 44-47.

Panofsky, H.A. and J.A. Dutton, 1984: *Atmospheric Turbulence: models and methods for engineering applications.* Wiley, New York, 397 pp.

Parilla, G., A. Lavin, H. Bryden, M. Garcia and R. Millard, 1984: Rising temperature in the subtropical North Atlantic Ocean over the past 35 years. *Nature*, **369**, 48 - 51.

Parker, D. E., P. D. Jones, C. K. Folland and A. Bevan, 1994: Interdecadal changes of surface temperature since the late 19th century. *J. Geophys. Res.*, **99**, 14377 - 14399.

Parkinson, C.L. and W.M. Washington ,1979: A large-scale numerical model of sea ice.  *J. Geophys. Res.,* **84**, 311-337.

Parkinson, C.L., Comiso, J.C., Zwally, H.J., Cavalieri, D.J., Gloersen, P., and Campbell, W.J., 1987: *Arctic Sea Ice, 1973-1976: Satellite Passive-Microwave Observations,* NASA SP-489, National Aeronautics and Space Administration, Washington, D.C.

Parrish, D. F., and J. C. Derber, 1992: The National Meteorological Center's spectral statistical interpolation analysis system.  *Mon. Wea. Rev.*, **120**, 1747-1763.

Pascal, R. W. and S. A. Josey, 2000: Accurate radiometric measurement of the atmospheric longwave flux at the sea surface. *J. Atmos. & Oceanic Tech.*, *(accepted).*

Paulson, C. A., and J. J. Simpson, 1977: Irradiance measurements in the upper ocean, *J. Phys. Oceanogr.*, **7**, 952-956.

Paulson, C.A. and J.J. Simpson, 1981: The temperature difference across the cool skin of the ocean. *J. Geophys. Res.*, **86**, 11044-11054.

Paulson, C.A., 1970: The mathematical representation of wind speed and temperature profiles in the unstable atmospheric surface layer. *J. Appl. Meteor.*, **9**, 857-861.

Payne, R.E., 1972: Albedo of the sea surface. *J. Atmos. Sci.*, **29**, 959-970.

Persson, P.O.G., D. Ruffieux and C.W. Fairall, 1997: recalculations of pack ice and lead surface energy budgets during the Arctic Leads Experiment (LEADEX) 1992. *J. Geophys. Res.,* **102**, 25085-25089.

Petersen, W. A., R. C. Cifelli, S. A. Rutledge, B. S. Ferrier, and B. F. Small,  1999:  Shipborne dual-Doppler operations during TOGA COARE: integrated observations of storm kinetics and electrification. *Bull. Amer. Meteor. Soc.*, **80**, 81-96.

Peterson E.W., and L.Hasse, 1987: Did the Beaufort scale or the wind climate change? *J. Phys. Oceanogr.*, **17**, 1071-1074.

Pfaendtner, J., S. Bloom, D. Lamich, M. Seablom, M. Sienkiewicz, J. Stobie and A. da Silva, 1995: *Documentation of the Goddard Earth Observing System (GEOS) Data Assimilation System – Version 1.* NASA Tech. Memo. 104606, vol. 4, Goddard Space Flight Center, Greenbelt, MD 20771, 44 pp.

Philipona,R., C. Frohlich and Ch Betz, 1995: Characterization of pyrgeometers and the accuracy of atmospheric long-wave radiation measurements. *Appl Opt.*, **34**, 1598-1605.

Phillips, T., 1994: *A Summary Documentation of the AMIP Models.*  PCMDI Report 18, Lawrence Liver-more National Laboratory, Livermore, CA, 343 pp ( see http://www-pcmdi.llnl.gov/modeldoc/amip/01toc.html )

Pilewskie, P., and F. P. J. Valero, 1995:  Direct observations of excess solar absorption by clouds. *Science*, **267**, 1626-1629.

Pinker, R. T., I. Laszlo, C. H. Whitlock, and T. P. Charlock, 1995: Radiative flux opens new window on climate research.  *EOS Trans. Amer. Geophys. Union*, **76**, 145-158.

Pinker, R.T., and I. Laszlo, 1992: Modeling surface solar irradiance for satellite applications on a global scale. *J. Appl. Meteor.*, **31**, 194-211.

Pinto, J.O. and J.A. Curry, 1997: Role of radiative transfer in the modelled mesoscale development of summertime arctic stratus. *J. Geophys. Res.,* **102**, 13861-13872.

Planton, S., G. Caniaux, and H. Giordani, 2000: Surface fluxes. in *Proc. Conf.  2$^{nd}$ Intl. Conf. on Reanalyses*, Reading, England, 23-27 Aug. 1999.  WCRP-109 (WMO/TD 985) WMO, Geneva, 111 – 114.

Pollard, R.T. and K.J.H. Thomas, 1989: Vertical circulation revealed by diurnal heating of the upper ocean in late winter.  Part 1: Observations. *J. Phys. Oceanogr.*, **19**, 269-278.

Pond S., D.B. Fissel and C.A. Paulson, 1974: A note on bulk aerodynamic coefficients for sensible heat and moisture fluxes. *Boundary-Layer Meteor.*, **6**, 333-339.

Post, M.J and Coauthors, 1998: The Combined Sensor Program: an air-sea science mission in the central and western Pacific ocean. *Bull. Amer. Meteor. Soc,* **78**, 2797-2815.

Price, J.F., R.A. Weller and R. Pinkel, 1986: Diurnal cycling: observations and models of the upper ocean response to diurnal heating, cooling and wind mixing. *J. Geophys. Res*., **91**, 8411-8427.

Rago, T.A., and H.T.Rossby, 1987: Heat transport into the Atlantic Ocean north of 32N latitude. *J.Phys.Oceanogr.*, **17**, 854-871.

Ramage, C. S., 1987: Secular change in reported surface wind speeds over the ocean. *J. Climate Appl. Meteor.*, **26**, 525-528.

Ramanathan, V., B. Subasilar, G. J. Zhang, W. Conant, R. D. Cess, J. T. Kiehl, H. Grassl, and L. Shi, 1995: Warm pool budget and shortwave cloud forcing: A missing physics? *Science*, **267**, 499-503.

Rayner, N.A., E.B. Horton, D.E. Parker, C.K. Folland and R.B. Hackett, 1996: *Version 2.2 of the Global sea-Ice and Sea Surface Temperature Data Set, 1903-1994.* Climate Research Technical Note No. 74, unpublished doc. available from the Meteorological Office, London Road, Bracknell, U.K..

Redelsperger, J.L., F. Guichard, and S. Mondon, 2000: A parameterization of mesoscale enhancement of surface fluxes for large scale models. *J. Climate*, **13**, 402-421.

Reed, R.K., 1977: On estimating insolation over the ocean. *J. Phys. Ocean.*, **7**, 482-485.

Renfrew, I. A., G. W. K. Moore, P. S. Guest and K. Bumke, 2000: A comparison of surface-layer, surface heat flux and surface momentum flux observations over the Labrador Sea with ECMWF analyses and NCEP reanalyses. *Submitted to J. Climate*.

Reynaud T., P. Legrang, H. Mercier and B. Barnier, 1998: A new analysis of hydrographic data in the Atlantic and its application to an inverse modelling study. International WOCE Newsletter, 32, 29-32.

Reynolds, R. M., 1998: The ARM project: contribution to the Tropical Western Pacific Site Scientific Plan. (unpublished manuscript).

Reynolds, R. W. and D. S. Marsico, 1993: An improved real time global sea surface temperature analysis. *J. Climate*, **6**, 114-119.

Reynolds, R. W. and T. M. Smith, 1994: Improved global sea surface temperature analyses using optimum interpolation. *J. Climate* **7**, 929 - 948.

Reynolds, R. W., 1988: A real time global sea surface temperature analysis. *J. Climate*, **1,** 75-86.

Reynolds, R. W., 1993: Impact of Mount Pinatubo aerosols on satellite-derived sea surface temperatures. *J. Climate*, **6**, 768 - 774.

Reynolds, R. W., 1999: Specific contributions to the observing system: Sea Surface Temperatures. *CLIMAR 99, WMO Workshop on Advances in Marine Climatology*, Vancouver, 8 - 15 Sept. 1999, 330 - 339.

Rieder, K. F. and J. A. Smith, 1998: Removing wave effects from the wind stress vector. *J. Geophys. Res.*, **103** (C1), 1363 - 1374.

Rigor, I., R. Colony, and S. Martin, 2000: Variations in surface air temperatures over the Arctic Ocean from 1979 to 1997, J. Climate,13: (5) 896-914.

Roberts, R. E., J. A. Selby and L. M. Bibermann, 1976: Infrared continuum absorption by atmospheric water vapor in the 8-12 micro-meter window. *Appl. Optics,* **15,** 2085-2090.

Rodda, J.C. and S.W. Smith, 1986: The significance of the systematic error in rainfall measurement for assessing wet deposition. *Atmospheric Environment*, **20**, 1059-1064

Rodwell, M.J., D.P.Rowell, and C.K.Folland, 1999: Oceanic forcing of the wintertime North Atlantic Oscillation and European climate. *Nature*, **398**, 320-323.

Rogers, C. D. and C. D. Walshaw, 1966: The computation of infrared cooling rate in planetary atmospheres, *Quart. J. Roy. Meteor. Soc.* **92**, 67 – 92.

Rogers, E., and L.F.Bossart, 1986: An investigation of explosively deepening oceanic cyclones. *Mon. Wea.Rev.*, **114**, 702-718.

Roland, J.R., 1976: Comparison of two different raindrop disdrometers. 17th Conf. on Radar Meteor., Seattle WA, Amer. Meteor. Soc., 398-405.

Rosatti, A., and K. Miyakoda, 1988. A general circulation model for upper ocean simulations. *J. Phys. Oceanog.*, **18**, 1601-1626.

Rossow, W. B., L. C. Garder, P.-J. Lu, and A. Walker, 1991: *International Satellite Cloud Climatology Project (ISCCP) documentation of cloud data.* WMO/TD-No. 266, Revised March 1991, WMO, Geneva, 76 pp. plus three appendices.

Rossow, W.B., and A.A. Lacis, 1990: Global, seasonal cloud variations from satellite radiance measurements. II: Cloud properties and radiative effects. *J. Climate*, **3**, 1204-1253.

Rossow, W.B., and R.A. Schiffer, 1991: ISCCP cloud data products. *Bull. Amer. Meteor. Soc.*, **72**, 2-20.

Rossow, W.B., and R.A. Schiffer, 1999: Advances in understanding clouds from ISCCP. *Bull. Amer. Meteor. Soc.*, **80,** (11), 2261–2288.

Rossow, W.B., and Y-C. Zhang, 1995: Calculation of surface and top-of-atmosphere radiative fluxes from physical quantities based on ISCCP datasets, Part II: Validation and first results. *J. Geophys. Res.*, **100**, 1167-1197 (contact wrossow@giss.nasa.gov for access to these data).

Rossow, W.B., L.C. Garder and A.A. Lacis, 1989: Global, seasonal cloud variations from satellite radiance measurements. Part I: Sensitivity of analysis. *J. Climate*, **2**, 419-462.

Rothrock, D.A., and J. Zhang, 1997: Surface downwelling radiative fluxes: Ice model sensitivities and data accuracies, Workshop on Polar Processes in Global Climate, 13-15 November 1996, Cancun, Mexico, *Amer. Meteor. Soc.*, **D(VT)200**, 119-121.

Roullet, G., and G. Madec, 2000. Salt conservation, free surface and varying volume: a new formulation for Ocean GCMs. *J. Geophys. Res., in press.*

Ruprecht, E., 1993: Observation and analysis of global rainfall. *Energy and Water Cycles in the Climate System,* E.Rashke and D.Jacob, Eds., NATO ASI SeriesI, vol. **5**, Springer, 165-185.

Russell, C.A., C.W. Fairall, O.P.G. Persson, E.L. Andreas, P.S. Guest, R. Lindsay, H.A. Eide and T. Horst, 1999a: Intercomparison of downward longwave flux measurements during the first two months of SHEBA. pp. 314-318, *Proc. 5$^{th}$ conf. on polar meteor. and oceanography*, 10-15 Jan. 1999, Dallas, TX, Amer. Meteor. Soc., Boston, MA.

Russell, C.A., C.W. Fairall, O.P.G. Persson, E.L. Andreas, P.S. Guest, R. Lindsay and T. Delany, 1999b: Intercomparison and normalization of five Eppley Pyrgeometer IR fluxes during April-May, 1998 at SHEBA. *Proc. 10$^{th}$ conf. on atmospheric radiation*, 28 June-2 July 1999, Madison Wis., Amer. Meteor. Soc., Boston, MA.

Rutledge, S.A., R. Cifelli, C. DeMott, W. Petersen, T. Rickenbach, J. Lutz, R. Bowie, M. Strong and E. Williams, 1993: The shipboard deployment of the MIT C-band radar during TOGA-COARE. *Proc. 26$^{th}$ Inter. Conf. On Radar Met.*, 24-28 May 1993, Norman, OK, Amer. Meteor. Soc., Boston, MA.

Salby, M. L. and P. Callaghan, 1997: Sampling error in climate properties derived from satellite measurements: Consequences of undersampled diurnal variability. *J. Climate*, **10**, 18 - 36.

Sanders, J.W., 1976: A growth-stage scaling model for the wind-driven sea, *Dtsch. Hydrogr. Z.*, **29**, 136-161.

Saunders, P.M., 1967: The temperature at the ocean-air interface, *J. Atmos. Sci.* **24**, 269-273.

Sauvageot, H., 1994: Rainfall measurement by radar: a review. *Atmos. Res.*, **35**, 27-54.

Schanz, L. and P. Schlüssel, 1997: Atmospheric back radiation in the Tropical Pacific. *Meteor. Atmos. Phys.*, **63**, 217 - 226.

Schiano, M. E., R. Santoleri, F. Bignami, R. M. Leonardi, S. Marullo and E. Boehm, 1993: Air-sea interaction measurements in the west Mediterranean Sea during the Tyrrhenian Eddy Multi-Platform Observations Experiment. *J. Geophys. Res.*, **98** (C2), 2461 - 2474.

Schlichting, H, 1969: *Boundary Layer Theory* (6th edition), McGraw-Hill, New York, 747 pp.

Schlüssel, P. and H. Luthardt, 1991: Surface wind speeds over the north sea from special sensor microwave / imager observations. *J. Geophys. Res.*, **96**, 4845 - 4853.

Schlüssel, P., 1989: Satellite-derived low-level atmospheric water-vapour content from synergy of AVHRR with HIRS. *Int.J.RemoteSens.*, **10**, 705-721.

Schlüssel, P., 1995: Passive Fernerkundung der unteren Atmosphäre und der Meeresoberfläche aus dem Weltraum. *Berichte aus dem Zentrum für Meeres-und Klimaforschung, Reihe A: Meteorologie, 20*, 175 pp. [Available from Universität Hamburg Meteorologisches Institut, Bundesstraße 55, 20146 Hamburg, Germany].

Schlüssel, P., and Emery W. 1990: Atmospheric water-vapor over oceans from SSM/I measurements *Int. J. Rem. Sensing* **11** (5) 753-766

Schlüssel, P., L. Schanz, and G. Englisch, 1995: Retrieval of latent heat flux and longwave irradiance at the sea surface from SSM/I and AVHRR measure-ments. *Advanced Space Research*, **16**, 107-116.

Schmetz, J., 1989: Towards a surface radiation climatology: retrieval of downward irradiances from satellites. *Atmos. Res.*, **23**, 287 - 321.

Schubert, S.D., and R.B. Rood, 1995: *Proceedings of the Workshop of the GEOS-1 Five Year Assimil-ation*. NASA Tech. Mem. 104606, Vol. 7, Goddard Space Flight Center Greenbelt, MD, 201 pp.

Schubert, S.D., C.-K. Park, C.-Y. Wu, W. Higgins, Y. Kondratyeva, A. Molod, L. Takacs, M. Seablom, and R. Rood, 1995: *A Multiyear Assimilation with the GEOS-1 System: Overview and Results*. NASA Tech. Mem. 104606, Vol. 6, Goddard Space Flight Center Greenbelt, MD, 183 pp. (see also http://dao.gsfc.nasa.gov/experiments/assim54A.html )

Schulz, J. and V. Jost, 2000: A New satellite-Derived Freshwater Flux Climatology: The Hamburg Ocean Atmosphere Parameters and Fluxes from Satellite Data, *(submitted to J. Climate)*.

Schulz, J., 1993a: Fernerkundung des latenten Wärmeflusses an der Meeresoberfläche. Ph.D. dissertation, Universität Hamburg, 108 pp. [*Berichte aus dem Zentrum für Meeres- und Klimaforschung, Reihe A: Meteorologie*, Nr. 4.]

Schulz, J., 1993b: Latent heat flux at the air-sea interface from a combination of SSM/I with AVHRR data. *Proc. 6th AVHRR data user's meeting,* Belgirate,

Italy, 179 - 185. [EUMETSAT publication: EUM P 12, ISSN 1015 9576]

Schulz, J., J. Meywerk, S. Ewald, and P. Schlüssel, 1997: Evaluation of Satellite-derived Latent Heat Fluxes. *Journal of Climate*, **10**, 2782-2795.

Schulz, J., P. Schlüssel, H. Graßl, 1993: Water vapour in the atmospheric boundary layer over oceans from SSM/I measurements. *Int. J. Remote Sens.*, **14**, 2773 - 2789.

Schwarzkopf, M. D., and S. B. Fels, 1991: The simplified exchange method revisited: An accurate rapid method for computation of infrared cooling rates and fluxes. *J. Geophys. Res.*, **96**, 9075-9096.

Schweiger, A.J., R.W. LIndsay, J.R. Key and J.A. Francis. 1999. Arctic Clouds in Multiyear Satellte Data Sets. *Geophysical Research Letters*, **26**, No.13, 1845-1848.

Seckel, G. R. and F. H. Beaudry, 1973: The radiation from sun and sky over the Pacific Ocean (Abstract). *Trans. Am. Geophys. Union*, **54**, 1114.

Serreze, M.C., Hurst, C.M., 2000: Representation of mean Arctic precipitation from NCEP-NCAR and ERA reanalyses, *J. Climate* **13** (1) 182-201.

Servain, J., J. N. Stricherz, and D. M. Legler, 1996: TOGA Pseudo-stress Atlas 1985-1994 Volume I: Tropical Atlantic. Centre ORSTOM, Plouzané, France, 158 pp.

Servain,J., A.J.Busalacchi, M.J.McPhaden, A.D.Moura, G.Reverdin, M.Vianna and S.E.Zebiak, 1998: A Pilot Research Moored Array in the Tropical Atlantic (PIRATA). *Bull. Am. Met.. Soc.*, **79**, 2019-2031.

Shaw, J. A., J. H. Churnside and E. R. Westwater, 1991: An Infrared Spectrometer for Ground-Based Profiling of Atmospheric Temperature and Humidity. *Proc. SPIE Int'l. Symp. on Optical Appl. Sci. and Engineering*, July 21 - 26, 1991, San Diego, CA, **1540**, 681-686.

Sheppard, B.E. and P.I. Joe, 1994: Comparison of raindrop size distribution by a Joss-Waldvogel disdrometer. *J. Atmos. Oceanic Technol.*, **11**, 874-887.

Sheppard, B.E., 1990: Effect of irregularities in the diameter classification of raindrops by the Joss-Waldvogel disdrometer. *J. Atmos. Oceanic Technol.*, **7**, 180-183.

Shin, K.-S. and G. R. North, 1988: Sampling error study for rainfall estimate by satellite using a stochastic model. *J. Appl. Met.*, **27**, 1218 - 1231.

Shine, K.P., 1984: Parameterization of the shortwave flux over high albedo surfaces as a function of cloud thickness and surface albedo. *Quart. J. Roy. Meteor. Soc.*, **110**, 747-764.

Shinoda, T., H. H. Hendon, and J. Glick, 1999: Intraseasonal surface fluxes in the tropical western Pacific and Indian Oceans from NCEP reanalyses. *Mon. Wea. Rev.*, **127**, 678-693.

Short, D. A., R. A. Kucera, B. S. Ferrier, J. C. Gerlach, S. A. Rutledge and O. W. Thiele, 1997: Shipboard radar rainfall patterns within the TOGA COARE IFA. *Bull. Amer. Meteor. Soc.*, **78**, 2817-2836.

Siefridt L., B. Barnier, K. Béranger and H. Roquet, 1999: Evaluation of operational ECMWF analyses surface heat fluxes: impact of parameterisation changes during 1986-95, *J. Marine Sys., ***19**, 113-135.

Simpson, J. J., A. Schmidt and A. Harris, 1998: Improved cloud detection in Along Track Scanning Radiometer (ATSR) data over the ocean. *Rem. Sensing of Environment*, **65**(1), 1-24

Simpson, J.J. and C.A. Paulson, 1979: Mid-ocean observations of atmospheric radiation. *Quart. J. R. Met. Soc.*, **105**, 487-502.

Slingo, J., and P. Delecluse, 1999: Scale interactions and the tropical atmosphere-ocean system. *Proc. Conference TOGA coupled ocean-atmosphere response experiment (COARE)*. WMO/TD-No.940, WMO, Geneva, 59-69.

Slutz, R. J., S. J. Lubker, J. D. Hiscox, S. D. Woodruff, R. L. Jenne, D. H. Joseph, P. M. Steurer and J. D. Elms, 1985: *COADS, Comprehensive Ocean--Atmosphere Data Set, Release 1.* Climate Research Program, Environmental Research Laboratory, Boulder, CO 262 pp.

Smith, E. A., & co-authors 1998: Results of WetNet PIP-2 project. *J. Atmos. Sci.*, **55**, 1483 - 1536.

Smith, S. D., & co-authors, 1992: Sea surface wind stress and drag coefficients: the HEXOS results. *Boundary-Layer Meteor.*, **60**, 109-142.

Smith, S. D., 1980: Wind stress and heat flux over the ocean in gale force winds. *J. Phys. Oceanog.*, **10**, 709-726.

Smith, S. D., 1988: Coefficients for sea surface wind stress, heat flux, and wind profiles as a function of wind speed and temperature. *J. Geophys. Res.*, **93**, 15467-15472.

Smith, S. D., 1989: Water vapor flux at the sea surface. *Boundary-Layer Meteor.*, **47**, 277-293.

Smith, S. R., C. Harvey, and D. M. Legler, 1996a: *Handbook of Quality Control Procedures and Methods for Surface Meteorology Data.* WOCE Report 141/96, COAPS Report 96-1, WOCE Data Assembly Center, COAPS, Florida State University, Tallahassee, FL 32306-2840, 56 pp.

Smith, S. R., D. M. Legler, and K. V. Verzone, 1999: Quantifying uncertainties in NCEP reanalysis using high-quality research vessel observations. *CLIMAR 99, WMO Workshop on Advances in Marine Climatology*, Vancouver, 8 - 15 Sept. 1999, 223-230.

Smith, T. M., R. W. Reynolds, R. E. Livezey and D. C. Stokes, 1996b: Reconstruction of historical sea surface temperatures using empirical orthogonal functions. *J. Climate*, **9**, 1403 - 1420.

Smith, W.L. & co-authors, 1996c: Observations of the infrared radiative properties of the ocean: implications for the measurement of sea surface temperature via satellite remote sensing. *Bull. Amer. Meteor. Soc.*, **77**, 41-51.

Smull, B. F., and M. J. McPhaden, 1998: Comparison of NCEP/NCAR and ECMWF reanalysed fields with TOGA TAO buoy observations over the tropical Pacific. *Proceedings of the 1st WCRP Intl. Conf. on Reanalyses.* 27-31 Oct. 1997, Silver Spring, MD, USA, WCRP-104, WMO/TD-876. WMO, Geneva, 227-230.

Smyth, W.D., D. Hebert and J.N. Moum, 1996: Local ocean response to a multiphase westerly wind burst – 2. Thermal and freshwater responses. *J. Geophys. Res.*, **101**, 22513-22533.

Soloviev, A.V. and P. Schluessel, 1994: Parameterization of the cool skin of the ocean and of the air-ocean gas transfer on the basis of modelling surface renewal. *J. Phys. Oceanog.*, **24**, 1339-1346.

Soloviev, A.V. and P. Schluessel, 1996: Evolution of cool skin and direct air-gas transfer coefficient during daytime. *Boundary-Layer Meteor.*, **77** 45-68.

Soman, V. V., J. B. Valdés, G. R. North, 1995: Satellite sampling and the diurnal cycle statistics of Darwin rainfall data. *J. Appl. Met.*, **34**, 2481 - 2490.

Sorbjan, Z., 1997: Comments on "A convective transport theory for surface fluxes". *J. Atmos. Sci.*, **54**, 576-578.

Speer, K.G., J.Holfort, T.Reynaud, G.Siedler, 1996: South Atlantic Heat Transport at 11° S. In: *The South Atlantic present and past circulation*, G. Welen & G. Siedler eds., Springer Verlag, Berlin.

Spencer, R. W., 1993: Global oceanic precipitation from the MSU during 1979-91 and comparison to other climatologies. *J. Climate*, **6**, 1301 - 1326.

Spinhirne, J. D., 1993: Micro Pulse Lidar. *IEEE Trans. Geo. Rem. Sens.*, **31**, 48-55.

Stamnes, K., S.-C. Tsay, W. Wiscombe, and K. Jayaweera, 1988: Numerically stable algorithm for discrete-ordinates-method radiative transfer in multiple scattering and emitting layered media. *Appl. Opt.*, **27**, 2502-2509.

Staneva, J.V., E.V. Stanev, and N.H.Rachev, 1995: Heat balance estimates using atmospheric analysis data: A case study for the Black Sea. *J. Geophys. Res.*, **100**, 18581-18596.

Steiner, M. and R.A. Houze, 1997: Sensitivity of the estimated monthly convective rain fraction to the choice of Z-R relation. *J. Appl. Meteor.*, **36**, 452-462.

Stendel, M., and K. Arpe, 1997: *Evaluation of the hydrological cycle in reanalyses and observations.* Max-Planck-Institut für Meteorologie, Report 228, Hamburg, Germany, 52 pp.

Stephens, G. L., and S.-C. Tsay, 1990: On the cloud absorption anomaly. *Quart. J. Roy. Meteor. Soc.*, **116**, 671-704.

Stephens. G. L., and T. J. Greenwald, 1991: Observations of the earth's radiation budget in relation to atmospheric hydrology. Part II: Cloud effects and cloud feedback. *J. Geophys. Res.*, **96**, 15325-15340.

Sterl, A., G.J. Komen, P.D. Cotton 1998: Fifteen years of global wave hindcasts using winds from the European Centre for Medium-Range Weather Forecasts reanalysis: Validating the reanalyzed winds and assessing the wave climate. *J. Geophys. Res.*, **103**, 5477-5492.

Stogryn, A. P., C. T. Butler, and T. J. Bartolac, 1994: Ocean surface wind retrievals from special microwave imager data with neural networks. *J. Geophys. Res.*, **99**, 981 - 984.

Stokes, G. M., and S. E. Schwartz, 1994: The Atmospheric Radiation Measurement Program (ARM) Program: Programmatic Background and Design of the Cloud and Radiation Test Bed. *Bull. Amer. Meteor. Soc.,* **75**, 1201-1221.

Stone, R., T. Mefford, E. Dutton, D. Longenecker, B. Halter and D. Endres, 1996: *Surface radiation and meteorological measurements: January 1992 to December 1994.* NOAA Data Report ERL-CMDL-11, 81pp.

Stricherz, J. N., D. M. Legler, and J. J. O'Brien, 1997: *TOGA Pseudo-Stress Atlas 1985-1994: II Tropical Pacific Ocean.* COAPS/Florida State University. COAPS Report 97-2, 162 pp.

Stuhlmann, R., M. Rieland and E. Raschke, 1990: An improvement of the IMGK model to derive total and diffuse solar-radiation at the surface from satellite data. *J. Appl. Meteor.*, **29**, 586-603.

Stull, R. B., 1988: *An Introduction to Boundary Layer Meteor.*.Kluwer Academic Publishers, Dordrecht, Holland.

Stull, R. B., and Eloranta 1984: Boundary-Layer Experiment – 1983, *Bull. Amer. Meteor. Soc.* **65**: (5) 450-456.

Stull, R.B., 1994: A convective transport theory for surface fluxes. *J. Atmos. Sci.*, **51**, 3-32.

Stull, R.B., 1997: Reply to Sorbjan's comments. *J. Atmos. Sci.*, **54**, 579.

Swift, C. T. and R. E. McIntosh, 1983: Considerations for microwave remote sensing of ocean- surface salinity. *IEEE Trans.Geosci.Rem.Sens.*, **21**, 480 – 491.

Sykes, R.I., D.S. Henn and W.S. Lewellen, 1993: Surface-layer description under free-convection conditions. *Quart. J. Roy. Meteor. Soc.*, **119**, 409-421

Takacs, L. L., A. Molod, and T. Wang, 1994: *Documentation of the Goddard Earth Observing System (GEOS) General Circulation Model-Version 1.* NASA Tech. Mem. 104606, Vol. 1, Goddard Space Flight Center Greenbelt, MD, 100 pp.

Takara, E., and R. G. Ellingson, 2000:  Broken cloud field longwave scattering effects. *J. Atmos. Sci.*, **57**, 1298-1310.

Tanimoto, Y., N.Iwasaka, and K.Hanava, 1997: Relationships between sea surface temperature, the atmospheric circulation, and air-sea fluxes on multiply time scales. *J.Met.Soc.Japan*, **75**, 831-849.

Tanre, D., C. Deroo, P. Duhaut, M. Herman, J-J. Morcrette, J. Perbos and P-Y. Deschamps, 1990: Description of a computer code to simulate the satellite signal in the solar spectrum. *Int. J. Remote Sensing*, **11**, 659-668.

Tarpley, J.D., 1979: Estimating incident solar radiation at the surface from geostationary satellite data. *J. Appl. Meteor.*, **18**, 1172-1181.

Taylor, P. K. and M. J. Yelland, 2000a: A note on the apparent "imbalance" term in the Turbulent Kinetic Energy Budget. *J.Atmos.Oceanic Tech.*,**17**, 82-89.

Taylor, P. K. and M. J. Yelland, 2000b: Comments on: On the effect of ocean waves on the kinetic energy balance and consequences for the inertial dissipation technique. *J. Phys. Oceanogr. (submitted).*

Taylor, P. K., 1984: The determination of surface fluxes of heat and water by satellite microwave radiometry and *in situ* measurements. *Large-scale oceanographic experiments and satellites*, C. Gautier and M. Fieux, Eds., D. Reidel, 223-246.

Taylor, P. K., and M. A. Yelland, 2000c: The dependence of sea surface roughness on the height and steepness of the waves. *J.PhysOceanogr.,(in press).*

Taylor, P. K., E. C. Kent and S. A. Josey, 1999c: The accuracy of sea surface temperature data from Voluntary Observing Ships. *in Report of the OOPC/AOPC Workshop on Global Sea Surface Temperature Data Sets.*  (Palisades, N.Y., USA, 2-4 November 1998). Report GCOS-57, GOOS-79, WMO/TD 978, WMO Geneva., Annex III, 51 -54.

Taylor, P. K., E. C. Kent, M. J. Yelland and B. I. Moat, 1995: The Accuracy of Wind Observations from Ships. *Proc. Internat. COADS Winds Workshop*, Kiel, Germany, 31 May - 2 June, 1994, Env. Res. Labs., NOAA, Boulder, Colorado  (also at http://www.cdc.noaa.gov/coads/kiel/ ), 132 - 155.

Taylor, P. K., E. C. Kent, M. J. Yelland and B. I. Moat, 1999a: The Accuracy Of Marine Surface Winds From Ships And Buoys. *CLIMAR 99, WMO Workshop on Advances in Marine Climatology*, Vancouver, 8 - 15 Sept. 1999,  59 - 68.

Taylor, P. K., E. F. Bradley, C. W. Fairall, L. Legler, J. Schulz, R. A. Weller and G. H. White, 1999d: Surface Fluxes and Surface Reference Sites. *Proc.*

*Symp. The Ocean Observing System for Climate - Oceanobs 99*, St Raphael, 25 - 27 October, 1999.

Taylor, P. K., S. A. Josey and E. C. Kent, 1999e: A comparison of climatological, model derived and observed air-sea flux values for the COARE area. *Conf. on the TOGA Coupled Ocean-Atmosphere Response Experiment (COARE),* Boulder, Co., USA, 7-14 July 1998, WCRP-107, WMO/TD 940, WMO, 249 - 250.

Taylor, P. K., S. A. Josey and E. C. Kent, 1999f: Observations of Ocean Surface Fluxes:  Means and Variability. *Seminar on Atmosphere-surface interaction*, Reading, 8-12 September 1997, ECMWF, Reading, UK, 1 - 31.

Taylor, P.K., M.J.Yelland, F.W.Dobson and R.J.Anderson, 1999b: Storm Wind  Study II: Wind Stress Estimates from Buoy and Ship. in *Proc. Symp. On the Wind-driven Air-sea Interfaces* (Ed. M.L. Banner), Univ. of New South Wales, Sydney,  11-15 Jan., 353 - 354.

Tiedtke, M., 1983: The sensitivity of the time-mean large-scale flow to cumulus convection in the ECMWF model. *ECMWF Workshop on Convection in large-scale Models*, 28 Nov.-1 Dec. 1983, ECMWF, Reading, UK, 297-316.

Tiedtke, M., 1989: A comprehensive mass flux scheme for cumulus parameterization in large-scale models. *Mon. Wea. Rev.*, **117**, 1779-1800.

Tiedtke, M., 1993: Representation of clouds in large-scale models. *Mon. Wea. Rev.*, **121**, 3040-3061.

Timmermann, A., Latif M., Grotzner A., Voss R. 1999: Modes of climate variability as simulated by a coupled general circulation model. Part I: ENSO-like climate variability and its low-frequency modulation *Climate Dynamics* **15**: (8) 605-618.

Toba, Y., N. Iida, H. Kawamura, N. Ebuchi and I.S.F. Jones, 1990: Wave dependance of sea-surface wind stress. *J. Phys. Oceanog.*, **20**, 705-721.

Tobin, D. C., & co-authors, 1999: Downwelling spectral radiance observations at the SHEBA ice station: Water vapor continuum measurements from 17 to 26 micrometer.  *J. Geophys. Res.*, **104**, 2081-2092.

Tokay, A., and D.A. Short, 1996: Evidence from tropical raindrop spectra of the origin of rain from stratiform versus convective clouds. *J. Applied Meteor.*, **35**, 355-371.

Trenberth K.E., and Guillemot C.J. 1998: Evaluation of the atmospheric moisture and hydrological cycle in the NCEP/NCAR reanalyses *Climate Dyn.* **14** 213-231.

Trenberth, K. E. and A. Solomon, 1994: The global heat balance: heat transports in the atmosphere and ocean. *Climate Dyn.*, **10**, 107 - 134.

Trenberth, K. E., 1998: The heat budget of the atmosphere and ocean. *Proc. 1st WCRP Intl. Conf. on Reanalyses.*  27-31 Oct. 1997, Silver Spring, MD, USA, WCRP-104, WMO/TD-876.  WMO, Geneva, 17-20.

Trenberth, K. E., J. M. Caron, and D. P. Stepaniak, 2000a:  The atmospheric energy budget and implications for surface fluxes and ocean heat transports.  *Submitted to J. Climate.*

Trenberth, K. E., W. G. Large and J. G. Olson, 1989: The Effective Drag Coefficient For Evaluating Wind Stress Over The Oceans. *Journal of Climate*, **2**(12), 1507-1516.

Trenberth, K.E. and C.J. Guillemot, 1998: Evaluation of the atmospheric moisture and hydrological cycle in

the NCEP/NCAR reanalyses. *Climate Dyn.*, **14**, 213-231.

Trenberth, K.E., D. P. Stepaniak, J. W. Hurrell, and M. Fiorino, 2000b: Quality of reanalyses in the tropics. *Submitted to J. Climate.*

Trishchenko, A. P., and Z. Li, 1999: On the determination of shortwave cloud radiative forcing. *Proc. AMS Tenth Conf. on Atmospheric Radiation,* Madison WI (June 28 - July 2, 1999), 141-144.

Troen, I., and L. Mahrt, 1986: A simple model of the atmospheric boundary layer: Sensitivity to surface evaporation. *Bound.-Layer Meteor.*, **37**, 129-148.

Tsukamoto, O., and H. Ishida, 1995: Turbulent flux measurements and energy budget analysis over the equatorial Pacific during TOGA-COARE IOP. *J. Meteor. Soc. Japan*, **73**, 557-568.

Tucker, G. B., 1961: precipitation over the North Atlantic Ocean. *Quart.J.Roy.Meteor.Soc.*,**87**,147-158.

Uppala, S., J. K. Gibson, M. Fiorino, A. Hernandez, P. Kallberg, X. Li, K. Onogi, and S. Saarinen, 2000 : ECMWF second generation reanalysis: ERA40. *Proc. Conf. 2nd Intl. Conf. on Reanalyses*, Reading, England, 23-27 Aug. 1999. WCRP-109 (WMO/TD 985) WMO, Geneva, 9 - 13.

Valero, F. P. J., P. Minnis, S. K. Pope, A. Bucholtz, B. C. Bush, D. R. Doelling, W. L. Smith, Jr., and X. Dong, 2000: The absorption of solar radiation by the atmosphere as determined using satellite, aircraft, and surface data during the ARM Enhanced Short-wave Experiment (ARESE). *J. Geophys. Res.*, **105**, 4743-4758.

Valero, F. P. J., R. D. Cess, M. Zhang, S. K. Pope, A. Bucholtz, B. Bush, and J. Vitko, 1997: Absorption of solar radiation by the cloudy atmosphere: Interpretations of collocated aircraft measurements. *J. Geophys. Res.*, **102**, 29,917-29,927.

Valero, F. P. J., W. J. Y. Gore, and L. P. M. Giver, 1982: Radiative flux measurements in the troposphere. *Appl. Opt.*, **21**, 831-838.

Verschell, M. A., M. A. Bourassa, D. E. Weissman, and J. J. O'Brien, 1999: Ocean model validation of the NASA scatterometer winds. *J. Geophys. Res.*, **104**, 11359-11373.

Vorosmarty C. J., Fekete B., and Tucker B.A., 1996. *Global River Discharge Data Base* (RivDIS v1.0), IHP-V Theme 1, Unesco 1996.

Waliser D. E. , W. D. Collins, and S. P. Anderson, 1996: An estimate of the surface shortwave cloud forcing over the western Pacific during TOGA COARE *Geophys. Res. Lett.* **23**: (5) 519-522.

Walton, C. C., Pichel W.G., Sapper J.F., and May D.A., 1998: The development and operational application of nonlinear algorithms for the measurement of sea surface temperatures with the NOAA polar-orbiting environmental satellites *J. Geophys. Res.* **103**: (C12) 27999-28012.

WAMDI group: Hasselmann, S., & co-authors, 1988: The WAM model - a third generation ocean wave prediction model. *J Phys, Oceanogr.*, **8**, 1775-1810.

Wang, T., K.B.Earnshaw and R.S.Lawrence, 1978: Simplified optical path-average rain gauge. *Applied Optics*, **17**, 385-390.

Wang, T., K.B.Earnshaw and R.S.Lawrence, 1979: Path-averaged measurements of rain rate and raindrop size distribution using a fast-response optical sensor. *J. Applied Meteor.*, **18**, 654-660.

Ward, M.N., 1992: Provisionally corrected surface wind data, worldwide ocean-atmosphere surface fields, and Sahelian rainfall variability. *J.Climate*,**5**, 454-475.

Ward, N.M. and B.J.Hoskins, 1996: Near surface wind over the Global Ocean 1949-1988. *J.Climate*, **9**, 1877-1895.

Warren *et al.*, 1988 *Global Distribution of Total Cloud Cover and Cloud Type Amounts over the Ocean* (for digital version see http://cdiac.ESD.ORNL.GOV/ndps/ndp026.html )

WCRP, 1985: *Report on the third session of the JSC/CCCO TOGA Scientific Steering Group.* WMO/TD-No. 81, WCP-107, 26pp.

WCRP, 1989: *WOCE Surface Flux Determinations - A strategy for in situ measurements.* Working Group on *in situ* measurements for Fluxes WCRP-23 (WMO/TD No.304), WMO, Geneva.

WCRP, 1990: *Scientific plan for the TOGA Coupled Ocean-Atmosphere Response Experiment,* WCRP Pub. 3 Addendum (WMO/TD 64 Addendum), WMO.

WCRP, 2000: *Proc. Conf. 2nd Intl. Conf. on Reanalyses*, Reading, England, 23-27 Aug. 1999. WCRP-109 (WMO/TD 985) WMO, Geneva.

Weare, B.C., and P.T.Strub, 1981: The significance of sampling biases on calculated monthly mean oceanic surface heat fluxes. *Tellus*, **33**, 211-224.

Webb, E. K., 1970: Profile relationships: the log-linear range and extension to strong stability, *Quart. J. Roy. Meteor. Soc.* **96** (407) 67 – 90.

Webb, E.K., G.I. Pearman and R. Leuning, 1980: Correction of flux measurements for density effects due to heat and water vapor transport. *Quart. J. Roy. Meteor. Soc.,* **106**, 85-100.

Webster, P.J. and R. Lukas, 1992; TOGA COARE. The coupled ocean atmosphere response experiment. *Bull. Am. Meteor. Soc.* **72**, 1377-1416.

Webster, P.J., C.A. Clayson and J.A. Curry, 1996: Clouds, radiation, and the diurnal cycle of sea surface temperature in the tropical western Pacific. *J. Climate,* **9**, 1712-1730.

Weller, R. A. and P. K. Taylor, 1999: A Strategy for Marine Meteorological and Air-Sea Flux Observation. *Preprint volume: 3rd Symp. on Integrated Observing Systems*, Dallas, Texas, Jan., 1999, AMS, Boston.

Weller, R. A. and S. P. Anderson, 1996: Surface Meteor. and air-sea fluxes in the western equatorial Pacific warm pool during the TOGA Coupled Ocean-Atmosphere Experiment. *Journal of Climate*, **9**, 1959 - 1990.

Weller, R. A., D. L. Rudnick and N. J. Brink, 1995: Meteorological variability and air-sea fluxes at a closely spaced array of surface moorings. *J. Geophys. Res.*, **100**(C3), 4867 - 4883.

Weller, R. A., M. F. Baumgartner, S. A. Josey, A. S. Fischer and J. Kindle, 1998: Atmospheric forcing in the Arabian Sea during 1994-1995 : observations and comparisons with climatology and models. *Deep Sea Research II*, **45**, 1961 - 1999.

Weller, R.A., S.P.Anderson, H.W. Wijesekera, C.A.Paulson, M.F.Cronin, and L.M.Rothstein, 1999: Oceanic response to buoyancy flux and wind stress during COARE. *Proc. Conf. TOGA coupled ocean-atmosphere response experiment (COARE).* WMO/TD-No.940, WMO, Geneva, 43-58.

Wells, N. C. and S. King-Hele, 1990: Parameterization of tropical ocean heat flux. *Quart. J. Roy. Meteor. Soc.*, **116**, 1213 - 1224.

Wentz, F. J. and R. W. Spencer, 1998: SSM/I rain retrievals within a unified all-weather ocean algorithm. *J. Atmos. Sci.*, **55**, 1613 - 1627.

Wentz, F. J., 1975: A two-scale scattering model for foam free sea microwave brightness temperatures. *J. Geophys. Res.*, **80**, 3441 - 3446.

Wentz, F. J., 1989: *User's manual SSM/I geophysical tapes.* Tech. Rep. 060989, 16 pp [available from Remote Sensing Systems, Santa Rosa, CA, USA].

Wentz, F. J., 1994: *User's manual SSM/I-2 geophysical tapes,* RSS Tech. Rep. 070194, 44pp. [from Remote Sensing Systems, Santa Rosa, CA, USA].

Wentz, F. J., 1997: A well calibrated ocean algorithm for SSM/I. *J. Geophys. Res.*, **102**, 8703 - 8718.

White, G. and A. da Silva, 1998: An intercomparison of surface marine fluxes from GEOS-1/DAS, ECMWF /ERA and NCEP/NCAR reanalyses. *9th Conf. On Interaction of the Sea and Atmos.*,11-16 Jan., Phoenix, AZ. Amer. Meteor. Soc., Boston, MA, 20-23.

White, G. and S. Saha, 1999: Estimation of the global energy and water cycle from global data assimilation. *Global Energy and Water Cycles*, K. A. Browning and R. J. Gurney, ed., Cambridge University Press, Cambridge, UK, 55-60.

White, G. H., 1995: An Intercomparison of Prec-ipitation and Surface Fluxes from Operational NWP Analysis/Forecast Systems. *CAS/JSC Working Group on Numerical Experimentation Report 22*. WMO/TD-723. WMO, Geneva, 33 pp +figs.

White, G., 1996b: Fluxes from operational analysis/forecast systems and the NCEP/NCAR reanalysis. *WCRP Workshop on Air-Sea Flux Fields for Forcing Ocean Models and Validating GCMs*, Reading, England, 24-27 Oct. 1995,WMO/TD-762. WMO, Geneva, 131-137.

White, G., 2000: Long-term trends in the NCEP/NCAR reanalysis. *2nd Intl. Conf. on Reanalyses,* Reading, England, 23-27 Aug. 1999. WCRP-109 (WMO/TD 985) WMO, Geneva, 54 - 57.

White, G., ed., 1996a: *WCRP Workshop on Air-Sea Flux Fields for Forcing Ocean Models and Validating GCMs*. Reading, England, 14-17 Oct. 1995. WMO, Geneva, WMO/TD-No. 762, 184 pp.

Whitlock, C. H., & co-authors, 1995: First global WCRP short wave Surface radiation Budget dataset. *Bull. Amer. Meteor. Soc.*, **76**, 905-922.

Wick, G.A., 1995: Evaluation of the variability and predictability of the bulk-skin sea surface temperature difference with application to satellite-measured sea surface temperature. *Ph.D. Thesis,* Dept. of Aerospace Engineering Sciences, University of Colorado. 146 pp.

Wick, G.A., W.J. Emery, L.H. Kantha, and P. Schlussel, 1996: The behavior of the bulk – skin sea surface temperature difference under varying wind speed and heat flux. *J. Phys. Ocean.*, **26**, 1969-1988.

Wielicki, B. A., and B. Barkstrom, 1991: Clouds and the Earth's Radiant Energy System (CERES): An Earth Observing System Experiment. *Second Symp. on Global Change Studies,* New Orleans, LA, Jan. 14-18, 1991, 11-16.

Wijffels, S.E., R.W.Scmitt, H.Bryden and A. Stigebrand, 1992: Transport of freshwater by the Ocean. *J.Phys. Oceanogr.*, **22**, 155-162.

Wild M., A. Ohmura, H. Gilgen, E. Roeckner 1995: Validation Of General-Circulation Model Radiative Fluxes Using Surface Observations. *J Climate* **8** (5 Part 2) 1309-1324.

Wild, M., 1999: Discrepancies between model-calculated and observed shortwave atmospheric absorption in areas with high aerosol loadings. *J. Geophys. Res.*, **104**, 27,361-27,373.

Wild, M., 2000: Assessment of surface and atmospheric radiation budgets in the ECMWF/NCEP/NASA reanalyses using collocated surface and satellite data. *Proc. Conf. 2nd Intl. Conf. on Reanalyses*, Reading, England, 23-27 Aug. 1999. WCRP-109 (WMO/TD 985) WMO, Geneva, 181 - 184.

Wild, M., A. Ohmura, H. Gilgen, and J. J. Morcrette, 1998: Assessment of the ECMWF reanalysis radiative fluxes using surface observations. *Proc. 1st WCRP Intl. Conf. on Reanalyses.* 27-31 Oct. 1997, Silver Spring, MD, USA, WCRP-104, WMO/TD-876. WMO, Geneva, 69-72.

Wilkerson, J.C. and M.D. Earle, 1990: A study of differences between environmental reports by ships in the voluntary observing program and measurements from NOAA buoys. *J. Geophys. Res.*, **95**, 18,225-18,268.

Williams, C. R., W.L. Ecklund, K. S. Gage, E. R. Westwater, and J. B. Snider, 1995: Comparison of integrated liquid water content derived from a 915 MHz wind profiler and a dual frequency microwave radiometer in the tropics, *Preprint vol. 27th Conf. on Radar Meteor.,* Vail, CO, 279-280, Oct., 1995.

Williams, C.R., W.L. Ecklund, P. Johnson and K.S. Gage, 1999: Precipitation climatology observed with profilers during TOGA-COARE. *Proc. Conf. on the TOGA Coupled Ocean-Atmosphere Response Experiment (COARE98), Boulder CO, 7-14 July 1998,* pp. 191-192, WCRP-107, WMO, Geneva.

WMO, 1970: *The Beaufort scale of wind force (technical and operational aspects).*, World Meteorological Organisation, Geneva, 22 pp.

WMO, 1985: Instruments and observing methods Report No. 25. *Workshop on the correction of precipitation measurements*, Zurich, Switzerland, 1-3 April 1985 (B. Sevruk, Ed.), WMO/TD – No. 104, 288 pp.

WMO, 1989: Instruments and observing methods Report No. 48. *International workshop precipitation measurements,* St. Moritz, Switzerland, 3-7 December 1989 (B. Sevruk, Ed.), WMO/TD – No. 328, 584 pp.

WMO, 1990: *International list of selected, supplementary and auxiliary ships,* World Meteorological Organisation, Geneva.

Wolter, K., 1997: Trimming problems and remedies in COADS. *J.Climate.*, **10**, 1980-1997.

Woodruff, S. D., R. J. Slutz, R. L. Jenne and P. M. Steurer, 1987: A comprehensive ocean-atmosphere data set. *Bul. Amer. Meteor. Soc.* , **68** , 1239-1250.

Woodruff, S. D., S. J. Lubker, K. Wolter, S. J. Worley and J. D. Elms, 1993: Comprehensive Ocean-Atmosphere Data Set (COADS) release 1a: 1980-92. *Earth System Monitor*, **4**, 4 - 8.

Woodruff, S.D., H.F.Diaz, J.D.Elms, S.J.Worley, 1998: COADS Release 2 data and metadata enhancements for improvements of marine surface flux fields. *Phys. Chem. Earth* , 23, 5/6, 517-526.

World Climate Research Programme, 1990: *Global Precipitation Climatology Project: Implementation and data management plan.* WMO/TD-No. 367, WMO, Geneva, 47pp.

Wright, P.B. 1988: *An atlas based on the COADS data set: Fields of mean wind, cloudiness and humidity at the surface of the global ocean.* Rep. No.14 Max-Planck-Institut für Meteorologie, Hamburg.

Wu, J., 1968: Laboratory studies of wind-wave interactions. *J. Fluid Mech.*, **34**, 91-111.

Wu, J., 1980: Wind-stress coefficients over sea surface near neutral conditions – a revisit. *J. Phys. Oceanog.*, **10**, 727-740.

Wu, J., 1994: The sea surface is aerodynamically rough even under light winds. *Boundary-Layer Meteor.*, **69**, 149-158.

Wu, S. T. and A. K. Fung, 1972: A noncoherent model for microwave emissions and backscattering from the sea surface. *J. Geophys. Res.*, **77**, 5917 - 5929.

Wu, Z., and K. Li, 1995: Wind speed discontinuity related to Beaufort wind observations and its influence on latent heat flux. *Proc. Internat. COADS Winds Workshop*, Kiel, Germany, 1994. Ed. H.Diaz and H.-J.Isemer, NOAA-ERL, IFM (Kiel), 212-231.

Wunsch, C., 1984: An eclectic Atlantic Ocean circulation model. Part 1: The meridional flux of heat. *J. Phys. Ocean.*, **14**, 1712-1733.

Xie, P. and P. A. Arkin, 1997: Global precipitation: a 17-year monthly analysis based on gauge observations, satellite estimates, and numerical model outputs. *Bull. Amer. Meteor. Soc.*, **78**, 2539 - 2558.

Xie, P. and P. A. Arkin, 1998: Global monthly precipitation estimates from satellite-observed outgoing longwave radiation. *J. Climate*, **11**, 137 - 164.

Xie, P., and P. A. Arkin, 1996: Analyses of global monthly precipitation using gauge observations, satellite estimates and numerical model predictions. *J. Climate*, **9**, 840-858.

Yanai, M., S. Esbensen and J.H. Chu, 1973: Determination of bulk properties of tropical cloud clusters from large-scale heat and moisture budgets. *J. Atmos. Sci.*, **30**, 611-627.

Yang, D., B. E. Goodison, J. R. Metcalfe, V. S. Golubev, R. Bates, T. Pangburn and C. L. Hanson, 1998: Accuracy of NWS 8" standard nonrecording precipitation gauge: Results and application of WMO comparison. *J. Atmos. Oceanic Tech.*, **15**, 54-68.

Yau, M.K., and M. Jean, 1989: Synoptic aspects and physical processes in the rapidly intensifying cyclone of 6-8 March 1986. *Atmosphere-Ocean*, **27**, 59-86.

Yelland M.J. and P.K.Taylor, 1996: Wind stress measurements from the open ocean. *J. Phys. Oceanogr.*, **26**, 541-558.

Yelland, M. J., 2000: A direct comparison of open ocean and coastal wind stress measurements. *(unpublished manuscript)*.

Yelland, M. J., B. I. Moat, P. K. Taylor, R. W. Pascal, J. Hutchings and V. C. Cornell, 1998: Measure-ments of the open ocean drag coefficient corrected for air flow disturbance by the ship. *J. Phys. Oceanogr.*, **28**, 1511 - 1526.

Young, I.R. and G.J. Holland, 1996: *Atlas of the Oceans: Wind and Wave Climate*, Pergamon Press, 241 pp.

Young, I.R., 1999: Seasonal variability of the global ocean wind and wave climate, *Int. J. Climatol.*, **19**, 931-950.

Yu, L. S., and P. Malonotte-Rizzoli, 1998: Inverse modeling of seasonal variations in the North Atlantic Ocean. *J. Phys. Oceanogr.*, **28**, 902-922.

Yu, L., and J. J. O'Brien, 1995: Variational data assimilation for determining the seasonal net surface heat flux using a tropical Pacific ocean model. *J. Phys. Oceanogr.*, **25**, 2319-2343.

Zavody, A. M., M. R. Gorman, D. J. Lee, D. Eccles, C. T. Mutlow and D. T. Llewellyn-Jones, 1994: The ATSR data processing scheme developed for the EODC. *Int.J.Remote Sensing*, **15**, 827 - 843.

Zender, C. S., B. Bush, S. K. Pope, A. Bucholtz, W. D. Collins, J. T. Kiehl, F. P. J. Valero and J. J. Vitko, 1997: Atmospheric absorption during the Atmospheric Radiation Measurement (ARM) enhanced shortwave experiment (ARESE). *J. Geophys. Res.*, **102**(D25), 29901 - 29917.

Zeng, L. and G. Levy, 1995: Space and time aliasing structure in monthly mean polar-orbiting satellite data. *J. Geophys. Res.*, **100**, 5133-5142.

Zeng, L. X. and R. A. Brown, 1998: Scatterometer observations at high wind speeds. *J. Appl. Meteor.*, **37**, 1412 - 1420.

Zeng, X. ; Zhao, M. ; Dickinson, R. E. ; He, Y. 1999 A multiyear hourly sea surface skin temperature data set derived from the TOGA TAO bulk temperature and wind speed over the tropical pacific *J. Geophys. Res.*, **104**, 1525 – 1536.

Zeng, X., M. Zhao, and R. E. Dickinson, 1998: Intercomparison of bulk aerodynamical algorithms for the computation of sea surface fluxes using TOGA COARE and TAO data. *J. Climate*, **11**, 2628-2644.

Zhang, G.J. and M.J. McPhaden, 1995: The relationship between sea surface temperature and latent heat flux in the equatorial Pacific. *J. Climate*, **8**, 589-605.

Zhang, G.J., 1995: Use of monthly mean data to compute surface turbulent fluxes in the Tropical Pacific. *J. Climate*, **8**, 3084-3090.

Zhang, Y-C., W.B. Rossow and A.A. Lacis, 1995: Calculation of surface and top-of-atmosphere radiative fluxes from physical quantities based on ISCCP datasets, Part I: Method and sensitivity to input data uncertainties. *J. Geophys. Res.*, **100**, 1149-1165.

Zillmann, J. W., 1972: A study of some aspects of the radiation and the heat budgets of the southern hemisphere oceans., Bureau of Meteor., Department of the Interior, Canberra,  Australia.

Zipser, E. J.,  and R. H. Johnson, 1998: Systematic errors in radiosonde humidities: A global problem? *Proc. 10th Symp. on Meteorol. Obs.*, 11-16 Jan., Phoenix, Amer. Meteor. Soc., Boston, MA, 72-73.

Zolina, O., and S.K.Gulev, 1998: Intercomparison of the NCEP Reanalysis winds to the instrumental measurements and VOS observations in the North Atlantic, In: *First International Conference on Reanalyses*, WMO/TD-876, WMO, 298-301.

Zupanski, M., and E. Kalnay, 1999: Principles of data assimilation. *Global Energy and Water Cycles*, K. A. Browning and R. J. Gurney, ed., Cambridge University Press, Cambridge, UK, 48-52.

Zwally, H.J., Comiso, J.C., Parkinson, C.L., Campbell, W.J., Carsey, F.D., and Gloersen, P., 1983: *Antarctic Sea Ice, 1973-1976: Satellite Passive-Microwave Observations*, NASA SP-459, Washington, D.C.

## APPENDIX A.  MEMBERS OF THE WORKING GROUP ON AIR-SEA FLUXES

Dr. Sergey Gulev (co-chair),
P.P.Shirshov Institute of Oceanology,
RAS
36 Nakhimovsky Ave.,
117218 Moscow,
Russia

Peter K. Taylor  (co-chair),
James Rennell Division (254/27)
Southampton Oceanography Centre,
European Way,
Southampton, SO14 3ZH,
United Kingdom

Dr. Bernard Barnier
LEGI
Institut de Mécanique de Grenoble
BP53, 38041, Grenoble Cedex,
France

Dr. E. Frank Bradley
CSIRO, Land and Water,
GPO Box 1666,
Canberra, ACT 2601,
Australia

Dr. Tom Charlock
Atmospheric Sciences Division
Mail Stop 420
NASA Langley Research Center
Hampton,  VA 23681-0001,
USA

Dr. Peter Gleckler
PCMDI,
Lawrence Livermore National Lab,
P.O. Box 808, L-264
University of California,
Livermore,  CA, 94551,
USA

Prof. Masahisa Kubota
School of Marine Science and
Technology,Tokai University
Orido,
Shimizu,
Shizuoka  424-8610.
JAPAN

Dr. Kunio Kutsuwada,
School of Marine Science and Technology,
Tokai University
3-20-1, Orido,
Shimizu,  Shizuoka 424-8610,
Japan

Dr. David Legler
COAPS, Florida State University
2035 E.Paul Dirac Drive
R.M.Johnson Bldg. - Suite 200
Tallahassee, FL 32306-2840,
USA

Dr. Ralf Lindau
Institut für Meereskunde
Duesternbrooker Weg. 20,
D-24105  Kiel,
Germany

Dr. Drew Rothrock
Applied Physics Laboratory,
University of Washington,
1013 NE 40th Streeet,
Seattle,   WA 98105,
USA

Dr. Joerg Schulz
Deutsches Zentrum für Luft- und Raumfahrt
DFD-US KP
Linder Hoehe
D-51170 Koeln,
Germany

Dr. Arlindo da Silva
Data Assimilation Office
Goddard Space Flight Center,
Greenbelt,
Maryland, 20771,
USA

Dr. Andreas Sterl
KNMI,
PO Box 201
3730 AE De Bilt,
The Netherlands

Dr. Glenn White
W/NMC2, WWB, Rm.207
National Centers for Environmental
Prediction
5200 Auth Rd.
Washington, D.C. 20233, USA

## APPENDIX B.   CATALOGUE OF FLUX DATA SETS AND FLUX RELATED PRODUCTS

### B.1 Introduction

This Appendix give details of how to access the catalogue, the catalogue contents, and the information which should be submitted for each catalogue entry.

### B.2 Accessing the Catalogue

The Catalogue of Flux products is available on the Internet at
http://www-pcmdi.llnl.gov/airseawg/
and also mirrored at
http://www.lmd.jussieu.fr/pcmdi-mirror/airseawg/
and at
http://www.bom.gov.au/bmrc/clch/pcmdi-mirror/airseawg/

It is intended that this catalogue should be continued to be maintained following the end of the Working Groups term of office.

### B.3 Preliminary Initial Contents List

Arctic Global Radiation (AGR-1) Data Set of point observations

Arctic Global Radiation (AGR-2) Gridded Data Set

Arctic Ocean Radiative Fluxes

Atlas and Ardizzone SSMI-derived winds

CERSAT

ECMWF Operational Analyses

ERA-15 Reanalysis

FSU Tropical pseudo stress analyses

GEOS1 Reanalysis

Gridded Daily and Monthly Arctic Atmospheric and Surface Data from TOVS

HOAPS fluxes from satellite

IABP/POLES 2-m air temperature data set

IfM Fluxes and Flux Related Data Set

IORAS/IFM North Atlantic wave and wave dependent wind stress

Japanese Ocean Flux data sets with Use of Remote sensing Observations

NCEP-1 Reanalysis

NCEP-2 Reanalysis

NMC/NCEP Operational Analyses

OCEANOR wave fields

ORSTOM Tropical Atlantic Pseudo-stress and Sea Surface Temperature Analyses

Polar Radiation Fluxes

SOC Satellite altimeter significant wave height global climatology

SOC Climatology

UWM/COADS Climatology

WAM cycle 4 data obtained with ECMWF Re-Analysis winds

WAM wave hindcasts using ERA winds

WOCE Surface Meteorology Data

### B.4 Information to be Submitted

Table B.1 (overleaf) shows the categories of information which are required for a product entry and for a verification data set such as an air-sea interaction experiment.

| PRODUCT DATA SET | EXPERIMENT DATA SET |
|---|---|
| Name: | Area: |
| Geographical area: | Time Period: |
| Time period: | **VARIABLES:** |
| Grid: (space/time) | platforms |
| Resolution:(space/time; note that this may be less than the grid spacing) | instruments (accuracies) |
| **VARIABLES:** | **FLUXES:** |
| Formulae used | measured (method) |
| Data sources | calculated (formulae) |
| Corrections applied | **AVAILABILITY** |
| **AVAILABILITY:** | How/Where |
| How/where: | Formats |
| Format(s) | References |
| **DOCUMENTATION:** | **DOCUMENTATION** |
| Product documentation: | Comments |
| Reference list: | |
| **COMMENTS:** | |
| (including notes on strengths/weaknesses and results of quality tests where these are available) | |

## APPENDIX C. ACRONYMS AND ABBREVIATIONS

| | |
|---|---|
| 4DVAR | 4D variational assimilation |
| ADM | Angular Distribution Models |
| ADCP | Acoustic Doppler Current Profiler |
| AERI | Atmospheric Emitted Radiance Interferometer |
| AES | (Canadian) Atmospheric Environment Service |
| AGCM | Atmospheric General Circulation Model |
| AIDJEX | Artic Ice Dynamics Joint Experiment |
| AIP | Algorithm Intercomparison Projects ( of GPCP) |
| AMIP | Atmospheric Model Intercomparison Project |
| AMSR | Advanced Scanning Microwave Radiometer |
| AOGCM | Atmospheric Ocean General Circulation Model (coupled model) |
| ARESE | ARM Enhanced Shortwave Experiment |
| ARGO | (experiment to deploy drifting buoys for ocean data assimilation) |
| ARKTIS'93 | Polarstern Arctic cruises |
| ARM | Atmospheric Radiation Measurement program |
| ARPEGE | Action de Recherche Petite Echelle Grande Echelle - French climate model |
| ASTEX | Atlantic Stratocumulus Transformation Experiment |
| ATLAS | Autonomous Temperature Line Acquisition System |
| ATOVS | Advanced TIROS Operational Vertical Sounder |
| ATSR | Along-Track Scanning Radiometer |
| AVHRR | Advanced Very High Resolution Radiometer |
| BOMEX | Barbados Oceanographic Meteorological Experiment |
| BDRF | Bi-Directional Reflectance Function |
| BSRN | Baseline Surface Radiation Network |
| CAGEX | CERES/ARM/GEWEX experiment |
| CART | (ARM) Cloud and Radiation Testbed |
| CASP | Canadian Atlantic Storm Project |
| CASPR | Cloud and Surface Parameter Retrieval system |
| CCN | Cloud Condensation Nuclei |
| CDAS | Climate Data Assimilation System |
| CDC | (US) Climate Diagnostics Center |
| CEAREX | Coordinated Eastern Arctic Experiment |
| CEPEX | Central Equatorial Pacific Experiment |
| CERES | Clouds and the Earth's Radiant Energy System |
| CERSAT | Centre ERS-1 d'Archivage et de Traitement |
| CFD | Computational Fluid Dynamics |
| CIMO | WMO Commission for Instruments and Methods of Observation |
| CLASS | (ARM radiosonde type) |
| CMAP | CPC Merged Analysis of Precipitation |
| CMDL | (NOAA) Climate Monitoring and Diagnostics Laboratory |
| CMMIV | Beaufort Scale defined by Commision for Marine Meteorology 4th Session |

| | |
|---|---|
| CMR-5 | Compressed Marine Reports--Product 5 (of COADS) |
| COADS | Comprehensive Ocean-Atmosphere Data Set |
| COAPS | Center for Ocean Atmosphere Prediction Studies (FSU) |
| COARE | Coupled Ocean-Atmosphere Response Experiment |
| COLA . | Centre for Ocean-Land-Atmosphere Studies |
| COMPARE | CERES Ocean Measurement Platform for Aerosol and Radiation Evaluation |
| CPC | Climate Prediction Center |
| CSIRO | Commonwealth Scientific and Industrial Reserch Organisation (Australia) |
| CTD | Conductivity Temperature and Depth (instrument) |
| CTT | Convective Transport Theory |
| DAAC | Distributed Active Archive Center |
| DAO | Data Assimilation Office |
| DMSP . | Defense Meteorological Satellite Program |
| DOE | Department of Energy |
| DSD | Drop Size Distribution |
| ECHAM3 | European Centre model with HAMburg physics (version 3) |
| ECMWF | European Centre for Medium Range Weather Forecasting |
| ENSO | El Niño / Southern Oscillation |
| EOF | Empirical Orthogonal Function |
| EOS-AM1 | Earth Observation System AM1 satellite (now Terra) |
| ERA15 | ECMWF 15 year reanalysis |
| ERBE | Earth Radiation Budget Experiment |
| ERI | Engine Room Intake |
| ERICA | Experiment on Rapidly Intensifying Cyclones over the Atlantic |
| ERS-1 | European Remote Sensing satellite |
| ESA | European Space Agency |
| ESTAR | Electrically Scanning Thinned Array Radiometer |
| EUMETSAT | European Meteorological Satellite agency |
| EUROWAVE | (system for diagnosis and forecasting of waves in European coastal areas) |
| FASINEX | Frontal Air-Sea Interaction Experiment |
| FIFE | First ISCCP Field Experiment |
| FNOC | Fleet Numerical Oceongraphy Center |
| FSU | Florida State University |
| FTIR | Fourier Transform Infrared Instrument |
| FTP | File Transfer Protocol |
| GALE | Genesis of Atlantic Lows Experiment |
| GARP | Global Atmospheric Research Programme |
| GATE | GARP Atlantic Tropical Experiment |
| GCI | Global Cloud Imagery |
| GCM's | General Circulation Models |
| GCOS | Global Climate Observing System |
| GEBA | Global Energy Balance Archive |
| GEOS1 | first Goddard Earth Observation System reanalysis |
| GEOSAT | (altimetric satelllite) |
| GEWEX | Global Energy and Water Cycle Experiment |

| | | | | |
|---|---|---|---|---|
| GIN | Greenland/Iceland/Norwegian Seas | | METEOSAT | [European] geostationary meteorological satellite |
| GISS | Godard Institute for Space Studies | | MFWT . | Meridional Fresh Water Transport |
| GISST | Global Ice and Sea Surface Temperature (project) | | MHT | Meridional Heat Transport |
| GMS | [Japanese] Geostationary Meteorological Satellite | | MJO | Madden-Julian oscillation |
| GODAE | Global Ocean Data Assimilation Experiment | | MODIS | MODerate resolution Imaging Spectro-radiometer |
| GOES-E/W | [US] geostationary meteorological satellites | | MSTG | COADS Monthly Summary Trimmed Groups |
| GOOS | Global Ocean Observing System | | MSU | Microwave Sounding Unit |
| GPCP | Global Precipitation Climatology Project | | MWSR | Microwave Water Substance Radiometer |
| GPI | Geostationary Precipitation Index | | NAO | North Atlantic Oscillation |
| GPS | Global Positioning System | | NASA | (US) National Aeronautics and Space Administration |
| GRDC | Global Runoff Data Centre | | NCAR | (US) National Center for Atmospheric Research |
| GSFC | Goddard Space Flight Centre | | | |
| GTS | Global Telecommunications System | | NCAR CCM3 | NCAR Community Climate Model (version 3) |
| HadCM3 | Hadley Centre Climate Model (version 3) | | | |
| HEXMAX | (main HEXOS field experiment) | | NCAR-ATD | NCAR Atmospheric Technology Division |
| HEXOS | Humidity Exchange Over the Sea (experiment program) | | NCAR-CSM | NCAR Climate System Model |
| HIRS | High-resolution Infrared Radiation Sounder | | NCEP | (US) National Centers for Environmental Prediction |
| HOAPS | Hamburg Ocean Atmosphere Parameters and Fluxes from Satellite Data | | NCEP1/NCEP2 | NCEP/NCAR reanalyses |
| | | | NDBC | (US) National Data Buoy Center |
| IABP/POLES | International Arctic Buoy Programme/Polar Exchange at the Sea Surface | | NESDIS | (US) National Environmental Satellite Data and Information Service |
| | | | NHF | Net Heat Flux |
| ICE | International Cirrus Experiment | | NIP | Normal Incidence Pyrheliometer |
| ICRCCM | Intercomparison of Radiation Codes in Climate Models | | NLW | Net Long Wave |
| | | | NMC | National Meteorological Centre (now NCEP) |
| IFREMER | Institut Français de la Researche sur la Mer | | NOAA | (US) National Oceanic and Atmospheric Administration |
| IfM | Institut für Mereskunde Kiel | | | |
| IHP | International Hydrography Program | | NOAA/ETL | NOAA Environment Technology Laboratory |
| IMET | Improved Meteorology (WHOI instrumentation package) | | NODC | National Oceanographic Data Center |
| | | | NPO | North Pacific Oscillation |
| IOP | Intensive Observation Phase | | NSCAT | NASA Scatterometer |
| IPCC | International Panel on Climate Change | | NSW | Net Short Wave |
| IR | InfraRed | | NWP | Numerical Weather Prediction |
| ISCCP | International Satellite Cloud Climatology Project | | OCL | Ocean Climate Laboratory |
| | | | ODA | Ocean Data Assimilation |
| ITCZ | Inter-Tropical Convergence Zone | | ODBS | (Japan) Ocean data Buoy System |
| JASIN | Joint Air-Sea Interaction Experiment | | ODGP | Ocean Data Gathering Programme |
| JASMINE | Joint Air Sea Monsoon Experiment | | OGCM | Ocean General Circulation Model |
| JMA . | Japan Meteorological Agency | | OI | Optimal Interpolation |
| JONSWAP | Joint North Sea Wave Project | | OLR | Outgoing Longwave Radiation |
| JSC | Joint Scientific Committee (of the WCRP) | | OPAICE | (French Ocean and ICE model) |
| KNMI | Koninklijk Nederlands Meteorologisch Instituut | | OPI | OLR based Precipitation Index |
| | | | ORG | Optical Raingauge |
| KWAJEX | TRMM validation Experiment around Kwajalein island | | ORSTOM | (Institut français de recherche scientifique pour le développement en coopération) |
| LabSea | Labrador Sea Deep Convection Experiment | | OWS | Ocean Weather Ship |
| | | | P-ALACE | Profiling Autonomous Lagrangian Circulation Explorer |
| LBLRTM | Line-By-Line Radiative Transfer Models | | | |
| LEADEX | (Remote Sensing of Lead Properties in the Arctic) | | PCMDI | Program for Climate Model Diagnosis and Intercomparison |
| LMD | Laboratoire de Mètèorologie Dynamique (Paris, france) | | PI | Principal Investigator |
| | | | PIP | Precipitation Intercomparison Project |
| LMR | Long Marine Records | | PIR | Eppley precision infrared radiometer |
| LOWTRAN7 | (radiation transfer code) | | PIRATA | Pilot Research Moored Array in the Tropical Atlantic |
| LSG | Large Scale Geostrophic model | | | |
| LW | Longwave | | PNA | Pacific-North American pattern |
| MBT | Mechanical Bathythermograph | | PR | Precipitation Radar |
| MCSST | Multi Channel Sea Surface Temperature | | PROBE | Pilot Radiation Observation Experiment |
| MCTEX | Maritime Continent Thunderstorm Experiment. | | PROVOR | (FRENCH PROFILING FLOAT) |
| | | | PRT | platinum resistance thermometer |

| | | | | |
|---|---|---|---|---|
| QuikScat | (NASA Scatterometry Satellite) | | SW | Shortwave |
| RADARSAT | (Canadian Scatterometry Satellite) | | SWH | Significant Wave Height |
| RAMS | (Valero radiometer) | | SWS-2 | Storm Wave Study - 2 |
| RAPS | Rotating Azimuth Plane Scanning | | TAO | Tropical Atmosphere Ocean Array |
| RGPS | RADARSAT Geophysical Processor System | | TIROS | Television InfraRed Observational Satellite |
| RH | Relative Humidity | | TMI | TRMM Microwave Imager |
| RHS | Right Hand Side | | TOA | Top Of the Atmosphere |
| RMS/rms | Root Mean Square | | TOGA | Tropical Ocean Global Atmosphere |
| RRTM | Rapid Radiative Transfer Model | | TOMS | Total Ozone Measuring System |
| RTM | Radiative Transfer Model | | TOPEX/POSEIDON (Altimetric satellite system) | |
| RTNEPH | (United States Air Force) Real-Time Nephanalysis | | TOVS | TIROS Operational Vertical Sounder |
| SAR | Synthetic Apperture Radar | | TRITON | (West Pacific buoy array) |
| SBUV | Solar Backscatter UltraViolet | | TRMM | Tropical Rainfall Measuring Mission |
| SBWR | Ship Borne Wave Recorder | | TWP | ARM Tropical West Pacific |
| ScaRaB | Scanner for Radiation Budget | | UCAR | University Corporation for Atmospheric Research |
| SCOPE | San Clemente Ocean Probing Experiment | | UKMO | United Kingdom Meteorological Office |
| SCOR | Scientific Committee on Ocean Research | | URL | Internet address (Uniform Resource Locator) |
| SCSMEX | South China Sea Monsoon Experiment | | UWM | University of Wisconsin-Milwaukee |
| SECTIONS | Energetically Active Zones of the Ocean (EAZO) and Climate Variability experiment programme | | VIRS | Visible and Infrared Scanner |
| | | | VISSR | Visible Infra Red Spin-Scan Radiometer (on GMS) |
| SEMAPHORE | Structure des Echanges Mer-Atmosphere, Proprietes des Heterogeneites Oceaniques: researche Experimentale | | VOS | Voluntary Observing Ships |
| | | | VSOP-NA | VOS Special Observing Programme - North Atlantic |
| SHEBA | Surface Heat Budget of the Arctic Ocean | | VTPR | Vertical temperature Profile Radiometer |
| SMMR | Scanning Multichannel Microwave Radiometer | | WAM | Wave Model |
| | | | WAMDI | Wave Model Development and Implementation group |
| SMOS | Soil Moisture and Ocean Salinity | | WCRP | World Climate Research Programme |
| SOC | Southampton Oceanography Centre | | WGASF | Working Group on Air-Sea Fluxes |
| SOFIA | Surface of the Ocean, Fluxes and Interactions with the Atmosphere | | WGNE | Working Group on Numerical Experimentation |
| SRB | surface radiation budget | | WHOI | Woods Hole Oceanographic Institution |
| SRB | Surface Radiation Budget | | WMO | World Meteorological Organisation |
| SSI | spectral statistical interpolation | | WOCE | World Ocean Circulation Experiment |
| SSM/I | Special Sensor Microwave/Imager | | WOCE AIMS | WOCE Analysis Interpretation Modelling and Synthesis |
| SSS | Sea Surface Salinity | | WRR | World Radiation Reference |
| SSST | Sea Surface SkinTemperature | | XBT | Expendable Bathy-Thermograph |
| SST | Sea Surface Temperature | | XCTD | Expendable CTD |
| SVD | Singular Vector Decomposition | | | |